The Structure of Measurements and States in Quantum Theory

Habilitationsschrift

vorgelegt von

Dr. rer. nat. Matthias Kleinmann

eingereicht bei der Naturwissenschaftlich–Technischen Fakultät

der Universität Siegen

Siegen, 2019

gedruckt auf alterungsbeständigem holz- und säurefreiem Papier

SUMMARY

This thesis concerns the structure of quantum theory as the fundamental contemporary theoretical framework of physics. Prior to quantum theory, the underlying frameworks for most of fundamental physics had been the frameworks of classical mechanics and classical statistics. In a broad sense, such frameworks provide the means to describe and model situations that occur in physics. They allow to study abstract systems like the harmonic oscillator, concrete systems like the orbits of planets, or fundamental interactions as for the electromagnetic theory. The major difference between classical physics and quantum physics is how such systems are modeled. Most notably, while classical theory is centered around stable configurations and the description of the dynamics of a system, quantum theory is much richer by adding the notion of a state of the system and treating measurements in an explicit manner. Of course, the state of a system is a notion that is also present in classical theory, for example, as a point in phase space. And it is also possible to formulate a theory of measurements in classical physics. However, quantum states and quantum measurements are central to quantum theory and both are those concepts that are the least similar to classical theory. Quantum states describe the physical situation in an abstract sense, but they are not a literal description of the properties of the system. Quantum measurements are a theoretical concept that provides the interface between the formalism of quantum theory and the direct observations in an experiment.

With this central role of states and measurements in quantum theory and the abstract nature of them, enhancing our knowledge of the structure of both is an important endeavor. This thesis focuses on the structure of what states and measurements are according to the formalism of quantum theory itself. The most radical approach to quantum theory is the operational approach, particular predominant in the field of quantum information science and the neighboring field of foundations of quantum theory. Here, abstract quantum systems are studied and the experimental realization of particular concepts are often a lesser concern. This situation coevolved with the experimental advances in quantum optics, which nowadays provides us with control over physical systems to a level that abstract concepts, for example qubits, are commonly available for experimentation. This also marks the exciting transition from a point, where quantum theory is predominately used to describe physical phenomena to a theory that is ready to be used in engineering—a step that is reminiscent to the transition from a naive understanding of, for example, electromagnetic forces to the full fleshed theory of electromagnetism that allows us to build and enhance sophisticated devices such as the electric motor.

Consequently, this thesis is focused on abstract notions of states and measurements. A very general mathematical framework for a theory to capture both notions is the operational framework of general probabilistic theories. This framework is so broad that it captures quantum theory and classical probability theory as special cases. The generalization is achieved by considering an abstraction of the real vector space of Hermitian operators and an abstraction of the concept of positive semidefiniteness. These two concepts are basically enough to recover the skeleton of quantum theory, but general probabilistic theories generalize this to be applicable to virtually any conceivable operational theory. One can now ask: What is the role of quantum theory within this framework? Which concepts are native to quantum theory, and which concepts are due to the fact that quantum theory is an instance of the general probabilistic theories? This perspective is a central motivation for this thesis.

An important catalyst for the research in this thesis is the question, whether or not a theo-

retical concept, for example quantum contextuality or entanglement, is experimentally relevant. That is, whether a concept is experimentally testable, at least in principle. Eventually, this requires to consider the data from experiments, and in the ideal case this is possible without going into the details of the experimental realization. Having access to the experimental data, one can ask surprisingly simple questions, for example, is the experimental data compatible with the existence of a quantum state and the assumed measurements? This brings basic statistical analysis to the world of quantum optical experiments and enables us to study and dissect experiments on the basis of raw data.

Quantum measurements

In quantum theory, observable quantities are represented by Hermitian operators on a Hilbert space [1]. Let us consider the calculation of the expectation value of the energy $\langle E \rangle$. For this, we need the state of the system, ρ, and the operator representing the energy observable, in this case the Hamilton operator H. Then the simple formula

$$\langle E \rangle = \operatorname{tr}(\rho H) \tag{1}$$

holds. Its right hand side has a clear mathematical meaning and involves the mathematical representations of the quantum state and the energy observable. However, this does not yet give a good interpretation of the left hand side. In order to obtain this, we use the spectral decomposition of the Hamilton operator,[1] $H = \sum_j^n E_j \Pi_j$ with n distinct energy eigenvalues E_j and Π_j orthogonal projections, $\Pi_j = \Pi_j^\dagger = \Pi_j^2$. We can now write

$$\langle E \rangle = \sum_j^n E_j \operatorname{tr}(\rho \Pi_j) = \sum_j^n E_j p_j, \tag{2}$$

with $p_j = \operatorname{tr}(\rho \Pi_j)$. Born [2] identified p_j to be the probability to observe the energy E_j. We hence can understand the energy expectation value as a mean value in a Bernoulli-type experiment with n outcomes, where to each outcome j the energy E_j is associated. These outcomes are consequently in one-to-one correspondence with the projectors Π_j. We refer to the family of projectors $(\Pi_j)_j^n$ as a (sharp) quantum measurement and we identify the outcomes of the measurement with the projectors Π_j. The characteristic properties of such families are (i) all Π_j are orthogonal projections and (ii) they sum to identity, $\sum_j \Pi_j = \mathbb{1}$.

If we now implement a quantum measurement, what is the state after the measurement? There are at least three possible answers to this question: (i) No sensible state can be associated. (ii) The state depends on the implementation of the measurement apparatus. (iii) The state is given according to Lüders' rule. From a practical perspective, (i) is often the most reasonable answer, for example, for a photon detected by a camera. In other situations, (ii) is the correct, but the answer is too generic to provide further insights into the nature of quantum measurements. Answer (iii) is the one that can be found in many textbooks and is in a certain sense the most conservative one. Specifically, Lüders' rule [3] (also sometimes attributed to von Neumann) states that if a system in state ρ is measured using the measurement $(\Pi_j)_j$ and the measurement result j is ignored, then the state after the measurement is computed according to the map

$$\Lambda_{\text{ignore}} \colon \rho \mapsto \sum_j \Pi_j \rho \Pi_j. \tag{3}$$

If the measurement result is incorporated into the quantum state and the measurement result

[1] Here and in the following we always assume the underlying Hilbert space to be finite dimensional.

was j, then the rule becomes reminiscent of a Bayesian update,

$$\Lambda_j \colon \rho \mapsto \frac{\Pi_j \rho \Pi_j}{p_j}, \tag{4}$$

allowing for the relation $\Lambda_{\text{ignore}} = \sum_j p_j \Lambda_j$.

Quantum states

General quantum states are conveniently represented by a density operator ρ. If ρ is of rank one, then ρ is a pure state and often represented by a normalized vector $|\psi\rangle$, such that $\rho = |\psi\rangle\langle\psi|$. In general, pure states are superpositions $|\psi\rangle = \sum_i \psi_i |i\rangle$ of the basis states $|i\rangle$. This superposition is one of the main features of quantum theory where it differs from classical theory. It becomes particularly intriguing, when we consider situations where the quantum state describes a composite system, composed of two or more distinguishable parties or degrees of freedom. Then, the Hilbert space of the system has a natural tensor product structure, $\mathcal{H} = \mathcal{H}_A \otimes \mathcal{H}_B \otimes \cdots$, and it features entangled states. A pure state $\rho = |\psi\rangle\langle\psi|$ is entangled, if it is a superposition for any product basis $(|i, j, \ldots\rangle)_{i,j,\ldots}$ of the Hilbert space. That is, $|\psi\rangle$ is entangled [4,5] if it is not a product state, $|\psi\rangle \neq |\psi_A\rangle \otimes |\psi_B\rangle \otimes \cdots$. For mixed states, a state is entangled if it is not separable, that is, if it cannot be written as a convex combination of product states [6]. The structure of entanglement has been analyzed in detail [7].

An important concept in relation to entanglement is the paradigm of local operations and classical communication (LOCC) [7, 8]. This refers to a situation where parties can locally manipulate their part of the global system by adding and discarding auxiliary systems, performing unitary transformations, and performing measurements. In contrast, global operations that would require an interaction between the parties are not allowed—with the exception of the exchange of classical information, for example the broadcast of measurement outcomes. An LOCC protocol can consist of an arbitrary number of rounds of communication and local operations. An important aspect in the analysis of quantum entanglement is to study of how states can be transformed by means of LOCC, either deterministically or with nonvanishing probability. This leads to the definition of entanglement classes and entanglement monotones [7].

Besides this theoretical analysis, there is also the practical concern how one can provide evidence for the preparation of an entangled state [9]. This can be, for example, the mere proof of entanglement, the verification of a state being in a particular entanglement class, or the full measurement of the density operator. Entanglement detection can be used to prove good experimental control over multipartite quantum systems, since for most scenarios, creating entangled states is a difficult task and it is an important step towards full quantum control over a system.

In such an experiment, the state is subjected to different measurements, or measurement settings. Typically, these measurements are chosen to be local measurements, such that party A performs measurements $(\Pi_{a,j})_j$ from a family labeled by a, etc. This yields the correlations

$$p(i, j, \ldots | a, b, \ldots) = \operatorname{tr}[\rho(\Pi_{a,i} \otimes \Pi_{b,j} \otimes \cdots)], \tag{5}$$

for all combinations $(a, b, \ldots)$ of measurements performed in the experiment. Depending on the experimental situation, the correlations might not be fully available, but are coarse-grained due to experimental limitations, for example, if only the total angular momentum can be measured. In either way, in order to prove the entangled nature of an experimentally prepared state, methods are required that allow to infer this property from the obtained data. In the most extreme case, the projectors in Eq. (5) span the full set of Hermitian operators. Then Eq. (5) can be inverted to yield the full quantum state ρ. This is the case quantum state tomography.

1 Quantum contextuality

Quantum contextuality is a notorious nonclassical feature of quantum measurements. It expresses the fact that the outcomes of quantum measurements cannot be predetermined without specifying a measurement context. More precisely, quantum contextuality is a property of a set measurement outcomes $\{\Pi_\alpha \mid \alpha \in \mathcal{A}\}$. If this set is carefully chosen, then it is impossible to find an assignment $v\colon \mathcal{A} \to \{0,1\}$, such that

$$\sum_{\alpha\in\mathcal{C}} \Pi_\alpha = \mathbb{1} \quad \text{implies} \quad \sum_{\alpha\in\mathcal{C}} v(\alpha) = 1 \tag{6}$$

and[2]

$$\sum_{\alpha\in\mathcal{C}'} \Pi_\alpha \leq \mathbb{1} \quad \text{implies} \quad \sum_{\alpha\in\mathcal{C}'} v(\alpha) \leq 1 \tag{7}$$

for any subset $\mathcal{C}$ of $\mathcal{A}$. Specifically, if $\mathcal{C}$ satisfies the first condition in Eq. (7), then it is specifies a measurement context and $(\Pi_\alpha)_{\alpha\in\mathcal{C}}$ forms an incomplete measurement. If the first condition in Eq. (6) is satisfied, then $(\Pi_\alpha)_{\alpha\in\mathcal{C}}$ defines a complete measurement. Both conditions together enforce that v assigns exactly one outcome to a complete measurement and not more than one outcome to an incomplete measurement. By assumption this is not true for all contexts simultaneously and therefore either the outcomes of some measurements are not predetermined or the assignment must depend on the context, that is, v must depend on the context $\mathcal{C}$. The first example of a set where no assignment v exists is due to Kochen and Specker [10] and requires $|\mathcal{A}| = 117$ projectors and. The smallest possible such set has only 18 projectors [11].

In contrast, if an assignment v exists, then it constitutes a deterministic noncontextual model for the according set of projectors [10]. This is very similar to the local hidden variable models discussed by Bell [12]. For each such noncontextual model v, we obtain a vector $\vec{p} = [v(\alpha)]_\alpha$ and the set of all models for a specific set of projectors defines then the vertices of a polytope $\mathcal{P} \subset \mathbb{R}^{|\mathcal{A}|}$. The points in $\mathcal{P}$ correspond to statistical mixtures of noncontextual assignments, again in close analogy to the considerations of Bell. It is now possible that there exists a quantum state ρ, such that $\vec{q}_\rho = [\mathrm{tr}(\Pi_\alpha\rho)]_\alpha$ is not in $\mathcal{P}$. Then, this is an instance of quantum contextuality: One can find an affine function $I\colon \mathbb{R}^{|\mathcal{A}|} \to \mathbb{R}$, such that $I(\vec{p}) \leq 0$ holds for any $\vec{p} \in \mathcal{P}$ but $I(\vec{q}_\rho) > 0$. Consequently, the function I gives rise to the noncontextuality inequality $I(\vec{p}) \leq 0$. The simplest such inequality uses only 5 projectors [13]. There exist even cases where $\vec{q}_\rho \in \mathcal{P}$ does not hold for any quantum state ρ. Then, this is an instance of a state-independent noncontextuality inequality, the simplest of which uses 13 projectors [14].

The structure of state-independent quantum contextuality

A scenario for state-independent contextuality in particular exhibits contextual behavior for systems in the completely mixed quantum state, $\rho = \mathbb{1}/\,\mathrm{tr}(\mathbb{1})$. In Publ. [**P17**] we give a counterexample to the reverse statement, namely that there is a noncontextuality inequality that is violated for the completely mixed quantum state, but not for all quantum states [**P17**].

The question arises, which sets of projectors allow for state-independent contextuality. This is answered in Publ. [**P17**] where we present necessary and sufficient conditions for the case where all projectors are of rank one. These conditions allow for an exhaustive search for state-independent contextuality scenarios. We prove in Publ. [**P17**] that if the dimension of the underlying Hilbert space is $d = 3$, then the smallest such set must have 13 projectors. Dimension $d = 3$ is special, because the possible sets of projectors satisfy very limiting constraints. We extend this result in Publ. [**P18**] to arbitrary dimensions. For this, new tools in graph theory are developed

[2] Here $X \leq Y$ for operators X and Y refers to $Y - X$ being positive semidefinite.

and in a computer based search we analyze the order of 10^{11} graphs. As result, we find that the smallest set of rank-one projectors must still have 13 projectors [**P18**].

Conversely, given a set of projectors that exhibits state-independent contextuality, which is the optimal inequality for which the statistical significance of a quantum violation can be maximal? This is addressed in Publ. [**P8**] and solved by reducing it to a linear optimization problem. Using this method, it is shown that well-known inequalities are not optimal and new, optimal inequalities are provided in Publ. [**P8**].

Contextuality as experimentally verifiable phenomenon

Contextuality as a property of quantum theory is a well-established concept, but is it also a property that can be verified in an experiment? Such an experiment would test a prediction of quantum theory itself, and not a particular model within quantum theory. Therefore, it is desirable that the validity of quantum theory is not assumed in the evaluation of the experiment. This, in turn, implies that the same measurement outcome α occurring in different measurement contexts $\mathcal{C}_1$ and $\mathcal{C}_2$ can be identified as same projector [11, 15–18]. However, different measurements tend to have very different implementations in an experiment and this is in conflict with the assumption that the assignment v is noncontextual.

There are at least three approaches to resolve this conflict. First, it might be possible to find situations where there is a convincing argument that a projector, albeit part of different measurements, has to have the same physical implementation, for example, by representing an orientation in space [10, 18]. However, such a situation is difficult to achieve. Second, one can refrain to a weak notion of equivalence, namely, if it is not possible to achieve a distinction in an experiment between different implementations, then one infers that the corresponding classical model assigns the same value to those implementations. This seemingly benign assumption leads to a quite different notion of contextuality [19]. Thirdly, one can choose a sequential implementation. Here one implements a sequence of compatible measurements such that the effective joint measurement yields the desired measurement. This method is used in the majority of the experimental implementations, for example in Refs. [**P1**, 20–25]. It requires two extra constraints on the sequential measurements: The measurement apparatuses must follow Lüders' rule and all measurements within a sequence must be compatible. Neither of these assumptions is directly testable in an experiment and, even more concerning, neither of these assumptions can be perfectly satisfied due to experimental imperfections.

In our approach to these problems we make plausible assumptions on the underlying reasons for any discrepancy, by employing appropriate noncontextual models. In Publ. [**P3**], three major models are worked out that can achieve this goal. One of these methods ("First Approach") was used in the first modern experimental verification of quantum contextuality [**P1**]. In this experiment, two ions in a linear Paul trap are subjected to sequential measurements, according to the Peres–Mermin scenario [26, 27]. We extend this model to include even more general noncontextual models in Publ. [**P12**]. There we also show that a renewed evaluation of the data from Publ. [**P1**] still gives strong evidence against these extended noncontextual models. Other models are discussed in Refs. [28, 29]. Conversely, some experimental violations of noncontextuality inequalities use implementations that are not suitable to provide convincing evidence for quantum contextuality, as we point out in Publ. [**P10**].

Memory cost of quantum contextuality

In the realization of quantum contextuality as sequential measurements, it is worth to analyze how quantum theory achieves the contextual behavior. In a measurement sequence the quantum state undergoes a state change that depends on the measurement as well as on the measurement outcome. In this sense, it seems that the quantum system is used as memory to store information

in order to achieve the contextual behavior. This raises the question, whether quantum contextuality in sequential measurements is merely due to the memory of the quantum system and whether a classical machine with memory can exhibit contextual behavior.

It has to be noted that on the one hand, an n-level quantum systems cannot store more classical information than an n-state classical system [30], but on the other hand, simulating a qubit can already require unbounded classical memory [31]. Therefore it is not clear, whether a classical machine with n states would be able to simulate the contextual behavior of an n-level quantum system. In Publ. [**P6**] we address this question. To this end we consider a variant of the Peres–Mermin contextuality scenario, in which the contextual behavior is due to the deterministic correlations between the measurements in a sequence. Using only these deterministic predictions, we find that quantum contextuality cannot be simulated on a corresponding classical system. This result relies on arbitrary sequences of measurements restricted such that any consecutive pair is composed of compatible measurements. Hence, contextuality has a memory footprint if quantum systems and classical systems are compared.

In the canonical scenario of quantum contextuality, only sequences of mutually jointly measurable measurements are used. For this case and the deterministic predictions, no quantum advantage is found [**P6**]. However, one can also consider all predictions, including also those which occur only with a certain probability. For this we define in Publ. [**P24**] the memory of a stochastic mixture of stochastic classical machines [32]. For the canonical Peres–Mermin scenario, we proof that such a mixture can simulate any probabilistic prediction of quantum theory.

In order to go one step further, we connect the idea of memory cost with more general situations where repeatability and sharpness are not required. In Publ. [**P13**] we find that even then one can make conclusions about the minimal dimension of the underlying Hilbert space. Further methods to bound the dimension of the Hilbert space are discussed in Refs. [33–36]. In a complementary approach, investigated in Publ. [**P14**], we analyze the situation where the measurements are projective but the dimension of the Hilbert space is arbitrary. Although there is no requirement on the compatibility of subsequent measurements, there are still nontrivial bounds on the obtainable values of noncontextuality inequalities and related scenarios.

2 General probabilistic theories

So far we mostly considered sharp quantum measurements, that is, families of projectors that are a resolution of identity. However, the set of valid quantum measurements on a given Hilbert space is much larger and encompasses the set of generalized measurements [37, 38], defined as families $(E_j)_j$ with $E_j \geq 0$ and $\sum_j E_j = \mathbb{1}$. The elements E_j are the effects of the generalized measurement.

Interestingly, the set of effects is sufficient to describe the very core of quantum theory. To see this, we describe only situations, where a system is in a state ρ and subject to a measurement $(E_j)_j$. We consider the real vectors space V_{QT} of Hermitian operators and within this vectors space we identify the cone V_{QT}^+ of positive semidefinite operators. We have $(E_j)_j \subset V_{\mathrm{QT}}^+$ and we can write the quantum state as the linear map $\omega\colon A \mapsto \mathrm{tr}(\rho A)$ on V. The characteristic properties of ω are positivity, $A \geq 0$ implies $\omega(A) \geq 0$, and normalization, $\omega(\mathbb{1}) = 1$. These two conditions are also sufficient for a linear map ω to be generated by a quantum state ρ. Hence the structure of the quantum states is dictated by the structure of quantum effects and quantum theory on a given Hilbert space is already characterized by the triple $(V_{\mathrm{QT}}, V_{\mathrm{QT}}^+, u_{\mathrm{QT}})$ with $u_{\mathrm{QT}} = \mathbb{1}$. From a mathematical point of view, this triple forms an order unit vector space [39, 40]. From a physics point of view, this language is tailored to capture the notion of a broad class of physical theories [**P15**, 41–44]: There are much more order unit vector spaces then the ones constructed from quantum theory and they all allow for a basic interpretation as a theory with states, measurements and also general operations. The theories that arise from this mathematical formalism

(and variants thereof) are the general probabilistic theories. The predictions within the general probabilistic theories can vastly differ from those of quantum theory, for example, it is possible to obtain correlations in a Bell-type experiment that cannot be reached with any quantum system [45] and consequently have never been observed. The fact that general probabilistic theories contain quantum theory only as a special case gives rise to a challenge for as well as a chance to our understanding of quantum theory. This is linked to the question, why all physical systems can be described by order unit vector spaces that arise from Hilbert spaces. Since, so far, we only considered systems on a very basic level, it is conceivable that when we incorporate more and more desiderata on a physical theory into the mathematical framework we can eventually arrive at quantum theory. This program has a rich history and several lists of desiderata (or axioms) have been found that narrow down the set of general probabilistic theories [41–43, 46–49].

In this thesis I take a different point of view. One can understand quantum theory as the specific instance of general probabilistic theories that is relevant for formulating our current understanding of physics. This is in analogy to, for example, Maxwell's theory of electromagnetism being a particular theory within all possible field theories. In this setting, one can explore how quantum theory is special, and which properties are characteristic to quantum theory.

Lüders' rule

Sharp measurements play a central role in quantum theory and it is therefore desirable to translate this concept to the language of general probabilistic theories. It can be shown that several natural definition of sharpness can be defined, which all coincide in quantum theory but are different in particular general probabilistic theories, cf. Publ. **[P15]**, Section 2.2. One of the most characteristic features of sharp quantum measurement is the existence of Lüders' rule in analogy to Eq. (4). This can be formulated in the Heisenberg picture, so that a measurement transforms all future measurements. Then Lüders' rule for an effect e can be formulated as the transformation that is such that no finer effect f (that is, $e - f \in V^+$) is disturbed by a preceding measurement of e. This definition is introduced and studied in in Publ. **[P15]**. A similar concept is investigated in Ref. [50].

Emergence of bipartite quantum correlations

Classical mechanics is a good approximation for most macroscopic phenomena. Hence it is no surprise that quantum mechanics emerged when experimental access to microscopic phenomena became available. If we now assume that quantum theory is not the ultimate theory of physics, but is to be superseded by some of the general probabilistic theories, then why did we not yet see any deviation from the predictions of quantum theory? Stated in a different way, if in the future another fundamental theory is needed, why is quantum theory in such precise agreement with our observations? In Publ. **[P9]** we provided a possible answer to this question: Quantum theory could be the universal emerging theory of any general probabilistic theory. The underlying assumption is that we do not have access to all possible measurements but only to those, which span a low-dimensional subspace. Then, using Dvoretzky's theorem [51], we show that the emerging bipartite correlations are—with high probability—in arbitrary good agreement with the correlations predicted by quantum theory.

The structure of n-outcome measurements

A central object in a general probabilistic theory is the set of effects, that is, the set

$$V_u^+ = \{e \in V^+ \mid u - e \in V^+\}. \tag{8}$$

It is important to realize that this set does not yet specify the set of allowed measurements. It is true that for any allowed measurement $(e_j)_j$, each effect e_j must be in V_u^+. However, the converse might not always hold true. From an operational point of view, there are two simple methods that allow us to construct from one measurement another measurement. First, for a measurement $(e_j)_j$, if η is a map from the indices $\{ j \}$ to another set of indices $\{ k \}$, then the measurement $(f_k)_k$ can be achieved by simple relabeling, yielding

$$f_k = \sum_{j:\, \eta(j)=k} e_j. \tag{9}$$

This guarantees, in particular, that if f is an effect of some measurement $(e_j)_j$, then also the measurement $(f, u - f)$ can be achieved. Second, it is possible to make convex combinations of measurement with the same index set, that is, if $(e_{n,j})_j$ are measurements labeled by n, then for some arbitrary probability distribution $(p_n)_n$ we obtain the measurement $(f_j)_j$ with

$$f_j = \sum_n p_n e_{n,j}. \tag{10}$$

If the set of all n-outcome measurements is known, then from these requirements one can construct a minimal set of achievable m-outcome measurements for $m > n$, exactly by applying the above two methods to the set of known measurements. Any such m-outcome measurement is called n-ary. The binary measurements are generated from all measurements $(e, u - e)$ with $e \in V_u^+$. This construction is operationally the smallest set conceivable. However, in quantum theory, this is not how the set of m-outcome measurements is constructed. There, the set of admissible measurements is given by any possible measurement $(e_j)_j \subset V_e^+$ and is hence the largest set possible.

In Publ. [**P19**] we show that the maximal and minimal sets of quantum measurements are different and that this difference can be tested in a bipartite Bell-type experiment. We identify experiments that (inadvertently) already have provided evidence for the assertion. In Publ. [**P21**] we show that it is even possible to find 3-outcome measurements on a qubit that are not binary within quantum theory. This is also verified in an experiment using photons, cf. Publ. [**P21**]. In Publ. [**P19**] we show that for any n, there are m-outcome quantum measurements that cannot be explained by any n-ary measurements, not only from quantum theory, but from any general probabilistic theory. An experimental test of this property would therefore constitute a theory independent test on the structure of measurements, but the results in Publ. [**P19**] are not yet experimentally feasible. In Publ. [**P25**] we further elaborate on this topic and provide strong Bell-type inequalities that allow to verify that the correlations obtained from $(n + 1)$-outcome quantum measurements cannot have originated from any n-ary measurement even if from a general probabilistic theory. A violation of one of these inequalities has been verified in an experiment using photons, cf. Publ. [**P26**].

3 Entanglement characterization and detection

Entanglement is a feature of a composed quantum systems and a state is entangled if and only if it cannot be obtained by means of an LOCC protocol from a product state. Before I discuss my results directly on entanglement theory, let me first consider a family of mutually orthogonal product states. Since each of these states can be produced locally, it should also be possible to decide locally, or by means of LOCC, in which of the states a system is. Surprisingly, this is not possible with unit probability and a counterexample was provided in Ref. [52]. The technical difficulty in proving this result is that the number of rounds in an LOCC protocol can be unbounded. It might even be possible to find an infinite family of protocols (possible each with

an unbounded number of rounds), such that the limiting protocol can achieve perfect discrimination, while no protocol in the family can. In fact, it is known that the topological closure of all LOCC protocols does not coincide with the set of protocols that can be implemented in a finite number of rounds [53]. This issue has already been discussed farsightedly in Ref. [52]. In Publ. [**P5**] we provide a rigorous version of the proof in Ref. [52] and extend the technique to work on almost arbitrary families of states.

Distance measures between states and entanglement classes

When we aim to quantify how entangled a quantum state $|\psi\rangle$ is, a natural idea is to measure the distance between this state and the set of all product states. The geometric measure of entanglement follows exactly this idea [54] and is given by

$$E_g(\psi) = 1 - \max_{\phi} |\langle\psi|\phi\rangle|^2, \tag{11}$$

where the maximization is over all product states $|\phi\rangle$. For mixed states this measure is extended via the usual convex roof construction, cf. Ref. [9], Section 4.1.2. Already for pure states, the maximization is a difficult nonlinear optimization problem. However, if the state is symmetric, that is, invariant under permutation of the parties, this maximization simplifies dramatically. In Publ. [**P2**] we prove that the product state yielding the maximal overlap is necessarily symmetric. While at first sight this result might seem natural, there are counterexamples for the same problem over real Hilbert spaces. We also extend our results to the maximization $\langle\phi|X|\phi\rangle$, when the operator X is permutationally symmetric.

Entanglement detection with spin-observables

Entanglement has applications that reach beyond its mathematical definition and its operational interpretation. A particular intriguing property of entangled states is that they can improve the precision in metrological tasks; for a review, cf. Ref. [55]. The characteristic quantity to measure the metrological usefulness of a state ρ with respect to a unitary $U_\theta = \exp(-iA\theta)$ is the quantum Fisher information $\mathcal{F}_Q(\rho, A)$, where larger values indicate better performance in determining the phase parameter θ.

Typically, the generator A takes the form of a local Hamiltonian. An example are the components of the total angular momentum $J_\ell = \frac{1}{2}\sum_k {\sigma^{(k)}}_\ell$ for n qubits, where ${\sigma^{(k)}}_\ell$ is the Pauli operator in $(\ell = x, y, z)$-direction, acting on the kth qubit. Then U_θ represents the n-fold local evolution of the system. If ρ is a suitably entangled state, then the metrological performance can be vastly improved compared to a simple product state. For this reason, it is of practical relevance to determine the metrological usefulness of a system. On the one hand, there exist simple lower bounds on the quantum Fisher information based on the components of the total angular momentum J_ℓ, in particular in form of the inequality [56]

$$\mathcal{F}_Q(\rho, J_y) \geq \langle J_z\rangle^2/(\Delta J_x)^2, \tag{12}$$

where $(\Delta J_x)^2$ denotes the variance of J_x. On the other hand, if the state has at most k-partite entanglement, then

$$\mathcal{F}_Q[\rho, J_\ell] \leq k\, n \tag{13}$$

holds [56].

In Publ. [**P22**] we show how this entanglement criterion can be improved by a modification of the quantum Fisher information. In Publ. [**P23**] we find a tight lower bound for the quantum Fisher information that outperforms the bound in Eq. (12) and can be computed for many situations. We also show how our methods can be applied to realistic experimental scenarios and

we demonstrate this on existing experimental data. In Publ. [**P27**] we use related methods to find an entanglement criterion tailored for a specific experiment with entangled clouds of ultracold atoms. In this experiment, a Bose–Einstein condensate was prepared and then divided into two spatially separated clouds. Using our methods, it was then possible to prove entanglement between these two clouds by measuring the angular momentum observables for each cloud.

A conspicuous property of Eq. (12) is its occurrence of the variance in the denominator. The fact that the variance of an operator cannot simply vanish is expressed in the Robertson–Schrödinger inequality, $(\Delta A)^2(\Delta B)^2 \geq \frac{1}{4}|\langle[A,B]\rangle|^2$. However, this inequality depends on the quantum state and in finite dimensions it is always possible to have the right hand side equal to zero, even if A and B do not commute. In order to overcome this dependence on the quantum state, there exists a different class of uncertainty relations, the entropic uncertainty relations [57]. The archetypal entropic uncertainty relation is due to Maassen and Uffink and is expressed for two measurement bases $(|a_i\rangle)_i$ and $(|b_i\rangle)_i$. Using the Shannon entropy $S[(p_i)_i] = -\sum_i p_i \log(p_i)$, this relation is given by [58]

$$S[(\langle a_i|\rho|a_i\rangle)_i] + S[(\langle b_i|\rho|b_i\rangle)_i] \geq -2\log(\max_{i,j}|\langle a_i|b_j\rangle|). \tag{14}$$

In Publ. [**P7**] we show that this inequality is always tight if the two measurement bases are stabilizer bases and that tightness occurs for any of the basis states. Stabilizer bases are a generalization of graph states, a class of states with very distinct entanglement properties [59]. We furthermore study a class of entropic uncertainty relations that are generalized to a collection of anticommuting observables.

4 Evaluation of experimental data

Several publications included in this thesis contain an experimental demonstration of a theoretical prediction [**P1**, **P4**, **P21**, **P26**, **P27**]. The data obtained in these experiments is typically very clean in the sense that it depends only weakly on the experimental setup or only on parameters that are very well known, for example the orientation of a polarization measurement for photons. However, most of these experiments can only collect a rather low number of samples, so that the statistical fluctuations dominate over the uncertainty originating in the lack of knowledge over parameters in the experiment. For these reasons, the statistical evaluation of the data becomes an important aspect.

Measurement schemes with improved statistical properties

It can be beneficial to already incorporate data evaluation concerns into the design of an experiment. A powerful tool to verify the entanglement of a state are entanglement witnesses [9]. An entanglement witness is a Hermitian operator W with $\langle W\rangle \geq 0$ for all separable states, but $\langle W\rangle < 0$ for some entangled states. In particular, Bell inequalities can be reformulated as entanglement witnesses. In an experiment, the aim is to verify $\langle W\rangle < 0$ with a high statistical significance $\mathcal{S} = -\langle W\rangle/(\Delta W)$. In Publ. [**P4**] we show that for pure quantum states, W can be always improved to yield a higher significance, unless it is already an eigenstate of $\langle W\rangle$. Since in many situations the target state is a pure state, this is a widely applicable result. However, one also has to consider that the observable W is in most cases not directly accessible, but has to be measured in a particular decomposition of local observables, such that $W = \sum_i A_i \otimes B_i \otimes \cdots$. In an experiment, each term in the sum is measured separately, and hence each term suffers from statistical fluctuations. We show that in this situation, even under different models for experimental imperfections, a careful choice of the observable W and its decomposition can increase

the statistical significance [**P4**]. This effect is also demonstrated in an experiment with photons [**P4**].

In general, measuring a single observable is by far not enough to verify the properties of a quantum state. A notoriously demanding case are bound entanglement states. Roughly speaking, a bipartite quantum state is bound entangled if it is entangled, but even if both parties share an arbitrary number of those bound entangled states, they cannot produce a single maximally entangled state of the form $|\psi\rangle = (|01\rangle - |10\rangle)/\sqrt{2}$ using only local manipulations, cf. Ref. [7], Section XII. Several experiments have been performed with the aim to demonstrate a preparation of such a state, cf. Publ. [**P28**] for a discussion. A main difficulty is that in low dimensional Hilbert spaces, the set of bound entangled states is a rather small region within the set of density operators. Hence one has to find a state that is particularly robust to experimental imperfections and one needs to find a statistical hypothesis test that allows one to decide whether the experimental data can provide evidence for the preparation of a bound entangled state. In Publ. [**P28**] we develop methods to efficiently find bound entangled states that are particularly well-suited for experimental detection. Based on the noncentral χ^2-distribution we develop a statistically robust hypothesis test and we find that a rigorous experiment is within current experimental capabilities.

Statistical tools for quantum state tomography

Quite often, experiments obtain full tomographic data, however, with a rather low number of samples. The data consists then of the relative frequencies of occurrence $f(i, j, \dots | a, b, \dots)$ for each outcome and each measurement setting. The frequencies are distributed according to the probabilities $p(i, j, \dots | a, b, \dots)$ in Eq. (5). Since p depends linearly on ρ, it is tempting to replace p by f in Eq. (5) and to invert the equation in order to obtain an estimate for ρ. Apart from minor technical details, such a procedure is valid in principle and is called linear inversion or unconstrained least squares [60]. A more sophisticated method is the maximum likelihood reconstruction [61], where the estimated density operator is the operator that maximizes the likelihood $\mathcal{L}(\rho|f) = \mathrm{Prob}(f|\rho)$. In order to ensure that the solution is a valid quantum state, the optimization is restricted accordingly. The main criticism to this method is that it does not yield a confidence region. This problem is most commonly overcome by the bootstrapping method [62], where one simulates the experiment based on the data in order to approximate the distribution of the reconstructed states. In turn, this allows one to estimate the variance. This method is the most commonly used method for the evaluation of the data in quantum state tomography.

However, maximum likelihood estimation and bootstrapping do not yield reliable estimates: In Publ. [**P16**] we show that in realistic scenarios this method is biased and the estimated error bar does not even contain the true state. In addition, we observe a tendency of the method to reconstruct states that are more entangled than the actual states in the experiment. We explain and explore this phenomenon in Publs. [**P16**, **P20**]. As an alternative we suggest to use the linear inversion scheme and provide practical methods for computing confidence intervals. Other computable error regions for density operators have been suggested recently [63–65].

The main assumption that enters the analysis of tomographic data is the characterization of the measurements. To which extend this characterization is valid has to be estimated from the experimental setup. However, one can use the experimental data in order verify this assumption. There are two major reasons why this is possible. First, in most situations, the measurement outcomes form an overcomplete set, that is, already a smaller subset of the projectors (or effect operators) would span the set of Hermitian operators. Hence, there are certain linear relations between the operators, which lead to linear relations between the probabilities $p(i, j, \dots | a, b, \dots)$. These relations need to be satisfied by the observed frequencies within the error margin. This can be tested, for example, using Hoeffding's tail inequality [66] or Wilks theorem [67]. We introduce

this method in Publ. [**P11**] and show that it can be successfully applied to experimental data.

Second, we can use that the two defining constraints of a density operator are normalization and positive semidefiniteness. The former condition is automatically satisfied due to the normalization of frequencies. The latter condition, however, is usually not satisfied for linear inversion, in particular if the experimental state is close to a pure state. This is the case because then many eigenvalues are close to zero and due to statistical fluctuations some of them can become negative [68]. However, within the statistical uncertainty, the experimental data has to be compatible with a positive semidefinite operator. We show that this property is efficiently tested by testing whether different fractions of the data yield a significant negative expectation value $\langle\eta|\rho|\eta\rangle$ for the same vector $|\eta\rangle$ [**P11**]. This second test turns out to be even more efficient than the first one and can detect already very small deviations in the alignment of the measurement settings.

Contributions to Publications

For all publications, I participated in the development of the results, verified the statements and findings, and contributed to the writing of the manuscript. Below, I specify my main contributions to each publication. [**P1**] I developed the model for the imperfect measurements and contributed to the design of the experiment. [**P2**] I proved the main result and analyzed the translationally invariant case. [**P3**] I developed the definitions, the first error model, and the hidden variable model explaining all quantum-mechanical predictions. [**P4**] I proved the observation and developed the error model. [**P5**] I provided the definitions, developed and proved the main theorem, and studied the examples. [**P6**] I developed the concept and definition of memory cost, provided the automatons for the Peres–Mermin square, and proved the theorems. [**P7**] I developed the proofs for the statements in Sections IV and V. [**P8**] I developed and formulated the method for optimizing the inequalities and optimized the specific inequalities. [**P9**] I developed the main result and the statement of the propositions and proved the propositions. [**P10**] I analyzed the problems in the criticized experiment. [**P11**] I developed the central idea, the witness tests, the discussion of the negative eigenvalues, the likelihood ratio test, and performed the data analysis. [**P12**] I developed the problem statement and the hidden variable model. [**P13**] I developed the concept, provided the "the simplified method," and performed the according numerical analysis. [**P14**] I proved the results in Sections II–IV. [**P15**] I am the sole author. [**P16**] I developed the problem statement, analyzed the numerical results, and proved the proposition. [**P17**] I proved the theorems, in particular Theorems 3 and 4 and I wrote the computer code for proving Theorem 4. [**P18**] I developed the techniques to prove the main result, in particular Lemmas 2 and 3 and I wrote the computer code for searching all graphs. [**P19**] I discovered and proved the main theorem and performed the numerical analysis of the experiments. [**P20**] I developed the results and the presentation of the section "Systematic Errors in Quantum Experiments" (cf. also Publ. [**P16**]). [**P21**] I developed the inequality, was closely involved in the design of the experiment, and analyzed the data. [**P22**] I derived Observation 2 and extended the inequality to fluctuating particle numbers. [**P23**] I proofed the main result in Section II and Observation 2 and developed the numerical analysis for the Dicke states. [**P24**] I developed the problem statement, the definition of the mixtures of automatons, proved the main result, and provided the methods in the appendix. [**P25**] I developed and implemented the concepts and the methods to find the inequalities and analyzed the resulting inequalities. [**P26**] I provided the theory part, was closely involved in the design of the experiment, and evaluated the data. [**P27**] I improved the derivation of the entanglement criterion and contributed to the evaluation of the data. [**P28**] I analyzed the problem, provided the methods for constructing the bound entangled ball, and developed the methods for the statistical evaluation.

References

[1] J. von Neumann, *Mathematische Grundlagen der Quantenmechanik*, (Springer, Berlin, 1932).

[2] M. Born, Zur Quantenmechanik der Stoßvorgänge, Z. Physik **37**, 863 (1926).

[3] G. Lüders, Über die Zustandsänderung durch den Meßprozeß, Ann. Phys. (Leipzig) **443**, 322 (1951).

[4] A. Einstein, B. Podolsky, and N. Rosen, Can quantum-mechanical description of physical reality be considered complete?, Phys. Rev. **47**, 777 (1935).

[5] E. Schrödinger, Discussion of probability relations between separated systems, Math. Proc. Cambridge Phil. Soc. **31**, 555 (1935).

[6] R.F. Werner, Quantum states with Einstein–Podolsky–Rosen correlations admitting a hidden-variable model, Phys. Rev. A **40**, 4277 (1989).

[7] R. Horodecki, P. Horodecki, M. Horodecki, and K. Horodecki, Quantum entanglement, Rev. Mod. Phys. **81**, 865 (2009).

[8] C.H. Bennett, D.P. DiVincenzo, J.A. Smolin, and W.K. Wootters, Mixed-state entanglement and quantum error correction, Phys. Rev. A **54**, 3824 (1996).

[9] O. Gühne and G. Tóth, Entanglement detection, Phys. Rep. **474**, 1 (2009).

[10] S. Kochen and E.P. Specker, The problem of hidden variables in quantum mechanics, J. Math. Mech. **17**, 59 (1967).

[11] A. Cabello, J.M. Estebaranz, and G. García-Alcaine, Bell–Kochen–Specker theorem: A proof with 18 vectors, Phys. Lett. A **212**, 183 (1996).

[12] J.S. Bell, On the Einstein Podolsky Rosen paradox, Physics **1**, 195 (1964).

[13] A.A. Klyachko, M.A. Can, S. Binicioğlu, and A.S. Shumovsky, Simple test for hidden variables in spin-1 systems, Phys. Rev. Lett. **101**, 020403 (2008).

[14] S. Yu and C.H. Oh, State-independent proof of Kochen–Specker theorem with 13 rays, Phys. Rev. Lett. **108**, 030402 (2012).

[15] D. Meyer, Finite precision measurement nullifies the Kochen–Specker theorem, Phys. Rev. Lett. **83**, 3755 (1999).

[16] R. Clifton and A. Kent, Simulating quantum mechanics by non-contextual hidden variables, Proc. R. Soc. London A **456**, 2101 (2000).

[17] C. Simon, M. Żukowski, H. Weinfurter, and A. Zeilinger, Feasible "Kochen–Specker" experiment with single particles, Phys. Rev. Lett. **85**, 1783 (2000).

[18] J.-Å. Larsson, A Kochen–Specker inequality, Europhys. Lett. **58**, 799 (2002).

[19] R.W. Spekkens, Contextuality for preparations, transformations, and unsharp measurements, Phys. Rev. A **71**, 052108 (2005).

[20] H. Bartosik, J. Klepp, C. Schmitzer, S. Sponar, A. Cabello, H. Rauch, and Y. Hasegawa, Experimental test of quantum contextuality in neutron interferometry, Phys. Rev. Lett. **103**, 040403 (2009).

[21] E. Amselem, M. Rådmark, M. Bourennane, and A. Cabello, State-independent quantum contextuality with single photons, Phys. Rev. Lett. **103**, 160405 (2009).

[22] B.H. Liu, Y.F. Huang, Y.X. Gong, F.W. Sun, Y.S. Zhang, C.F. Li, and G.C. Guo, Experimental demonstration of quantum contextuality with nonentangled photons, Phys. Rev. A **80**, 044101 (2009).

[23] O. Moussa, C.A. Ryan, D.G. Cory, and R. Laflamme, Testing contextuality on quantum ensembles with one clean qubit, Phys. Rev. Lett. **104**, 160501 (2010).

[24] R. Lapkiewicz, P. Li, C. Schaeff, N.K. Langford, S. Ramelow, M. Wieśniak, and A. Zeilinger, Experimental non-classicality of an indivisible quantum system, Nature (London) **474**, 490 (2011).

[25] M. Jerger, Y. Reshitnyk, M. Oppliger, A. Potočnik, M. Mondal, A. Wallraff, K. Goodenough, S. Wehner, K. Juliusson, N.K. Langford, and A. Fedorov, Contextuality without nonlocality in a superconducting quantum system, Nat. Commun. **7**, 12930 (2016).

[26] A. Peres, Incompatible results of quantum measurements, Phys. Lett. A **151**, 107 (1990).

[27] N.D. Mermin, Simple unified form for the major no-hidden-variables theorems, Phys. Rev. Lett. **65**, 3373 (1990).

[28] A. Winter, What does an experimental test of quantum contextuality prove or disprove?, J. Phys. A **47**, 424031 (2014).

[29] J.V. Kujala, E.N. Dzhafarov, and J.-Å. Larsson, Necessary and sufficient conditions for an extended noncontextuality in a broad class of quantum mechanical systems, Phys. Rev. Lett. **115**, 150401 (2015).

[30] A.S. Holevo, Bounds for the quantity of information transmitted by a quantum communication channel, Probl. Inf. Transm. **9**, 177 (1973).

[31] E.F. Galvão and L. Hardy, Substituting a qubit for an arbitrarily large number of classical bits, Phys. Rev. Lett. **90**, 087902 (2003).

[32] A. Paz, *Introduction to Probabilistic Automata*, (Academic, New York, 1971).

[33] J. Hoffmann, C. Spee, O. Gühne, and C. Budroni, Structure of temporal correlations of a qubit, New J. Phys. **20**, 102001 (2018).

[34] R. Gallego, N. Brunner, C. Hadley, and A. Acín, Device-independent tests of classical and quantum dimensions, Phys. Rev. Lett. **105**, 230501 (2010).

[35] N. Brunner, M. Navascués, and T. Vértesi, Dimension witnesses and quantum state discrimination, Phys. Rev. Lett. **110**, 150501 (2013).

[36] J.I. de Vicente, Shared randomness and device-independent dimension witnessing, Phys. Rev. A **95**, 012340 (2017).

[37] P. Busch, P.J. Lahti, and P. Mittelstaedt, *The Quantum Theory of Measurement*, (Springer-Verlag, Berlin Heidelberg, 1991).

[38] T. Heinosaari and M. Ziman, *The Mathematical Language of Quantum Theory: From Uncertainty to Entanglement*, (Cambridge University Press, Cambridge New York, 2012).

[39] E.M. Alfsen, *Compact convex sets and boundary integrals*, (Springer-Verlag, Berlin Heidelberg, 1971).

[40] V.I. Paulsen and M. Tomforde, Vector spaces with an order unit, Indiana Univ. Math. J. **58**, 1319 (2009).

[41] G. Ludwig, *An Axiomatic Basis for Quantum Mechanics*, Vol. I–II, (Springer-Verlag, Berlin Heidelberg, 1987).

[42] L. Masanes and M.P. Müller, A derivation of quantum theory from physical requirements, New J. Phys. **13**, 063001 (2011).

[43] G. Chiribella, G.M. D'Ariano, and P. Perinotti, Informational derivation of quantum theory, Phys. Rev. A **84**, 012311 (2011).

[44] G. Chiribella and X. Yuan, Bridging the gap between general probabilistic theories and the device-independent framework for nonlocality and contextuality, Inf. Comput. **250**, 15 (2016).

[45] S. Popescu and D. Rohrlich, Quantum nonlocality as an axiom, Found. Phys. **24**, 379 (1994).

[46] P. Mittelstaedt, *The Interpretation of Quantum Mechanics and the Measurement Process*, (Cambridge University Press, Cambridge New York, 1998).

[47] L. Hardy, Quantum theory from five reasonable axioms, arXiv:quant-ph/0101012.

[48] B. Dakić and Č. Brukner, Quantum theory and beyond: Is entanglement special?, in *Deep Beauty. Understanding the Quantum World through Mathematical Innovation*, edited by H. Halvorson (Cambridge University Press, New York, 2011), p. 365.

[49] P.A. Höhn and C.S.P. Wever, Quantum theory from questions, Phys. Rev. A **95**, 012102 (2017).

[50] G. Chiribella and X. Yuan, Measurement sharpness cuts nonlocality and contextuality in every physical theory, arXiv:1404.3348.

[51] V.D. Milman and G. Schechtman, *Asymptotic Theory of Finite Dimensional Normed Spaces*, (Springer-Verlag, Berlin Heidelberg, 1986).

[52] C.H. Bennett, D.P. DiVincenzo, C.A. Fuchs, T. Mor, E. Rains, P.W. Shor, J.A. Smolin, and W.K. Wootters, Quantum nonlocality without entanglement, Phys. Rev. A **59**, 1070 (1999).

[53] E. Chitambar, D. Leung, L. Mančinska, M. Ozols, and A. Winter, Everything you always wanted to know about LOCC (but were afraid to ask), Commun. Math. Phys. **328**, 303 (2014).

[54] T.-C. Wei and P.M. Goldbart, Geometric measure of entanglement and applications to bipartite and multipartite quantum states, Phys. Rev. A **68**, 042307 (2003).

[55] G. Tóth and I. Apellaniz, Quantum metrology from a quantum information science perspective, J. Phys. A **47**, 424006 (2014).

[56] L. Pezzé and A. Smerzi, Entanglement, nonlinear dynamics, and the Heisenberg limit, Phys. Rev. Lett. **102**, 100401 (2009).

[57] S. Wehner and A. Winter, Entropic uncertainty relations—a survey, New J. Phys. **12**, 025009 (2010).

[58] H. Maassen and J.B.M. Uffink, Generalized entropic uncertainty relations, Phys. Rev. Lett. **60**, 1103 (1988).

[59] M. Hein, W. Dür, J. Eisert, R. Raussendorf, M. Van den Nest, and H.J. Briegel, Entanglement in graph states and its applications, in: *Quantum computers, algorithms and chaos*, Proceedings of the International School of Physics, Enrico Fermi No. 162, edited by G. Casati, D.L. Shepelyansky, P. Zoller, and G. Benenti (IOS, Amsterdam, 2006), p. 115.

[60] D.F.V. James, P.G. Kwiat, W.J. Munro, and A.G. White, Measurement of qubits, Phys. Rev. A **64**, 052312 (2001).

[61] Z. Hradil, Quantum-state estimation, Phys. Rev. A **55**, R1561 (1997).

[62] B. Efron and R.J. Tibshirani, *An Introduction to the Bootstrap*, (Chapman & Hall, London, 1994).

[63] T. Sugiyama, P.S. Turner, and M. Murao, Precision-guaranteed quantum tomography, Phys. Rev. Lett. **111**, 160406 (2013).

[64] M. Guta, J. Kahn, R. Kueng, and J.A. Tropp, Fast state tomography with optimal error bounds, arXiv:1809.11162.

[65] J. Wang, V.B. Scholz, and R. Renner, Confidence polytopes in quantum state tomography, arXiv:1808.09988.

[66] W. Hoeffding, Probability inequalities for sums of bounded random variables, J. Am. Stat. Assoc. **58**, 301 (1963).

[67] S.S. Wilks, *Mathematical Statistics*, (John Wiley & Sons, New York London, 1962).

[68] L. Knips, C. Schwemmer, N. Klein, J. Reuter, G. Tóth, and H. Weinfurter, How long does it take to obtain a physical density matrix?, arXiv:1512.06866.

PUBLICATIONS

[P1] G. Kirchmair, F. Zähringer, R. Gerritsma, M. Kleinmann, O. Gühne, A. Cabello, R. Blatt, and C.F. Roos, State-independent experimental test of quantum contextuality, Nature (London) **460**, 494 (2009). ► p. 19

[P2] R. Hübener, M. Kleinmann, T.-C. Wei, C. González-Guillén, and O. Gühne, Geometric measure of entanglement for symmetric states, Phys. Rev. A **80**, 032324 (2009). ► p. 25

[P3] O. Gühne, M. Kleinmann, A. Cabello, J.-Å. Larsson, G. Kirchmair, F. Zähringer, R. Gerritsma, and C.F. Roos, Compatibility and noncontextuality for sequential measurements, Phys. Rev. A **81**, 022121 (2010). ► p. 31

[P4] B. Jungnitsch, S. Niekamp, M. Kleinmann, O. Gühne, H. Lu, W.-B. Gao, Y.-A. Chen, Z.-B. Chen, and J.-W. Pan, Increasing the statistical significance of entanglement detection in experiments, Phys. Rev. Lett. **104**, 210401 (2010). ► p. 47

[P5] M. Kleinmann, H. Kampermann, and D. Bruß, Asymptotically perfect discrimination in the local-operation-and-classical-communication paradigm, Phys. Rev. A **84**, 042326 (2011). ► p. 53

[P6] M. Kleinmann, O. Gühne, J.R. Portillo, J.-Å. Larsson, and A. Cabello, Memory cost of quantum contextuality, New J. Phys. **13**, 113011 (2011). ► p. 61

[P7] S. Niekamp, M. Kleinmann, and O. Gühne, Entropic uncertainty relations and the stabilizer formalism, J. Math. Phys. **53**, 012202 (2012). ► p. 79

[P8] M. Kleinmann, C. Budroni, J.-Å. Larsson, O. Gühne, and A. Cabello, Optimal inequalities for state-independent contextuality, Phys. Rev. Lett. **109**, 250402 (2012). ► p. 89

[P9] M. Kleinmann, T.J. Osborne, V.B. Scholz, and A.H. Werner, Typical local measurements in generalized probabilistic theories: Emergence of quantum bipartite correlations, Phys. Rev. Lett. **110**, 040403 (2013). ► p. 95

[P10] E. Amselem, M. Bourennane, C. Budroni, A. Cabello, O. Gühne, M. Kleinmann, J.-Å. Larsson, and M. Wieśniak, Comment on "State-independent experimental test of quantum contextuality in an indivisible system", Phys. Rev. Lett. **110**, 078901 (2013). ► p. 101

[P11] T. Moroder, M. Kleinmann, P. Schindler, T. Monz, O. Gühne, and R. Blatt, Certifying systematic errors in quantum experiments, Phys. Rev. Lett. **110**, 180401 (2013). ► p. 103

[P12] J. Szangolies, M. Kleinmann, and O. Gühne, Tests against noncontextual models with measurement disturbances, Phys. Rev. A **87**, 050101(R) (2013). ► p. 109

[P13] C. Budroni, T. Moroder, M. Kleinmann, and O. Gühne, Bounding temporal quantum correlations, Phys. Rev. Lett. **111**, 020403 (2013). ► p. 115

[P14] O. Gühne, C. Budroni, A. Cabello, M. Kleinmann, and J.-Å. Larsson, Bounding the quantum dimension with contextuality, Phys. Rev. A **89**, 062107 (2014). ► p. 123

[P15] M. Kleinmann, Sequences of projective measurements in generalized probabilistic models, J. Phys. A: Math. Theor. **47**, 455304 (2014). ► p. 135

[**P16**] C. Schwemmer, L. Knips, D. Richart, H. Weinfurter, T. Moroder, M. Kleinmann, and O. Gühne, Systematic errors in current quantum state tomography tools, Phys. Rev. Lett. **114**, 080403 (2015). ► p. 149

[**P17**] A. Cabello, M. Kleinmann, and C. Budroni, Necessary and sufficient condition for quantum state-independent contextuality, Phys. Rev. Lett. **114**, 250402 (2015). ► p. 157

[**P18**] A. Cabello, M. Kleinmann, and J.R. Portillo, Quantum state-independent contextuality requires 13 rays, J. Phys. A: Math. Theor. **49**, 38LT01 (2016). ► p. 163

[**P19**] M. Kleinmann and A. Cabello, Quantum correlations are stronger than all nonsignaling correlations produced by n-outcome measurements, Phys. Rev. Lett. **117**, 150401 (2016). ► p. 171

[**P20**] O. Gühne, M. Kleinmann, and T. Moroder, Analysing multiparticle quantum states, in: *Quantum [Un]Speakables II*, edited by R. Bertlmann and A. Zeilinger (Springer, 2016) p. 345. ► p. 177

[**P21**] E.S. Gómez, S. Gómez, P. González, G. Cañas, J.F. Barra, A. Delgado, G.B. Xavier, A. Cabello, M. Kleinmann, T. Vértesi, and G. Lima, Device-independent certification of a nonprojective qubit measurement, Phys. Rev. Lett. **117**, 260401 (2016). ► p. 197

[**P22**] G. Vitagliano, I. Apellaniz, M. Kleinmann, B. Lücke, C. Klempt, and G. Tóth, Entanglement and extreme spin squeezing of unpolarized states, New J. Phys. **19**, 013027 (2017). ► p. 203

[**P23**] I. Apellaniz, M. Kleinmann, O. Gühne, and G. Tóth, Optimal witnessing of the quantum Fisher information with few measurements, Phys. Rev. A **95**, 032330 (2017). ► p. 221

[**P24**] G. Fagundes and M. Kleinmann, Memory cost for simulating all quantum correlations of the Peres–Mermin scenario, J. Phys. A: Math. Theor. **50**, 325302 (2017). ► p. 235

[**P25**] M. Kleinmann, T. Vértesi, and A. Cabello, Proposed experiment to test fundamentally binary theories, Phys. Rev. A **96**, 032104 (2017). ► p. 243

[**P26**] X.-M. Hu, B.-H. Liu, Y. Guo, G.-Y. Xiang, Y.-F. Huang, C.-F. Li, G.-C. Guo, M. Kleinmann, T. Vértesi, and A. Cabello, Observation of Stronger-than-Binary Correlations with Entangled Photonic Qutrits, Phys. Rev. Lett. **120**, 180402 (2018). ► p. 249

[**P27**] K. Lange, J. Peise, B. Lücke, I. Kruse, G. Vitagliano, I. Apellaniz, M. Kleinmann, G. Tóth, and C. Klempt, Entanglement between two spatially separated atomic modes, Science **360**, 416 (2018). ► p. 255

[**P28**] G. Sentís, J.N. Greiner, J. Shang, J. Siewert, and M. Kleinmann, Bound entangled states fit for robust experimental verification, Quantum **2**, 113 (2018). ► p. 265

All publications are reproduced as they appear on arXiv.org. The reproduced articles concur with the published articles as cited above.

State-independent experimental test of quantum contextuality

G. Kirchmair[1,2], F. Zähringer[1,2], R. Gerritsma[1,2], M. Kleinmann[1],
O. Gühne[1,3], A. Cabello[4], R. Blatt[1,2], and C. F. Roos[1,2*]
[1] *Institut für Quantenoptik und Quanteninformation, Österreichische Akademie der Wissenschaften, Otto-Hittmair-Platz 1, A-6020 Innsbruck, Austria*
[2] *Institut für Experimentalphysik, Universität Innsbruck, Technikerstr. 25, A-6020 Innsbruck, Austria*
[3] *Institut für theoretische Physik, Universität Innsbruck, Technikerstr. 25, A-6020 Innsbruck, Austria*
[4] *Departamento de Física Aplicada II, Universidad de Sevilla, E-41012 Sevilla, Spain*

(Dated: November 24, 2009)

The question of whether quantum phenomena can be explained by classical models with hidden variables is the subject of a long lasting debate[1]. In 1964, Bell showed that certain types of classical models cannot explain the quantum mechanical predictions for specific states of distant particles[2]. Along this line, some types of hidden variable models have been experimentally ruled out[3, 4, 5, 6, 7, 8, 9]. An intuitive feature for classical models is non-contextuality: the property that any measurement has a value which is independent of other compatible measurements being carried out at the same time. However, the results of Kochen, Specker, and Bell[10, 11, 12] show that non-contextuality is in conflict with quantum mechanics. The conflict resides in the structure of the theory and is independent of the properties of special states. It has been debated whether the Kochen-Specker theorem could be experimentally tested at all[13, 14]. Only recently, first tests of quantum contextuality have been proposed and undertaken with photons[15] and neutrons[16, 17]. Yet these tests required the generation of special quantum states and left various loopholes open. Here, using trapped ions, we experimentally demonstrate a state-independent conflict with non-contextuality. The experiment is not subject to the detection loophole and we show that, despite imperfections and possible measurement disturbances, our results cannot be explained in non-contextual terms.

PACS numbers:

Hidden variable models assert that the result $v(A)$ of measuring the observable A on an individual quantum system is predetermined by a hidden variable λ. Two observables A and B are mutually compatible, if the result of A does not depend on whether B is measured before, after, or simultaneously with A and vice versa. Non-contextuality is the property of a hidden variable model that the value $v(A)$ is determined, regardless of which other compatible observable is measured jointly with A. As a consequence, for compatible observables the relation $v(AB) = v(A)v(B)$ holds. Kochen and Specker showed that the assumption of non-contextuality cannot be reconciled with quantum mechanics. A considerable simplification of the original Kochen-Specker argument by Mermin and Peres[18, 19] uses a 3×3 square of observables A_{ij} with possible outcomes $v(A_{ij}) = \pm 1$, where the observables in each row or column are mutually compatible. Considering the products of rows $R_k = v(A_{k1})v(A_{k2})v(A_{k3})$ and columns $C_k = v(A_{1k})v(A_{2k})v(A_{3k})$, the total product would be $\prod_{k=1,2,3} R_k C_k = 1$, since any $v(A_{ij})$ appears twice in the total product.

In quantum mechanics, however, one can take a four-level quantum system, for instance two spin-$\frac{1}{2}$-particles, and the following array of observables,

$$\begin{array}{ccc} A_{11} = \sigma_z^{(1)} & A_{12} = \sigma_z^{(2)} & A_{13} = \sigma_z^{(1)} \otimes \sigma_z^{(2)} \\ A_{21} = \sigma_x^{(2)} & A_{22} = \sigma_x^{(1)} & A_{23} = \sigma_x^{(1)} \otimes \sigma_x^{(2)} \\ A_{31} = \sigma_z^{(1)} \otimes \sigma_x^{(2)} & A_{32} = \sigma_x^{(1)} \otimes \sigma_z^{(2)} & A_{33} = \sigma_y^{(1)} \otimes \sigma_y^{(2)}. \end{array} \quad (1)$$

Here, $\sigma_i^{(k)}$ denotes the Pauli matrix acting on the k-th particle, and all the observables have the outcomes ± 1. Moreover, in each of the rows or columns of (1), the observables are mutually commuting and can be measured simultaneously or in any order. In any row or column, their measurement product R_k or C_k equals 1, except for the third column where it equals -1. Hence, quantum mechanics yields for the product $\prod_{k=1,2,3} R_k C_k$ a value of -1, in contrast to non-contextual models.

To test this property, it has to be expressed as an inequality since no experiment yields ideal quantum measurements. Recently, it has been shown that the inequality

$$\langle \mathcal{X}_{\rm KS} \rangle = \langle R_1 \rangle + \langle R_2 \rangle + \langle R_3 \rangle + \langle C_1 \rangle + \langle C_2 \rangle - \langle C_3 \rangle \leq 4 \quad (2)$$

holds for all non-contextual theories[20], where $\langle \cdots \rangle$ denotes the ensemble average. Quantum mechanics predicts for *any* state that $\langle \mathcal{X}_{\rm KS} \rangle = 6$, thereby violating inequality (2). For an experimental test, an ensemble of quantum states Ψ needs to be prepared and each realization subjected to the measurement of one of the possible sets of compatible observables. Here, it is of utmost importance that all measurements of A_{ij} are

*Electronic address: christian.roos@uibk.ac.at

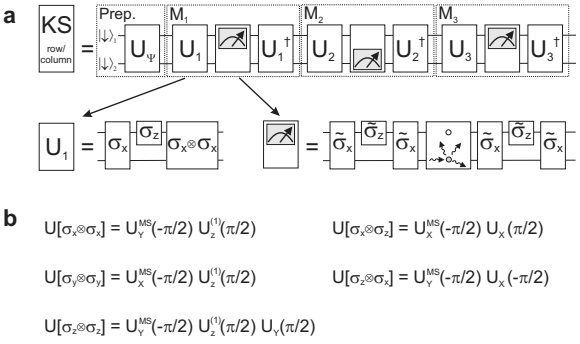

FIG. 1: Experimental measurement scheme. **a** For the measurement of the jth row (column) of the Mermin-Peres square (1), a quantum state is prepared on which three consecutive QND measurements M_k, $k = 1, 2, 3$, are performed measuring the observables A_{jk} (A_{kj}). Each measurement consists of a composite unitary operation U_k that maps the observable of interest onto one of the single-qubit observables $\sigma_z^{(1)}$ or $\sigma_z^{(2)}$ which are measured by fluorescence detection. To this end, the quantum state of the qubit that is not to be detected is hidden[22] in the $D_{5/2}$-Zeeman state manifold by a composite π-pulse transferring the $|\downarrow\rangle$ state's population to the auxiliary state $|a\rangle \equiv |D_{5/2}, m = 5/2\rangle$ prior to fluorescence detection. After the detection, the qubit state is restored. In the lower line, σ_i, $\tilde{\sigma}_i$ symbolize the Hamiltonian acting on the qubit or on the subspace spanned by $\{|\downarrow\rangle, |a\rangle\}$. The unitary operations U are synthesized from single-qubit and maximally entangling gates. **b** All mapping operations U_k employed for measuring the five two-qubit spin correlations $\sigma_i^{(1)} \otimes \sigma_j^{(2)}$ require an entangling gate. Here, we list the gate decompositions of $U[\sigma_i^{(1)} \otimes \sigma_j^{(2)}]$ used in the experiments where $U_X(\theta) \equiv U(\theta, \phi = 0)$ and $U_Y(\theta) \equiv U(\theta, \phi = \pi/2)$.

context-independent[20], i.e., A_{ij} must be detected with a quantum non-demolition (QND) measurement that provides no information whatsoever about any other co-measurable observable.

Experiments processing quantum information with trapped ions[21] are particularly well-suited for this purpose as arbitrary two-qubit quantum states Ψ can be deterministically generated by laser-ion interactions and measured with near-unit efficiency[6]. Two ionic energy levels are defined to represent the qubit basis states $|\uparrow\rangle$ and $|\downarrow\rangle$, which are eigenstates of the observable σ_z. The qubit is measured by electron shelving[21] projecting onto $|\uparrow\rangle$ or $|\downarrow\rangle$. Measurement of any other observable A_{ij} is reduced to detecting $\sigma_z^{(k)}$, k=1 or 2, by applying a suitable unitary transformation U to the state Ψ prior to measuring $\sigma_z^{(k)}$, and its inverse $U^\dagger$ after the measurement (see Fig. 1 and Methods). With these basic tools, any set of observables can be sequentially measured in an arbitrary temporal order.

For the experiment, a pair of $^{40}Ca^+$ ions is trapped in a linear Paul trap with axial and radial vibrational frequencies of $\omega_{ax} = (2\pi)\,1.465$ MHz and $\omega_r \approx (2\pi)\,3.4$ MHz and Doppler-cooled by exciting the $S_{1/2} \leftrightarrow P_{1/2}$ and $P_{1/2} \leftrightarrow D_{3/2}$ dipole transitions. Optical pumping initializes an ion with a fidelity of 99.5% to the qubit state $|\downarrow\rangle \equiv |S_{1/2}, m = 1/2\rangle$, the second qubit state being $|\uparrow\rangle \equiv |D_{5/2}, m = 3/2\rangle$. The qubit is coherently manipulated[23] by an ultrastable, narrowband laser coherently exciting the $S_{1/2} \leftrightarrow D_{5/2}$ quadrupole transition in a magnetic field of $B = 4$ Gauss. Single-qubit light-shift gates $U_z^{(1)}(\theta) = \exp(-i\frac{\theta}{2}\sigma_z^{(1)})$ are realized by an off-resonant beam impinging on ion 1 with a beam waist of 3 μm and a k-vector perpendicular to the ion string. A second beam, illuminating both ions with equal strength at an angle of 45° with respect to the ion crystal, serves to carry out gate operations that are symmetric under qubit exchange. Collective single-qubit gates $U(\theta, \phi) = \exp(-i\frac{\theta}{2}(\sigma_\phi^{(1)} + \sigma_\phi^{(2)}))$, where $\sigma_\phi = \cos(\phi)\sigma_x + \sin(\phi)\sigma_y$, are realized by resonantly exciting the qubit transition and controlling the phase ϕ of the laser light. If instead a bichromatic light field near-resonant with the upper and lower sideband transitions of the axial centre-of-mass (COM) mode is used, a Mølmer-Sørensen gate[24] $U^{MS}(\theta, \phi) = \exp(-i\frac{\theta}{2}\sigma_\phi^{(1)} \otimes \sigma_\phi^{(2)})$ is implemented[23, 25]. We achieve a maximally entangling gate ($\theta = \pi/2$) capable of mapping $|\downarrow\downarrow\rangle$ to $|\downarrow\downarrow\rangle + ie^{-i2\phi}|\uparrow\uparrow\rangle$ with a fidelity of about 98% even for Doppler-cooled ions in a thermal state with an average of $\bar{n}_{ax,COM} \approx 18$ vibrational quanta. This property is of crucial importance as the experiment demands gate operations subsequent to quantum state detection by fluorescence measurements which do not preserve the motional quantum number. The set of elementary gates[26] $\{U_z^{(1)}(\theta), U(\theta, \phi), U^{MS}(\theta, \phi)\}$ is sufficient to construct the two-qubit unitary operations needed for creating various input states Ψ and mapping the observables A_{ij} to $\sigma_z^{(k)}$ for read-out (see Methods).

Equipped with these tools, we create the singlet state $\Psi = (|\uparrow\downarrow\rangle - |\downarrow\uparrow\rangle)/\sqrt{2}$ by applying the gates $U_z^{(1)}(\pi)U(\frac{\pi}{2}, \frac{3\pi}{4})U^{MS}(\frac{\pi}{2}, 0)$ to the initial state $|\downarrow\downarrow\rangle$ and measure consecutively the three observables of a row or column of the Mermin-Peres square. The results obtained for a total of 6,600 copies of Ψ are visualized in Fig. 2. The three upper panels show the distribution of measurement results $\{v(A_{i1}), v(A_{i2}), v(A_{i3})\}$, their products as well as the expectation values $\langle A_{ij}\rangle$ for the observables appearing in the rows of (1), the three lower panels show the corresponding results for the columns of the square. All of the correlations have a value close to $+1$ whereas $\langle C_3\rangle = -0.913$. By adding them up and subtracting $\langle C_3\rangle$, we find a value of $\langle \mathcal{X}_{KS}\rangle = 5.46(4) > 4$, thus violating equation (2).

To test the prediction of a state-independent violation, we repeated the experiment for nine other quantum states of different purity and entanglement. Figure 3 shows that indeed a state-independent violation of the Kochen-Specker inequality occurs, $\langle \mathcal{X}_{KS}\rangle$ ranging from 5.23(5) to 5.46(4). We also checked that a violation of (2) occurs irrespective of the temporal order of the measurement triples. Figure 4 shows the results for all possible permutations of the rows and columns of (1) based on 39,600 realizations of the singlet state. When combining

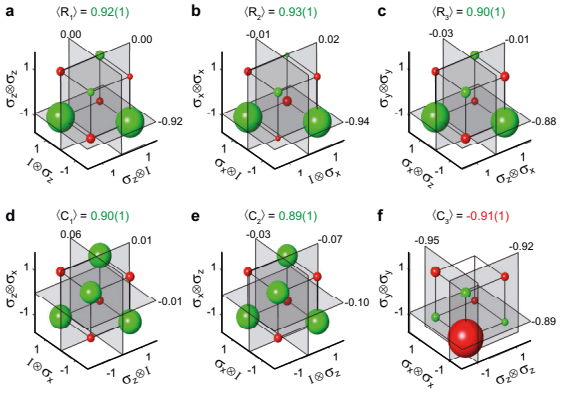

FIG. 2: Measurement correlations for the singlet state. **a** This subplot visualizes the consecutive measurement of the three observables $A_{11} = \sigma_z^{(1)}$, $A_{12} = \sigma_z^{(2)}$, $A_{13} = \sigma_z^{(1)} \otimes \sigma_z^{(2)}$ corresponding to row 1 of the Mermin-Peres square. The measurement is carried out on 1,100 preparations of the singlet state. The volume of the spheres on each corner of the cube represents the relative frequency of finding the measurement outcome $\{v_1, v_2, v_3\}$, $v_i \in \{\pm 1\}$. The color of the sphere indicates whether $v_1 v_2 v_3 = +1$ (green) or -1 (red). The measured expectation values of the observables A_{1j} are indicated by the intersections of the shaded planes with the axes of the coordinate system. The average of the measurement product $\langle R_1 \rangle$ is given at the top. **b-f** Similarly, the other five subplots represent measurements of the remaining rows or columns of the Mermin-Peres square. Subplot **f** demonstrates that the singlet state is a common eigenstate of the observables $\sigma_x^{(1)} \otimes \sigma_x^{(2)}$, $\sigma_y^{(1)} \otimes \sigma_y^{(2)}$, $\sigma_z^{(1)} \otimes \sigma_z^{(2)}$, as only one of the spheres has a considerable volume. Taking into account all the results, we find $\langle \mathcal{X}_{KS} \rangle = 5.46(4)$ in this measurement. Error bars, 1σ.

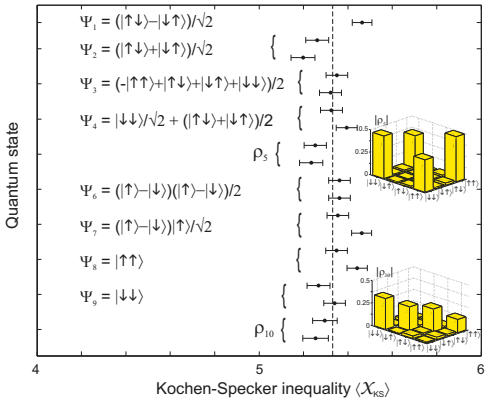

FIG. 3: State-independence of the Kochen-Specker inequality. The Kochen-Specker inequality was tested for ten different quantum states, including maximally entangled (Ψ_1-Ψ_3), partially entangled (Ψ_4) and separable (Ψ_6-Ψ_9) almost pure states as well as an entangled mixed state (ρ_5) and an almost completely mixed state (ρ_{10}). All states are analysed by quantum state tomography which yields for the experimentally produced states Ψ_1-Ψ_4, Ψ_6-Ψ_9 an average fidelity of 97(2)%. For all states, we obtain a violation of inequality (2) which demonstrates its state-independent character, the dashed line indicating the average value of $\langle \mathcal{X}_{KS} \rangle$. Error bars, 1σ (6,600 state realizations per data point).

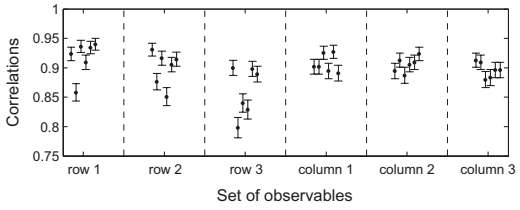

FIG. 4: Permutation within rows and columns of the Mermin-Peres square. As the three observables of a set are commuting, the temporal order of their measurements should have no influence on the measurement results. The figure shows the measured absolute values of the products of observables for any of the six possible permutations. By combining the results for the measurement of rows and columns, we obtain 36 values for the Kochen-Specker inequality ranging from 5.22 to 5.49, the average value given by 5.38. The scatter in the experimental data is caused by experimental imperfections that affect different permutations differently. For the measurements shown here, in total 39,600 copies of the singlet state were used.

the correlation results for the 36 possible permutations of operator orderings in equation (1), we find an average of $\langle \mathcal{X}_{KS} \rangle = 5.38$. Because of experimental imperfections, the experimental violation of the Kochen-Specker inequality falls short of the quantum-mechanical prediction. The dominating error source are imperfect unitary operations, in particular the entangling gates applied up to six times in a single experimental run.

All experimental tests of hidden-variable theories are subject to various possible loopholes. In our experiment, the detection loophole does not play a role, as the state of the ions are detected with near-perfect efficiency. From the point of view of a hidden variable theory, still objections can be made: In the experiment, the observables are not perfectly compatible and since the observables are measured sequentially, it may be that the hidden variables are disturbed during the sequence of measurements, weakening the demand to assign to any observable a fixed value independently of the context.

Nevertheless, it is possible to derive inequalities for classical non-contextual models, wherein the hidden variables are disturbed during the measurement process (see Methods). More specifically, it can be proved that then the probabilities of measurement outcomes obey the inequality

$$\begin{aligned} \langle \mathcal{X}_{DHV} \rangle \;=\; & \langle A_{12}A_{13} \rangle + \langle A_{22}A_{23} \rangle + \langle A_{12}A_{22} \rangle - \langle A_{13}A_{23} \rangle \\ & -2p^{\mathrm{err}}[A_{13}A_{12}A_{13}] - 2p^{\mathrm{err}}[A_{23}A_{22}A_{23}] \\ & -2p^{\mathrm{err}}[A_{22}A_{12}A_{22}] - 2p^{\mathrm{err}}[A_{23}A_{13}A_{23}] \leq 2. \end{aligned} \tag{3}$$

Here, $\langle A_i A_j\rangle = \langle v(A_i)v(A_j)\rangle$ denotes the ensemble average, if A_i is measured before A_j and $p^{\rm err}[A_iA_jA_i]$ denotes the probability that measuring A_j introduces a change on the value of A_i if the sequence $A_iA_jA_i$ is measured. To test this inequality, we prepared the state $\Psi \propto |\uparrow\uparrow\rangle + i\gamma|\downarrow\uparrow\rangle + \gamma|\uparrow\downarrow\rangle + i|\downarrow\downarrow\rangle$ where $\gamma = \sqrt{2}-1$, and measured the Mermin-Peres square with σ_y and σ_z exchanged. We find for the whole square the value $\langle \mathcal{X}_{KS}\rangle = 5.22(10) > 4$, and for Eq. (3) the value $\langle \mathcal{X}_{DHV}\rangle = 2.23(5) > 2$. This proves that even disturbances of the hidden variables for not perfectly compatible measurements cannot explain the given experimental data.

In principle, our analysis of measurement disturbances and dynamical hidden variable models can be extended to the full Mermin-Peres square, however, the experimental techniques have to be improved to find a violation there. Our findings show already unambiguously that the experimentally observed phenomena cannot be described by non-contextual models. Remarkably, here the experimental observation of counter-intuitive quantum predictions did not require the preparation of specific entangled states with non-local correlations. We expect this result to stimulate new applications of quantum contextuality for quantum information processing[27, 28, 29, 30].

Methods

Quantum state detection. The quantum state of a single ion is detected by illuminating both ions with light near the $S_{1/2} \leftrightarrow P_{1/2}$ transition frequency for $250\,\mu$s. To prevent the quantum information of the other ion from being read out, its $|\downarrow\rangle$ state population is transferred to (from) the $D_{5/2}, m = 5/2$ level before (after) the fluorescence measurement. The parameters of the read-out laser are set such that it keeps the axial COM-mode in the Lamb-Dicke regime[21] with $\bar{n}_{COM} \approx 18$. By combining the counts of two photomultipliers, we observe a Poissonian distribution of photon counts in the detection window with average count numbers $n_\uparrow \approx 7.8$ and $n_\downarrow \approx 0.07$ in the bright and dark state, respectively. Setting the detection threshold to 1.5 counts, the conditional probabilities for wrong quantum state assignments amount to $p(\uparrow|\downarrow) \approx 0.24\%$ and $p(\downarrow|\uparrow) \approx 0.39\%$. At the end of the detection interval, the ion is optically pumped on the $S_{1/2} \leftrightarrow P_{1/2}$ to prevent leakage of population from the qubit level $|\downarrow\rangle$ to the state $|S_{1/2}, m = -1/2\rangle$.

QND measurements of spin correlations. Quantum non-demolition measurements of observables A_{ij} that measure spin correlations are carried out by mapping the subspace $\mathcal{H}^+_{A_{ij}} = \{\psi | A_{ij}\psi = \psi\}$ onto the subspace $\mathcal{H}^+_{\sigma_z^{(2)}} = \{\psi|\sigma_z^{(2)}\psi = \psi\}$ prior to the fluorescence measurement of $\sigma_z^{(2)}$. This is achieved by applying a unitary state transformation U_{ij} satisfying $A_{ij} = U_{ij}^\dagger \sigma_z^{(2)} U_{ij}$ to the two-qubit state of interest. To decompose U_{ij} into the elementary gate operations available in our setup, we use a gradient-ascent based numerical search routine[26]. After measurement of $\sigma_z^{(2)}$, the inverse operation $U_{ij}^\dagger$ completes the QND measurement.

Modeling imperfect measurements. To deal with the case of imperfect measurements from a hidden variable viewpoint, let us assume that there is a hidden variable λ which simultaneously determines the probabilities of the results of all sequences of measurements. Such probabilities are written as $p[A^{(1)+}, B^{(2)-}; AB]$ etc., denoting the probability for the result $A^{(1)} = +1$ and $B^{(2)} = -1$ when measuring first A and then B. Then the probabilities fulfill

$$p[(A^{(1)+}; A) \wedge (B^{(1)+}; B)] \;\le\; p[A^{(1)+}, B^{(2)+}; AB] + p[(B^{(1)+}; B) \wedge (B^{(2)-}; AB)]. \quad (4)$$

This inequality holds because if λ is such that it contributes to $p[(A^{(1)+}; A) \wedge (B^{(1)+}; B)]$, then either the value of B stays the same when measuring A and λ contributes to $p[A^{(1)+}, B^{(2)+}; AB]$, or it is flipped and it contributes to $p[(B^{(1)+}; B) \wedge (B^{(2)-}, AB)]$. The term $p[A^{(1)+}, B^{(2)+}; AB]$ is directly measurable and we estimate the other term by assuming

$$p[(B^{(1)+}; B) \wedge (B^{(2)-}; AB)] \le p[B^{(1)+}, B^{(3)-}; BAB]. \quad (5)$$

This inequality means that the disturbance of a predetermined value of B caused by the measurement of B and A should be larger than the disturbance due to measurement of A alone, as the former includes additional experimental procedures compared with the latter. The probability $p[B^{(1)+}, B^{(3)-}; BAB]$ is experimentally accessible and combining Eq. (4) and (5) we obtain a measurable upper bound on $p[(A^{(1)+}; A) \wedge (B^{(1)+}; B)]$. Then, starting from the Clauser-Horne-Shimony-Holt-type inequality[20] $\langle AB\rangle + \langle CD\rangle + \langle AC\rangle - \langle BD\rangle \le 2$ which holds for simultaneous or undisturbed measurements, using the above bounds and the notation $p^{\rm err}[BAB] = p[B^{(1)+}, B^{(3)-}; BAB] + p[B^{(1)-}, B^{(3)+}; BAB]$, one arrives at the inequality (3), which then holds for sequences of measurements.

Acknowledgements

We gratefully acknowledge support by the Austrian Science Fund (FWF), by the European Commission (SCALA, OLAQUI and QICS networks + Marie-Curie program), by the Institut für Quanteninformation GmbH, by the Spanish MCI Project No. FIS2008-05596 and the Junta de Andalucía Excellence Project No. P06-FQM-02243. This material is based upon work supported in part by IARPA.

[1] Einstein, A., Podolsky, B. & Rosen, N., Can quantum-mechanical description of physical reality be considered complete? *Phys. Rev.* **47**, 777–780 (1935).

[2] Bell, J. S., On the Einstein-Podolsky-Rosen Paradox. *Physics* **1**, 195–200 (1964).

[3] Aspect, A., Dalibard, J., & Roger, G., Experimental test of Bell's inequalities using time-varying analyzers. *Phys. Rev. Lett.* **49**, 1804–1807 (1982).

[4] Tittel, W., Brendel, J., Zbinden, H. & N. Gisin, N., Violation of Bell inequalities by photons more than 10 km apart. *Phys. Rev. Lett.* **81**, 3563–3566 (1998).

[5] Weihs, G., Jennewein, T., Simon, C., Weinfurter, H., & Zeilinger A., Violation of Bell's inequality under strict Einstein locality conditions. *Phys. Rev. Lett.* **81**, 5039–5043 (1998).

[6] Rowe, M. A. *et al.*, Experimental violation of a Bell's inequality with efficient detection. *Nature* **409**, 791–794 (2001).

[7] Gröblacher, S., Paterek, T., Kaltenbaek, R., Brukner, Č., Żukowski, M., Aspelmeyer, M., & Zeilinger, A., An experimental test of non-local realism. *Nature* **446**, 871–875 (2007).

[8] Branciard, C., Brunner, N., Gisin, N., Kurtsiefer, C., Lamas-Linares, A., Ling, A., & Scarani V., Testing quantum correlations versus single-particle properties within Leggett's model and beyond. *Nat. Phys.* **4**, 681–685 (2008).

[9] Matsukevich, D. N. , Maunz, P., Moehring, D. L., Olmschenk, S., & Monroe, C., Bell inequality violation with two remote atomic qubits, *Phys. Rev. Lett.* **100**, 150404 (2008).

[10] Specker, E., Die Logik nicht gleichzeitig entscheidbarer Aussagen, *Dialectica* **14**, 239–246 (1960).

[11] Bell, J. S., On the problem of hidden variables in quantum mechanics. *Rev. Mod. Phys.* **38**, 447–452 (1966).

[12] Kochen, S., & Specker, E. P., The problem of hidden variables in quantum mechanics. *J. Math. Mech.* **17**, 59–87 (1967).

[13] Cabello, A., & García-Alcaine, G., Proposed experimental tests of the Bell-Kochen-Specker theorem. *Phys. Rev. Lett.* **80**, 1797-1799 (1998).

[14] Meyer, D. A., Finite precision measurement nullifies the Kochen-Specker theorem. *Phys. Rev. Lett.* **83**, 3751–3754 (1999).

[15] Huang, Y.-F., Li, C.-F., Zhang, Y.-S., Pan, J.-W. & Guo, G.-C., Experimental test of the Kochen-Specker theorem with single photons. *Phys. Rev. Lett.* **90**, 250401 (2003).

[16] Hasegawa, Y., Loidl, R., Badurek, G., Baron, M., & Rauch, H., Quantum contextuality in a single-neutron optical experiment. *Phys. Rev. Lett.* **97**, 230401 (2006).

[17] Bartosik, H., *et al.*, Experimental test of quantum contextuality in neutron interferometry. arXiv:0904.4576 (2009).

[18] Peres, A., Incompatible results of quantum measurements. *Phys. Lett. A* **151**, 107–108 (1990).

[19] Mermin, N. D., Simple unified form for the major no-hidden-variables theorems. *Phys. Rev. Lett.* **65**, 3373–3376 (1990).

[20] Cabello, A., Experimentally testable state-independent quantum contextuality. *Phys. Rev. Lett.* **101**, 210401 (2008).

[21] Häffner, H., Roos, C. F., & Blatt, R., Quantum computing with trapped ions. *Phys. Rep.* **469**, 155–203 (2008).

[22] Roos, C. F. *et al.*, Control and measurement of three-qubit entangled states. *Science* **304**, 1478–1480 (2004).

[23] Kirchmair, G. *et al.*, Deterministic entanglement of ions in thermal states of motion. *New J. Phys.* **11**, 023002 (2009).

[24] Mølmer, K., & Sørensen, A., Multiparticle entanglement of hot trapped ions. *Phys. Rev. Lett.* **82**, 1835–1838 (1999).

[25] Benhelm, J., Kirchmair, G., Roos, C. F., & Blatt, R., Towards fault-tolerant quantum computing with trapped ions. *Nat. Phys.* **4**, 463–466 (2008).

[26] Nebendahl, V., Häffner, H., & Roos, C. F., Optimal control of entangling operations for trapped-ion quantum computing. *Phys. Rev. A* **79**, 012312 (2009).

[27] Bechmann-Pasquinucci, H., & Peres, A., Quantum cryptography with 3-state systems. *Phys. Rev. Lett.* **85**, 3313–3316 (2000).

[28] Galvão, E. F., *Foundations of Quantum Theory and Quantum Information Applications*. Ph. D. thesis, Oxford University, 2002.

[29] Nagata, K., Kochen-Specker theorem as a precondition for secure quantum key distribution. *Phys. Rev. A* **72**, 012325 (2005).

[30] Spekkens, R. W., Buzacott, D. H., Keehn, A. J., Toner, B., and Pryde, G. J., Preparation contextuality powers parity-oblivious multiplexing. *Phys. Rev. Lett.* **102**, 010401 (2009).

The geometric measure of entanglement for symmetric states

Robert Hübener,[1] Matthias Kleinmann,[2] Tzu-Chieh Wei,[3] Carlos González-Guillén,[4] and Otfried Gühne[2,1]

[1]*Institut für Theoretische Physik, Universität Innsbruck, Technikerstraße 25, 6020 Innsbruck, Austria*
[2]*Institut für Quantenoptik und Quanteninformation, Österreichische Akademie der Wissenschaften, Otto Hittmair-Platz 1, 6020 Innsbruck, Austria*
[3]*Institute for Quantum Computing and Department of Physics and Astronomy, University of Waterloo, Waterloo N2L 3G1, Canada*
[4]*Dpto. Análisis Matemático & IMI, Universidad Complutense de Madrid, 28040 Madrid, Spain*

Is the closest product state to a symmetric entangled multiparticle state also symmetric? This question has appeared in the recent literature concerning the geometric measure of entanglement. First, we show that a positive answer can be derived from results concerning symmetric multilinear forms and homogeneous polynomials, implying that the closest product state can be chosen to be symmetric. We then prove the stronger result that the closest product state to any symmetric multiparticle quantum state is *necessarily* symmetric. Moreover, we discuss generalizations of our result and the case of translationally invariant states, which can occur in spin models.

PACS numbers: 03.67.Mn, 02.10.Xm, 03.67.-a

I. INTRODUCTION

Entanglement is a key phenomenon in quantum mechanics and its quantification is vital for the field of quantum information theory. Many entanglement measures have been proposed for the two-particle as well as for the multiparticle case [1, 2]. Virtually all of the proposed entanglement measures, however, suffer a serious drawback: They are very difficult to compute as their definition contains optimizations over certain states or quantum information protocols [3]. Such optimizations can be performed successfully for special cases only, for instance, if the density matrix under investigation possesses a high symmetry or belongs to a special family, e.g., with low rank [4].

An often-used entanglement measure for multiparticle systems is the geometric measure of entanglement [5]. For a given multiparticle state $|\psi\rangle$, one first considers the closest fully separable state $|\phi\rangle = |a\rangle|b\rangle|c\rangle\cdots$ in terms of the overlap

$$G(\psi) = \max_{|\phi\rangle=|a\rangle|b\rangle|c\rangle\cdots} |\langle\psi|\phi\rangle|, \tag{1}$$

and then defines the geometric measure of the pure state as

$$E_G(|\psi\rangle) = 1 - G(\psi)^2. \tag{2}$$

Sometimes, the geometric measure for pure states is also taken as $\varepsilon_G(|\psi\rangle) = -2\log_2 G(\psi)$. Based on this definition, the geometric measure is extended to mixed states via the convex roof construction: For a given density matrix ϱ one minimizes over all possible decompositions of ϱ into pure states $\varrho = \sum_k p_k\,|\phi_k\rangle\langle\phi_k|$, where the p_k form a probability distribution,

$$E_G(\varrho) \;=\; \min_{p_k,|\phi_k\rangle} \sum_k p_k E_G(|\phi_k\rangle). \tag{3}$$

Clearly, also this optimization is not straightforward to compute.

The geometric measure has become one of the widely used entanglement measures for the multiparticle case. It fulfills all the desired properties of an entanglement monotone [5]. Moreover, it has a physical interpretation of quantifying the difficulty in distinguishing multiparticle quantum states by local means [6]. It has also been used to study quantum phase transitions in spin models [7, 8] and the usefulness of states as resources for measurement based quantum computation [9]. The value of E_G has been computed for many pure states [10, 11, 12], and the convex roof for some important cases has been calculated in Refs. [5, 13].

If one considers the optimization problem in Eq. (1), a natural question arises whether for a symmetric state $|\psi\rangle$ the closest product state can be chosen symmetric, i.e., $|\phi\rangle = |a\rangle|a\rangle|a\rangle\cdots$. If this is true, it drastically simplifies the calculation of the geometric measure for pure symmetric states, as the number of parameters in this optimization then does not depend on the number of particles anymore. Recently this problem drew considerable attention in quantum information theory and some effort was made to prove it. For example, it has been used as a conjecture in Ref. [5]. In Ref. [11] it has been proved for two particles that there is always a symmetric state which gives the maximum value (but it can happen that also non-symmetric states yield the same value) and a first attempt for the N-particle case was given. Quite recently, special cases of this conjecture have been verified [14], and related conjectures have been formulated [15].

In this paper, we investigate the conjecture from several perspectives. We show that a result on N-homogeneous polynomials over Banach spaces can be applied to the above problem and proves that the maximum in Eq. (1) can be achieved by a symmetric state. However, this result does not allow to conclude that only symmetric solutions exist. We then go on to show that the optimal state maximizing $G(\psi)$ is *necessarily* symmetric for three or more particles. Finally, we will discuss con-

sequences and generalizations of our results, concerning, among others, the maximization of the expectation value of symmetric positive operators.

II. THE MAIN RESULT

In this section we will first apply a result from the theory of homogeneous polynomials to the conjecture, proving that a symmetric state attains the maximum. Then we proof a stronger version, stating that the maximizing state is necessarily symmetric. Let us fix our notation. We write the overlap with a product state as an evaluation of a corresponding N-linear form, i.e.,

$$\langle\psi|\alpha_1,\alpha_2,\ldots,\alpha_N\rangle =: \psi(\alpha_1,\alpha_2,\ldots,\alpha_N). \tag{4}$$

A symmetric state $|\psi\rangle$ then corresponds to a symmetric N-linear form ψ. For a k-level system, the vectors α_i are elements of $\mathbb{C}^k$ and we will always assume they are normalized. Furthermore, the expression $\alpha \equiv \beta$ denotes equality up to a phase, i.e., there is a phase φ such that $\alpha = e^{i\varphi}\beta$.

For any symmetric N-linear form there exists an associated N-homogeneous polynomial $\hat{\psi}$ [16] by virtue of the mapping

$$\hat{\psi}\colon \alpha \mapsto \psi(\alpha,\ldots,\alpha). \tag{5}$$

The norm of this polynomial is defined by

$$\|\hat{\psi}\| = \max_{\alpha}|\hat{\psi}(\alpha)|. \tag{6}$$

In this context the quantity $G(\psi)$ we introduced above is denoted by $\|\psi\|$.

The relation between the norms $\|\hat{\psi}\|$ and $\|\psi\|$ is studied in the theory of polynomials over Banach spaces, cf. Ref. [17]. For a Banach space $\mathcal{E}$ the *polarization constant* $c(N,\mathcal{E})$ is the smallest positive number such that

$$\|\psi\| \leq c(N,\mathcal{E})\|\hat{\psi}\| \tag{7}$$

holds for every symmetric N-linear form ψ over $\mathcal{E}$.

For finite dimensional real and complex Hilbert spaces this polarization constant is known to be 1, cf. Ref. [18, 19]. An exhaustive discussion can be found in Ref. [17]. In our particular case $\mathcal{E} = \mathbb{C}^k$ it follows that symmetric product states maximize the overlap with any symmetric state, but leaves open if also non-symmetric states attain the maximal value. This is in fact never the case for $N \geq 3$, as we summarize in

Lemma 1. *Let $\psi \neq 0$ be a symmetric N-linear form over $\mathbb{C}^k$ with $N \geq 3$ and let the vectors $\alpha_1,\ldots,\alpha_N$ maximize $|\psi|$, i.e.,*

$$G(\psi) = |\psi(\alpha_1,\alpha_2,\ldots,\alpha_N)|. \tag{8}$$

Then the vectors α_k are equal up to a phase, in other words, the span of $\alpha_1,\ldots,\alpha_N$ is one-dimensional.

In order to prove Lemma 1, we will first consider the situation where $N = 2$. The following Lemma and its proof were already given Ref. [11], however, the proof provides some observations that are essential in order to establish our main result.

Lemma 2 ([11])**.** *For any symmetric two-linear form ψ over $\mathbb{C}^k$ we can find a vector α such that*

$$G(\psi) = |\psi(\alpha,\alpha)|. \tag{9}$$

Rephrasing the statement of the Lemma, when maximizing $|\psi|$ for two particles, the maximum can by reached by a symmetric choice of vectors, although a solution maximizing $|\psi|$ is not necessarily symmetric.

Proof of Lemma 2. In a fixed orthonormal basis $\{b_i\}$ the symmetric quadratic form ψ is represented by a symmetric matrix $\Psi_{ij} := \psi(b_i,b_j)$. Then we have $\psi(\alpha,\beta) = \alpha^T\Psi\beta$, where on the right-hand side α and β are column vectors with coefficients in the basis $\{b_i\}$. For a complex symmetric matrix $\Psi = \Psi^T$ Takagi's factorization theorem [20] states that Ψ can be written as

$$\Psi = U^T D U, \tag{10}$$

with a unitary matrix U and a diagonal matrix $D = \mathrm{diag}(r_1,\ldots,r_k)$ where the non-negative values r_i are in decreasing order, $r_1 \geq r_2 \geq \cdots \geq r_k \geq 0$. In this form, a symmetric choice of α and β maximizing $|\psi|$ becomes evident, namely $\alpha \equiv \beta \equiv U^\dagger e_1$ where $e_1 = (1,0,\ldots,0)^T$. Hence $G(\psi) = r_1$. □

Let us make some remarks on the remaining freedom in the choice of α and β. First, we note that if $r_1 > r_2$ the only choice to reach the maximum r_1 is the one given in the proof above. Hence for this case the maximizing solution is unique (up to a phase) and symmetric.

Otherwise, consider the case $r_1 = r_2 = \cdots = r_d$. We then say ψ is degenerate and define $R_1 := \mathrm{span}_{\mathbb{C}}(\{e_1,\ldots,e_d\})$. If $G(\psi) = |\psi(\alpha,\beta)|$, we can always write $\alpha \equiv U^\dagger e^*$ and $\beta \equiv U^\dagger e$ with some $e \in R_1$, where the vector $e^* \in R_1$ denotes the vector obtained from e by complex conjugation in the given basis. The case that $e \equiv e^*$ then corresponds to the symmetric solutions.

The symmetric maximizing solutions therefore correspond via U to real vectors in R_1 (up to a phase), and having a non-symmetric solution $\alpha \not\equiv \beta$ of the maximization implies degeneracy. Moreover, in case of degeneracy we find a continuum of inequivalent asymmetric as well as symmetric solutions. The following observation will be needed in the main proof and expresses this fact.

Observation 3. *Given a symmetric two-linear form ψ with*

$$G(\psi) = |\psi(\alpha,\beta)|, \tag{11}$$

where $\beta \not\equiv \alpha$, we can always find two orthonormal vectors δ_1 and δ_2, such that:

(i) δ_1 *and* δ_2 *span the same space as* α *and* β*, in particular* $\alpha, \beta \in \mathrm{span}_{\mathbb{C}}(\{\delta_1, \delta_2\})$.

(ii) We have $G(\psi) = |\psi(\delta_1, \delta_1)| = |\psi(\delta_2, \delta_2)| = |\psi(\eta, \eta)| = |\psi(\mu, \mu')|$*, where*

$$\begin{aligned} \eta &:= (\delta_1 + \delta_2)/\sqrt{2}, \\ \mu &:= (\delta_1 + i\delta_2)/\sqrt{2}, \\ \mu' &:= (\delta_1 - i\delta_2)/\sqrt{2}. \end{aligned} \tag{12}$$

(iii) The vectors $\delta_1, \delta_2, \eta, \mu'$ *do not equal* α*, even modulo a phase.*

Proof. Consider $G(\psi) = |\psi(\alpha, \beta)| = |\psi(U^\dagger e^*, U^\dagger e)|$ with the unitary matrix U from Takagi's factorization of Ψ, where $e \not\equiv e^*$ as $\beta \not\equiv \alpha$ by assumption. We can choose two real orthonormal vectors f_1, f_2 such that $\mathrm{span}_{\mathbb{C}}(\{f_1, f_2\}) = \mathrm{span}_{\mathbb{C}}(\{e, e^*\})$. They can be obtained from the real and imaginary parts of e and e^* [21]. Hence

$$\delta_1 = U^\dagger f_1 \text{ and } \delta_2 = U^\dagger f_2 \tag{13}$$

is a valid choice of orthonormal vectors fulfilling (i), each providing a symmetric maximization of $|\psi|$. The vectors δ_1, δ_2 as well as the vectors η, μ, μ' derived from δ_1, δ_2 fulfill (ii) by construction, according to the observations above and because $\eta = U^\dagger(f_1 + f_2)/\sqrt{2}$, where $(f_1 + f_2)/\sqrt{2} \in R_1$ (likewise for μ, μ'). Finally, we have enough freedom to choose f_1, f_2 to satisfy (iii). □

After these preliminaries, we are ready to prove Lemma 1:

Proof of Lemma 1. The proof consists of two parts. In Part I we prove the case $N = 3$. In Part II we extend the result to arbitrary $N > 3$.

Part I. Assume a maximizing set of vectors $\{\alpha, \beta, \gamma\}$ has been found,

$$G(\psi) = |\psi(\alpha, \beta, \gamma)|. \tag{14}$$

We show that the assumption $\dim[\mathrm{span}_{\mathbb{C}}(\{\alpha, \beta, \gamma\})] \neq 1$ leads to $\psi = 0$.

Without losing generality, we hence assume that $\gamma \not\equiv \beta$. Then we have a degenerate quadratic form $\psi(\alpha, \cdot, \cdot\cdot)$. Using Lemma 2 we obtain a symmetric maximizing solution $\sigma \not\equiv \alpha$ (due to $\gamma \not\equiv \beta$, σ is not unique). Hence we have $G(\psi) = |\psi(\alpha, \sigma, \sigma)|$. From Observation 3, applied to the quadratic form $\psi(\cdot, \cdot\cdot, \sigma)$, we take the vectors $\delta_1, \delta_2, \eta, \mu, \mu'$ with the properties as stated. With these vectors we define the 2×2-matrices A, B, N, M via

$$\begin{aligned} A_{kl} &:= \psi(\delta_1, \delta_k, \delta_l), \\ B_{kl} &:= \psi(\delta_2, \delta_k, \delta_l), \\ N_{kl} &:= \psi(\eta, \delta_k, \delta_l) = (A_{kl} + B_{kl})/\sqrt{2}, \\ M_{kl} &:= \psi(\mu, \delta_k, \delta_l) = (A_{kl} + iB_{kl})/\sqrt{2}. \end{aligned} \tag{15}$$

As $\sigma, \delta_1, \delta_2, \eta$, and μ' are in $\mathrm{span}_{\mathbb{C}}(\{\delta_1, \delta_2\})$ the matrices A, B, N, M correspond to two-forms which assume the maximum $r_1 = G(\psi)$ on this span. Since $\delta_1, \delta_2, \eta, \mu' \not\equiv \sigma$, the quadratic forms A, B, N, M are degenerate with the value r_1. In terms of the Takagi factorization, we can write $A = U_A^T D U_A$ and $B = U_B^T D U_B$, etc. with $D = \mathrm{diag}(r_1, r_1)$. It follows that $A^\dagger A = B^\dagger B = N^\dagger N = M^\dagger M = D^2$, which implies $A^\dagger B + B^\dagger A = i(A^\dagger B - B^\dagger A) = 0$. Hence $B^\dagger A = 0$, which is only possible for $\psi = 0$.

Part II. The extension to the case $N > 3$ is proved as follows. If $G(\psi) = |\psi(\alpha_1, \alpha_2, \ldots, \alpha_N)|$ we define a symmetric 3-linear form by

$$\psi_{\hat{k}} := \psi(\hat{\alpha}_1, \hat{\alpha}_2, \ldots, \hat{\alpha}_k, \ldots, \alpha_N) \tag{16}$$

where $\hat{\alpha}_i$ denotes omission, i.e., $\alpha_1, \alpha_2, \alpha_k$ are omitted. As in Part 1, we have $G(\psi) = |\psi_{\hat{k}}(\alpha_1, \alpha_2, \alpha_k)|$ and thus $\alpha_1 \equiv \alpha_2 \equiv \alpha_k$ for all k. Hence all vectors $\alpha_1, \ldots, \alpha_N$ must be the same up to a phase. □

Lemma 1 is stated for N-linear forms over a complex vector space. If $|\psi\rangle$ is real, one can also consider the maximization over real product vectors. In general this will yield a different result than the complex case [22]. Since the polarization constant is 1 also in the real case, one can find a a symmetric state among the real product states which attains the maximum. In contrast to the complex case, the maximizing state is, however, not necessarily symmetric for three particles. A counterexample is $|\psi\rangle = (|001\rangle + |010\rangle + |100\rangle - |111\rangle)/2$ where the maximum of $1/2$ is also attained by $|\phi\rangle = |001\rangle$.

The following Lemma provides an additional very simple proof that $c(N, \mathcal{H}) = 1$ for $N = 2^\ell$, and is based on a symmetrization procedure.

Lemma 4. *Let* ψ *be a symmetric* N*-linear form with* $N = 2^\ell$ *and let the vectors* $\alpha_1, \ldots, \alpha_N$ *maximize* $|\psi|$*. Then there exists a normalized vector* ζ *in the span of* $\alpha_1, \ldots, \alpha_N$ *such that*

$$|\psi(\alpha_1, \ldots, \alpha_N)| = |\psi(\zeta, \ldots, \zeta)|. \tag{17}$$

This statement holds for real and complex Hilbert spaces.

Proof. Let $\langle \cdot, \cdot\cdot \rangle$ denote the scalar product and we define the constant $\Lambda = \psi(\alpha_1, \alpha_2, \alpha_3, \ldots)$. Then $\psi(\cdot, \alpha_2, \alpha_3, \ldots) = \Lambda \langle \alpha_1, \cdot \rangle$ and $\psi(\alpha_1, \cdot, \alpha_3, \ldots) = \Lambda \langle \alpha_2, \cdot \rangle$ (cf. Eq. (6) in Ref. [5]). Using the symmetry and linearity of ψ we arrive at

$$\psi(\cdot, \beta_1, \alpha_3, \ldots) = \Lambda \langle \beta_1, \cdot \rangle \tag{18}$$

and hence

$$\Lambda = \psi(\beta_1, \beta_1, \alpha_3, \ldots), \tag{19}$$

where $\beta_1 = (\alpha_1 + \alpha_2)/||\alpha_1 + \alpha_2||$. (If $\alpha_1 = -\alpha_2$, we set $\beta_1 = \alpha_1$ and replace Λ by $-\Lambda$.)

We now repeat this procedure, first yielding $\Lambda = \psi(\beta_1, \beta_1, \beta_3, \beta_3, \ldots)$ and then $\Lambda = \psi(\gamma_1, \gamma_1, \gamma_1, \gamma_1, \ldots)$, where β_3 is defined analogously to β_1 and $\gamma_1 = (\beta_1 + \beta_3)/||\beta_1 + \beta_3||$. In the second step we applied the symmetrization to the first and third argument as well as to the second and fourth argument. Since $N = 2^\ell$, we can complete this symmetrization and arrive at $\Lambda = \psi(\zeta, \ldots, \zeta)$ for some ζ in the span of $\alpha_1, \ldots, \alpha_N$. □

III. DISCUSSION

A. Physical interpretation of the proof

An interpretation of the proof of Lemma 1 in physical terms is the following. The matrices A, B, N and M in Eq. (15) are representations of the state $|\psi\rangle$, after one site has been measured out and the remaining state has been projected onto a two-dimensional subspace. The values r_i correspond to Schmidt coefficients of this remaining state and, as they are equal, the state corresponds to a Bell state. The proof of Lemma 1 shows that for qubits it is impossible to create a state of three particles that is both symmetric and always results in a Bell-pair like state after an arbitrary measurement on one site.

B. Translationally invariant states

It is interesting to ask whether also for translationally invariant states the maximum is attained in a symmetric state, as such states occur naturally in the analysis of spin models. This has sometimes been assumed when investigating the geometric measure in condensed matter systems.

First, a counterexample for this conjecture is the state

$$|\psi\rangle = \frac{1}{\sqrt{2}}(|0101\rangle + |1010\rangle) \tag{20}$$

for which the closest separable states are the non-symmetric states $|0101\rangle$ and $|1010\rangle$. In fact, one can find translationally invariant states which are orthogonal to any symmetric product state, e.g., $|\psi\rangle \sim (|0101\rangle - |0011\rangle +$ all translations).

This situation gets worse as the number of particles increases. Let $\mathcal{T}$ denote the subspace of translationally invariant states for N qukits and let $\mathcal{S} \subset \mathcal{T}$ be the permutationally symmetric subspace. Then any state in $\mathcal{X} = \mathcal{T} \cap \mathcal{S}^{\perp}$ – the orthocomplement of $\mathcal{S}$ in $\mathcal{T}$ – has a vanishing overlap with any symmetric product state, hence the closest product state is not symmetric. The dimension of $\mathcal{T}$ is given by [23]

$$\dim(\mathcal{T}) = \frac{1}{N}\sum_{j|N} \varphi(j)\, k^{N/j}, \tag{21}$$

where φ denotes Euler's totient function and the summation is over all divisors j of N. For $\mathcal{S}$ we have

$$\dim(\mathcal{S}) = \binom{N+k-1}{k-1}. \tag{22}$$

Therefore, if $N \gg k$ then the dimension of the subspace $\mathcal{X}$ is roughly given by $(k^N - N^k)/N$ and the fraction of states where the conjecture holds shrinks rapidly as the number of particles increases.

Concerning the analysis of entanglement in spin models, this shows that the assumption that the closest separable state to the ground state is symmetric, has to be handled with care. For some models, it seems to be true [8, 24], for other models (like the Majumdar-Ghosh model [25]) one can directly check that it is wrong.

C. Operators of higher rank

We now consider generalizations of our results. Let $\Pi_{\mathcal{S}}$ be the projector onto the symmetric subspace $\mathcal{S}$. An operator A is *permutationally symmetric* if it acts on the symmetric subspace only, i.e., it fulfills $A = \Pi_{\mathcal{S}} A \Pi_{\mathcal{S}}$. A is called *permutationally invariant* if it is invariant under permutation of the particles (the latter is a weaker condition than the former [26]). We hence define for an observable X

$$\begin{aligned} \hat{G}(X) &:= \max_{|\varphi\rangle = |a\rangle|b\rangle|c\rangle\cdots} |\langle\varphi|X|\varphi\rangle| \\ \hat{G}_{\mathcal{S}}(X) &:= \max_{|\varphi\rangle = |a\rangle\cdots|a\rangle} |\langle\varphi|X|\varphi\rangle| \end{aligned} \tag{23}$$

Such optimizations occur naturally in the construction of entanglement witnesses or in the estimation of entanglement measures via Legendre transforms [2].

To study the relation of these quantities, we can write $\langle\varphi|X|\varphi\rangle = \mathrm{Tr}\left[X\,|\varphi\rangle\langle\varphi|\right]$ as an evaluation of a corresponding N-linear form ξ over $\mathfrak{H}^k$ (the Banach space of Hermitian matrices of dimension k equipped with the trace norm) due to

$$\xi(A_1, \ldots, A_N) = \mathrm{Tr}\left[X A_1 \otimes \cdots \otimes A_N\right]. \tag{24}$$

Then any permutationally invariant operator X corresponds to a symmetric N-linear form ξ and an N-homogeneous polynomial $\hat{\xi}$. We now define $\|\xi\|$ and $\|\hat{\xi}\|$ analogously to Section II (using $\|A\| = 1$ as normalization condition). It is straightforward to see that $\hat{G}(X) = \|\xi\|$ and $\hat{G}_{\mathcal{S}}(X) = \|\hat{\xi}\|$. As the polarization constant can be shown to be [27]

$$c(N, \mathfrak{H}^k) = N^N/N! \quad \text{for} \quad N \leq k, \tag{25}$$

the quotient $\hat{G}(X)/\hat{G}_{\mathcal{S}}(X)$ can get arbitrarily large as N and k increase.

At the end of this section, we will provide a further explicit example. Let us first discuss some cases where symmetry assumptions do hold:

Corollary 5. *(i) If X is a positive permutationally symmetric observable then $\hat{G}(X)$ can be attained by a symmetric state.*
(ii) If X is a permutationally invariant N-qubit observable that contains only full correlation terms, then $\hat{G}(X)$ can be attained by a symmetric state.

Proof. (i) We note that

$$\hat{G}(X) \leq \max_{|\psi\rangle = |b_1\rangle\cdots|b_n\rangle} \max_{|\varphi\rangle = |a_1\rangle\cdots|a_n\rangle} |\langle\varphi|X|\psi\rangle|. \tag{26}$$

Fixing $|\psi\rangle$, the (unnormalized) state $X|\psi\rangle = \Pi_{\mathcal{S}} X \Pi_{\mathcal{S}}|\psi\rangle$ is symmetric and by virtue of Lemma 1 the maximum

is reached by a symmetric state $|a,\ldots,a\rangle$. Repeating the reasoning with the fixed state $|\varphi\rangle = |a,\ldots,a\rangle$, we get $\hat{G}(X) \leq \max_{|b\rangle} \max_{|a\rangle} |\langle a,\ldots,a|X|b,\ldots,b\rangle|$. The fact that for positive operators $2|\langle\alpha|P|\beta\rangle| \leq \langle\alpha|P|\alpha\rangle + \langle\beta|P|\beta\rangle \leq 2\max\{\langle\alpha|P|\alpha\rangle, \langle\beta|P|\beta\rangle\}$ holds for arbitrary $|\alpha\rangle$ and $|\beta\rangle$ proves that $\hat{G}(X) \leq \hat{G}_{\mathcal{S}}(X)$, hence $\hat{G}(X) = \hat{G}_{\mathcal{S}}(X)$.

(ii) An N-qubit operator X contains only full correlation terms if $X = \sum_{i,j,\ldots\in\{x,y,z\}} \lambda_{ij\ldots}\sigma_i \otimes \sigma_j \otimes \cdots$. Note that here $\sigma_0 = \mathbb{1}$ does not occur; a physically relevant and well known example for such an operator X is the Mermin inequality. As X is permutationally invariant, λ is equivalent to a symmetric N-linear form over $\mathbb{R}^3$. The Bloch representation for qubits implies that here the maximization is equivalent to finding $\max_{r_i\in\mathbb{R}^3} |\lambda(r_1, r_2, \ldots, r_N)|$ where the vectors r_i are the corresponding Bloch vectors. Since the polarization constant for real Hilbert spaces is 1 [17, 18, 19], the assertion follows. □

Let us conclude with some examples where symmetry assumptions do not hold. If X is symmetric but not positive, then the maximum $\hat{G}(X)$ is, in general, not attained by a symmetric state. A counterexample for two qubits is $X = 6\,|\psi^+\rangle\langle\psi^+| - |00\rangle\langle 00| - 2\,|11\rangle\langle 11|$ with $|\psi^+\rangle = (|01\rangle + |10\rangle)/\sqrt{2}$. Then $\hat{G}(X) = 3$ (we can take $|\phi_0\rangle = |01\rangle$) while the maximum for symmetric product states is 34/15. Also, if X is permutationally invariant (and even positive) then the maximum $\hat{G}(X)$ is, in general, not attained by a symmetric state. A counterexample is the singlet state, $X = |\psi^-\rangle\langle\psi^-|$ with $|\psi^-\rangle = (|01\rangle - |10\rangle)/\sqrt{2}$. This operator is invariant under permutation of the particles, but it does not act on the symmetric space. It has $\hat{G}(X) = 1/2$, but restriction to the symmetric $|\phi\rangle$ would yield again $\hat{G}(X) = 0$. This clarifies some questions raised in Ref. [15].

IV. CONCLUSION

In conclusion, we have discussed a widely used conjecture concerning the geometric measure of entanglement. Our results not only simplify the calculation of the geometric measure for symmetric states, but they also have applications to subjects in condensed matter physics. Furthermore, from a mathematical perspective, the quantity G, as defined in the introduction, is known as the injective tensor norm [28]. On the one hand, this norm is of central importance in tensor analysis, since there are, as Grothendieck showed, fourteen inequivalent natural tensor norms derivable from G [29]. On the other hand, this norm has also occurred in the discussion of the maximal output purity of quantum channels [30]. So we believe that the study of tensor norms can yield further interesting insights in quantum information theory.

We thank A. Abdesselam, A. Harrow, M. Murao, R. Orus, D. Pérez-García, S. Virmani and R.F. Werner for discussions. This work has been supported by the FWF (START prize) and the EU (OLAQUI, QICS, SCALA). TCW acknowledges support from IQC, NSERC and ORF. CGG acknowledges financial support from the Spanish grants I-MATH, MTM2008-01366, CCG08-UCM/ESP-4394 and Beca-COMPLUTENSE2006.

[1] M. Plenio and S. Virmani, Quant. Inf. Comp. **7**, 1 (2007); R. Horodecki *et al.*, Rev. Mod. Phys. **81**, 865 (2009).
[2] O. Gühne and G. Tóth, Phys. Reports **474**, 1 (2009).
[3] A well-known exception is the entanglement of formation (or the concurrence) for two qubits, see W.K. Wootters, Phys. Rev. Lett. **80**, 2245 (1998).
[4] B.M. Terhal and K.G.H. Vollbrecht, Phys. Rev. Lett. **85**, 2625 (2000); P. Rungta and C. M. Caves, Phys. Rev. A **67**, 012307 (2003); R. Lohmayer *et al.*, Phys. Rev. Lett. **97**, 260502 (2006); T.-C. Wei, Phys. Rev. A **78**, 012327 (2008).
[5] T.-C. Wei and P.M. Goldbart, Phys. Rev. A **68**, 042307 (2003).
[6] M. Hayashi *et al.*, Phys. Rev. Lett. **96**, 040501 (2006).
[7] T.-C. Wei *et al.*, Phys. Rev. A **71**, 060305(R) (2005); R. Orus, Phys. Rev. Lett. **100**, 130502 (2008); R. Orus, S. Dusuel, and J. Vidal, Phys. Rev. Lett. **101**, 025701 (2008); Y. Nakata, D. Markham, and M. Murao, Phys. Rev. A **79**, 042313 (2009).
[8] T.-C. Wei, arXiv:0810.2564.
[9] D. Gross, S. Flammia, J. Eisert, Phys. Rev. Lett. **102**, 190501 (2009); M.J. Bremner, C. Mora, and A. Winter Phys. Rev. Lett. **102**, 190502 (2009).
[10] D. Markham, A. Miyake, and S. Virmani, New J. Phys. **9**, 194 (2007); J.J. Hilling and A. Sudbery, arXiv:0905.2094.
[11] M. Hayashi *et al.*, Phys. Rev. A **77**, 012104 (2008).
[12] L. Tamaryan, D.K. Park and S. Tamaryan, Phys. Rev. A **77**, 022325 (2008); S. Tamaryan, T.-C. Wei, and D. Park, arXiv:0905.3791.
[13] O. Gühne, F. Bodoky, and M. Blaauboer, Phys. Rev. A **78**, 060301(R) (2008).
[14] M. Hayashi *et al.*, arXiv:0905.0010; T.-C. Wei and S. Severini, arXiv:0905.0012.
[15] P. Gawron *et al.*, arXiv:0905.3646.
[16] A polynomial P is N-homogeneous if $P(\lambda x) = \lambda^N P(x)$.
[17] S. Dineen, *Complex Analysis on Infinite Dimensional Spaces*, Springer, London-Berlin-Heidelberg, (1999).
[18] O. D. Kellogg, Math. Z. **27**, 55 (1928); S. Banach, Ann. Polon. Math **12**, 116 (1933).
[19] L. Hörmander, Math. Scand. **2**, 55 (1954).
[20] T. Takagi, Japanese J. Math. **1**, 83 (1927); see also R. Horn and C. Johnson, *Matrix Analysis*, (Cambridge University Press 1999), p. 204.
[21] Note that e and e^* are vectors with complex conjugated elements, i.e., $e = e_r + ie_i$ and $e^* = e_r - ie_i$ where $e_r, e_i \in \mathbb{R}^k$. Hence e_r, e_i is an example for a real basis, being linearly independent since $e \not\equiv e^*$. In fact, any real orthonormal basis of $\mathrm{span}_{\mathbb{C}}(\{e_r, e_i\})$ can be used as

f_1, f_2, as long as they fulfill (iii).

[22] An example of a for four-qubit state where the maximizations over real and complex product vectors differ is $|\psi\rangle = [|0000\rangle + |0001\rangle + |0010\rangle + |0100\rangle + |1000\rangle - 2(|1110\rangle + |1101\rangle + |1011\rangle + |0111\rangle)]/\sqrt{21}$.

[23] G. Pólya, Acta Math. **68**, 145 (1937).

[24] See Chapter 5 (Fig. 5.3) in T.-C. Wei, PhD-thesis, arXiv:0905.2467.

[25] C.K. Majumdar and D.K. Ghosh, J. Math. Phys. **10**, 1388 (1969).

[26] G. Tóth and O. Gühne, Phys. Rev. Lett. **102**, 170503 (2009).

[27] One can embed isometrically l_1^k (i.e., $\mathbb{R}^k$ with norm $\|\cdot\|_1$) into $\mathfrak{H}^k$ by a direct mapping into the diagonal. As $c(N, l_1^k) = N^N/N!$ for $N \leq k$ [17] and on the other hand $c(N, \mathcal{E}) \leq N^N/N!$ for any Banach space $\mathcal{E}$, we have $c(N, \mathfrak{H}^k) = N^N/N!$ for $N \leq k$.

[28] A. Defant and K. Floret, *Tensor Norms and Operator Ideals*, (North-Holland, 1993).

[29] A. Grothendieck, Bol. Soc. Mat. São Paulo **8**, 1 (1956).

[30] R.F. Werner and A.S. Holevo, J. Math. Phys. **43**, 4353 (2002).

Compatibility and noncontextuality for sequential measurements

Otfried Gühne,[1,2] Matthias Kleinmann,[1] Adán Cabello,[3] Jan-Åke Larsson,[4]
Gerhard Kirchmair,[1,5] Florian Zähringer,[1,5] Rene Gerritsma,[1,5] and Christian F. Roos[1,5]

[1]*Institut für Quantenoptik und Quanteninformation, Österreichische Akademie der Wissenschaften, Technikerstr. 21A, A-6020 Innsbruck, Austria*
[2]*Institut für Theoretische Physik, Universität Innsbruck, Technikerstr. 25, A-6020 Innsbruck, Austria*
[3]*Departamento de Física Aplicada II, Universidad de Sevilla, E-41012 Sevilla, Spain*
[4]*Institutionen för Systemteknik och Matematiska Institutionen, Linköpings Universitet, SE-581 83 Linköping, Sweden*
[5]*Institut für Experimentalphysik, Universität Innsbruck, Technikerstr. 25, A-6020 Innsbruck, Austria*

(Dated: January 5, 2010)

A basic assumption behind the inequalities used for testing noncontextual hidden variable models is that the observables measured on the same individual system are perfectly compatible. However, compatibility is not perfect in actual experiments using sequential measurements. We discuss the resulting "compatibility loophole" and present several methods to rule out certain hidden variable models which obey a kind of extended noncontextuality. Finally, we present a detailed analysis of experimental imperfections in a recent trapped ion experiment and apply our analysis to that case.

PACS numbers: 03.65.Ta, 03.65.Ud, 42.50.Xa

I. INTRODUCTION

Since the early days of quantum mechanics (QM), it has been debated whether or not QM can be completed with additional hidden variables (HVs), which would eventually account for the apparent indeterminism of the results of single measurements in QM, and may end into a more detailed deterministic description of the world [1–3]. The problem of distinguishing QM from HV theories, however, cannot be addressed unless one makes additional assumptions about the structure of the HV theories. Otherwise, for a given experiment, one can just take the observed probability distributions as a HV model [4]. Moreover, there are explicit HV theories, such as Bohmian mechanics [5, 6], which can reproduce all experiments up to date.

In the 1960s, it was found out that HV models reproducing the predictions of QM should have some peculiar and highly nonclassical properties. The most famous result in this direction is Bell's theorem [7]. Bell's theorem states that local HV models cannot reproduce the quantum mechanical correlations between local measurements on some entangled states. In principle, the theorem just states a conflict between two descriptions of the world: QM and local HV models. However, the proof of Bell's theorem by means of an inequality involving correlations between measurements on distant systems, which is satisfied by any local HV model, but is violated by some quantum predictions [8], allows us to take a step further and test whether or not the world itself can be described by local HV models [9–13]. More recently, a similar approach has been used to test whether or not the world can be reproduced with some specific nonlocal HV models [14–16].

A second seminal result on HV models reproducing QM is the Kochen-Specker (KS) theorem [17–19]. To motivate it, one first needs the notion of compatible measurements: two or more measurements are compatible, if they can be measured jointly on the same individual system without disturbing each other (i.e., without altering their results). Compatible measurements can be made simultaneously or in any order, and can be repeated any number of times on the same individual system and always must give the same result independently of the initial state of the system.

Second, one needs the notion of noncontextuality. A context is a set of compatible measurements. A physical model is called noncontextual if it assigns to a measurement a result independently of which other compatible measurements are carried out. There are some scenarios where the assumption of noncontextuality is specially plausible. For instance, in the case of measurements on distant systems, or in the case that the measurements concern different degrees of freedom of the same system and the degrees of freedom can be accessed independently.

In a nutshell, the KS theorem states that noncontextual HV models cannot reproduce QM. This impossibility occurs already for a single three-level system, so it is not related to entanglement.

There have been several proposals to test the KS theorem [20–24], but there also have been debates whether the KS theorem can be experimentally tested at all [25–34]. Nevertheless, first experiments have been performed, but these experiments required some additional assumptions [35–37, 45]. Furthermore, the notion of contextuality has been extended to state preparations [38] and experimentally investigated [39].

Quite recently, several inequalities have been proposed which hold for all noncontextual models, but are violated in QM, potentially allowing for a direct test [40–43]. A remarkable feature of some noncontextuality inequalities is that the violation is independent of the quantum state of the system [42, 43]. In this paper, we will call these

inequalities KS inequalities, since the proof of the KS theorem in Ref. [19] is also valid for any quantum state of the system. Very recently, several experiments have found violations of noncontextual inequalities [44–48]. Three of these experiments have found violations of a KS inequality for different states [44, 46] or for a single (maximally mixed) state [48]. In these experiments, compatible observables are measured sequentially.

The measurements in any experiment are never perfect. In tests of noncontextuality inequalities, these imperfections can be interpreted as a failure of the assumption that the observables measured sequentially on the same system are perfectly compatible. What if this compatibility is not perfect? We will refer to this problem as the "compatibility loophole". The main aim of this paper is to give a detailed discussion of this loophole and demonstrate that, despite of this loophole, still classes of HV models which obey a generalized definition of noncontextuality can be experimentally ruled out.

The paper is organized as follows: In Sec. II we give precise definitions of compatibility and noncontextuality, focusing on the case of sequential measurements. We also review some inequalities which have been proposed to test noncontextual HV models.

In Sec. III we discuss the case of not perfectly compatible observables. We first derive an inequality which holds for any HV model, however, this inequality is not experimentally testable. Then, we consider several possible extensions of noncontextuality. By that, we mean replacing our initial assumption of noncontextuality for perfectly compatible observables by a new one, which covers also nearly compatible observables and implies the usual noncontextuality if the measurements are perfectly compatible. We then present several experimentally testable inequalities which hold for HV models with some generalized version of noncontextuality, but which are violated in QM. One of these inequalities has already been found to be violated in an experiment [44]. In Sec. IV we present details of this experiment.

In Sec. V we present two explicit contextual HV models which violate all investigated inequalities. These models, which do not satisfy the assumptions of extended noncontextuality, are useful to understand which counterintuitive properties a HV model must have to reproduce the quantum predictions. Other contextual HV models for contextuality experiments have been proposed in Ref. [49]. Finally, in Sec. VI, we conclude and discuss consequences of our work for future experiments.

II. HIDDEN VARIABLE MODELS AND NONCONTEXTUALITY

A. Joint or sequential measurements

In the scenario originally used for discussing noncontextuality [19], a measurement device is treated as a single device producing outcomes for several compatible measurements (i.e., a context). When treating the measurement device in this manner, the whole context is needed to produce any output at all. In this joint measurement, one of the settings of the measurement device is always specifically associated with one of the outcomes, in the sense that another measurement device exists that takes only that setting as input and gives an identical outcome as output. This is checked by repeatedly making a joint measurement and the corresponding compatible single measurements in any possible order. This is at the basis of the noncontextuality argument. The argument goes: *precisely because* another context-less device exists that can measure the outcome of interest, there is good reason to assume that this outcome is independent of the context in the joint measurement.

In this paper we discuss sequential individual measurements, rather than joint measurements. It might be argued that the version of the noncontextuality assumption needed in this scenario is more restrictive on the HV model than the version used for joint measurements. This would mean that a test using a sequential setup would be weaker than a test using a joint measurement setup, because it would rule out fewer HV models. However, the motivation for assuming non-contextuality even in the joint measurement setup is the existence of the individual measurements and their compatibility and repeatability when combined with joint context-needing measurements. Therefore, the assumptions needed in the sequential measurements setting are equally well-motivated as the assumptions needed in the joint measurement setting.

In fact, the sequential setting is closer to the actual motivation of assuming noncontextuality: there exist individual context-less measurement devices that give the same results as the joint measurements, *and we actually use them in experiment*. Furthermore, from an experimental point of view, a changed context in the joint measurement device corresponds to a physically entirely different setup even for the unchanged setting within the context, so it is difficult to maintain that the outcome for the unchanged setting is unchanged from physical principles [18, 50]. Motivating physically unchanged outcomes is much easier in the sequential setup, since the device used is physically identical for the unchanged setting.

Therefore, in this paper we consider the situation where sequences of measurements are made on an individual physical system. Throughout the paper, we consider only dichotomic measurements with outcomes ± 1, but the results can be generalized to arbitrary measurements. The question is: under which conditions can the results of such measurements be explained by a HV model? More precisely, we ask which conditions a HV model has to violate in order to reproduce the quantum predictions.

B. Notation

The following notation will be used in the discussed HV models: λ is the HV, drawn with a distribution $p(\lambda)$ from a set Λ. The distribution summarizes all information about the past, including all preparation steps and all measurements already performed. Causality is assumed, so the distribution is independent of any event in the future. It rather determines all the probabilities of the results of all possible future sequences of measurements. We assume that, for a fixed value of the HV, the outcomes of future sequences of measurements are deterministic, hence all indeterministic behavior stems from the probability distribution. This is similar to the investigation of Bell inequalities, where any stochastic HV model can be mapped onto a deterministic one where the HV is not known [4, 51].

In an experiment, one first prepares a "state" via certain preparation procedures (which may include measurements). One always regards a state preparation as a procedure which can be repeated. At the HV level, it will therefore lead to an experimentally accessible probability distribution $p_{\exp}(\lambda)$. The HV model hence enables the experimenter to repeatedly prepare the same distribution. In a single instance of an experiment, one obtains a state determined by a single value λ of the HV. The probability for this instance is distributed according to the distribution $p_{\exp}(\lambda)$, and reflects the inability of the experimenter to control which particular value of the HVs has been prepared in a single instance.

Continuing, we denote by A_i the measurement of the observable (or measurement device) A at the position i in the sequence. For example, $A_1B_2C_3$ denotes the sequence of measuring A first, then B, and finally C. An outcome from a measurement, e.g., B_2 from the above sequence, is denoted $v(B_2|A_1B_2C_3)$. The product of three outcomes is denoted $v(A_1B_2C_3) = v(A_1|A_1B_2C_3)v(B_2|A_1B_2C_3)v(C_3|A_1B_2C_3)$. Given a probability distribution $p(\lambda)$, we write probabilities $p(B_2^+|A_1B_2C_3)$ [or $p(B_2^+C_3^-|A_1B_2C_3)$] for the probability of obtaining the value $B_2 = +1$ (and $C_3 = -1$) when the sequence $A_1B_2C_3$ is measured. One can also consider mean values like $\langle B_2|A_1B_2C_3\rangle = p(B_2^+|A_1B_2C_3) - p(B_2^-|A_1B_2C_3)$, or the mean value of the complete sequence, $\langle A_1B_2C_3\rangle = p[v(A_1B_2C_3) = +1] - p[v(A_1B_2C_3) = -1]$.

C. Compatibility of measurements

In the simplest case, compatibility is a relation between a pair of measurements, A and B. For that, let $\mathcal{S}_{AB}$ denote the (infinite) set of all sequences, which use only measurements of A and B, that is, $\mathcal{S}_{AB} = \{A_1, B_1, A_1A_2, A_1B_2, B_1A_2, \ldots\}$. Then, we formulate:

Definition 1.—Two observables A and B are compatible if the following two conditions are fulfilled:

(i) For any instance of a state (i.e. for any λ) and for any sequence $S \in \mathcal{S}_{AB}$, the obtained values of A and B remain the same,

$$v(A_k|S) = v(A_l|S), \tag{1a}$$
$$v(B_m|S) = v(B_n|S), \tag{1b}$$

where k, l, m, n are all possible indices for which the considered observable is measured at the positions k, l, m, n in the sequence S. [Equivalently, we could require that $p(A_k^+A_l^-|S) = 0$, etc., for all preparations corresponding to some $p_{\exp}(\lambda)$.]

(ii) For any state preparation [i.e., for any $p_{\exp}(\lambda)$], the mean values of A and B during the measurement of any two sequences $S_1, S_2 \in \mathcal{S}_{AB}$ are equal,

$$\langle A_k|S_1\rangle = \langle A_l|S_2\rangle, \tag{2a}$$
$$\langle B_m|S_1\rangle = \langle B_n|S_2\rangle. \tag{2b}$$

Clearly, conditions (i) and (ii) are necessary conditions for compatible observables, in the sense that two observables which violate any of them cannot reasonably called compatible.

It is important to note that the compatibility of two observables is experimentally testable by repeatedly preparing all possible $p_{\exp}(\lambda)$. The fact that this set is infinite is not a specific problem here, as any measurement device or physical law can only be tested in a finite number of cases. A crucial point in a HV model is that the set of all experimentally accessible probability distributions $p_{\exp}(\lambda)$ might not coincide with the set of all possible distributions $p(\lambda)$. We will discuss this issue in Sec. III D.

It should be noted that the conditions (i) and (ii) are not minimal, cf. Appendix A for a discussion. In particular, we emphasize that (ii) does not necessarily follow from (i), as we illustrate by the following example: Consider a HV model where, for any λ, all $v(A_k|S)$ are $+1$ when the first measurement in S is A_1, while they are -1 when the first measurement is B_1. The values $v(B_m|S)$ are always $+1$. Then, condition (i) is fulfilled, while (ii) is violated, since $\langle A\rangle = 1$ but $\langle A_2|B_1A_2\rangle = -1$.

Let us compare our definition of compatibility to the notion of "equivalent measurements" introduced by Spekkens in Ref. [38]. In this reference, two measurements are called equivalent if, for any state preparation, the probability distributions of the measurement outcomes for both measurements are the same. This is similar to our condition (ii), but disregards repeated measurements on individual systems as in (i). Interestingly, using this notion and POVMs, one can prove the contextuality of a quantum-mechanical two-level system [38].

Finally, it should be added that the notion of compatibility is extended in a straightforward manner to three or more observables. For instance, if three observables A, B, C are investigated, one considers the set $\mathcal{S}_{ABC}$ of all measurement sequences involving measurements of A, B, or C and extends the conditions (i) and (ii) in an obvious way. This is equivalent to requiring the pairwise compatibility of A, B, C, cf. Appendix A.

D. Definition of noncontextuality for sequential measurements

Noncontextuality means that the value of any observable A does not depend on which other compatible observables are measured jointly with A. For our models, we formulate noncontextuality as a condition on a HV model as follows:

Definition 2.—Let A and B be observables in a HV model, where A is compatible with B. We say that the HV model is noncontextual if it assigns, for any λ, an outcome of A which is independent of whether B is measured before or after A, that is,

$$v(A_1) = v(A_2|B_1A_2). \tag{3}$$

Hence, for these sequences we can write down $v(A)$ as being independent of the sequence. If the condition is not fulfilled, we call the model contextual.

It is important to note that the condition (3) is an assumption about the model and — contrary to the definition of compatibility — not experimentally testable. This is due to the fact that for a given instance of a state (corresponding to some unknown λ) the experimenter has to decide whether to measure A or B first.

From this definition and the time ordering, it follows immediately that, if A is compatible with B and A is also compatible with C, then for noncontextual models

$$v(A_1|A_1B_2) = v(A_2|B_1A_2) = v(A_1|A_1C_2) = v(A_2|C_1A_2). \tag{4}$$

holds. This is the often used definition of noncontextual models, stating that the value of A does not depend on whether B or C is measured before, jointly with, or after it.

This definition can directly be extended to three or more compatible observables. For instance, if $\{A, B, C\}$ are compatible, then noncontextuality means that for any λ,

$$\begin{aligned} v(A_1) &= v(A_2|B_1A_2) = v(A_2|C_1A_2) \\ &= v(A_3|B_1B_2A_3) = v(A_3|B_1C_2A_3) \\ &= v(A_3|C_1B_2A_3) = v(A_3|C_1C_2A_3). \end{aligned} \tag{5}$$

Of course, the equalities in the second and third line follow, if the first line holds for any λ and the HV model allows to see the measurement of B_1 or C_1 as a preparation step. Again, if $\{A, a, \alpha\}$ is another set of compatible observables, one can derive consequences similar to Eq. (4).

E. Inequalities for noncontextual HV models

Here we will discuss several previously introduced inequalities involving compatible measurements, which hold for any noncontextual HV model, but which are violated for certain states and observables in QM. Later, these inequalities are extended to the case where the observables are not perfectly compatible.

1. CHSH-like inequality

To derive a first inequality, consider the mean value

$$\langle \chi_{\text{CHSH}} \rangle = \langle AB \rangle + \langle BC \rangle + \langle CD \rangle - \langle DA \rangle. \tag{6}$$

If the measurements in each average are compatible [i.e., the pairs (A, B), (B, C), (C, D), and (D, A) are compatible observables)], then a noncontextual HV model has to assign a fixed value to each measurement, and the model predicts

$$|\langle \chi_{\text{CHSH}} \rangle| \leq 2. \tag{7}$$

In QM, on a two-qubit system, one can take the observables

$$\begin{aligned} A &= \sigma_x \otimes \mathbb{1}, \qquad B = \mathbb{1} \otimes \frac{(\sigma_z + \sigma_x)}{\sqrt{2}}, \\ C &= \sigma_z \otimes \mathbb{1}, \qquad D = \mathbb{1} \otimes \frac{(\sigma_z - \sigma_x)}{\sqrt{2}}, \end{aligned} \tag{8}$$

then, the measurements in each sequence are commuting and hence compatible, but the state

$$|\phi^+\rangle = (|00\rangle + |11\rangle)/\sqrt{2} \tag{9}$$

leads to a value of $\langle \chi_{\text{CHSH}} \rangle = 2\sqrt{2}$, therefore not allowing any noncontextual description. The choice of the observables in Eq. (8) is, however, by no means unique, if one transforms all of them via the same global unitary transformation, another set is obtained, and the state leading to the maximal violation does not need to be entangled. In fact, the two-qubit notation is only chosen for convenience and could be replaced by a formulation with a single party using a four-level system. For example, if we take the observables

$$\begin{aligned} A &= \sigma_x \otimes \sigma_x, \qquad B = \frac{1}{\sqrt{2}} \begin{pmatrix} 1 & 1 & 0 & 0 \\ 1 & -1 & 0 & 0 \\ 0 & 0 & -1 & 1 \\ 0 & 0 & 1 & 1 \end{pmatrix}, \\ C &= \sigma_z \otimes \mathbb{1}, \qquad D = \frac{1}{\sqrt{2}} \begin{pmatrix} 1 & -1 & 0 & 0 \\ -1 & -1 & 0 & 0 \\ 0 & 0 & -1 & -1 \\ 0 & 0 & -1 & 1 \end{pmatrix}, \end{aligned} \tag{10}$$

then, the measurements in each sequence are commuting and hence compatible, but the product state

$$|\Psi\rangle = |x^+\rangle|0\rangle = (|00\rangle + |10\rangle)/\sqrt{2} \tag{11}$$

leads to a value of $\langle \chi_{\text{CHSH}} \rangle = 2\sqrt{2}$, therefore not allowing any noncontextual description.

2. The KCBS inequality

As a second inequality, we take the pentagram inequality introduced by Klyachko, Can, Binicioğlu, and Shumovsky (KCBS) [41]. Here, one takes five dichotomic

observables and considers

$$\langle \chi_{\mathrm{KCBS}} \rangle = \langle AB \rangle + \langle BC \rangle + \langle CD \rangle + \langle DE \rangle + \langle EA \rangle. \quad (12)$$

If the observables in each mean value are compatible and noncontextuality is assumed, it can be seen that

$$\langle \chi_{\mathrm{KCBS}} \rangle \geq -3 \quad (13)$$

holds. However, using appropriate measurements on a three-level system, there are qutrit states which give a value of $\langle \chi_{\mathrm{KCBS}} \rangle = 5 - 4\sqrt{5} \approx -3.94$, also leading to contradiction with noncontextuality.

3. An inequality from the Mermin-Peres square

For the third inequality, we take the one introduced in Ref. [42]. Consider the mean value

$$\begin{aligned} \langle \chi_{\mathrm{KS}} \rangle =& \langle ABC \rangle + \langle abc \rangle + \langle \alpha\beta\gamma \rangle + \langle Aa\alpha \rangle + \langle Bb\beta \rangle \\ & - \langle Cc\gamma \rangle. \end{aligned} \quad (14)$$

If the measurements in each expectation value are compatible, then any noncontextual HV model has to assign fixed values to each of the nine occurring measurements. Then, one can see that

$$\langle \chi_{\mathrm{KS}} \rangle \leq 4. \quad (15)$$

However, on a two-qubit system, one can choose the observables of the Mermin-Peres square [52, 53]

$$\begin{array}{lll} A = \sigma_z \otimes \mathbb{1}, & B = \mathbb{1} \otimes \sigma_z, & C = \sigma_z \otimes \sigma_z, \\ a = \mathbb{1} \otimes \sigma_x, & b = \sigma_x \otimes \mathbb{1}, & c = \sigma_x \otimes \sigma_x, \\ \alpha = \sigma_z \otimes \sigma_x, & \beta = \sigma_x \otimes \sigma_z, & \gamma = \sigma_y \otimes \sigma_y. \end{array} \quad (16)$$

The observables in any row or column commute and are therefore compatible. Moreover, the product of the observables in any row or column equals $\mathbb{1}$, apart from the last column, where it equals $-\mathbb{1}$. Hence, for any quantum state,

$$\langle \chi_{\mathrm{KS}} \rangle = 6 \quad (17)$$

holds. The remarkable fact in this result is that it shows that any quantum state reveals nonclassical properties if the measurements are chosen appropriately.

III. NOT PERFECTLY COMPATIBLE MEASUREMENTS

In any real experiment, the measurements will not be perfectly compatible. Hence, the notion of noncontextuality does not directly apply. The experimental violation of inequalities like (7), (13), and (15) proves that one cannot assign to the measurement devices independent outcomes ± 1. However, a model that is not trivially in conflict with QM also has to explain the measurement results of sequences of incompatible observables, such as e.g. the results from measuring A_1C_2 for the observables of the CHSH-like inequality. Therefore, it is not straightforward to find out which are the implications of these violations on the structure of the possible HV models. The reason is that the assumption that incompatible measurements have predetermined independent outcomes is not physically plausible.

To deal with this problem, we will derive extended versions of the inequalities (7), (13), and (15), which are valid even in the case of imperfect compatibility. We will first derive an inequality which is an extension of inequality (7) and which holds for any HV model. This inequality, however, contains terms which are not experimentally accessible. Then, we investigate how these terms can be connected to experimental quantities, if certain assumptions about the HV model are made. We will present three types of testable inequalities, the first two start from condition (i) of Definition 1, while the third one uses condition (ii).

First we consider nearly compatible observables. We show that, if the observables fulfill the condition (i) of Definition 1 to some extent and if assumptions about the dynamics of probabilities in a HV model are made, then these HV models can be experimentally refuted.

In the second approach, we consider the case that a certain finite number of compatibility tests has been made. For some runs of the experiment the tests are successful [i.e., no error occurs when checking condition (i)], and in some runs errors occur. We then assume that the subset of HVs, where noncontextuality holds is at least as large as the subset where the compatibility tests are successful. We then show that HV models of this type can, in principle, be refuted experimentally.

Finally, in the third approach, we also consider assumptions about the possible distributions $p_{\mathrm{exp}}(\lambda)$, and show that if the condition (ii) of Definition 1 is nearly fulfilled, then again this type of HV models can experimentally be ruled out.

We will discuss these approaches using the CHSH-like inequality (7). At the end of the section, we will also explain how the inequalities (13) and (15) have to be modified, in order to test these different types of HV models.

A. CHSH-like inequality for all HV models

To start, consider a HV model with a probability distribution $p(\lambda)$ and let $p[(A_1^+|A_1)$ and $(B_1^+|B_1)]$ denote the probability of finding A^+ if A is measured first and B^+ if B is measured first. This probability is well defined in all HV models of the considered type, but it is impossible to measure it directly, as one has to decide whether one measures A or B first. Our aim is now to connect it to probabilities arising in sequential measurements, as this will allow us to find contradictions between HV models and QM.

First, note that

$$p[(A_1^+|A_1) \text{ and } (B_1^+|B_1)] \leq p[A_1^+, B_2^+|A_1B_2] + \\ + p[(B_1^+|B_1) \text{ and } (B_2^-|A_1B_2)]. \quad (18)$$

This inequality is valid because if λ is such that it contributes to $p[(A_1^+|A_1) \text{ and } (B_1^+|B_1)]$, then either the value of B stays the same when measuring A_1B_2 (hence λ contributes to $p[A_1^+, B_2^+|A_1B_2]$) or the value of B is flipped and λ contributes to $p[(B_1^+|B_1) \text{ and } (B_2^-|A_1B_2)]$. The first term $p[A_1^+, B_2^+|A_1B_2]$ is directly measurable as a sequence, but the second term is not experimentally accessible.

Let us rewrite

$$\langle AB\rangle = 1 - 2p[(A_1^+|A_1) \text{ and } (B_1^-|B_1)] \\ -2p[(A_1^-|A_1) \text{ and } (B_1^+|B_1)], \quad (19)$$

as the mean value obtained from the probabilities $p[(A_1^\pm|A_1) \text{ and } (B_1^\pm|B_1)]$. Then, using Eq. (18), it follows that

$$\langle A_1B_2\rangle - 2p^{\text{flip}}[AB] \leq \langle AB\rangle \leq \langle A_1B_2\rangle + 2p^{\text{flip}}[AB], \quad (20)$$

where we used $p^{\text{flip}}[AB] = p[(B_1^+|B_1) \text{ and } (B_2^-|A_1B_2)] + p[(B_1^-|B_1) \text{ and } (B_2^+|A_1B_2)]$. This $p^{\text{flip}}[AB]$ can be interpreted as a probability that A flips a predetermined value of B.

Furthermore, using Eqs. (6) and (7), we obtain

$$|\langle \mathcal{X}_{\text{CHSH}}\rangle| \leq 2(1 + p^{\text{flip}}[AB] + p^{\text{flip}}[CB] \\ + p^{\text{flip}}[CD] + p^{\text{flip}}[AD]), \quad (21)$$

where

$$\langle \mathcal{X}_{\text{CHSH}}\rangle := \langle A_1B_2\rangle + \langle C_1B_2\rangle + \langle C_1D_2\rangle - \langle A_1D_2\rangle. \quad (22)$$

Inequality (21) holds for any HV model and is the generalization of inequality (7). Note that for perfectly compatible observables, the flip terms in inequality (21) vanish if the assumption of noncontextuality is made. Then, this results in inequality (7).

B. First approach: Constraints on the disturbance and the dynamics of the HV

The terms $p^{\text{flip}}[AB]$, etc. in inequality (21) are not experimentally accessible. Now we will discuss how they can be experimentally estimated when some assumptions on the HV model are made.

In order to obtain an experimentally testable version of inequality (21), we will assume that

$$p[(B_1^+|B_1) \text{ and } (B_2^-|A_1B_2)] \\ \leq p[(B_1^+|B_1) \text{ and } (B_1^+, B_3^-|B_1A_2B_3)] \\ \equiv p[B_1^+, B_3^-|B_1A_2B_3]. \quad (23)$$

This assumption is motivated by the experimental procedure: Let us assume that one has a physical state, for which one surely finds B_1^+ if B_1 is measured first, but finds B_2^- if the sequence A_1B_2 is measured. Physically, one would explain this behavior as a disturbance of the system due to the experimental procedures when measuring A_1. The left-hand side of Eq. (23) can be viewed as the amount of this disturbance. The right-hand side quantifies the disturbance of B when the sequence $B_1A_2B_3$ is measured. In real experiments, it can be expected that this disturbance is larger than when measuring A_1B_2, because of the additional experimental procedures involved. Note that in real experiments, a measurement of B will also disturb the value of B itself, as can be seen from the fact that sometimes the values of B_1 and B_2 will not coincide, if the sequence B_1B_2 is measured.

It should be stressed, however, that we do not assume that the set of HV values giving $[(B_1^+|B_1) \text{ and } (B_2^-|A_1B_2)]$ is contained in the set giving $(B_1^+, B_3^-|B_1A_2B_3)$, the assumption only relates the sizes of these two sets.

In addition, by a similar reasoning, the assumption (23) may be relaxed to

$$p[(B_1^+|B_1) \text{ and } (B_2^-|A_1B_2)] \leq p[B_1^+, B_k^-|B_1SA_{k-1}B_k], \quad (24)$$

where S is a given finite sequence of measurements from $\mathcal{S}_{AB}$. Again, if the measurements are nearly compatible, this type of HV models can be ruled out experimentally.

Assumption (23) gives an measurable upper bound to $p^{\text{flip}}[AB]$. One directly has

$$|\langle \mathcal{X}_{\text{CHSH}}\rangle| \leq 2(1 + p^{\text{err}}[B_1A_2B_3] + p^{\text{err}}[B_1C_2B_3] \\ + p^{\text{err}}[D_1C_2D_3] + p^{\text{err}}[D_1A_2D_3]), \quad (25)$$

where we used

$$p^{\text{err}}[B_1A_2B_3] = p[B_1^+, B_3^-|B_1A_2B_3] + p[B_1^-, B_3^+|B_1A_2B_3], \quad (26)$$

denoting the total disturbance probability of B when measuring $B_1A_2B_3$.

The point of this inequality is that if the observable pairs (A, B), (C, B), (C, D), and (A, D) fulfill approximately the condition (i) in the definition of compatibility, the terms p^{err} will become small, and a violation of inequality (25) can be observed. In Ref. [44] it was found that $\langle \mathcal{X}_{\text{CHSH}}\rangle - 2(p^{\text{err}}[B_1A_2B_3] + p^{\text{err}}[B_1C_2B_3] + p^{\text{err}}[D_1C_2D_3] + p^{\text{err}}[D_1A_2D_3]) = 2.23(5)$. Hence this experiment cannot be described by HV models which fulfill Eq. (23), see also Section IV.

C. Second approach: Assuming noncontextuality for the set of HVs where the observables are compatible

Let us discuss a different approach to obtain experimentally testable inequalities. For that, consider the

case that the experimenter has measured a (finite) set of sequences in $\mathcal{S}_{AB}$ in order to test the validity of condition (i) in the definition of compatibility. He finds that the conditions are violated or fulfilled with certain probabilities. In terms of the HV model, there is a certain subset $\Lambda_{AB} \subset \Lambda$ of all HVs where *all* tests in the finite set of experimentally performed compatibility tests succeed and through the observed probabilities the experimenter can estimate the volume of this set.

In this situation, one can assume that, for each HV $\lambda \in \Lambda_{AB}$ (where all the measured compatibility requirements are fulfilled), the assumption of noncontextuality is also valid. More precisely, one can assume that $v(A_1|A_1B_2) = v(A_2|B_1A_2)$ in Eq. (3) holds for all $\lambda \in \Lambda_{AB}$. One may support this assumption if one considers noncontextuality as a general property of nature, since this is the usual noncontextuality assumption for the HV model where the HVs are restricted to Λ_{AB}.

To see that this assumption leads to an experimentally testable inequality, consider the case where the experimenter has tested all sequences up to length three, that is all sequences from $\mathcal{S}_{AB}^{(3)} = \{A_1A_2A_3, A_1A_2B_3, \ldots, B_1B_2B_3\}$ and has determined, for each of them, the probability $p^{\text{err}}(S)$ that some measurement, which is performed two or three times in the sequence is disturbed. For sequences like $B_1A_2B_3$, this is exactly $p^{\text{err}}[B_1A_2B_3]$ defined in Eq. (26). However, now we have additional error terms like $p^{\text{err}}[B_1B_2A_3] = p[B_1^+, B_2^-|B_1B_2A_3] + p[B_1^-, B_2^+|B_1B_2A_3]$ and $p^{\text{err}}[B_1B_2B_3] = 1 - p[B_1^+, B_2^+B_3^+|B_1B_2B_3] - p[B_1^-, B_2^-B_3^-|B_1B_2B_3]$, etc. These probabilities are not completely independent: due to the time ordering, a λ that contributes to $p^{\text{err}}[B_1B_2A_3]$ (or $p^{\text{err}}[A_1A_2B_3]$) will also contribute to $p^{\text{err}}[B_1B_2B_3]$ (or $p^{\text{err}}[A_1A_2A_3]$). Consequently, relations like $p^{\text{err}}[B_1B_2A_3] \leq p^{\text{err}}[B_1B_2B_3]$ hold.

Let us define

$$p^{\text{err}}[\mathcal{S}_{AB}^{(3)}] = \Big(\sum_{S\in\mathcal{S}_{AB}^{(3)}} p^{\text{err}}[S]\Big) - p^{\text{err}}[B_1B_2A_3] - p^{\text{err}}[A_1A_2B_3]. \tag{27}$$

Here, we have excluded two p^{err} in the sum, as the λ's which contribute to them are already counted in other terms. With this definition, for a given distribution $p_{\text{exp}}(\lambda)$, a lower bound to the probability of finding a λ where condition (i) from Definition 1 is fulfilled, is

$$p[\Lambda_{AB}] \geq 1 - p^{\text{err}}[\mathcal{S}_{AB}^{(3)}]. \tag{28}$$

From that and the assumption that $v(A_1|A_1B_2) = v(A_2|B_1A_2)$ on Λ_{AB}, it directly follows that

$$p^{\text{flip}}[AB] \leq p^{\text{err}}(\mathcal{S}_{AB}^{(3)}), \tag{29}$$

giving a measurable upper bound to $p^{\text{flip}}[AB]$. Finally, the experimentally testable inequality

$$\begin{aligned}|\langle \mathcal{X}_{\text{CHSH}}\rangle| \leq 2(1 &+ p^{\text{err}}[\mathcal{S}_{AB}^{(3)}] + p^{\text{err}}[\mathcal{S}_{CB}^{(3)}] \\ &+ p^{\text{err}}[\mathcal{S}_{CD}^{(3)}] + p^{\text{err}}[\mathcal{S}_{AD}^{(3)}])\end{aligned} \tag{30}$$

holds. This inequality is similar to inequality (25), but it contains more error terms. Nevertheless, a violation of this inequality in ion-trap experiments might be feasible in the near future (see Sec. IV).

This result deserves two further comments. First, in the derivation we assumed a pointwise relation; namely, for all $\lambda \in \Lambda_{AB}$, the noncontextuality assumption $v(A_1|A_1B_2) = v(A_2|B_1A_2)$ holds. Of course, we could relax this assumption by assuming only that the volume of the set where $v(A_1|A_1B_2) = v(A_2|B_1A_2)$ holds is not smaller than the volume of Λ_{AB}. Under this condition, Eq. (30) still holds.

Second, when comparing the second approach with the first one, one finds that the first one is indeed a special case of the second one. In fact, from a mathematical point of view, the first approach is the same as the second one, if in the second approach only the compatibility test $S = B_1A_2B_3$ is performed. Consequently, inequality (25) is weaker than (30). However, note that the first approach came from a different physical motivation. Further, assuming a pointwise relation for the first approach is very assailable, as only one compatibility test is made. But, as we have seen, a relation between the volumes suffices. A pointwise relation can only be motivated if all experimentally feasible compatibility tests are performed.

D. Third approach: Certain probability distributions cannot be prepared

The physical motivation of the third approach is as follows: The experimenter can prepare different probability distributions $p_{\text{exp}}(\lambda)$ and check their properties. For instance, he can test to which extent the condition (ii) in Definition 1 is fulfilled. However, in a general HV model there might be probability distributions $p(\lambda)$ that do not belong to the set of experimentally accessible $p_{\text{exp}}(\lambda)$. One might be tempted to believe that this difference is negligible and that the properties that can be verified for the $p_{\text{exp}}(\lambda)$ hold also for some of the $p(\lambda)$. In this approach we will show that this belief can be experimentally falsified. More specifically, we show that if only four conditional probability distributions have the same properties as all $p_{\text{exp}}(\lambda)$, then a contradiction with QM occurs.

So let us assume that the experimenter has checked that the observables A and B fulfill condition (ii) in Definition 1 approximately. He has found that

$$|\langle B_1|B_1A_2\rangle - \langle B_2|A_1B_2\rangle| \leq \varepsilon_{AB} \tag{31}$$

for all possible (or, at least, a large number of) $p_{\text{exp}}(\lambda)$. This means that, for experimentally accessible distributions $p_{\text{exp}}(\lambda)$, one has that

$$\begin{aligned}|p(B_1^+|B_1A_2) - p(B_2^+|A_1B_2)| &\leq \varepsilon_{AB}/2, \\ |p(B_1^-|B_1A_2) - p(B_2^-|A_1B_2)| &\leq \varepsilon_{AB}/2,\end{aligned} \tag{32}$$

as can be seen by direct calculation.

Let us consider the flip probability $p^{\text{flip}}[AB] = p[(B_1^+|B_1) \text{ and } (B_2^-|A_1B_2)] + p[(B_1^-|B_1) \text{ and } (B_2^+|A_1B_2)]$ again. Here, the probability p stems from the initial probability distribution $p(\lambda)$. One can consider the conditional probability distributions $q^{\pm}(\lambda)$ which arise from $p(\lambda)$ if the result of B_1 is known. Physically, the conditional distributions describe the situation for an observer, who knows that the experimenter has prepared $p(\lambda)$ but has the additional information that measurement of B_1 will give $+1$ or -1. With that, we can rewrite

$$\begin{aligned} p^{\text{flip}}[AB] = q^+(B_2^-|A_1B_2)p(B_1^+|B_1) \\ + q^-(B_2^+|A_1B_2)p(B_1^-|B_1). \end{aligned} \tag{33}$$

Now let us assume that these conditional probability distributions have the same properties as all accessible distributions $p_{\text{exp}}(\lambda)$. Then, the bounds in Eq. (32) also have to hold for $q^{\pm}$. Since $p(B_1^+|B_1) + p(B_1^-|B_1) = 1$, it follows directly that $p^{\text{flip}}[AB] \leq \varepsilon_{AB}/2$. Hence, under the assumption that some conditional probability distributions in the HV model have similar properties as the preparable $p_{\text{exp}}(\lambda)$, the inequality

$$\langle \mathcal{X}_{\text{CHSH}} \rangle \leq 2 + \varepsilon_{AB} + \varepsilon_{CB} + \varepsilon_{CD} + \varepsilon_{AD} \tag{34}$$

holds. A violation of it implies that, in a possible HV model, certain conditional probability distributions have to be fundamentally different from experimentally preparable distributions.

Again, this result deserves some comments. First, note that the tested bound in Eq. (32) does not have to hold for all probability distributions in the theory. In an experiment testing Eq. (34) with some $\hat{p}_{\text{exp}}(\lambda)$ only assumptions about four conditional probability distributions (corresponding to two possible second measurements with two outcomes) have to be made. In fact, assuming Eq. (32) for δ-distributions (i.e., a fixed HV λ) is not very physical, as in this case the left-hand side of these equations is 0 or 1.

Second, finding an experimental violation of Eq. (34) shows that these four distributions have properties significantly different from all preparable $p_{\text{exp}}(\lambda)$. In other words, one may conclude that in a possible HV model describing such an experiment, it must be forbidden to prepare $\hat{p}_{\text{exp}}(\lambda)$ with additional information about the result of B or D.

To make this last point more clear, consider the situation where the experimenter has prepared $\hat{p}_{\text{exp}}(\lambda)$ and a second physicist has the additional knowledge that the result of B_1 will be $+1$, if it would be measured as a first instance. Both physicists disagree on the probability distribution $\hat{p}_{\text{exp}}$ and q^+, but that is not the central problem because this occurs in any classical model as well. The point is that q^+ cannot be prepared: If the experimenter measures B_1 and keeps only the cases where he finds $+1$ he obtains a new experimentally accessible probability distribution $\tilde{p}_{\text{exp}}$. But this will not be the same as the probability distribution q^+, because in this case, the first measurement has already been made.

E. Application to the KCBS inequality and the KS inequality (15)

In the previous discussion, we used the CHSH like inequality (7) to develop our ideas. Clearly, one could also start from inequalities (13) and (15) to obtain testable inequalities for the types of HV models discussed above.

For the KCBS inequality (12) this can be done with the same methods as before, since the KCBS inequality uses only sequences of two measurements, as the CHSH inequality (7). A generalization of Eq. (34) is

$$\begin{aligned} \langle \mathcal{X}_{\text{KCBS}} \rangle := \langle A_1B_2 \rangle + \langle C_1B_2 \rangle + \langle C_1D_2 \rangle + \langle E_1D_2 \rangle \\ + \langle E_1A_2 \rangle \geq -3 - (\varepsilon_{AB} + \varepsilon_{CB} + \varepsilon_{CD} + \varepsilon_{ED} + \varepsilon_{EA}). \end{aligned} \tag{35}$$

Generalizations of Eqs. (25) and (30) can also be written down in a similar manner.

Also for the KS inequality (15), one can deduce generalizations, which exclude certain types of HV models. The main problem here is to estimate a term like $\langle A_1B_2C_3 \rangle$. First, an inequality corresponding to Eq. (18) is

$$\begin{aligned} p[(A_1^+|A_1) \text{ and } (B_1^+|B_1) \text{ and } (C_1^+|C_1)] \\ \leq\ p[A_1^+, B_2^+, C_3^+|A_1B_2C_3] + \\ + p[(B_1^+|B_1) \text{ and } (B_2^-|A_1B_2)] \\ + p[(C_1^+|C_1) \text{ and } (C_3^-|A_1B_2C_3)], \end{aligned} \tag{36}$$

which holds again for any HV model. Then, a direct calculation gives that one has

$$\begin{aligned} \langle ABC \rangle \leq \langle A_1B_2C_3 \rangle + 4p^{\text{flip}}[AB] + 4p^{\text{flip}}[(AB)C] \\ \langle ABC \rangle \geq \langle A_1B_2C_3 \rangle - 4p^{\text{flip}}[AB] - 4p^{\text{flip}}[(AB)C], \end{aligned} \tag{37}$$

where

$$\begin{aligned} p^{\text{flip}}[(AB)C] = p[(C_1^+|C_1) \text{ and } (C_3^-|A_1B_2C_3)] \\ + p[(C_1^-|C_1) \text{ and } (C_3^+|A_1B_2C_3)]. \end{aligned} \tag{38}$$

Given these bounds, one arrives at testable inequalities, provided assumptions on the HV model are made as in the three approaches above. If Eq. (23) is assumed, one can directly estimate $p^{\text{flip}}[AB] \leq p^{\text{err}}[A_1B_2]$ and

$$\begin{aligned} p^{\text{flip}}[(AB)C] \leq p^{\text{err}}[(AB)C] \\ = p[C_1^+C_4^-|C_1A_2B_3C_4] + p[C_1^-C_4^+|C_1A_2B_3C_4]. \end{aligned} \tag{39}$$

Then, if one writes down the generalized form of Eq. (15), then there are more correction terms than in Eq. (25). Moreover, they involve sequences of length four. On average, these p^{err} terms have to be smaller than $2/48 \approx 0.0417$ in order to allow a violation. Consequently, an experimental test is very demanding (see also the discussion in subsection IV C). Finally, generalizations in the sense of Eqs. (30 and 34) can also be derived in a similar manner.

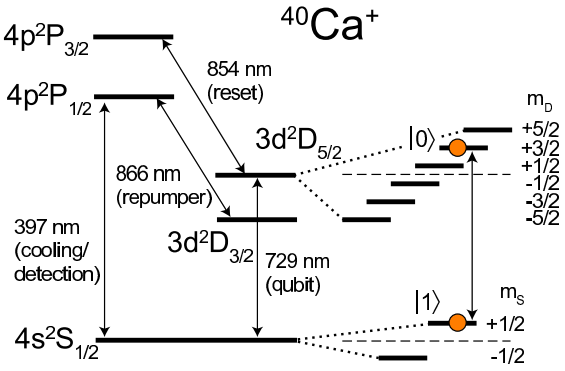

FIG. 1: Partial level scheme of $^{40}Ca^{+}$ showing the relevant energy levels and the laser wavelengths needed for coupling the states. The D-states are metastable with a lifetime of about 1s. A magnetic field of about 4 Gauss is applied to lift the degeneracy of the Zeeman states. The states $|0\rangle$, $|1\rangle$ used for encoding quantum information are indicated in the figure.

IV. EXPERIMENTAL IMPLEMENTATION

Experimental tests of noncontextual HV theories have been carried out with photons [35–37, 45, 46], neutrons [37, 45], laser-cooled trapped ions [44], and liquid-state nuclear magnetic resonance systems [48]. In the experiments with photons and neutrons, single particles were prepared and measured in a four-dimensional state space composed of two two-dimensional state spaces describing the particle's polarization and the path it was following. In contrast, in a recent experiment with trapped ions [44], a composite system comprised of two trapped ions prepared in superpositions of two long-lived internal states was used for testing the KS theorem. In the following, we will describe this experiment and present details about the amount of noncompatibility of the observables implemented.

A. Experimental methods

Trapped laser-cooled ions are advantageous for these kinds of measurements because of the highly efficient quantum state preparation and measurement procedures trapped ions offer. In Ref. [44], a pair of $^{40}Ca^{+}$ ions was prepared in a state space spanned by the states $|00\rangle$, $|01\rangle$, $|10\rangle$, $|00\rangle$, where $|1\rangle = |S_{1/2}, m_S = 1/2\rangle$ is encoded in a Zeeman ground state and $|0\rangle = |D_{5/2}, m_D = 3/2\rangle$ in a long-lived metastable state of the ion (see Fig. 1).

A key element for both preparation and measurement are laser-induced unitary operations that allow for arbitrary transformations on the four-dimensional state space. For this, the entangling operation $U^{MS}(\theta,\phi) = \exp(-i\frac{\theta}{2}\sigma_\phi \otimes \sigma_\phi)$ where $\sigma_\phi = \cos(\phi)\,\sigma_x + \sin(\phi)\,\sigma_y$ is realized by a bichromatic laser field off-resonantly coupling to transitions involving the ions' center-of-mass mode along the weakest axis of the trapping potential [54]. In addition, collective single-qubit gates $U(\theta,\phi) = \exp[-i\frac{\theta}{2}(\sigma_\phi \otimes \mathbb{1} + \mathbb{1} \otimes \sigma_\phi)]$ are realized by resonantly coupling the states $|0\rangle$, $|1\rangle$. Finally, the single-qubit gate $U_z(\theta) = \exp(-i\frac{\theta}{2}\sigma_z)$ is implemented by a strongly focused laser inducing a differential light-shift on the states of the first ion. This set of operations, $\mathcal{S} = \{U_z(\theta), U(\theta,\phi), U^{MS}(\theta,\phi)\}$, which is sufficient for constructing arbitrary unitary operations, can be used for preparing the desired input states $|\psi\rangle$.

A measurement of σ_z by a state projection onto the basis states $|0\rangle$, $|1\rangle$ on one of the ions is carried out by illuminating the ion with laser light coupling the $S_{1/2}$ ground state to the short-lived excited state $P_{1/2}$ and detecting the fluorescence emitted by the ion with a photomultiplier. Population in $P_{1/2}$ decays back to $S_{1/2}$ within a few nanoseconds so that thousands of photons are scattered within a millisecond if the ion was originally in the state $|1\rangle$. If it is in state $|0\rangle$, it does not couple to the light field and therefore scatters no photons. In the experiment, we assign the state $|1\rangle$ to the ion if more than one photon is registered during a photon collection period of 250μs. In this way, the observables $\sigma_z \otimes \mathbb{1}$ and $\mathbb{1} \otimes \sigma_z$ can be measured.

To measure further observables like $\sigma_i \otimes \mathbb{1}$, $\mathbb{1} \otimes \sigma_j$, or $\sigma_i \otimes \sigma_j$, the quantum state ρ to be measured is transformed into $U\rho U^\dagger$ by a suitable unitary transformation U prior to the state detection. Measuring the value of $\sigma_z \otimes \mathbb{1}$ on the transformed state is equivalent to measuring the observable $A = U^\dagger(\sigma_z \otimes \mathbb{1})U$ on the original state ρ. The measurement is completed by applying the inverse operation $U^\dagger$ after the fluorescence measurement. The purpose of this last step is to map the projected state onto an eigenstate of the observable A. In this way, any observable A with two pairs of degenerate eigenvalues can be measured. The complete measurement, consisting of unitary transformation, fluorescence detection and back transformation, constitutes a quantum nondemolition measurement of A. Each measurement of a quantum state yields one bit of information which carries no information about other compatible observables.

B. Measurement results

The measurement procedure outlined above is very flexible and can be used to consecutively measure several observables on a single quantum system as illustrated by the following example. To test inequality Eq. (14) for the observables of the Mermin-Peres square (16), the quantum state $|\psi\rangle = |11\rangle/\sqrt{2} + e^{i\frac{\pi}{4}}(|01\rangle + |10\rangle)/2$ is prepared by a applying the sequence of gates $U^{MS}(-\pi/2, \pi/4)U^{MS}(-\pi/2, 0)U(\pi/2, 0)$ to the initial state $|11\rangle$. The correlations that are found for a sequence of measurements $A_1B_2C_3$, where $A_1 = \sigma_z \otimes \sigma_z$, $B_2 = \sigma_x \otimes \sigma_x$, and $C_3 = \sigma_y \otimes \sigma_y$ are shown in Fig. 2. For this measurement, 1100 copies of the state were created and measured. Each corner of the sphere corresponds to a measurement outcome (v_1, v_2, v_3) where $v_k = \pm 1$ is the measurement result for the kth observable. The

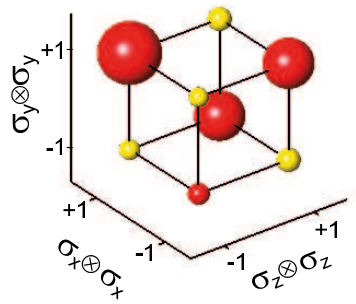

FIG. 2: Measurement correlations for a sequence of measurements $A_1B_2C_3$ with $A_1 = \sigma_z \otimes \sigma_z$, $B_2 = \sigma_x \otimes \sigma_x$, and $C_3 = \sigma_y \otimes \sigma_y$ for a partially entangled input state. The colors indicates whether $v_1v_2v_3 = +1$ (yellow spheres) or $v_1v_2v_3 = -1$ (red spheres). The volume of a sphere is proportional to the likelihood of finding the corresponding measurement outcome (v_1, v_2, v_3).

relative frequencies of the measurement outcomes are indicated by the volume of the spheres attached to the corners, and the colors indicates whether $v_1v_2v_3 = +1$ or $v_1v_2v_3 = -1$. For perfect state preparation and measurements, one would expect to observe always $v_1v_2v_3 = -1$. Due to experimental imperfections, the experiment yields $\langle v_1v_2v_3\rangle = -0.84(2)$. Nevertheless, the experimental results nicely illustrate the quantum measurement process: the first measurement gives $\langle\sigma_z \otimes \sigma_z\rangle = 0.00(2)$, i.e. the state $|\psi\rangle$ is equally likely to be projected onto $|\Psi_+\rangle = |11\rangle$ $(v_1 = +1)$ and onto $|\Psi_-\rangle = (|01\rangle + |10\rangle)/\sqrt{2}$ $(v_1 = -1)$. In the latter case, the projected state $|\Psi_-\rangle$ is an eigenstate of $\sigma_x \otimes \sigma_x$ and $\sigma_y \otimes \sigma_y$ so that these measurements give definite results $v_2 = +1$ and $v_3 = +1$ (upper left corner of Fig. 2). In the former case, the projected state is not an eigenstate of $\sigma_x \otimes \sigma_x$ and $v_2 = +1$ and $v_3 = -1$ are found with equal likelihood. In this case, v_2 and v_3 are random but correlated with $v_2v_3 = 1$ (the other two strongly populated corners of Fig. 2).

In Ref. [44], also the other rows and columns of the Mermin-Peres square (16) were measured for the state $|\psi\rangle$, and a violation of Eq. (14) was found with $\langle\chi_{\rm KS}\rangle = 5.36(4)$. Also different input states were investigated to check that the violation is indeed state-independent. The fact that the result falls short of the quantum mechanical prediction of $\langle\chi_{\rm KS}\rangle = 6$ is due to imperfections in the measurement procedure. These imperfections could be incorrect unitary transformations, but also errors occurring during the fluorescence measurement.

An instructive test consists in repeatedly measuring the same observable on a single quantum system and analyzing the measurement correlations. Table I shows the results of five consecutive measurements of $A = \sigma_z \otimes \mathbb{1}$ on a maximally mixed state based on 1100 experimental repetitions.

As expected, the correlations $\langle A_iA_{i+k}|A_1 \ldots A_5\rangle$ are independent of the measurement number i within the error bars. However, the correlations become smaller and smaller the bigger k gets. Table II shows another set of measurements correlations $\langle A_iA_j|A_1 \ldots A_5\rangle$, where $A = \sigma_x \otimes \sigma_x$. Here, the correlations are slightly smaller, since entangling interactions are needed for mapping A onto $\sigma_z \otimes \mathbb{1}$, which is experimentally the most demanding step.

TABLE I: Measurement correlations $\langle A_iA_j|A_1 \ldots A_5\rangle$ between repeated measurements of $A = \sigma_z \otimes \mathbb{1}$ for a maximally mixed state. Observing a correlation of $\langle A_iA_j|A_1 \ldots A_5\rangle = \alpha_{ij}$ means that the probability for the measurement results of A_i and A_j to coincide equals $(\alpha_{ij} + 1)/2$.

Measurement	2	3	4	5
1	0.97(1)	0.97(1)	0.96(1)	0.95(1)
2		0.97(1)	0.97(1)	0.96(1)
3			0.98(1)	0.98(1)
4				0.98(1)

TABLE II: Measurement correlations $\langle A_iA_j|A_1 \ldots A_5\rangle$ between repeated measurements of $A = \sigma_x \otimes \sigma_x$ for a maximally mixed state. Observing a correlation of $\langle A_iA_j|A_1 \ldots A_5\rangle = \alpha_{ij}$ means that the probability for the measurement results of A_i and A_j to coincide equals $(\alpha_{ij} + 1)/2$.

Measurement	2	3	4	5
1	0.94(1)	0.88(1)	0.82(2)	0.80(2)
2		0.93(1)	0.87(2)	0.84(2)
3			0.90(1)	0.87(2)
4				0.93(1)

It is also interesting to compare the correlations $\langle A_1A_3|A_1A_2A_3\rangle$ with the correlations $\langle A_1A_3|A_1B_2A_3\rangle$ for an observable B that is compatible with A. For $A = \sigma_x \otimes \sigma_x$ and $B = \sigma_z \otimes \sigma_z$, we find $\langle A_1A_3|A_1A_2A_3\rangle = 0.88(1)$ and $\langle A_1A_3|A_1B_2A_3\rangle = 0.83(2)$ when measuring a maximally mixed state; i.e., it seems that the intermediate measurement of B perturbs the correlations slightly more than an intermediate measurement of A. Similar results are found for a singlet state, where $\langle A_1A_3|A_1A_2A_3\rangle = 0.92(1)$, $\langle B_1B_3|B_1B_2B_3\rangle = 0.91(1)$, but $\langle A_1A_3|A_1B_2A_3\rangle = 0.90(1)$, and $\langle B_1B_3|B_1A_2B_3\rangle = 0.89(1)$. Because of $\langle B_1B_3|B_1A_2B_3\rangle = 1-2p^{\rm err}(B_1A_2B_3)$, correlations of the type $\langle B_1B_3|B_1A_2B_3\rangle$ are required for checking inequality (25) that takes into account disturbed HVs.

C. Experimental limitations

There are a number of error sources contributing to imperfect state correlations, the most important being:

(i) *Wrong state assignment based on fluorescence data.* During the 250 μs detection period of the current experiment, the number of detected photons has a Poissonian distribution with an average number of $\overline{n}_{|1\rangle} = 8$ photons

if the ion is in state $|1\rangle$. If the ion is in state $|0\rangle$, it does not scatter any light, however, light scattered from trap electrodes gives rise to a Poissonian distribution with an average number of $\overline{n}_{|0\rangle} = 0.08$ photons. These photon count distributions slightly overlap. The probability of detecting 0 or 1 photons even though the ion is in the bright state, is 0.3%. The probability of detecting more than one photon if the ion is in the dark state is also 0.3%. Therefore, if the threshold for discriminating between the dark and the bright state is set between 1 and 2, the probability for wrongly assigning the quantum state is 0.3%. Making the detection period longer would reduce this error but increase errors related to decoherence of the other ion's quantum state that is not measured.

(ii) *Imperfect optical pumping.* During fluorescence detection, the ion leaves the computational subspace $\{|0\rangle, |1\rangle\}$ if it was in state $|1\rangle$ and can also populate the state $|S_{1/2}, m_S = -1/2\rangle$. To prevent this leakage, the ion is briefly pumped on the $S_{1/2} \leftrightarrow P_{1/2}$ transition with σ_+-circularly polarized light to pump the population back to $|1\rangle$. Due to imperfectly set polarization and misalignment of the pumping beam with the quantization axis, this pumping step fails with a probability of about 0.5%.

(iii) *Interactions with the environment.* Due to the non-zero differential Zeeman shift of the states used for storing quantum information, superposition states dephase in the presence of slowly fluctuating magnetic fields. In particular, while measuring one ion by fluorescence detection, quantum information stored in the other ion dephases. We partially compensate for this effect by spin-echo-like techniques [55] that are based on a transient storage of superposition states in a pair of states having an opposite differential Zeeman shift as compared to the states $|0\rangle$ and $|1\rangle$. A second interaction to be taken into account is spontaneous decay of the metastable state $|0\rangle$ which however only contributes an error of smaller than 0.1%.

(iv) *Imperfect unitary operations.* The mapping operations are not error-free. This concerns in particular the entangling gate operations needed for mapping the eigenstate subspace of a spin correlation $\sigma_i \otimes \sigma_j$ onto the corresponding subspaces of $\sigma_z \otimes \mathbb{1}$. For this purpose, a Mølmer-Sørensen gate operation $U^{MS}(\pi/2, \phi)$ [54, 56] is used. This gate operation has the crucial property of requiring the ions only to be cooled into the Lamb-Dicke regime. In the experiments, the center-of-mass mode used for mediating the gate interaction is in a thermal state with an average of 18 vibrational quanta. In this regime, the gate operation is capable of mapping $|11\rangle$ onto a state $|00\rangle + e^{i\phi}|11\rangle$ with a fidelity of about 98%. Taking this fidelity as being indicative of the gate fidelity, one might expect errors of about 4% in each measurement of spin correlations $\sigma_i \otimes \sigma_j$ as the gate is carried out twice, once before and once after the fluorescence measurement.

These error sources prevented us from testing a generalization of inequality (15) as discussed in subsection III E. Measurement of the correlations $\langle B_1 B_3 | B_1 A_2 B_3 \rangle$ and $\langle C_1 C_4 | C_1 A_2 B_3 C_4 \rangle$ resulted in error terms p^{err} that were about 0.06 for sequences involving three measurements and about 0.1 for sequences with four measurements, i. e. twice as big as required for observing a violation of (15). However, the experimental errors were small enough to demonstrate a violation of the CHSH-like inequality (25), valid for nonperfectly compatible observables [44]. A test of the inequality (30) would become possible if the error rates could be further reduced.

V. CONTEXTUAL HV MODELS

In this section we will introduce two HV models which are contextual in the sense of Eq. (3) and violate the inequalities discussed in Sec. II. We first discuss a simple model which violates inequality (25), and then a more complex one, which reproduces all measurement results for a (finite-dimensional) quantum mechanical system. These models are useful to point out which counterintuitive properties a HV model must have to reproduce the quantum predictions, and which further experiments can rule out even these models.

A. A simple HV model leading to a violation of inequality (25)

We will show here that violation of inequality (25) can be achieved simply by allowing the HV model to remember what measurements have been performed and what the outcome was. The basic idea of the model is very simple (cf. the more complicated presentation in [49]).

The task is to construct a simple HV model for our four dichotomic observables A, B, C, and D. The HV λ is taken to be a quadruple with entries taken from the set $\{+, -, \oplus, \ominus\}$, the latter two cases will be called "locked" in what follows, signifying that the value is unchanged whenever a compatible measurement is made. For convenience, we can write $\lambda = (A^+, B^+, C^+, D^+)$ or $\lambda = (A^+, B^-, C^\oplus, D^\ominus)$, etc, and we take the initial distribution to be probability 1/2 of either (A^+, B^+, C^+, D^+) or (A^-, B^-, C^-, D^-). The measurement of an observable is simply reporting the appropriate sign, and locking the value in the position. To make the model contextual, we add the following mechanism:

(a) If A is measured, then the sign of D is reversed and locked unless it is locked.

(b) If D is measured, then the sign of A is reversed and locked unless it is locked.

For the case $\lambda = (A^+, B^+, C^+, D^+)$, the measurement results when measuring inequality (25) will be as follows.

(i) Measurement of A_1 will yield A_1^+ and $\lambda = (A^\oplus, B^+, C^+, D^\ominus)$, and for the next measurement one obtains B_2^+ or D_2^-.

(ii) Measurement of B_1 will yield B_1^+ and $\lambda = (A^+, B^\oplus, C^+, D^+)$, and further one obtains $A_2^+ B_3^+$ or $C_2^+ B_3^+$.

(iii) Measurement of C_1 will yield C_1^+ and $\lambda = (A^+, B^+, C^\oplus, D^+)$, and we'll obtain B_2^+ or D_2^+ afterwards.

(iv) Measurement of D_1 will yield D_1^+ and $\lambda = (A^\ominus, B^+, C^+, D^\oplus)$, and we'll obtain $C_2^+ D_3^+$ or $A_2^- D_3^+$. The last is because a measurement of A_2 will not change $D^\oplus$ since it is locked. In this case, after a measurement of A_2 the HVs are $\lambda = (A^\ominus, B^+, C^+, D^\oplus)$.

The case $\lambda = (A^-, B^-, C^-, D^-)$ is the same with reversed signs. This means that

$$\langle A_1 B_2 \rangle = \langle C_1 B_2 \rangle = \langle C_1 D_2 \rangle = -\langle A_1 D_2 \rangle = 1, \tag{40}$$

and

$$\begin{aligned} p^{\mathrm{err}}[B_1 A_2 B_3] = p^{\mathrm{err}}[B_1 C_2 B_3] = p^{\mathrm{err}}[D_1 C_2 D_3] \\ = p^{\mathrm{err}}[D_1 A_2 D_3] = 0. \end{aligned} \tag{41}$$

Hence, this model leads to the maximal violation of Eq. (25).

In this model, the observables A and D are compatible in the sense of Definition 1, but they maximally violate the noncontextuality condition in Eq. (3). It is easy to verify that $p^{\mathrm{flip}}[AD] = 1$, so that the assumption (23) does not hold. We argue that in this model, the change in the outcome D cannot be explained as merely due to a disturbance of the system from the experimental procedures when measuring A_1. It should therefore be no surprise that the inequality (25) is violated by the model. Finally, note that a model behavior like this would create problems in any argument to establish noncontextuality via repeatability of compatible measurements, even for joint measurements as discussed in Section IIA, and not only in the sequential setting used here.

B. A HV model explaining all quantum mechanical predictions

Let us now introduce a detailed HV model which reproduces all the quantum predictions for sequences of measurements. In a nutshell, this contextual HV model is a translation of a machine that classically simulates a quantum system.

We consider the case that only dichotomic measurements are performed on the quantum mechanical system. Therefore, any observable A decomposes into $A = \Pi_+^A - \Pi_-^A$ with orthogonal projectors Π_+ and Π_-. For a mixed state ϱ, a measurement of this observable produces the result $+1$ with probability $p(A^+) = \mathrm{tr}(\Pi_+^A \rho)$, and the result -1 with probability $p(A^-) = \mathrm{tr}(\Pi_-^A \rho)$. In addition, the measurement apparatus will modify the quantum state according to

$$\varrho \mapsto \frac{\Pi_\pm^A \varrho \Pi_\pm^A}{\mathrm{tr}(\Pi_\pm^A \varrho)}, \tag{42}$$

depending on the measurement result ± 1.

This behavior can exactly be mimicked by a HV model, if we allow the value of the HV to be modified by the action of the measurement. If $\mathcal{H}$ is the Hilbert space of the quantum system, we use two types of HVs. First, we use parameters $0 \leq \lambda^A < 1$, $0 \leq \lambda^B < 1$, etc. for each observable A, B, etc. and second we use a normalized vector $|\psi\rangle \in \mathcal{H}$.

Then, for given values of all these parameters, we associate to any observable the measurement result as follows: We define $q^A = \langle \psi | \Pi_-^A | \psi \rangle$ and let the model predict the measurement result: -1 if $\lambda^A < q^A$, and $+1$ if $q^A \leq \lambda^A$. Furthermore, depending on the measurement result, the values of the HVs λ^A and $|\psi\rangle$ change according to

$$\lambda^A \mapsto \begin{cases} \dfrac{\lambda^A}{q^A} & \text{if } \lambda^A < q^A, \\ \dfrac{\lambda^A - q^A}{1 - q^A} & \text{if } \lambda^A \geq q^A, \end{cases} \tag{43}$$

and

$$|\psi\rangle \mapsto \begin{cases} \dfrac{\Pi_-^A |\psi\rangle}{\sqrt{q^A}} & \text{if } \lambda^A < q^A, \\ \dfrac{\Pi_+^A |\psi\rangle}{\sqrt{1 - q^A}} & \text{if } \lambda^A \geq q^A. \end{cases} \tag{44}$$

Let us now fix the initial probability distribution of the HVs. The experimentally accessible probability distributions $p(\lambda^A, \lambda^B, \ldots; \psi)$ shall not depend on the parameters λ^A, $\lambda^B, \ldots$, that is, $p(\lambda^A, \lambda^B, \ldots; \psi) = p(\lambda'^A, \lambda'^B, \ldots; \psi)$. Hence we write $p(\psi) = \int d\lambda^A d\lambda^B \cdots p(\lambda^A, \ldots; \psi)$. The probability distribution $p(\psi)$ and the measure $d\psi$ are chosen such that

$$\varrho_p = \int d\psi \; p(\psi) |\psi\rangle\langle\psi| \tag{45}$$

is the corresponding quantum state.

We now verify that this model indeed reproduces the quantum predictions. If the initial distribution is p, then the probability to obtain the result -1 for A is given by

$$\begin{aligned} p_-^A &= \int_{\lambda^A < q^A} d\lambda^A d\psi \; p(\psi) = \int d\psi \; \langle \psi | \Pi_-^A | \psi \rangle \, p(\psi) \\ &= \mathrm{tr}(\rho_p \Pi_-^A), \end{aligned} \tag{46}$$

and hence is in agreement with the quantum prediction. Due to the transformations in Eq. (43) and Eq. (44), the probability distribution changes by the action of the measurement, $p \mapsto p'$. The new distribution p' again

does not depend on λ^A and, in case of the measurement result -1, we have

$$p'(\psi) = \frac{1}{p_-^A} \int d\psi' {q'}^A \, \delta \left(|\psi\rangle - \frac{\Pi_-^A |\psi'\rangle}{\sqrt{{q'}^A}} \right) p(\psi'), \quad (47)$$

where δ denotes Dirac's δ-distribution and ${q'}^A = \langle\psi'|\Pi_-^A|\psi'\rangle$. The new corresponding mixed state is given by

$$\begin{aligned} \varrho_{p'} &= \int d\psi \; p'(\psi) |\psi\rangle\langle\psi| \\ &= \frac{1}{p_-^A} \int d\psi' \; p(\psi') \Pi_-^A |\psi'\rangle\langle\psi'| \Pi_-^A \\ &= \frac{\Pi_-^A \varrho_p \Pi_-^A}{\mathrm{tr}(\varrho_p \Pi_-^A)}. \end{aligned} \quad (48)$$

This demonstrates that the transformation in Eq. (42) is suitably reproduced by $\varrho_p \mapsto \varrho_{p'}$. An analogous calculation can be performed for the measurement result $+1$.

Let us illustrate that this model is actually contextual, as defined in Eq. (3). As an example, we choose two commuting observables $A = \Pi_+^A - \Pi_-^A$ and $B = \Pi_+^B - \Pi_-^B$ with the property that, for some pure state $|\psi\rangle$, we have $\langle\psi|A_1 B_2|\psi\rangle = +1$, while $\langle\psi|B|\psi\rangle < 1$. An example would be $A = \sigma_z \otimes \mathbb{1}$ and $B = -\mathbb{1} \otimes \sigma_z$ with $|\psi\rangle$ being the singlet state. Then, after a measurement of A_1, the result of a subsequent measurement of B_2 is fixed and hence independent of λ^B. However, if B is measured without a preceding measurement of A, then the result of B will be -1 if $\lambda^B < \langle\psi|\Pi_-^B|\psi\rangle$, and $+1$ else. Hence, in our particular model, given the preparation of $|\psi\rangle$, $v(B_1)$ depends on λ^B, while $v(B_2|A_1 B_2)$ only depends on λ^A. However, the model does not allow special correlations between λ^A and λ^B and hence the model is contextual, i.e., necessarily there are experimentally accessible values of the HVs, such that Eq. (3) is violated.

VI. CONCLUSIONS

Experimental quantum contextuality is a potential source of new applications in quantum information processing, and a chance to expand our knowledge on the reasons why quantum resources outperform classical ones. In some sense, experimental quantum contextuality is an old discipline, since most Bell experiments are just experiments ruling out noncontextual HV models, since they do not fulfill the required spacelike separation needed to invoke locality as a physical motivation behind the assumption of noncontextuality. The possibility of observing state-independent quantum contextuality, however, is a recent development. It shows that the power of QM is not necessarily in some particular states, but also in some sets of measurements which can reveal nonclassical behavior of any quantum state.

These experiments must satisfy some requirements which are not explicitly needed for tests of Bell inequalities. An important requirement is that one has to test experimentally, to which extent the implemented measurements are indeed compatible. In this paper, we have discussed how to deal with the inevitable errors, preventing us from implementing perfectly compatible measurements. The problem of not-perfectly compatible observables is not fatal, but should be taken into account with care.

We have presented three approaches how additional requirements can be used to exclude the possibility of noncontextual explanations of the experimental results, and we have applied them to three specific inequalities of particular interest: a CHSH-like noncontextuality inequality using sequential measurements on individual systems, which can be violated by specific states of four or more levels, a KCBS noncontextuality inequality using sequential measurements on individual systems, which can be violated by specific states of three or more levels, and a KS inequality coming from the Mermin-Peres square which is violated by any state of a four-level system. Similar methods can be applied to any noncontextuality inequality, irrespective of the number of sequential measurements or the dimensionality of the Hilbert space.

The main motivation was to provide experimentalists with inequalities to rule out noncontextual HV models unambiguously, if some additional assumptions are made. We have shown that a recent experiment with trapped ions already ruled out some of these HV models. By providing examples of HV models, we have seen that these extra assumptions are not necessarily satisfied by very artificial HV models. Nevertheless they lead to natural extensions of the assumption of noncontextuality, and allow us to reach conclusions about HV models in realistic experiments with nonperfect devices. An interesting line of future research will be to investigate how these extra assumptions can be replaced by fundamental physical principles such as locality in experiments where the system under observation is entangled with a distant system on which additional measurements can be performed.

Acknowledgments

The authors thank R. Blatt, J. Emerson, B.R. La Cour, O. Moussa, and R.W. Spekkens for discussions and acknowledge support by the Austrian Science Fund (FWF), the European Commission (SCALA, OLAQUI and QICS networks and the Marie-Curie program), the Institut für Quanteninformation GmbH, the Spanish MCI Project No. FIS2008-05596, and the Junta de Andalucía Excellence Project No. P06-FQM-02243. A.C. and J.-Å. L. thank the IQOQI for its hospitality. This material is based upon work supported in part by IARPA.

Appendix

In Sec. II C we discussed the notion of compatibility for subsequent measurements. In this Appendix we provide two examples which demonstrate that both parts of Definition 1 are independent. We then show that the statement of compatibility can be simplified to involve sequences of length 2 only.

a. Mutual independence of Definition 1 (i) and Definition 1 (ii). For an example that (i) does not include (ii), assume that the expectation value of A depends on whether the first measurement in the sequence is A or B. Then $\langle A_1|A_1B_2\rangle \neq \langle A_2|B_1A_2\rangle$ and hence condition (ii) is violated. However, such a model is not in conflict with condition (i), if once A was measured, the value of A stays unchanged for the rest of the sequence.

For the converse, assume a HV model where the expected value $\langle A\rangle$ does not depend on the results of any previous measurement. Then, for any sequence and any k, $\langle A\rangle = \langle A_k|S\rangle$ and, hence, condition (ii) is satisfied. However, $p(A_1^+A_2^-|A_2A_2) > 0$, unless $\langle A_1A_2\rangle = 1$, and thus condition (i) is violated.

b. Compatibility for sequences of length 2. Assume that, for any preparation procedure, A and B obey

$$\langle A_1\rangle = \langle A_2|A_1A_2\rangle = \langle A_2|B_1A_2\rangle, \tag{49}$$

i.e., condition (ii) of Definition 1 is satisfied for sequences of length 2. Then, for a sequence S of length k we have either $S = S'B$ or $S = S'A$, where S' is a sequence of length $k-1$. In a measurement of S, we can consider S' to be part of the preparation procedure and then apply Eq. (49). It follows that $\langle A_{k+1}|SA\rangle = \langle A_k|S'A\rangle$ and eventually $\langle A_{k+1}|SA\rangle = \langle A_1\rangle$ by induction.

In a similar fashion we reduce condition (i) of Definition 1 for dichotomic observables. For an experimentally accessible probability distribution $p_{\rm exp}(\lambda)$, we denote by $\tilde{p}_{\rm exp}(\lambda)$ the distribution obtained by a measurement of A and a postselection of the result $+1$. Then, for a sequence S of length k,

$$\begin{aligned} p(A_1^+A_{k+2}^-|ASA) &= \tilde{p}(A_{k+1}^-|SA)\,p(A_1^+|A_1) \\ &= \tilde{p}(A_1^-|A)\,p(A_1^+|A) \\ &= p(A_1^+A_2^-|A_1A_2), \end{aligned} \tag{50}$$

where for the second equality we used that $\langle A_{k+1}|SA\rangle = \langle A_1\rangle$ holds for $\tilde{p}$. It follows that a set of dichotomic observables Ξ is compatible if and only if, for any preparation and any $A, B \in \Xi$, $\langle A_1A_2\rangle = 1$ and Eq. (49) holds. In particular, this proves the assertion that pairwise compatibility of three or more observables is equivalent to an extended definition of compatibility involving sequences of all compatible observables.

[1] J. von Neumann, Ann. of Math. **32**, 191 (1931).
[2] A. Einstein, B. Podolsky, and N. Rosen, Phys. Rev. **47**, 777 (1935).
[3] N. Bohr, Phys. Rev. **48**, 696 (1935).
[4] R. F. Werner and M. M. Wolf, Quantum Inf. Comput. **1**(3), 1 (2001).
[5] D. Bohm and B. J. Hiley, *The Undivided Universe. An Ontological Interpretation of Quantum Theory* (Routledge, London, 1993).
[6] P. R. Holland, *The Quantum Theory of Motion. An Account of the de Broglie-Bohm Causal Interpretation of Quantum Mechanics* (Cambridge University Press, Cambridge, UK, 1993).
[7] J. S. Bell, Physics (Long Island City, NY) **1**, 195 (1964).
[8] J. F. Clauser, M. A. Horne, A. Shimony, and R. A. Holt, Phys. Rev. Lett. **23**, 880 (1969), *ibid.* **24**, 549 (1970).
[9] A. Aspect, J. Dalibard, and G. Roger, Phys. Rev. Lett. **49**, 1804 (1982).
[10] G. Weihs, T. Jennewein, C. Simon, H. Weinfurter, and A. Zeilinger, Phys. Rev. Lett. **81**, 5039 (1998).
[11] M. A. Rowe, D. Kielpinski, V. Meyer, C. A. Sackett, W. M. Itano, C. Monroe, and D. J. Wineland, Nature (London) **409**, 791 (2001).
[12] D. N. Matsukevich, P. Maunz, D. L. Moehring, S. Olmschenk, and C. Monroe, Phys. Rev. Lett. **100**, 150404 (2008).
[13] W. Rosenfeld, M. Weber, J. Volz, F. Henkel, M. Krug, A. Cabello, M. Żukowski, and H. Weinfurter, Adv. Sci. Lett. **2**, 469 (2009).
[14] A. J. Leggett, Found. Phys. **33**, 1469 (2003).
[15] S. Gröblacher, T. Paterek, R. Kaltenbaek, Č. Brukner, M. Żukowski, M. Aspelmeyer, and A. Zeilinger, Nature (London) **446**, 871 (2007); *ibid.* **449**, 252 (2007).
[16] C. Branciard, N. Brunner, N. Gisin, C. Kurtsiefer, A. Lamas-Linares, A. Ling, and V. Scarani, Nat. Phys. **4**, 681 (2008).
[17] E. Specker, Dialectica **14**, 239 (1960).
[18] J. S. Bell, Rev. Mod. Phys. **38**, 447 (1966).
[19] S. Kochen and E. P. Specker, J. Math. Mech. **17**, 59 (1967).
[20] S. M. Roy and V. Singh, Phys. Rev. A **48**, 3379 (1993).
[21] A. Cabello and G. García-Alcaine, Phys. Rev. Lett. **80**, 1797 (1998).
[22] C. Simon, M. Żukowski, H. Weinfurter, and A. Zeilinger, Phys. Rev. Lett. **85**, 1783 (2000).
[23] C. Simon, Č. Brukner, and A. Zeilinger, Phys. Rev. Lett. **86**, 4427 (2001).
[24] J.-Å. Larsson, Europhys. Lett. **58**, 799 (2002).
[25] D. A. Meyer, Phys. Rev. Lett. **83**, 3751 (1999).
[26] A. Kent, Phys. Rev. Lett. **83**, 3755 (1999).
[27] N. D. Mermin, quant-ph/9912081.
[28] R. Clifton and A. Kent, Proc. R. Soc. London, Ser. A **456**, 2101 (2000).
[29] H. Havlicek, G. Krenn, J. Summhammer, and K. Svozil, J. Phys. A **34**, 3071 (2001).
[30] D. M. Appleby, Phys. Rev. A **65**, 022105 (2002).

[31] A. Cabello, Phys. Rev. A **65**, 052101 (2002).
[32] T. Breuer, in *Non-locality and Modality*, edited by T. Placek and J. Butterfield (Kluwer Academic, Dordrecht, Holland, 2002), p. 195.
[33] T. Breuer, Phys. Rev. Lett. **88**, 240402 (2002).
[34] J. Barrett and A. Kent, Stud. Hist. Phil. Sci. Part B: Stud. Hist. Philos. Mod. Phys. **35**, 151 (2004).
[35] M. Michler, H. Weinfurter, and M. Żukowski, Phys. Rev. Lett. **84**, 5457 (2000).
[36] Y.-F. Huang, C.-F. Li, Y.-S. Zhang, J.-W. Pan, and G.-C. Guo, Phys. Rev. Lett. **90**, 250401 (2003).
[37] Y. Hasegawa, R. Loidl, G. Badurek, M. Baron, and H. Rauch, Phys. Rev. Lett. **97**, 230401 (2006).
[38] R. W. Spekkens, Phys. Rev. A **71**, 052108 (2005).
[39] R. W. Spekkens, D. H. Buzacott, A. J. Keehn, B. Toner, and G. J. Pryde, Phys. Rev. Lett. **102**, 010401 (2009).
[40] A. Cabello, S. Filipp, H. Rauch, and Y. Hasegawa, Phys. Rev. Lett. **100**, 130404 (2008).
[41] A. A. Klyachko, M. A. Can, S. Binicioğlu, and A. S. Shumovsky, Phys. Rev. Lett. **101**, 020403 (2008).
[42] A. Cabello, Phys. Rev. Lett. **101**, 210401 (2008).
[43] P. Badziąg, I. Bengtsson, A. Cabello, and I. Pitowsky, Phys. Rev. Lett. **103**, 050401 (2009).
[44] G. Kirchmair, F. Zähringer, R. Gerritsma, M. Kleinmann, O. Gühne, A. Cabello, R. Blatt, and C. F. Roos, Nature (London) **460**, 494 (2009).
[45] H. Bartosik, J. Klepp, C. Schmitzer, S. Sponar, A. Cabello, H. Rauch, and Y. Hasegawa, Phys. Rev. Lett. **103**, 040403 (2009).
[46] E. Amselem, M. Rådmark, M. Bourennane, and A. Cabello, Phys. Rev. Lett. **103**, 160405 (2009).
[47] B. H. Liu, Y. F. Huang, Y. X. Gong, F. W. Sun, Y. S. Zhang, C. F. Li, and G. C. Guo, Phys. Rev. A **80**, 044101 (2009).
[48] O. Moussa, C. A. Ryan, D. G. Cory, and R. Laflamme, arXiv:0912.0485.
[49] B. R. La Cour, Phys. Rev. A **79**, 012102 (2009).
[50] J. S. Bell, Found. Phys. **12**, 989 (1982).
[51] A. Peres, Found. Phys. **29**, 589 (1999).
[52] A. Peres, Phys. Lett. A **151**, 107 (1990).
[53] N. D. Mermin, Phys. Rev. Lett. **65**, 3373 (1990).
[54] G. Kirchmair, J. Benhelm, F. Zähringer, R. Gerritsma, C. F. Roos, and R. Blatt, New J. Phys. **11**, 023002 (2009).
[55] H. Häffner, C. F. Roos, and R. Blatt, Phys. Rep. **469**, 155 (2008).
[56] A. Sørensen and K. Mølmer, Phys. Rev. Lett. **82**, 1971 (1999).

Increasing the statistical significance of entanglement detection in experiments

Bastian Jungnitsch,[1] Sönke Niekamp,[1] Matthias Kleinmann,[1] Otfried Gühne,[1,2]
He Lu,[3] Wei-Bo Gao,[3] Yu-Ao Chen,[3,4] Zeng-Bing Chen,[3] and Jian-Wei Pan[3,4]

[1]*Institut für Quantenoptik und Quanteninformation, Österreichische Akademie der Wissenschaften, Technikerstraße 21A, A-6020 Innsbruck, Austria*
[2]*Institut für Theoretische Physik, Universität Innsbruck, Technikerstraße 25, A-6020 Innsbruck, Austria*
[3]*Hefei National Laboratory for Physical Sciences at Microscale and Department of Modern Physics, University of Science and Technology of China, Hefei, Anhui 230026, China*
[4]*Physikalisches Institut, Ruprecht-Karls-Universität Heidelberg, Philosophenweg 12, 69120 Heidelberg, Germany*

(Dated: March 30, 2010)

Entanglement is often verified by a violation of an inequality like a Bell inequality or an entanglement witness. Considerable effort has been devoted to the optimization of such inequalities in order to obtain a high violation. We demonstrate theoretically and experimentally that such an optimization does not necessarily lead to a better entanglement test, if the statistical error is taken into account. Theoretically, we show for different error models that reducing the violation of an inequality can improve the significance. Experimentally, we observe this phenomenon in a four-photon experiment, testing the Mermin and Ardehali inequality for different levels of noise. Furthermore, we provide a way to develop entanglement tests with high statistical significance.

PACS numbers: 03.65 Ud, 03.67 Mn

Introduction — Quantum theory is a statistical theory, predicting in general only probabilities for experimental results. Consequently, in most experiments observing quantum effects, several copies of a quantum state are generated and individually measured to determine the desired probabilities. As only a finite number of states can be generated, this leads to an unavoidable statistical error. The particularly low generation rate in certain experiments demands a careful statistical treatment; a fact that is well known from particle physics [1, 2].

In quantum information processing, many of today's experiments aim at the generation of entanglement, which is considered to be a central resource [3, 4]. So far, entanglement of up to ten qubits has been achieved using trapped ions or photons [5, 6]. For the experimental verification of entanglement, often inequalities for the correlations — such as Bell inequalities or entanglement witnesses — are used [4], in which a violation indicates entanglement. The maximization of this violation has been investigated in detail, cf. Refs. [4, 7]. In fact, making such inequalities more sensitive is a crucial step in order to allow advanced experiments with more particles.

In this paper we demonstrate theoretically and experimentally that such an optimization does not necessarily lead to a better entanglement test, if the statistical nature of quantum theory is taken into account. It was already noted [8] that, when aiming at ruling out local realism, highly entangled states do not necessarily deliver a stronger test than weakly entangled states, but this does not answer the question which inequality to use for a given state and it remains unclear how to apply it to actual error models used in experiments. Also, most of the different entanglement detection methods compared in Ref. [9] cannot be applied to multiparticle systems.

Theoretically, we show for different error models that decreasing the violation of an inequality can improve the significance. Also, we demonstrate this phenomenon in a four-photon experiment, measuring the Mermin and the Ardehali inequality. We find that the former inequality leads to a higher significance than the latter, despite a lower violation. Finally, we discuss the physical origin of this phenomenon and provide methods to construct entanglement tests with a high statistical significance.

Statement of the problem — A witness $\mathcal{W}$ is an observable which has a non-negative expectation value on all separable states (i.e., states which can be written as a mixture of product states, $\varrho = \sum_k p_k |a_k, b_k\rangle\langle a_k, b_k|$ with some probabilities p_k). Hence, a negative expectation value of a witness signals entanglement. Similarly, a Bell inequality $\langle\mathcal{B}\rangle \leq C_{\mathrm{lhv}}$, where $\mathcal{B}$ is a sum of certain correlation terms, holds if the measurement outcomes can originate from a local hidden variable (LHV) model. As separable states allow a description by LHV models, a violation of a Bell inequality implies the presence of entanglement.

In both cases, we define $\mathcal{V}$ as the violation of the corresponding inequality. That is, for a witness we have $\mathcal{V}(\mathcal{W}) = -\langle\mathcal{W}\rangle$ while for a Bell inequality $\mathcal{V}(\mathcal{B}) = \langle\mathcal{B}\rangle - C_{\mathrm{lhv}}$. Then, the significance of an entanglement test can be defined as

$$\mathcal{S} = \frac{\mathcal{V}}{\mathcal{E}} \tag{1}$$

where $\mathcal{E}$ is the statistical error for the experiment. Clearly, $\mathcal{E}$ depends on the particular experimental implementation and on the error model used. Nevertheless, in any experiment $\mathcal{S}$ is a well characterized quantity; its notion is widely used in the literature, when the violation is expressed in terms of "standard deviations", also

in other fields of physics [1].

Previously, much effort has been devoted to improving entanglement tests in order to achieve a higher violation. For instance, for entanglement witnesses a mature theory how to optimize witnesses has been developed [7]. Here, for a given witness $\mathcal{W}$ one tries to find a positive operator P, such that $\mathcal{W}' = \mathcal{W} - P$ is still a witness. In order to have a more significant result, however, one can either increase $\mathcal{V}$ in Eq. (1) or decrease $\mathcal{E}$. It is a central result of this paper that decreasing $\mathcal{E}$ is often superior.

Variance as the error — Let us first consider a simple model, in which we take the square root of the variance as the error of a witness,

$$\mathcal{E}(\mathcal{W}) = \Delta(\mathcal{W}) = \sqrt{\langle \mathcal{W}^2 \rangle - \langle \mathcal{W} \rangle^2}. \tag{2}$$

An experimentally relevant model will be discussed below. This simple model already demonstrates that the standard optimization of witnesses is often not the appropriate approach to increase the significance:

Observation. Let $\varrho = |\psi\rangle\langle\psi|$ be a pure state detected by the witness $\mathcal{W}$. Then, one can always increase the significance of $\mathcal{W}$ at the expense of optimality (i.e., by *adding* a positive operator). With this method one can make the significance arbitrarily large.

Namely, one needs to find a positive observable P, such that $|\psi\rangle$ is an eigenstate of $\mathcal{W}' = \mathcal{W} + P$; then the error vanishes. Indeed, such a P can be found (see Appendix).

Multi-photon experiments — Let us now consider a realistic situation, in which other and more specific error models are used. As our later implementation uses multi-photon entanglement, we concentrate on this type of experiments but our ideas can also be applied to other implementations, such as trapped ions.

The basic experimental quantities are the numbers of detection events n_i of the different detectors i. From these data, all other quantities such as correlations or mean values of observables are derived.

In the standard error model for photonic experiments [6, 10], the counts are assumed to be distributed according to a Poissonian distribution, whose mean value is given by the observed value. That is, for a certain measurement outcome i one sets the mean value as $\langle n_i \rangle = n_i$ and the error as $\mathcal{E}(n_i) = \sqrt{n_i}$ (being the standard deviation of a Poissonian distribution). In general, for a function $f = f(n_i)$ of several counts, Gaussian error propagation is applied to obtain the error (see below).

To give an example, consider a two-qubit correlation

$$\mathcal{M} = \alpha Z_1 Z_2 + \beta Z_1 \mathbb{1}_2 + \gamma \mathbb{1}_1 Z_2. \tag{3}$$

Here and in the following, Z_k (or $\mathbb{1}_k$) denotes the Pauli matrix σ_z (or the identity matrix) acting on the kth qubit and tensor product symbols are omitted. $\langle \mathcal{M} \rangle$ can be determined by measuring in the common eigenbasis of all three terms in $\mathcal{M}$, i.e., by projecting onto $|00\rangle, |01\rangle, |10\rangle$ and $|11\rangle$. Repeating this with many copies of the state will lead to count numbers n_{kl} with $k, l = 0$ or 1 and to count rates $p_{kl} = n_{kl}/n_{\mathrm{tot}}$, where $n_{\mathrm{tot}} = n_{00} + n_{01} + n_{10} + n_{11}$ is the total number of events. The mean value $\langle \mathcal{M} \rangle$ can be written as a linear combination of p_{kl}, namely $\langle \mathcal{M} \rangle = \lambda_{00} p_{00} + \lambda_{01} p_{01} + \lambda_{10} p_{10} + \lambda_{11} p_{11}$ with $\lambda_{00} = \alpha + \beta + \gamma, \lambda_{01} = -\alpha + \beta - \gamma, \lambda_{10} = -\alpha - \beta + \gamma$, and $\lambda_{11} = \alpha - \beta - \gamma$. Then, according to Gaussian error propagation, the squared error is given by [11]

$$\mathcal{E}(\mathcal{M})^2 = \sum_{k,l} \Big[\frac{\partial \langle \mathcal{M} \rangle}{\partial n_{kl}} \Big]^2 \mathcal{E}(n_{kl})^2 = \sum_{k,l} \Big[\frac{\lambda_{kl}}{n_{\mathrm{tot}}} - \frac{\langle \mathcal{M} \rangle}{n_{\mathrm{tot}}} \Big]^2 n_{kl}. \tag{4}$$

Let us finally discuss the underlying assumptions of this error model. The first main assumption is that the n_{kl} are Poisson distributed and their errors are uncorrelated. This is well motivated by the experimental observations. Moreover, Gaussian error propagation stems from a Taylor expansion of the function f. Finally, if one interprets the standard deviation as a confidence interval, one tacitly assumes that the distribution is Gaussian, as for other distributions the connection is not so direct. If the number of events for all detectors is sufficiently large (e.g. $n_{kl} \gtrsim 10$), however, the Poissonian distribution is approximated well by a Gaussian distribution.

Bell inequalities for four particles — Let us now discuss the Mermin and Ardehali inequality as experimentally relevant examples. First, we consider

$$\mathcal{B}_{\mathrm{M}} = X_1 X_2 X_3 X_4 - [X_1 X_2 Y_3 Y_4 + \text{ perm.}] + Y_1 Y_2 Y_3 Y_4, \tag{5}$$

where the bracket $[\dots]$ is meant as a sum over all permutations of $X_1 X_2 Y_3 Y_4$ that yield distinct operators. For states allowing an LHV description, the Mermin inequality $\langle \mathcal{B}_{\mathrm{M}} \rangle \leq 4$ holds [12]. We wrote $\mathcal{B}_{\mathrm{M}}$ with the Pauli matrices as observables, since they are used later, however, one might replace them by arbitrary dichotomic measurements.

Second, we consider the Ardehali inequality $\langle \mathcal{B}_{\mathrm{A}} \rangle \leq 2\sqrt{2}$ [13], where

$$\begin{aligned} \mathcal{B}_{\mathrm{A}} = (&X_1 X_2 X_3 A_4 + X_1 X_2 X_3 B_4 \\ &- [X_1 Y_2 Y_3 A_4 + \text{ perm.}] - [X_1 Y_2 Y_3 B_4 + \text{ perm.}] \\ &- [X_1 X_2 Y_3 A_4 + \text{ perm.}] + [X_1 X_2 Y_3 B_4 + \text{ perm.}] \\ &+ Y_1 Y_2 Y_3 A_4 - Y_1 Y_2 Y_3 B_4) / \sqrt{2}. \end{aligned} \tag{6}$$

Here, the sums in square brackets include all distinct permutations on the first three qubits. We set $A_4 = (X_4 + Y_4)/\sqrt{2}$ and $B_4 = (X_4 - Y_4)/\sqrt{2}$, but again, the observables can remain arbitrary [14].

The Mermin and Ardehali inequality reveal the non-local correlations of the four-qubit GHZ state,

$$|GHZ_4\rangle = \frac{1}{\sqrt{2}} (|0000\rangle + |1111\rangle). \tag{7}$$

For this state we have $\langle \mathcal{B}_{\mathrm{M}} \rangle = \langle \mathcal{B}_{\mathrm{A}} \rangle = 8$. As the bound for LHV models for the Ardehali inequality is smaller,

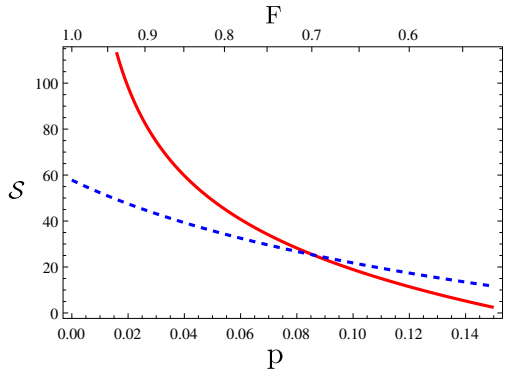

FIG. 1: Significance $\mathcal{S}$ for the Mermin (red, solid) and the Ardehali inequality (blue, dashed) for bit-flip noise. On the horizontal axes, we show the bit-flip probability and the corresponding fidelity with respect to a perfect GHZ state. We assumed that the experimenter prepares 8000 instances of a GHZ state and chooses either to measure the eight terms of the Mermin inequality (each term with 1000 realizations of the state) or the 16 terms of the Ardehali inequality with 500 states per correlation term. See text for further details.

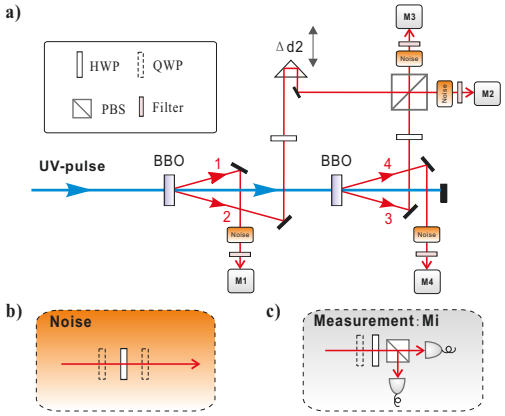

FIG. 2: Scheme of the experimental setup. **a**. The setup to generate the required four-photon GHZ state. Femtosecond laser pulses ($\approx$ 200 fs, 76 MHz, 788 nm) are converted to ultraviolet pulses through a frequency doubler LiB_3O_5 (LBO) crystal (not shown). The pulses go through two main β-barium borate (BBO) crystals (2 mm), generating two pairs of photons. The observed two-fold coincidence count rates are about 1.6×10^4/s with a visibility of 96% (94%) in the H/V (+/−) basis. **b**. Setup for engineering the bit-flip noise. **c**. The measurement setup.

the violation $\mathcal{V}$ is larger. This may lead to the opinion that the Ardehali inequality is "better" than the Mermin inequality for the state $|GHZ_4\rangle$.

However, this belief is easily shattered, if the significance $\mathcal{S}$ is considered as the relevant figure of merit. This can be seen directly from Eq. (4). The GHZ state is an eigenstate for each of the correlation measurements in the Mermin inequality (they are so-called stabilizing operators of the GHZ state). Hence, if the Mermin inequality for a perfect GHZ state is measured, we have in the last term of Eq. (4) for each case k, l either $\lambda_{kl} = \langle \mathcal{M} \rangle$ (since the mean value is an eigenvalue) or $n_{kl} = 0$, hence $\mathcal{E}(\mathcal{M})$ vanishes. The Ardehali inequality, however, does not contain stabilizer terms and the error remains finite.

For an experimental application it is important that the Mermin inequality leads to a higher significance than the Ardehali inequality, even if noise is introduced [15]. To see this, we considered bit-flip noise, which can easily be simulated in experiment. Therefore, we used a perfect GHZ state whose qubits are locally affected by the bit-flip operation f with probability p, i.e. $f(\varrho_i) = (1-p)\varrho_i + pX_i\varrho_i X_i$ for each qubit i. In Fig. 1, we plotted the significance $\mathcal{S}$ versus the fidelity F of the noisy state w.r.t. a perfect GHZ state, i.e. $F = \langle GHZ_4|\varrho_{exp}|GHZ_4\rangle$, and versus the bit-flip probability p. For $F \geq 0.70$ the Mermin inequality is more significant (for the 6-qubit versions of these inequalities [12, 13], this changes to $F \geq 0.40$). As can be seen from Eq. (4), the fact that one witness is more significant than the other one is independent of the total particle number. Moreover, a calculation for white noise yields very similar values ($F \geq 0.72$ for 4 qubits, $F \geq 0.41$ for 6 qubits). This suggests that the effect does not depend on details of the noise. Note that the threshold value for white noise vanishes exponentially fast for an increasing number of qubits.

Experimental setup — Spontaneous down conversion has been used to produce the desired four-photon state [see Fig. 2(a)]. With the help of polarizing beam splitters (PBSs), half-wave plates (HWPs) and conventional photon detectors, we prepare a four-qubit GHZ state, where $|0\rangle = |H\rangle$ ($|1\rangle = |V\rangle$) denotes horizontal (vertical) polarization. We have chosen the bit-flip noise channel to demonstrate the theory introduced in this paper. As shown in Fig. 2(b), the noisy quantum channels are engineered by one HWP sandwiched with two quarter-wave plates (QWPs) [16]. The HWP is switched randomly between $+\theta$ and $-\theta$ and the QWPs are set at 0° with respect to the vertical direction. In this way, the noise channel can be engineered with a bit-flip probability $p = \sin^2(2\theta)$. The Pauli matrix measurements required in the Bell test can be implemented by a combination of HWP, QWP and PBS [see Fig. 2(c)]. The fidelity of the prepared GHZ state is obtained via $F = \frac{1}{2}(\langle|0000\rangle\langle 0000| + |1111\rangle\langle 1111|\rangle) + \frac{1}{16}\langle \mathcal{B}_M \rangle$. Without added noise, its value is $F = 0.84 \pm 0.01$.

Experimental results — For different noise levels, the experimental results of the violation, the statistical error and the significance are shown in Table I. The first observation is that, when there is no engineered noise, the violation of the Mermin inequality is smaller than the violation of the Ardehali inequality. Its significance, however, is larger than that of the Ardehali inequality; this proves that testing the Mermin inequality is a better choice to characterize the entanglement in this case.

θ	p	$\mathcal{V}(\mathcal{B}_M)$	$\mathcal{E}(\mathcal{B}_M)$	$\mathcal{S}(\mathcal{B}_M)$	$\mathcal{V}(\mathcal{B}_A)$	$\mathcal{E}(\mathcal{B}_A)$	$\mathcal{S}(\mathcal{B}_A)$
$\pm 0°$	0	2.37	0.05	44.3	3.65	0.10	35.0
$\pm 2°$	0.005	2.00	0.06	33.4	3.14	0.11	29.2
$\pm 4°$	0.019	1.57	0.07	23.7	2.48	0.11	21.8
$\pm 6°$	0.043	1.13	0.07	16.2	2.05	0.11	17.8
$\pm 8°$	0.076	0.67	0.08	8.8	1.63	0.12	13.7

TABLE I: Experimental values of the violation, the statistical error and the significance for different values of θ (and the corresponding p). $\mathcal{V}(\mathcal{B}_M)$, $\mathcal{E}(\mathcal{B}_M)$, $\mathcal{S}(\mathcal{B}_M)$ represent the values of $\mathcal{V}$, $\mathcal{E}$ and $\mathcal{S}$ in testing the Mermin inequality; $\mathcal{V}(\mathcal{B}_A)$, $\mathcal{E}(\mathcal{B}_A)$, $\mathcal{S}(\mathcal{B}_A)$ represent the corresponding values for the Ardehali inequality. Each setting $X_1X_2X_3X_4$ etc. in the Mermin inequality is measured for 800 s, while each setting $X_1X_2X_3A_4$ etc. in the Ardehali inequality is measured for 400 s. The average total count number for each inequality is about 7500.

Secondly, when the noise level increases, the significance in the Mermin inequality decreases more quickly. When $\theta = \pm 6°, \pm 8°$, the significance for the Ardehali inequality is already larger than that for the Mermin inequality. Due to the experimental imperfections, the initial state to which the noise is added is not the perfect GHZ state. However, assuming an initial state like $\varrho(p = 0) = \alpha|0000\rangle\langle 0000| + \beta|1111\rangle\langle 1111| + \gamma(|0000\rangle\langle 1111| + |1111\rangle\langle 0000|) + \frac{\lambda}{16}\mathbb{1}$, where $\alpha = 0.362, \beta = 0.522, \gamma = 0.398, \lambda = 0.12$ reproduces that for $p \leq 0.019$ the Mermin inequality is more significant.

Discussion — We have proved that it can be favorable to use an entanglement witness or a Bell inequality that results in a lower violation. We confirmed this experimentally using four-photon GHZ states. Our results show that the usual way of optimizing witnesses will not necessarily lead to more powerful tools for the analysis of many-particle experiments. It is important to note that when the number of photons in multi-photon experiments is increased the count rates decrease; consequently, the statistical error becomes more and more relevant.

Our results provide a direction to find powerful entanglement tests for low count rates: the observed effect relied on the fact that in the Mermin inequality only stabilizer measurements were made. There are already powerful approaches available to construct witnesses from stabilizer observables [17] and also other Mermin-like or Ardehali-like Bell inequalities have been explored [18]. Consequently, these approaches are promising candidates for developing sensitive analysis tools. Further, inequalities similar to witnesses have been proposed and used to characterize quantum gate fidelities [19], which is another application of our theory. Finally, we believe that results on statistical confidence from other fields of physics (e.g. [2]) can give new insights in advanced experiments on quantum information processing.

We thank A. Cabello, R. Gill, O. Gittsovich, D. James, J.-Å. Larsson and C. Roos for discussions and acknowledge support by the FWF (START Prize), the EU (SCALA, OLAQUI, QICS, Marie Curie Excellence Grant), the NNSFC, the NFRP (2006CB921900), the CAS, the ICP at HFNL, and the A. v. Humboldt Foundation.

Appendix — To prove the Observation, we use as an ansatz for the improved witness $\mathcal{W}' = \mathcal{W} + \gamma P$, where $\gamma > 0$ and P is a positive observable with unit trace. For small γ, we expand $-\frac{\langle \mathcal{W}'\rangle}{\Delta(\mathcal{W}')} = -\frac{\langle \mathcal{W}\rangle}{\Delta(\mathcal{W})} + \gamma \frac{\langle \mathcal{W}\rangle}{2\Delta^3(\mathcal{W})}\Big[\langle \mathcal{W}P + P\mathcal{W}\rangle - 2\frac{\langle \mathcal{W}^2\rangle}{\langle \mathcal{W}\rangle}\langle P\rangle\Big] + O(\gamma^2)$. Maximizing this expression over all positive P with $\mathrm{Tr}(P) = 1$ is equivalent to minimizing $\mathrm{Tr}(QP)$, where $Q = \varrho\mathcal{W} + \mathcal{W}\varrho - 2\langle \mathcal{W}^2\rangle/\langle \mathcal{W}\rangle\varrho$. Hence the optimal P is a one-dimensional projector $P = |\varphi\rangle\langle\varphi|$, where $|\varphi\rangle$ is an eigenvector corresponding to the minimal eigenvalue of Q. We still have to show that this minimal eigenvalue is negative. To this end, we make the ansatz $|\varphi\rangle = \alpha|\psi\rangle + \beta|\psi^\perp\rangle$, where $\langle\psi|\psi^\perp\rangle = 0$. We then have to minimize $\mathrm{Tr}(QP) = 2\,\mathrm{Re}(\alpha^*\beta\langle\psi|\mathcal{W}|\psi^\perp\rangle) - 2|\alpha|^2\frac{\Delta^2_\psi(\mathcal{W})}{\langle\psi|\mathcal{W}|\psi\rangle}$. We can always choose the phases of α and β such that $\mathrm{Re}(\ldots)$ is negative. Therefore the optimal $|\psi^\perp\rangle$ is the vector orthogonal to $|\psi\rangle$ which maximizes $|\langle\psi|W|\psi^\perp\rangle|$, i.e., $|\psi^\perp_{\mathrm{opt}}\rangle = [\mathbf{1} - |\psi\rangle\langle\psi|]\mathcal{W}|\psi\rangle/\Delta_\psi(\mathcal{W})$. Furthermore, we can always choose the moduli of α and β such that the negative term $2\,\mathrm{Re}(\ldots)$ dominates the positive second term. This shows that the minimal eigenvalue of Q is negative.

For finite γ we can iterate this procedure. We always find the same $|\psi^\perp_{\mathrm{opt}}\rangle$ (though α and β will be different in each iteration step). Thus, we make the ansatz $\gamma P = a|\psi\rangle\langle\psi| + b|\psi^\perp_{\mathrm{opt}}\rangle\langle\psi^\perp_{\mathrm{opt}}| + c|\psi\rangle\langle\psi^\perp_{\mathrm{opt}}| + \mathrm{h.c.}$ for the final result of the iteration. If we choose $c = -\Delta_\psi(\mathcal{W})$, $ab \geq |c|^2$, and $a, b > 0$, then γP is positive, $|\psi\rangle$ is an eigenstate of $\mathcal{W}'$, and $\Delta_\psi(\mathcal{W}')$ is zero, so $\mathcal{S}$ diverges. □

[1] For an overview of the different approaches, see C. Amsler *et al.* (Particle Data Group), Phys. Lett. B **667**, 1 (2008) or the proceedings of PHYSTAT2003, available at `http://slac.stanford.edu/econf/C030908/proceedings.html`.

[2] G.J. Feldman and R.D. Cousins, Phys. Rev. D **57**, 3873 (1998).

[3] R. Horodecki *et al.*, Rev. Mod. Phys. **81**, 865 (2009); M. Plenio and S. Virmani, Quant. Inf. Comp. **7**, 1 (2007).

[4] O. Gühne and G. Tóth, Phys. Reports **474**, 1 (2009).

[5] H. Häffner *et al.*, Nature **438**, 643 (2005); W.B. Gao *et al.*, arXiv:0809.4277.

[6] C.-Y. Lu *et al.*, Nature Physics **3**, 91 (2007).

[7] M. Lewenstein *et al.*, Phys. Rev. A **62**, 052310 (2000); P. Hyllus and J. Eisert, New J. Phys. **8**, 51 (2006); G. Tóth *et al.*, New J. Phys. **11**, 083002 (2009).

[8] W. van Dam, R.D. Gill, and P. Grünwald, IEEE-Transactions on Information Theory **51**, 2812 (2005); A. Acín, R.D. Gill, and N. Gisin, Phys. Rev. Lett. **95**, 210402 (2005); R.D. Gill, IMS Lecture Notes Monograph Series **55**, 135 (2007), math/0610115.

[9] J.B. Altepeter *et al.*, Phys. Rev. Lett. **95**, 033601 (2005).

[10] D.F.V. James *et al.*, Phys. Rev. A **64**, 052312 (2001).
[11] In Ref. [10] the second term, $-\langle\mathcal{M}\rangle/n_{\rm tot}$, is omitted, leading to a systematic overestimation of the standard deviation. Such an overestimation is problematic, if the claim is that certain state properties (e.g. having a negative partial transpose) are not significant. This can occur, e.g. in the analysis of bound entanglement, see A. Elias and M. Bourennane, Nature Phys. **5**, 748 (2009).
[12] N. Mermin, Phys. Rev. Lett. **65**, 1838 (1990).
[13] M. Ardehali, Phys. Rev. A **46**, 5375 (1992).
[14] Indeed, with the given choice of observables the operators $\mathcal{B}_{\rm M}$ and $\mathcal{B}_{\rm A}$ are identical within quantum mechanics. However, the use of A and B within the Ardehali inequality results in a more restrictive test for LHV models.
[15] This is also important, as for nearly perfect GHZ states, some count numbers n_{kl} will be close to zero. Then, the interpretation of the statistical error as a confidence interval may be questioned.
[16] Y.-A. Chen *et al.*, Phys. Rev. Lett. **96**, 220504 (2006).
[17] G. Tóth and O. Gühne, Phys. Rev. Lett. **94**, 060501 (2005).
[18] V. Scarani *et al.*, Phys. Rev. A **71**, 042325 (2005); A. Cabello, O. Gühne, and D. Rodriguez, *ibid.* **77** 062106 (2008); O. Gühne and A. Cabello, *ibid.* **77**, 032108 (2008).
[19] H.F. Hofmann, Phys. Rev. Lett. **94**, 160504 (2005); W.-B. Gao *et al.*, Phys. Rev. Lett. **104**, 020501 (2010);

Asymptotically perfect discrimination in the LOCC paradigm

M. Kleinmann,[1,2] H. Kampermann,[3] and D. Bruß[3]

[1] *Department Physik, Universität Siegen, Walter-Flex-Str. 3, D-57068 Siegen, Germany*
[2] *Institut für Quantenoptik und Quanteninformation, Österreichische Akademie der Wissenschaften, Technikerstr. 21A, A-6020 Innsbruck, Austria*
[3] *Institut für Theoretische Physik III, Heinrich-Heine-Universität Düsseldorf, D-40225 Düsseldorf, Germany*

We revisit the problem of discriminating orthogonal quantum states within the local quantum operation and classical communication (LOCC) paradigm. Our particular focus is on the asymptotic situation where the parties have infinite resources and the protocol may become arbitrarily long. Our main result is a necessary condition for perfect asymptotic LOCC discrimination. As an application, we prove that for complete product bases, unlimited resources are of no advantage. On the other hand, we identify an example, for which it still remains undecided whether unlimited resources are superior.

PACS numbers: 03.65.Ud, 03.67.Ac, 03.67.Hk

I. INTRODUCTION

An important concept in quantum information theory is the paradigm known as "local operations and classical communication" (LOCC). It specifies the operational power of two or more parties which only have local access to a distributed quantum system but are equipped with a classical communication channel. A typical question now is, whether a certain task that usually is trivial to perform with global access can be accomplished within this restricted set of operations. Prominent such examples are entanglement distillation, entanglement transformations, or local state discrimination, and results from such examples have strong influence on central topics in quantum information theory, e.g. in entanglement classification and quantification or in quantum communication theory [1, 2].

Here, we will focus on the local discrimination of orthogonal states, i.e., states, which can be discriminated perfectly by a global measurement. This situation has been studied extensively in the literature, cf. e.g. Ref. [3–11], and some of the results are quite counter-intuitive. For example, it is always possible to perfectly discriminate two arbitrary orthogonal states [12], while there exist product bases which cannot be discriminated perfectly by means of LOCC [13].

An LOCC discrimination protocol in general consists of several rounds, where in each round one party performs a measurement and communicates the results to all parties. Due to the existence of "weak measurements" [14, 15] it is not clear that perfect discrimination can be achieved in a finite number of such rounds. From a physical point of view, the question of perfect distinguishability is not particularly meaningful, since unavoidable experimental imperfections will always impede perfect measurement results. Rather it would be interesting to know, whether with increasing experimental effort, one can get arbitrarily close to perfect discrimination. This asymptotic case has already been noticed and approached in Ref. [13], but to our knowledge only in Ref. [16] this question has been considered again, while the majority of the work on LOCC discrimination explicitly is limited to perfect discrimination in a finite number of rounds (cf. e.g. Ref. [7–11]) or to the more general class of stochastic LOCC measurements (or separable measurements [17]), cf. e.g. Ref. [3–6]. So far it is actually unclear whether the asymptotic consideration may yield a different result than the finite analysis.

In this contribution, we now revisit the problem of perfect discrimination by asymptotic LOCC. Our main result is a general necessary condition for such a discrimination to be possible, cf. Proposition 1. The proof of this result uses a variant of the protocol splitting technique introduced in Ref. [13]. We, however, do not rely on a continuous measurement process, but rather show that a finite enlargement of the protocol suffices in order to employ the protocol splitting. As an application of Proposition 1, we show that a product basis can be discriminated asymptotically if and only if it can be discriminated by finite means. This also gives an analytical proof of the numerical findings in Ref. [13]. (A similar result regarding unextendible product bases was stated in Ref. [16], however we question the validity of this proof, cf. our Remark below Proposition 2.) Finally, we study an example provided by Duan *et al.* [18], for which it is known that it cannot be discriminated by any finite protocol, while it can be discriminated perfectly by stochastic LOCC. For this example, using our result, we cannot exclude that asymptotic LOCC could achieve perfect discrimination.

Our paper is organized as follows: In Sec. II we thoroughly define our notion of asymptotic LOCC discrimination and analyze possible generalizations. In Sec. III we prove our main result, which is summarized in Proposition 1. We then discuss two examples in Sec. IV before we conclude in Sec. V.

II. ASYMPTOTIC LOCC DISCRIMINATION

In our scenario we aim at discriminating a certain family of multipartite mixed states (ρ_μ), where ρ_μ are

density operators on a finite-dimensional Hilbert space $\mathcal{H} = \bigotimes_r \mathcal{H}^{(r)}$. We will first define a general notion of finite LOCC measurements and then describe the transition from those finite measurements to the asymptotic situation.

A. Finite LOCC measurements

The most general quantum measurement with n outcomes is described by a positive operator valued measure (POVM), i.e., a finite family (E_k) of n positive semi-definite operators (or *effects*) on $\mathcal{H}$ obeying $\sum_k E_k = \mathbb{1}$. The probability to obtain the outcome k for a state ρ_μ is then given by $\mathrm{tr}(\rho_\mu E_k)$. Hence a measurement can be written as the mapping $\mathfrak{E}\colon X \mapsto (\mathrm{tr}[XE_k])$ from the set of operators into $\mathbb{C}^n$, where $0 \leq \mathfrak{E}(\rho)_k \leq 1$ for any state ρ.

Any POVM can be implemented by a physical measurement device and vice versa, any such device corresponds to a unique POVM. If the physical setup is limited to the LOCC paradigm then each effect E_k will be a sum of positive semi-definite product operators [13, 19],

$$E_k = \sum_j \bigotimes_r E_{k,j}^{(r)} \text{ with } E_{k,j}^{(r)} \geq 0. \tag{1}$$

However, as first shown by Bennett *et al.* in Ref. [13], the converse statement does not hold in general.

We call a measurement a *finite LOCC measurement*, if it can be implemented by an LOCC protocol, using only finite dimensional ancilla systems, measurements with a finite number of outcomes and which is guaranteed to terminate after a certain number of rounds. The intuition behind this restriction is a realistic experimental setup, where the effective dimension of the Hilbert space shall be finite, the classical communication channel has limited capacity, and the experiment cannot be kept stable for an infinite time span.

B. Deviation from perfect discrimination

For our goal of perfect discrimination of orthogonal states, we now measure the deviation from perfect discrimination $d(\mathfrak{E})$ for an arbitrary measurement $\mathfrak{E}$. Therefore we assume that for some fixed set of states (ρ_μ), $d(\mathfrak{E})$ is a non-negative real number such that $d(\mathfrak{E}) = 0$ implies that $\mathfrak{E}$ achieves perfect discrimination of (ρ_μ). Then we define the *asymptotic deviation* $\hat{d}$ as the infimum of d over all finite LOCC measurements. In particular, if $\hat{d} = 0$ then for any deviation $\varepsilon > 0$ we can find a finite LOCC measurement $\mathfrak{E}^\varepsilon$, such that $d(\mathfrak{E}^\varepsilon) < \varepsilon$.

The deviation measure has to be chosen carefully, as a trivial (but meaningful) choice for the deviation is e.g. the measure d_{finite}, which yields 1 whenever the measurement fails to achieve perfect discrimination and 0 in the case of perfect discrimination. Then $\hat{d}_{\mathrm{finite}} = 0$ if and only if there exists a finite LOCC measurement that achieves perfect discrimination.

Typically we would be rather interested, whether e.g. the mean failure probability could approach zero as the LOCC measurement becomes more and more expensive. We thus define the deviation measure $d_{\mathrm{mf}}(\mathfrak{E})$ to be the minimal mean failure probability over any possible classical post-processing of $\mathfrak{E}$, i.e.,

$$d_{\mathrm{mf}}(\mathfrak{E}) = 1 - \sum_k \max_\mu (p_\mu \mathfrak{E}(\rho_\mu)_k), \tag{2}$$

with some arbitrary *a priori* probabilities $p_\mu > 0$ obeying $\sum_\mu p_\mu = 1$. (The interpretation of this measure is as follows: Assume that the state ρ_μ is prepared with probability p_μ and we use the measurement $\mathfrak{E}$ in order to learn about the index μ. Given the measurement result k, the strategy which minimizes the probability of a failure is the one in which we announce the index μ maximizing $p_\mu \mathfrak{E}(\rho_\mu)_k$.)

In Ref. [13], in contrast, an entropy based measure was used for the deviation measure, namely the conditional entropy

$$d_{\mathrm{ce}}(\mathfrak{E}) = H(S|K) \equiv H(S,K) - H(K) \tag{3}$$

where S is the random variable, determining the index μ of the state ρ_μ, K is the random variable for the measurement outcome k, and $H(X)$ denotes the Shannon entropy of a random variable X. However, $\hat{d}_{\mathrm{ce}} = 0$ already implies $\hat{d}_{\mathrm{mf}} = 0$ since $d_{\mathrm{ce}}(\mathfrak{E}) \geq d_{\mathrm{mf}}(\mathfrak{E})$ holds for any measurement $\mathfrak{E}$ [20].

— At this point the moderately impatient reader may directly skip to our main result summarized in Proposition 1. Otherwise, allow us to introduce some additional notation:

First we combine the *a priori* probabilities p_μ and the states ρ_μ to *weighted* states $\gamma_\mu \equiv p_\mu \rho_\mu$. For a moment let us assume, that the measure d is defined for arbitrary families of N weighted states with $\sum_\mu \mathrm{tr}\,\gamma_\mu = 1$ (this will be guaranteed by property (ia) of regular measures we are about to define). Then we write $d(\mathfrak{E}) \equiv d[\mathfrak{E}; (\gamma_\mu)]$ and let for an operator A

$$d(\mathfrak{E}|A) = \begin{cases} d[\mathfrak{E}; (A\gamma_\mu A^\dagger / p_A)]) & \text{if } p_A > 0 \\ d[\mathfrak{I}; (\gamma_\mu)] & \text{else,} \end{cases} \tag{4}$$

where $p_A = \sum_\mu \mathrm{tr}(A\gamma_\mu A^\dagger)$ and $\mathfrak{I}\colon X \mapsto \mathrm{tr}[X]$ is the trivial measurement. (The operator A in this definition shall correspond to the Kraus operator of a measurement result, i.e. $A^\dagger A$ is an effect of a POVM. Then $d(\mathfrak{E}|A)$ denotes the deviation, given that we have performed a certain POVM and obtained the result with effect $A^\dagger A$.)

Although we will focus on the measure d_{mf}, most parts of our method apply to general regular deviation measures: We call a deviation measure d for N states *regular*, if the following conditions are satisfied:

(ia) The measure $d[\mathfrak{E};(\gamma_\mu)]$ only depends on $p(\mu,k)\equiv\mathfrak{E}(\gamma_\mu)_k$; d is well-defined for all probability distributions $p(\mu,k)$ with $p(\mu,k)\geq 0$ and $\sum_{\mu,k}p(\mu,k)=1$.

(ib) For a fixed number of measurement outcomes, d is bounded and continuous in $p(\mu,k)$.

(ii) A classical post-processing [21] Π acts non-decreasing, i.e., $d(\Pi\circ\mathfrak{E})\geq d(\mathfrak{E})$.

(iii) If a measurement is performed in two stages, then optimal post-selection after the first stage acts non-increasing. That is, if $\mathfrak{E}$ is of the form $\mathfrak{E}\colon\rho\mapsto\bigoplus_k\mathfrak{E}_k(A_k\rho A_k^\dagger)$ with $\sum_k A_k^\dagger A_k=\mathbb{1}$ and measurements $\mathfrak{E}_k$, then $d(\mathfrak{E})\geq\min_k d(\mathfrak{E}_k|A_k)$.

We mention, that condition (iii) is satisfied for d_{mf} and d_{ce} due to $d(\mathfrak{E})=\sum_k p_{A_k}d(\mathfrak{E}_k|A_k)$ for either measure; d_{mf} and d_{ce} in particular are regular. On the other hand, the measure d_{finite} satisfies all conditions but the continuity condition in (ib).

III. A NECESSARY CONDITION FOR PERFECT ASYMPTOTIC DISCRIMINATION

In this section we will derive our main result, Proposition 1, which states a necessary condition for perfect discrimination by asymptotic LOCC, $\hat{d}_{\mathrm{mf}}=0$. We present this proof in four steps: As a prelude we will start with pseudo-weak measurements, a technique that will become important for the protocol splitting method. The protocol splitting (cf. Ref. [13]) then achieves a split of the protocol into stage I and a continuation of stage I. This in turn allows to genuinely bound $\hat{d}$, cf. Eqns. (12) and (13). Finally we specialize this intermediate result to the regular deviation measure d_{mf}, yielding Proposition 1.

A. Prelude: Pseudo-weak measurements

Given a POVM (E_k) we define for $b_k\geq 0$ and $\beta\equiv 1/(1+\sum_k b_k)$ the POVM (E_k^{pw}) and the family of POVMs $(E_{(k),\ell}^{\mathrm{rc}})$ via

$$E_k^{\mathrm{pw}}=\beta\,(b_k\mathbb{1}+E_k), \tag{5a}$$

$$E_{(k),\ell}^{\mathrm{rc}}=\beta\,(b_k+\delta_{k,\ell})(E_k^{\mathrm{pw}})^{-1/2}E_\ell(E_k^{\mathrm{pw}})^{-1/2}, \tag{5b}$$

with $\delta_{k,l}=1$ if $k=l$ and zero else — if $b_k=0$, we let $E_{(k),l}^{\mathrm{rc}}=\delta_{k,l}\mathbb{1}$. A measurement of (E_k^{pw}) is a *pseudo-weak* implementation of (E_k), while we will refer to $(E_{(k),\ell}^{\mathrm{rc}})$ as the *recovery* measurement for outcome k. Indeed, an application of the recovery measurement after the pseudo-weak measurement on $|\psi\rangle$ results in

$$U_{k,\ell}\sqrt{E_{(k),\ell}^{\mathrm{rc}}}\sqrt{E_k^{\mathrm{pw}}}|\psi\rangle=\sqrt{\beta\,(b_k+\delta_{k,l})}\,\sqrt{E_\ell}\,|\psi\rangle, \tag{6}$$

with $U_{k,\ell}$ a unitary originating from the polar decomposition. In particular, if the outcome of the pseudo-weak measurement is ignored, the (weighted) state for outcome ℓ is identical to the state obtained by the original measurement in the case of outcome ℓ.

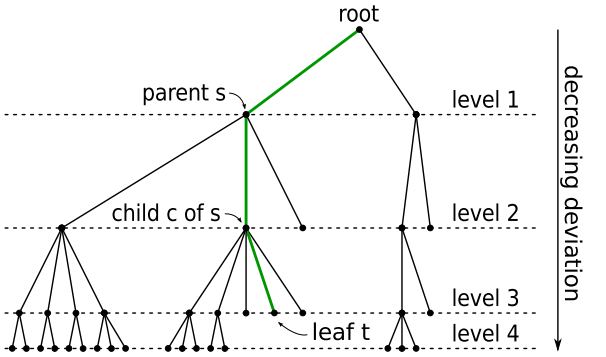

FIG. 1. Example of a 4-leveled tree graph which represents an LOCC measurement with at most 4 steps. The branch $B(t)$ (thick green) connects the leaf t with the root node and hence consists of the root node, node s and its child c and the leaf t.

Let us now consider a completely positive and trace preserving (CPTP) map Λ described by Kraus operators (A_k), $\Lambda\colon\rho\mapsto\sum_k A_k\rho A_k^\dagger$. With $A_k=V_k\sqrt{E_k}$ a polar decomposition of A_k (where $V_k^\dagger V_k=\mathbb{1}$), this map corresponds to a measurement of the POVM (E_k) and a subsequent application of V_k and hence we can use the above method to obtain a pseudo-weak implementation (A_k^{pw}) of (A_k) via $A_k^{\mathrm{pw}}=\sqrt{E_k^{\mathrm{pw}}}$. The recovery step is then a CPTP map described by $(A_{(k),\ell}^{\mathrm{rc}})$ with $A_{(k),\ell}^{\mathrm{rc}}=V_\ell U_{k,\ell}\sqrt{E_{(k),\ell}^{\mathrm{rc}}}$.

B. Protocol splitting

In general, a finite LOCC protocol consists of a certain number of steps, where in each step a particular party applies a family (Λ_k) of local quantum operations $\Lambda_k\colon\rho\mapsto A_k\rho A_k^\dagger$ with $\Lambda=\sum_k\Lambda_k$ trace preserving. These quantum operations depend on the course of the protocol so far and the measurement result k is always communicated to all parties. This situation can be depicted by a tree graph (cf. Fig. 1), where the children of each node correspond to a particular operation Λ_k, a level in the tree represents a particular protocol step, and each branch corresponds to a particular course of the protocol.

Hence, a finite LOCC protocol can be represented by a tree graph with root element, where to each node s of the tree, an operator $A_{(s)}$ is associated. (The associated operator for the root node is the identity operator.) For each node, the associated child operators $(A_{(c)})$ shall form a family of Kraus operators of a local CPTP map, i.e., all operators in $(A_{(c)})$ act only non-trivially on some

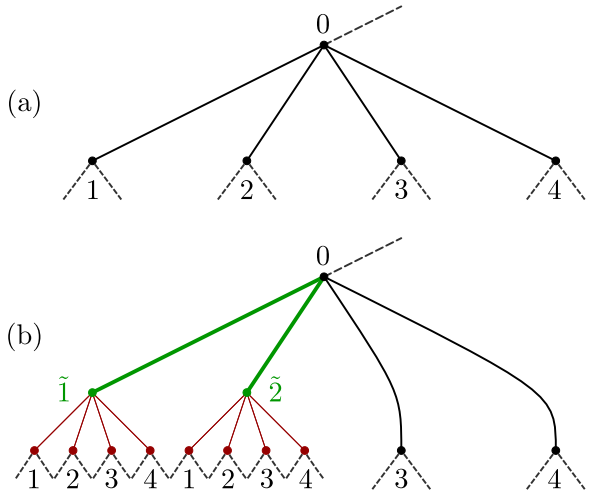

FIG. 2. Introduction of a pseudo-weak measurement and recovery step. Assume that $d(\mathfrak{I}|A_{B(1)}) \leq d(\mathfrak{I}|A_{B(2)}) < \delta$, while $\delta \leq d(\mathfrak{I}|A_{B(3)}) \leq d(\mathfrak{I}|A_{B(4)})$ in the original situation (a). In (b) the pseudo-weak measurement was introduced with $b_{(1)}$ and $b_{(2)}$ such that $d(\mathfrak{I}|A_{B(\tilde{1})}) = d(\mathfrak{I}|A_{B(\tilde{2})}) = \delta$ (thick green), while the operators at nodes 3 and 4 remain —up to a prefactor— unchanged. Then for the nodes $\tilde{1}$ and $\tilde{2}$ a recovery step is introduced (thin red), such that —up to a prefactor— in effect the original operators from the nodes 1 to 4 occur. Finally the according parts of the original protocol are added to the outcomes of the recovery measurements (dashed gray).

particular party. Then for any path P in this tree we associate an operator A_P as the product of the operators in reversed ordering: If $P = (s_1, \ldots, s_m)$, where s_k is the parent of s_{k+1}, then $A_P = A_{(s_m)} \cdots A_{(s_1)}$. Note that A_P is a product operator. For a node s we then denote by $B(s)$ the path connecting the root element with s (including the root element and s).

For an arbitrary δ with $0 < \delta < d(\mathfrak{I})$ (again, $\mathfrak{I}\colon X \mapsto \mathrm{tr}[X]$) we modify the protocol in an iterative procedure as follows (cf. Fig. 2). For any node s we denote by $D_\delta(s)$ the set of child nodes for which the deviation dropped below δ, i.e.,

$$D_\delta(s) = \{c \text{ is child of } s \mid d(\mathfrak{I}|A_{B(c)}) < \delta\}. \tag{7}$$

Let s be a node with non-empty set $D_\delta(s)$ but $d(\mathfrak{I}|A_{B(a)}) > \delta$ for any $a \in B(s)$. For such a node, the associated child operators $(A_{(c)})$ are replaced by the pseudo-weak implementation $(A^{\mathrm{pw}}_{(c)})$ with the parameters $(b_{(c)})$ (cf. Sec. III A) chosen such that $d(\mathfrak{I}|A^{\mathrm{pw}}_{(c)}A_{B(s)}) = \delta$ for all $c \in D_\delta(s)$ and $b_{(c)} = 0$ else. This is always possible, since regular deviation measures are continuous and the pseudo-weak measurement smoothly interpolates between $A_{(c)} \equiv V_{(c)}\sqrt{A^\dagger_{(c)}A_{(c)}}$ and $V_{(c)}$ for $b_{(c)} = 0 \ldots \infty$. For the nodes in $D_\delta(s)$ we add the recovery step as an additional level (the recovery measurement for the remaining child nodes would be trivial). After the recovery measurement, the according part of the original protocol is appended.

This procedure is repeated, until for all nodes s either $D_\delta(s)$ is empty or there exists an $a \in B(s)$ with $d(\mathfrak{I}|A_{B(a)}) = \delta$. It is important to note, that this procedure terminates after a finite number of steps. This is the case, since the number of candidates subject to modification decreases in each step of the procedure; the recovery levels are only introduced when $d(\mathfrak{I}|A_{B(s)}) = \delta$.

We denote by *stage I* of the protocol the part that does not enter the recovery steps, but rather terminates as soon as $d(\mathfrak{I}|A_{B(s)}) = \delta$ in the modified protocol.

C. Analysis of the best-case deviation

For the moment we only consider stage I of the modified protocol (with parameter δ). As an abbreviation we define for each leaf k of this stage the shorthand $A_k := A_{B(k)}$. Let us now define the set

$$S_\delta = \{k \text{ is leaf} \mid d(\mathfrak{I}|A_k) = \delta\}. \tag{8}$$

Due to our modification of the protocol, $k \notin S_\delta$ only if k was already a leaf in the original protocol with $d(\mathfrak{I}|A_k) > \delta$.

For each leaf k we let $\mathfrak{E}_k$ be the continuation of stage I of the modified protocol. With Π being the post-processing that "forgets" all results of any pseudo-weak measurement introduced by the protocol splitting (this are those results with parameter $b_{(c)} > 0$), the measurement

$$\mathfrak{E}\colon \rho \mapsto \Pi[\textstyle\bigoplus_k \mathfrak{E}_k(A_k \rho A_k^\dagger)] \tag{9}$$

is equivalent to the original protocol. Hence, due to property (ii) and (iii) of regular measures d, we have

$$d(\mathfrak{E}) \geq \min_k d(\mathfrak{E}_k|A_k) \geq \min[\delta, \min_{k\in S_\delta} d(\mathfrak{E}_k|A_k)]. \tag{10}$$

We now consider the case of $\hat{d} = 0$, i.e., for any $\varepsilon > 0$ there exists a protocol $\mathfrak{E}^\varepsilon$ with $d(\mathfrak{E}^\varepsilon) < \varepsilon$. Then for any δ with $0 < \delta < d(\mathfrak{I})$ and any ε with $0 < \varepsilon < \delta$ we have

$$\varepsilon > d(\mathfrak{E}^\varepsilon) \geq \min_{k\in S_\delta} d(\mathfrak{E}_k|A_k). \tag{11}$$

(Note that $\mathfrak{E}_k$ and A_k depend on δ and $\mathfrak{E}^\varepsilon$.) The right-hand side of this inequality can be further lower bounded by

$$y_\delta = \inf\{d(\mathfrak{G}|\sqrt{E}) \mid \mathfrak{G} \text{ is a finite LOCC measurement, } E \in M_\delta\}, \tag{12a}$$

where

$$\mathcal{M}_\delta = \{E \text{ is a product operator} \mid E \geq 0, \textstyle\sum_\mu \mathrm{tr}(\gamma_\mu E) = 1, \text{ and } d(\mathfrak{I}|\sqrt{E}) = \delta\}. \tag{12b}$$

This is a lower bound, since any $\mathfrak{E}_k$ is a finite LOCC measurement, $A_k^\dagger A_k/p_{A_k} \in \mathcal{M}_\delta$ [cf. Eq. (4); the case $p_{A_k} = 0$ cannot occur due to $\delta < d(\mathfrak{I})$], and due to property (ia) of regular deviation measures. We have an intermediate result:

$$\hat{d} = 0 \text{ only if } y_\delta = 0 \text{ for any } 0 < \delta < d(\mathfrak{I}). \tag{13}$$

The main use of this result is the reverse statement, where $y_\delta > 0$ for some δ shows that $\hat{d} > 0$. In this case we are not interested in the actual value of y_δ, and we therefore now aim to eliminate the infimum in the expression for y_δ.

D. Specialization to d_{mf}

The special property of the measure d_{mf}, as defined in Eq. (2), we are about to exploit is, that for the discrimination of N states, it is never advantageous to choose a measurement with more than N outcomes (for more than N outcomes one could always combine the results for which $\max_\nu p_\nu \mathfrak{E}(\rho_\nu)_k$ is achieved at $\mu = \nu$). Therefore, in order to make the set of measurements in the definition of y_δ [cf. Eq. (12a)] a compact set, we extend the allowed measurements to arbitrary global measurements [22], but at the same time consider only measurements with at most N outcomes.

We also assume that the kernels of the states (γ_μ) do not share a product vector, i.e., $\bigcap_\mu \ker \gamma_\mu$ contains no product vector (except 0). Let $E \in \mathcal{M}_\delta$, as defined in Eq. (12b), have the spectral decomposition $E = \sum_j e_j |j\rangle\langle j|$, where $|j\rangle$ are product vectors. Then with $R = \sum_\mu \gamma_\mu$ we have

$$1 = \operatorname{tr}(RE) \geq \min_j(\langle j|R|j\rangle) \max_j e_j \geq \eta_R \max_j e_j. \tag{14}$$

where $\eta_R = \inf \langle \xi|R|\xi\rangle$, with the infimum taken over *all* product vectors $|\xi\rangle$. Since the kernel of R contains no product vector, $\eta_R > 0$ and hence $e_j \leq 1/\eta_R$. This in turn shows that we can replace the condition $E \geq 0$ by the compact condition $\mathbb{1}/\eta_R \geq E \geq 0$. Due to the condition $\sum_\mu \operatorname{tr} \gamma_\mu E = 1$, we have $d(\mathfrak{I}|\sqrt{E}) = d[\mathfrak{I}; (\sqrt{E}\gamma_\mu\sqrt{E})]$ which shows due to the continuity of d, that the condition $d(\mathfrak{I}|\sqrt{E}) = \delta$ defines a compact set. Hence $\mathcal{M}_\delta$ as defined in Eq. (12b) itself is a compact set.

Together with the continuity of regular measures, it follows that $\hat{d}_{\mathrm{mf}} = 0$ only if there exists an operator E in $\mathcal{M}_\delta$ and a measurement $\mathfrak{G}$ with $d(\mathfrak{G}|\sqrt{E}) = 0$. Hence the states $(\sqrt{E}\gamma_\mu\sqrt{E})$ can be perfectly discriminated and thus are mutually orthogonal, i.e. $\operatorname{tr}(\gamma_\mu E \gamma_\nu E) = 0$ for $\mu \neq \nu$.

Finally, our argument is independent of the *a priori* probabilities $p_\mu > 0$, and we hence can choose them to be all equal (this maximizes $d_{\mathrm{mf}}(\mathfrak{I})$ to $1/N$ and hence the range of δ). The boundary cases $\delta = 0$ and $\delta = d_{\mathrm{mf}}(\mathfrak{I})$ are trivial to fulfill. Letting $\chi = 1 - \delta$, we arrive at our main result:

Proposition 1. *Let (ρ_μ) be a family of N states, such that $\bigcap_\mu \ker \rho_\mu$ contains no product vector (except 0).*

Then (ρ_μ) can be discriminated perfectly by asymptotic LOCC, $\hat{d}_{\mathrm{mf}} = 0$, only if for all χ with $1/N \leq \chi \leq 1$ there exists a product operator $E \geq 0$ obeying $\sum_\mu \operatorname{tr}(E\rho_\mu) = 1$, $\max_\mu \operatorname{tr}(E\rho_\mu) = \chi$, and $\operatorname{tr}(E\rho_\mu E\rho_\nu) = 0$ for $\mu \neq \nu$.

This necessary condition does not imply perfect discrimination for finite LOCC, as we will demonstrate in Section IV B. We mention, that the Proposition basically holds for any regular deviation measure d, for which the optimal general measurement strategy for N arbitrary states can be achieved using at most a certain fixed number of effects.

Note, that the precondition in Proposition 1 is not robust under trivial local embeddings: If a local Hilbert space $\mathcal{H}^{(s)}$ is extended to $\mathcal{H}^{(s)} \oplus \mathcal{H}'$, this condition will be violated. However, if $E' \in \mathcal{M}_\delta$, then the projection onto the original space $E' \mapsto E$ is still in $\mathcal{M}_\delta$ and $d(\mathfrak{G}|\sqrt{E}) = d(\mathfrak{G}|\sqrt{E'})$. Therefore, in the Proposition the embedding Hilbert space $\mathcal{H} = \bigotimes_r \mathcal{H}^{(r)}$ should be chosen as small as possible.

IV. EXAMPLES

A. Product bases

Let $(|\psi_\mu\rangle)$ be an orthonormal product basis of an N-dimensional Hilbert space $\mathcal{H} = \bigotimes_r \mathcal{H}^{(r)}$. We assume that the states $(|\psi_\mu\rangle\langle\psi_\mu|)$ can be discriminated by asymptotic LOCC and hence for any χ with $1/N \leq \chi \leq 1$ there exists an operator E obeying the conditions in Proposition 1. For $1/N < \chi < 1/(N-1)$, this operator E must be of full rank, but cannot be a multiple of the identity operator.

We choose some decompositions $|\psi_\mu\rangle = \bigotimes_r |\omega_\mu^{(r)}\rangle$ and $E = \bigotimes_r E^{(r)}$ with $E^{(r)} \geq 0$. Since $\langle\psi_\nu|E|\psi_\mu\rangle = 0$ if and only if $\mu \neq \nu$, it follows that $E|\psi_\mu\rangle = f_\mu|\psi_\mu\rangle$ with $f_\mu > 0$. Hence for any r we have $E^{(r)}|\omega_\mu^{(r)}\rangle = f_\mu^{(r)}|\omega_\mu^{(r)}\rangle$ with $f_\mu^{(r)} > 0$. It follows that a local measurement of the *observable* $E^{(r)}$ does not change any of the input states. Since for some subsystem s, the observable $E^{(s)}$ is not proportional to the identity operator, the measurement of $E^{(s)}$ separates the set of states in at least two non-empty subsets. Each of the subsets is again an orthonormal product basis of a subspace of $\mathcal{H}$ and each of the subsets inherits the property that it can be discriminated by asymptotic LOCC. By induction we arrive at

Proposition 2. *If a complete (product) basis can be discriminated perfectly by asymptotic LOCC ($\hat{d}_{\mathrm{mf}} = 0$) then it can already be discriminated perfectly by a finite LOCC measurement.*

Since $\hat{d}_{\mathrm{mf}} > 0$ implies $\hat{d}_{\mathrm{ce}} > 0$ [cf. Eqns. (2) and (3)], this Proposition in particular yields an analytical proof of the result of Bennett *et al.* in Ref. [13]. Unfortunately,

it is not straightforward to extend this type of argument to the situation of an unextendible product basis (then $|\psi_\mu\rangle$ is not necessarily an eigenstate of E.).

Remark. In Ref. [16] a proof was given that unextendible product bases cannot be discriminated by asymptotic LOCC. (Since a complete basis is also unextendible, this includes Proposition 2 as a special case.) While the statement is likely to hold, the proof given there is incomplete. In particular we question the argument below Eq. (16), showing that the quotient "M_N/c_N" converges to a constant for "$N \to \infty$" (in this expression N denotes the number of steps until the protocol is aborted). The argument for this convergence is quite general and should hold whenever finite discrimination is not possible (more precisely, if any local measurement either destroys orthogonality or is trivial). For the example in Sec. IV B, however, the quotient would diverge, since "c_N" is zero in this case.

B. When Proposition 1 does not decide

The previous example showed that for a wide class of examples, asymptotic LOCC does not provide an advantage over LOCC with finite resources. In this section we give an explicit example for which Proposition 1 does not help to decide whether perfect discrimination via asymptotic LOCC can be performed.

We aim to discriminate the following three mutually orthogonal states on a two-qubit system:

$$\begin{aligned} |\psi_1\rangle &= |00\rangle, \\ |\psi_2\rangle &\propto 2|01\rangle - (\sqrt{3}+1)|10\rangle - \sqrt{6}\sqrt[4]{3}|11\rangle, \\ |\psi_3\rangle &\propto 2|01\rangle - (\sqrt{3}-1)|10\rangle + \sqrt{2}\sqrt[4]{3}|11\rangle. \end{aligned} \tag{15}$$

In Ref. [18], Example 1 [23], it has been demonstrated, that this set of vectors can be discriminated perfectly by stochastic LOCC, while there exists no perfect discrimination strategy for LOCC in a finite number of steps. In fact, a local effect that does not destroy orthogonality is necessarily proportional to the identity operator.

The only state that is orthogonal to all $|\psi_\mu\rangle$ is entangled and hence we can apply Proposition 1. However, in the Appendix we construct an operator E_χ for $\frac{1}{3} \leq \chi \leq 1$, which satisfies the conditions from Proposition 1. Hence our necessary condition for perfect discrimination by asymptotic LOCC is satisfied, but Proposition 1 does not provide a sufficient criterion.

V. CONCLUSIONS

We considered the case of asymptotic local operations and classical communication for the discrimination of mutually orthogonal states and derived a necessary condition for perfect asymptotic discrimination to be possible. Our analysis yielded a general necessary condition, cf. Proposition 1, which consists of the existence of a certain product operator. As an example we showed, that any complete basis of product states can be discriminated perfectly by asymptotic LOCC if and only if they can already be discriminated in a finite number of rounds (cf. Proposition 2).

Our result allows to relatively easily exclude whether a family of states can be discriminated by asymptotic LOCC, however it is still unclear whether infinite resources can be of any advantage. Although the general intuition might be, that for perfect discrimination the asymptotic case is not superior, we identified an example, which could be a counter-example for this case as our necessary condition is fulfilled. However, as a sufficient criterion is not available, this question remains open.

ACKNOWLEDGMENTS

We thank O. Gittsovich, O. Gühne, B. Jungnitsch, B. Kraus, T. Moroder, S. Niekamp, and A. Thiel for helpful discussions. This work has been supported by the DFG and the Austrian Science Fund (FWF): Y376 N16 (START Prize) and SFB FOQUS.

Appendix: Construction of E_χ

In this Appendix we provide an operator E_χ for the states defined in Eq. (15). This operator satisfies the conditions from Proposition 1. We first define the local qubit-operator A_χ via

$$\begin{aligned} \langle 0|A_\chi|0\rangle &= -(12\sqrt{3}-21)\chi + 3\sqrt{3} - 3, \\ \langle 1|A_\chi|1\rangle &= (6\sqrt{3}-12)\chi - 2\sqrt{3} + 6, \\ \langle 0|A_\chi|1\rangle &= \sqrt{2\sqrt{3}-3}[(5\sqrt{3}-3)\chi - 2\sqrt{3}], \\ \langle 1|A_\chi|0\rangle &= \langle 0|A_\chi|1\rangle^*, \end{aligned} \tag{A.1}$$

and the diagonal operators B_χ and C_χ via

$$\begin{aligned} \langle 0|B_\chi|0\rangle &= 20\chi + 2\tilde{\chi} - 4, \\ \langle 1|B_\chi|1\rangle &= (12-\sqrt{3})\chi + \tilde{\chi} + \sqrt{3} - 1, \end{aligned} \tag{A.2}$$

and

$$\begin{aligned} \langle 0|C_\chi|0\rangle &= -(4+3\sqrt{3})\chi - \tilde{\chi} + 3\sqrt{3} + 5, \\ \langle 1|C_\chi|1\rangle &= \langle 1|B_\chi|1\rangle, \end{aligned} \tag{A.3}$$

where

$$\tilde{\chi} = \sqrt{(115-8\sqrt{3})\chi^2 - (46-10\sqrt{3})\chi - 2\sqrt{3} + 4}. \tag{A.4}$$

Then with

$$\tilde{E}_\chi = \begin{cases} B_\chi \otimes C_\chi & \text{if } \chi < 1/2 \\ A_\chi \otimes |1\rangle\langle 1| & \text{else.} \end{cases} \tag{A.5}$$

we finally let $E_\chi = \tilde{E}_\chi / \sum_\mu \langle \psi_\mu | \tilde{E}_\chi | \psi_\mu \rangle$. One readily verifies that E_χ has the desired properties.

[1] R. Horodecki, P. Horodecki, M. Horodecki, and K. Horodecki, Rev. Mod. Phys. **81**, 865 (2009).
[2] O. Gühne and G. Tóth, Phys. Rep. **474**, 1 (2009).
[3] S. Ghosh, G. Kar, A. Roy, A. Sen(De), and U. Sen, Phys. Rev. Lett. **87**, 277902 (2001).
[4] B. M. Terhal, D. P. DiVincenzo, and D. W. Leung, Phys. Rev. Lett. **86**, 5807 (2001).
[5] M. Horodecki, A. Sen(De), U. Sen, and K. Horodecki, Phys. Rev. Lett. **90**, 047902 (2003).
[6] S. Ghosh, G. Kar, A. Roy, and D. Sarkar, Phys. Rev. A **70**, 022304 (2004).
[7] Y.-X. Chen and D. Yang, Phys. Rev. A **64**, 064303 (2001).
[8] P.-X. Chen and C.-Z. Li, Phys. Rev. A **68**, 062107 (2003); Phys. Rev. A **70**, 022306 (2004).
[9] M. Nathanson, J. Math. Phys. **46**, 062103 (2005).
[10] J. Watrous, Phys. Rev. Lett. **95**, 080505 (2005).
[11] R. Duan, Y. Xin, and M. Ying, Phys. Rev. A **81**, 032329 (2010).
[12] J. Walgate, A. J. Short, L. Hardy, and V. Vedral, Phys. Rev. Lett. **85**, 4972 (2000).
[13] C. H. Bennett, D. P. DiVincenzo, C. A. Fuchs, T. Mor, E. Rains, P. W. Shor, J. A. Smolin, and W. K. Wootters, Phys. Rev. A **59**, 1070 (1999).
[14] M. Renninger, Z. f. Phys. A **158**, 417 (1960).
[15] R. H. Dicke, Am. J. Phys. **49**, 925 (1981).
[16] S. De Rinaldis, Phys. Rev. A **70**, 022309 (2004).
[17] A stochastic LOCC measurement is a measurement that can be implemented by means of LOCC with a certain probability $p > 0$, while with probability $1 - p$ the measurement will fail. Stochastic LOCC measurements are exactly those with separable effects as in Eq. (1) and hence the alternative name *separable measurements* has also been used.
[18] R. Duan, Y. Feng, Y. Xin, and M. Ying, IEEE Trans. Inform. Th. **55**, 1320 (2009).
[19] H. Barnum, M. A. Nielsen, and B. Schumacher, Phys. Rev. A **57**, 4153 (1998).
[20] In order to see this, note that for any probability distribution $P = (p_\mu)$ we have $1-\max_\mu p_\mu \leq -\log_b \max_\mu p_\mu \leq H(P)$ for any base $1 < b \leq \mathrm{e}$.
[21] A classical post-processing can be described by a stochastic matrix $\pi_{\ell|k}$ with $\sum_\ell \pi_{\ell|k} = 1$, such that $\Pi[\mathfrak{E}(\rho)]_\ell = \sum_k \pi_{\ell|k} \mathfrak{E}(\rho)_k$.
[22] Using global measurements yields a rather rough estimate. One could also choose the set of fully separable measurements as defined in Eq. (1). Then Proposition 1 would contain the additional restriction, that the states must allow a discrimination by separable measurements after result E. This condition, however, is difficult to evaluate and hence we only cover the simpler case of global measurements here.
[23] We chose $\alpha = \pi/12$, $\beta = \pi/6$, and $\tan\gamma = 3^{-1/4}$ and different local bases.

MEMORY COST OF QUANTUM CONTEXTUALITY

MATTHIAS KLEINMANN[1,2], OTFRIED GÜHNE[1,2,3], JOSÉ R PORTILLO[4], JAN-ÅKE LARSSON[5] AND ADÁN CABELLO[6,7]

Abstract. The simulation of quantum effects requires certain classical resources, and quantifying them is an important step in order to characterize the difference between quantum and classical physics. For a simulation of the phenomenon of state-independent quantum contextuality, we show that the minimal amount of memory used by the simulation is the critical resource. We derive optimal simulation strategies for important cases and prove that reproducing the results of sequential measurements on a two-qubit system requires more memory than the information carrying capacity of the system.

1. Introduction

According to quantum mechanics, the result of a measurement may depend on which other compatible observables are measured simultaneously [1–3]. This property is called contextuality and is in contrast to classical physics, where the answer to a single question does not depend on which other compatible questions are asked at the same time.

Contextuality can be seen as complementary to the well known nonlocality of distributed quantum systems [4]. Both phenomena can be used for information processing tasks, albeit the applications of contextuality are far less explored [5–12]. Although contextuality and nonlocality can be considered as signatures of nonclassicality, they can be simulated by classical models [3, 13–15]. However, while nonlocal classical models violate a fundamental physical principle (the bounded speed of information), it is not clear whether contextual classical models violate any fundamental principle. Moreover, while the resources needed in order to imitate quantum nonlocality have been extensively investigated [16–18], there is no similar knowledge about the resources needed to simulate quantum contextuality.

In any model which exhibits contextuality in sequential measurements, the system will eventually attain different internal states during certain measurement sequences. These states can be considered as *memory* — a model attaining the minimal number of states is then memory-optimal and defines the memory cost. In this paper we investigate the memory cost as the critical resource in a classical simulation of quantum contextuality and we construct memory-optimal models for relevant cases. The amount of required memory increases as we consider more and more contextuality constraints. This can be used to quantify contextuality in a given quantum setting. We show that certain scenarios breach the amount of two

[1] Institut für Quantenoptik und Quanteninformation, Österreichische Akademie der Wissenschaften, Technikerstr. 21A, A-6020 Innsbruck, Austria.
[2] Universität Siegen, Fachbereich Physik, Walter-Flex-Straße 3, D-57068 Siegen, Germany.
[3] Institut für Theoretische Physik, Universität Innsbruck, Technikerstr. 25, A-6020 Innsbruck, Austria.
[4] Departamento de Mathemática Aplicada I, Universidad de Sevilla, E-41012 Sevilla, Spain.
[5] Institutionen för Systemteknik och Matematiska Institutionen, Linköpings Universitet, SE-581 83 Linköping, Sweden.
[6] Departamento de Física Aplicada II, Universidad de Sevilla, E-41012 Sevilla, Spain.
[7] Department of Physics, Stockholm University, S-10691 Stockholm, Sweden.

bits needed for the simulation of two qubits. This demonstrates that the memory needed to simulate only a small set of measurements on a quantum system may exceed the information that can be transmitted using this system (given by the Holevo bound [19]) — a similar effect was observed so far only for the classical simulation of a *unitary* evolution [20].

2. Scenario

We focus on the following set of two-qubit observables, also known as the Peres-Mermin (PM) square [4, 21],

$$\begin{bmatrix} A & B & C \\ a & b & c \\ \alpha & \beta & \gamma \end{bmatrix} = \begin{bmatrix} \sigma_z \otimes \mathbb{1} & \mathbb{1} \otimes \sigma_z & \sigma_z \otimes \sigma_z \\ \mathbb{1} \otimes \sigma_x & \sigma_x \otimes \mathbb{1} & \sigma_x \otimes \sigma_x \\ \sigma_z \otimes \sigma_x & \sigma_x \otimes \sigma_z & \sigma_y \otimes \sigma_y \end{bmatrix}, \tag{1}$$

where σ_x, σ_y, and σ_z denote the Pauli operators. The square is constructed such that the observables within each row and column commute and are hence compatible, and the product of the operators in a row or column yields $\mathbb{1}$, except for the last column where it yields $-\mathbb{1}$. Thus the product of the measurement results for each row and column will be $+1$ except in the third column where it will be -1. In contrast, for a noncontextual model the measurement result for each observable must not depend on whether the observable is measured in the column or row context. Hence the number of rows and columns yielding a product of -1 is always even, as any observable appears twice.

Similar to the Bell inequalities for local models, any noncontextual model satisfies the inequality

$$\langle \chi \rangle \equiv \langle ABC \rangle + \langle abc \rangle + \langle \alpha\beta\gamma \rangle + \langle Aa\alpha \rangle + \langle Bb\beta \rangle - \langle Cc\gamma \rangle \leq 4, \tag{2}$$

while for perfect observables quantum mechanics (QM) predicts $\langle \chi \rangle = 6$ [22]. Here, the term $\langle ABC \rangle$ denotes the average value of the product of the outcomes of A, B, and C, if these observables are measured simultaneously or in sequence on the same quantum system. The violation is independent of the quantum state, which emphasizes that the phenomenon is a property of the set of observables rather than of a particular quantum state.

Recently, this inequality has been experimentally tested using trapped ions [23], photons [24], and nuclear magnetic resonance systems [25]. The results show a good agreement with the quantum predictions. In these experiments, the observables are measured in a sequential manner. Since the observed results cannot be explained by a model using only preassigned values, the system necessarily attains different states during some particular sequences, i.e., the system memorizes previous events. (Note that also in QM the system attains different states during the measurement sequences.) This leads to our central question: *How much memory is required in order to simulate quantum contextuality?*

3. A first model

Before we formulate the previous question more precisely, let us provide an example of a model that simulates the contextuality in the PM square. We assume that the system can only attain 3 different physical states S_1, S_2, and S_3 (e.g. discrete points in phase-space). Let us associate a table to each state via

$$S_1 : \begin{bmatrix} + & + & (+,2) \\ + & + & (+,3) \\ + & + & + \end{bmatrix}, \quad S_2 : \begin{bmatrix} + & (+,1) & + \\ - & + & - \\ - & (-,3) & + \end{bmatrix}, \quad S_3 : \begin{bmatrix} + & - & - \\ (+,1) & + & + \\ (-,2) & - & + \end{bmatrix}. \tag{3}$$

Those tables define the model's behavior in the following way: If e.g. the system is in state S_1 and we measure the observable γ, consider the first table at the

position of γ (i.e., the last entry in the third row). The $+$ sign at this position indicates that the measurement result will be $+1$, while the system stays in state S_1. If we continue and measure C, we encounter the entry $(+, 2)$ which indicates the measurement result $+1$ and a subsequent change to the state S_2. Being in state S_2, the second table defines the behavior for the next measurement: For instance a measurement of c yields now the result -1 and the system stays in state S_2.

Thus, starting in state S_1, the measurement results for the sequence γCc are $+1, +1, -1$, so that the product is -1 in accordance with the quantum prediction. It is straightforward to verify that this model yields $\langle \chi \rangle = 6$. In addition, the observables within each context are compatible in the sense that in sequences of the form AA, ABA, or $A\alpha aA$, the first and last measurement of A yields the same output. In fact this particular model is *memory-optimal* (cf. Theorem 1) and we assign the symbol $\mathcal{A}_3$ to it.

4. Memory cost of classical models

Any model that reproduces contextuality eventually predicts that the system attains different states during some measurement sequences. As an omniscient observer one would know the state prior to each measurement and could include it in the measurement record. Thus, knowing the state of the system, one can predict the measurement outcome as well as the state of the system that will occur prior to the next measurement. Thus we can write any model that explains the outcomes of sequential measurements in the same fashion as we did for $\mathcal{A}_3$.

Taking a different point of view, any such model can be considered to be an automaton with finitely many internal states, taking inputs (measurement settings) and yielding outputs (measurement results). In our notation, the output depends not only on the internal state, but also on the input. Such automatons are known as Mealy machines [26, 27].

The quantum predictions add restrictions on such an automaton and thus increase the number of internal states needed. As a simple example we could require that an automaton reproduces the quantum predictions from the rows and columns in the PM square. That is, for all sequences in the set

$$\mathscr{Q}_{\mathrm{rc}} = \{ABC, abc, \alpha\beta\gamma, Aa\alpha, Bb\gamma, Cc\gamma, \text{ and permutations}\}, \tag{4}$$

we require that the automaton must yield an output that matches the quantum prediction. For example, QM predicts for the sequence ABC that the output is either $+1, +1, +1$ or one of the permutations of $+1, -1, -1$.

More generally, if $\mathscr{Q}$ denotes a set of measurement sequences, we say that an automaton $\mathcal{A}$ *obeys* the set $\mathscr{Q}$ if the output for any sequence in $\mathscr{Q}$ matches the quantum prediction — i.e., if for any sequence in $\mathscr{Q}$, the output of $\mathcal{A}$ could have occurred with a nonvanishing probability according to the quantum scenario. We say that a sequence *yields a contradiction* if the output of this sequence cannot occur according to QM. Hereby we consider all quantum predictions from any initial state (it would also suffice to only consider the completely mixed state $\varrho = \mathbb{1}/\operatorname{tr}[\mathbb{1}]$). Furthermore, we assume that prior to the measurement of a sequence, the automaton always is re-initialized. This ensures that the output of the automaton is independent of any action prior to the selected measurement sequence. Note that we only consider the *certain* quantum predictions which occur with a probability of 1, while e.g. in the PM square we do not require that for the sequence $A\gamma$ the probability of obtaining $+1, +1$ is equal to the probability of obtaining $+1, -1$. Finally, if an automaton with k states $S_1, \ldots, S_k$ obeys $\mathscr{Q}$ and there exists no automaton with less states obeying $\mathscr{Q}$, we define the *memory cost* of $\mathscr{Q}$ to be $\mathrm{M}(\mathscr{Q}) = \log_2(k)$.

5. Contextuality conditions

Our definition of memory cost so far applies to arbitrary situations, even those in which contextuality does not directly play a role. In contrast, contextuality of sequential measurements corresponds to the particular feature, that certain sequences of mutually compatible observables cannot be explained by a model with preassigned values (cf. Ref. [28] for a detailed discussion). The contextuality conditions for observables $X_1, X_2, \ldots$ thus arise from the set of all sequences of mutually compatible observables,

$$\mathscr{Q}_{\text{context}} = \{X_1 X_2 \ldots \mid X_\ell \text{ mutually compatible}\}. \tag{5}$$

If the choice of observables $X_1, X_2, \ldots$ exhibits contextuality, then $\mathrm{M}(\mathscr{Q}_{\text{context}}) > 0$. — In the case of the PM square, $\mathscr{Q}_{\text{context}}$ surely contains all the row and column sequences that we included in $\mathscr{Q}_{\text{rc}}$. In addition, however, $\mathscr{Q}_{\text{context}}$ contains e.g. the sequences AA, ABA, and $A\alpha aA$, for which QM predicts with certainty a repetition of the value of A in the first and last instance. Note, that the set $\mathscr{Q}_{\text{context}}$ also contains more complicated sequences like $ACABCA$ for which QM predicts with certainty that the values of A (C) in the first, third and sixth (second and fifth) measurement coincide, and that product of the outcome for ABC yields $+1$.

A particular feature of contextuality is that one can find observables that exhibit contextuality independent of the actual preparation (the initial state) of the quantum system. Consequently, one may consider an extended preparation procedure of the automaton, where the experimenter performs additional measurements between the initialization of the automaton and the actual sequence. The experimenter would e.g. measure the sequence $bABC$ but consider the measurement of the observable b to be actually part of the preparation procedure. We write $\lfloor b \rfloor ABC$ for a sequence where we are not interested in the result of b. If $\mathscr{Q}_{\text{all}}$ denotes the set of all sequences with observables $X_1, X_2, \ldots$, we write

$$\mathscr{Q}'_{\text{context}} = \{\lfloor T \rfloor S \mid S \in \mathscr{Q}_{\text{context}}, T \in \mathscr{Q}_{\text{all}}\} \tag{6}$$

for the set of all sequences in $\mathscr{Q}_{\text{context}}$, including arbitrary preparation procedures.

For the contextuality in the PM square, the automaton $\mathcal{A}_3$ obeys $\mathscr{Q}_{\text{context}}$, while no automaton with less than 3 states can obey $\mathscr{Q}_{\text{context}}$, cf. Appendix A for details. We did not specify an initial state for $\mathcal{A}_3$ and indeed the contextuality conditions are obeyed for any initial state. We summarize:

Theorem 1. *The memory cost for the contextuality correlations $\mathscr{Q}'_{\text{context}}$ in the PM square is $\log_2(3) \approx 1.58$ bits; $\mathrm{M}(\mathscr{Q}'_{\text{context}}) = \mathrm{M}(\mathscr{Q}_{\text{context}}) = \log_2(3)$. Consequently, the automaton $\mathcal{A}_3$ is memory-optimal.*

6. Compatibility conditions

The set $\mathscr{Q}_{\text{context}}$ contains all sequences of mutually compatible observables, but does not contain sequences like $ABaA$, for which QM also predicts that both occurring values of A are the same. Sequences of this form enforce that all observables compatible with an observable Y must not change the measurement result of Y. This can be covered by the set of all compatibility conditions

$$\mathscr{Q}_{\text{compat}} = \{Y \lfloor X_1 X_2 \ldots \rfloor Y \mid X_\ell \text{ compatible to } Y\}, \tag{7}$$

and a convincing test of contextuality must also test the correlations due to this set of sequences. Again we define $\mathscr{Q}'_{\text{compat}}$ to include arbitrary preparation procedures.

The automaton $\mathcal{A}_3$ does not obey $\mathscr{Q}_{\text{compat}}$, since e.g. starting with state S_1, the sequence $B\lfloor C\beta \rfloor B$ yields the record $+1, \lfloor +1, -1, \rfloor -1$ and hence violates the assumption of compatibility; similar sequences can be found for any initial state. We show in Appendix D that no automaton with three states can obey simultaneously

$\mathscr{Q}'_{\text{compat}}$ and $\mathscr{Q}'_{\text{context}}$ and hence $\mathrm{M}(\mathscr{Q}'_{\text{compat}}$ and $\mathscr{Q}'_{\text{context}}) \geq 2$. However, there exist automata with four internal states which obey $\mathscr{Q}'_{\text{compat}}$ and $\mathscr{Q}'_{\text{context}}$. As an example of such an automaton we define $\mathcal{A}_4$ via

$$S_1\colon \begin{bmatrix} + & + & (+,2) \\ + & + & (+,3) \\ + & + & + \end{bmatrix},\quad S_2\colon \begin{bmatrix} + & + & + \\ - & + & - \\ (-,4) & (+,1) & + \end{bmatrix},$$
$$S_3\colon \begin{bmatrix} + & - & - \\ + & + & + \\ (+,1) & (-,4) & + \end{bmatrix},\quad S_4\colon \begin{bmatrix} + & - & (-,3) \\ - & + & (-,2) \\ - & - & + \end{bmatrix}. \tag{8}$$

Similar to the situation for $\mathcal{A}_3$, the initial state for the automaton $\mathcal{A}_4$ can be chosen freely; we refer to Appendix B for details. So we have:

Theorem 2. *The memory cost of for the contextuality and compatibility correlations in the PM square is two bits;* $\mathrm{M}(\mathscr{Q}'_{\text{compat}}$ *and* $\mathscr{Q}'_{\text{context}}) = 2$. *Consequently, the automaton* $\mathcal{A}_4$ *is memory-optimal.*

7. Extended Peres-Mermin square

There are, however, further contextuality effects for two qubits which then require more than two bits for a simulation. Namely, in Ref. [29] an extension of the PM square has been introduced, involving 15 different observables in 15 different contexts. The argument goes as follows: Consider the 15 observables of the type $\sigma_\mu \otimes \sigma_\nu$ where $\mu, \nu \in \{0, x, y, z\}$ and $\sigma_0 = \mathbb{1}$ and the case $\mu = \nu = 0$ is excluded. In this set there are 12 trios of mutually compatible observables such that the product of their results is always $+1$, like $[\sigma_x \otimes \mathbb{1}, \mathbb{1} \otimes \sigma_y, \sigma_x \otimes \sigma_y]$ and $[\sigma_x \otimes \sigma_y, \sigma_y \otimes \sigma_x, \sigma_z \otimes \sigma_z]$, and three trios of mutually compatible observables such that the product of their results is always -1, like $[\sigma_x \otimes \sigma_y, \sigma_y \otimes \sigma_z, \sigma_z \otimes \sigma_x]$. This leads to 15 contexts in total. Similar to the usual PM square, one can derive an state independent inequality. For this inequality, QM predicts a value of 15 for the total sum, while noncontextual models have a maximal value of 9, cf. Ref. [29] and Appendix E for details.

One may argue that this new contextuality argument is stronger than the usual PM square [29]. Does a simulation of it require more memory than the original PM square? Indeed, this is the case:

Theorem 3. *The memory cost for the contextuality and compatibility correlations in the extended version of the PM square is strictly larger than two bits.*

More precisely, according to Eqns. (5) and (7) we define the contextuality sequences $\mathscr{Q}'_{\text{compat},15}$ and compatibility sequences $\mathscr{Q}'_{\text{context},15}$ for the 15 observables in the extension of the PM square. Then, the theorem states that $\mathrm{M}(\mathscr{Q}'_{\text{compat},15}$ and $\mathscr{Q}'_{\text{context},15}) > 2$. The proof is based on the following idea: If one considers the 15 contexts in the extended square then they can be arranged in a collection of 10 distinct squares, each similar to the usual PM square. The contextuality in this arrangement is strong enough such that for each fixed assignment of the output, one must have *three* contradictions for one of the 10 usual PM squares. One can show, however, that any four-state solution obeying $\mathscr{Q}'_{\text{context}}$ and $\mathscr{Q}'_{\text{compat}}$ is similar to $\mathcal{A}_4$, in which for no fixed state one has three contradictions. The full proof is given in Appendix E.

Although in this paper we are mainly concerned about the memory cost of contextuality, we mention that the simulation of all certain quantum predictions of the PM square already requires more than two bits of memory. In fact, any four-state automaton that obeys $\mathscr{Q}'_{\text{compat}}$ and $\mathscr{Q}'_{\text{context}}$ is up to some symmetries of the form

of $\mathcal{A}_4$ (cf. Appendix E, Proposition 5), but for $\mathcal{A}_4$ the sequence $\lfloor\beta\rfloor ab\lfloor C\rfloor c$ yields a contradiction. This proves that $\mathrm{M}(\mathscr{Q}_{\mathrm{all}}) > 2$.

On the other hand, QM itself suggests an automaton for simulating contextuality. If e.g. we choose the pure state $|\phi\rangle\langle\phi|$ defined by $A|\phi\rangle = B|\phi\rangle = |\phi\rangle$ as initial state, then this state and all the states occurring during measurement sequences define an (nondeterministic) automaton. By a straightforward calculation one finds that this automaton attains 24 different states if we consider the set of all sequences $\mathscr{Q}_{\mathrm{all}}$. By a suitable elimination of the nondeterminism, we can readily reduce the number of states to 10 (cf. Appendix F) yielding an upper bound on the required memory and hence $2 < \mathrm{M}(\mathscr{Q}_{\mathrm{all}}) \leq \log_2(10) \approx 3.32$.

8. Conclusions

We have investigated the amount of memory needed in order to simulate quantum contextuality in sequential measurements. We determined the memory-optimal automata for important cases and have proven that the simulation of contextuality phenomena for two qubits requires more than two classical bits of memory. However, the maximal amount of classical information that can be stored and retrieved in two qubits is well known to be limited to two bits [19]. This implies that any classical model of such a system either would allow to store and retrieve more than two bits or would have inaccessible degrees of freedom. (An example of the latter is $\mathcal{A}_3$, since one cannot perfectly infer the initial state from the results of any measurement sequence.)

It should be emphasized that our analysis is about the memory that is needed to classically simulate the *certain* predictions from measurement *sequences* on a quantum system. In contrast, one may ask how many different states are needed to merely explain the observed expectation values [30–35]. However, the number of states needed in this scenario measures the number of different initial configurations of the system, while we have shown that even for a fixed initial configuration, the system must eventually attain a certain number of states during measurement sequences. Similarly, it has been demonstrated that a hybrid system of one qubit and one classical bit of memory is *on average* superior to a classical system having only access to a single bit of memory [36] – while we show in Theorem 1, that for a two-qubit system, even the certain predictions cannot be simulated with one classical bit of memory.

Our work provides a link between information theoretical concepts on the one side and quantum contextuality and the Kochen-Specker theorem on the other side. While for Bell's theorem such connections are well explored and have given deep insights into QM [18, 37, 38], for contextuality many questions remain open: If an experiment violates some noncontextuality inequality up to a certain degree, but not maximally, what memory is required to simulate this behavior? Can nondeterministic machines help to simulate contextuality? What amount of memory and randomness is required to simulate all quantum effects in the PM square, especially in the distributed setting [12]? Finally, for quantum non-locality it has been extensively investigated why QM does not exhibit the maximal non-locality [37, 38]. A similar situation occurs for quantum contextuality — can concepts from information theory also help to understand the nonmaximal violation in this situation?

Acknowledgments

The authors thank E. Amselem, P. Badziąg, J. Barrett, I. Bengtsson, M. Bourennane, Č. Brukner, P. Horodecki, A. R. Plastino, M. Rådmark, and V. Scholz for discussions. This work has been supported by the Austrian Science Fund (FWF): Y376

N16 (START Prize) and SFB FOQUS, the MICINN Projects MTM2008-05866 and FIS2008-05596, the Wenner-Gren Foundation, and the EU (QICS, NAMEQUAM, Marie Curie CIG 293993/ENFOQI).

Appendix A. $\mathcal{A}_3$ is optimal

We already defined the set of row and column sequences $\mathscr{Q}_{\rm rc}$ in Eq. (4). Another natural constraint is given by the set of repeated measurements

$$\mathscr{Q}_{\rm repeat} = \{AA, BB, CC, aa, bb, cc, \alpha\alpha, \beta\beta, \gamma\gamma\}, \tag{9}$$

where we expect for any of these pairs that the results in the first and the second measurement coincide. Both sets $\mathscr{Q}_{\rm rc}$ and $\mathscr{Q}_{\rm repeat}$ obviously are subsets of the set of contextuality sequences $\mathscr{Q}_{\rm context}$ of the PM square. Nevertheless, an automaton that simultaneously obeys $\mathscr{Q}_{\rm rc}$ and $\mathscr{Q}_{\rm repeat}$ already possesses more than two internal states, i.e. M($\mathscr{Q}_{\rm rc}$ and $\mathscr{Q}_{\rm repeat}$) > 1. In order to see this, assume that the automaton has only two internal states and without loss of generality that it starts in state S_1. We consider the case where in the last column there must be a prescribed state change in order to avoid a contradiction, i.e., in S_1 the product of the assignments of $Cc\gamma$ is $+1$, contrary to the quantum prediction. Note that there always exists at least one row or column with such a contradiction, and that the proof for any row or column follows the same lines. If there is only one state change (say after a measurement of γ), then, while measuring the sequence $Cc\gamma$, the automaton would remain in S_1 until after the last output and therefore yield a contradiction. If there are two (or more) state changes in the last column (say c and γ), both must go to S_2. Then, the constraints from $\mathscr{Q}_{\rm repeat}$ require that γ has the same values in S_1 and S_2 (this is also true for c). But then the sequence $Cc\gamma$ in $\mathscr{Q}_{\rm rc}$ will yield a contradiction. Thus a two-state automaton cannot obey both, $\mathscr{Q}_{\rm rc}$ and $\mathscr{Q}_{\rm repeat}$.

On the other hand, $\mathcal{A}_3$ is an example of a 3 state automaton, which obeys $\mathscr{Q}_{\rm rc}$ and $\mathscr{Q}_{\rm repeat}$. In fact $\mathcal{A}_3$ obeys $\mathscr{Q}'_{\rm context}$. In order to see this, it is enough to show, that for any choice of the initial state, the automaton will obey $\mathscr{Q}_{\rm context}$. So we assume that S_1 is the initial state; the reasoning for S_2 and S_3 is similar. If we now measure a sequence with observables from the first row only, we may jump between the states S_1 and S_2, but the output for all observables in the first row are the same for either state. A similar argument holds for all rows and the first and second column. For a sequence with measurements from the third column, assume that the first observable in the sequence, that is not γ, is the observable c. Then the state changes to S_3, in which the last column does not yield a contradiction. Since only the output C was changed, but C was not measured so far, we cannot get any contradiction. A similar argument can be used for the case where the first observable in the sequence, that is not γ, is the observable C.

In summary, since any automaton that obeys $\mathscr{Q}_{\rm context}$ has at least 3 states and $\mathcal{A}_3$ is a 3 state automaton obeying the larger set $\mathscr{Q}'_{\rm context}$, we have shown that $\mathcal{A}_3$ is memory-optimal for either set.

Appendix B. $\mathcal{A}_4$ obeys $\mathscr{Q}'_{\rm context}$ and $\mathscr{Q}'_{\rm compat}$

In this Appendix we demonstrate that the automaton $\mathcal{A}_4$ indeed obeys $\mathscr{Q}'_{\rm context}$ and $\mathscr{Q}'_{\rm compat}$. The proof for $\mathscr{Q}'_{\rm context}$ is completely analogous to the one in Appendix A.

For $\mathscr{Q}'_{\rm compat}$, we consider a fixed observable, e.g. B. Then S_1 and S_2 yield $+1$ while S_3 and S_4 give -1. However, using arbitrary measurements compatible to B, (i.e., A, B, C, b, and β) we can never reach S_3 or S_4 if we start from S_1 or S_2 and *vice versa*. Hence no contradiction occurs for any sequence of the type $\lfloor T \rfloor B \lfloor X_1 X_2 \ldots \rfloor B$. A similar argument holds for all observables, if we note in

addition that e.g. after a measurement of C the automaton can only be in S_2 or S_3.

Appendix C. Definitions and basic rules used in the optimality proofs

As we already did in the main text, we denote the observables from the PM square by

$$\begin{bmatrix} A & B & C \\ a & b & c \\ \alpha & \beta & \gamma \end{bmatrix}. \tag{10}$$

Furthermore, we denote the rows of the square by $\mathbf{R}_i$, and the columns by $\mathbf{C}_i$. The value table of each memory state i is denoted by T_i and the update table by U_i. We write an entry of zero in U_i, if the state does not change for that observable. Furthermore, we write measurement sequences as $A_1^+ B_2^- C_2^- a_3^+$ meaning that when the sequence $ABCa$ was measured, the results were $+,-,-,+$, and the memory was initially in state S_1 and changed like $S_1 \mapsto S_2 \mapsto S_2 \mapsto S_3$.

It will be useful for our later discussion to note some rules about the structure of the value and update tables.

1. *Sign flips:* Let us assume that we have an automaton obeying $\mathscr{Q}'_{\text{context}}$ and $\mathscr{Q}'_{\text{compat}}$ (or some subset of those sets) and pick a 2×2 square of observables (e.g., the set $\{A, B, a, b\}$ or $\{A, B, \alpha, \beta\}$ or $\{A, C, \alpha, \gamma\}$). Then, if we flip in each T_i the signs corresponding to these observables, we will obtain another valid automaton.

   This holds true, because the mentioned sign flips do not change any of the certain quantum predictions from $\mathscr{Q}'_{\text{context}}$ or $\mathscr{Q}'_{\text{compat}}$. This rule will allow us later to fix one or two entries in a given value table T_i.
2. *Number of contradictions:* Any table T_i contains either one, three, or five contradictions to the row and column constraints.

   This follows directly from that fact that any fixed assignment fulfills $\prod_k \mathbf{R}_k \mathbf{C}_k = +1$, while the row and column constraints require $\prod_k \mathbf{R}_k \mathbf{C}_k = -1$.
3. *Condition for fixing the memory:* Let us assume that we have an automaton obeying $\mathscr{Q}'_{\text{context}}$ and let there be a table T_i which assigns to an observable (say A) a value different from all other tables. Then, the update table U_i must contain only zeroes in the corresponding row and column (here, $\mathbf{R}_1$ and $\mathbf{C}_1$).

   The observables in the row and column correspond to compatible observables, which are not allowed to change the value of the first observable. However, any change of the memory state would change the value, as T_i is the only table with the initial assignment.
4. *Contradictions and transformations:* Let us assume that we have an automaton obeying $\mathscr{Q}'_{\text{context}}$ and let there be in T_i some contradiction in the column $\mathbf{C}_j$ (or the row $\mathbf{R}_j$). Then, in the update table U_i there cannot be two zeroes in the the column $\mathbf{C}_j$ (or the row $\mathbf{R}_j$).

   If there were two zeroes, it could happen that one measures two entries of $\mathbf{C}_j$ without changing the memory state. But then measuring the third one will reveal the contradiction in T_i. (Note that the automaton first provides the result and then updates its state.)
5. *Contradictions and other tables:* Let us assume that we have an automaton obeying $\mathscr{Q}'_{\text{context}}$ and let there be in T_i a contradiction in the column $\mathbf{C}_j$ (or the row $\mathbf{R}_j$). Then, there must be two different tables T_k and T_l where in both the column $\mathbf{C}_j$ has no contradictions anymore, but the assignments of T_k and T_l differ in two observables of $\mathbf{C}_j$. Furthermore, in the column

$\mathbf{C}_j$ of the update table U_i there must be two entries leading to two different states.

First, note that there must be at least one other table T_k where the contradiction does not exist anymore. This follows from the fact that we may measure $\mathbf{C}_j$ starting from the memory state i. After having made these measurements, we arrive at some state k, and from the contextuality correlations $\mathscr{Q}'_{\text{context}}$ it follows that $\mathbf{C}_j$ in T_k has no contradiction.

The table T_k differs from T_i in at least one observable X in $\mathbf{C}_j$. On the other hand, starting from T_i one might measure X as a first observable. Then, making further measurements on $\mathbf{C}_j$ one must arrive at a table T_l without a contradiction. Since T_k and T_l have both no contradiction, they must differ in at least two places, one of them being X. Finally, if the column $\mathbf{C}_j$ in U_i would only have entries of zero and k, then $\mathbf{C}_j$ in T_k could not differ from T_i. This eventually leads to a contradiction and hence proves the last assertion.

Appendix D. $\mathcal{A}_4$ is memory-optimal

Here, we proof the optimality of the 4-state automaton $\mathcal{A}_4$, in the sense of obeying $\mathscr{Q}'_{\text{context}}$ and $\mathscr{Q}'_{\text{compat}}$ with a minimum number of states. We use the definitions and rules as introduced in Appendix C.

Let us assume that we would have a three-state automaton obeying $\mathscr{Q}'_{\text{context}}$. T_1 has a contradiction, and we can assume, without loss of generality, that it is $\mathbf{C}_3$. Then, according to Rule 1 we can, without loss of generality, assume that all entries in $\mathbf{C}_3$ are "+". Together with Rule 5 this leads to the conclusion that the three states T_i are, without loss of generality, of the form:

$$T_1\colon \begin{bmatrix} & + \\ & + \\ & + \end{bmatrix}, \qquad T_2\colon \begin{bmatrix} & + \\ & + \\ & - \end{bmatrix}, \qquad T_3\colon \begin{bmatrix} & + \\ & - \\ & + \end{bmatrix}, \tag{11a}$$

$$U_1\colon \begin{bmatrix} & 2 \\ & 3 \end{bmatrix}, \qquad U_2\colon \begin{bmatrix} & & 0 \\ & & 0 \\ 0 & 0 & 0 \end{bmatrix}, \qquad U_3\colon \begin{bmatrix} 0 & 0 & 0 \\ & & 0 \end{bmatrix}. \tag{11b}$$

Here, empty places in the tables mean that the corresponding entries are not yet fixed. The table U_1 follows from Rule 5, and U_2 and U_3 follow from Rule 3.

Which can be the entries corresponding to the observables a and b in U_2? Since T_3 assigns a different value to c than T_2, there cannot be a "3" at these entries, otherwise, a sequence like $c_2^+ a_2^? c_3^-$ would lead to a contradiction to the conditions of $\mathscr{Q}_{\text{context}}$.

But there can also not be a "1" at these entries, because then the sequence $c_2^+ a_2^? \gamma_1^+ c_3^-$ yields a contradiction to $\mathscr{Q}_{\text{compat}}$, since a and γ are compatible with c. So the entries of $\mathbf{R}_2$ in U_2 must be zero, as there are only three states in the memory. A similar argument can be applied to U_3, showing that here $\mathbf{R}_3$ must be zero.

So the tables have to be of the form

$$T_1\colon \begin{bmatrix} & + \\ & + \\ & + \end{bmatrix}, \qquad T_2\colon \begin{bmatrix} & + \\ & + \\ & - \end{bmatrix}, \qquad T_3\colon \begin{bmatrix} & + \\ & - \\ & + \end{bmatrix}, \tag{12a}$$

$$U_1\colon \begin{bmatrix} & 2 \\ & 3 \end{bmatrix}, \qquad U_2\colon \begin{bmatrix} 0 & 0 & 0 \\ 0 & 0 & 0 \\ 0 & 0 & 0 \end{bmatrix}, \qquad U_3\colon \begin{bmatrix} 0 & 0 & 0 \\ 0 & 0 & 0 \\ 0 & 0 & 0 \end{bmatrix}. \tag{12b}$$

Now, according to Rule 4, the contradictions in T_2 as well as in T_3 can only be in $\mathbf{R}_1$. But, according to Rule 5, if there is a contradiction in $\mathbf{R}_1$ of T_2, there must be two different T_i and T_j where there is no contradiction in $\mathbf{R}_1$. But there is only one table left, namely T_1, and we arrive at a contradiction.

Appendix E. Proof that the classical simulation of the extended PM square requires more than two bits of memory

Let us now discuss the extended PM square from Ref. [29]. Again, we refer to Appendix C for basic definitions and rules. As already mentioned, one considers for that the array of observables

$$\begin{bmatrix} & \chi_{01} & \chi_{02} & \chi_{03} \\ \chi_{10} & \chi_{11} & \chi_{12} & \chi_{13} \\ \chi_{20} & \chi_{21} & \chi_{22} & \chi_{23} \\ \chi_{30} & \chi_{31} & \chi_{32} & \chi_{33} \end{bmatrix} = \begin{bmatrix} & \mathbb{1}\otimes\sigma_x & \mathbb{1}\otimes\sigma_y & \mathbb{1}\otimes\sigma_z \\ \sigma_x\otimes\mathbb{1} & \sigma_x\otimes\sigma_x & \sigma_x\otimes\sigma_y & \sigma_x\otimes\sigma_z \\ \sigma_y\otimes\mathbb{1} & \sigma_y\otimes\sigma_x & \sigma_y\otimes\sigma_y & \sigma_y\otimes\sigma_z \\ \sigma_z\otimes\mathbb{1} & \sigma_z\otimes\sigma_x & \sigma_z\otimes\sigma_y & \sigma_z\otimes\sigma_z \end{bmatrix}. \tag{13}$$

These observables can be grouped into trios, in which the observables commute and their product equals $\pm\mathbb{1}$. Nine trios are of the form $\{\chi_{k0}, \chi_{kl}, \chi_{0l}\}$, three trios where the product equals $+\mathbb{1}$ are $\{\chi_{11}, \chi_{23}, \chi_{32}\}$, $\{\chi_{12}, \chi_{21}, \chi_{33}\}$, and $\{\chi_{13}, \chi_{22}, \chi_{31}\}$. Three trios where the product equals $-\mathbb{1}$ are $\{\chi_{11}, \chi_{22}, \chi_{33}\}$, $\{\chi_{12}, \chi_{23}, \chi_{31}\}$, and $\{\chi_{13}, \chi_{21}, \chi_{32}\}$. From this, one can derive the inequality

$$\begin{aligned} \textstyle\sum_{k,l} \langle \chi_{k0}\chi_{kl}\chi_{0l}\rangle + \langle \chi_{11}\chi_{23}\chi_{32}\rangle + \langle \chi_{12}\chi_{21}\chi_{33}\rangle + \\ + \langle \chi_{13}\chi_{22}\chi_{31}\rangle - \langle \chi_{11}\chi_{22}\chi_{33}\rangle - \langle \chi_{12}\chi_{23}\chi_{31}\rangle - \\ - \langle \chi_{13}\chi_{21}\chi_{32}\rangle \leq 9 \end{aligned} \tag{14}$$

for noncontextual models, while QM predicts a value of 15, independently of the state.

First note that in this new inequality 15 terms (or contexts) occur but any noncontextual model can fulfill the quantum prediction for only 12 of them at most, so three contradictions cannot be avoided. One can directly check that in the whole construction of the inequality, 10 different PM squares occur. Nine of them are a simple rewriting of the usual PM square, while the tenth comes from the observables χ_{kl} with $k, l \neq 0$. Any of the 15 terms in the inequality contributes to four of these PM squares.

Any value table for the 15 observables leads to assignments to the 15 contexts, but it has at least three contradictions. As any context contributes to four PM squares, this would lead to 12 contradictions in the 60 contexts of the 10 PM squares, if we consider them separately. Since in a PM square the number of contradictions cannot be two (Rule 2), this means that one of the PM squares has to have three contradictions.

Let us now assume that we have a valid automaton for this extended PM square with four memory states. Of course, this would immediately give a valid four-state automaton of any of the 10 PM squares. For one of these PM squares, at least one table has to have *three* contradictions. So it suffices to prove the following Lemma:

Lemma 4. *There is no four-state automaton obeying $\mathscr{Q}'_{compat}$ and $\mathscr{Q}'_{context}$, where one table T_i has three contradictions.*

In course of proving this Lemma we will also prove the following:

Proposition 5. *The four-state automaton $\mathcal{A}_4$ is unique, up to some permutation or sign changes.*

To prove the Lemma, we proceed in the following way: Without loss of generality, we can assume that the first three tables T_i look like the T_i in Eq. (11a). Then,

we can add a fourth table T_4. For the last column of this table, there are $2^3 = 8$ possible values. We will investigate all eight possibilities and show that either we arrive directly at a contradiction, or that only an automaton similar to $\mathcal{A}_4$ is possible, in which any table has only one contradiction. This proves the Lemma.

We will first deal with the four cases, where T_4 has also a contradiction in $\mathbf{C}_3$. This will lead to Observation 6, which will be useful in the following four cases.

Case 1: *For T_4 one has $[C, c, \gamma] = [+\,+\,+]$:*
In this case, a simple application of the previous rules implies that several entries are fixed:

$$T: \begin{bmatrix} & & + \\ & & + \\ & & + \end{bmatrix}, \begin{bmatrix} & & + \\ & & + \\ & & - \end{bmatrix}, \begin{bmatrix} & & + \\ & & - \\ & & + \end{bmatrix}, \begin{bmatrix} & & + \\ & & + \\ & & + \end{bmatrix}, \tag{15}$$

$$U: \begin{bmatrix} & & \\ & & 2 \\ & & 3 \end{bmatrix}, \begin{bmatrix} & & 0 \\ 0 & 0 & 0 \\ 0 & 0 & 0 \end{bmatrix}, \begin{bmatrix} & & 0 \\ 0 & 0 & 0 \\ 0 & 0 & 0 \end{bmatrix}, \begin{bmatrix} & & \\ & & 2 \\ & & 3 \end{bmatrix}. \tag{16}$$

Here and in the following, we write the T_i and U_i just as a row for notational simplicity, starting from T_1 to T_4. The entries in U_1 and U_4 are fixed from the following reasoning: Let us assume that one measures c in T_1, then, since the values $C(T_i)$ are the same in all T_i, one has to change immediately to a table with no contradiction in $\mathbf{C}_3$, and where the value of c is still the same. The only possibility is T_2. Furthermore, $\mathbf{R}_2$ in U_2 and $\mathbf{R}_3$ in U_3 must be zero due to the same argument which led to Eq. (12b).

It follows (Rule 4) that T_2 and T_3 have both exactly one contradiction, which must be in $\mathbf{R}_1$. So, in $\mathbf{R}_1$ of U_2 there must be the entries "1" and "4" [an entry "3" would not solve the problem, because in $\mathbf{R}_1(T_3)$ has also a contradiction]. As we can still permute the first and second column, we can without loss of generality assume that the first row in U_2 is $[1\ \ 4\ \ 0]$. Due to Rule 1, we can also assume, without loss of generality, that $A(T_2) = +$. Similarly, in $\mathbf{R}_1(U_3)$ there must be the entries "1" and "4", resulting in two different cases:

If $\mathbf{R}_1(U_3) = [1\ 4\ 0]$, we must have the following tables,

$$T: \begin{bmatrix} + & & + \\ & & + \\ & & + \end{bmatrix}, \begin{bmatrix} + & - & + \\ & & + \\ & & - \end{bmatrix}, \begin{bmatrix} + & - & + \\ & & - \\ & & + \end{bmatrix}, \begin{bmatrix} & - & + \\ & & + \\ & & + \end{bmatrix}, \tag{17}$$

$$U: \begin{bmatrix} & & \\ & & 2 \\ & & 3 \end{bmatrix}, \begin{bmatrix} 1 & 4 & 0 \\ 0 & 0 & 0 \\ 0 & 0 & 0 \end{bmatrix}, \begin{bmatrix} 1 & 4 & 0 \\ 0 & 0 & 0 \\ 0 & 0 & 0 \end{bmatrix}, \begin{bmatrix} & & \\ & & 2 \\ & & 3 \end{bmatrix}. \tag{18}$$

where the added values in $\mathbf{R}_1$ of the T_i follow from $\mathbf{R}_1(U_2)$ and $\mathbf{R}_1(U_3)$.

Now, if we start from T_2 and measure the sequence $a_2 A_2 a_1$, we see that we must have $a(T_1) = a(T_2)$. Similarly, from T_3 we can measure $a_3 A_3 a_1$, implying that $a(T_1) = a(T_2) = a(T_3)$. Similarly, we find that $b(T_2) = b(T_3) = b(T_4)$. But this gives a contradiction: In $\mathbf{R}_2(T_2)$ and $\mathbf{R}_2(T_3)$ there is no contradiction and $c(T_2) \neq c(T_3)$. Therefore, it cannot be that $a(T_2) = a(T_3)$ and at the same time $b(T_2) = b(T_3)$.

As the second case, we have to consider the possibility that $\mathbf{R}_1(U_3) = [4\ 1\ 0]$. Then, also the values of $\mathbf{R}_1(T_3)$ must be interchanged, $\mathbf{R}_1(T_3) = [-\,+\,+]$. Then, starting from T_2, the sequence $\alpha_2 A_2 \gamma_1 \alpha_3$ shows directly that $\alpha(T_2) = \alpha(T_3)$. Similarly, starting from T_3, the sequence $a_3 A_3 c_4 a_2$ shows that $a(T_2) = a(T_3)$. But since $A(T_2) \neq A(T_3)$, this is a contradiction.

Case 2: *For T_4 one has $[C, c, \gamma] = [+\,-\,-]$:*
As in Case 1, one can directly see that several entries are fixed:

$$T: \begin{bmatrix} & & + \\ & & + \\ & & + \end{bmatrix}, \begin{bmatrix} & & + \\ & & + \\ & & - \end{bmatrix}, \begin{bmatrix} & & + \\ & & - \\ & & + \end{bmatrix}, \begin{bmatrix} & & + \\ & & - \\ & & - \end{bmatrix}, \tag{19}$$

$$U: \begin{bmatrix} & & \\ & & 2 \\ & & 3 \end{bmatrix}, \begin{bmatrix} & & 0 \\ 0 & 0 & 0 \\ 0 & 0 & 0 \end{bmatrix}, \begin{bmatrix} & & 0 \\ 0 & 0 & 0 \\ 0 & 0 & 0 \end{bmatrix}, \begin{bmatrix} & & \\ & & 3 \\ & & 2 \end{bmatrix}. \tag{20}$$

The zeroes in U_2 and U_3 come from the following argumentation: Starting from T_1, the measurement sequence $c_1^+ X_2 c_?$ with X compatible to c shows that in $\mathbf{R}_2(U_2)$ and $\mathbf{C}_3(U_2)$ there can be no "3" or "4". But there can be also no "1", because then the sequence $c_1^+ X_2 \gamma_1 c_3^-$ would lead to a contradiction. Therefore, $\mathbf{R}_2(U_2)$ and $\mathbf{C}_3(U_2)$ have to be zero. Starting from T_4 and measuring γ one can similarly prove that the entries for $\mathbf{R}_3(U_2)$ have to be zero and analogous arguments prove also the zeroes in U_3.

It is now clear (Rule 4) that the contradictions in T_2 and T_3 have to be in $\mathbf{R}_1$ and the missing entries in U_2 and U_3 can only be "4" and "1". As we still can permute the first and second column, there are only two possibilities:

Case 2A: First, we consider the case that $\mathbf{R}_1(U_2) = \mathbf{R}_1(U_3) = [1\ 4\ 0]$. As in Case 1, we can directly see that $a(T_2) = a(T_1) = a(T_3)$ and $b(T_2) = b(T_4) = b(T_3)$. Hence, $\mathbf{R}_2(T_2)$ and $\mathbf{R}_2(T_3)$ differ exactly in the value of c, but in both cases there is no contradiction in $\mathbf{R}_2$. This is not possible.

Case 2B: Second, we consider the case that the first rows of U_2 and U_3 differ, and we take $\mathbf{R}_1(U_2) = [1\ 4\ 0]$ and $\mathbf{R}_1(U_3) = [4\ 1\ 0]$. Then, we apply Rule 1 to fix for $A(T_3) = a(T_3) = +$. Then, the tables have to be:

$$T: \begin{bmatrix} - & - & + \\ & - & + \\ & + & + \end{bmatrix}, \begin{bmatrix} - & + & + \\ & & + \\ & & - \end{bmatrix}, \begin{bmatrix} + & - & + \\ + & - & - \\ + & + & + \end{bmatrix}, \begin{bmatrix} + & + & + \\ + & & - \\ + & & - \end{bmatrix}, \tag{21}$$

$$U: \begin{bmatrix} & & \\ & & 2 \\ & & 3 \end{bmatrix}, \begin{bmatrix} 1 & 4 & 0 \\ 0 & 0 & 0 \\ 0 & 0 & 0 \end{bmatrix}, \begin{bmatrix} 4 & 1 & 0 \\ 0 & 0 & 0 \\ 0 & 0 & 0 \end{bmatrix}, \begin{bmatrix} & & \\ & & 3 \\ & & 2 \end{bmatrix}. \tag{22}$$

Here, $\mathbf{C}_2(T_1)$ and $\mathbf{C}_1(T_4)$ come from measurement sequences like $a_3^+ A_3^+ a_4^+$, starting from T_3.

Again, we have two possibilities for the value of b in T_2. If we set $b(T_2) = -$, then all values in all T_i are fixed and each table has exactly one contradiction. This is, up to some relabeling, the four-state automaton $\mathcal{A}_4$ from the main text (indeed, this is the way how this solution was found). If we set $b(T_2) = +$, then also all T_i can be filled, and we must have:

$$T: \begin{bmatrix} - & - & + \\ + & - & + \\ - & + & + \end{bmatrix}, \begin{bmatrix} - & + & + \\ + & + & + \\ - & + & - \end{bmatrix}, \begin{bmatrix} + & - & + \\ + & - & - \\ + & + & + \end{bmatrix}, \begin{bmatrix} + & + & + \\ + & + & - \\ + & + & - \end{bmatrix}, \tag{23}$$

$$U: \begin{bmatrix} & 3 & 2 \\ 2 & & 3 \end{bmatrix}, \begin{bmatrix} 1 & 4 & 0 \\ 0 & 0 & 0 \\ 0 & 0 & 0 \end{bmatrix}, \begin{bmatrix} 4 & 1 & 0 \\ 0 & 0 & 0 \\ 0 & 0 & 0 \end{bmatrix}, \begin{bmatrix} & 2 & 3 \\ 3 & & 2 \end{bmatrix}. \tag{24}$$

Here, the tables T_1 and T_4 have three contradictions (two new ones in $\mathbf{R}_2$ and $\mathbf{R}_3$) and the new entries in U_1 and U_4 must be introduced according to Rule 5 [note that $a(T_i)$ and $\beta(T_i)$ are for all tables the same]. Then, however, starting from T_1, the sequence $\alpha_1^- A_2^- \gamma_1^+ \alpha_3^+$ shows that this is not valid solution.

Case 3: *For T_4 one has $[C, c, \gamma] = [- + -]$:*
In this case, a simple reasoning according to the usual rules fixes the entries:

$$T: \begin{bmatrix} & + \\ & + \\ & + \end{bmatrix}, \begin{bmatrix} & + \\ & + \\ & - \end{bmatrix}, \begin{bmatrix} & + \\ & - \\ & + \end{bmatrix}, \begin{bmatrix} & - \\ & + \\ & - \end{bmatrix}, \tag{25}$$

$$U: \begin{bmatrix} & \\ & \\ & 3 \end{bmatrix}, \begin{bmatrix} & \\ & \\ & \end{bmatrix}, \begin{bmatrix} & & 0 \\ 0 & 0 & 0 \\ & & 0 \end{bmatrix}, \begin{bmatrix} 0 & 0 & 0 \\ & & 0 \\ & & 0 \end{bmatrix}. \tag{26}$$

Here we have an obvious contradiction in T_4/U_4: $\mathbf{C}_3(T_4)$ contains a contradiction, but (due to Rule 3) one is not allowed to change the memory state when measuring it. Therefore, the memory can never be in the state 4. But then, one would have effectively a three-state solution, which is not possible, as we know already.

Case 4: *For T_4 one has $[C, c, \gamma] = [- - +]$:*
This is the same as Case 3, where $\mathbf{R}_2$ and $\mathbf{R}_3$ have been interchanged.

Now we have dealt with all the cases, where T_4 contains a contradiction in $\mathbf{C}_3$, just as T_1. We have seen that in this cases there can only be a solution if each table contains exactly one contradiction, and this solution is unique, up to some permutations or sign flips. Moreover, we could have made the same discussion with rows instead of columns. Therefore from the first four cases we can state an observation which will be useful in the remaining four cases:

Observation 6. *If in any four-state solution two tables T_i and T_j have both a contradiction in the same column $\mathbf{C}_k$ (or row $\mathbf{R}_k$), then there has to be exactly one contradiction in each value table of the automaton.*

So, if there is a four-state solution where one table has three contradictions, then it cannot be that two tables have both a contradiction in the same column or row.

Then we can proceed with the remaining cases.

Case 5: *For T_4 one has $[C, c, \gamma] = [+ + -]$:*
This is the critical case, as it is difficult to distinguish the tables T_2 and T_4 here. First, the following entries are directly fixed:

$$T: \begin{bmatrix} & + \\ & + \\ & + \end{bmatrix}, \begin{bmatrix} & + \\ & + \\ & - \end{bmatrix}, \begin{bmatrix} & + \\ & - \\ & + \end{bmatrix}, \begin{bmatrix} & + \\ & + \\ & - \end{bmatrix}, \tag{27}$$

$$U: \begin{bmatrix} & 2 \\ & 3 \end{bmatrix}, \begin{bmatrix} & & 0|4 \\ 0|4 & 0|4 & 0|4 \\ & & 0|4 \end{bmatrix}, \begin{bmatrix} & & 0 \\ 0 & 0 & 0 \\ 0 & 0 & 0 \end{bmatrix}, \begin{bmatrix} & \\ & \\ & 0|2 \\ & 0|2 \end{bmatrix}. \tag{28}$$

Here, $c(U_1) = 2$ has been chosen without loss of generality. It is clear that $c(U_1) = 2$ or $c(U_1) = 4$, as T_2 and T_4 are equivalent at the beginning, we can choose T_2 here. The entries of the type $_{i|j}$ in U_2 and U_4 mean that the numbers can be i or j, but nothing else. The values of $c(U_2)$ [and $c(U_4)$] cannot be 1, because then the sequence $c_2^+\gamma_1^+c_3^-$ directly reveals a contradiction. Furthermore, the zeroes in $\mathbf{R}_3(U_3)$ and $\mathbf{R}_2(U_3)$ follow similarly as Eq. (12b) or from Rule 3. In addition, $C(U_2) \neq 1$, because otherwise the sequence $c_1^+C_2^+\gamma_1^+$ reveals a contradiction to the PM conditions. Also, $C(U_2) \neq 3$, because of $c_1^+C_2^+c_3^-$. Similarly, 1 and 3 are excluded as values for $a(U_2)$ and $b(U_2)$, due to the sequences $c_1^+a_2\gamma_1^+c_3^-$ and $c_1^+a_2^+c_3^-$.

Furthermore, we can use our Observation 6: If in a four-state solution one column has a contradiction in two of the T_i, then there can be only one contradiction in

any T_i. Here we can use it as follows: It is clear that T_3 has its contradiction in $\mathbf{R}_1$. Since we aim to rule out a four-state solution where one table has three contradictions, we can assume that there is no contradiction in $\mathbf{R}_1$ in all the other T_i (especially in T_2 and T_3). Otherwise, we would already know that no solution exists with three contradictions in a table. We can distinguish two cases:

Case 5A: Let us assume that $\gamma(U_2) = 0$. Then, the tables must read:

$$T: \begin{bmatrix} & + \\ & + \\ & + \end{bmatrix}, \begin{bmatrix} & + \\ & + \\ & - \end{bmatrix}, \begin{bmatrix} & + \\ & - \\ & + \end{bmatrix}, \begin{bmatrix} & + \\ & + \\ & - \end{bmatrix}, \tag{29}$$

$$U: \begin{bmatrix} & 2 \\ & 3 \end{bmatrix}, \begin{bmatrix} & & 0|4 \\ 0|4 & 0|4 & 0|4 \\ 0|4 & 0|4 & 0 \end{bmatrix}, \begin{bmatrix} & & 0 \\ 0 & 0 & 0 \\ 0 & 0 & 0 \end{bmatrix}, \begin{bmatrix} & \\ & 0|2 \\ & 0|2 \end{bmatrix}. \tag{30}$$

The new entries in U_2 follow from $\gamma(U_2) = 0$ in combination with $\gamma(T_1) = \gamma(T_3) \neq \gamma(T_2)$.

Due to Rule 5, the table T_2 must have a contradiction in $\mathbf{C}_1$, $\mathbf{C}_2$, or $\mathbf{R}_1$. From Observation 6, we can assume that it is not in $\mathbf{R}_1$. Due to possible permutations of $\mathbf{C}_1$ and $\mathbf{C}_2$ we further assume without loss of generality that the contradiction is in $\mathbf{C}_1$. Then we have:

$$U: \begin{bmatrix} & 2 \\ & 3 \end{bmatrix}, \begin{bmatrix} 1 & & 0|4 \\ 4 & 0|4 & 0|4 \\ 0|4 & 0|4 & 0 \end{bmatrix}, \begin{bmatrix} & & 0 \\ 0 & 0 & 0 \\ 0 & 0 & 0 \end{bmatrix}, \begin{bmatrix} & \\ & 0|2 \\ & 0|2 \end{bmatrix}. \tag{31}$$

We cannot have $A(U_2) = 3$, since there is a contradiction in $\mathbf{R}_1(T_3)$ and $C(T_i) = +$ for all tables. In addition, due to Rule 5, it is not possible that $A(U_2) = 4$. Finally, we choose $a(U_2) = 4$, the other option would be $\alpha(U_2) = 4$, this will be discussed below.

From Observation 6 we can conclude that $\mathbf{C}_1(T_1)$ and $\mathbf{C}_1(T_4)$ do not contain contradictions, since $\mathbf{C}_1(T_2)$ contains already a contradiction. So $\mathbf{C}_1(T_1)$ and $\mathbf{C}_1(T_4)$ must differ in two places (Rule 5). One of these places must be $A(T_1) \neq A(T_4)$. Let us assume that the second one is $a(T_1) \neq a(T_4)$, the other case $[\alpha(T_1) \neq \alpha(T_4)]$ will be discussed below. Then, we can conclude that in $\mathbf{R}_1(U_1)$ and $\mathbf{C}_1(U_1)$ we cannot have the entries "2" and "4", and in $\mathbf{R}_2(U_4)$ and $\mathbf{C}_1(U_4)$ we cannot have the entries "2" and "1". To see this, note that we must have $A(T_2) = A(T_1) \neq A(T_4)$ and, if $B(U_1) = 2$, we can consider the measurement sequence $A_2B_1a_2A_4$ or, if $B(U_1) = 4$, the sequence $A_2B_1A_4$ etc. Hence, we have:

$$U: \begin{bmatrix} 0 & 0 & 0 \\ 0|3 & & 2 \\ 0|3 & & 3 \end{bmatrix}, \begin{bmatrix} 1 & & 0|4 \\ 4 & 0|4 & 0|4 \\ 0|4 & 0|4 & 0 \end{bmatrix}, \begin{bmatrix} & & 0 \\ 0 & 0 & 0 \\ 0 & 0 & 0 \end{bmatrix}, \begin{bmatrix} 0|3 & & \\ 0|3 & 0|3 & 0 \\ 0|3 & & 0|2 \end{bmatrix}.$$

Here, we used in $\mathbf{R}_1(U_1)$ that $\mathbf{R}_1(T_3)$ has a contradiction and $C(T_i) = +$ for all tables, so it is not possible to go there.

Now, by Rule 1, we may fix $A(T_2) = a(T_2) = +$. Then we arrive at

$$T: \begin{bmatrix} + & + & + \\ & & + \\ & & + \end{bmatrix}, \begin{bmatrix} + & + & + \\ + & + & + \\ - & + & - \end{bmatrix}, \begin{bmatrix} & & + \\ & & - \\ & & + \end{bmatrix}, \begin{bmatrix} - & - & + \\ + & & + \\ - & & - \end{bmatrix}, \tag{32}$$

$$U: \begin{bmatrix} 0 & 0 & 0 \\ 0|3 & & 2 \\ 0|3 & & 3 \end{bmatrix}, \begin{bmatrix} 1 & & 0|4 \\ 4 & 0|4 & 0|4 \\ 0|4 & 0|4 & 0 \end{bmatrix}, \begin{bmatrix} & & 0 \\ 0 & 0 & 0 \\ 0 & 0 & 0 \end{bmatrix}, \begin{bmatrix} 0|3 & & 0|2 \\ 0 & 0 & 0 \\ 0|3 & & 0|2 \end{bmatrix}. \tag{33}$$

Here, we must have $A(T_4) = \alpha(T_4)$ since $\mathbf{C}_1(T_4)$ has no contradiction. Furthermore, $\mathbf{R}_1(T_4)$ has no contradiction due to Observation 6. The values of $\mathbf{R}_2(U_4)$

are determined by considering sequences like $c_4a_4c_?$; and $C(U_4) \neq 3$, because of $c_4^+C_4c_3^-$, and $C(U_4) \neq 1$, because of $c_4^+C_4\gamma_1c_3^-$.

In addition, we can conclude that $A(U_4) = 0$ and $B(U_4) = 0$, since $\mathbf{R}_1(T_3)$ has a contradiction and $C(T_i) = +$ for all tables, so it is not possible to go there. Then we can fill T_4 completely. Then, also $C(U_4) = 0$, otherwise the sequence $B_4^-C_4^+B_2^+$ gives a contradiction. If we had $\alpha(U_4) = 3$, then we must have $A(T_4) = A(T_3) = -$ and, consequently (Rule 5) $B(U_3) = 1$ or 2, but then the sequence $A_4^-\alpha_4^-B_3^+A_{1|2}^+$ leads to a contradiction, so $\alpha(U_4) = 0$. In summary, we have:

$$T: \begin{bmatrix} + & + & + \\ & & + \\ & & + \end{bmatrix}, \begin{bmatrix} + & + & + \\ + & + & + \\ - & + & - \end{bmatrix}, \begin{bmatrix} & & + \\ & & - \\ & & + \end{bmatrix}, \begin{bmatrix} - & - & + \\ + & + & + \\ - & - & - \end{bmatrix}, \tag{34}$$

$$U: \begin{bmatrix} 0 & 0 & 0 \\ 0|3 & & 2 \\ 0|3 & & 3 \end{bmatrix}, \begin{bmatrix} 1 & & 0|4 \\ 4 & 0|4 & 0|4 \\ 0|4 & 0|4 & 0 \end{bmatrix}, \begin{bmatrix} & & 0 \\ 0 & 0 & 0 \\ 0 & 0 & 0 \end{bmatrix}, \begin{bmatrix} 0 & 0 & 0 \\ 0 & 0 & 0 \\ 0 & & 0|2 \end{bmatrix}. \tag{35}$$

Now T_1 is the only candidate for a table with three contradictions. In order to obey Observation 6, the only possibilities for contradictions are $\mathbf{C}_2$, $\mathbf{C}_3$, and $\mathbf{R}_2$, since T_4 has its contradiction in $\mathbf{R}_3$. Especially, there must be a contradiction in $\mathbf{C}_2(T_1)$. Then, in order to obey Rule 5, we must have:

$$T: \begin{bmatrix} + & + & + \\ & & + \\ & & + \end{bmatrix}, \begin{bmatrix} + & + & + \\ + & + & + \\ - & + & - \end{bmatrix}, \begin{bmatrix} - & + & + \\ & & - \\ & & + \end{bmatrix}, \begin{bmatrix} - & - & + \\ + & + & + \\ - & - & - \end{bmatrix}, \tag{36}$$

$$U: \begin{bmatrix} 0 & 0 & 0 \\ 0|3 & 2|3 & 2 \\ 0|3 & 2|3 & 3 \end{bmatrix}. \begin{bmatrix} 1 & & 0|4 \\ 4 & 0|4 & 0|4 \\ 0|4 & 0|4 & 0 \end{bmatrix}, \begin{bmatrix} 4 & 1|2 & 0 \\ 0 & 0 & 0 \\ 0 & 0 & 0 \end{bmatrix}, \begin{bmatrix} 0 & 0 & 0 \\ 0 & 0 & 0 \\ 0 & & 0|2 \end{bmatrix}. \tag{37}$$

However, if $b(U_1) = 3$, then the sequence $B_1^+b_1A_3B_4^-$ leads to a contradiction, while, if $\beta(U_1) = 3$, then the sequence $B_1^+\beta_1A_3B_4^-$ leads to a problem.

Finally, if we would have taken $\alpha(U_2) = 4$ or $\alpha(T_1) \neq \alpha(T_4)$ the proof would proceed along the same lines, but this time the contradiction in T_4 would be in the second row.

Case 5B: Let us assume that $\gamma(U_2) = 4$. Then, many entries on U_4 are fixed and we have:

$$T: \begin{bmatrix} & & + \\ & & + \\ & & + \end{bmatrix}, \begin{bmatrix} & & + \\ & & + \\ & & - \end{bmatrix}, \begin{bmatrix} & & + \\ & & - \\ & & + \end{bmatrix}, \begin{bmatrix} & & + \\ & & + \\ & & - \end{bmatrix}, \tag{38}$$

$$U: \begin{bmatrix} & & 2 \\ & & 3 \end{bmatrix}, \begin{bmatrix} & & 0|4 \\ 0|4 & 0|4 & 0|4 \\ & & 4 \end{bmatrix}, \begin{bmatrix} & & 0 \\ 0 & 0 & 0 \\ 0 & 0 & 0 \end{bmatrix}, \begin{bmatrix} & & 0|2 \\ 0|2 & 0|2 & 0|2 \\ 0|2 & 0|2 & 0|2 \end{bmatrix}. \tag{39}$$

Here we cannot have $a(U_4) = 1$, due the sequences $c_2\gamma_2a_4c_1$ [if $c(U_2) = 0$] or $c_2a_4c_1$ [if $c(U_2) = 4$], and also not $a(U_4) = 3$, due to similar sequences. The same arguments apply to $b(U_4)$. The entries in $\mathbf{R}_3(U_4)$ and $\mathbf{C}_3(4)$ come from possible sequences like $\gamma_4\alpha_4\gamma_?$ if $\gamma(U_4) = 0$ or $\gamma_4\gamma_2\alpha_4\gamma_?$ if $\gamma(U_4) = 2$.

But then the proof can proceed exactly as in the Case 5A, with T_2 and T_4 interchanged: The only significant difference comes from $c(U_1) = 2 \neq 4$, but this was never used in the proof.

Case 6: *For T_4 one has $[C, c, \gamma] = [+ - +]$:*
This is the same as the Case 5 with a permutation of $\mathbf{R}_2$ and $\mathbf{R}_3$.

Case 7: *For T_4 one has $[C, c, \gamma] = [- + +]$:*
In this case, the tables read:

$$T: \begin{bmatrix} & + \\ & + \\ & + \end{bmatrix}, \begin{bmatrix} & + \\ & + \\ & - \end{bmatrix}, \begin{bmatrix} & + \\ & - \\ & + \end{bmatrix}, \begin{bmatrix} & - \\ & + \\ & + \end{bmatrix}, \tag{40}$$

$$U: \begin{bmatrix} & 2 \\ & 3 \end{bmatrix}, \begin{bmatrix} & & 0 \\ {\scriptstyle 0|4} & {\scriptstyle 0|4} & 0 \\ 0 & 0 & 0 \end{bmatrix}, \begin{bmatrix} & & 0 \\ 0 & 0 & 0 \\ {\scriptstyle 0|4} & {\scriptstyle 0|4} & 0 \end{bmatrix}, \begin{bmatrix} 0 & 0 & 0 \\ {\scriptstyle 0|2} & {\scriptstyle 0|2} & 0 \\ {\scriptstyle 0|3} & {\scriptstyle 0|3} & 0 \end{bmatrix}. \tag{41}$$

Here, the entries in U_1 have been chosen without loss of generality: From Rule 4 and 5 it follows that one can restrict the attention to the cases where $\mathbf{C}_3(U_1) = [\ \ , 2, 3]$, $\mathbf{C}_3(U_1) = [\ \ , 2, 4]$, or $\mathbf{C}_3(U_1) = [\ \ , 4, 3]$. We only consider the first possibility, in the other cases the proof is analogous and is left to the gentle reader as an exercise. The zeroes in U_2, U_3, and U_4 come from Rule 3. The entries $_{0|2}$ in U_4 come from possible measurement sequences like $c_4 a_4 c_3$ or $c_4 a_4 \gamma_1 c_3$ which prove that there cannot be the entries "3" or "1". The other entries can be derived accordingly.

From Rule 5, it follows that in T_4 the contradiction cannot be in the rows, so it has to be in the first or second column. Let us assume, without loss of generality, that it is in $\mathbf{C}_1(T_4)$. Further, we can assume without loss of generality, that the values A and a in T_4 are both "+". Then, the tables can be more specified as

$$T: \begin{bmatrix} & + \\ & + \\ & + \end{bmatrix}, \begin{bmatrix} + & & + \\ + & + & + \\ + & - & - \end{bmatrix}, \begin{bmatrix} + & & + \\ - & + & - \\ - & - & + \end{bmatrix}, \begin{bmatrix} + & - & - \\ + & + & + \\ - & - & + \end{bmatrix}, \tag{42}$$

$$U: \begin{bmatrix} & 2 \\ & 3 \end{bmatrix}, \begin{bmatrix} {\scriptstyle 0|1} & & 0 \\ 0 & {\scriptstyle 0|4} & 0 \\ 0 & 0 & 0 \end{bmatrix}, \begin{bmatrix} {\scriptstyle 0|1} & & 0 \\ 0 & 0 & 0 \\ 0 & {\scriptstyle 0|4} & 0 \end{bmatrix}, \begin{bmatrix} 0 & 0 & 0 \\ 2 & {\scriptstyle 0|2} & 0 \\ 3 & {\scriptstyle 0|3} & 0 \end{bmatrix}. \tag{43}$$

To see this, one first fills T_4, then, together with the entries of $\mathbf{C}_1(U_4)$, many values of T_2 and T_3 are fixed. The entries $_{0|1}$ are justified similar to the reasoning above.

In T_2 as well as in T_3 the contradiction has to be either in $\mathbf{R}_1$ or $\mathbf{C}_2$. However, there cannot be a contradiction in $\mathbf{R}_1$. To see this, assume that there were a contradiction in $\mathbf{R}_1(T_2)$. Then, starting from T_2 we may measure the sequence $C_2 A_2 B$ or $C_2 B_2 A$. According to Rule 5, we must end in two different T_i. But the memory state can never change to T_4 [because $C(T_4) = -$]. So we must have $B(U_2) = 3$, but this will not escape the contradiction, since the values for A and C coincide in T_2 and T_3. So there is only T_1 left, and we arrive at a contradiction.

Consequently, the contradictions have to be both in $\mathbf{C}_2(T_2)$ and $\mathbf{C}_2(T_3)$. In principle, our Observation 6 implies already that we cannot find a solution with three contradictions in one table. But one can also directly prove that there is no solution at all. We have:

$$T: \begin{bmatrix} + & + & + \\ & + & + \\ & - & + \end{bmatrix}, \begin{bmatrix} + & + & + \\ + & + & + \\ + & - & - \end{bmatrix}, \begin{bmatrix} + & + & + \\ - & + & - \\ - & - & + \end{bmatrix}, \begin{bmatrix} + & - & - \\ + & + & + \\ - & - & + \end{bmatrix}, \tag{44}$$

$$U: \begin{bmatrix} & & 2 \\ & & 3 \end{bmatrix}, \begin{bmatrix} {\scriptstyle 0|1} & 1 & 0 \\ 0 & 4 & 0 \\ 0 & 0 & 0 \end{bmatrix}, \begin{bmatrix} {\scriptstyle 0|1} & 1 & 0 \\ 0 & 0 & 0 \\ 0 & 4 & 0 \end{bmatrix}, \begin{bmatrix} 0 & 0 & 0 \\ 2 & {\scriptstyle 0|2} & 0 \\ 3 & {\scriptstyle 0|3} & 0 \end{bmatrix}. \tag{45}$$

Here, we must have $B(T_1) = B(T_2) = B(T_3) = +$ due to measurement sequences like $B_2^+ B_1^+$ or $B_3^+ B_1^+$ and $\beta(T_1) = \beta(T_2)$ due to $\beta_2^- B_2^+ \beta_1^-$ and $b(T_1) = b(T_3)$ due to $b_3^+ B_3^+ b_1^+$. But then, starting from T_2, the sequence $\beta_2^- B_2^+ b_1^+$ reveals a contradiction to the PM conditions.

Case 8: *For T_4 one has $[C, c, \gamma] = [---]$:*
In this case, we directly have:

$$T: \begin{bmatrix} & & + \\ & & + \\ & & + \end{bmatrix}, \begin{bmatrix} & & + \\ & & + \\ & & - \end{bmatrix}, \begin{bmatrix} & & + \\ & & - \\ & & + \end{bmatrix}, \begin{bmatrix} & & - \\ & & - \\ & & - \end{bmatrix}, \tag{46}$$

$$U: \begin{bmatrix} & & 2 \\ & & 3 \end{bmatrix}, \begin{bmatrix} & & 0 \\ 0 & 0 & 0 \\ 0 & 0 & 0 \end{bmatrix}, \begin{bmatrix} & & 0 \\ 0 & 0 & 0 \\ 0 & 0 & 0 \end{bmatrix}, \begin{bmatrix} 0 & 0 & 0 \\ & & 0 \\ & & 0 \end{bmatrix}. \tag{47}$$

Starting from T_2 we may measure the sequence C_2A_2B or C_2B_2A. According to Rule 5, we must end in two different T_i. But the memory state can neither change to T_4 [because $C(T_4) = -$] nor to T_3 [as $\mathbf{R}_1(T_3)$ contains a contradiction]. So there is only T_1 left, and we arrive at a contradiction.

In summary, by considering all eight different cases we have shown that no four-state solution exists in which one table has three contradictions. This proves the claim.

Appendix F. A 10-state automaton obeying all sequences

In this Appendix we show an example of a 10-state automaton that obeys the set of all sequences $\mathscr{Q}_{\text{all}}$. For that, we define 10 eigenstates of two compatible observables. We let $|A^-B^+\rangle$ be a quantum state with $A|A^-B^+\rangle = -|A^-B^+\rangle$ and $B|A^-B^+\rangle = +|A^-B^+\rangle$. In this fashion we define the 10 states $|A^+B^+\rangle$, $|A^-B^+\rangle$, $|C^+c^+\rangle$, $|C^-c^+\rangle$, $|\gamma^+\beta^+\rangle$, $|\gamma^-\beta^+\rangle$, $|\alpha^+a^+\rangle$, $|\alpha^-a^+\rangle$, $|a^+b^+\rangle$, and $|B^+b^+\rangle$. Any measurement of an observable from the PM square projects with finite probability any state of the set onto another state of the set. If e.g. the automaton is in state $|A^-B^+\rangle$ and we measure c, QM predicts a chance of 50% to get the outcome $+1$ yielding the state $|C^-c^+\rangle$, and a 50% chance to obtain -1 and the state $|C^-c^-\rangle$. The former state is in the set of the 10 states and hence our automaton would return $+1$ and change to the state $|C^-c^+\rangle$. We furthermore define that, if both states predicted by QM are in the set of the 10 states, then we prefer the state corresponding to the output of $+1$. Together with an arbitrary choice of the initial state, this completes the definition of the automaton. By construction, this automaton is deterministic and obeys $\mathscr{Q}_{\text{all}}$.

References

[1] Specker, E. *Dialectica* **14**(2–3), 239–246 (1960).
[2] Kochen, S. and Specker, E. P. *J. Math. Mech.* **17**(1), 59–87 (1967).
[3] Bell, J. S. *Rev. Mod. Phys.* **38**(3), 447–452 (1966).
[4] Mermin, N. D. *Phys. Rev. Lett.* **65**(27), 3373 (1990).
[5] Heywood, P. and Redhead, M. L. G. *Found. Phys.* **13**(5), 481–499 (1983).
[6] Bechmann-Pasquinucci, H. and Peres, A. *Phys. Rev. Lett.* **85**(15), 3313–3316 (2000).
[7] Spekkens, R. W. *Phys. Rev. Lett.* **101**(2), 020401 (2008).
[8] Cabello, A. *Phys. Rev. Lett.* **104**(22), 220401 (2010).
[9] Aharon, N. and Vaidman, L. *Phys. Rev. A* **77**(5), 052310 (2008).
[10] Svozil, K. *Phys. Rev. A* **79**(5), 054306 (2009).
[11] Svozil, K. CDMTCS Research Report Series 353, MAR (2009).
[12] Horodecki, K., Horodecki, M., Horodecki, P., Horodecki, R., Pawłowski, M., and Bourennane, M. arXiv:1006.0468.
[13] Bell, J. S. *Found. Phys.* **12**(10), 989–999 (1982).
[14] La Cour, B. R. *Phys. Rev. A* **79**(1), 012102 (2009).

[15] Khrennikov, A. Y. *Contextual Approach to Quantum Formalism.* Springer, Berlin, (2009).
[16] Toner, B. F. and Bacon, D. *Phys. Rev. Lett.* **91**(18), 187904 (2003).
[17] Pironio, S. *Phys. Rev. A* **68**(6), 062102 (2003).
[18] Buhrman, H., Cleve, R., Massar, S., and de Wolf, R. *Rev. Mod. Phys.* **82**(1), 665 (2010).
[19] Holevo, A. S. *Probl. Inf. Trans.* **9**(3), 177–183 (1973).
[20] Galvão, E. F. and Hardy, L. *Phys. Rev. Lett.* **90**(8), 087902 (2003).
[21] Peres, A. *Phys. Lett. A* **151**(3–4), 107–108 (1990).
[22] Cabello, A. *Phys. Rev. Lett.* **101**(21), 210401 (2008).
[23] Kirchmair, G. et al. *Nature (London)* **460**(7254), 494–497 (2009).
[24] Amselem, E., Rådmark, M., Bourennane, M., and Cabello, A. *Phys. Rev. Lett.* **103**(16), 160405 (2009).
[25] Moussa, O., Ryan, C. A., Cory, D. G., and Laflamme, R. *Phys. Rev. Lett.* **104**(16), 160501 (2010).
[26] Mealy, G. H. *Bell Systems Technical J.* **34**, 1045 (1955).
[27] Roth Jr., C. H. *Fundamentals of Logic Design.* Thomson, Stanford, CT, (2009).
[28] Gühne, O. et al. *Phys. Rev. A* **81**(2), 022121 (2010).
[29] Cabello, A. *Phys. Rev. A* **82**(3), 032110 (2010).
[30] Harrigan, N., Rudolph, T., and Aaronson, S. arXiv:0709.1149.
[31] Dakić, B., Šuvakov, M., Paterek, T., and Brukner, Č. *Phys. Rev. Lett.* **101**(19), 190402 (2008).
[32] Vértesi, T. and Pál, K. F. *Phys. Rev. A* **79**(4), 042106 (2009).
[33] Brukner, Č. and Zeilinger, A. *Found. Phys.* **39**, 677–689 (2009).
[34] Galvão, E. F. *Phys. Rev. A* **80**(2), 022106 (2009).
[35] Gallego, R., Brunner, N., Hadley, C., and Acín, A. *Phys. Rev. Lett.* **105**(23), 230501 (2010).
[36] Brukner, Č., Taylor, S., Cheung, S., and Vedral, V. arXiv:quant-ph/0402127.
[37] Brassard, G. et al. *Phys. Rev. Lett.* **96**(25), 250401 (2006).
[38] Pawłowski, M. et al. *Nature (London)* **461**(7267), 1101–1104 (2009).

Entropic uncertainty relations and the stabilizer formalism

Sönke Niekamp, Matthias Kleinmann, and Otfried Gühne
Universität Siegen, Fachbereich Physik, Walter-Flex-Straße 3, D-57068 Siegen, Germany and
Institut für Quantenoptik und Quanteninformation, Österreichische Akademie der Wissenschaften, Technikerstraße 21a, A-6020 Innsbruck, Austria

(Dated: 2 February 2012)

Entropic uncertainty relations express the quantum mechanical uncertainty principle by quantifying uncertainty in terms of entropy. Central questions include the derivation of lower bounds on the total uncertainty for given observables, the characterization of observables that allow strong uncertainty relations, and the construction of such relations for the case of several observables. We demonstrate how the stabilizer formalism can be applied to these questions. We show that the Maassen–Uffink entropic uncertainty relation is tight for the measurement in any pair of stabilizer bases. We compare the relative strengths of variance-based and various entropic uncertainty relations for dichotomic anticommuting observables.

I. INTRODUCTION

In quantum mechanics, one cannot predict a measurement outcome with certainty unless the system is in an eigenstate of the observable being measured. It follows that if two or more observables have no common eigenstate, it is not possible to prepare the system such that for each observable only one measurement outcome can occur. This is known as the uncertainty principle,[1–4] which is quantitatively formulated in terms of uncertainty relations.

Uncertainty relations not only describe a fundamental quantum mechanical concept, but have also found application, e. g., in quantum cryptography[5–7] and entanglement detection.[8–10] Entropic uncertainty relations[11–15] have turned out to be particularly useful. More recently, the uncertainty principle has also been formulated in terms of majorization relations.[16] In Ref. 17, Berta *et al.* derived an entropic uncertainty relation for a system which is entangled to a quantum memory. Access to this memory can then be used to lower the uncertainties of measurements on the system. This relation has been the subject of recent experiments.[18,19]

Historically, the first and still the most celebrated uncertainty relation was given by Heisenberg[1,2] and applies to canonically conjugate observables such as position and momentum, stating that $\Delta^2(q)\Delta^2(p) \geq \hbar^2/4$. It was generalized to arbitrary observables in the form of Robertson's[3] uncertainty relation $\Delta^2(A)\Delta^2(B) \geq |\langle[A,B]\rangle|^2/4$. On closer inspection, the latter does not have all desirable properties of an uncertainty relation, in particular since it is trivial for any eigenstate of either observable. Robertson's relation has also been generalized to the case of more than two observables.[20,21]

A different approach is based on the idea of quantifying uncertainty by the entropy of the probability distribution for the measurement outcomes.[11–15] As a consequence, the resulting uncertainty relations depend only on the eigenstates, but not on the eigenvalues of the observables. That is, they are independent of the labelling of the measurement results, which in finite dimensions is essentially arbitrary. For this reason, entropic uncertainty relations can be regarded as a more natural formulation of the uncertainty principle, at least in the case of finitely many measurement outcomes, which we consider here. For a review of entropic uncertainty relations see, e. g., Ref. 15.

An entropic uncertainty relation [see Eq. (6) for an example] gives a lower bound on the sum of the entropies for the measurement outcomes of some observables on a quantum state. This bound necessarily depends on the observables, but preferably is independent of the state. For the case of two observables, such bounds have been determined, e. g., in Refs. 12–14. Finding the best bound is in general not easy. Putting differently, the question here is a characterization of observables which admit strong uncertainty relations. So far, most results apply to the case of two observables only,[15,22] despite the generalization of the theory to several observables being an interesting problem.

In this article, we demonstrate how the stabilizer formalism[23] can be applied to these questions. This formalism provides an efficient description of certain many-qubit states, including highly entangled ones. In the field of quantum information theory, stabilizer stabilizer states and the more special case of graph states are widely used. For example, a particular class of graph states, namely, cluster states, serve as a universal resource for measurement-based quantum computation.[24,25] Cluster states are also interesting because they are particularly robust against decoherence, independently of the system size.[26,27] Graph states have been employed as codewords of error-correcting codes.[28] Finally, the stabilizer formalism has been used for entanglement detection.[29]

Using the stabilizer formalism, we first investigate the question for which observables the Maassen–Uffink uncertainty relation [see Eq. (6)] is tight. We show that this is the case for the measurement in any two stabilizer bases. We then turn our attention to the many-observable setting, focussing on dichotomic anticommuting observables. Generalizing a result by Wehner and Winter,[22] we provide a systematic construction of uncertainty relations. The family of uncertainty relations we obtain con-

tains both entropic and variance-based ones. We compare the relative strengths of these relations. Finally, we apply them to the stabilizing operators of two stabilizer states.

This article is organized as follows: In Sec. II, we introduce our notation and review previous results. This includes a short introduction to stabilizers and graph states. Section III contains our results on measurements in stabilizer bases, and Sec. IV those on several dichotomic anticommuting observables. In Sec. V, the latter are applied to the stabilizing operators of two stabilizer states. Finally, Sec. VI is devoted to a discussion of the results.

II. STATEMENT OF THE PROBLEM

A. Entropic uncertainty relations

We consider the following general situation: when measuring an observable A on a state ρ, the measurement outcome a_i occurs with probability $p_i = \mathrm{Tr}(\Pi_i \rho)$, where $A = \sum_{i=1}^{m} a_i \Pi_i$ is the spectral decomposition of the observable and the a_i are mutually distinct. For an entropy function S, we denote by $S(A|\rho)$ the entropy of this probability distribution $P = (p_1, \ldots, p_m)$. In this article, we will use the Shannon entropy

$$S^S(P) = -\sum_{i=1}^{m} p_i \log(p_i) \tag{1}$$

as well as the min-entropy

$$S^{\min}(P) = -\log(\max_i p_i) \tag{2}$$

and the Tsallis entropy

$$S_q^T(P) = \frac{1 - \sum_{i=1}^{m} (p_i)^q}{q-1}, \qquad q > 1. \tag{3}$$

In the limit $q \to 1$, the Tsallis entropy gives the Shannon entropy. We use the logarithm to base 2 throughout.

We are interested in uncertainty relations for a family of observables $\{A_1, \ldots, A_L\}$ of the form

$$\frac{1}{L} \sum_{k=1}^{L} S(A_k|\rho) \geq c_{\{A_k\}}, \tag{4}$$

where S is an entropy function. The lower bound $c_{\{A_k\}}$ may depend on the observables, but shall be independent of the state. For a given set of observables, an uncertainty relation is called tight, if a state ρ_0 exists that attains the lower bound, $1/L \sum_{k=1}^{L} S(A_k|\rho_0) = c_{\{A_k\}}$.

Clearly the entropy of an observable depends only on its eigenstates and is independent of its eigenvalues, as long as they are nondegenerate. We will therefore not distinguish between a nondegenerate observable A and its eigenbasis $\mathcal{A}$. The Shannon entropy satisfies $0 \leq S^S(\mathcal{A}|\rho) \leq \log(m)$, where m is the length of the basis $\mathcal{A}$. If we choose for ρ one of the basis states of $\mathcal{A}_k$, we have $1/L \sum_{k=1}^{L} S(\mathcal{A}_k|\rho) \leq \log(m)(L-1)/L$, because in this case the entropy is zero for one basis and upper bounded by $\log(m)$ for the remaining $L-1$ bases. This implies that for the Shannon entropy the right-hand side of Eq. (4) cannot exceed $\log(m)(L-1)/L$. An uncertainty relation that reaches this limit is called maximally strong, and the corresponding measurements are called maximally incompatible.[15] In other words, maximal incompatibility means that if the outcome of one measurement is certain, the outcomes of the remaining measurements are completely random.

A related notion is mutual unbiasedness. Two orthonormal bases $|a_i\rangle$ and $|b_i\rangle$, $i = 1, \ldots, d$, are called mutually unbiased if

$$\big|\langle a_i|b_j\rangle\big| = \frac{1}{\sqrt{d}}, \tag{5}$$

for all i and j. Pairwise mutual unbiasedness is a necessary, but for more than two bases not a sufficient condition for the existence of a maximally strong uncertainty relation.[15]

For the Shannon entropies of $L = 2$ measurement bases, Maassen and Uffink[14] have proven the following result:

Maassen–Uffink uncertainty relation. *For any two measurement bases $\mathcal{A} = \{|a_i\rangle\}$ and $\mathcal{B} = \{|b_i\rangle\}$,*

$$\frac{1}{2}[S^S(\mathcal{A}|\rho) + S^S(\mathcal{B}|\rho)] \geq -\log\big(\max_{i,j} |\langle a_i|b_j\rangle|\big). \tag{6}$$

In the case of mutually unbiased bases the Maassen–Uffink relation is maximally strong and thus tight, equality holding for any of the basis states. (Note that for two arbitrary observables the entropy sum is in general not minimized by an eigenstate of either of them.[30])

B. The stabilizer formalism and graph states

As our main tool, we will employ the stabilizer formalism. This formalism allows to describe certain many-qubit states, among them graph states, in an efficient manner. For a review of this topic see, e. g., Ref. 23.

The n-qubit Pauli group consists of all tensor products of n Pauli matrices, including the identity, with prefactors ± 1 and $\pm \mathrm{i}$. Any commutative subgroup of the Pauli group that has 2^n elements and does not contain $-\mathbb{1}$ has a unique common eigenstate with eigenvalue $+1$. This state is called stabilizer state; the group is called the stabilizer group and the group elements are called the stabilizing operators of the state. The stabilizer group defines in fact a complete basis of common eigenstates, the stabilizer state being one of them. We refer to this basis as stabilizer basis. Any basis state is again a stabilizer state, whose stabilizer group is obtained from the original one by flipping the signs of some of its elements.

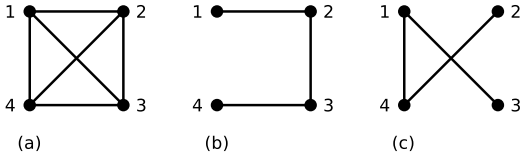

FIG. 1. Graphs of the graph states discussed in the text.

The most important examples of stabilizer states are graph states. In fact, it can be shown that any stabilizer state is equivalent to a graph state under a local unitary operation (more specifically, a local Clifford operation).[23] A graph state is described by a simple undirected graph, whose vertices represent qubits and whose edges represent the interactions that have created the graph state from a product state [see Fig. 1 for examples]. More precisely, with the completely disconnected n-vertex graph, we associate the state $|+\rangle^{\otimes n}$, where $|+\rangle$ is the eigenvector of σ_x with eigenvalue $+1$. An edge between two vertices stands for the controlled phase gate applied to the corresponding pair of qubits, which in the standard σ_z-basis is $C = \mathrm{diag}(1,1,1,-1)$. The stabilizing operators of a graph state can immediately be read off the graph: with qubit i, we associate the operator

$$K_i = \sigma_x^{(i)} \prod_{j\in N(i)} \sigma_z^{(j)}, \tag{7}$$

the product being over the neighbourhood $N(i)$ of vertex i, that is, all vertices directly connected to it by an edge. Here $\sigma_x^{(i)}$ and $\sigma_z^{(i)}$ denote the Pauli matrices σ_x and σ_z acting on qubit i. The operators K_i generate the stabilizer group. Any state of the stabilizer basis (here called graph state basis) can be obtained from the graph state by applying the operation σ_z on a subset of the qubits.

As an example, let us consider the graphs in Fig. 1 (a) and (b). The generators of the stabilizer group of the first state are $K_1 = \sigma_x \otimes \sigma_z \otimes \sigma_z \otimes \sigma_z$, $K_2 = \sigma_z \otimes \sigma_x \otimes \sigma_z \otimes \sigma_z$, $K_3 = \sigma_z \otimes \sigma_z \otimes \sigma_x \otimes \sigma_z$, and $K_4 = \sigma_z \otimes \sigma_z \otimes \sigma_z \otimes \sigma_x$; for the second state, they are $K_1 = \sigma_x \otimes \sigma_z \otimes \mathbb{1} \otimes \mathbb{1}$, $K_2 = \sigma_z \otimes \sigma_x \otimes \sigma_z \otimes \mathbb{1}$, $K_3 = \mathbb{1} \otimes \sigma_z \otimes \sigma_x \otimes \sigma_z$, and $K_4 = \mathbb{1} \otimes \mathbb{1} \otimes \sigma_z \otimes \sigma_x$. Under local unitary operations, the corresponding graph states are equivalent to the 4-qubit Greenberger–Horne–Zeilinger (GHZ) state $|\mathrm{GHZ}_4\rangle = (|0000\rangle + |1111\rangle)/\sqrt{2}$ and the 4-qubit linear cluster state $|\mathrm{C}_4\rangle = (|0000\rangle + |0011\rangle + |1100\rangle - |1111\rangle)/2$, respectively.

III. A STRONG UNCERTAINTY RELATION FOR STABILIZER BASES

In this section, we investigate the conditions under which the Maassen–Uffink uncertainty relation is tight. We show that this is the case for the measurement in any two stabilizer bases.

We shall need the following lemma:

Lemma 1. *If a pair of bases $\mathcal{A} = \{|a_i\rangle\}$ and $\mathcal{B} = \{|b_i\rangle\}$ satisfies*

$$\big|\langle a_i|b_j\rangle\big| \in \{0, r\} \quad \forall\, i,j \tag{8}$$

for some r, then the Maassen–Uffink relation Eq. (6) for the measurement in these bases is tight. Equality occurs for any of the basis states.

Proof. For $\rho = |b_{j_0}\rangle\langle b_{j_0}|$ the Maassen–Uffink relation reads

$$-\sum_i p_i \log(p_i) \geq -\log(\max_i p_i) \quad \text{where } p_i = \big|\langle a_i|b_{j_0}\rangle\big|^2. \tag{9}$$

Note that the right-hand side is the min-entropy of the probability distribution p_i. By assumption $p_i \in \{0, r^2\}$ for all i. It follows that equality holds. □

The main result of this section is the following theorem:

Theorem 2. *For the measurement in a pair of stabilizer bases, the Maassen–Uffink uncertainty relation Eq. (6) is tight. The bound is attained by any of the basis states.*

The proof is based on a result on mutually unbiased bases, which is due to Bandyopadhyay *et al.* (see the proof of Theorem 3.2 in Ref. 31):

Theorem 3 (Ref. 31)**.** *Let C_1 and C_2 each be a set of d commuting unitary $d \times d$-matrices. Furthermore assume that $C_1 \cap C_2 = \{\mathbb{1}\}$ and that all matrices in $C_1 \cup C_2$ are pairwise orthogonal with respect to the Hilbert–Schmidt scalar product. Then the eigenbases defined by either set of matrices are mutually unbiased.*

Proof of Theorem 2. Throughout the proof we consider two stabilizing operators that differ only by a minus sign as equal. Let S_1 and S_2 be the two stabilizer groups and define $C_0 = S_1 \cap S_2$. Then C_0 is a subgroup of both S_1 and S_2. We consider the factor groups $C_1 = S_1/C_0$ and $C_2 = S_2/C_0$. The groups C_0, C_1, and C_2 are all stabilizer groups, though the spaces stabilized by them are in general not one-dimensional. This gives us a decomposition of the Hilbert space $\mathcal{H} = \mathcal{H}_0 \otimes \mathcal{H}_{12}$, where C_0 acts trivially on $\mathcal{H}_{12}$ and C_1 and C_2 act trivially on $\mathcal{H}_0$. By the previous theorem, C_1 and C_2 define mutually unbiased bases $|c_i^{(1)}\rangle$ and $|c_i^{(2)}\rangle$ of $\mathcal{H}_{12}$. It follows that the stabilizer bases can be written as $|s_{ij}^{(1)}\rangle = |c_i^{(0)}\rangle \otimes |c_j^{(1)}\rangle$ and $|s_{ij}^{(2)}\rangle = |c_i^{(0)}\rangle \otimes |c_j^{(2)}\rangle$, respectively, where $|c_i^{(0)}\rangle$ is the basis of $\mathcal{H}_0$ defined by C_0. The stabilizer bases thus satisfy the condition of Lemma 1 with $r = (\dim H_{12})^{-1/2}$. □

In Appendix A, we give an alternative proof that does not require the result on mutually unbiased bases. In Appendix B, we develop a method to calculate the right-hand side of the uncertainty relation explicitly for certain classes of graph states.

IV. UNCERTAINTY RELATIONS FOR SEVERAL DICHOTOMIC ANTICOMMUTING OBSERVABLES

Little is known about uncertainty relations for more than two measurements[15] (see, however, Ref. 32). Following Wehner and Winter,[22] we will concentrate on dichotomic anticommuting observables. An observable is called dichotomic if it has exactly two distinct eigenvalues. We will always normalize dichotomic observables such that their eigenvalues are ± 1. In other words, these observables square to the identity.

The following result has been called a meta-uncertainty relation,[15,22] for reasons that soon will become apparent.

Lemma 4. *Let $A_1, \ldots, A_L$ be observables which anticommute pairwise $\{A_k, A_\ell\} = 0$ for $k \neq \ell$ and which have eigenvalues ± 1. Then $\sum_{k=1}^{L} \langle A_k \rangle^2 \leq 1$, or equivalently,*

$$\sum_{k=1}^{L} \Delta^2(A_k) \geq L - 1, \tag{10}$$

where $\Delta^2(A) = \langle (A - \langle A \rangle)^2 \rangle$ is the variance of A.

The following proof of this lemma was given in Ref. 29. For an alternative proof, based on the Clifford algebra, see Ref. 22.

Proof. Choose real coefficients $\lambda_1, \ldots, \lambda_L$ with $\sum_{k=1}^{L} \lambda_k^2 = 1$. Because of anticommutativity and $A_k^2 = \mathbb{1}$, we have $(\sum_{k=1}^{L} \lambda_k A_k)^2 = \sum_{k=1}^{L} \lambda_k^2 A_k^2 = \sum_{k=1}^{L} \lambda_k^2 \mathbb{1} = \mathbb{1}$ and thus $|\sum_{k=1}^{L} \lambda_k \langle A_k \rangle| = |\langle \sum_{k=1}^{L} \lambda_k A_k \rangle| \leq 1$ for all states, since for any observable $\langle X \rangle^2 \leq \langle X^2 \rangle$. Interpreting the expression $\sum_{k=1}^{L} \lambda_k \langle A_k \rangle$ as the euclidian scalar product of the vector of coefficients λ_k and the vector of expectation values $\langle A_k \rangle$, and noting that the vector of coefficients λ_k is an arbitrary unit vector, we see that the vector $\langle A_k \rangle$ has a length less than or equal to 1. Observing $\sum_{k=1}^{L} \langle A_k^2 \rangle = L$, we obtain the lemma. □

The converse implication is also true in the following sense, as was already shown in Ref. 22:

Lemma 5. *Let $A_1, \ldots, A_L$ be dichotomic anticommuting observables as above, and let $a_1, \ldots, a_L$ be real numbers with $\sum_{k=1}^{L} a_k^2 \leq 1$. Then there exists a quantum state ρ such that the numbers a_k are the expectation values of the observables, $a_k = \mathrm{Tr}(A_k \rho)$.*

Proof. Consider the state $\rho = \frac{1}{d}(\mathbb{1} + \sum_{k=1}^{L} a_k A_k)$, where d is the dimension of the Hilbert space. Because of the properties of the observables, $\mathrm{Tr}(A_k A_\ell) = d\delta_{k\ell}$. Furthermore, the observables A_k are traceless: $\mathrm{Tr}(A_k) = \mathrm{Tr}(A_k A_\ell A_\ell) = \mathrm{Tr}(A_\ell A_k A_\ell) = -\mathrm{Tr}(A_k A_\ell A_\ell) = -\mathrm{Tr}(A_k)$. This shows that the state ρ has the desired expectation values. It remains to show that $\rho \geq 0$. But in the proof of the previous lemma, we have already seen that $|\sum_{k=1}^{L} a_k \langle A_k \rangle| \leq 1$. □

The meta-uncertainty relation is thus the best possible bound on the expectation values of the observables. Note that in the case of one qubit and the three Pauli matrices, it reduces to the Bloch sphere picture. The relation has also been used to study monogamy relations for Bell inequalities.[33] Generalizing Wehner and Winter's result for the Shannon entropy,[22] we can derive entropic uncertainty relations for various entropies from it.

Let A be an observable with eigenvalues ± 1 and $x = [\mathrm{Tr}(A\rho)]^2$ its squared expectation value. Then the probability distribution for the measurement outcomes of A is given by $P = (\frac{1+\sqrt{x}}{2}, \frac{1-\sqrt{x}}{2})$ or $P = (\frac{1-\sqrt{x}}{2}, \frac{1+\sqrt{x}}{2})$. Any entropy S, being invariant under permutation of P, is thus a function of x, which we denote by $\widetilde{S}$,

$$\widetilde{S}(x) = S(A|\rho) = S\big((\frac{1 \pm \sqrt{x}}{2}, \frac{1 \mp \sqrt{x}}{2})\big). \tag{11}$$

We say that the entropy S is concave in the squared expectation value if the function $\widetilde{S}$ is concave. This property is the crucial condition for the following entropic uncertainty relation. We shall also assume that for the peaked probability distribution, the entropy has the value zero, $\widetilde{S}(1) = 0$.

Theorem 6. *Let $A_1, \ldots, A_L$ be observables which anticommute pairwise $\{A_k, A_\ell\} = 0$ for $k \neq \ell$ and which have eigenvalues ± 1 and let S be an entropy which is concave in the squared expectation value (that is, an entropy for which the function $\widetilde{S}$ defined in Eq. (11) is concave). Then*

$$\min_{\rho} \frac{1}{L} \sum_{k=1}^{L} S(A_k|\rho) = \frac{L-1}{L} S_0, \tag{12}$$

where $S_0 = S\big((\frac{1}{2}, \frac{1}{2})\big)$ is the entropy value of the flat probability distribution.

Proof. For the case of the Shannon entropy the proof was given in Ref. 22. Let $x_k = [\mathrm{Tr}(A_k \rho)]^2$. Lemma 4 states that $\vec{x}$ lies in the simplex defined by $\sum_{k=1}^{L} x_k \leq 1$ and $x_k \geq 0$. As the function $\widetilde{S}$ is concave on the interval $[0, 1]$, the function $\vec{x} \mapsto \sum_k \widetilde{S}(x_k)$ is concave on the simplex. Thus it attains its minimum at an extremal point of the simplex, that is, $x_k = 1$ for one k and $x_\ell = 0$ for $\ell \neq k$. At an extremal point, $1/L \sum_{k=1}^{L} \widetilde{S}(x_k) = S_0(L-1)/L$. □

Before commenting on the implications of this theorem, we discuss which entropies satisfy the requirement of being concave in the squared expectation value. For the Shannon entropy, this was already shown in Ref. 22. The Tsallis entropy can be treated analogously, though one has to distinguish between different parameter ranges.

Lemma 7. *The Tsallis entropy S_q^T of a dichotomic observable is concave in the squared expectation value (that is, the function $\widetilde{S}_q^T$ defined as in Eq. (11) is concave on the interval $[0, 1]$) for parameter values $1 < q < 2$ and $3 < q$, but convex for $2 < q < 3$.*

Proof. Explicitly,

$$\widetilde{S}_q^T(x) = \frac{1}{q-1}\Big[1 - \Big(\frac{1+\sqrt{x}}{2}\Big)^q - \Big(\frac{1-\sqrt{x}}{2}\Big)^q\Big]. \quad (13)$$

For $q = 2$ and $q = 3$, this function is easily seen to be linear. For the second derivative, we obtain

$$\partial_x^2 \widetilde{S}_q^T(x) = \frac{q}{q-1}\frac{1}{2^{q+2}}\frac{1}{x^{3/2}}\Big\{(1+\sqrt{x})^{q-2}\big[1-\sqrt{x}(q-2)\big] - (1-\sqrt{x})^{q-2}\big[1+\sqrt{x}(q-2)\big]\Big\}. \quad (14)$$

Substituting $y = \sqrt{x}$ and omitting the prefactor (which is always positive), we arrive at the function

$$f_q(y) = (1+y)^{q-2}[1-y(q-2)] - (1-y)^{q-2}[1+y(q-2)]. \quad (15)$$

Observing that $f_q(0) = 0$, we note that $f_q(y)$ is positive (negative) for all $0 < y \leq 1$ if its derivative $f_q'(y)$ is positive (negative) for all $0 < y \leq 1$. The derivative is given by

$$f_q'(y) = -(q-2)(q-1)y\big[(1+y)^{q-3} - (1-y)^{q-3}\big]. \quad (16)$$

For $1 < q < 2$, the prefactor $-(q-2)(q-1)$ is positive and the term in the square brackets is negative; for $2 < q < 3$, the prefactor is negative and the term in the brackets is still negative; for $q > 3$, the prefactor is negative and the term in the brackets positive. This proves the lemma. □

Let us add some remarks on the theorem. The Shannon entropy has the required concavity in the squared expectation value, and the resulting uncertainty relation is the one found by Wehner and Winter.[22] For the Tsallis entropy S_q^T, we have to distinguish between different parameter ranges: for parameter values $q = 2$ and $q = 3$ this entropy is, up to a constant factor, equal to the variance, $S_2^T(A|\rho) = 1/2\Delta^2(A)$ and $S_3^T(A|\rho) = 3/8\Delta^2(A)$, and the uncertainty relation is equivalent to the meta-uncertainty relation itself. Thus it is the optimal uncertainty relation for these observables. The relation based on the Shannon entropy is strictly weaker.

In Lemma 7, we have shown that the Tsallis entropy satisfies the condition of Theorem 6 for parameter values $1 < q \leq 2$ and $3 \leq q$. The entropy value for the flat probability distribution, which determines the bound, is $S_0 = (1 - 2^{1-q})/(q-1)$. In the special case of the observables σ_x and σ_y and parameter $q \in [2n-1, 2n]$ with $n \in \mathbb{N}$, the uncertainty relation was derived before in Footnote 32 of Ref. 9.

As we remarked above, Lemmas 4 and 5 provide a complete characterization of the set of expectation values of dichotomic anticommuting observables which can originate from valid quantum states. Deriving uncertainty relations from them means approximating this set from the outside. This is illustrated in Fig. 2.

In the parameter range $2 < q < 3$, the Tsallis entropy does not satisfy the condition for the theorem (see Lemma 7). An exceptional behaviour of the Tsallis entropy in this parameter range was also reported in Ref. 9. The collision entropy or Rényi entropy of order 2 and the min-entropy do not satisfy the condition either. The uncertainty relations for these entropies given in Ref. 22 also follow from the meta-uncertainty relation, but do not fit into this scheme.

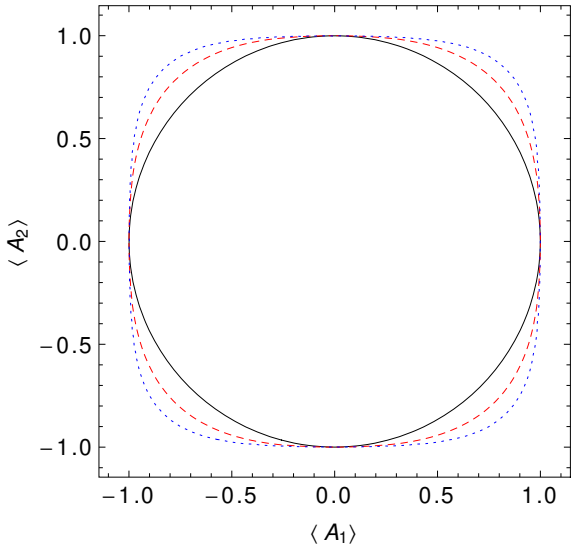

FIG. 2. Bounds on the expectation values $(\langle A_1\rangle, \langle A_2\rangle)$ for two dichotomic anticommuting observables provided by different uncertainty relations. The black solid line corresponds to the meta-uncertainty relation Lemma 4, which can also be understood as an entropic uncertainty relation for the Tsallis entropy with parameter value $q = 2$ or $q = 3$. The red dashed line and the blue dotted line correspond to the entropic uncertainty relation Theorem 6 for the Shannon entropy and the Tsallis entropy with $q = 8$, respectively.

In the following section, we will apply Theorem 6 to the stabilizing operators of two stabilizer states.

Uncertainty relations for several observables can also be constructed without requiring anticommutativity: applying a result by Mandayam *et al.*[32] to a set of stabilizer bases $\mathcal{A}_1, \ldots, \mathcal{A}_L$ with basis vectors denoted by $\mathcal{A}_k = \{|a_i^{(k)}\rangle\}_i$, one finds for their min-entropies

$$\frac{1}{L}\sum_{k=1}^{L} S^{\min}(\mathcal{A}_k|\rho) \geq -\log\Big[\frac{1+r(L-1)}{L}\Big], \quad (17)$$

where

$$r = \max_{k\neq\ell}\max_{i,j}\big|\langle a_i^{(k)}|a_j^{(\ell)}\rangle\big| \quad (18)$$

is the maximal overlap of the basis states. We omit the proof, since this relation readily follows from Appendix C.1 of Ref. 32.

V. AN UNCERTAINTY RELATION FOR STABILIZING OPERATORS

In this section, we will apply the uncertainty relation for anticommuting dichotomic observables (Theorem 6) to the elements of a pair of stabilizer groups.

Let S and T be two n-qubit stabilizer groups. Throughout this section, we consider two operators as equal if they differ only by a minus sign. Define $\widetilde{S} = S \setminus T$ and $\widetilde{T} = T \setminus S$. Let $M = \widetilde{S} \cup \widetilde{T}$ be the symmetric difference of S and T and denote its elements by $A_1, \ldots, A_L$. In Theorem 10, we will give a lower bound on $1/L \sum_{k=1}^{L} S(A_k|\rho)$.

We begin by proving the following lemma.

Lemma 8. *Let S be a stabilizer group and g a Pauli operator (that is, a tensor product of Pauli matrices and the identity matrix) which anticommutes with an element $s_0 \in S$. Then g anticommutes with exactly half of the elements of S.*

Proof. Choose any $s_1 \in S$ with $s_1 \neq s_0$ and let $s_2 = s_0 s_1$. We will now show that g anticommutes with s_2 if it commutes with s_1 and vice versa. Consider first the case $[s_1, g] = 0$. The identity $\{AB, C\} = A[B, C] + \{A, C\}B$ shows that $\{s_2, g\} = \{s_0 s_1, g\} = s_0[s_1, g] + \{s_0, g\}s_1 = 0$. Consider now the case $\{s_1, g\} = 0$. Using the same identity, we obtain $s_0[s_2, g] = \{s_0 s_2, g\} - \{s_0, g\}s_2 = \{s_1, g\} - \{s_0, g\}s_2 = 0$ and thus $[s_2, g] = 0$. We now iterate this procedure by choosing $s_3 \in S \setminus \{s_0, s_1, s_2\}$ and using it in place of s_1. (Note that $s_0 s_3 \neq s_1$ and $\neq s_2$.) The operator s_0 is kept fixed during the whole iteration. In this way, S can be divided into pairs of observables, each consisting of one element commuting with g and one anticommuting with g. Note that s_0 forms a pair with the identity. □

Excluding the trivial case $S = T$, any element of T anticommutes with at least one element of S, since at most 2^n orthogonal (with respect to the Hilbert–Schmidt scalar product) unitary $2^n \times 2^n$-matrices can commute pairwise (see, e. g., Ref. 31). Thus $L = |M|$ varies from 2^n to $2(2^n - 1)$.

We will now see, using only combinatorical reasoning, that this lemma implies that M can be divided into anticommuting pairs. We shall need the following combinatorical result:

Marriage theorem. *Consider a bipartite graph, that is, two disjoint sets of vertices U and V and a collection of edges, each connecting a vertex in U with a vertex in V. We consider the case of $|U| = |V|$. Then the graph contains a perfect matching, that is, the vertices can be divided into disjoint pairs of connected vertices, if and only if the following marriage condition is fulfilled: For each subset U' of U, the set V' of vertices in V connected to vertices in U' is at least as large as U'.*

This theorem was first proven in Ref. 34.

Lemma 9. *The symmetric difference M of any two stabilizer groups S and T can be divided into anticommuting pairs of operators.*

Proof. We show that the marriage condition is fulfilled. Let S' be any subset of $\widetilde{S}$. Consider first the case $|S'| > 2^{n-1}$. Then any $t \in T$ anticommutes with at least one $s \in S'$, because any such t anticommutes with exactly 2^{n-1} elements of $\widetilde{S}$. Thus the number of $t \in \widetilde{T}$ anticommuting with at least one $s \in S'$ is $|\widetilde{T}| = |\widetilde{S}| \geq |S'|$. Consider now the case $|S'| \leq 2^{n-1}$. For any $s \in S'$, we then find 2^{n-1} elements of $\widetilde{T}$ anticommuting with s. Thus the number of $t \in \widetilde{T}$ anticommuting with at least one $s \in S'$ is $2^{n-1} \geq |S'|$. □

We are now ready to state the main result of this section.

Theorem 10. *Let $M = \{A_1, \ldots, A_L\}$ be the symmetric difference of two stabilizer groups. Then*

$$\frac{1}{L} \sum_{k=1}^{L} S(A_k|\rho) \geq \frac{1}{2} S_0 \tag{19}$$

holds, where S is an entropy which is concave in the squared expectation value (that is, an entropy for which the function $\widetilde{S}$ defined in Eq. (11) is concave) and S_0 is the entropy value of the flat probability distribution. Any basis state of either stabilizer basis attains the lower bound.

Proof. Due to Theorem 6 the uncertainty relation $S(A_k|\rho) + S(A_\ell|\rho) \geq S_0$ holds for any anticommuting pair A_k, A_ℓ. Lemma 9 states that M consists of $L/2$ such pairs. This shows the uncertainty relation. The density matrix of the stabilizer state defined by the group $T = \{T_k\}$ is given by

$$\rho_T = \frac{1}{2^n} \sum_{k=1}^{2^n} T_k \tag{20}$$

(see, e. g., Ref. 23). Thus

$$\mathrm{Tr}(A_k \rho_T) = \frac{1}{2^n} \sum_{\ell=1}^{2^n} \mathrm{Tr}(A_k T_\ell) = 0 \quad \text{for all} \quad A_k \notin T, \tag{21}$$

showing $S(A_k|\rho_T) = S_0$ for $L/2$ observables A_k. □

This relation is not maximally strong. This is due to the fact that some of the observables commute.

VI. CONCLUSION

We demonstrated how the stabilizer formalism can be combined with the theory of entropic uncertainty relations. We focussed on two problems: the characterization of pairs of measurement bases which give rise to strong

uncertainty relations and the generalization of the theory to the many-observable setting.

Concerning the first question, we showed that for the measurement in any two stabilizer bases the Maassen–Uffink relation is tight (Theorem 2). We also demonstrated how the stabilizer formalism can be used to compute the overlap of the basis states, which gives the lower bound on the entropy sum.

Concerning the second question, we generalized a result by Wehner and Winter on the Shannon entropy for several dichotomic anticommuting observables to a larger class of entropies (Theorem 6). Comparing the strengths of these uncertainty relation, we saw that entropic relations are not necessarily stronger than variance-based ones. Indeed, in the case of dichotomic anticommuting observables the variance-based uncertainty relation is optimal in the sense that it exactly describes the set of expectation values which can originate from valid quantum states. As an application of Theorem 6, we derived an uncertainty relation for the elements of two stabilizer groups (Theorem 10).

ACKNOWLEDGMENTS

We thank Bastian Jungnitsch, Oleg Gittsovich, Tobias Moroder, and Gemma De las Cuevas for helpful discussions, and Maarten Van den Nest for pointing out Refs. 35 and 36. Furthermore, we thank the associate editor and an anonymous referee for helpful comments, in particular for a simple proof of Lemma 7. This work has been supported by the Austrian Science Fund (FWF): Y376-N16 (START prize) and the EU (Marie Curie CIG 293993/ENFOQI).

Appendix A: Alternative proof of Theorem 2

In this appendix, we give an alternative proof of Theorem 2, which is not based on any previous results on mutually unbiased bases. Let $S = \{S_k\}$ and $T = \{T_k\}$ be two n-qubit stabilizer groups with stabilizer states $|S\rangle$ and $|T\rangle$. Define $S^+ = S \cap T$, where, unlike in the first proof, we consider two operators as distinct if they differ by a minus sign. Also define $S^- = S \cap -T$. Both S^+ and $S^+ \cup S^-$ are easily seen to be subgroups of S. By Lagrange's theorem $|S^+| = 2^p$ and $|S^+ \cup S^-| = 2^q$ with some $p \in \{1, 2, \ldots, n\}$ and $q \in \{p, p+1, \ldots, n\}$. The projectors onto the stabilizer states are given by

$$|S\rangle\langle S| = \frac{1}{2^n} \sum_{k=1}^{2^n} S_k \tag{A1}$$

and similarly for $|T\rangle$ (see, e. g., Ref. 23). Thus

$$\begin{aligned} \big|\langle S|T\rangle\big|^2 &= \frac{1}{2^{2n}} \sum_{k,\ell=1}^{2^n} \mathrm{Tr}(S_k T_\ell) \\ &= \frac{1}{2^n}\big(|S^+| - |S^-|\big) \\ &= \frac{1}{2^n}(2^{p+1} - 2^q) \\ &= \begin{cases} 2^{q-n} & \text{for } p = q, \\ 0 & \text{for } p = q-1. \end{cases} \end{aligned} \tag{A2}$$

The case $p < q - 1$ cannot occur since it would give a negative value of $|\langle S|T\rangle|^2$ and thus lead to a contradiction.

Consider now another state $|T'\rangle$ of the stabilizer basis of T. This state is again a stabilizer state, whose stabilizing operators are equal to those of $|T\rangle$ up to some minus signs. In particular $S^+ \cup S^-$ and thus q are the same for $|T\rangle$ and for $|T'\rangle$, and Lemma 1 applies. □

Appendix B: A recurrence relation for the overlap of two graph state bases

In this appendix, we derive a recurrence relation for the scalar products $\langle G_i^{(1)}|G_j^{(2)}\rangle$ of two graph state bases $|G_i^{(1)}\rangle$ and $|G_i^{(2)}\rangle$ and use it to determine the Maassen–Uffink bound for certain classes of graph states. Recall that any of these basis states is obtained from the state $|+\rangle^{\otimes n}$ by applying first controlled phase gates $C = \mathrm{diag}(1, 1, 1, -1)$ and then local phases σ_z. Since all these operations commute, we can move all phase gates in the scalar product $\langle G_i^{(1)}|G_j^{(2)}\rangle$ to the right and all local phases to the left. This corresponds to replacing $G^{(1)}$ by the empty or completely disconnected graph and $G^{(2)}$ by the "sum modulo 2" of the graphs $G^{(1)}$ and $G^{(2)}$. Similarly, it does not restrict the set of values of $\langle G_i^{(1)}|G_j^{(2)}\rangle$ if we consider only one state of the basis $|G_j^{(2)}\rangle$, such as the graph state $|G^{(2)}\rangle$ itself. The graph state basis of the empty graph consists of all tensor products of the eigenstates of σ_x. We can write those states as $H^{\otimes n}|\vec{y}\rangle$, where $H = \frac{1}{\sqrt{2}}\left(\begin{smallmatrix} 1 & 1 \\ 1 & -1 \end{smallmatrix}\right)$ is the Hadamard gate and $|\vec{y}\rangle$ for $\vec{y} \in \mathbb{F}_2^n$ is a state of the standard basis in binary notation.

[As the Hadamard gate is a local Clifford operation, the state $H^{\otimes n}|G^{(2)}\rangle$ is a stabilizer state. This shows that the scalar products $\langle G_i^{(1)}|G^{(2)}\rangle$ can be understood as the coefficients of a stabilizer state with respect to the standard basis. It has been shown that for any stabilizer state these coefficients are 0, ±1, and ±i, up to a global normalization (see Theorem 5 and the paragraph below in Ref. 35. For an alternative proof, see Ref. 36.) This constitutes yet another proof of Theorem 2 for the case of graph state bases.]

As an example, consider the graphs in Fig. 1 (a) and (b). Up to local unitaries, the corresponding graph states

are the 4-qubit GHZ state and the 4-qubit linear cluster state, but the uncertainty relation is not invariant under these local unitary operations. By the above remark the Maassen–Uffink bound for the corresponding bases is equal to the bound for the empty graph and the "sum" of the graphs, which in our case is given by Fig. 1 (c). The latter is again equal to the graph (b), up to a permutation of vertices.

Let us return to the explicit calculation of the overlaps. In the standard basis, we have

$$H^{\otimes n}|\vec{y}\rangle = \frac{1}{2^{n/2}} \sum_{\vec{x}\in\mathbb{F}_2^n} (-1)^{\sum_i y_i x_i} |\vec{x}\rangle. \tag{B1}$$

The adjacency matrix of an n-qubit graph is the symmetric $n \times n$-matrix A whose entry A_{ij} is 1 if there is an edge between vertices i and j and 0 if there is not. It thus provides a complete description of the graph state, which we will therefore denote by $|G_A\rangle$. The representation of this state in the standard basis is (see Proposition 2.14 in Ref. 37)

$$|G_A\rangle = \frac{1}{2^{n/2}} \sum_{\vec{x}\in\mathbb{F}_2^n} (-1)^{\sum_{i<j} x_i A_{ij} x_j} |\vec{x}\rangle. \tag{B2}$$

The scalar products are thus given by

$$\begin{aligned} R_n(\vec{y}, A) &\coloneqq \langle \vec{y}|H^{\otimes n}|G_A\rangle \\ &= \frac{1}{2^n} \sum_{\vec{x}\in\mathbb{F}_2^n} (-1)^{\sum_i y_i x_i + \sum_{i<j} x_i A_{ij} x_j}. \end{aligned} \tag{B3}$$

To derive a recurrence relation, we write

$$\vec{x} = \begin{pmatrix} \xi \\ \vec{x}\,' \end{pmatrix}, \quad \vec{y} = \begin{pmatrix} \upsilon \\ \vec{y}\,' \end{pmatrix}, \quad A = \begin{pmatrix} 0 & \vec{a}\,'^t \\ \vec{a}\,' & A' \end{pmatrix} \tag{B4}$$

and obtain

$$\begin{aligned} R_n(\vec{y}, A) &= \frac{1}{2^n} \sum_{\xi\in\{0,1\}} \sum_{\vec{x}\,'\in\mathbb{F}_2^{n-1}} (-1)^{\upsilon\xi + \sum_i y_i' x_i' + \xi \sum_i a_i' x_i' + \sum_{i<j} x_i' A_{ij}' x_j'} \\ &= \frac{1}{2^n} \sum_{\vec{x}\,'\in\mathbb{F}_2^{n-1}} (-1)^{\sum_i y_i' x_i' + \sum_{i<j} x_i' A_{ij}' x_j'} + \frac{1}{2^n}(-1)^{\upsilon} \sum_{\vec{x}\,'\in\mathbb{F}_2^{n-1}} (-1)^{\sum_i (y_i' + a_i') x_i' + \sum_{i<j} x_i' A_{ij}' x_j'} \\ &= \frac{1}{2} R_{n-1}(\vec{y}\,', A') + (-1)^{\upsilon} \frac{1}{2} R_{n-1}(\vec{y}\,' + \vec{a}\,', A'). \end{aligned} \tag{B5}$$

This is the desired recurrence relation.

We already know that $R_{n-1}(\vec{y}\,', A') \in \{0, \pm r_{A'}, \pm \mathrm{i} r_{A'}\}$ for all $\vec{y}$ for some $r_{A'}$ Since the coefficients R are real, $R_{n-1}(\vec{y}\,', A') \in \{0, \pm r_{A'}\}$. Thus we have $R_n(\vec{y}, A) \in \{0, \pm\frac{1}{2} r_{A'}, \pm r_{A'}\}$. This shows that either $r_A = \frac{1}{2} r_{A'}$ or $r_A = r_{A'}$, depending on $\vec{a}\,'$.

The Maassen–Uffink relation for the graph state bases is maximally strong if and only if $r = 2^{-n/2}$. On the other hand, r is an integer multiple of 2^{-n} (even 2^{1-n}). One can see this by induction with the recurrence relation. This shows that this uncertainty relation is never maximally strong for graph state bases with an odd number of qubits.

We will now use the recurrence relation to compute r for certain classes of states, and by doing so, construct maximally strong uncertainty relations for all even numbers of qubits. We assume one graph to be empty and vary only the other one. The application of the recurrence relation is particularly easy if $R_{n-1}(\vec{y}\,', A')$ is independent of $\vec{y}\,'$, up to a sign.

First we show by induction that for the fully connected graph with an even number n of qubits, we have $R_n(\vec{y}, A) = \pm 2^{-n/2}$ for all $\vec{y}$. For $n = 2$, we have $r_2 = 1/2$. Assume the assertion to be true for $n - 2$. Let A, A', and A'' be the fully connected adjacency matrices for n, $n - 1$, and $n - 2$ qubits, respectively, and $\vec{a}\,' = (1, 1, \ldots, 1) \in \mathbb{F}_2^{n-1}$, $\vec{a}\,'' = (1, 1, \ldots, 1) \in \mathbb{F}_2^{n-2}$ and similarly for $\vec{0}$. Then

$$\begin{aligned} R_n(\vec{0}, A) &= \frac{1}{2} R_{n-1}(\vec{0}\,', A') + \frac{1}{2} R_{n-1}(\vec{a}\,', A') \\ &= \frac{1}{2}\Big[\frac{1}{2} R_{n-2}(\vec{0}\,'', A'') + \frac{1}{2} R_{n-2}(\vec{a}\,'', A'')\Big] \\ &\quad + \frac{1}{2}\Big[\frac{1}{2} R_{n-2}(\vec{a}\,'', A'') - \frac{1}{2} R_{n-2}(\vec{0}\,'', A'')\Big] \\ &= \frac{1}{2} R_{n-2}(\vec{a}\,'', A'') \\ &= \pm\frac{1}{2}\frac{1}{2^{(n-2)/2}} = \pm\frac{1}{2^{n/2}}. \end{aligned} \tag{B6}$$

This implies that $R_n(\vec{y}, A) \in \{0, \pm 2^{-n/2}\}$ for all $\vec{y}$. But because of normalization, $R_n(\vec{y}, A) = 0$ is not possible. This shows the assertion. For the fully connected graph with an odd number of qubits, we have

$$\begin{aligned} R_n(\vec{y}, A) &= \frac{1}{2} R_{n-1}(\vec{y}\,', A') \pm \frac{1}{2} R_{n-1}(\vec{y}\,' + \vec{a}\,', A') \\ &\in \big\{0, \pm\frac{1}{2^{(n-1)/2}}\big\}. \end{aligned} \tag{B7}$$

The generalization of the state in Fig. 1 (b), which is equivalent under local unitary operations to the linear

cluster state, can be treated in exactly the same way, and we obtain the same results for r_n.

[1] W. Heisenberg, Z. Phys. **43**, 172 (1927), for an English translation by J. A. Wheeler and W. H Zurek see: "The physical content of quantum kinematics and mechanics," in *Quantum Theory and Measurement*, edited by J. A. Wheeler and W. H Zurek (Princeton University Press, Princeton, 1983) pp. 62–84.

[2] E. H. Kennard, Z. Phys. **44**, 326 (1927).

[3] H. P. Robertson, Phys. Rev. **34**, 163 (1929).

[4] P. Busch, T. Heinonen, and P. Lahti, Physics Reports **452**, 155 (2007).

[5] M. Koashi, J. Phys.: Conf. Ser. **36**, 98 (2006).

[6] I. Damgård, S. Fehr, R. Renner, L. Salvail, and C. Schaffner, in *Advances in Cryptology – CRYPTO 2007*, Lecture Notes in Computer Science, Vol. 4622, edited by A. Menezes (Springer, Berlin, 2007) pp. 360–378.

[7] M. Koashi, New J. Phys. **11**, 045018 (2009).

[8] H. F. Hofmann and S. Takeuchi, Phys. Rev. A **68**, 032103 (2003).

[9] O. Gühne and M. Lewenstein, Phys. Rev. A **70**, 022316 (2004).

[10] O. Gühne, Phys. Rev. Lett. **92**, 117903 (2004).

[11] I. Białynicki-Birula and J. Mycielski, Commun. Math. Phys. **44**, 129 (1975).

[12] D. Deutsch, Phys. Rev. Lett. **50**, 631 (1983).

[13] K. Kraus, Phys. Rev. D **35**, 3070 (1987).

[14] H. Maassen and J. B. M. Uffink, Phys. Rev. Lett. **60**, 1103 (1988).

[15] S. Wehner and A. Winter, New J. Phys. **12**, 025009 (2010).

[16] M. H. Partovi, Phys. Rev. A **84**, 052117 (2011).

[17] M. Berta, M. Christandl, R. Colbeck, J. M. Renes, and R. Renner, Nat. Phys. **6**, 659 (2010).

[18] R. Prevedel, D. R. Hamel, R. Colbeck, K. Fisher, and K. J. Resch, Nat. Phys. **7**, 757 (2011).

[19] C.-F. Li, J.-S. Xu, X.-Y. Xu, K. Li, and G.-C. Guo, Nat. Phys. **7**, 752 (2011).

[20] H. P. Robertson, Phys. Rev. **46**, 794 (1934).

[21] D. A. Trifonov, Eur. Phys. J. B **29**, 349 (2002).

[22] S. Wehner and A. Winter, J. Math. Phys. **49**, 062105 (2008).

[23] M. Hein, W. Dür, J. Eisert, R. Raussendorf, M. Van den Nest, and H. J. Briegel, in *Quantum Computers, Algorithms and Chaos*, Proceedings of the International School of Physics Enrico Fermi No. 162, edited by G. Casati, D. L. Shepelyansky, P. Zoller, and G. Benenti (IOS Press, Amsterdam, 2006) p. 115, arXiv:quant-ph/0602096.

[24] R. Raussendorf and H. J. Briegel, Phys. Rev. Lett. **86**, 5188 (2001).

[25] R. Raussendorf, D. E. Browne, and H. J. Briegel, Phys. Rev. A **68**, 022312 (2003).

[26] W. Dür and H.-J. Briegel, Phys. Rev. Lett. **92**, 180403 (2004).

[27] M. Hein, W. Dür, and H.-J. Briegel, Phys. Rev. A **71**, 032350 (2005).

[28] D. Schlingemann and R. F. Werner, Phys. Rev. A **65**, 012308 (2001).

[29] G. Tóth and O. Gühne, Phys. Rev. A **72**, 022340 (2005).

[30] G. Ghirardi, L. Marinatto, and R. Romano, Phys. Lett. A **317**, 32 (2003).

[31] S. Bandyopadhyay, P. O. Boykin, V. Roychowdhury, and F. Vatan, Algorithmica **34**, 512 (2002).

[32] P. Mandayam, S. Wehner, and N. Balachandran, J. Math. Phys. **51**, 082201 (2010).

[33] P. Kurzyński, T. Paterek, R. Ramanathan, W. Laskowski, and D. Kaszlikowski, Phys. Rev. Lett. **106**, 180402 (2011).

[34] P. Hall, J. London Math. Soc. **10**, 26 (1935).

[35] J. Dehaene and B. De Moor, Phys. Rev. A **68**, 042318 (2003).

[36] M. Van den Nest, Quant. Inf. Comp. **10**, 258 (2010).

[37] M. Van den Nest, *Local equivalence of stabilizer states and codes*, Ph.D. thesis, Katholieke Universiteit Leuven (2005), ftp://ftp.esat.kuleuven.be/pub/SISTA/mvandenn/reports/05-99.ps.

Optimal inequalities for state-independent contextuality

Matthias Kleinmann,[1,*] Costantino Budroni,[2,1,†] Jan-Åke Larsson,[3,‡] Otfried Gühne,[1,§] and Adán Cabello[2,¶]

[1] *Naturwissenschaftlich-Technische Fakultät, Universität Siegen, Walter-Flex-Straße 3, D-57068 Siegen,Germany*
[2] *Departamento de Física Aplicada II, Universidad de Sevilla, E-41012 Sevilla, Spain*
[3] *Institutionen för Systemteknik, Linköpings Universitet, SE-58183 Linköping, Sweden*

Contextuality is a natural generalization of nonlocality which does not need composite systems or spacelike separation and offers a wider spectrum of interesting phenomena. Most notably, in quantum mechanics there exist scenarios where the contextual behavior is independent of the quantum state. We show that the quest for an optimal inequality separating quantum from classical noncontextual correlations in an state-independent manner admits an exact solution, as it can be formulated as a linear program. We introduce the noncontextuality polytope as a generalization of the locality polytope, and apply our method to identify two different tight optimal inequalities for the most fundamental quantum scenario with state-independent contextuality.

PACS numbers: 03.65.Ta, 03.65.Ud

Introduction.—The investigation of the operational differences between quantum mechanics and classical mechanics resulted 1964 in the discovery of Bell's inequalities [1]. Such inequalities constrain the correlations obtained from spacelike-separated measurements and are satisfied by any local hidden variable (HV) model but are violated by quantum mechanics. For every measurement scenario, there exists a minimal set of inequalities, called *tight* Bell inequalities, which provide also sufficient conditions: If all tight inequalities are satisfied, then there exists a local HV model reproducing the corresponding set of correlations [2, 3].

Mathematically speaking, each tight Bell inequality corresponds to a facet of the locality polytope [3]. This means that it is an $(p-1)$-dimensional face of the p-dimensional polytope obtained as a convex hull of the vectors representing local assignments to the results of the considered measurements. Such a polytope gives all classical probabilities associated to a local model for a given measurement scenario, and its facets give precisely the boundaries of the polytope. In this sense, tight inequalities separate classical from nonclassical correlations perfectly.

Similarly, noncontextuality inequalities [4–6] are constraints on the correlations among the results of compatible observables, which are satisfied by any noncontextual HV model. While the violation of Bell inequalities reveals nonlocality, the violation of noncontextuality inequalities reveals contextuality [7, 8], which is a natural generalization of nonlocality privileging neither composite systems (among other physical systems), nor spacelike-separated measurements (among other compatible measurements), nor entangled states (among other quantum states).

All Bell inequalities are noncontextuality inequalities, but there are two features of noncontextuality inequalities which are absent in Bell inequalities. One is that noncontextuality inequalities may be violated by simple quantum systems such as single qutrits [4]. These violations have recently been experimentally observed with photons [9]. The other is that the violation can be independent of the quantum state of the systems [5, 6], thus it reveals state-independent contextuality (SIC). The latter has been demonstrated recently with ququarts (four-level quantum systems) using ions [10], photons [11], and nuclear magnetic resonance [12].

The notion of tightness naturally applies also to noncontextuality inequalities. Tight noncontextuality inequalities are the facets of the correlation polytope of compatible observables as we will explain below. Compared with the locality polytope, the difference is in the notion of compatibility, since now one no longer considers only collections of spacelike-separated measurements, but admits more generally the measurement of a *context*, i.e., a collection of mutually compatible measurements. For a given contextuality scenario, the corresponding set of tight inequalities gives necessary and sufficient conditions for the existence of a noncontextual model.

For example, the three inequalities with state-independent violation introduced in Ref. [5], are all tight. These inequalities are only violated for ququarts (two of the inequalities) and eight-level quantum systems (the third inequality), but not for qutrits. Another example of a tight inequality is the noncontextuality inequality for qutrits of Klyachko *et al.* [4], which indeed was derived by means of the correlation polytope method. However, this latter inequality does not have a state-independent quantum violation.

Obtaining all tight inequalities is, in general, a hard task. The correlation polytope is characterized by the number of settings and outcomes of the considered scenario. While there are algorithms that find all the facets of a given polytope, the time required to compute them grows exponentially as the number of settings increases. Therefore, this method can only be applied to simple cases with a reduced number of settings [2, 4, 13]. Given the facets of the polytope, in a next step one can try to find quantum observables that exhibit a maximal gap between the maximal noncontextual value and the quantum

prediction.

In this paper we approach the problem differently. For many situations, the quantum observables are already known, and it remains to find inequalities that are tight and optimal and, in addition, may exhibit SIC. Thus we first describe the noncontextuality polytope for a given set of observables and a given list of admissible contexts. A noncontextuality inequality is then an affine hyperplane that does not intersect this polytope. We then introduce a method for maximizing the state-independent quantum violation via linear programming. The resulting linear program can be solved with standard optimization routines, and the optimality of the solution is guaranteed. As an application we derive the optimal inequality for several state independent scenarios, in particular analyzing a recently discovered qutrit scenario [14]. Using our method, we find noncontextuality inequalities with state-independent violation and the fewest number of observables and contexts. These inequalities turn out to be in addition tight and hence provide the most fundamental examples of inequalities with state-independent violation.

Contextuality scenarios, the noncontextuality polytope, and noncontextuality inequalities.—We start from some given dichotomic [15] quantum observables $A_1, A_2, \ldots, A_n$. A context $\underline{\mathfrak{c}}$ is then a set of indices, such that A_k and A_ℓ are compatible whenever $k, \ell \in \underline{\mathfrak{c}}$, i.e., $[A_k, A_\ell] = 0$. For example if A_1 and A_2 are compatible, then valid contexts would be $\{1\}$, $\{2\}$, and $\{1, 2\}$. As we see below, it may be interesting to consider only a certain admissible subset $\mathfrak{C}$ of the set of all possible contexts $\{\underline{\mathfrak{c}}\}$. The observables $A_1, \ldots, A_n$, together with the list of admissible contexts $\mathfrak{C}$, form the contextuality scenario.

The set of all (contextual as well as noncontextual) correlations for such a scenario can be represented by the following standard construction. We first use that, if A_k and A_ℓ are compatible, then the expectation value of A_k is not changed whether or not A_ℓ is measured in the same context. Thus, instead of considering all correlations, it suffices to only consider the vector $\vec{v} = (v_{\underline{\mathfrak{c}}} \mid \underline{\mathfrak{c}} \in \mathfrak{C})$, where $v_{\underline{\mathfrak{c}}}$ is the expectation value of the product of the values of the observables indexed by $\underline{\mathfrak{c}}$. For example, for the contexts $\{1\}$, $\{2\}$, $\{1, 2\}$, a contextual HV model may with equal probability assign the values $\{+1\}$, $\{+1\}$, $\{-1, +1\}$, or $\{-1\}$, $\{-1\}$, $\{+1, -1\}$, respectively, yielding $\vec{v} \equiv (v_1, v_2, v_{1,2}) = (1/2, 1/2, -1)$.

In the simplest *noncontextual* HV model, however, each observable has a fixed assignment $\vec{a} \equiv (a_1, \ldots, a_n) \in \{-1, 1\}^n$ for the observables $A_1, \ldots, A_n$, and accordingly each entry in $\vec{v}$ is exactly the product of the assigned values, i.e., $v_{\underline{\mathfrak{c}}} = \prod_{k \in \underline{\mathfrak{c}}} a_k$. The most general noncontextual HV model predicts fixed assignments $\vec{a}^{(i)}$ with probabilities p_i, and hence the set of correlations that can be explained by a noncontextual HV models is characterized by the convex hull of the models with fixed assignments, thus forming the noncontextuality polytope.

Then, a noncontextuality inequality is an affine bound on the noncontextuality polytope, i.e., a real vector $\vec{\lambda}$ such that $\eta \geq \vec{\lambda} \cdot \vec{v}$ for all correlation vectors v that originate from a noncontextual model:

$$\eta \geq \sum_{\underline{\mathfrak{c}} \in \mathfrak{C}} \lambda_{\underline{\mathfrak{c}}} \prod_{k \in \underline{\mathfrak{c}}} a_k, \tag{1}$$

for any assignment $\vec{a} \equiv (a_1, \ldots, a_n) \in \{-1, 1\}^n$.

In quantum mechanics, in contrast, the measurement of the entry $v_{\underline{\mathfrak{c}}}$ corresponds to the expectation value $\langle \prod_{k \in \underline{\mathfrak{c}}} A_k \rangle_\rho$, where ρ specifies the quantum state. Thus the value of $\vec{\lambda} \cdot \vec{v}$ predicted by quantum mechanics is given by $\langle T(\vec{\lambda}) \rangle_\rho$, with

$$T(\vec{\lambda}) = \sum_{\underline{\mathfrak{c}} \in \mathfrak{C}} \lambda_{\underline{\mathfrak{c}}} \prod_{k \in \underline{\mathfrak{c}}} A_k. \tag{2}$$

If the expectation value exceeds the noncontextual limit η, then the inequality demonstrates contextual behavior, yielding the quantum violation

$$\mathcal{V} = \frac{\max_\rho \langle T(\vec{\lambda}) \rangle_\rho}{\eta} - 1. \tag{3}$$

An inequality is optimal, if the violation is maximal for the given contextuality scenario. In general, this optimization is difficult to perform and it is not always clear that an optimal inequality also yields the most significant violation [16].

Optimal state independent violation and tight inequalities.—However, if we require a state independent violation of the inequality, without loss of generality, $T(\vec{\lambda}) = \mathbb{1}$ and hence the optimization over the quantum state ϱ vanishes. Then, the coefficient vector $\vec{\lambda}$ and the noncontextuality bound η are optimal if η is minimal under the constraint $T(\vec{\lambda}) = \mathbb{1}$ and if the inequalities in Eq. (1) are satisfied. That is, we ask for a solution $(\eta^*, \vec{\lambda}^*)$ of the optimization problem

$$\begin{aligned} \text{minimize:} \quad & \eta, \\ \text{subject to:} \quad & T(\vec{\lambda}) = \mathbb{1} \text{ and} \\ & \text{Eq. (1) holds for all } \vec{a}. \end{aligned} \tag{4}$$

This optimization problem is a linear program and such programs can be solved efficiently by standard numerical techniques and optimality is then guaranteed. We implemented this optimization using CVXOPT [17] for Python, which allows us to study inequalities with up to $n = 21$ observables and $|\mathfrak{C}| = 131$ contexts. Note that this program also solves the feasibility problem, whether a contextuality scenario exhibits SIC at all. This is the case, if and only if the program finds a solution with $\eta < 1$ and thus $\mathcal{V} > 0$.

The optimal coefficients $\vec{\lambda}^*$ are, in general, not unique but rather form a polytope defined by Eq. (1) with $\eta =$

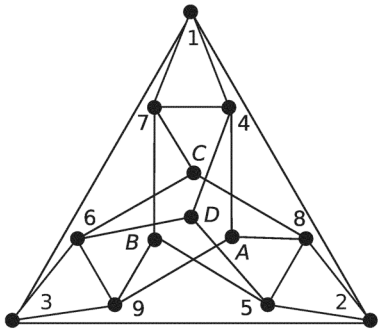

$v_1 = (1,0,0)$ $v_5 = (1,0,-1)$ $v_A = (-1,1,1)$
$v_2 = (0,1,0)$ $v_6 = (1,-1,0)$ $v_B = (1,-1,1)$
$v_3 = (0,0,1)$ $v_7 = (0,1,1)$ $v_C = (1,1,-1)$
$v_4 = (0,1,-1)$ $v_8 = (1,0,1)$ $v_D = (1,1,1)$
$v_9 = (1,1,0)$

FIG. 1. Graph of the compatibility relations between the observables for the Yu-Oh scenario. Nodes represent vectors $|v_i\rangle$ [or the observables A_i defined in (5)] and edges represent orthogonality (or compatibility) relations.

$\underline{\mathfrak{c}}$	YO	opt_2	opt_3	$\underline{\mathfrak{c}}$	YO	opt_2	opt_3	$\underline{\mathfrak{c}}$	YO	opt_2	opt_3
1	2	2	1	A-D	2	1	2	3, 9	−1	−2	−1
2	2	3	1	1,2	−1	−1	−2	4, 7	−1	0	−1
3	2	3	1	1,3	−1	−1	−2	5, 8	−1	−2	−1
4	2	1	1	1,4	−1	−1	−1	6, 9	−1	−2	−1
5	2	2	1	1,7	−1	−1	−1	$*$,A-D	−1	−1	−2
6	2	2	1	2,3	−1	−2	−2	1,2,3	–	–	0
7	2	1	1	2,5	−1	−2	−1	1,4,7	–	–	−3
8	2	2	1	2,8	−1	−2	−1	2,5,8	–	–	−3
9	2	2	1	3,6	−1	−2	−1	3,6,9	–	–	−3

TABLE I. Coefficients $\lambda_{\underline{\mathfrak{c}}}$ of inequalities for the Yu-Oh scenario. The column $\underline{\mathfrak{c}}$ labels the different contexts, YO the coefficients in the inequality of Ref. [14], opt_2 an optimal tight inequality with contexts of maximal size 2, opt_3 an optimal tight inequality with contexts of all sizes. For compactness, the coefficients in the column YO have been multiplied by 50/3, for the column opt_2 by 52/3 and for the column opt_3 by 83/3. The row labeled "A–D" shows the coefficients for the contexts $\{A\}$, $\{B\}$, $\{C\}$, $\{D\}$ and the row labeled "$*$,A–D" shows the coefficients for $\{4,A\}$, $\{8,A\}$, $\{9,A\}$, $\{5,B\}$, $\{7,B\}$, $\{9,B\}$, $\{6,C\}$, $\{7,C\}$, $\{8,C\}$, $\{4,D\}$, $\{5,D\}$, $\{6,D\}$.

η^*. This leaves the possibility to find optimal inequalities with further special properties. There are at least two important properties that one may ask for. Firstly, from an experimental point of view, it would be desirable to have some of the coefficients $\lambda_{\underline{\mathfrak{c}}} = 0$, since then the context $\underline{\mathfrak{c}}$ does not need to be measured. In general, it will depend on the experimental setup, which coefficients $\lambda_{\underline{\mathfrak{c}}} = 0$ yield the greatest advantage. For the sequential measurement schemes it is natural to choose the longest measurement sequences. Secondly, there might be *tight* inequalities among the optimal solutions: An inequality is tight, if the affine hyperplane given by the solutions of $\eta = \vec{\lambda} \cdot \vec{x}$ is tangent to a facet of the noncontextuality polytope. This property can be readily checked using Pitowsky's construction [3]: Denote by p the affine dimension of the noncontextuality polytope and choose those assignments $\vec{a}$, for which Eq. (1) is saturated. Then, the inequality is tangent to a facet if and only if the affine space spanned by the vertices $\vec{v} \equiv (\prod_{k \in \underline{\mathfrak{c}}} a_k \mid \underline{\mathfrak{c}} \in \mathfrak{C})$ is $(p-1)$-dimensional.

Furthermore, we mention that the condition of state independence might be loosened to only require that the quantum violation is *at least* $\mathcal{V}$ for all quantum states. This corresponds to replacing the condition $T(\vec{\lambda}) = \mathbb{1}$ by the condition that $T(\vec{\lambda}) - \mathbb{1}$ is positive semidefinite. Then, the linear program in Eq. (4) becomes a semidefinite program, which still can be solved by standard numerical methods with optimality guaranteed. However, for the examples that we consider in the following, the semidefinite and the linear program yield the same results.

Most fundamental noncontextuality inequalities.—We now apply our method to the SIC scenario for a qutrit system introduced by Yu and Oh [14]. Qutrit systems are of fundamental interest, since no smaller quantum system can exhibit a contextual behavior [8]. It has been shown, that this scenario is the simplest possible SIC scenario for a qutrit [18].

For a qutrit system, the dichotomic observables are of the form

$$A_i = \mathbb{1} - 2|v_i\rangle\langle v_i|. \tag{5}$$

In the Yu-Oh scenario, there are 13 observables defined by the 13 unit vectors $|v_i\rangle$ provided in Fig. 1. In the according graph, each operator is represented by node $i \in V$ of the graph $G = (V, E)$ and an edge $(i,j) \in E$ indicates that $|v_i\rangle$ and $|v_j\rangle$ are orthogonal, $\langle v_j|v_i\rangle = 0$, so that A_i and A_j are compatible. The original inequality takes into account all contexts of size one and two, $\mathfrak{C}_{\text{YO}} = \{\{1\}, \ldots, \{D\}\} \cup E$ and the coefficients were chosen to $\lambda_{\underline{\mathfrak{c}}} = -3/50$ if $\underline{\mathfrak{c}} \in E$ and $\lambda_{\underline{\mathfrak{c}}} = 6/50$ else. This yields an inequality with a state-independent quantum violation of $\mathcal{V} = 1/24 \approx 4.2\%$.

With the linear program we find that the maximal violation for the contexts $\mathfrak{C}_{\text{YO}}$ is $\mathcal{V} = 1/12 \approx 8.3\%$ and thus twice that of the inequality in Ref [14]. Interestingly, among the optimal coefficients $\vec{\lambda}^*$ there is a solution which is tight and for which the coefficients $\lambda_{4,7}$ vanishes, cf. Table I, column "opt_2" for the list coefficients. We find that up to symmetries, $\lambda_{4,7}$ is the only context that can be omitted while still preserving optimality.

In order to demonstrate the practical advantage, let us discuss the recent experimental values obtained for the Yu-Oh scenario [19, FIG. 2]. For those values, the original Yu-Oh inequality is violated by 3.7 standard deviations. But if the same data is evaluated using our optimal inequality "opt_2", the violation increases to 7.5

standard deviations. We mention, however, that the particular experimental setup implements the same observable in different context differently, thus easily allowing a noncontextual HV model explaining the data [20]. A setup avoiding such problems is described in Ref. [21].

The maximal contexts in the Yu-Oh scenario are of size three, and hence it is possible to include also the corresponding terms in the inequality, i.e., we extend the contexts $\mathfrak{C}_{\mathrm{YO}}$ by the contexts $\{1,2,3\}$, $\{1,4,7\}$, $\{2,5,8\}$, and $\{3,6,9\}$. Since this increases the number of parameters in the inequality, there is a chance that this case allows an even higher violation. In fact, the maximal violation is $\mathcal{V} = 8/75 \approx 10.7\%$. Again, it is possible to find tight inequalities with vanishing coefficients, and in particular the context $\{1,2,3\}$ can be omitted; the list of coefficients is given in Table I, column "opt_3".

Further examples.—Our method is applicable to all SIC scenarios, providing the optimal inequality. We mention two further examples: (i) The "extended Peres-Mermin square" uses as observables all 15 products of Pauli operators on a two-qubit system, $(\sigma_\mu \otimes \sigma_\nu)$ [22]. The optimal violation is $\mathcal{V} = 2/3$, where only contexts of size three need to be measured and $\lambda_{\underline{\mathfrak{C}}} = 1/15$, except $\lambda_{xx,yy,zz} = \lambda_{xz,yx,zy} = \lambda_{xy,yz,zx} = -1/15$. Among the optimal solutions no simpler inequality exists. (ii) The 18 vector proof [23] of the Kochen-Specker theorem uses a ququart system and 18 observables of the form (5). For contexts up to size 2 the maximal violation is $\mathcal{V} = 1/17 \approx 5.9\%$ (cf. [24]), while including all context the maximal violation is $\mathcal{V} = 2/7 \approx 28.6\%$ (cf. [5]). The situation where only contexts up to size 3 are admissible has not yet been studied and we find numerically a maximal violation of $\mathcal{V} \approx 14.3\%$.

Conclusions.—Contextuality is suspected to be one of the fundamental phenomena in quantum mechanics. While it can be seen as the underlying property of the nonlocal behavior of quantum mechanics, so far no methods for a systematic investigation have been developed. We here showed that Pitowsky's polytope naturally generalizes to the noncontextual scenario and hence the question of a full characterization of this noncontextuality polytope arises. This can be done via the so-called tight inequalities. On the other hand, among the most striking aspects where contextuality is more general than nonlocality is that the former can be found to be independent of the quantum state. For this state-independent scenario, we showed that the search for the optimal inequality reduces to a linear program, which can be solved numerically with optimality guaranteed. We studied several cases of this optimization and find that in all those instances one can construct noncontextuality inequalities with a state independent violation that are, in addition, tight. This is in particular the case for the most fundamental scenario of state independent contextuality [14] and we presented two essentially different inequalities—one involves at most contexts of size two, the other of size three. We hence lifted the Yu-Oh scenario to the same fundamental status as the CHSH Bell inequality [25], which is the simplest scenario for nonlocality. Our state-independent tight inequalities are particularly suitable for experimental tests and hence we expect that they stimulate experiments to finally observe SIC in qutrits [21].

The authors thank J. R. Portillo for checking some calculations. This work was supported by the Spanish Project No. FIS2011-29400, the EU (Marie-Curie CIG 293933/ENFOQI), the Austrian Science Fund (FWF): Y376-N16 (START prize), and the BMBF (CHIST-ERA network QUASAR).

* matthias.kleinmann@uni-siegen.de
† cbudroni@us.es
‡ jan-ake.larsson@liu.se
§ otfried.guehne@uni-siegen.de
¶ adan@us.es

[1] J. S. Bell, Physics **1**, 195 (1964).
[2] A. Fine, Phys. Rev. Lett. **48**, 291 (1982).
[3] I. Pitowsky, *Quantum Probability-Quantum Logic* (Springer, Berlin, 1982).
[4] A. A. Klyachko, M. A. Can, S. Binicioğlu, and A. S. Shumovsky, Phys. Rev. Lett. **101**, 020403 (2008).
[5] A. Cabello, Phys. Rev. Lett. **101**, 210401 (2008).
[6] P. Badziąg, I. Bengtsson, A. Cabello, and I. Pitowsky, Phys. Rev. Lett. **103**, 050401 (2009).
[7] E. Specker, Dialectica **14**, 239 (1960).
[8] J. S. Bell, Rev. Mod. Phys. **38**, 447 (1966); S. Kochen and E. P. Specker, J. Math. Mech. **17**, 59 (1967).
[9] R. Łapkiewicz, P. Li, C. Schaeff, N. K. Langford, S. Ramelow, M. Wieśniak, and A. Zeilinger, Nature (London) **474**, 490 (2011); J. Ahrens, E. Amselem, A. Cabello, and M. Bourennane, (unpublished).
[10] G. Kirchmair, F. Zähringer, R. Gerritsma, M. Kleinmann, O. Gühne, A. Cabello, R. Blatt, and C. F. Roos, Nature (London) **460**, 494 (2009).
[11] E. Amselem, M. Rådmark, M. Bourennane, and A. Cabello, Phys. Rev. Lett. **103**, 160405 (2009).
[12] O. Moussa, C. A. Ryan, D. G. Cory, and R. Laflamme, Phys. Rev. Lett. **104**, 160501 (2010).
[13] I. Pitowsky and K. Svozil, Phys. Rev. A **64**, 014102 (2001); D. Collins and N. Gisin, J. Phys. A: Math. Gen. **37**, 1775 (2004).
[14] S. Yu and C. H. Oh, Phys. Rev. Lett. **108**, 030402 (2012).
[15] Dichotomy is not a restriction, since using the spectral decomposition $X = \sum \lambda_i \Pi_i$ the observable X can be replaced by the dichotomic observables $X_i = 2\Pi_i - \mathbb{1}$.
[16] B. Jungnitsch, S. Niekamp, M. Kleinmann, O. Gühne, H. Lu, W.-B. Gao, Y.-A. Chen, Z.-B. Chen, and J.-W. Pan, Phys. Rev. Lett. **104**, 210401 (2010).
[17] "CVXOPT," http://abel.ee.ucla.edu/cvxopt/.
[18] A. Cabello, arXiv:1112.5149v2.
[19] C. Zu, Y.-X. Wang, D.-L. Deng, X.-Y. Chang, K. Liu, P.-Y. Hou, H.-X. Yang, and L.-M. Duan, Phys. Rev. Lett. **109**, 150401 (2012).
[20] O. Gühne, M. Kleinmann, A. Cabello, J.-Å. Larsson, G. Kirchmair, F. Zähringer, R. Gerritsma, and C. F.

Roos, Phys. Rev. A **81**, 022121 (2010).
[21] A. Cabello, E. Amselem, K. Blanchfield, M. Bourennane, and I. Bengtsson, Phys. Rev. A **85**, 032108 (2012).
[22] A. Cabello, Phys. Rev. A **82**, 032110 (2010).
[23] A. Cabello, J. M. Estebaranz, and G. García-Alcaine, Phys. Lett. A **212**, 183 (1996).
[24] S. Yu and C. Oh, arXiv:1112.5513v1.
[25] J. F. Clauser, M. A. Horne, A. Shimony, and R. A. Holt, Phys. Rev. Lett. **23**, 880 (1969); Phys. Rev. Lett. **24**, 549 (1970).

Typical local measurements in generalised probabilistic theories: emergence of quantum bipartite correlations

Matthias Kleinmann,[1,*] Tobias J. Osborne,[2,†] Volkher B. Scholz,[3,2,‡] and Albert H. Werner[2,§]

[1] *Naturwissenschaftlich-Technische Fakultät, Universität Siegen, Walter-Flex-Straße 3, 57068 Siegen, Germany*
[2] *Institut für Theoretische Physik, Leibniz Universität Hannover, Appelstraße 2, 30167 Hannover, Germany*
[3] *Institut für Theoretische Physik, ETH Zurich, Wolfgang-Pauli-Strasse 27, 8093 Zurich, Switzerland*

(Dated: 15 May 2012)

What singles out quantum mechanics as the fundamental theory of Nature? Here we study local measurements in generalised probabilistic theories (GPTs) and investigate how observational limitations affect the production of correlations. We find that if only a subset of *typical* local measurements can be made then all the bipartite correlations produced in a GPT can be simulated to a high degree of accuracy by quantum mechanics. Our result makes use of a generalisation of Dvoretzky's theorem for GPTs. The tripartite correlations can go beyond those exhibited by quantum mechanics, however.

PACS numbers: 03.65.Ta, 03.65.Ud

Introduction.—The continued success of quantum mechanics (QM) strongly implies that it is the fundamental description of Nature. However, it could still be that QM is simply a very good effective theory which breaks down if we are able to perform experiments with sufficiently high energy and precision. In this case QM would need to be replaced by a more general "post-quantum" theory. In particular *generalised probabilistic theories* (GPTs) [1–5] have received considerable attention recently, both as a foil to better understand the features of QM, and as a powerful abstract way to reason about correlations and locality. These investigations have lead to many interesting results, including simplified and improved cryptographic schemes and primitives [6, 7].

If Nature is actually described by a theory other than QM then the natural question arises: why is QM such a good effective theory? A natural answer, which we investigate here, is that experimental imperfections prevent us from observing any post-quantum phenomena.

Suppose that Nature is described by a GPT with a high-dimensional state space and corresponding high-dimensional set of all possible measurements. Observational limitations, such as detector resolution, mean that it is impossible to access most of these theoretically possible measurements. If physically implementable measurements are those chosen from some *typical* subset (a precise definition is given in the sequel) then we show that the *bipartite* correlations arising in any experiment can be modelled, to a high degree of precision, by those of QM. Note that the tripartite and multipartite correlations could go beyond those exhibited by QM: a sufficiently refined experiment involving three or more particles could exhibit behavior going beyond that possible within QM.

It is interesting to contrast our setting with that of *decoherence*, which models the passage from the microscopic to the macroscopic *classical* world [8, 9]. The crucial difference here is that decoherence arises from the correlations developed between a given particle and many other inaccessible particles (in the GPT framework it is rather likely that decoherence will always leads to an effective classical theory). By way of contrast, we consider only a few particles in isolation: roughly speaking, we study the case where only the "local dimensions" are effectively truncated.

Our argument builds on several important prior ideas. The first arises from the search [10–13] for an axiomatic derivation of QM: it was realised that a reasonable physical theory should allow for the convex combination of different possible measurements, and hence the underlying sets of both states and measurements should be *dual* convex bodies. These developments have lead to the identification of generalised probabilistic theories as a general framework to study theories of physics going beyond QM.

The second cornerstone of our argument is the *concentration of measure phenomenon* [14, 15] epitomized by Dvoretzky's theorem which states, roughly, that a random low-dimensional section of a high-dimensional convex body looks approximately spherical. This powerful result has already found myriad applications in quantum information theory, e.g., in quantum Shannon theory [16, 17], and quantum computational complexity theory [18, 19]. Here we adapt the "tangible" version of Dvoretzky's theorem for our purposes.

The final idea we exploit is the observation that *spherical* state spaces can be simulated by *sections* of quantum mechanical state spaces [20]. As will become evident, our approach owes much to the recent work [21, 22] showing that bipartite correlations may be modelled by QM when the constituents locally obey QM.

Here we exploit these three core ideas to obtain our

Main result. *If the local measurements in a GPT are chosen from a typical section of the convex body of all possible measurements then, with a high degree of accu-*

racy, they do not yield any post-quantum prediction for the bipartite scenario.

More specifically, we require that the physically implementable measurements are in essence given by the section of the convex body of all measurements with a low-dimensional $O(n)$-*typical* subspace. This means that the accessible measurements span a subspace and the choice of this subspace is not particular among all other subspaces of the same dimension. This is a core assumption in our argument. Although we restrict our attention here to the case of a $O(n)$-typical subspaces, it is likely that our result extends to a much wider variety of typicality notions.

Our argument then implies that for most measurements given by low-dimensional subspaces the outcomes can be explained using quantum mechanics. Hence we argue that those measurement devices revealing any post-quantum behavior are extremely difficult to build—since the choice of the right subspace requires extreme fine tuning.

Probabilistic physical theories, ordered vector spaces.— It is useful to formulate GPTs in the mathematical language of *ordered vector spaces* [2, 23, 24]: we begin with the description of the single-party state space and local measurements. The system is always assumed to be in a *state* ω, which encodes the probabilities of each outcome of all the possible measurements that may be performed. The set of all possible states, *state space*, is denoted Ω. Since any *probabilistic* combination of states is, in principle, preparable, Ω is a convex set. We always assume that Ω is represented as a subset of $\mathbb{R}^n$.

A state $\omega \in \Omega$ assigns a probability to each *outcome* of any possible measurement; a measurement outcome is represented by a map $f : \Omega \to [0, 1]$. This map respects probabilistic mixtures of states, meaning that $f(p\omega_1 + (1-p)\omega_2) = pf(\omega_1) + (1-p)f(\omega_2)$. Extending each map linearly allows us to conclude that measurement outcomes are elements of the *dual space* V to $\mathbb{R}^n$. Any such f is called an *effect*. A special effect is the *unit effect* e defined by $e(\omega) = 1$ for all $\omega \in \Omega$. The unit effect represents a measurement with a single outcome: this is certain to occur regardless of what the state is. Convex combinations of effects are themselves assumed to be legal effects, so the set of effects is a convex subset of the *dual* vector space V. A *measurement* with M outcomes is then a set of effects $\{f_j\}_{j=1}^M$ summing to the unit effect $e = \sum_{j=1}^M f_j$. This ensures that outcome probabilities of measurements sum to one. It is convenient to introduce the *cone* generated by the zero effect, the unit effect, and all other effects, i.e., the set $V^+ \equiv \{tf \,|\, t \geq 0, f \text{ is an effect}\}$.

The triple (V, V^+, e) is known as an *ordered unit vector space* and encodes all of the theoretically possible local effects of a GPT. Throughout the following we regard (V, V^+, e) as the fundamental defining representation of a GPT with state space as a derived concept (i.e., Ω is henceforth *defined* as the set of all positive linear functionals ω on V such that $e(\omega) = 1$). It is convenient to assume a further property, namely, that the triple (V, V^+, e) is *Archimedean*. This means that if $te+f \in V^+$ for all $t > 0$, then $f \in V^+$. Such *Archimedean ordered unit vector* spaces are referred to as *AOU spaces* in the sequel. The Archimedean axiom is a kind of closure assumption which allows us, for example, to construct the order norm $\|f\|_+ \equiv \inf\{t \,|\, te \pm f \in V^+, t \geq 0\}$. All ordered vector spaces can be *Archimedeanised* [25], and from now on we assume that the effects of a GPT are suitably represented by an AOU space.

An important example of a GPT is that of *quantum mechanics* itself: an n-level quantum system is described by an AOU space where $V \subset M_n(\mathbb{C})$ is the set of $n \times n$ hermitian matrices. The effects are then the matrices $F \in V$ with $0 \leq F \leq \mathbb{1}$ and the unit is $e \equiv \mathbb{1}$. The cone V^+ generated by these effects is hence given by the positive semidefinite matrices. One can verify that the triple (V, V^+, e) is Archimedean. State space Ω is given by $\{F \mapsto \mathrm{tr}(\rho F) \,|\, \rho \in V^+, \mathrm{tr}(\rho) = 1\}$ and the order norm $\|A\|_+$ is given by the largest singular value of A.

Sections of GPTs.—Here we study the effective theories arising from GPTs when only a subset of the possible effects may be implemented. For this purpose it is useful to introduce the notion of a linear map between AOU spaces: we say that a linear map $\varphi \colon V \to W$ between two AOU spaces (V, V^+, e_V) and (W, W^+, e_W) is *positive* if $\varphi(V^+) \subset W^+$ and φ is *unital* when $\varphi(e_V) = e_W$.

Our definition of a *section* of a GPT/AOU space W is then motivated by the observation that if we can only implement some subset of the effects in W^+ then we can implement any convex combination of them. A particular example of such a restriction is the *intersection* of W^+ with some subspace $V \subset W$. Since we can always apply the "do nothing" measurement, we require the subspace V to contain e_W. Abstractly, a section of (W, W^+, e_W) is defined to be a positive unital injection $\phi : V \hookrightarrow W$ such that $\phi(V^+) = W^+ \cap \mathrm{im}\,\phi$. This last condition has the consequence that the left inverse ϕ^{-1} is also a positive unital linear map.

When restricted to a section of a GPT (W, W^+, e_W) the state space of the section (V, V^+, e_V) is given by a *quotient* of the state space of W, i.e., $\Omega_V = \Omega_W / \sim$, where the equivalence relation is determined by $\omega \sim \sigma$ if $f(\omega) = f(\sigma)$ for all $f \in V$. This quotient is the *shadow* of the convex body Ω_W on the subspace V.

We now describe the AOU space playing the central role in our argument. This space is given by triple $(\mathbb{R}^{n+1}, C^+_{n+1}(c), (1, \vec{0}))$ where $C^+_{n+1}(c)$ denotes the $(n+1)$-dimensional Euclidean cone with length-diameter ratio $c : 2$, i.e.,

$$C^+_{n+1}(c) = \{(t, \vec{x}) \in \mathbb{R}_+ \times \mathbb{R}^n \mid t \geq c\|\vec{x}\|_2\}, \qquad (1)$$

of which $e = (1, \vec{0})$ is the order unit.

It is a nontrivial fact that this space can be embedded into a quantum system, i.e., it is a section of QM. The argument is due to Tsirelson [20] and proceeds as follows. Let $m = n/2$ if n is even and $m = (n+1)/2$ for odd n and define $\gamma_1, \ldots, \gamma_{2m} \in M_{2^m}(\mathbb{C})$ via $\gamma_{2j-1} = \sigma_z^{(1)} \cdots \sigma_z^{(j-1)} \sigma_x^{(j)}$ and $\gamma_{2j} = \sigma_z^{(1)} \cdots \sigma_z^{(j-1)} \sigma_y^{(j)}$, where we've employed the standard Pauli matrix notation and juxtaposition indicates an implicit tensor product. Consider the positive unital injection

$$\varphi \colon (t, \vec{x}) \mapsto t\mathbb{1} + c \sum_j x_j \gamma_j, \tag{2}$$

(The positivity follows from $2t\,\varphi(t,\vec{x}) = \varphi(t,\vec{x})^2 + (t^2 - c^2\|x\|_2^2)\,\mathbb{1} \geq 0$, arising from $\gamma_j\gamma_k + \gamma_k\gamma_j = 2\delta_{jk}\mathbb{1}$). Since φ is an injection, it has a left-inverse

$$\varphi' \colon A \mapsto (\operatorname{tr} A, \operatorname{tr}(A\gamma_i)/c))/2^m, \tag{3}$$

which is again positive. (Let $x_i \equiv \operatorname{tr}(A\gamma_i)$, so that $\operatorname{tr}(A) - c\|\vec{x}/c\|_2 = \operatorname{tr}[A\varphi(1, -(\vec{x}/\|\vec{x}\|_2)/c)] \geq 0$, since both matrices in the trace are already positive.)

Multipartite systems.—We now discuss how to form joint systems in the GPT framework. Suppose Alice and Bob are each in possession of a GPT (V_A, V_A^+, e_A) and (V_B, V_B^+, e_B), respectively, which describes the purely *local* measurements for each party. The *joint GPT* is then *defined* to be the AOU space $(V_A \otimes V_B, V_{AB}^+, e_A \otimes e_B)$ where, in order to proceed, we must specify how to construct the cone $V_{AB}^+ \equiv$ "$(V_A \otimes V_B)^+$". There are an infinite variety of possibilities, however, we may restrict our attention to the following two extremal definitions [26]. The first corresponds to the *maximal tensor product* $(V_A \otimes_{\max} V_B)^+$ which is defined to be the Archimedeanisation of the cone $\{\sum_{j=1}^k f_j \otimes g_j \,|\, f_j \in V_A^+, g_j \in V_B^+, k \in \mathbb{N}\}$ and the second to the *minimal tensor product* $(V_A \otimes_{\min} V_B)^+ \equiv \{u \in V_A \otimes V_B \,|\, (\omega_A \otimes \omega_B)(u) \geq 0, \text{for all } \omega_A \in \Omega_A \text{ and } \omega_B \in \Omega_B\}$.

By way of contrast, the tensor product used in the formation of joint systems in quantum mechanics is neither the minimal nor maximal one, but is rather strictly in between: $(V_A \otimes_{\max} V_B)^+ \subset (V_A \otimes_{\mathrm{QM}} V_B)^+ \subset (V_A \otimes_{\min} V_B)^+$. The quantum mechanical tensor cone V_{AB}^+ is given by the set of positive semidefinite operators in $M_{n_A}(\mathbb{C}) \otimes M_{n_B}(\mathbb{C})$. The state space $\Omega_{AB}^{\min}$ corresponding to $(V_A \otimes_{\min} V_B)^+$ is precisely the set of *separable states* and the state space $\Omega_{AB}^{\max}$ corresponding to $(V_A \otimes_{\max} V_B)^+$ is given by the set of all positive semidefinite operators W with $\operatorname{tr}(W) = 1$ which satisfy $\operatorname{tr}(WA \otimes B) \geq 0$, $\forall A, B \geq 0$. This set is dual to the set of *entanglement witnesses* [27] and includes all legal density operators as well as some operators with negative eigenvalues. Even though the state space $\Omega_{AB}^{\max}$ in the case where our local GPTs are QM is strictly larger than quantum mechanical state space, results of [21, 22] show that it does not give rise to any bipartite correlations going beyond QM. The following proposition is a slight generalization of this statement, dealing with (local) sections of quantum systems.

Proposition 1. *Consider two AOU spaces (V_A, V_A^+, e_A) and (V_B, V_B^+, e_B) which are sections of quantum systems with according positive unital injections φ_A and φ_B into an n_A-level (respectively, n_B-level) quantum system. Assume, without loss of generality, that $n_A \leq n_B$. Then for any positive unital bilinear map $\omega_{AB} \colon V_A \times V_B \to \mathbb{R}$ there exists a state σ_{AB} of the composite quantum system AB and a positive unital automorphism ψ on B such that $\omega_{AB}(f,g) = \operatorname{tr}(\sigma_{AB}\ \varphi_A(f) \otimes (\psi \circ \varphi_B)(g))$.*

Proof. By assumption the map $\omega'_{AB}(M_A, M_B) \mapsto \omega_{AB}(\varphi_A^{-1}(M_A), \varphi_B^{-1}(M_B))$ is positive and unital on the quantum systems A, B. Hence the statement reduces to the case where φ_A and φ_B are both the identity mapping. A proof for this case was given by Barnum et al. [21]. □

We stress that the existence of positive unital left inverse maps φ_A^{-1} and φ_B^{-1} is essential for this result to hold. Indeed, in the case of a hypothetical nonlocal box [28], it is impossible to find positive unital maps into quantum such that there left inverse is also positive and hence non-local boxes allow post-quantum behavior. It is also important to note that Proposition 1 does not generalize to more than two parties [22].

Typical sections, main result.—Consider an arbitrary pair of n-dimensional GPTs A and B and suppose that we are only able to access a *typical section* of the set of local effects for A (respectively, B). This is modelled by the intersection of V_A^+ (respectively, V_B^+) with a typical k-dimensional subspace, $k \ll n$. To do this abstractly we choose a bijection T between V and $\mathbb{R}^n$ and consider a random linear injection $X \colon \mathbb{R}^k \hookrightarrow \mathbb{R}^n$ such that the random variable $X(\vec{x})$ is distributed according to the uniform measure on the Euclidean $(n-1)$-sphere of radius $\|\vec{x}\|_2$. (That is, X is an $O(n)$-random rotation of an embedded fiducial k-dimensional subspace.) We call

$$Q(t, \vec{x}) = te + TX(\vec{x}) \tag{4}$$

a *centered random section* of $\mathbb{R}^{k+1}$ into V and it ensures that every subspace corresponding to a typical choice of measurement settings contains the neutral effect e. Since only convex combinations of e with $TX(\mathbb{R}^k)$ are feasible, we now study the cone $V^+ \cap Q(\mathbb{R}_+, \mathbb{R}^k)$.

The following result captures the *concentration of measure* phenomenon for our setting.

Proposition 2. *Let (V, V^+, e) be an n-dimensional AOU space and $0 < \varepsilon < 1$. Then for $k \leq \mathcal{O}(\varepsilon^2 \log n)$ there exists a $k+1$ dimensional centered random section Q of V, such that, with high probability,*

$$Q(C_{k+1}^+(1+\varepsilon)) \subset V^+ \cap Q(\mathbb{R}_+, \mathbb{R}^k) \subset Q(C_{k+1}^+(1-\varepsilon)). \tag{5}$$

Proof. At the heart of the proof is the following "tangible" version of Dvoretzky's theorem [14, 17, 29]: If $\eta\colon S^{n-1} \to \mathbb{R}$ is a Lipschitz function with constant L and central value 1 (with respect to the uniform spherical measure on S^{n-1}), then for every $\varepsilon > 0$, if $E \subset \mathbb{R}^n$ is a random subspace of dimension $k \leq k_0 = c_0 \varepsilon^2\, n/L^2$, we have, that

$$\text{Prob}\left[\sup_{S^{n-1}\cap E} |\eta(\vec{x}) - 1| > \varepsilon\right] \leq c_1 \mathrm{e}^{-c_2 k_0}, \qquad (6)$$

where c_0, c_1, and c_2 are absolute constants.

For our scenario, we use $\eta(\vec{z}) = \inf\{t > 0 \mid te + T\vec{z} \in V^+\}$ with T chosen such that η has a mean (which is a particular central value) of 1 on the $(n-1)$-dimensional Euclidean sphere and that the Lipschitz constant L of η is bounded via $L \leq c'\sqrt{n/\log n}$ for some absolute constant c'. This is always possible, as can be seen following the proof of Theorem 4.3 in [29]: First, by a Lemma of Dvoretzky and Rogers [14, Theorem 3.4], the bijection T can be chosen such that for all canonical vectors $\vec{e}_k$ with $k \leq n/2$ it holds that $\|T\vec{e}_k\|_+ \geq \|T\|/4$. Without loss of generality we may assume in addition that η has mean 1. Then, for a vector of normal distributed variables $\vec{g}$ and due to $\|T\vec{z}\|_+ = \max\{\eta(\vec{z}), \eta(-\vec{z})\}$ and [29, Eqns. (4.14, 4.18)] we find,

$$\begin{aligned} 2\sqrt{n} \geq 2\mathbb{E}\eta(\vec{g}) \geq \mathbb{E}\|T\vec{g}\|_+ &\geq \mathbb{E}\max_k |g_k|\, \|T\vec{e}_k\|_+ \\ &\geq \mathbb{E}\max_{k\leq n/2} |g_k|\, \|T\vec{e}_k\|_+ \geq c''\sqrt{\log(n/2)}\, \|T\|/4. \end{aligned} \qquad (7)$$

On the other hand, η is a sublinear function and thus

$$\begin{aligned} |\eta(\vec{z}_1) - \eta(\vec{z}_2)| &\leq \max\{\eta(\vec{z}_1 - \vec{z}_2), \eta(\vec{z}_2 - \vec{z}_1)\} \\ &= \|T(\vec{z}_1 - \vec{z}_2)\|_+ \leq \|T\|\, \|\vec{z}_1 - \vec{z}_2\|_2, \end{aligned} \qquad (8)$$

which eventually shows $L \leq c'\sqrt{n/\log n}$.

Now, by virtue of Dvoretzky's theorem, the following holds with high probability. For all $\vec{x} \neq 0$ with $\xi \equiv \|\vec{x}\|_2 \leq 1/(1+\varepsilon)$, we have $\eta[X(\vec{x}/\xi)] \leq 1 + \varepsilon \leq 1/\xi$, and hence $Q(1, \vec{x}) = [e/\xi + TX(\vec{x}/\xi)]\xi \in V^+$. Conversely, for all $\vec{x}$ with $\xi \equiv \|\vec{x}\|_2 > 1/(1-\varepsilon)$, we have $\eta[X(\vec{x}/\xi)] \geq 1 - \varepsilon > 1/\xi$, i.e., $Q(1, \vec{x}) \notin V^+$. The converse statement completes the proof. □

Thus, with high accuracy, the effective theory corresponding to a low-dimensional $O(n)$-typical section of a local GPT looks like a Euclidean AOU space, cf. Fig. 1 for an illustration. The cones $Q(C^+_{k+1}(1 \pm \varepsilon))$ give a very accurate description of the typical section, since by linearity all observable probabilities may at most deviate by $\mathscr{O}(\varepsilon)$. Combining this with our previous finding, namely that Euclidean cones are sections of QM, and hence, in view of Proposition 1, all bipartite correlations of their maximal tensor product may be simulated within QM, we arrive at our anticipated main result. Conversely, due to an argument by Tsirelson [20], all bipartite dichotomic correlations can be explained within an Euclidean cone of appropriate dimension. Our result reduces to this dichotomic case, since already our description of a GPT by an AOU space is essentially limited to the dichotomic case.

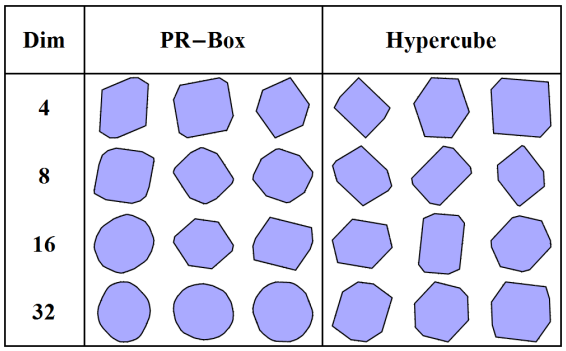

FIG. 1. Typical two-dimensional sections of a hypercube and of the effect space of a PR-Box in various dimensions. In both cases an increasing rounding of the corners of the sections can be observed. However in the case of a hypercube, which is the extremal situation for Dvoretzky's theorem, there is still an appreciable probability for non-rounded sections, due to low dimensionality.

Finally we briefly discuss the situation of a generalized Popescu-Rohrlich (PR) box, which exhibits (in some sense) the "maximal" possible post-quantum correlations [28]. Such boxes are locally described by an AOU vector space over $\mathbb{R}^n$ with cone $\text{PR}^+ = \{(t, \vec{x}) \mid t \geq \sum_i |x_i|\}$ and neutral element $(1, \vec{0})$. By virtue of Proposition 2, the fraction of 3-dimensional sections from a 55×10^6-dimensional box with a post-quantum behavior of more than $\pm 3\%$ is as low as 10^{-6}[30].

Conclusions.—We have presented a mechanism whereby observable bipartite correlations of an arbitrary post-quantum theory could be, with high accuracy, compatible with those exhibited by quantum mechanics. Our argument exploited the concentration of measure phenomenon and hence works for any typical low-dimensional section of a generalised probabilistic theory. We argued that such typical sections arise due to a lack of ultra-precise experimental control, in which case it would be virtually impossible to observe any post-quantum behavior, even if the fundamental theory of Nature wasn't quantum mechanics. This is complementary to the emergence of classicality from quantum mechanics via decoherence [8, 9], since we consider only a pair of (microscopic) objects, rather than an ensemble of objects. Our argument indicates that there is another option for a refinement of today's physics: we might be missing hidden post-quantum structures due to an ignorance of the correct measurement directions.

We thank O. Gühne, A. Ahlbrecht, and C. Budroni for helpful discussions and the Centro de Ciencias de Be-

nasque, where part of this work has been done, for its hospitality during the workshop on quantum information 2012. This work has been supported by the Austrian Science Fund (FWF): Y376-N16 (START prize), the BMBF (CHIST-ERA network QUASAR), the EU (Marie-Curie CIG 293933/ENFOQI, Coquit, QFTCMPS), V.B.S. is supported by an ETH postdoctoral fellowship and the SNF through the National Centre of Competence in Research Quantum Science and Technology. This work was supported, in part, by the cluster of excellence EXC 201 "Quantum Engineering and Space-Time Research", by the Deutsche Forschungsgemeinschaft (DFG).

* matthias.kleinmann@uni-siegen.de
† tobias.osborne@itp.uni-hannover.de
‡ scholz@phys.ethz.ch
§ albert.werner@itp.uni-hannover.de

[1] H. Barnum, J. Barrett, M. Leifer, and A. Wilce, Phys. Rev. Lett. **99**, 240501 (2007).
[2] H. Barnum and A. Wilce, Electron. Notes Theor. Comput. Sci. **270**, 3 (2011).
[3] J. Barrett, Phys. Rev. A **75**, 032304 (2007).
[4] L. Masanes and M. P. Müller, New J. Phys. **13**, 063001 (2011).
[5] G. Chiribella, G. M. D'Ariano, and P. Perinotti, Phys. Rev. A **81**, 062348 (2010).
[6] J. Barrett, L. Hardy, and A. Kent, Phys. Rev. Lett. **95**, 010503 (2005).
[7] E. Hänggi, R. Renner, and S. Wolf, in *EUROCRYPT* (2010) pp. 216–234.
[8] M. Navascués and H. Wunderlich, Proc. R. Soc. A **466**, 881 (2010).
[9] P. Kurzyński, A. Soeda, R. Ramanathan, A. Grudka, J. Thompson, and D. Kaszlikowski, "Experimental undecidability of macroscopic quantumness," (2012), arXiv:1111.2696v2.
[10] G. Ludwig, *An Axiomatic Basis for Quantum Mechanics*, Vol. I-II (Springer-Verlag, Berlin Heidelberg, 1987).
[11] P. Mittelstaedt, *The Interpretation of Quantum Mechanics and the Measurement Process* (Cambridge University Press, 1998).
[12] L. Hardy, "Quantum theory from five reasonable axioms," (2001), arXiv:quant-ph/0101012v4.
[13] E. M. Alfsen and F. W. Shultz, *Geometry of State Spaces of Operator Algebras* (Springer, 2003).
[14] V. D. Milman and G. Schechtman, *Asymptotic theory of finite dimensional normed spaces*, Lecture Notes in Mathematics, Vol. 1200 (Springer-Verlag, Berlin, 1986).
[15] M. Talagrand, Inst. Hautes Études Sci. Publ. Math. **81**, 73 (1995).
[16] P. Hayden, D. W. Leung, and A. Winter, Comm. Math. Phys. **265**, 95 (2006).
[17] G. Aubrun, S. Szarek, and E. Werner, Comm. Math. Phys. **305**, 85 (2011).
[18] M. J. Bremner, C. Mora, and A. Winter, Phys. Rev. Lett. **102**, 190502 (2009).
[19] D. Gross, S. T. Flammia, and J. Eisert, Phys. Rev. Lett. **102**, 190501 (2009).
[20] B. S. Tsirel'son, Zap. Nauchn. Sem. Leningrad. Otdel. Mat. Inst. Steklov. (LOMI) **142**, 174 (1985), (Russian, English translation [31]).
[21] H. Barnum, S. Beigi, S. Boixo, M. B. Elliott, and S. Wehner, Phys. Rev. Lett. **104**, 140401 (2010).
[22] A. Acín, R. Augusiak, D. Cavalcanti, C. Hadley, J. K. Korbicz, M. Lewenstein, L. Masanes, and M. Piani, Phys. Rev. Lett. **104**, 140404 (2010).
[23] E. M. Alfsen, *Compact convex sets and boundary integrals*, Ergebnisse der Mathematik und ihrer Grenzgebiete No. 57 (Springer, Berlin, 1971).
[24] V. I. Paulsen, *Completely bounded maps and operator algebras*, Cambridge Studies in Advanced Mathematics No. 78 (Cambridge University Press, Cambridge, 2002).
[25] V. I. Paulsen and M. Tomforde, Indiana Univ. Math. J. **58**, 1319 (2009).
[26] K. H. Han, "Tensor products and nuclearity of ordered vector spaces with archimedean order unit," (2009), arXiv:0906.1858v1.
[27] M. Horodecki, P. Horodecki, and R. Horodecki, Phys. Lett. A **223**, 1 (1996).
[28] S. Popescu and D. Rohrlich, Found. Phys. **24**, 379 (1994).
[29] G. Pisier, *The volume of convex bodies and Banach space geometry*, Cambridge Tracts in Mathematics No. 94 (Cambridge University Press, Cambridge, 1989).
[30] Those estimates stem from estimating the constants c_0, c_1, and c_2 in the original proofs. Numerically estimations yield much better bounds and the dimension can be estimated to be ≈ 2000 .
[31] B. S. Tsirel'son, J. Soviet Math. **36**, 557 (1987).

Comment on "State-Independent Experimental Test of Quantum Contextuality in an Indivisible System"

In this Comment we argue that the experiment described in the recent Letter [1] does not allow to make conclusions about contextuality. Our main criticism is that the measurement of the observables as well as the preparation of the state manifestly depend on the chosen context. Contrary to that, contextuality is about the behavior of the *same* measurement device in different experimental contexts (cf. e.g. Ref. [2–4]).

The authors aim to experimentally demonstrate that the noncontextuality assumption is violated by quantum systems. Specifically, they report a violation of the noncontextuality inequality recently introduced by Yu an Oh [5], which is of the form

$$\sum_k \langle A_k \rangle - \frac{1}{4} \sum_{(k,\ell)\in E} \langle A_k A_\ell \rangle \leq 8. \qquad (1)$$

The notation $\langle A_k A_\ell \rangle$ is an abbreviation denoting the expectation value of the product of the outcomes of the observables A_k and A_ℓ. This inequality holds for any noncontextual model, i.e., any model having preassigned values for each observable A_k, irrespective of the measurement context (the different pairs $A_k A_\ell$). Therefore, the experimenter must convincingly argue that the assignment of the observables is independent of the context. This is a central point in any experimental test of contextuality. For the argument leading to Eq. (1) it is thus crucial that (i) the same symbol A_k always corresponds to the same measurement and (ii) the expectation value is evaluated always for the same state of the system.

In Table I, we list the different measurement procedures that have been used in the experiment, as provided by the supplementary material of the Letter. Clearly, except for A_{z_1} and $A_{y_3^-}$, none of the observables is measured context independently. In particular, the observables A_{h_α} ($\alpha = 0, 1, 2, 3$) are measured in each context differently, violating condition (i). In addition the input states are chosen differently for different contexts—an approach that has not been investigated before and directly violates condition (ii).

Since no experimental data or discussion concerning these issues is provided in the Letter, the only means to conclude that those different procedures actually correspond to the same physical observable is to invoke previous knowledge about the functioning of the optical devices. However, since the setup is operated on a single photon level, this actually requires to employ their quantum mechanical description. But then the experiment can merely be used to verify the predictions of quantum mechanics *within* the framework of quantum mechanics, rather than a to provide a proof of contextual behavior.

	z_1	z_2	z_3	y_1^-	y_2^-	y_3^-	y_1^+	y_2^+	y_3^+	h_1	h_2	h_3	h_0
z_1	1	1	1	1			1						
z_2	1a	?	1a		3			3					
z_3	1a'	1a'	?			2a'			2a'				
y_1^-	1b'			1b'			1b'			X2			X2
y_2^-		3b'			3b'			3b'			Y2		Y2
y_3^-			2			2			2			2	2
y_1^+	1b			1b			1b				X5	X4	
y_2^+		3b			3b			3b		Y4		Y5	
y_3^+			2a			2a			?	4	5		
h_1				X2d				Y4c	4c	4c			
h_2					Y2d		X5c		5c		5c		
h_3						2d	X4c	Y5c				2d	
h_0				X2c	Y2c	2c							2c

TABLE I. Different realizations of the 13 observables in the different contexts. In each row k, the entries correspond to the different experimental realizations of the observable A_k depending on the context, i.e., for column ℓ in the context $\langle A_k A_\ell \rangle$, for $\ell = k$ in the single observable context $\langle A_k \rangle$. In the entries, the number corresponds to the setting of HWP5 (1: 0°, 2: 25.5°, 3: 45°, 4: −22.5°, 5: 67.5°) and the lower case letter to the setting of HWP6 (a: 0°, b: 22.5°, c: 17.63°, d: −17.63°). Where only the number occurs, the setting of HWP6 does not influence the observable, since the observable was measured using Detector 1; if Detector 3 was used, a prime is added. An X denotes a change of the input state prior to measurement by swapping $|0\rangle$ and $|2\rangle$, while Y denotes a swap of $|1\rangle$ and $|2\rangle$. For $\langle A_{z_2} \rangle$, $\langle A_{z_3} \rangle$, and $\langle A_{y_3^+} \rangle$ it is not clear from the material which setting was used in the experiment.

E. Amselem[♂], M. Bourennane[♂], C. Budroni[♀], A. Cabello[♁], O. Gühne[♀], M. Kleinmann[♀], J.-Å. Larsson[♂], and M. Wieśniak[♃].

[♂]Department of Physics, Stockholm University, S-10691 Stockholm, Sweden; [♀]Naturwissenschaftlich-Technische Fakultät, Universität Siegen, Walter-Flex-Straße 3, D-57068 Siegen, Germany; [♁]Departamento de Física Aplicada II, Universidad de Sevilla, E-41012 Sevilla, Spain; [♂]Institutionen för Systemteknik, Linköpings Universitet, SE-58183 Linköping, Sweden; [♃]Institute of Theoretical Physics and Astrophysics, University of Gdańsk, 80-952 Gdańsk, Poland.

[1] C. Zu, Y.-X. Wang, D.-L. Deng, X.-Y. Chang, K. Liu, P.-Y. Hou, H.-X. Yang, and L.-M. Duan, Phys. Rev. Lett. **109**, 150401 (2012).
[2] J. S. Bell, Rev. Mod. Phys. **38**, 447 (1966).
[3] A. Peres, J. Phys. A: Math. Gen. **24**, L175 (1991).
[4] N. D. Mermin, Rev. Mod. Phys. **65**, 803 (1993).
[5] S. Yu and C. H. Oh, Phys. Rev. Lett. **108**, 030402 (2012).

Certifying experimental errors in quantum experiments

Tobias Moroder,[1,2] Matthias Kleinmann,[1] Philipp Schindler,[3] Thomas Monz,[3] Otfried Gühne,[1,2] and Rainer Blatt[2,3]

[1] *Naturwissenschaftlich-Technische Fakultät, Universität Siegen, Walter-Flex-Str. 3, D-57068 Siegen, Germany*
[2] *Institut für Quantenoptik und Quanteninformation, Österreichische Akademie der Wissenschaften, Technikerstr. 21A, A-6020 Innsbruck, Austria*
[3] *Institut für Experimentalphysik, Universität Innsbruck, Technikerstr. 25, A-6020 Innsbruck, Austria*

When experimental errors are ignored in an experiment, the subsequent analysis of its results becomes questionable. We develop tests to detect systematic errors in quantum experiments where only a finite amount of data is recorded and apply these tests to tomographic data taken in an ion trap experiment. We put particular emphasis on quantum state tomography and present three detection methods: the first two employ linear inequalities while the third is based on the generalized likelihood ratio.

PACS numbers: 03.65.Ta, 03.65.Wj, 06.20.Dk, 42.50.Dv

Introduction.—Measurements are central to acquiring information about the underlying system in any quantum experiment. However, for quantum systems of increased complexity, the analysis of all measurement data gets challenging when one deals with both statistical and systematic errors. Statistical errors refer to the intrinsic problem that true probabilities are never accessible in any experiment but are merely approximated from count rates which lead to relative frequencies. A well-known example where statistical effects play a dominant role is quantum state tomography [1]: the task to determine an unknown state by means of appropriate measurements. Here the deviations between probabilities and relative frequencies cause severe problems in the actual state reconstruction, since naïvely using the frequencies in Born's rule easily leads to unphysical "density operators," meaning that some eigenvalues are negative. This problem can be circumvented by reconstruction principles that explicitly account for statistical effects [2, 3].

The analysis is generally further complicated because of additional systematic errors, *e.g.*, caused by drifts in the state generation, misalignment in the measurements or fluctuations of external parameters. To reconstruct the state from the observed data one requires an operator assignment for each classical outcome of the performed measurements. This measurement model is essential, not just for quantum state tomography, but also to certify state characteristics like entanglement via entanglement witnesses [4, 5] or applications as quantum key distribution to prove security in the calibrated device scenario [6]. However, in a real experiment the measured observables might deviate from this employed description due to systematic errors. This mismatch can have severe impact on the analysis and can lead to, for instance, spurious entanglement detection as exemplified in Ref. [7] or insecurity in quantum key distribution [8, 9]. Though deviations of this kind have been discussed and partially countermeasured by different techniques [10–14], it has not yet been investigated how to distinguish them from statistical errors. An exception is Ref. [15], where drifts in the source are detected by measurements on subsequent states.

In this Letter we present experimentally and theoretically three methods to detect whether systematic errors are statistically significant, *i.e.*, if there is merely a small probability that the observed results were generated by statistical effects only. In that case, the model becomes questionable and further analysis must involve a refined model or include other means of treating systematic errors. We emphasize that the techniques outlined below can only falsify but never verify that systematic errors are absent. Some errors, as, for example, depolarizing noise, are not detectable without further calibration. Still, we recommend that these tests are applied before reconstructing actual quantum states since they serve as additional systematic error checks after calibrating the setup. Three procedures are presented in detail, the first two use linear inequalities that are satisfied if no systematic errors are present, while the third is based on the likelihood ratio [17, 18]. Note that other techniques from hypothesis testing, like the prediction-based-ratio analysis [19] or the chi-square goodness-of-fit [20], provide alternative procedures to test for systematic errors.

Tomography setting.—A common tomography protocol uses 3^n possible combinations of Pauli operators on n qubits and one measures locally the respective expectation values in the associated eigenbasis which provides 2^n distinct outcomes, yielding a total of $3^n \times 2^n = 6^n$ different outcomes. Note that an n-qubit density operator is already determined by $4^n - 1$ parameters, *i.e.*, this measurement scheme collects an overcomplete data set. This tomography protocol is known as the Pauli measurement scheme [3] which has been used for n-qubit systems in ion traps [21] or photonic setups [22].

More generally, we consider a tomography protocol with measurements for different settings labeled by s and which registers the respective frequencies $f_k^s = m_k^s/N_\mathrm{s}$, where m_k^s denotes the counts of the specific outcome k in N_s repetitions of this experiment. The repetitions N_s are assumed to be equal for each setting. The observables M_k^s are the attributed measurement operators and

they span the complete operator space in order to enable a full reconstruction of the density operator. Most often this set is overcomplete, *i.e.*, the operators are not independent of each other which can be expressed in terms of linear identities $\sum c_k^s M_k^s = 0$ using real coefficients c_k^s. The set of probabilities consistent with this quantum model are all distributions $P_{\mathrm{qm}}(k|s) = \mathrm{tr}(\rho M_k^s)$ that can be written using a density operator ρ.

Witness test.—The set of distributions consistent with the assumed quantum model can be characterized by linear inequalities. This is in analogy to entanglement witnesses [5, 16] for separable states or Bell inequalities [23] for local hidden variable models. Consider a set of real coefficients $w = w_k^s$ that define a positive semidefinite operator via $\sum w_k^s M_k^s = Z_w \succeq 0$, *i.e.*, all eigenvalues are non-negative. Then for each such w the expectation value of any probability distribution from the quantum model P_{qm} satisfies

$$w \cdot P_{\mathrm{qm}} \equiv \sum_{s,k} w_k^s P_{\mathrm{qm}}(k|s) = \mathrm{tr}(\rho Z_w) \geq 0. \qquad (1)$$

Thus a distribution P with $w \cdot P < 0$ is incompatible with the assumed quantum model, and any such distribution can be detected by a set of coefficients w of the described form (even with partial information [24]). Thus we refer to w as a witness for systematic errors, but note that its associated operator Z_w is not an entanglement witness.

Equation (1) is formulated on the level of probabilities which are not accessible in the experiment. Nevertheless one can replace the probabilities by the observed frequencies $f = f_k^s$ and consider the sample mean $w \cdot f \equiv \sum w_k^s f_k^s$ of the witness. Then $w \cdot f \geq 0$ does not need to hold anymore because statistical effects can produce a negative value. However, the probability to observe large deviations from the true mean is bounded and decreases exponentially with the number of performed repetitions. A quantitative statement is given by Hoeffding's tail inequality [25], as similarly used for example in efficient fidelity estimation [26, 27]. We emphasize that this inequality is even valid for small data sets containing only few or no counts for certain outcomes.

Proposition 1.—Consider a witness $w = w_k^s$ obeying $\sum w_k^s M_k^s = Z_w \succeq 0$. If the data are generated by the quantum model $P_{\mathrm{qm}}(k|s) = \mathrm{tr}(\rho M_k^s)$, then for all $t > 0$,

$$\mathrm{Prob}[w \cdot f \leq -t] \leq \exp(-2t^2 N_{\mathrm{s}}/C_w^2) \qquad (2)$$

with $C_w^2 = \sum_s (w_{\max}^s - w_{\min}^s)^2$, where $w_{\max/\min}^s$ are the optima for setting s over all outcomes k. A proof is given in the appendix.

The interpretation is as follows: Suppose that one carries out an experiment for a previously chosen witness w and fixed error probability α, which one still tolerates before one announces a systematic error. Using Proposition 1 one computes the necessary violation $t_\alpha = \sqrt{-C_w^2 \log(\alpha)/2N_{\mathrm{s}}}$. If one now registers frequencies f_{obs} with $w \cdot f_{\mathrm{obs}} \leq -t_\alpha$, then the probability that any error-free experiment would produce such data is less than α and one says that a systematic error is significant at significance level α. However, for given data it is more common to report the smallest α such that the systematic error is significant. This is also called the p-value in hypothesis testing [17]. Proposition 1 states that this p-value has an upper bound of $\exp[-2(w \cdot f_{\mathrm{obs}})^2 N_{\mathrm{s}}/C_w^2]$ if $w \cdot f_{\mathrm{obs}} < 0$.

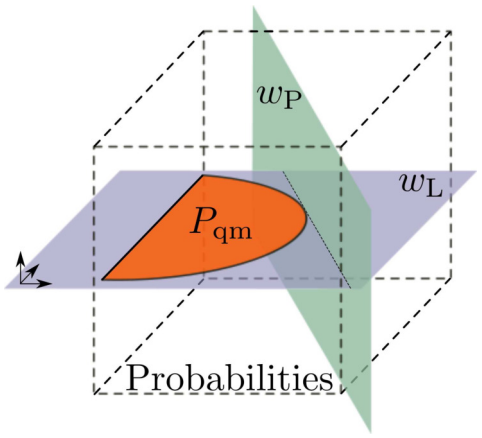

FIG. 1. The admissible probabilities from the quantum model P_{qm} typically form a convex, lower dimensional subset within all possible probability distributions (dashed cube). This dimension reduction stems from additional linear relations that a probability distribution from the quantum model must fulfil. These relations are checked by witnesses w_{L}, while w_{P} verify positivity of the density operator.

Witness structure.—Each witness w as defined above can be decomposed into two conceptually different parts. One that solely verifies positivity of an underlying density operator, denoted as w_{P}, and into another part w_{L} that only checks the linear dependencies within the assumed measurement operators, such that one obtains $w = w_{\mathrm{P}} + w_{\mathrm{L}}$. It turns out that these two parts of the witness are orthogonal. Note that the witness w_{P} uniquely describes the operator $\sum w_{\mathrm{P}k}^s M_k^s = Z_w$, while the witness w_{L} (and also $-w_{\mathrm{L}}$) vanishes due to the linear relations $\sum w_{\mathrm{L}k}^s M_k^s = 0$. Figure 1 gives a schematic picture of this situation.

Issue of negative eigenvalues.—The above framework provides an answer to the issue of negative eigenvalues in linear inversion, since it is connected to witnesses of the type w_{P}. Linear inversion refers to the state reconstruction process in which one estimates the unknown density operator by using the observed frequencies in Born's rule $\mathrm{tr}(\rho M_k^s) = f_k^s$. Since this set of linear equations is typically not exactly solvable because of overcompleteness one selects the operator ρ_{ls} which minimizes the least squares, $\sum [f_k^s - \mathrm{tr}(\rho_{\mathrm{ls}} M_k^s)]^2$. As one ignores the positivity constraint this operator ρ_{ls} will often represent

an invalid density operator because some eigenvalues are negative, *i.e.*, $\langle\psi|\rho_{\rm ls}|\psi\rangle < 0$.

Proposition 2.—Let $\rho_{\rm ls}$ be the linear inversion using least squares and consider a given vector $|\psi\rangle$. If the data are generated by the quantum model $P_{\rm qm}(k|s) = {\rm tr}(\rho M_k^s)$, then for all $t > 0$,

$$\text{Prob}[\langle\psi|\rho_{\rm ls}|\psi\rangle \leq -t\,] \leq \exp(-2t^2 N_{\rm s}/C_w^2) \qquad (3)$$

with C_w^2 as given in Proposition 1 computed from the unique $w_{\rm P}$ satisfying $\sum w_{{\rm P}k}^s M_k^s = |\psi\rangle\langle\psi|$. A proof is given in the appendix.

This proposition shows that the probability to successfully guess a state $|\psi\rangle$, independently of the recorded data, where $\rho_{\rm ls}$ has a negative expectation value is exponentially suppressed.

Likelihood ratio test.—In addition to the attributed quantum model $P_{\rm qm}(k|s) = {\rm tr}(\rho M_k^s)$ we can also describe the observations with a more general model assumption of independent distributions $P_{\rm ind}(k|s) = p_k^s \geq 0$ and $\sum_k p_k^s = 1$ for each setting s. The question whether the observed data set is compatible with the assumed quantum model can now be addressed by comparing the maximal likelihoods of either model [17].

For that, we start from the likelihood for a distribution P given the observed frequencies f, which is $L(P) = \prod_{k,s} P(k|s)^{N_{\rm s} f_k^s}$ ignoring the multinomial prefactor. A quantum state $\rho_{\rm ml}$ that maximizes the likelihood $L(P)$ is considered to be a good estimate for the physical state [1, 2]. In contrast, for the model with all independent distributions, the optimum is given by $p_k^s = f_k^s$. Since the quantum model is contained in this more general model, the likelihood of any quantum model can at best be equal to this optimal likelihood. Thus one finds $L(f) \geq L[{\rm tr}(\rho_{\rm ml} M_k^s)]$ or equivalently, a non-negative log-likelihood ratio $\lambda_{\rm qm} = 2\log L(f) - 2\log L[{\rm tr}(\rho_{\rm ml} M_k^s)]$.

The likelihood ratio test is based on the observation, that if the data are indeed generated from the quantum model then the probability for outcomes which satisfy $\lambda_{\rm qm} \geq t$ decreases rapidly if t exceeds a certain value. Wilks' theorem [28] states that this ratio is distributed according to a chi-square distribution already for moderately large samples. However this theorem does not directly apply to $\lambda_{\rm qm}$ because of the positivity constraint; but it works for the slightly larger model where one performs the optimization (rather than over quantum models) over probabilities $P_{\rm nqm}(k|s) = {\rm tr}(X M_k^s)$ that can be written in terms of a Hermitian operator X. Note that X can have negative eigenvalues, indicated by the subscript "n", while still obeying the positivity constraints ${\rm tr}(X M_k^s) \geq 0$ for the measurements M_k^s. With $X_{\rm ml}$ being a corresponding optimum we now study the log-likelihood ratio

$$\lambda_{\rm nqm} = 2\log L(f) - 2\log L[{\rm tr}(X_{\rm ml} M_k^s)]. \qquad (4)$$

Proposition 3.—If the data are generated by the d-dimensional quantum model $P_{\rm qm}(k|s) = {\rm tr}(\rho M_k^s)$ with K outcomes for each of the S settings, then for all $t > 0$, as $N_{\rm s} \to \infty$,

$$\text{Prob}[\lambda_{\rm nqm} \geq t] \to Q(\Delta/2, t/2), \qquad (5)$$

with the dimension deficit $\Delta = (K-1)S - (d^2-1)$ and the regularized incomplete gamma function Q [29]. A proof is given in the appendix.

The interpretation and application is analogous to Proposition 1. Though Proposition 3 is only a strict statement in the asymptotic case $N_{\rm s} \to \infty$, Eq. (5) gives reliable values already for moderately large $N_{\rm s}$, as we will demonstrate below.

Experimental setup—Experimentally, we study tomographic data from an ion trap quantum processor encoding qubits in the ground and the metastable state of $^{40}{\rm Ca}^+$ ions where each ion represents a qubit. Details on the experimental setup can be found in Ref. [30]. Single ions can be addressed with a tightly focused, off-resonant beam. Here the ac-Stark effect induces an operation of the form $\exp(-i\Omega_l \tau \sigma_{z,l}/2)$ on ion l, with the Rabi frequency Ω_l determined by detuning and intensity, and pulse duration τ. Combined with collective, resonant operations on all qubits, state tomography according to the Pauli measurement scheme can be implemented on the trapped-ion quantum register.

In an experimental realization, the finite width of the focused beam results in residual ion-light interaction on next-neighbor qubits. The Rabi frequency of ion k when addressing ion j can be described by the addressing matrix $\Omega_{j,k}$. Thus the operation on the qubit register can then be written as $\exp(-i\sum_k \Omega_{j,k}\tau\sigma_{z,k}/2)$. The addressing quality can be quantified with a cross-talk parameter $\epsilon = \max_{j\neq k}(\Omega_{j,k}/\Omega_{j,j})$, which can be increased by defocusing the addressed laser beam.

Using this setup we perform tomography on various states and investigate whether the obtained data suffer from any kind of systematic errors. This includes data for Greenberger-Horne-Zeilinger states on 4 ions, $|GHZ\rangle = (|0000\rangle + |1111\rangle)/\sqrt{2}$, where we intentionally increased the cross-talk ϵ to test the presented techniques, a large data set on a two-qubit Bell state $|\psi^-\rangle = (|01\rangle - |10\rangle)/\sqrt{2}$ and measurements on the ground state $|SSSS\rangle = |1111\rangle$. Moreover we re-analyse observations on a W-state on 5 qubits, $|W\rangle = (|00001\rangle + |00010\rangle + |00100\rangle + |01000\rangle + |10000\rangle)/\sqrt{5}$ and a bound-entangled (BE) Smolin state [31].

Empirical findings.— At first we implement the witness test, see Table I. Let us stress that Proposition 1 does not allow us to determine and to evaluate the witness w from the same data. If one would do so then one effectively employs $\min_w w \cdot f$ instead of $w \cdot f$ as required in Proposition 1. Because of that we divide the observed data into two equally sized parts, yielding frequencies f_1 and f_2. Afterwards we use the first part f_1 to determine a reasonable witness w, which is evaluated on the second part, $w \cdot f_2$. Here we choose either of the

State	n	N_s	ϵ	w_L	w_P	LR	LR*
GHZ	4	750	0.20 *	97%	10^{-6}%	10^{-10}%	10^{-9}%
		750	0.12 *	100%	10^{-7}%	0.024%	0.14%
		600	< 0.03	79%	81%	0.91%	4.1%
Bell	2	61650	< 0.03	100%	100%	50%	49%
SSSS	4	2600	$< 0.03^\dagger$	48%	84%	0.037%	0.008%
BE	4	5200	< 0.03	99%	14%	35%	36%
W	5	100	0.04	49%	91%	(0.081%)	5.5%

TABLE I. Systematic error analysis for various experimental data according to different tests, *i.e.*, w_L and w_P refer to the witness test, while LR corresponds to the likelihood ratio test. The values are upper bounds on the p-value of each test. The specifications are: n number of qubits, N_s number of measurements per setting, ϵ measured cross-talk parameter. LR* is obtained using a parametric bootstrapping method [32] with 1000 samples. For data marked with * we manually increased the cross-talk, while † have been intensity fluctuations.

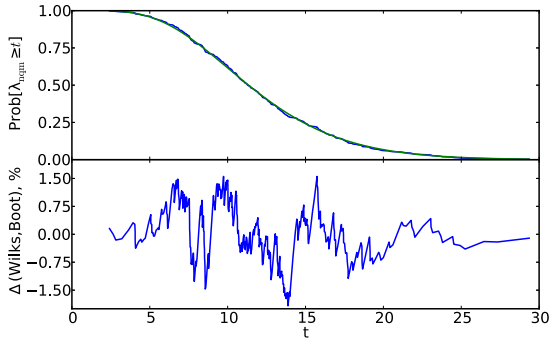

FIG. 2. Fraction of runs with a log-likelihood ratio $\lambda_{\mathrm{nqm}} \geq t$ from a 411-fold repetition of the Bell-state experiment. In the upper graph, the shaky blue line corresponds to the experimental data, while the smooth green line is the prediction according to Wilks' theorem. The lower graph shows the difference between both curves.

two types of witnesses testing positivity w_P or linear dependencies w_L. As witness w_P we select the witness that corresponds to the projector onto the smallest eigenvalue on the linear inversion ρ_{ls} using the first data set f_1. For the linear dependencies we use $w_L = -f_1 + \mathrm{tr}(\rho_{ls} M_k^s)$, because it gives the largest negative expectation value $w_L \cdot f_1$ on the first data. Note that the employed choices are not necessarily optimal [33]. If the observed value $w \cdot f_2$ is negative, we ask for the statistical significance as explained after Proposition 1. If we choose a significance level of for instance $\alpha = 0.1\%$, the witness w_P reliably detects the artificially introduced cross-talk for the GHZ-state experiments, while w_L is less powerful for these examples.

The likelihood ratio test, as a third method, is best suited for a larger number of samples, since Proposition 3 makes only a strict statement for $N_s \to \infty$. In Figure 2 we compare the empirical distribution between a two-qubit Bell experiment using 150 samples per setting and the predicted distribution according to Wilks' theorem. Hence for the two-qubit case this number might already be sufficiently close to this limit. This observation is further supported by a comparison with a bootstrapping method [32] (see appendix) which produces similar results as the ones obtained from Proposition 3. Based on these observations we are confident that the results using Proposition 3 for finite N_s are trustworthy for all data from Table I except for the W-state, which has a too low number of samples. Evaluating the experimental data we detect again the manually increased cross-talk in the GHZ experiments, but now also some discrepancies in the SSSS experiment, which occurred because of intensity fluctuations during the experiment [34].

Conclusion and outlook.—Tomographic reconstruction of quantum states can be problematic since nonphysical properties, such as negative eigenvalues, might occur. One possible solution is to use reconstruction schemes, which by construction result in a valid state. Then, however, serious concerns remain, since negative eigenvalues can also be a signature of systematic errors. We have provided tests which can be used to distinguish systematic from statistical errors in quantum experiments. These tests were shown to recognize systematic errors in real tomographic data from ion trap experiments.

Though we formulated our result for the case of state tomography, our methods can be applied to other assumptions like the nonsignaling condition in Bell experiments. From the more general perspective, many experiments in physics aim to determine parameters in an assumed theoretical model. Our results show that it is possible to give rigorous estimates on whether the assumed model class is inappropriate.

We thank K.M.R. Audenaert, K. Banaszek, M. Cramer, O. Gittsovich, S. Glancy, M. Guta, D. Gross, B. Jungnitsch, H. Kampermann, E. Knill, S. Niekamp and Y. Zhang for stimulating discussions. The authors are grateful for the opportunity to participate in the Heraeus Summer School "Modern Statistical Methods in QIP", where parts of this research have been developed. This work has been supported by the Austrian Science Fund FWF (START prize No. Y376-N16, SFB FoQuS No. F4002-N16), the EU (AQUTE, Marie Curie CIG 293993/ENFOQI), the BMBF (CHIST-ERA network QUASAR), the Institut für Quanteninformation GmbH and by the European Research Council. This research was funded by the Office of the Director of National Intelligence (ODNI), Intelligence Advanced Research Projects Activity (IARPA), through the Army Research Office grant W911NF-10-1-0284. All statements of fact, opinion or conclusions contained herein are those of the authors and should not be construed as representing the official views or policies of IARPA, the ODNI, or the U.S. Government.

[1] M. G. A. Paris and J. Řeháček, eds., *Quantum state estimation* (Springer Berlin Heidelberg, 2004).
[2] Z. Hradil, Phys. Rev. A **55**, R1561 (1997).
[3] D. F. V. James, P. G. Kwiat, W. J. Munro, and A. G. White, Phys. Rev. A **64**, 052312 (2001).
[4] M. Lewenstein, B. Kraus, J. I. Cirac, and P. Horodecki, Phys. Rev. A **62**, 052310 (2000).
[5] B. Terhal, Phys. Lett. A **271**, 319 (2000).
[6] V. Scarani, H. Bechmann-Pasquinucci, N. J. Cerf, M. Dušek, N. Lütkenhaus, and M. Peev, Rev. Mod. Phys. 81 **81**, 1301 (2009).
[7] A. Acín, N. Gisin, and L. Masanes, Phys. Rev. Lett. **97**, 120405 (2006).
[8] B. Qi, C. H. F. Fung, H. K. Lo, and X. Ma, Quantum Inf. Comput. **7**, 73 (2007).
[9] L. Lydersen, C. Wiechers, C. Wittmann, D. Elser, J. Skaar, and V. Makarov, Nature Photonics **4**, 686 (2010).
[10] P. Lougovski, S. J. van Enk, K. S. Choi, S. B. B Papp, H. Deng, and H. J. Kimble, New J. Phys. **11**, 063029 (2009).
[11] T. Moroder, O. Gühne, N. J. Beaudry, M. Piani, and N. Lütkenhaus, Phys. Rev. A **81**, 052342 (2010).
[12] J. D. Bancal, N. Gisin, Y.-C. Liang, and S. Pironio, Phys. Rev. Lett. **106**, 250404 (2011).
[13] T. Moroder and O. Gittsovich, Phys. Rev. A **85**, 032301 (2012).
[14] D. Rosset, R. Ferretti-Schöbitz, J.-D. Bancal, N. Gisin, and Y.-C. Liang, Phys. Rev. A **86**, 062325 (2012).
[15] L. Schwarz and S. J. van Enk, Phys. Rev. Lett. **106**, 180501 (2011).
[16] M. Horodecki, P. Horodecki, and R. Horodecki, Phys. Lett. A **223**, 1 (1996).
[17] K. Knight, *Mathematical Statistics* (Chapman and Hall/CRC Press, London, 2000).
[18] R. Blume-Kohout, J. O. S. Yin, and S. J. van Enk, Phys. Rev. Lett. **105**, 170501 (2010).
[19] Y. Zhang, S. Glancy, and E. Knill, Phys. Rev. A **84**, 062118 (2011).
[20] A. F. Mood, *Introduction to the Theory of Statistics* (McGraw-Hill, New York, 1974).
[21] H. Häffner, W. Hänsel, C. F. Roos, J. Benhelm, D. Chekal kar, M. Chwalla, T. Körber, U. D. Rapol, M. Riebe, P. O. Schmidt, C. Becher, O. Gühne, W. Dür, and R. Blatt, Nature **438**, 643 (2005).
[22] N. Kiesel, C. Schmid, G. Tóth, E. Solano, and H. Weinfurter, Phys. Rev. Lett. **98**, 063604 (2007).
[23] A. Peres, Found. of Phys. **29**, 589 (1999).
[24] T. Moroder, M. Keyl, and N. Lütkenhaus, J. Phys. A: Math. Theor. **41**, 275302 (2008).
[25] W. Hoeffding, J. Am. Stat. Assoc. **58**, 301 (1963).
[26] S. T. Flammia and Y.-K. Liu, Phys. Rev. Lett. **106**, 230501 (2011).
[27] M. P. da Silva, O. Landon-Cardinal, and D. Poulin, Phys. Rev. Lett. **107**, 210404 (2011).
[28] S. S. Wilks, *Mathematical Statistics* (John Wiley & Sons, New York, London, 1962).
[29] Explicitly, $Q(s,x) = \int_x^\infty y^{s-1}\mathrm{e}^{-y}\mathrm{d}y / \int_0^\infty y^{s-1}\mathrm{e}^{-y}\mathrm{d}y$; the function $1 - Q(\Delta/2, t/2)$ is the cumulative distribution function of a chi-square distribution with Δ degrees of freedom.
[30] F. Schmidt-Kaler, H. Häffner, S. Gulde, M. Riebe, G. P. T. Lancaster, T. Deuschle, C. Becher, W. Hänsel, J. Eschner, C. F. Roos, and R. Blatt, Applied Physics B: Lasers and Optics **77**, 789 (2003).
[31] J. T. Barreiro, P. Schindler, O. Gühne, T. Monz, M. Chwalla, C. F. Roos, M. Hennrich, and R. Blatt, Nature Physics **6**, 943 (2010).
[32] B. Efron and R. J. Tibshirani, *An Introduction to the Bootstrap* (Chapman & Hall, 1994).
[33] B. Jungnitsch, S. Niekamp, M. Kleinmann, O. Gühne, H. Lu, W. B. Gao, Y.-A. Chen, Z.-B. Chen, and J.-W. Pan, Phys. Rev. Lett. **104**, 210401 (2010).
[34] The optimizations are done using the solver `cp` from the Python package CVXOPT.

Appendix

Proof of Proposition 1.—The proposition uses Hoeffding's tail inequality [25] and the property that valid quantum distributions P_{qm} have a non-negative expectation value $w \cdot f \geq 0$ due to Eq. (1). Hoeffding's inequality states that the sample mean $\bar{X} = \sum X_i/N$ of N independent, not necessarily identical distributed, bounded random variables X_i with $\mathrm{Prob}[X_i \in [a_i, b_i]] = 1$ for $i = 1, \ldots N$ satisfies

$$\mathrm{Prob}[\bar{X} - \mathbb{E}(\bar{X}) \leq -t] \leq \exp[-2N^2t^2/\sum(b_i - a_i)^2] \quad (6)$$

for all $t > 0$ and $\mathbb{E}(\bar{X})$ denoting the mean value of $\bar{X}$. In order to prove the proposition we identify $\bar{X}$ with the sample mean of the witness. This is achieved as follows:

Suppose that Y_i^s denotes the random variable associated with the i-th repetition of the measurement setting s. In case of the measurement outcome k, Y_i^s takes the value Sw_k^s where S denotes the total number of measurement settings. It is bounded between $Y_i^s \in [Sw_{\min}^s, Sw_{\max}^s]$. Then the sample mean of all these variables

$$\bar{Y} = \frac{1}{SN_{\mathrm{s}}} \sum_{s,i} Y_i^s \quad (7)$$

yields values

$$\frac{1}{SN_{\mathrm{s}}} \sum_{s,k} Sw_k^s m_k^s = \sum_{s,k} w_k^s f_k^s = w \cdot f, \quad (8)$$

where m_k^s denotes the counts of the specific outcome k in N_{s} repetitions of the measurement settings s.

Using Hoeffding's inequality together with the property that $\mathbb{E}(\bar{Y}) = w \cdot P_{\mathrm{qm}} \geq 0$ holds for any valid quantum distribution P_{qm} due to Eq. (1) one arrives at

$$\begin{aligned} \mathrm{Prob}[w \cdot f \leq -t] &= \mathrm{Prob}[\bar{Y} \leq -t] && (9)\\ &\leq \mathrm{Prob}[\bar{Y} - \mathbb{E}(\bar{Y}) \leq -t] && (10)\\ &\leq \exp[-2t^2 N_{\mathrm{s}}/C_s^2], && (11) \end{aligned}$$

with $C_s^2 = \sum_s (w_{\max}^s - w_{\min}^s)^2$. The first inequality holds because the set of all outcomes satisfying $\bar{Y} < -t$ is a

subset of $\bar{Y} - \mathbb{E}(\bar{Y}) \leq -t$. This concludes the proof of the proposition.

Proof of Proposition 2.—In order to prove the proposition we show $\langle\psi|\rho_{\rm ls}|\psi\rangle = w_{\rm P} \cdot f$, which can then be used in Proposition 1 to obtain the final statement.

Given a valid decomposition w satisfying $\sum w_k^s M_k^s = |\psi\rangle\langle\psi|$ one obtains

$$\langle\psi|\rho_{\rm ls}|\psi\rangle = \sum w_k^s \operatorname{tr}(M_k^s \rho_{\rm ls}) = \sum w_k^s f_{{\rm P}k}^{\ s} \tag{12}$$

$$= w \cdot f_{\rm P} = w_{\rm P} \cdot f, \tag{13}$$

together with the solution of least squares $\operatorname{tr}(M_k^s \rho_{\rm ls}) = f_{{\rm P}k}^{\ s}$.

Proof of Proposition 3.—We start by a rough statement of Wilks' theorem (cf. *e.g.*, 13.8.1 in Ref. [28]). Suppose that we have a family of models, that is sufficiently smoothly parameterized by an open set $\Omega \subset \mathbb{R}^r$ and let A be a subspace of $\mathbb{R}^r$ of dimension $r - \Delta$. If we draw N' samples from our model with some (unknown) parameter $z \in A \cap \Omega$, then the distribution of the log-likelihood ratio

$$\lambda_A = 2 \log \sup_{x \in \Omega} L(x) - 2 \log \sup_{y \in A \cap \Omega} L(y) \tag{14}$$

converges to the χ^2_Δ distribution as $N' \to \infty$. Hence,

$$\lim_{N' \to \infty} \operatorname{Prob}[\lambda_A \geq t] = Q(\Delta/2, t/2). \tag{15}$$

For our model, the set of parameters Ω is given by $\tilde{p}_k^s$ with $k = 1, \ldots, K-1$, $s = 1, \ldots, S$ obeying $\tilde{p}_k^s > 0$ and $\sum_k \tilde{p}_k^s < 1$. Furthermore, we let A be the subspace where $q_k^s = \operatorname{tr}(X M_k^s)$ for some Hermitian matrix X. We now basically arrived at Proposition 3. It only remains to change the notation from $\tilde{p}_k^s$ to p_k^s via $p_K^s = 1 - \sum_k \tilde{p}_k^s$ and to admit a more relaxed notation by essentially writing $\max_{x \in \overline{\Omega}}$ instead of $\sup_{x \in \Omega}$.

Bootstrapping for Table I.—We first calculate the maximum likelihood state $\rho_{\rm ml}$ from the measured data and then simulate the tomographic process using that state. From the simulated data we then calculate the log-likelihood ratio $\lambda_{\rm nqm}$. We repeat this procedure 1000 times and compare the distribution with the predicted chi-square distribution. In our examples, the distribution matches always almost perfectly, however with a slightly different parameter Δ. We then determine Δ' to be such, that $Q(\Delta'/2, m) = 1/2$, where m is the median of the sampled distribution. Using Δ', we obtain the values of the column LR* of Table I.

Tests against noncontextual models with measurement disturbances

Jochen Szangolies,[1,2,*] Matthias Kleinmann,[2,†] and Otfried Gühne[2,‡]

[1] *Institut für Theoretische Physik III, Heinrich-Heine-Universität Düsseldorf, D-40225 Düsseldorf, Germany*
[2] *Naturwissenschaftlich-Technische Fakultät, Universität Siegen, Walter-Flex-Straße 3, D-57068 Siegen, Germany*

The testability of the Kochen-Specker theorem is a subject of ongoing controversy. A central issue is that experimental implementations relying on sequential measurements cannot achieve perfect compatibility between the measurements and that therefore the notion of noncontextuality does not apply. We demonstrate by an explicit model that such compatibility violations may yield a violation of noncontextuality inequalities, even if we assume that the incompatibilities merely originate from context-independent noise. We show, however, that this problem can be circumvented by combining the ideas behind Leggett-Garg inequalities with those of the Kochen-Specker theorem.

PACS numbers: 03.65.Ta, 03.65.Ud

I. INTRODUCTION

Bell's theorem [1] is a famous no-go result that provides constraints on the program of interpreting quantum mechanics as an incomplete theory in the sense of Einstein, Podolsky, and Rosen [2]. It is expressed via inequalities that are fulfilled by any local realistic theory, but which are predicted to be violated by quantum mechanics. Experimentally, it is indeed found that quantum mechanics violates these inequalities for certain entangled states [3, 4]. Similar to Bell, Leggett and Garg [5] have proposed inequalities that are fulfilled by theories that satisfy a criterion of *macroscopic realism*, meaning that a system always occupies one of the states accessible to it. Under the further assumption of measurement non-invasiveness, the correlations between measurements performed on the system at different points in time obey a bound that is violated by quantum mechanics.

A third no-go result is provided by the Kochen-Specker theorem [6, 7]. Essentially, it replaces Bell's assumption of locality with the condition of noncontextuality: the outcome of a measurement on a system should not depend on other compatible measurements performed on the same system. Here, two measurements are called compatible, if they can be measured simultaneously or in a temporal sequence without any disturbance. The Kochen Specker result contains Bell's theorem as a special case in which the measurements are performed at spatial separation [8]. It is, however, also applicable to single quantum systems; consequently, entanglement is not necessary for violations of noncontextuality. In fact, violations of Kochen-Specker inequalities occur for all quantum systems of dimension $d \geq 3$, independent of the initial quantum state [6].

However, in contrast to Bell's theorem, the Kochen-Specker theorem does not readily lend itself to experimental tests of quantum mechanics. The direct testability is stymied by the fact that, during each experiment, only one measurement context is accessible at any given time. This limitation can be overcome, however, because similarly to Bell's theorem, the Kochen-Specker theorem can be expressed using inequalities, though it was originally not cast into this form [9, 10]. This permits testing quantum contextuality by using measurements that are carried out sequentially.

But even in this formulation, the question of experimental testability poses further difficulties. The reason for this lies in the notion of contextuality, which only applies in the case of compatible observables. But in an experiment, this condition cannot be fulfilled perfectly; indeed, even measuring the same observable twice may yield different results. This is due to the unavoidable presence of noise during the measurement process, which leads to disturbances of the state. It has been argued that this inherent difficulty, together with a related issue concerning the finite precision of real measurements, nullifies the physical significance of the Kochen-Specker theorem [11–13].

Different strategies have been proposed to overcome this problem. In Ref. [13], the modification of Kochen-Specker inequalities through the introduction of error terms was considered (see also Ref. [14]). Given that the measurement-induced disturbances are cumulative, these terms compensate for the violations of compatibility. A related approach, addressing a similar loophole in experimental tests of Leggett-Garg inequalities, was proposed in Ref. [15]. On the other hand it was suggested in Ref. [16] to perform experiments on separate qutrits in order to forestall the possibility of violations of compatibility.

In this paper, we take a different approach. First, we consider the question: what does an experimentally observed violation of a noncontextuality inequality license us to conclude? By proposing an explicit model capturing the effects of noise-induced compatibility violations, we argue that to conclude contextuality from the violation alone is difficult to justify: the model produces violations of noncontextuality inequalities while being in-

*Electronic address: szangolies@thphy.uni-duesseldorf.de
†Electronic address: matthias.kleinmann@uni-siegen.de
‡Electronic address: otfried.guehne@uni-siegen.de

dependent of the measurement context, and thus, noncontextual in this sense. In particular, we show that even the introduction of error terms as proposed in Ref. [13] cannot settle the issue.

We then propose a way to circumvent this problem by taking into account the ideas of Leggett and Garg: imposing a suitable time-ordering onto the measurements, it turns out to be possible to formulate inequalities that cannot be violated within our framework, and thus, allow to rule out more general hidden-variable models under realistic experimental conditions.

This paper is organized as follows. In Section II, we briefly recall the notions of compatibility and contextuality. Then, we propose an explicit classical noise model capable of inducing compatibility violation in such a way as to violate contextuality inequalities. In Section III we show that the model cannot be ruled out by previous approaches. To remedy this problem, in Section IV we propose new inequalities, utilizing ideas from Leggett and Garg. These inequalities allow to rule out more general hidden variable models.

II. NONCONTEXTUAL MODELS

As a basis for our investigations we take a variant of the well-known Clauser-Horne-Shimony-Holt (CHSH) inequality [17]

$$\langle \chi_{\mathrm{CHSH}} \rangle = \langle AB \rangle + \langle BC \rangle + \langle CD \rangle - \langle DA \rangle \overset{NCHV}{\leq} 2 \overset{QM}{\leq} 2\sqrt{2}. \tag{1}$$

Each of the observables A, B, C, D has outcomes ± 1, and $\langle AB \rangle$ denotes the average over many repetitions obtained by measuring first A, then B, and then multiplying the results. If we assume that the observables in each context $\langle AB \rangle$, etc., are compatible, then $NCHV$ denotes the classical (noncontextual hidden-variable) bound, i.e., the value obtained if each of the observables is assumed to have a fixed value independently of which context it is measured in. The bound QM denotes the maximal value achievable in quantum mechanics [18]. The question now is: suppose one experimentally observes $\langle \chi_{\mathrm{CHSH}} \rangle > 2$. Is this sufficient to conclude contextual behavior?

First, we need to make the notions of compatibility and noncontextuality precise. Consider some observables $\mathcal{O} = \{A, B, C, \ldots\}$. Compatibility then means that within any sequence of measurements composed of these observables, the observed value does not depend on the point at which it is measured within the sequence. That is, for any sequence of compatible measurements $\mathcal{C}$, the observed value of O at the ith point in the sequence, $v_i(O|\mathcal{C})$, does not depend on i, i.e., $v_i(O|\mathcal{C}) = v_j(O|\mathcal{C})$ for all i and j. This formalizes the notion that measurement of one observable does not influence the measurement of any other observable.

Then, any set of compatible observables $\mathcal{C}$ is called a *context*. A theory is called *noncontextual*, if for all observables O and for all contexts $\mathcal{C}, \mathcal{C}'$ the observed value is independent of the context, i.e., $v(O|\mathcal{C}) = v(O|\mathcal{C}')$. Note that through the definition of a context, the notion of noncontextuality explicitly depends on compatibility.

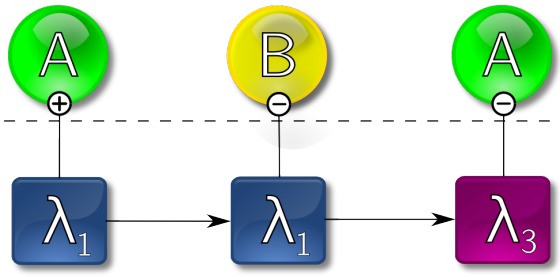

FIG. 1: Schematic representation of a sequence of measurements. Measurements A and B are performed sequentially on a system whose (hidden-variable) state λ evolves stochastically as indicated. Time runs left to right.

To approach the question, we construct a counterexample given by a simple model for noise-induced disturbances of the hidden-variable states. These hidden states λ_i are assumed to completely specify all possible experimental outcomes. In the present case, they can thus be indexed by the dichotomic outcomes of measurements of the observables $\mathcal{O} = \{A, B, C, D\}$: a given state is specified uniquely by a set of values $v(O) \in \{\pm 1\}$ for all $O \in \mathcal{O}$. For ease of notation, this set of values may be interpreted as a binary number, whose decimal value is used to index the state, i.e., $\lambda_2 = \lambda_{(++-+)}$ denotes the state that produces the measurement results $A = +1$, $B = +1$, $C = -1$ and $D = +1$. The model can be generalized by considering states that are convex combinations of the value attributions λ_i, such that the most general state can be written as a mixture $\sum_{i=0}^{(2^n)-1} p_i \lambda_i$, where $\sum_{i=0}^{(2^n)-1} p_i = 1$ and n denotes the number of observables.

The dynamics of this model now is such that after every measurement, the system may randomly execute a transition to a different state. Note that this transition does not depend on which measurement was carried out. This models the effect of noise introduced during measurement, i.e., after a noisy interaction with the system, further measurements will in general yield different results. We will now show that this is equivalent to the introduction of compatibility violations in a realistic experiment, and, crucially, that these violations may lead to false positives in Kochen-Specker tests.

Consider the evolution depicted in Fig. 1: a measurement of the observable A is made on a system in the state λ_1, consequently producing the result $+1$. Subsequently, the observable B is measured, yielding -1. Then, the system undergoes a state transition to λ_3, and a subsequent measurement of A yields -1. Thus, compatibility is violated.

Of course, this model cannot suffice to capture all

quantum mechanical effects; in particular, for *a priori* incompatible observables, it is easy to show that its behavior differs from that of quantum mechanics: take a measurement sequence such as AAA. Without disturbances, both quantum mechanics and the model predict that the same result will be repeated three times; allowing for noise influences, there will be a small probability of disagreement. Measuring ACA, however, since A and C are not compatible, quantum mechanics predicts that the result for the second measurement of A must be random, while in our model, it will agree with the first result up to possible probabilistic state changes (i.e., in our model, the probability distribution from which the value of A is drawn will not differ whether it is the third measurement in the sequence AAA or in the sequence ACA). However, Kochen-Specker tests are always carried out within compatible sets of observables, and, since we are (for the moment) only investigating what can be concluded from such a test alone, this is not our concern here. Our main point is that this simple model can invalidate some ideas to make Kochen-Specker tests robust against noise.

Let us now consider what happens during a measurement of the left-hand side of Eq. (1) if violations of compatibility are present. Then, if we denote by A_i the observed value of A, given that the hidden variable state is λ_i, $\langle\chi_{\mathrm{CHSH}}\rangle$ can be calculated as follows:

$$\begin{aligned}\langle\chi_{\mathrm{CHSH}}\rangle &= \sum_{i,j}(A_iB_j + B_iC_j + C_iD_j - D_iA_j)p_{ij} \\ &\equiv \sum_{i,j} K_{ij}p_{ij}, \end{aligned} \tag{2}$$

where the p_{ij} denote the probability that the evolution of the system is $\lambda_i \to \lambda_j$, that is, that the state during the first measurement was λ_i, which transitioned to λ_j before the second one, and we have introduced the quantity $K_{ij} = A_iB_j + B_iC_j + C_iD_j - D_iA_j$. The maximum $K^{\max}$ of the coefficients K_{ij} provides the upper bound

$$\langle\chi_{\mathrm{CHSH}}\rangle = \sum_{i,j} K_{ij}p_{ij} \leq \max_{ij}\{K_{ij}\} \equiv K^{\max}. \tag{3}$$

Each K_{ij} represents the value of χ_{CHSH}, given the hidden variable evolution $\lambda_i \to \lambda_j$. It is easy to check that $K_{0,8} = 4$: $\lambda_0 = (++++)$ and $\lambda_8 = (-+++)$, and thus, $\langle AB\rangle = \langle BC\rangle = \langle CD\rangle = +1$, while $\langle DA\rangle = -1$. Hence, a simple model that after each measurement changes the system's state from λ_0 to λ_8 will maximally violate the CHSH inequality; if the change happens only with a certain probability p, obviously any value between 2 and 4 can be achieved.

It should be noted that despite the evolution of the hidden variable, this model is noncontextual in the sense that whether or not a state transition is effected does not depend on the measured context. It thus seems surprising that this model can violate the CHSH inequality, apparently indicating contextual behavior. However, strictly speaking, noncontextuality simply does not apply in this case, as it is defined only under the assumption of perfect compatibility.

III. CONNECTION WITH PREVIOUS WORKS

An approach to rein in the effects of compatibility violations was proposed in Ref. [13]. There, several classes of error terms were proposed, such that additional measurements may be performed in order to quantify the degree of failure of *a priori* compatible observables to be compatible in the actual experiment, i.e., the degree of influence a measurement of A has on the compatible measurement B, for example. We will concentrate, for the moment, on the first class of error terms from Ref. [13], which are those that have been experimentally implemented.

Based on an assumption of noise cumulation, that is, an assumption that additional measurements always lead to additional noise and thus a worse violation of compatibility, the inequality

$$\begin{aligned}\langle\chi_{\mathrm{CHSH}}\rangle - p^{\mathrm{err}}[BAB] - p^{\mathrm{err}}[CBC] \\ -p^{\mathrm{err}}[DCD] - p^{\mathrm{err}}[ADA] \leq 2,\end{aligned} \tag{4}$$

holds [13]. Here for instance $p^{\mathrm{err}}[BAB]$ is the probability that the second measurement of B in the sequence BAB disagrees with the first one.

However, it is clear that the model we discuss does not obey the assumption of cumulative noise: for an evolution such as $\lambda_0 \to \lambda_4 \to \lambda_0$, clearly both measurements of B in the sequence BAB agree, but if B were measured in the second place of the sequence, then it would have yielded a value opposite to the first. Thus, the model is not necessarily constrained by Inequality (4); and in fact, since the error terms all vanish for such an evolution, it is clear that the model can violate it.

Alternatively, it may be noted that while the original CHSH-inequality is only concerned with measurement sequences of length 2, the error terms contain only sequences of length 3, and thus, can only provide information about the system's behavior during such sequences. This criticism holds for the other two classes of error terms in Ref. [13] as well.

IV. MODIFIED INEQUALITIES

However, another approach, which does not need any additional measurements or further assumptions, is possible. This amounts to essentially applying the ideas of Leggett and Garg to contextuality inequalities. Rather than employing the original inequalities proposed in Ref. [5], it is convenient for our purposes to use a slightly different formulation. Consider two different measurements C and C', performed at two points in time. Then, $C(C + C') + C'(C - C') = \pm 2$, and thus

$A = \sigma_z \otimes \mathbb{1}$	$B = \mathbb{1} \otimes \sigma_z$	$C = \sigma_z \otimes \sigma_z$
$a = \mathbb{1} \otimes \sigma_x$	$b = \sigma_x \otimes \mathbb{1}$	$c = \sigma_x \otimes \sigma_x$
$\alpha = \sigma_z \otimes \sigma_x$	$\beta = \sigma_x \otimes \sigma_z$	$\gamma = \sigma_y \otimes \sigma_y$

TABLE I: The Peres-Mermin square, with the Pauli matrices σ_i, and the 2×2 identity matrix $\mathbb{1}$. The observables in all rows and columns commute, and the product of all rows and the first two columns is equal to $\mathbb{1}$, while for the last column, $Cc\gamma = -\mathbb{1}$.

$\langle C'C\rangle + \langle CC\rangle + \langle CC'\rangle - \langle C'C'\rangle \leq 2$, where $\langle CC'\rangle$ denotes the correlation between C, measured at t_1, and C', measured at t_2.

We can now impose a similar time-ordering of observables on Eq. (1), to get

$$\langle \chi_{\rm CHSH}\rangle = \langle AB\rangle + \langle CB\rangle + \langle CD\rangle - \langle AD\rangle \leq 2. \quad (5)$$

It is not hard to see that for Eq. (5), $K_{ij} \leq 2$ for all (i, j): if the first three terms are equal to $+1$, the fourth is necessarily equal to $+1$, as well. Hence, our model cannot violate Inequality (5), despite the violation of compatibility. Since in the case of a trivial evolution of the hidden variables, i.e. an evolution that leaves the state invariant, we recover the usual notion of (sequential) noncontextuality, an experimental test of Eq. (5) constitutes a test of quantum contextuality robust against the compatibility loophole.

It should be noted that the CHSH-inequality is not the only one that can be modified to hold in the case of compatibility violations: another important inequality proposed in Ref. [9] is based on the Peres-Mermin square ([19]; see Table I). Using the same reasoning as in the CHSH-case, the inequality

$$\begin{aligned}\langle \chi_{\rm PM}\rangle &= \langle ABC\rangle + \langle cab\rangle + \langle \beta\gamma\alpha\rangle \\ &+ \langle Aa\alpha\rangle + \langle \beta Bb\rangle - \langle c\gamma C\rangle \leq 4 \end{aligned} \quad (6)$$

holds also in the case of imperfect compatibility between observables. In quantum mechanics, a value of $\langle \chi_{\rm PM}\rangle = 6$ can be reached. Again, it is here the ordering of the measurement sequences that matters: the original inequality proposed in Ref. [9] followed the ordering indicated in Table I; but in this form, it is not hard to see that the inequality can be violated easily by our model. Interestingly, the ordering proposed here is also useful if the Mermin-Peres inequality should be used for estimating the dimension of a quantum system [20].

The importance of this scenario is that this inequality is state-independent, that is, one does not require a special quantum state for the violation (as is the case for the CHSH-inequality). Furthermore, an experiment using sequential measurements on trapped ions already implemented this scenario by measuring the observables in Table I in all possible permutations [14]. This experiment focused on the violation of the inequality as originally proposed in Ref. [9], and using this data, the observed value for Eq. (6) is $\langle \chi_{\rm PM}\rangle = 5.35(4)$.

Not every noncontextuality inequality can be modified this straightforwardly, though. For example, the Klyachko-Can-Binicioğlu-Shumovsky inequality [10]

$$\begin{aligned}\langle \chi_{\rm KCBS}\rangle =& \langle AB\rangle + \langle BC\rangle + \langle CD\rangle \\ &+ \langle DE\rangle + \langle EA\rangle \overset{NCHV}{\geq} -3 \overset{QM}{\geq} 5 - 4\sqrt{5}, \end{aligned} \quad (7)$$

which exhibits a quantum violation even for a single qutrit system, as demonstrated experimentally in Ref. [21], cannot be rearranged appropriately. Nevertheless, our approach can be generalized: the modified inequality

$$\begin{aligned}&\langle AB\rangle + \langle CB\rangle + \langle CD\rangle + \langle ED\rangle + \langle EA\rangle - \langle AA\rangle \\ &\overset{NCHV}{\geq} -4 \overset{QM}{\geq} 4 - 4\sqrt{5} \end{aligned} \quad (8)$$

holds for any noncontextual hidden-variable evolution. The reason for this is that it enforces the ordering conditions as in Eq. (5): to maximize the left hand side of Eq. (8), for instance A_i must equal E_j, as must A_j; however, then $A_i = A_j$, and thus, $\langle AA\rangle = 1$. This shows that even in the case of a single qutrit a Kochen-Specker test ruling out our model can be undertaken. However, one should note that due to this modification, the relative quantum violation shrinks, since the absolute violation stays the same, while the absolute value of the classical expectation increases. Finally, it should be noted that a similar inequality like Eq. (8) has already been used in Ref. [21] in order to compensate for the fact that in this setup the observable A was implemented in two different ways.

In fact, a recently proposed state-independent inequality violated by a single qutrit system [22] can be treated in the same way. This inequality features 13 observables $\{A^1, \ldots, A^{13}\}$, and the form that yields the maximum quantum violation is [23, 24]

$$\sum_i \Gamma_i \langle A^i\rangle + \sum_{ij} \Gamma_{ij} \langle A^i A^j\rangle \leq 16, \quad (9)$$

where the coefficients are as follows: $\Gamma_i = 1$ for $i \in \{4, 7, 10, \ldots, 13\}$, $\Gamma_i = 2$ for $i \in \{1, 5, 6, 8, 9\}$, and $\Gamma_i = 3$ for $i \in \{2, 3\}$; $\Gamma_{ij} = -1$ for $(i, j) \in \{(1, 2), (1, 3), (1, 4), (1, 7), (4, 10), (8, 10), (9, 10), (5, 11), (7, 11), (9, 11), (6, 12), (7, 12), (8, 12), (4, 13), (5, 13), (6, 13)\}$, $\Gamma_{ij} = -2$ for $(i, j) \in \{(2, 3), (2, 5), (2, 8), (3, 6), (3, 9), (5, 8), (6, 9)\}$, and $\Gamma_{ij} = 0$ else. By checking all possible hidden variable evolutions one verifies that the modified inequality [25]

$$\sum_i \Gamma_i \langle A^i\rangle + \sum_{ij} \Gamma_{ij} \langle A^i A^j\rangle + 4 \sum_i \langle A^i A^i\rangle \leq 68 \quad (10)$$

cannot be violated by noncontextually evolving models. However, since the maximum quantum value in this case is only $69 + \frac{1}{3}$, the relative violation is reduced to $\frac{1}{51} \approx 1.96\%$, compared to originally $\frac{1}{12} \approx 8.3\%$.

V. CONCLUSION

We have provided a novel approach to the compatibility problem in Kochen-Specker experiments. Using the idea of time-ordering, as first proposed by Leggett and Garg, we have derived new inequalities violated by quantum mechanics even in the case of imperfectly compatible measurements. This shows that with a careful ordering of the measurements classical models can be ruled out, which cannot be excluded with existing approaches [13]. Nevertheless, we are not claiming that our modified inequalities allow a test of the Kochen-Specker theorem free from the compatibility loophole. Our results, however, show that with a simple reordering of the measurements a significantly larger class of hidden-variable models can be ruled out.

We thank C. Roos for providing us with the data from their experiment, and C. Budroni and D. Bruß for valuable discussions. This work has been supported by the EU (Marie Curie CIG 293993/ENFOQI) and BMBF (projects QuOReP and QUASAR).

[1] J.S. Bell, Physics **1**, 195 (1964).
[2] A. Einstein, B. Podolsky, N. Rosen, Physical Review **41**, 777 (1935).
[3] A. Aspect, P. Grangier, G. Roger, Phys. Rev. Lett. **47**, 460 (1981); A. Aspect, P. Grangier, G. Roger, Phys. Rev. Lett. **49**, 91 (1982); A. Aspect, J. Dalibard, G. Roger, Phys. Rev. Lett. **49**, 1804 (1982).
[4] G. Weihs, T. Jennewein, C. Simon, H. Weinfurter, A. Zeilinger, Phys. Rev. Lett. **81**, 5039 (1998).
[5] A.J. Leggett, A. Garg, Phys. Rev. Lett. **54**, 857 (1985).
[6] S. Kochen, E. P. Specker, J. Math. Mech. **17**, 59 (1967).
[7] J. S. Bell, Rev. Mod. Phys. **38**, 447 (1966).
[8] N. D. Mermin, Rev. Mod. Phys. **65**, 803 (1993).
[9] A. Cabello, Phys. Rev. Lett. **101**, 210401 (2008).
[10] A. A. Klyachko, M. A. Can, S. Binicioğlu, A. S. Shumovsky, Phys. Rev. Lett. **101**, 020403 (2008).
[11] D. A. Meyer, Phys. Rev. Lett. **83**, 3751 (1999).
[12] A. Kent, Phys. Rev. Lett. **83**, 3755 (1999).
[13] O. Gühne, M. Kleinmann, A. Cabello, J-Å. Larsson, G Kirchmair, F. Zähringer, R. Gerritsma, C. F. Roos, Phys. Rev. A **81**, 022121 (2010).
[14] G. Kirchmair, F. Zähringer, R. Gerritsma, M. Kleinmann, O. Gühne, A. Cabello, R. Blatt, C. F. Roos, Nature **460**, 494 (2009).
[15] M. Wilde, A. Mizel, Found. Phys. **42**, 256 (2012).
[16] A. Cabello, M. Terra Cunha, Phys. Rev. Lett. **106**, 190401 (2011).
[17] J. F. Clauser, M. A. Horne, A. Shimony, and R. A. Holt, Phys. Rev. Lett. **23**, 880 (1969).
[18] B. S. Tsirelson, Lett. Math. Phys. **4**, 93 (1980).
[19] A. Peres, Phys. Lett. A **151**, 107 (1990); N. D. Mermin, Phys. Rev. Lett. **65**, 3373 (1990).
[20] O. Gühne, C. Budroni, A. Cabello, M. Kleinmann, and J.-Å. Larsson, arXiv:1302.2266.
[21] R. Lapkiewicz, P. Li, C. Schaeff, N.K. Langford, S. Ramelow, M. Wieśniak, and A. Zeilinger, Nature (London) **474**, 490 (2011).
[22] S. Yu, C. H. Oh, Phys. Rev. Lett **108**, 030402 (2012).
[23] M. Kleinmann, C. Budroni, J.-Å. Larsson, O. Gühne, A. Cabello, Phys. Rev. Lett. **109**, 250402 (2012).
[24] X. Zhang, M. Um, J. Zhang, S. An, Y. Wang, D.-l. Deng, C. Shen, L. Duan and K. Kim, Phys. Rev. Lett. **110**, 070401 (2013).
[25] There is no ordering ambiguity for the single measurements $\langle A^i \rangle$ since we consider disturbances to result from measurement interactions; a single measurement can always be considered to occur in the first position of a measurement sequence.

Bounding Temporal Quantum Correlations

Costantino Budroni,[1] Tobias Moroder,[1] Matthias Kleinmann,[1] and Otfried Gühne[1]

[1] *Naturwissenschaftlich-Technische Fakultät, Universität Siegen, Walter-Flex-Straße 3, D-57068 Siegen, Germany*

(Dated: July 17, 2013)

Sequential measurements on a single particle play an important role in fundamental tests of quantum mechanics. We provide a general method to analyze temporal quantum correlations, which allows us to compute the maximal correlations for sequential measurements in quantum mechanics. As an application, we present the full characterization of temporal correlations in the simplest Leggett-Garg scenario and in the sequential measurement scenario associated with the most fundamental proof of the Kochen-Specker theorem.

PACS numbers: 03.65.Ta, 03.65.Ud

Introduction.—The physics of microscopic systems is governed by the laws of quantum mechanics and exhibits many features that are absent in the classical world. The best-known result showing such a difference is due to Bell [1]. The assumptions of realism and locality lead to bounds on the correlations—the Bell inequalities, and these bounds are violated in quantum mechanics. Interestingly, this quantum violation is limited for many Bell inequalities and does not reach the maximal possible value. For instance, the Bell inequality derived by Clauser, Horne, Shimony, and Holt (CHSH) bounds the correlation [2]

$$\mathcal{B} = \langle A_1 \otimes B_1 \rangle + \langle A_1 \otimes B_2 \rangle + \langle A_2 \otimes B_1 \rangle - \langle A_2 \otimes B_2 \rangle, \quad (1)$$

where A_i and B_j are measurements on two different particles. On the one hand, local realistic models obey the CHSH inequality $\mathcal{B} \leq 2$, which is violated in quantum mechanics. On the other hand, the maximal quantum value is upper bounded by $\mathcal{B} \leq 2\sqrt{2}$, a result known as Tsirelson's bound [3]. Whereas this bound holds within quantum mechanics, it has turned out that hypothetical theories that reach the algebraic maximum $\mathcal{B} = 4$ without allowing faster-than-light communication are possible [4]. This raises the question of whether the bounded quantum value can be derived on physical grounds from fundamental principles. Partial results are available, and principles have been suggested that bound the correlations: in a world where maximal correlations are observed, the communication complexity is trivial [5], a principle established as information causality is violated [6], and there exists no reversible dynamics [7].

The question of how and why quantum correlations are fundamentally limited has been discussed mainly in the scenario of bipartite and multipartite measurements. What happens, however, if we shift the attention from spatially separated measurements to temporally ordered measurements? There is no need to measure on distinct systems as in Eq. (1), but rather, we may perform sequential measurements on the same system. Then, an elementary property of quantum mechanics becomes important: the measurement changes the state of the system. In fact, this allows us to temporally "transmit" a certain amount of information [8], and one would expect that the correlations in the temporal case can be larger than in the spatial situation.

We stress that sequential measurements also have been considered in the analysis of the question how quantum and classical mechanics are different, the most well-established results here are quantum contextuality (the Kochen-Specker theorem [9]) and macrorealism (Leggett-Garg inequalities [10]); cf. Fig. 1. The research in this fields has triggered experiments involving sequential measurements. For demonstrating such a contradiction between classical and quantum physics, e.g., the correlation

$$\begin{aligned}\mathcal{S}_5 =& \langle A_1 A_2 \rangle_{\text{seq}} + \langle A_2 A_3 \rangle_{\text{seq}} + \langle A_3 A_4 \rangle_{\text{seq}} + \langle A_4 A_5 \rangle_{\text{seq}} \\ & - \langle A_5 A_1 \rangle_{\text{seq}} \end{aligned} \quad (2)$$

has been considered [11, 12]. Here, $\langle A_i A_j \rangle_{\text{seq}}$ denotes a sequential expectation value that is the average of the product of the value of the observables A_i and A_j when first A_i is measured, and afterwards A_j. One can show that for macrorealistic theories as well as for noncontextual models the bound $\mathcal{S}_5 \leq 3$ holds, but in quantum mechanics, this can be violated.

Here however, we are rather interested in the fundamental bounds on the temporal quantum correlations, with no assumption about the compatibility of the observables. Special cases of this problem have been discussed before: for Leggett-Garg inequalities, maximal values for two-level systems have been derived [11, 13], and temporal inequalities similar to the CHSH inequality have been discussed [8, 14].

We provide a method that allows us to compute the maximal achievable quantum value for an arbitrary inequality and thus we solve the problem of bounding temporal quantum correlations. First, we will discuss a simple method, which can be used for expressions as in Eq. (2), where only sequences of two measurements are considered. Then, we introduce a general method which can be used for arbitrary sequential measurements, resulting in a complete characterization of the possible

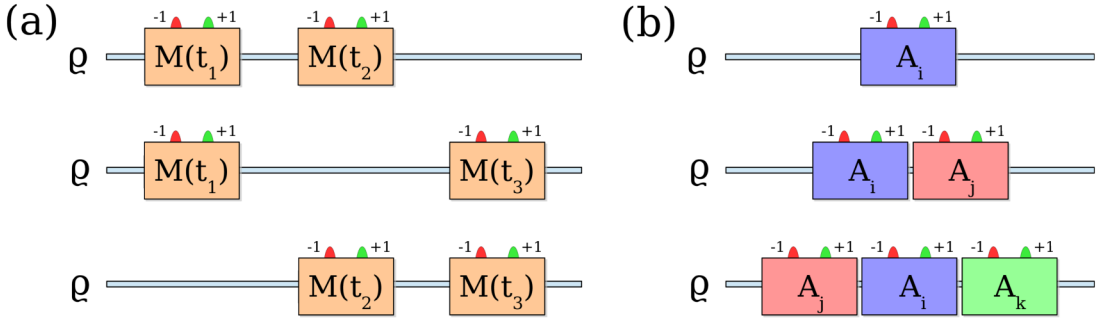

FIG. 1. Sequential measurements occur in two different scenarios. (a) In the Leggett-Garg scenario, one takes a single observable M that measures whether the physical system is in one of two possible macroscopic states. Then, one considers the correlations between these measurements at three different times, $\langle M(t_1)M(t_2)\rangle_{\text{seq}}$, $\langle M(t_1)M(t_3)\rangle_{\text{seq}}$, and $\langle M(t_2)M(t_3)\rangle_{\text{seq}}$. The values predicted by quantum mechanics contradict the assumption that the physical system is in any of these macroscopic states at any time and that the measurement reveals this state without disturbing it. (b) In the Kochen-Specker scenario one considers a set of observables A_i. Some of these observables are compatible and can therefore be measured simultaneously or in a sequence without any disturbance. Then one measures the correlations of simultaneous or sequential measurements of compatible observables, such as $\langle A_i\rangle_{\text{seq}}$, $\langle A_iA_j\rangle_{\text{seq}}$, and $\langle A_jA_iA_k\rangle_{\text{seq}}$. For these correlations, one finds that quantum mechanics contradicts the assumption of noncontextuality. This assumption states that the result of a measurement should not depend on which other compatible observables are measured along with it. It should be noted, however, that the situation considered in this Letter is more general than case (a) or (b), since no assumption about the time evolution or the compatibility of observables is made.

quantum values. Interestingly, our methods characterize temporal correlations exactly, whereas for the case of spatially separated measurements only converging approximations are known.

Projective measurements.—When determining the maximal value for sequential measurements as in Eq. (2) we consider projective measurements, as these are the standard textbook examples of quantum measurements. The underlying formalism has been established by von Neumann [15] and Lüders [16]. An observable A with possible results ±1 is described by two projectors Π_+ and Π_- such that $A = \Pi_+ - \Pi_-$. If the observable A is measured, the quantum state is projected onto the space of the observed result, i.e., $\varrho \mapsto \Pi_\pm\varrho\Pi_\pm/\mathrm{Tr}(\varrho\Pi_\pm)$. Applying this scheme to the case of sequential measurements, one finds that the sequential mean value can be written as

$$\langle A_iA_j\rangle_{\text{seq}} = \frac{1}{2}[\mathrm{Tr}(\varrho A_iA_j) + \mathrm{Tr}(\varrho A_jA_i)]. \qquad (3)$$

It is interesting to notice that for pairs of ±1-valued observables such a mean value does not depend on the order of the measurement [8].

The simplified method.—We first show how the maximal quantum mechanical value for an expression such as $\mathcal{S}_5$ in Eq. (2) can be determined. First, we consider a set $\mathcal{A} = \{A_i\}$ of ±1-valued observables and a general expression $C = \sum_{ij}\lambda_{ij}\langle A_iA_j\rangle_{\text{seq}}$. The correlations given in Eq. (2) are just a special case of this scenario. Then, we consider the matrix built up by the sequential mean values $X_{ij} = \langle A_iA_j\rangle_{\text{seq}}$. This matrix has the following properties: (i) it is real and symmetric, $X = X^T$, (ii) the diagonal elements equal one, $X_{ii} = 1$, and (iii) the matrix has no negative eigenvalue (or $v^TXv \geq 0$ for any vector v), denoted as $X \succeq 0$ (see Appendix A2). A similar construction for the matrix X, together with the optimization problem below, has been considered before in relation with Bell inequalities [17]. However, our method involves a different notion of correlations, namely that given by Eq. (3).

The main idea is now to optimize the expression $C = \sum_{ij}\lambda_{ij}X_{ij}$ over all matrices with the properties (i)–(iii) above. Hence, we consider the optimization problem

$$\text{maximize:} \sum_{ij}\lambda_{ij}X_{ij}, \qquad (4)$$
$$\text{subjected to:} X = X^T \succeq 0 \text{ and for all } i,\ X_{ii} = 1.$$

Since all matrices X that can originate from a sequence of quantum measurements will be of this form, one performs the optimization over a potentially larger set. Thus, the solution of this optimization is, in principle, just an upper bound on the maximal quantum value of $\mathcal{S}_5$. Note that the optimization itself can be done efficiently and is assured to reach the global optimum since it represents a so-called semidefinite program [18]. In the case of $\mathcal{S}_5$, this optimization can even be solved analytically and gives

$$\mathcal{S}_5 \leq \frac{5}{4}\left(1+\sqrt{5}\right) \approx 4.04. \qquad (5)$$

It turns out that appropriately chosen measurements on a qubit already reach this value (see Appendix A2 and Refs. [11, 19]). Hence, this upper bound is tight. More generally, one can prove that each matrix X with the above properties has a sequential quantum representation (see Appendix A2). Finally, note that if the observables in each sequence are required to commute, then the maximal quantum value for $\mathcal{S}_5$ is known to be $\Omega_{QM} = 4\sqrt{5} - 5 \approx 3.94$ [20, 21].

The general method.—The above method can only be used for correlations terms of sequences of at most two ± 1-valued observables. In the following, we discuss the conditions allowing a given probability distribution to be realized as sequences of measurements on a single quantum system in the general setting. We label as $\mathbf{r} = (r_1, r_2, \ldots, r_n)$ the results of an n-length sequence obtained by using the setting $\mathbf{s} = (s_1, s_2, \ldots, s_n)$. The ordering is such that r_1, s_1 label the result and the setting for the first measurement etc. The outcomes of any such sequence are sampled from the sequential conditional probability distribution

$$P(\mathbf{r}|\mathbf{s}) \equiv P_{\text{seq}}(r_1, r_2, \ldots, r_n|s_1, s_2, \ldots, s_n). \tag{6}$$

In the case of projective quantum measurements, each individual result r of any setting s is associated with a projector Π_r^s, which altogether satisfy two requirements: for each setting the operators must sum up to the identity, i.e., $\sum_r \Pi_r^s = \mathbb{1}$ and they satisfy the orthogonality relations $\Pi_r^s \Pi_{r'}^s = \delta_{rr'} \Pi_r^s$, where $\delta_{rr'}$ is the Kronecker symbol. Finally, after the measurement with the setting s and result r, the quantum state is transformed according to the rule $\varrho \mapsto \Pi_r^s \varrho \Pi_r^s / P(r|s)$.

In the following, we say that the a conditional probability distribution $P(\mathbf{r}|\mathbf{s})$ has a sequential projective quantum representation if there exists a suitable set of such operators Π_r^s and an appropriate initial state ϱ such that

$$P(\mathbf{r}|\mathbf{s}) = \text{Tr}[\Pi(\mathbf{r}|\mathbf{s})\Pi(\mathbf{r}|\mathbf{s})^\dagger \varrho], \tag{7}$$

with the shorthand $\Pi(\mathbf{r}|\mathbf{s}) = \Pi_{r_1}^{s_1} \Pi_{r_2}^{s_2} \cdots \Pi_{r_n}^{s_n}$.

Whether a given distribution $P(\mathbf{r}|\mathbf{s})$ indeed has such a representation can be answered via a so-called matrix of moments, which often appears in moment problems [17, 22–24]. This matrix, denoted as M in the following, contains the expectation value of the products of the above-used operators $\Pi(\mathbf{r}|\mathbf{s})$ at the respective position in the matrix. In order to identify this position we use as a label the abstract operator sequence $\mathbf{r}|\mathbf{s}$ for both row and column index. In this way the matrix is defined as

$$M_{\mathbf{r}|\mathbf{s};\mathbf{r}'|\mathbf{s}'} = \langle \Pi(\mathbf{r}|\mathbf{s}) \Pi(\mathbf{r}'|\mathbf{s}')^\dagger \rangle. \tag{8}$$

Whenever this matrix is indeed given by a sequential projective quantum representation, the matrix M satisfies two conditions: (a) linear relations of the form $M_{\mathbf{r}|\mathbf{s};\mathbf{k}|\mathbf{l}} = M_{\mathbf{r}'|\mathbf{s}';\mathbf{k}'|\mathbf{l}'}$ if the underlying operators are equal as a consequence of the properties of normalization and orthogonality of projectors, (b) $M \succeq 0$ since $v^\dagger M v \geq 0$ holds for any vector v, because such a product can be written as the expectation value $\langle CC^\dagger \rangle_\varrho \geq 0$ which is non-negative for any operator C. Finally, note that certain entries of this matrix are the given probability distribution, for instance, at the diagonal $M_{\mathbf{r}|\mathbf{s};\mathbf{r}|\mathbf{s}} = P(\mathbf{r}|\mathbf{s})$. The main point, however, is the converse statement: given a moment matrix with properties (a) and (b) above, the associated probability distribution $P(\mathbf{r}|\mathbf{s})$ always has a sequential projective quantum representation (see Appendix A3).

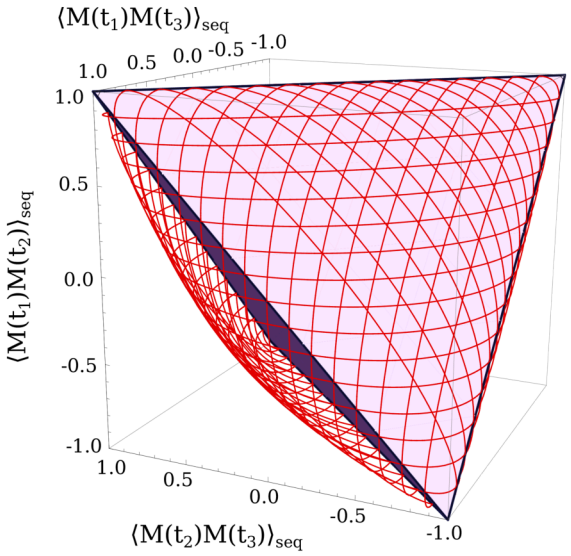

FIG. 2. Complete characterization of the possible quantum values for the simplest Leggett-Garg scenario. In this case, three different times are considered, resulting in three possible correlations $\langle M(t_1)M(t_2)\rangle_{\text{seq}}$, $\langle M(t_1)M(t_3)\rangle_{\text{seq}}$, and $\langle M(t_2)M(t_3)\rangle_{\text{seq}}$. In this three-dimensional space, the possible classical values form a tetrahedron, characterized by Eq. (9) and variants thereof. The possible quantum mechanical values form a strictly larger set with curved boundaries.

Hence, the search for quantum bounds represents again a semidefinite program. The fact that this characterization is sufficient is in stark contrast with the analogue technique in the spatial Bell-type scenario [22, 23], where one needs to use moment matrices of an increasing size n to generate better superset characterizations which only become sufficient in the limit $n \to \infty$. However, indirectly, the sufficiency of our method has already been proven in this context [23] (see Appendix A3).

Applications.—To demonstrate the effectiveness of our approach, we discuss four examples. First, we consider the original Leggett-Garg inequality

$$\begin{aligned}\mathcal{S} = \langle M(t_1)M(t_2)\rangle_{\text{seq}} + \langle M(t_2)M(t_3)\rangle_{\text{seq}} \\ -\langle M(t_1)M(t_3)\rangle_{\text{seq}} \leq 1.\end{aligned} \tag{9}$$

This bound holds for macrorealistic models, and it has been shown that in quantum mechanics values up to $\mathcal{S} = 3/2$ can be observed [10, 11, 13]. Our methods allow us not only to prove that this value is optimal for any dimension and any measurement, but also to, for instance, determine all values in the three-dimensional space of temporal correlations $\langle M(t_i)M(t_j)\rangle$, which can originate from quantum mechanics. The detailed description is given in Fig. 2, and the calculations are given in the Appendix A1.

Second, we consider generalizations of the Eq. (2) with a larger number of measurements, known as N-cycle inequality [20, 21],

$$\mathcal{S}_N = \sum_{i=0}^{N-2} \langle A_i A_{i+1}\rangle_{\text{seq}} - \langle A_{N-1}A_0\rangle_{\text{seq}}. \tag{10}$$

For this case, everything can be solved analytically (see Appendix A2) leading to the bound

$$\mathcal{S}_N \leq N\cos\left(\frac{\pi}{N}\right), \tag{11}$$

which can be reached by suitably chosen measurements. This value has already occurred in the literature [11, 19], but only qubits have been considered. Our proof shows that it is valid in arbitrary dimension. Note that the fact that the maximal value is obtained on a qubit system is not trivial, although the measurements are dichotomic. For Kochen-Specker inequalities with dichotomic measurements examples are known, where the maximum value cannot be attained in a two-dimensional system [19] and also for Bell inequalities this has been observed [26, 27].

As a third application, we consider the noncontextuality scenario recently discovered by S. Yu and C. H. Oh [28]. There, thirteen measurements on a three-dimensional system are considered, and a noncontextuality inequality is constructed, which is violated by any quantum state. It has been shown that this scenario is the simplest situation where state-independent contextuality can be observed [29], so it is of fundamental importance. We can directly apply our method to the original inequality by Yu and Oh, as well as recent improvements [30] and compute the corresponding Tsirelson-like bounds. We recall that our results are not directly related to the phenomenon of quantum contextuality, since no compatibiliy of the measurements is assumed, but they show the effectiveness of our method even on complex scenarios, namely, inequalities containing 37 or 41 terms, that involve sequential measurements. Our results are summarized in Table 1.

Another class of inequalities is given by the guess-your-neighbor's-input inequalities [31], which if viewed as multipartite inequalities, show no quantum violation but a violation with the use of postquantum no-signalling resources. We calculate the sequential bound for the case of measurement sequences of length three, instead of measurement on three parties. We consider

Ineq.	NCHV bound	State-independent quantum value	Algebraic maximum	**Sequential bound**
Yu-Oh	16	$50/3 \approx 16.67$	50	17.794
Opt2	16	$52/3 \approx 17.33$	52	20.287
Opt3	25	$83/3 \approx 27.67$	65	32.791

TABLE I. Bounds on the quantum correlations for the Kochen-Specker inequalities in the most basic scenario. Three inequalities were investigated: First, the original inequality proposed in Ref. [28] and the optimal inequalities from Ref. [30] with measurement sequences of length two (Opt2) and length three (Opt3). For each inequality, the following numbers are given: the maximum value for noncontextual hidden variable (NCHV) models, the state-independent quantum violation in three-dimensional systems (obtained in Refs. [28, 30]), the algebraic maximum and the maximal value that can be attained in quantum mechanics for the sequential measurements. The latter bound is higher than the state independent quantum value, since the observables do not have to obey the compatibility relations occurring in the Kochen-Specker theorem. Notice that the sequential bound is obtained as a maximization over the set of possible observables and states, thus it is in general state-dependent. Interestingly, in all cases the maximal quantum values are significantly below the algebraic maximum.

$$\begin{aligned} P(000|000) + P(110|011) + P(011|101) \\ +P(101|110) \leq \Omega_{C,Q} \leq \Omega_S \leq \Omega_{NS}, \end{aligned} \tag{12}$$

with the notation $P(r_1, r_2, r_3|s_1, s_2, s_3)$ as before, and possible results and settings $r_i \in \{0, 1\}$ and $s_i \in \{0, 1\}$. We find that

$$\Omega_S \approx 1.0225, \tag{13}$$

while it is known that $\Omega_{C,Q} = 1$ and $\Omega_{NS} = \frac{4}{3}$, where the indices C, Q, S, NS label, respectively, the classical, quantum, sequential and no-signalling bounds. So, in this case, the bound for sequential measurements is higher than the bound for spatially separated measurements. This also highlights the greater generality of our method in comparison with the results of Ref. [8]: there, only temporal inequalities with sequences of length two have been considered, where in addition the measurements can be split in two separate groups. In this case it turned out that the bounds were always reached with commuting observables. Our examples show that this is usually not the case, when longer measurement sequences are considered.

Discussion and conclusions.—For interpreting our results, let us note that our scenario is more general than the scenarios considered by Leggett and Garg and Kochen and Specker. Leggett and Garg consider a special time evolution $\varrho(t) = U(t)\varrho(0)U^\dagger(t)$, which is mapped in the Heisenberg picture onto the observables. In our case,

the observables are not connected via unitaries; this corresponds to a more general time evolution. Compared with the Kochen-Specker scenario, our approach is more general since it does not assume that the measurements in a sequence are commuting. Nevertheless, if one wishes to connect existing noncontextuality inequalities to information processing tasks, it is important to know the maximal quantum values (also if the observables do not commute), in order to characterize the largest quantum advantage possible.

Furthermore, we emphasize that in our derivation it was assumed that the measurements are described by projective measurements and this condition is indeed important. In fact, this sheds light on the role of projective measurements: one can easily construct classical devices with a memory, which give for sequential measurements as in Eq. (2) the algebraic maximum $\mathcal{S}_5 = 5$. These classical devices must also have a quantum mechanical description. Our results show, however, that in this quantum mechanical description more general than projective measurements must occur and a more general dynamical evolution than the projection is required. From this perspective, our results prove that the memory that can be encrypted in quantum systems by projective measurements is bounded.

Our results lead to the question of why quantum mechanics does not allow us to reach the algebraic maximum of temporal correlations, as long as projective measurements are considered. We believe that proper generalizations of concepts such as information causality and communication complexity might play a role here, but we leave this question for further research. A first step in explaining quantum mechanics from information theoretical principles lies in the precise characterization of all possible temporal quantum correlations, and our work presents an operational solution to this problem.

Acknowledgements.—We thank J.-D. Bancal, T. Fritz, Y.-C. Liang, G. Morchio, and M. Navascués for discussions. This work has been supported by the EU (Marie Curie CIG 293993/ENFOQI) and the BMBF (Chist-Era Project QUASAR).

A1: Discussion of the simplest Leggett-Garg scenario

In this part we provide some further details about how to determine the set of possible quantum values for the simplest non-trivial Leggett-Garg scenario as shown in Fig. 2 of the main text. Here it is assumed that one can measure an observable M at three different time instances t_1, t_2, t_3 as shown in Fig. 1 of the main text, which gives rise to three different observables $A_i = M(t_i)$ with $i = 1, 2, 3$.

However, rather than being interested in determining the full sequential probability $P(\mathbf{r}|\mathbf{s})$ for all possible combinations we are here only interested in some limited information, namely only for the correlation space. This means that from a general distribution we only want to reproduce the correlations terms $\langle A_i A_j \rangle_{\text{seq}}$ with $1 \leq i < j \leq 3$ each defined by

$$\langle A_i A_j \rangle_{\text{seq}} = P(r_i = r_j | i, j) - P(r_i \neq r_j | i, j). \tag{14}$$

Thus we want to characterize the set

$$\begin{aligned} \mathcal{S}_{\text{qm}} = \{ & q_{ij} \in \mathbb{R}^3 : q_{ij} = \langle A_i A_j \rangle_{\text{seq}}, \\ & \langle A_i A_j \rangle_{\text{seq}} \text{ has projective quantum rep.} \}. \end{aligned} \tag{15}$$

For this we refer to problem given by Eq. 4 of the main text, with

$$X = \begin{bmatrix} 1 & \langle A_1 A_2 \rangle_{\text{seq}} & \langle A_1 A_3 \rangle_{\text{seq}} \\ \langle A_1 A_2 \rangle_{\text{seq}} & 1 & \langle A_2 A_3 \rangle_{\text{seq}} \\ \langle A_1 A_3 \rangle_{\text{seq}} & \langle A_2 A_3 \rangle_{\text{seq}} & 1 \end{bmatrix}. \tag{16}$$

Any matrix of this form has a sequential projective quantum representation if and only if X is positive semidefinite. However a matrix satisfies $X \succeq 0$ if and only if the determinant of all principal minors are non-negative. This gives

$$\begin{aligned} \mathcal{S}_{\text{qm}} = \{ & q_{ij} \in \mathbb{R}^3 : |q_{ij}| \leq 1, \\ & 1 + 2q_{12}q_{13}q_{23} \geq q_{12}^2 + q_{13}^2 + q_{23}^2 \}. \end{aligned} \tag{17}$$

which is the plotted region of Fig. 2 of the main text.

We mention that via the general method one can also in principle determine the achievable probability distribution of a general scenario. However, this requires the solution of a SDP with some unknown entries, and hence an analytic solution is in general not accessible.

A2: Detailed discussion of bounds for the N-cycle inequalities

We first need the general form [21] for Eq. (10) of the main text

$$\mathcal{S}_N(\gamma) = \sum_{i=0}^{N-1} \gamma_i \langle A_i A_{i+1} \rangle_{\text{seq}}, \tag{18}$$

where the indices are taken modulo N and $\gamma = (\gamma_0, \ldots, \gamma_{N-1}) \in \{-1, 1\}^N$ with an odd number of -1. Since any two assignments γ and γ' can be converted into each other via some substitutions $A_i \to -A_i$, the quantum bound does not depend on the particular choice of γ. For the case odd N, we can consider the expression

$$\mathcal{S}_N = -\sum_{i=0}^{N-1} \langle A_i A_{i+1} \rangle_{\text{seq}}, \tag{19}$$

with index i taken modulo N. The optimization problem in Eq. (4) of the main text, therefore, can be expressed as

$$\begin{aligned} \text{maximize:} \quad & \frac{1}{2}\mathrm{Tr}(WX) \\ \text{subjected to:} \quad & X = X^T \succeq 0 \text{ and } X_{ii} = 1 \text{ for all } i, \end{aligned} \tag{20}$$

where W is the circulant symmetric matrix

$$W = -\begin{bmatrix} 0 & 1 & \dots & 0 & 1 \\ 1 & 0 & 1 & & 0 \\ \vdots & 1 & 0 & \ddots & \vdots \\ 0 & & \ddots & \ddots & 1 \\ 1 & 0 & \dots & 1 & 0 \end{bmatrix}. \tag{21}$$

The condition $X \succeq 0$, i.e. $v^T X v \geq$ for any real vector v, follows from the fact that $\langle A_i A_j \rangle_{\text{seq}} = \frac{1}{2}\mathrm{Tr}[\varrho(A_i A_j + A_j A_i)]$ and the fact that the matrix $Y = \mathrm{Tr}[\varrho(A_i A_j)]$ fulfils $v^T Y v \geq$ for any real vector v, and X is the real part of Y.

By using the vector $\lambda = (\lambda_1, \dots, \lambda_N)$, the dual problem for the semidefinite program in Eq. (20) can be written as (see Ref. [18] for a general treatment and Ref. [17] for the discussion of a similar problem)

$$\begin{aligned} \text{minimize:} \quad & \mathrm{Tr}(diag(\lambda)) \\ \text{subjected to:} \quad & -\frac{1}{2}W + diag(\lambda) \succeq 0, \end{aligned} \tag{22}$$

where $diag(\lambda)$ denotes the diagonal matrix with entries $\lambda_1, \dots, \lambda_N$.

Let us denote with p and d optimal values for, respectively, the primal problem in Eq. (20) and the dual problem in Eq. (22). Then $d \geq p$. We shall provide a feasible solution for the dual problem with $d = N\cos(\frac{\pi}{N})$ and a feasible solution for the primal problem with $p = d$, this will guarantee the optimality of our primal solution.

We start by finding the maximum eigenvalue for W. Since W is a circulant matrix, its eigenvalues can be written as [32]

$$\mu_j = -2\cos\left(\frac{2\pi j}{N}\right) \tag{23}$$

for $j = 0, \dots, N-1$, and $\mu_{max} = 2\cos\left(\frac{\pi}{N}\right)$ the maximum eigenvalue.

For a pair of Hermitian matrices A, B, it holds $\mu_{min}(A+B) \geq \mu_{min}(A) + \mu_{min}(B)$, where μ_{min} denotes the minimum eigenvalue. Therefore, $\lambda = (\cos\left(\frac{\pi}{N}\right), \dots, \cos\left(\frac{\pi}{N}\right))$ is a feasible solution for the dual problem and $\mathrm{Tr}[diag(\lambda)] = N\cos\left(\frac{\pi}{N}\right)$, and $p \leq N\cos\left(\frac{\pi}{N}\right)$.

Now consider the matrix $X'_{ij} = (x_i, x_j)$, with $x_1, \dots, x_N$ unit vectors in a 2-dimensional space such that the angle between x_i and x_{i+1} is $\frac{N+1}{N}\pi$, and $(\cdot,\cdot)$ denoting the scalar product. Clearly, X' is positive semidefinite. Since $X'_{i,i+1} = -\cos\left(\frac{\pi}{N}\right)$, it follows that $p = d = N\cos\left(\frac{\pi}{N}\right)$ and the solution X' is optimal.

In order to prove that X' can be obtained as matrix of expectation values for sequential measurements, we define for a 3-dimensional unit vector $\vec{a}$ the observable $\sigma_a \equiv \vec{\sigma}\cdot\vec{a}$, where $\vec{\sigma}$ denotes the vector of the Pauli matrices. Then, by Eq. (3) of the main text, $\langle \sigma_a \sigma_b \rangle_{seq} = \vec{a}\cdot\vec{b}$, independently of the initial quantum state ϱ. In fact, explicit observables reaching this bound have already been discussed in the literature [11, 19].

For the case N even, we can consider the expression

$$\mathcal{S}_N = \sum_{i=0}^{N-2} \langle A_i A_{i+1} \rangle_{seq} - \langle A_0 A_{N-1} \rangle_{seq}, \tag{24}$$

and the maximization problem can be expressed as a SDP as in Eq. (20), with the proper choice of the matrix W. Such a SDP has been solved in Ref. [17]. The solution is analogous to the previous one: A set of observables, for a two-level system, saturating the bound, again, independently of the quantum state, is given by observables $A_i = \vec{\sigma}\cdot\vec{x_i}$, where the vectors x_i are on a plane with an angle $\frac{\pi}{N}$ separating x_i and x_{i+1}.

As opposed to the N odd case, such a bound can be also reached with commuting operators, this corresponds to the well known maximal violation of Braunstein-Caves inequalities [17].

The above results prove that the bound computed in Ref. [19] for sequential measurements on qubits, coinciding with the value explicitly obtained in Ref. [11], is valid for any dimension of the quantum system on which measurements are performed.

Finally, we stress that the construction of the above set of observables from the solution of the SDP, i.e., the matrix X or the set of vectors $\{x_i\}$ such that $X_{ij} = (x_i, x_j)$, is general. We recall that the vectors $\{x_i\}$ can be obtained, e.g., as the columns of the matrix $\sqrt{X}$ and, therefore, the dimension of the subspace spanned by them is equal to the rank of the matrix X. In the previous case, since we were dealing with vectors in dimension $d \leq 3$, we used the property of Pauli matrices

$$\{\sigma_a, \sigma_b\} \equiv \sigma_a\sigma_b + \sigma_b\sigma_a = 2(\vec{a}\cdot\vec{b})\mathbb{1}. \tag{25}$$

For matrices X with higher rank, the corresponding vectors $\{x_i\}$ will span a real vector space V of dimension $d > 3$. Now for general complex vector spaces V with a symmetric bilinear form $(\ ,\ )$, an analogue of Eq.(25), namely

$$\{A_v, A_u\} = 2(v,u)\mathbb{1}, \quad \text{for any } u, v \in V \tag{26}$$

can be established by a representation of associated Clifford algebra, cf. Ref. [33, 34]

As a consequence, for every positive semidefinite real matrix X with diagonal elements equal to 1, one can find

a set of unit vectors $\{x_i\}$ giving $X_{ij} = (x_i, x_j)$ and a set of ± 1-valued observables $\{A_i\}$, associated with $\{x_i\}$, such that

$$\langle A_i A_j \rangle_{seq} = \mathrm{Tr}\left[\frac{1}{2}\varrho(A_i A_j + A_j A_i)\right] = (x_i, x_j), \quad (27)$$

for all quantum states ϱ. In particular, if the rank of X is d, such operators can be chosen as $2^d \times 2^d$ Hermitian matrices [35]. This shows the completeness of the simplified method.

A3: Completeness of the general method

In this part we shortly comment on the completeness of the presented general method. As pointed out, this has already been proven indirectly in the context of the spatial bipartite case [23].

At first let us change slightly the notation in order to make it closer to the one used in Ref. [23]. In the following we do not explicitly consider the matrix M from the main text, but rather a slightly smaller matrix where one erases some trivial constraints. In the following the set $\{E_i\}$ contains all projectors Π_k^s, but one of the outcomes k from each setting s is left out. We also use a single subscript to identify setting and outcome. Then the matrix

$$\chi^n_{\mathbf{uv}} = \mathrm{Tr}[E(\mathbf{u})E(\mathbf{v})^\dagger \rho] \quad (28)$$

with $\mathbf{u} = (u_1, u_2, \ldots, u_l)$ is built from all products $E(\mathbf{u}) = E_{u_1} E_{u_2} \cdots E_{u_l}$ of the operators $\{E_i\}$ of at most length $l \leq n$, and the single extra "sequence" $\mathbf{u} = 0$ of the identity operator, $E(0) = \mathbb{1}$. Again this matrix has to satisfy linear relations parsed as $\chi^n_{\mathbf{uv}} = \chi^n_{\mathbf{u'v'}}$, if the operators fulfill $E(\mathbf{u})E(\mathbf{v})^\dagger = E(\mathbf{u'})E(\mathbf{v'})^\dagger$ as a consequence of the orthogonality properties of projectors, and that $\chi^n \succeq 0$.

That this matrix is positive semidefinite can be verified as follows: Let us first assume that there exists a sequential projective quantum representation. Consider the operator $C = \sum_{\mathbf{u}} c_{\mathbf{u}} E(\mathbf{u})^\dagger$ with arbitrary $c_{\mathbf{u}} \in \mathbb{C}$ and evaluate the expectation value of $CC^\dagger$, which provides

$$\mathrm{Tr}(CC^\dagger \varrho) = \sum_{\mathbf{u},\mathbf{v}} c_{\mathbf{u}} \mathrm{Tr}[E(\mathbf{u})^\dagger E(\mathbf{v})\varrho] c^*_{\mathbf{v}} \quad (29)$$

$$= \sum_{\mathbf{u},\mathbf{v}} c_{\mathbf{u}} \chi^n_{\mathbf{uv}} c^*_{\mathbf{v}} \geq 0. \quad (30)$$

The final inequality holds because $CC^\dagger \succeq 0$ and $\rho \succeq 0$ are both positive semidefinite operators. Since $c_{\mathbf{u}} \in \mathbb{C}$ are arbitrary the condition given by Eq. (30) means that $\chi^n \succeq 0$ is positive semidefinite.

For the reverse one needs a way to construct an explicit sequential projective quantum representation out of the matrix χ^n satisfying the above properties. For this, clearly more difficult part, we refer to Ref. [23] and just mention the solution. For the given positive semidefinite matrix χ^n one associates a set of vectors $\{|e_{\mathbf{u}}\rangle\}$ by the relation $\chi^n_{\mathbf{uv}} = \langle e_{\mathbf{u}} | e_{\mathbf{v}} \rangle$. From this set of vectors one now constructs an appropriate state and corresponding projective measurements by $\hat{\mathcal{H}} = \mathrm{span}(\{|e_{\mathbf{u}}\rangle\})$, $\hat{\rho} = |e_0\rangle\langle e_0|$, and $\hat{E}_i = \mathrm{proj}(\mathrm{span}(\{|e_{\mathbf{u}}\rangle : u_1 = i\}))$ where proj means the projector onto the given subspace. That these solution satisfies all the required constraints is shown in the proof of Theorem 8 of Ref. [23]. An analogous mathematical result, valid only for the case of dichotomic observables, has been presented also in Ref. [25].

In the spatial case considered in Ref. [23], some of these operators, additionally, have to commute since they should correspond to measurements onto different local parts. This cannot be inferred, in general, by a finite level χ^n and this is eventually the reason why in the spacial case arbitrary high order terms have to be considered. However, luckily, since in our situation the measurements of different settings may well fail to commute we can rely on a finite level n.

[1] J. S. Bell, Physics **1**, 195 (1964).
[2] J. F. Clauser, M. A. Horne, A. Shimony, and R. A. Holt, Phys. Rev. Lett. **23**, 880 (1969).
[3] B. C. Cirel'son, Lett. Math. Phys. **4**, 93 (1980).
[4] S. Popescu and D. Rohrlich, Found. Phys. **24**, 379 (1994).
[5] G. Brassard, H. Buhrman, N. Linden, A. A. Méthot, A. Tapp, and F. Unger, Phys. Rev. Lett. **96**, 250401 (2006).
[6] M. Pawłowski, T. Paterek, D. Kaszlikowski, V. Scarani, A. Winter, and M. Żukowski, Nature (London) **461**, 1101 (2009).
[7] D. Gross ,M. Müller, R. Colbeck, and C. O. Dahlsten, Phys. Rev. Lett. **104** 080402 (2010).
[8] T. Fritz, New J. Phys. **12**, 083055 (2010).
[9] S. Kochen and E. P. Specker, J. Math. Mech. **17**, 59 (1967).
[10] A.J. Leggett and A. Garg, Phys. Rev. Lett. **54**, 857 (1985).
[11] M. Barbieri, Phys. Rev. A **80**, 034102 (2009).
[12] A. A. Klyachko, M. A. Can, S. Binicioğlu, and A. S. Shumovsky, Phys. Rev. Lett. **101**, 020403 (2008).
[13] J. Kofler and C. Brukner, Phys. Rev. Lett. **101**, 090403 (2008).
[14] T. Fritz, J. Math. Phys. **51**, 052103 (2010).
[15] J. von Neumann, *Mathematische Grundlagen der Quantenmechanik* (Springer, Berlin, 1932).
[16] G. Lüders, Ann. Phys. (Leipzig) **8**, 322 (1951).
[17] S. Wehner, Phys. Rev. A **73**, 022110 (2006).
[18] L. Vandenberghe and S. Boyd, Semidefinite Programming, SIAM Rev. **38**, 49 (1996).
[19] O. Gühne, C. Budroni, A. Cabello, M. Kleinmann, and J.-Å. Larsson, arXiv:1302.2266.
[20] Y.-C. Liang, R. W. Spekkens, and H. M. Wiseman, Phys. Rep. **506**, 1 (2011).
[21] M. Araújo, M. T. Quintino, C. Budroni, M. Terra Cunha, and A. Cabello, arXiv:1206.3212.

[22] M. Navascués, S. Pironio, and A. Acín, Phys. Rev. Lett. **98**, 010401 (2007).
[23] M. Navascués, S. Pironio, and A. Acín, New J. Phys. **10**, 073013 (2008).
[24] A.C. Doherty, Y.-C. Liang, B. Toner, and S. Wehner, in *Proceedings of IEEE Conference on Computational Complexity, College Park, MD, 2008* (IEEE, New York 2008) p.199.
[25] S. Pironio, M. Navascués, and A. Acín, *SIAM J. Optim.* **20(5)**, 2157 (2010).
[26] K.F. Pál and T. Vértesi, Phys. Rev. A **82**, 022116 (2010).
[27] T. Moroder, J.-D. Bancal, Y.-C. Liang, M. Hofmann, and O. Gühne, Phys. Rev. Lett. **111**, 030501 (2013).
[28] S. Yu and C. H. Oh, Phys. Rev. Lett. **108**, 030402 (2012).
[29] A. Cabello, arXiv:1112.5149.
[30] M. Kleinmann, C. Budroni, J.-Å. Larsson, O. Gühne, and A. Cabello, Phys. Rev. Lett. **109**, 250402 (2012).
[31] M.L. Almeida, J.-D Bancal, N. Brunner, A. Acín, N. Gisin, and S. Pironio, Phys. Rev. Lett. **104**, 230404 (2010).
[32] R. M. Gray, Foundations and Trends in Communications and Information Theory, **2** 155 (2006).
[33] B. S. Tsirel'son, Zap. Nauchn. Sem. Leningrad. Otdel. Mat. Inst. Steklov. (LOMI) **142**, 174 (1985), (Russian, English translation [34]).
[34] B. S. Tsirel'son, J. Soviet Math. **36**, 557 (1987).
[35] O. Bratteli and D. W. Robinson, Operator Algebras and Quantum Statistical Mechanics Vol. 2, Springer (1997)

Bounding the quantum dimension with contextuality

Otfried Gühne,[1] Costantino Budroni,[1] Adán Cabello,[2] Matthias Kleinmann,[1] and Jan-Åke Larsson[3]

[1]*Naturwissenschaftlich-Technische Fakultät, Universität Siegen, Walter-Flex-Str. 3, D-57068 Siegen*
[2]*Departamento de Física Aplicada II, Universidad de Sevilla, E-41012 Sevilla, Spain*
[3]*Institutionen för Systemteknik och Matematiska Institutionen, Linköpings Universitet, SE-581 83 Linköping, Sweden*

(Dated: June 12, 2014)

We show that the phenomenon of quantum contextuality can be used to certify lower bounds on the dimension accessed by the measurement devices. To prove this, we derive bounds for different dimensions and scenarios of the simplest noncontextuality inequalities. The resulting dimension witnesses work independently of the prepared quantum state. Our constructions are robust against noise and imperfections, and we show that a recent experiment can be viewed as an implementation of a state-independent quantum dimension witness.

PACS numbers: 03.65.Ta, 03.65.Ud

I. INTRODUCTION

The recent progress in the experimental control and manipulation of physical systems at the quantum level opens new possibilities (e.g., quantum communication, computation, and simulation), but, at the same time, demands the development of novel theoretical tools of analysis. There are already tools which allow us to recognize quantum entanglement and certify the usefulness of quantum states for quantum information processing tasks [1, 2]. However, on a more fundamental level, there are still several problems which have to be addressed. For example, how can one efficiently test whether measurements actually access all the desired energy levels of an ion? How to certify that the different paths of photons in an interferometer can be used to simulate a given multi-dimensional quantum system? Similar questions arise in the analysis of experiments with orbital angular momentum, where high-dimensional entanglement can be produced [3, 4], or in experiments with electron spins at nitrogen-vacancy centers in diamond, where the quantumness of the measurements should be certified [5].

The challenge is to provide lower bounds on the *dimension* of a quantum system only from the statistics of measurements performed on it. More precisely, one certifies lower bounds on the dimension of the underlying Hilbert space, where the measurement operators act on. Such bounds can be viewed as lower bounds on the complexity and the number of levels accessed by the measurement devices: If the measurement operators act nontrivially only on a small subspace, then all measurements results can be modeled by using a low-dimensional quantum system only. Note that this is not directly related to the rank of a density matrix. In fact, a pure quantum state acting on a one-dimensional subspace only can still give rise to measurement results, which can only be explained assuming a higher-dimensional Hilbert space.

The problem of estimating the Hilbert space dimension has been considered in different scenarios, and slightly different notions of dimension were involved. Brunner and coworkers introduced the concept of quantum "dimension witnesses" by providing lower bounds on the dimension of composite systems from the violation of Bell inequalities [6, 7]. The nonlocal properties of the correlations produced are clearly the resource used for this task. As a consequence, even if the experimenter is able to access and manipulate many levels of her systems locally, but she is not able to entangle those levels, the above test fails to certify such a dimension. Such a task can therefore be interpreted as a test of the type of entanglement and correlations produced, namely, how many levels or degrees of freedom the experimenter is able to entangle.

In a complementary scenario, several different states of a single particle are prepared and different measurements are carried out [8–10]. This approach has also recently been implemented using photons [11, 12]. In this situation, the dimension of the system can be interpreted as the dimension of the set of states the experimenter is able to prepare.

As a third possibility, also the continuous time evolution can be used to bound the dimension of a quantum system [13]. In this case, the relevant notion of dimension is that of the set of states generated by the dynamical evolution of the system.

In this paper we focus on sequential measurements on a single system, a type of measurements used in tests of quantum contextuality, and we show how they can be used for bounding the dimension of quantum systems. Quantum contextuality is a genuine quantum effect leading to the Kochen-Specker theorem, which states that quantum mechanics is in contradiction to non-contextual hidden variable (NCHV) models [14–18]. In fact, already in the first formulation of the theorem the dimension plays a central role [14].

We derive bounds for the several important noncontextuality (NC) inequalities for different dimensions and scenarios. The experimental violation of these bounds automatically provides a lower bound on the dimension of the system, showing that NC inequalities can indeed be used as dimension witnesses. Remarkably, contextuality can be used as a resource for bounding the dimension of quantum systems in a state-independent way.

This illustrates clearly the difference with the existing schemes: Dimension witnesses derived according to Refs. [9, 10] certify the minimum classical or quantum dimension spanned by a set of preparations. They distinguish between classical and quantum dimension d, but, in general, not between quantum dimension d and classical dimension $d+1$. They require at least $d+1$ preparations to certify a dimension d. On the other side, dimension witnesses based on Bell's theorem or contextuality certify the minimum quantum dimension accessed by the measurement devices acting on a system prepared in the a single state. Contrary to the Bell scenario [6, 7], in our approach the initial state and its nonlocal properties play no role and the result of our test can directly be interpreted as the minimal number of levels accessed and manipulated by the measurement apparatus.

The paper is organized as follows. In Sec. I, we discuss the case of state-dependent noncontextuality inequalities, specifically, Klyachko, Can, Binicioğlu, and Shumovsky (KCBS) inequality [19]. In Sec. II, we discuss what happens when the sequences of measurements contain non-compatible measurements. In Sec. IV and Sec. V, we apply the same analysis to the case of state-independent noncontextuality inequalities, specifically, the Peres-Mermin (PM) inequality [20–22]. In Sec. VI, we discuss the case of imperfect measurements, then in Sec. VII we show how a recent experimental test of contextuality can be viewed as an implementation of our dimension witness.

II. THE KCBS INEQUALITY

We first turn to the state-dependent case. The simplest system showing quantum contextuality is a quantum system of dimension three [14]. The simplest NC inequality in three dimensions is the one introduced by Klyachko, Can, Binicioğlu, and Shumovsky (KCBS) [19]. For that, one considers

$$\langle \chi_{\text{KCBS}} \rangle = \langle AB \rangle + \langle BC \rangle + \langle CD \rangle + \langle DE \rangle + \langle EA \rangle, \quad (1)$$

where A, B, C, D, and E are measurements with outcomes -1 and 1, and the measurements in the same mean value $\langle \ldots \rangle$ are compatible [23], i.e., are represented in quantum mechanics by commuting operators. The mean value itself is defined via a sequential measurement: For determining $\langle AB \rangle$, one first measures A and then B on the same system, multiplies the two results, and finally averages over many repetitions of the experiment.

The KCBS inequality states that

$$\langle \chi_{\text{KCBS}} \rangle \overset{\text{NCHV}}{\geq} -3, \quad (2)$$

where the notation "$\overset{\text{NCHV}}{\geq} -3$" indicates that -3 is the minimum value for any NCHV theory. Here, noncontextuality means that the theory assigns to any observable (say, B) a value independent of which other compatible observable (here, A or C) is measured jointly with it.

In quantum mechanics, a value of $\langle \chi_{\text{KCBS}} \rangle = 5 - 4\sqrt{5} \approx -3.94$ can be reached on a three-dimensional system, if the observables and the initial state are appropriately chosen. This quantum violation of the NCHV bound does not increase in higher-dimensional systems [18, 24], and the violation of the KCBS inequality has been observed in recent experiments with photons [25, 26].

Given the fact that quantum contextuality requires a three-dimensional Hilbert space, it is natural to ask whether a violation of Eq. (2) implies already that the system is not two-dimensional. The following observation shows that this is the case:

Observation 1. Consider the KCBS inequality where the measurements act on a two-dimensional quantum system and are commuting, i.e., $[A, B] = [B, C] = [C, D] = [D, E] = [E, A] = 0$. Then, the classical bound holds:

$$\langle \chi_{\text{KCBS}} \rangle \overset{\text{2D,com.}}{\geq} -3. \quad (3)$$

Proof of Observation 1. First, if two observables A and B are compatible, then $|\langle A \rangle \pm \langle AB \rangle| \leq 1 \pm \langle B \rangle$. This follows from the fact that A and B have common eigenspaces and the relation holds separately on each eigenspace. Second, in two dimensions, if $[A, B] = 0 = [B, C]$, then either $B = \pm\mathbb{1}$ or $[A, C] = 0$. The reason is that, if B is not the identity, then it has two one-dimensional eigenspaces. These are shared with A and C, so A and C must be simultaneously diagonalizable.

Considering the KCBS operator χ_{KCBS}, the claim is trivial if $A, \ldots, E$ are all compatible, because then the relation holds separately on each eigenspace. It is only possible that not all of them commute if there are two groups in the sequence $\{A, B, C, D, E\}$ of operators separated by identity operators. Without loss of generality, we assume that the groups of commuting operators are $\{E, A\}$ and $\{C\}$ so that $B = b\mathbb{1} = \pm\mathbb{1}$ and $D = d\mathbb{1} = \pm\mathbb{1}$. This gives

$$\begin{aligned} \langle \chi_{\text{KCBS}} \rangle &= b\langle A \rangle + b\langle C \rangle + d\langle C \rangle + d\big(\langle E \rangle + d\langle EA \rangle\big) \\ &\geq b\langle A \rangle + b\langle C \rangle + d\langle C \rangle - 1 - d\langle A \rangle \\ &= (b-d)\langle A \rangle + (b+d)\langle C \rangle - 1 \geq -3 \end{aligned} \quad (4)$$

and proves the claim. In this argumentation, setting observables proportional to the identity does not change the threshold, but in general it is important to consider this case, as this often results in higher values. □

It should be added that Observation 1 can also be proved using a different strategy: Given two observables on a two-dimensional system, one can directly see that if they commute, then either one of them is proportional to the identity, or their product is proportional to the identity. In both cases, one has a classical assignment for some terms in the KCBS inequality and then one can check by exhaustive search that the classical bound holds. Details are given in the Appendix A1.

Furthermore, Observation 1 can be extended to generalizations of the KCBS inequality with more than five

observables [24]: For that, one considers

$$\langle \chi_N \rangle = \sum_{i=1}^{N-1} \langle A_i A_{i+1} \rangle + s \langle A_N A_1 \rangle, \tag{5}$$

where $s = +1$ if N is odd and $s = -1$ if N is even. For this expression, the classical bound for NCHV theories is given by $\langle \chi_N \rangle \geq -(N-2)$. In fact, the experiment in Ref. [25] can also be viewed as measurement of $\langle \chi_6 \rangle$.

The discussion of the possible mean values $\langle \chi_N \rangle$ in quantum mechanics differs for even and odd N. If N is odd, the maximal possible quantum mechanical value is $\langle \chi_N \rangle = \Omega_N \equiv -[3N \cos(\pi/N) - N]/[1 + \cos(\pi/N)]$ and this value can already be attained in a three-dimensional system [18, 24]. The proof of Observation 1 can be generalized in this case, implying that for two-dimensional systems the classical bound $\langle \chi_N \rangle \geq -(N-2)$ holds. So, for odd N, the generalized KCBS inequalities can be used for testing the quantum dimension.

If N is even, the scenario becomes richer: First, quantum mechanics allows to obtain values of $\langle \chi_N \rangle = \Omega_N \equiv -N \cos(\pi/N)$, but this time this value requires a four-dimensional system [24]. For two-dimensional quantum systems, the classical bound $\langle \chi_N \rangle \geq -(N-2)$ holds. For three-dimensional systems, one can show that if the observables A_i in a joint context are different ($A_i \neq \pm A_{i+1}$) and not proportional to the identity, then still the classical bound holds (for details see Appendix A2). However, if two observables are the same, e.g. $A_1 = -A_2$, then $\langle A_1 A_2 \rangle = -1$ and $\langle \chi_N \rangle = -1 + \langle \chi_{N-1} \rangle$. In summary, for even N, we have the following hierarchy of bounds

$$\langle \chi_N \rangle \overset{\text{2D,com.}}{\geq} -(N-2) \overset{\text{3D,com.}}{\geq} -1 + \Omega_{N-1} \overset{\text{4D,com.}}{\geq} \Omega_N. \tag{6}$$

Here, the notation $\overset{\text{2D,com.}}{\geq}$ etc. means that this bound holds for commuting observables in two dimensions. All these bounds are sharp. This shows that extended KCBS inequalities are even more sensitive to the dimension than the original inequality.

III. THE KCBS INEQUALITY WITH INCOMPATIBLE OBSERVABLES

In order to apply Observation 1 the observables must be compatible. Since this condition is not easy to guarantee in experiments [31], we should ask whether it is possible to obtain a two-dimensional bound for the KCBS inequality when the observables are not necessarily compatible. We can state:

Observation 2. If the observables $A, \ldots, E$ are dichotomic observables but not necessarily commuting, then, for any two-dimensional quantum system,

$$\langle \chi_{\text{KCBS}} \rangle \overset{\text{2D}}{\geq} -\frac{5}{4}(1 + \sqrt{5}) \approx -4.04. \tag{7}$$

This bound is sharp and can be attained for suitably chosen measurements.

The strategy of proving this bound is the following: If the observables are not proportional to the identity, one can write $A = |A^+\rangle\langle A^+| - |A^-\rangle\langle A^-|$ and $B = |B^+\rangle\langle B^+| - |B^-\rangle\langle B^-|$, and express $|A^+\rangle\langle A^+|$ and $|B^+\rangle\langle B^+|$ in terms of their Bloch vectors $|\mathfrak{a}\rangle$ and $|\mathfrak{b}\rangle$. Then, one finds that

$$\langle AB \rangle = 2|\langle A^+|B^+\rangle|^2 - 1 = \langle \mathfrak{a}|\mathfrak{b}\rangle. \tag{8}$$

This property holds for all projective measurements on two-dimensional systems and is, together with a generalization below [see Eq. (15)] a key idea for deriving dimension witnesses. Note that it implies that the sequential mean value $\langle AB \rangle$ is independent of the initial quantum state and also of the temporal order of the measurements [27]. Eq. (8) allows us to transform the KCBS inequality into a geometric inequality for three-dimensional Bloch vectors. Additional details of the proof are given in Appendix A3.

Observation 2 shows that the bound for NCHV theories can be violated already by two-dimensional systems, if the observables are incompatible. This demonstrates that experiments, which aim at a violation of Eq. (2) also have to test the compatibility of the measured observables, otherwise the violation can be explained without contextuality.

It must be added that Observation 2 cannot be used to witness the quantum dimension, since one can show that Eq. (7) holds for all dimensions [32]. As we see below, this difficulty can be surmounted by considering NC inequalities in which quantum mechanics reaches the algebraic maximum.

IV. THE PERES-MERMIN INEQUALITY

In order to derive the state-independent quantum dimension witnesses, let us consider the sequential mean value [20],

$$\begin{aligned} \langle \chi_{\text{PM}} \rangle =& \langle ABC \rangle + \langle bca \rangle + \langle \gamma\alpha\beta \rangle + \langle A\alpha a \rangle + \langle bB\beta \rangle \\ & - \langle \gamma cC \rangle, \end{aligned} \tag{9}$$

where the measurements in each of the six sequences are compatible. Then, for NCHV theories the bound

$$\langle \chi_{\text{PM}} \rangle \overset{\text{NCHV}}{\leq} 4 \tag{10}$$

holds. In a four-dimensional quantum system, however, one can take the following square of observables, known as the Peres-Mermin square [21, 22]

$$\begin{array}{lll} A = \sigma_z \otimes \mathbb{1}, & B = \mathbb{1} \otimes \sigma_z, & C = \sigma_z \otimes \sigma_z, \\ a = \mathbb{1} \otimes \sigma_x, & b = \sigma_x \otimes \mathbb{1}, & c = \sigma_x \otimes \sigma_x, \\ \alpha = \sigma_z \otimes \sigma_x, & \beta = \sigma_x \otimes \sigma_z, & \gamma = \sigma_y \otimes \sigma_y. \end{array} \tag{11}$$

These observables lead for any quantum state to a value of $\langle \chi_{\text{PM}} \rangle = 6$, demonstrating state-independent contextuality. The quantum violation has been observed in several recent experiments [28–30]. Note that the sequences

in Eq. (9) are defined such that each observable occurs either always in the first or always in the second or always in the third place of a measurement a sequence. This difference to the standard version does not matter at this point (since the observables in any row or column commute), but it will become important below.

The PM inequality is of special interest for our program since it is violated up to the algebraic maximum with four-dimensional quantum systems and the violation is state-independent. Therefore, this inequality is a good candidate for dimension witnesses without assumptions on the measurements. First, we can state:

Observation 3. If the measurements in the PM inequality are dichotomic observables on a two-dimensional quantum system and if the measurements in each mean value are commuting, then one cannot violate the classical bound,

$$\langle \chi_{\mathrm{PM}} \rangle \overset{\mathrm{2D,\,com.}}{\leq} 4. \tag{12}$$

If one considers the same situation on a three-dimensional system, then the violation is bounded by

$$\langle \chi_{\mathrm{PM}} \rangle \overset{\mathrm{3D,\,com.}}{\leq} 4(\sqrt{5}-1) \approx 4.94. \tag{13}$$

These bounds are sharp.

The idea for proving this statement is the following: If one considers the three commuting observables in each mean value and assumes that they act on a three-dimensional system, then three cases are possible: (a) one of the three observables is proportional to the identity, or (b) the product of two observables is proportional to the identity, or (c) the product of all three observables is proportional to the identity. One can directly show that if case (c) occurs in some mean value, then the classical bound $\langle \chi_{\mathrm{PM}} \rangle \leq 4$ holds. For the cases (a) and (b), one can simplify the inequality and finds that it always reduces to a KCBS-type inequality, for which we discussed already the maximal quantum values in different dimensions [see Eq. 6]. Details are given in Appendix A4.

V. THE PM INEQUALITY WITH INCOMPATIBLE OBSERVABLES

Let us now discuss the PM inequality, where the observables are not necessarily compatible. Our results allow us to obtain directly a bound:

Observation 4. Consider the PM operator in Eq. (9), where the measurements are not necessarily commuting projective measurements on a two-dimensional system. Then we have

$$\langle \chi_{\mathrm{PM}} \rangle \overset{\mathrm{2D}}{\leq} 3\sqrt{3} \approx 5.20. \tag{14}$$

Proof. One can directly calculate as in the proof of Observation 2 that for sequences of three measurements on a two-dimensional system

$$\langle ABC \rangle = \langle A \rangle \langle BC \rangle \tag{15}$$

holds. Here, $\langle A \rangle = \mathrm{tr}(\varrho A)$ is the usual expectation value, and $\langle BC \rangle$ is the state-independent sequential expectation value given in Eq. (8). With this, we can write:

$$\begin{aligned} \langle \chi_{\mathrm{PM}} \rangle =& \langle A \rangle (\langle BC \rangle + \langle \alpha a \rangle) + \langle b \rangle (\langle ca \rangle + \langle B \beta \rangle) \\ &+ \langle \gamma \rangle (\langle \alpha \beta \rangle - \langle cC \rangle). \end{aligned} \tag{16}$$

Clearly, this is maximal for some combination of $\langle A \rangle = \pm 1$, $\langle b \rangle = \pm 1$, and $\langle \gamma \rangle = \pm 1$. But for any of these choices, we arrive at an inequality that is discussed in Lemma 7 in Appendix A3. Note that due to Eq. (15) the order of the measurements matters in the definition of $\langle \chi_{\mathrm{PM}} \rangle$ in Eq. (9). This motivates our choice; in fact, for some other orders (e.g., $\langle \tilde{\chi}_{\mathrm{PM}} \rangle = \langle ABC \rangle + \langle bca \rangle + \langle \beta \gamma \alpha \rangle + \langle A \alpha a \rangle + \langle \beta b B \rangle - \langle \gamma c C \rangle$) Eq. (14) does not hold, and one can reach $\langle \tilde{\chi}_{\mathrm{PM}} \rangle = 1 + \sqrt{9 + 6\sqrt{3}} \approx 5.404$. □

The question arises whether a high violation of the PM inequality also implies that the system cannot be three-dimensional and whether a similar bound as Eq. (14) can be derived. While the computation of a bound is not straightforward, a simple argument shows already that measurements on a three-dimensional systems cannot reach the algebraic maximum $\langle \chi_{\mathrm{PM}} \rangle = 6$ for any quantum state: Reaching the algebraic maximum implies that $\langle ABC \rangle = 1$. This implies that the value of C is predetermined by the values of A and B and the value A of determines the product BC. As this holds for any quantum state, it directly follows that A, B, C (and all the other observables in the PM square) are diagonal in the same basis and commute, so the bound in Observation 3 holds. From continuity arguments it follows that there must be a finite gap between the maximal value of $\langle \chi_{\mathrm{PM}} \rangle$ in three dimensions and the algebraic maximum.

VI. IMPERFECT MEASUREMENTS

In actual experimental implementations the measurements may not be perfectly projective. It is therefore important to discuss the robustness of our method against imperfections.

Notice that, since we are considering sequential measurements, another possibility for maximal violation of the above inequalities is the use of a classical device with memory, able to keep track of the measurement performed and adjust the outcomes of the subsequent measurements accordingly in order to obtain perfect correlations or anti-correlations. However, as proved in Ref. [27] and also discussed in Ref. [32], such a classical device cannot be simulated in quantum mechanics via projective measurements, more general positive operator valued measures (POVMs) are necessary.

We therefore limit our analysis to some physically motivated noise models. A noisy projective measurement A may be modelled by a POVM with two effects of the type $E^+ = (1-p)\mathbb{1}/2 + p|A^+\rangle\langle A^+|$ and $E^- = (1-p)\mathbb{1}/2 + p|A^-\rangle\langle A^-|$. Then, the probabilities of the POVM can be interpreted as coming from the following procedure: With a probability of p one performs the

projective measurement and with a probability of $(1-p)$ one assigns a random outcome. For this measurement model, one can show that Observation 4 is still valid. Details and a more general POVM are discussed in Appendix A5. We add that the proof strongly depends on the chosen measurement order in $\langle \chi_{\rm PM} \rangle$ and that in any case assumptions about the measurement are made, so the dimension witnesses are not completely independent of the measurement device.

The above discussion shows that it is extremely important to test the extent to which the measurements are projective and whether they are compatible. This can be achieved by performing additional tests. For instance, one can measure observable A several times in a sequence $\langle AAA \rangle$ to test whether the measurement is indeed projective. In addition, one may measure the sequence $\langle ABA \rangle$ and compare the results of the two measurements of A, to test whether A and B are compatible. For NC inequalities it is known how this information can be used to derive correction terms for the thresholds [31], and similar methods can also be applied here.

VII. EXPERIMENTAL RESULTS

To stress the experimental relevance of our findings, let us discuss a recent ion-trap experiment [28]. There, the PM inequality has been measured with the aim to demonstrate state-independent contextuality. For our purpose, it is important that in this experiment also all permutations of the terms in the PM inequality have been measured. This allows also to evaluate our $\langle \chi_{\rm PM} \rangle$ with the order given in Eq. (9). Experimentally, a value $\langle \chi_{\rm PM} \rangle = 5.36 \pm 0.05$ has been found. In view of Observation 3, this shows that the data cannot be explained by commuting projective measurements on a three-dimensional system. Furthermore, Observation 4 and the discussion above prove that, even if the measurements are noisy and noncommuting, the data cannot come from a two-dimensional quantum system.

VIII. GENERALIZATIONS

Generalizations of our results to other inequalities are straightforward: Consider a general noncontextuality inequality invoking measurement sequences of length two and three. For estimating the maximal value for two-dimensional systems (as in Observations 2 and 4) one transforms all sequential measurements via Eqs. (8) and (15) into expressions with three-dimensional Bloch-vectors, which can be estimated. Also noise robustness for the discussed noise model can be proven, as this follows also from the properties of the Bloch vectors (cf. Proposition 12 in the Appendix). In addition, if a statement as in Observation 3 is desired, one can use the same ideas as the ones presented here, since they rely on general properties of commuting observables in three-dimensional space. Consequently, our methods allow to transform most of the known state-independent NC inequalities (for instance, the ones presented in Refs. [20, 33–35]) into witnesses for the quantum dimension.

IX. DISCUSSION AND CONCLUSION

We have shown that the two main noncontextuality inequalities - the KCBS inequality (Observation 1) and the Peres-Mermin inequality (Observation 3 and 4) - can be used as dimension witnesses. In particular, Observation 4 shows that the the Peres-Mermin inequality can be used to certify the dimension of a Hilbert space independently of the state preparation and in a noise robust way. Our methods allow the application of other inequalities, showing that contextuality can be used as a resource for dimension tests of quantum systems. Our tests are state-independent, in contrast to the existing tests. This can be advantageous in experimental implementations, moreover it shows that one can bound the dimension of quantum systems without using about the properties of the quantum state. We hope that our results stimulate further research to answer a central open question: For which tasks in quantum information processing is quantum contextuality a useful resource?

Acknowledgments

We thank Tobias Moroder and Christian Roos for discussions. This work was supported by the BMBF (Chist-Era network QUASAR), the EU (Marie Curie CIG 293992/ENFOQI), the FQXi Fund (Silicon Valley Community Foundation), the DFG, and the Project No. FIS2011-29400 (Spain).

Appendix

A1: Alternative proof of Observation 1

For an alternative proof of Observation 1, we need the following Lemma:

Lemma 5. If two dichotomic measurements on a two-dimensional quantum system commute $[A_i, A_{i+1}] = 0$, then either

(a) one of the observables is proportional to the identity, $A_i = \pm \mathbb{1}$ or $A_{i+1} = \pm \mathbb{1}$ or,

(b) the product of the two observables is proportional to the identity, $A_i A_{i+1} = \pm \mathbb{1}$.

Proof of Lemma 5. This fact can easily be checked: the observables A_i and A_{i+1} are diagonal in the same basis and the entries on the diagonal can only be ± 1. Then, only the two cases outlined above are possible. □

Alternative proof of Observation 1. With the help of Lemma 5 one can consider each term of the KCBS inequality and make there six possible replacements. For instance, the term $\langle AB\rangle$ may be replaced by $\langle AB\rangle \mapsto \pm\langle B\rangle$ (if one sets $A \mapsto \pm\mathbb{1}$) or $\langle AB\rangle \mapsto \pm\langle A\rangle$ (if one sets $B \mapsto \pm\mathbb{1}$) or $\langle AB\rangle \mapsto \pm 1$. This results in a finite set of $6^5 = 7776$ possible replacements. Some of them are contradictory and can be disregarded, e.g., if one sets $B \mapsto \mathbb{1}$ from the term $\langle AB\rangle$ and $C \mapsto \mathbb{1}$ from the term $\langle CD\rangle$, then one cannot set $\langle BC\rangle \mapsto -1$ anymore. For the remaining replacements, one can directly check with a computer that the $\langle\chi_{\rm KCBS}\rangle$ reduces to the classical bound. □

A2: Detailed discussion of the generalized KCBS inequalities

First, we prove the following statement:

Lemma 6. Consider the generalized KCBS operator

$$\langle\chi_N\rangle = \sum_{i=1}^{N-1}\langle A_iA_{i+1}\rangle - \langle A_NA_1\rangle \tag{17}$$

for N even, where the A_i are dichotomic observables on a three-dimensional system, which are not proportional to the identity. Furthermore, the commuting pairs should not be equal, that is $A_i \neq A_{i+1}$. Then, the bound

$$\langle\chi_N\rangle \geq -(N-2) \tag{18}$$

holds.

Proof of Lemma 6. From the conditions, it follows that the observables have to be of the form $A_i = \pm(\mathbb{1} - 2|a_i\rangle\langle a_i|)$ with $\langle a_i|a_{i+1}\rangle = 0$. This implies that the sequential measurements can be rephrased via $A_iA_{i+1} = \pm(\mathbb{1} - 2|a_i\rangle\langle a_i| - 2|a_{i+1}\rangle\langle a_{i+1}|)$. Let us first assume that the signs in front of the A_i are alternating, that is, $A_i = +(\mathbb{1} - 2|a_i\rangle\langle a_i|)$ for odd i and $A_i = -(\mathbb{1} - 2|a_i\rangle\langle a_i|)$ for even i. Then, a direct calculation leads to

$$\langle\chi_N\rangle = -(N-2) + 4\langle\sum_{k=2}^{N-1}|a_k\rangle\langle a_k|\rangle. \tag{19}$$

From this, $\langle\chi_N\rangle \geq -(N-2)$ follows, since the operator in the sum is positive semidefinite.

A general distribution of signs for the A_i results in a certain distribution of signs for the A_iA_{i+1}. If I denotes the set of index pairs $(k, k+1)$, where $A_kA_{k+1} = +(\mathbb{1} - 2|a_k\rangle\langle a_k| - 2|a_{k+1}\rangle\langle a_{k+1}|)$, then I has always an odd number of elements. We can then write:

$$\langle\chi_N\rangle = -(N-2) + 2(|I|-1) + 4\langle\sum_{k=1}^{N}\alpha_k|a_k\rangle\langle a_k|\rangle \tag{20}$$

where $\alpha_k = 1$ if both $(k,k+1) \notin I$ and $(k-1,k) \notin I$, $\alpha_k = 0$ if either $(k,k+1) \in I, (k-1,k) \notin I$ or $(k,k+1) \notin I, (k-1,k) \in I$, and $\alpha_k = -1$ if both $(k,k+1) \in I$ and $(k-1,k) \in I$.

It remains to show that the last two terms are non-negative. The main idea to prove this is to use the fact that an operator like $X = \mathbb{1} - |a_i\rangle\langle a_i| - |a_{i+1}\rangle\langle a_{i+1}|$ is positive semidefinite, since $|a_i\rangle$ and $|a_{i+1}\rangle$ are orthogonal.

More explicitly, let us first consider the case where the index pairs in I are connected and distinguish different cases for the number of elements in I. If $|I| = 1$, there are no k with $\alpha_k = -1$, so $2(|I|-1)+4\langle\sum_{k=1}^{N}\alpha_k|a_k\rangle\langle a_k|\rangle \geq 0$. If $|I| = 2$, then $I = \{(i-1,i),(i,i+1)\}$ and there is a single $\alpha_i = -1$. In this case, one has $2|I| + 4\langle\sum_{k=1}^{N}\alpha_k|a_k\rangle\langle a_k|\rangle \geq 0$. This is not yet the desired bound, but it will be useful later.

If $|I| = 3$, then $I = \{(i-1,i),(i,i+1),(i+1,i+2)\}$ and we have $\alpha_i = \alpha_{i+1} = -1$. But now, the fact that $X = \mathbb{1} - |a_i\rangle\langle a_i| - |a_{i+1}\rangle\langle a_{i+1}| \geq 0$ directly implies that $2(|I|-1) + 4\langle\sum_{k=1}^{N}\alpha_k|a_k\rangle\langle a_k|\rangle \geq 0$. If $|I| = 4$ there are three $\alpha_k = -1$ and we can use $X \geq 0$ two times, showing that again $2|I| + 4\langle\sum_{k=1}^{N}\alpha_k|a_k\rangle\langle a_k|\rangle \geq 0$. All this can be iterated, resulting in two different bounds, for $|I|$ odd and $|I|$ even.

To complete the proof, we have to consider a general I which does not necessarily form a single block. One can then consider the different blocks and, since $|I|$ is odd, at least one of the blocks contains an odd number of index pairs. Then, summing up the bound for the single blocks leads to $2(|I|-1) + 4\langle\sum_{k=1}^{N}\alpha_k|a_k\rangle\langle a_k|\rangle \geq 0$. □

Finally, in order to justify Eq. (6) in the main text for the three-dimensional case, we have to discuss what happens if one of the observables is proportional to the identity. However, then the mean value $\langle\chi_N\rangle$ reduces to inequalities which will be discussed later (see Lemma 9 in Appendix A4).

A3: Detailed proof of Observation 2

For computing the minimal value in two-dimensional systems, we need the following Lemma. Note that the resulting value has been reported before [36], so the main task is to prove rigorously that this is indeed optimal.

Lemma 7. Let $|\mathfrak{a}_i\rangle \in \mathbb{R}^3$ be normalized real three-dimensional vectors and define

$$\chi_N = \sum_{i=1}^{N}\langle\mathfrak{a}_i|\mathfrak{a}_{i+1}\rangle \text{ for } N \text{ odd}, \tag{21a}$$

$$\chi_N = -\langle\mathfrak{a}_1|\mathfrak{a}_2\rangle + \sum_{i=2}^{N}\langle\mathfrak{a}_i|\mathfrak{a}_{i+1}\rangle \text{ for } N \text{ even}. \tag{21b}$$

Then we have

$$\chi_N \geq -N\cos(\frac{\pi}{N}). \tag{22}$$

Proof of Lemma 7. We write $|\mathfrak{a}_i\rangle = \{\cos(\alpha_i), \sin(\alpha_i)\cos(\beta_i), \sin(\alpha_i)\sin(\beta_i)\}$ and then

we have

$$\chi_N = \sum_{i=1}^{N} [\pm] \Big[\cos(\alpha_i)\cos(\alpha_{i+1}) + \cos(\beta_i - \beta_{i+1})\sin(\alpha_i)\sin(\alpha_{i+1}) \Big], \qquad (23)$$

where the symbol $[\pm]$ denotes the possibly changing sign of the term with $i = 1$. Let us first explain why the minimum of this expression can be obtained by setting all the $\beta_i = 0$. Without losing generality, we can assume that $|\mathfrak{a}_1\rangle$ points in the x-direction, i.e., $\alpha_1 = 0$ and $\sin(\alpha_1) = 0$. Then, only $N-2$ terms of the type $\sin(\alpha_i)\sin(\alpha_{i+1})$ remain and all of them have a positive prefactor. For given values of β_i we can choose the signs of $\alpha_2, \ldots, \alpha_{N-1}$ such that all these terms are negative, while the other parts of the expression are not affected by this. Then, it is clearly optimal to choose $\beta_2 = \beta_3 = \ldots = \beta_N = 0$. This means that all the vectors lie in the x-y-plane.

Having set all $\beta_i = 0$, the expression is simplified to $\chi_N = \sum_{i=1}^{N} [\pm] \cos(\alpha_i - \alpha_{i+1})$. We use the notation $\delta_i = \alpha_i - \alpha_{i+1}$ and minimize $\sum_{i=1}^{N} [\pm] \cos(\delta_i)$ under the constraint $\sum_{i=1}^{N} \delta_i = 0$. Using Lagrange multipliers, it follows that $[\pm] \sin(\delta_i) = \lambda$ for all i.

If N is odd, this means that we can express any δ_i as $\delta_i = \pi/2 \pm \vartheta + 2\pi k_i$ with $\vartheta \geq 0$. From $\cos(\pi/2 + \vartheta + 2\pi k_i) = -\cos(\pi/2 - \vartheta + 2\pi k_i)$, it follows that the sign in front of the ϑ should be identical for all δ_i, otherwise, the expression is not minimized. Let us first consider the case that all signs a positive. From the condition $\sum_{i=1}^{N} \delta_i = 0$, it follows that $N(\pi/2) + N\vartheta + 2\pi K = 0$, with $K = \sum_{i=1}^{N} k_i$. Since we wish to minimize χ_N, the angles δ_i should be as close as possible to π, which means that $|\vartheta - \pi/2|$ should be minimal. This leads to the result that one has to choose $K = -(N \pm 1)/2$. Computing the corresponding ϑ leads to $\vartheta = \pi/2 \pm \pi/N$, which results in Eq. (22). If the signs in front of all ϑ are negative, one can make a similar argument, but this time has to minimize $|\delta_i + \pi|$ or $|\vartheta - 3\pi/2|$. This leads to the same solutions.

If N is even, one has for $i = 2, \ldots, N$ again $\delta_i = \pi/2 \pm \vartheta + 2\pi k_i$ and the first δ_1 can be written as $\delta_1 = -\pi/2 \pm \vartheta + 2\pi k_1$. One can directly see that if the signs in front of ϑ is positive (negative) for all $i = 2, \ldots, N$ it has to be positive (negative) also for $i = 1$. A direct calculation as before leads to $\vartheta = \pi/2 \pm \pi/N$ and, again, to the same bound of Eq. (22). □

Proof of Observation 2. Let us first assume that none of the observables is proportional to the identity, and consider a single sequential measurement $\langle AB \rangle$ of two dichotomic noncommuting observables $A = |A^+\rangle\langle A^+| - |A^-\rangle\langle A^-| = P_+^A - P_-^A$ and $B = |B^+\rangle\langle B^+| - |B^-\rangle\langle B^-| = P_+^B - P_-^B$. We can also express $|A^+\rangle\langle A^+|$ and $|B^+\rangle\langle B^+|$ in terms of their Bloch vectors $|\mathfrak{a}\rangle$ and $|\mathfrak{b}\rangle$. Then, we have that

$$\langle AB \rangle = 2|\langle A^+|B^+\rangle|^2 - 1 = \langle \mathfrak{a}|\mathfrak{b}\rangle. \qquad (24)$$

Note that this means that the mean value $\langle AB \rangle$ is independent of the initial quantum state. To see this relation, we write $\langle AB \rangle = \mathrm{tr}(P_+^B P_+^A \varrho P_+^A P_+^B) - \mathrm{tr}(P_-^B P_+^A \varrho P_+^A P_-^B) - \mathrm{tr}(P_+^B P_-^A \varrho P_-^A P_+^B) + \mathrm{tr}(P_-^B P_-^A \varrho P_-^A P_-^B)$. Using the fact that in a two-dimensional system $|\langle A^+|B^+\rangle|^2 = |\langle A^-|B^-\rangle|^2$ and $|\langle A^-|B^+\rangle|^2 = |\langle A^+|B^-\rangle|^2$ holds, and $\mathrm{tr}(\varrho) = 1$, this can directly be simplified to the above expression. Using the above expression, we can write $\langle \chi_{\mathrm{KCBS}} \rangle = \sum_{i=1}^{5} \langle \mathfrak{a}_i | \mathfrak{a}_{i+1} \rangle$. Then, Lemma 7 proves the desired bound.

It remains to discuss the case where one or more observables in the KCBS inequality are proportional to the identity. Let us first assume that only one observable, say A_1 is proportional to the identity. Then, if the Bloch vector of ϱ is denoted by $|\mathfrak{r}\rangle$ a direct calculation shows that the KCBS operator reads

$$\langle \chi_{\mathrm{KCBS}} \rangle = \langle \mathfrak{r}|\mathfrak{a}_2\rangle + \sum_{i=2}^{4} \langle \mathfrak{a}_i|\mathfrak{a}_{i+1}\rangle + \langle \mathfrak{a}_5|\mathfrak{r}\rangle, \qquad (25)$$

and Lemma 7 proves again the claim. If two observables A_i and A_j are proportional to the identity, the same rewriting can be applied, if A_i and A_j do not occur jointly in one correlation term. This is the case if $j \neq i \pm 1$. In the other case (say, $A_1 = \mathbb{1}$ and $A_2 = -\mathbb{1}$), one has $\langle A_1 A_2 \rangle = -1$ and can rewrite

$$\langle \chi_{\mathrm{KCBS}} \rangle = -1 - \langle \mathfrak{r}|\mathfrak{a}_2\rangle + \sum_{i=3}^{4} \langle \mathfrak{a}_i|\mathfrak{a}_{i+1}\rangle + \langle \mathfrak{a}_4|\mathfrak{r}\rangle, \qquad (26)$$

and Lemma 7 implies that $\langle \chi_{\mathrm{KCBS}} \rangle \geq -4\cos(\pi/4) - 1 = -2\sqrt{2} - 1 > -5\cos(\pi/5) = -5(1+\sqrt{5})/4$. If more than two observables are proportional to the identity, the bound can be proven similarly. □

A4: Proof of Observation 3

We need a whole sequence of Lemmata:

Lemma 8. If one has three dichotomic measurements $A_i, i = 1, 2, 3$ on a three-dimensional quantum system which commute pairwise $[A_i, A_j] = 0$, then either

(a) one of the observables is proportional to the identity, $A_i = \pm\mathbb{1}$ for some i or,

(b) the product of two observables of the three observables is proportional to the identity, $A_i A_j = \pm\mathbb{1}$ for some pair i, j or,

(c) The product of all three observables is proportional to the identity, $A_1 A_1 A_3 = \pm\mathbb{1}$.

Note that these cases are not exclusive and that for a triple of observables several of these cases may apply at the same time.

Proof of Lemma 8. This can be proven in the same way as Lemma 5, since all A_i are diagonal in the same basis. □

Lemma 9. For sequences of dichotomic measurements the following inequalities hold:

$$\eta_N \equiv \langle A_1\rangle + \sum_{i=1}^{N-1}\langle A_i A_{i+1}\rangle - \langle A_N\rangle \leq N-1. \qquad (27)$$

Here, it is always assumed that two observables which occur in the same sequence commute. Moreover, if we define

$$\zeta_N \equiv \sum_{i=1}^{N}\langle A_i A_{i+1}\rangle - \langle A_N A_1\rangle, \qquad (28)$$

then we have

$$\zeta_N \leq N-2 \qquad (29)$$

in two-dimensional systems, while for three-dimensional systems.

$$\zeta_3 \leq 1; \quad \zeta_4 \leq 2, \qquad (30)$$
$$\zeta_5 \leq \sqrt{5}(4-\sqrt{5}), \quad \zeta_6 \leq 1+\sqrt{5}(4-\sqrt{5}) = 4(\sqrt{5}-1),$$

holds.

Proof of Lemma 9. If we consider η_N for $N=2$ both observables commute and the claim $\langle A_1\rangle + \langle A_1A_2\rangle - \langle A_2\rangle \leq 1$ is clear, as it holds for any eigenvector. The bounds for general η_N follow by induction, where in each step of the induction $\langle A_N A_{N+1}\rangle - \langle A_{N+1}\rangle \leq 1 - \langle A_N\rangle$ is used, but this is nothing but the bound for $N=2$.

The bounds for ζ_N are just the ones derived for the generalized KCBS inequalities, see Eq. (6) in the main text and Appendix A2. □

Lemma 10. Consider the PM square with dichotomic observables on a three-dimensional system, where for one column and one row only the case (c) in Lemma 8 applies. Then, one cannot violate the classical bound and one has $\langle\chi_{\rm PM}\rangle \leq 4$.

Proof of Lemma 10. Let us consider the case that the condition holds for the first column and the first row, the other cases are analogous. Then, none of the observables A, B, C, a, α is proportional to the identity since, otherwise, case (a) in Lemma 8 would apply. These observables can all be written as

$$A = \pm(\mathbb{1} - 2|A\rangle\langle A|), \qquad (31)$$

with some vector $|A\rangle$, and the vector $|A\rangle$ characterizes the observable A up to the total sign uniquely. In this notation, two observables X and Y commute if and only if the corresponding vectors $|X\rangle$ and $|Y\rangle$ are the same or orthogonal. For our situation, it follows that the vectors $|A\rangle, |B\rangle$, and $|C\rangle$ form an orthonormal basis of the three-dimensional space, since if two of them were the same, then for the first row also the case (b) in Lemma 8 would apply. Similarly, the vectors $|A\rangle, |a\rangle$ and $|\alpha\rangle$ form another orthonormal basis of the three-dimensional space. We can distinguish two cases:

Case 1: The vector $|B\rangle$ is neither orthogonal nor parallel to $|a\rangle$. From this, it follows that $|B\rangle$ is also neither orthogonal nor parallel to $|\alpha\rangle$ and similarly, $|C\rangle$ is neither orthogonal nor parallel to $|a\rangle$ and $|\alpha\rangle$ and vice versa.

Let us consider the observable b in the PM square. This observable can be proportional to the identity, but if this is not the case, the corresponding vector $|b\rangle$ has to be parallel or orthogonal to $|B\rangle$ and $|a\rangle$. Since $|B\rangle$ and $|a\rangle$ are neither orthogonal nor parallel, it has to be orthogonal to both, which means that it is parallel to $|A\rangle$. Consequently, the observable b is either proportional to the identity or proportional to A. Similarly, all the other observables β, c, and γ are either proportional to the identity or proportional to A.

Let us now consider the expectation value of the PM operator $\langle\chi_{\rm PM}\rangle$ for some quantum state ϱ. We denote this expectation value as $\langle\chi_{\rm PM}\rangle_\varrho$ in order to stress the dependence on ϱ. The observable A can be written as $A = P_+ - P_-$, where P_+ and P_- are the projectors onto the positive or negative eigenspace. One of these projectors is one-dimensional and equals $|A\rangle\langle A|$, the other other one is two-dimensional. For definiteness, let us take $P_+ = |A\rangle\langle A|$ and $P_- = \mathbb{1} - |A\rangle\langle A|$.

Instead of ϱ, we may consider the depolarized state $\sigma = p_+\varrho_+ + p_-\varrho_-$, with $\varrho_\pm = P_\pm\varrho P_\pm/p_\pm$ and $p_\pm = {\rm tr}(P_\pm\varrho P_\pm)$. Our first claim is that, in our situation,

$$\langle\chi_{\rm PM}\rangle_\varrho = \langle\chi_{\rm PM}\rangle_\sigma = p_+\langle\chi_{\rm PM}\rangle_{\varrho_+} + p_-\langle\chi_{\rm PM}\rangle_{\varrho_-}. \qquad (32)$$

It suffices to prove this for all rows and columns separately. Since the observables in each column or row commute, we can first measure observables which might be proportional to A. For the first column and the first row the statement is clear: We first measure A and the result is the same for ϱ and σ. After the measurement of A, however, the state ϱ is projected either onto ϱ_+ or ϱ_-. Therefore, for the following measurements it does not matter whether the initial state was ϱ or σ. As an example for the other rows and columns, we consider the second column. Here, we can first measure β and then b and finally B. If β or b are proportional to A, then the statement is again clear. If both β and b are proportional to the identity, then the measurement of $\langle\beta b B\rangle_\varrho$ equals $\pm\langle B\rangle_\varrho$. Then, however, one can directly calculate that $\langle B\rangle_\varrho = \langle B\rangle_\sigma$, since B and A commute.

Having established the validity of Eq. (32), we proceed by showing that for for each term $\langle\chi_{\rm PM}\rangle_{\varrho_+}$ and $\langle\chi_{\rm PM}\rangle_{\varrho_-}$ separately the classical bound holds. For $\langle\chi_{\rm PM}\rangle_{\varrho_+}$ this is clear: Since $P_+ = |A\rangle\langle A|$, we have that $\varrho_+ = |A\rangle\langle A|$ and $|A\rangle$ is an eigenvector of all observables occurring in the PM square. Therefore, the results obtained in $\langle\chi_{\rm PM}\rangle_{\varrho_+}$ correspond to a classical assignment of ±1 to all observables, and $\langle\chi_{\rm PM}\rangle_{\varrho_+} \leq 4$ follows. For the other term $\langle\chi_{\rm PM}\rangle_{\varrho_-}$, the problem is effectively a two-dimensional one, and we can consider the restriction of the observables to the two-dimensional space, e.g., $\bar{A} = P_-AP_-$, etc. In this restricted space we have that $\bar{A}, \bar{b}, \bar{\beta}, \bar{c}$, and $\bar{\gamma}$ are all of them proportional to the identity and, therefore, result in a classical assignment ±1 independent of

ϱ_-. Let us denote these assignments by $\hat{A}, \hat{b}, \hat{\beta}, \hat{c}$, and $\hat{\gamma}$. Then, it remains to be shown that

$$\begin{aligned}\mathcal{Z} \;=\; & \hat{A}\big[\langle \bar{B}\bar{C}\rangle_{\varrho_-} + \langle \bar{\alpha}\bar{a}\rangle_{\varrho_-}\big] + \hat{b}\hat{c}\langle \bar{a}\rangle_{\varrho_-} \\ & + \hat{\beta}\hat{\gamma}\langle \bar{\alpha}\rangle_{\varrho_-} + \hat{b}\hat{\beta}\langle \bar{B}\rangle_{\varrho_-} - \hat{c}\hat{\gamma}\langle \bar{C}\rangle_{\varrho_-} \leq 4 \end{aligned} \quad (33)$$

for all classical assignments and for all states ϱ_-. For observables $\bar{B}$ and $\bar{C}$ we have furthermore that $\bar{B}\bar{C} = \pm\mathbb{1}$ (see Lemma 5), hence $\bar{B} = \pm\bar{C}$ and similarly $\bar{a} = \pm\bar{\alpha}$. If one wishes to maximize $\mathcal{Z}$ for the case $\hat{A} = +1$, one has to choose $\bar{B} = \bar{C}$ and $\bar{a} = \bar{\alpha}$. Then, the product of the four last terms in $\mathcal{Z}$ equals -1, and $\mathcal{Z} \leq 4$ holds. For the case $\hat{A} = -1$ one chooses $\bar{B} = -\bar{C}$ and $\bar{a} = -\bar{\alpha}$, but still the product of the four last terms in $\mathcal{Z}$ equals -1, and $\mathcal{Z} \leq 4$. This finishes the proof of the first case.

Case 2: The bases $|A\rangle, |B\rangle, |C\rangle$ and $|A\rangle, |a\rangle, |\alpha\rangle$ are (up to some permutations or signs) the same. For instance, we can have the case in which $|B\rangle = |a\rangle$ and $|C\rangle = |\alpha\rangle$; the other possibilities can be treated similarly.

In this case, since $|B\rangle$ and $|\alpha\rangle$ are orthogonal, the observable β has to be either proportional to the identity or proportional to A. For the same reason, c has to be either proportional to the identity or to A.

Let us first consider the case in which one of the observables β and c is proportional to A, say $\beta = \pm A$ for definiteness. Then, since $|\beta\rangle = |A\rangle$ and $|B\rangle$ are orthogonal, b can only be the identity or proportional to C. Similarly, γ can only be the identity or proportional to C. It follows that *all* nine observables in the PM square are diagonal in the basis $|A\rangle, |B\rangle, |C\rangle$, and all observables commute. Then, $\langle \chi_{\rm PM}\rangle \leq 4$ follows, as this inequality holds in any eigenspace.

Second, let us consider the case in which β and c are both proportional to the identity. This results in fixed assignments $\hat{\beta}$ and $\hat{c}$ for them. Moreover, B and a differ only by a sign $\hat{\mu}$ (that is, $a = \hat{\mu}B$) and C and α differ only by a sign $\hat{\nu}$ (i.e., $\alpha = \hat{\nu}C$). So we have to consider

$$\begin{aligned}\mathcal{X} \;=\; & \langle ABC\rangle + \hat{\mu}\hat{\nu}\langle ABC\rangle + \hat{\beta}\langle Bb\rangle \\ & + \hat{\mu}\hat{c}\langle Bb\rangle + \hat{\nu}\hat{\beta}\langle C\gamma\rangle - \hat{c}\langle C\gamma\rangle. \end{aligned} \quad (34)$$

In order to achieve $\mathcal{X} > 4$ one has to choose $\hat{\mu} = \hat{\nu}$, $\hat{\beta} = \hat{\mu}\hat{c}$, and $\hat{c} = -\hat{\nu}\hat{\beta}$. However, the later is equivalent to $\hat{\beta} = -\hat{\nu}\hat{c}$, showing that this assignment is not possible. Therefore, $\mathcal{X} \leq 4$ has to hold. This finishes the proof of the second case. □

Lemma 11. Consider the PM square with dichotomic observables on a three-dimensional system, where for one column (or one row) only the case (c) in Lemma 8 applies. Then, one cannot violate the classical bound and one has $\langle \chi_{\rm PM}\rangle \leq 4$.

Proof of Lemma 11. We assume that the condition holds for the first column. Then, none of the observables A, a, and α are proportional to the identity, and the corresponding vectors $|A\rangle, |a\rangle$, and $|\alpha\rangle$ form an orthonormal basis of the three-dimensional space.

The idea of our proof is to consider possible other observables in the PM square, which are not proportional to the identity, but also not proportional to A, a, or α. We will see that there are not many possibilities for the observables, and in all cases the bound $\langle \chi_{\rm PM}\rangle \leq 4$ can be proved explicitly.

First, consider the case that there *all* nontrivial observables in the PM square are proportional to A, a, or α. This means that all observables in the PM square are diagonal in the basis defined by $|A\rangle, |a\rangle$, and $|\alpha\rangle$, and all observables commute. But then the bound $\langle \chi_{\rm PM}\rangle \leq 4$ is clear.

Second, consider the case that there are several nontrivial observables, which are *not* proportional to A, a, or α. Without losing generality, we can assume that the first of these observables is B. This implies that $|B\rangle$ is orthogonal to $|A\rangle$ and lies in the plane spanned by $|a\rangle$ and $|\alpha\rangle$, but $|a\rangle \neq |B\rangle \neq |\alpha\rangle$. It follows for the observables b and β that they can only be proportional to the identity or to A (see Case 1 in Lemma 10). We denote this as $b = \hat{b}[A]$, where $[A] = A$ or $\mathbb{1}$, and $\hat{b}$ denotes the proper sign, i.e., $b = \hat{b}A$ or $b = \hat{b}\mathbb{1}$. Similarly, we write $\beta = \hat{\beta}[A]$.

Let us assume that there is a second nontrivial observable which is not proportional to A, a, or α (but it might be proportional to B). We can distinguish three cases:

(i) First, this observable can be given by C and C is not proportional to B. Then, this is exactly the situation of Case 1 in Lemma 10, and $\langle \chi_{\rm PM}\rangle \leq 4$ follows.

(ii) Second, this observable can be given by C. However, C is proportional to B. Then, $c = \hat{c}[A]$ and $\gamma = \hat{\gamma}[A]$ follows. Now the proof can proceed as in Case 1 of Lemma 10. One arrives to the same Eq. (33), with the extra condition that $\bar{B} = \pm\bar{C}$, which was deduced after Eq. (33) anyway. Therefore, $\langle \chi_{\rm PM}\rangle \leq 4$ has to hold.

(iii) Third, this observable can be given by c. Then, it cannot be proportional to B, since $|B\rangle$ is not orthogonal to $|a\rangle$. It first follows that $C = \hat{C}[a]$ and $\gamma = \hat{\gamma}[a]$. Combined with the properties of B, one finds that $C = \hat{C}\mathbb{1}$ and $b = \hat{b}\mathbb{1}$ has to hold. Then, the PM inequality reads

$$\begin{aligned}\mathcal{Y} \;=\; & \langle A\alpha a\rangle + \langle B(A\hat{C} + \hat{b}\hat{\beta}[A])\rangle \\ & + \hat{\beta}\hat{\gamma}\langle \alpha[A][a]\rangle + \langle c(\hat{b}a - \hat{C}\hat{\gamma}[a])\rangle. \end{aligned} \quad (35)$$

In this expression, the observables B and c occur only in a single term and a single context. Therefore, for any quantum state, we can obtain an upper bound on $\mathcal{Y}$ by replacing $B \mapsto \pm\mathbb{1}$ and $c \mapsto \pm\mathbb{1}$ with appropriately chosen signs. However, with this replacement, all observables occurring in $\mathcal{Y}$ are diagonal in the basis defined by $|A\rangle, |a\rangle$, and $|\alpha\rangle$, and $\mathcal{Y} = \langle \chi_{\rm PM}\rangle \leq 4$ follows.

In summary, the discussion of the cases (i), (ii), and (iii) has shown the following: It is not possible to have three nontrivial observables in the PM square, which are all of them not proportional to A, a, or α. If one has two of such observables, then the classical bound has been proven.

It remains to be discussed what happen if one has only one observable (say, B), which is not proportional to A, a, or α. However, then the PM inequality can be written

similarly as in Eq. (35), and B occurs in a single context. We can set again $B \mapsto \pm\mathbb{1}$ and the claim follows. □

Finally, we can prove our Observation 3:

Proof of Observation 3. Lemma 10 and Lemma 11 solve the problem, if case (c) in one column or row happens. Therefore, we can assume that in all columns and all rows only the cases (a) or (b) from Lemma 8 apply. However, in these cases, we obtain a simple replacement rule: For case (a), one of the observables has to be replaced with a classical value ± 1 and, for case (b), one of the observables can be replaced by a different one from the same row or column. In both cases, the PM inequality is simplified.

For case (a), there are six possible replacement rules, as one of the three observables must be replaced by ± 1. Similarly, for case (b), there are six replacement rules. Therefore, one obtains a finite number, namely $(6+6)^6$ possible replacements. As in the case of the KCBS inequality (see the alternative proof of Observation 1 in Appendix A1), some of them lead to contradictions (e.g., one may try to set $A = +\mathbb{1}$ from the first column, but $A = -\mathbb{1}$ holds due to the rule from the first row). Taking this into account, one can perform an exhaustive search of all possibilities, preferably by computer. For all cases, either the classical bound holds trivially (e.g., because the assignments require already, that one row is -1) or the PM inequality can be reduced, up to some constant, to one of the inequalities in Lemma 8. In most cases, one obtains the classical bound. However, in some cases, the PM inequality is reduced to $\langle \chi_{\mathrm{PM}} \rangle = \zeta_5 + 1$ or $\langle \chi_{\mathrm{PM}} \rangle = \zeta_6$. To give an example, one may consider the square

$$\begin{bmatrix} A & B & C \\ a & b & c \\ \alpha & \beta & \gamma \end{bmatrix} = \begin{bmatrix} A & \mathbb{1} & C \\ a & b & \mathbb{1} \\ \mathbb{1} & \beta & \gamma \end{bmatrix}, \tag{36}$$

which results in $\langle \chi_{\mathrm{PM}} \rangle = \zeta_6$ for appropriately chosen A_i. Therefore, from Lemma 9 follows that in three dimensions $\langle \chi_{\mathrm{PM}} \rangle = 4(\sqrt{5}-1) \approx 4.94$ holds and can indeed be reached. □

A5: Imperfect measurements

In this section we discuss the noise robustness of Observation 4. In the first subsection, we prove that Observation 4 also holds for the model of noisy measurements explained in the main text. In the second subsection, we discuss a noise model that reproduces the probabilities of the most general POVM.

A5.1: Noisy measurements

In order to explain the probabilities from a noisy measurement, we first consider the following measurement model: Instead of performing the projective measurement A, one of two possible actions are taken:

(a) with a probability p_A the projective measurement is performed, or

(b) with a probability $1-p_A$ a completely random outcome ± 1 is assigned independently of the initial state. Here, the results $+1$ and -1 occur with equal probability.

In case (b), after the assignment the physical system is left in one of two possible states ϱ^+ or ϱ^-, depending on the assignment. We will not make any assumptions on $\varrho^\pm$.

Before formulating and proving a bound on $\langle \chi_{\mathrm{PM}} \rangle$ in this scenario, it is useful to discuss the structure of $\langle \chi_{\mathrm{PM}} \rangle$ for the measurement model. A single measurement sequence $\langle ABC \rangle$ is split into eight terms: With a prefactor $p_A p_B p_C$ one has the value, which is obtained, if all measurements are projective; with a prefactor $p_A p_B (1-p_C)$ one has the value, where A and B are projective, and C is a random assignment, etc. It follows that the total mean value $\langle \chi_{\mathrm{PM}} \rangle$ is an affine function in the probability p_A (if all other parameters are fixed) and also in all other probabilities p_X for the other measurements. Consequently, the maximum of $\langle \chi_{\mathrm{PM}} \rangle$ is attained either at $p_A = 1$ or $p_A = 0$, and similarly for all the measurements. Therefore, for maximizing $\langle \chi_{\mathrm{PM}} \rangle$ it suffices to consider the finite set of cases where, for each observable, either always possibility (a) or always possibility (b) is taken. We can formulate:

Proposition 12. Consider noisy measurements as described above. Then, the bound from Observation 4

$$\langle \chi_{\mathrm{PM}} \rangle \leq 3\sqrt{3} \tag{37}$$

holds.

Proof. As discussed above, we only have to discuss a finite number of cases. Let us consider a single term $\langle ABC \rangle$. If C is a random assignment, then $\langle ABC \rangle = 0$, independently how A and B are realized. It follows that if C, β or a are random assignments, then $\langle \chi_{\mathrm{PM}} \rangle \leq 4$.

On the other hand, if A is a random assignment, then $\langle ABC \rangle = 0$ as well: (i) If B and C are projective, then the measurement of B and C results in the state independent mean value $\langle BC \rangle$ [see Eq. (8) in the main text]. This value is independent of the state $\varrho^\pm$ remaining after the assignment of A, hence $\langle ABC \rangle = \langle AB \rangle - \langle AB \rangle = 0$. (ii) If B is a random assignment, one can also directly calculate that $\langle ABC \rangle = 0$ and the case that (iii) C is a random assignment has been discussed already. Consequently, if A, b, or γ are random assignments, then $\langle \chi_{\mathrm{PM}} \rangle \leq 4$.

It remains to discuss the case that B, c, or α are random assignments while all other measurements are projective. First, one can directly calculate that if A, C are projective, and B is a random assignment, then

$$\langle ABC \rangle = \mathrm{tr}(\varrho A)\mathrm{tr}(CX), \tag{38}$$

with $X = (\varrho^+ - \varrho^-)/2$. If X is expressed in terms of Pauli matrices, then the length of its Bloch vector does

not exceed one, since the Bloch vectors of $\varrho^{\pm}$ are subnormalized.

The estimate of $\langle\chi_{\rm PM}\rangle$ can now proceed as in the proof of Observation 4, and one arrives at the situation of Lemma 7 in Appendix A3, where now the vectors are subnormalized, and not necessarily normalized. But still the bound from Lemma 7 is valid: If the smallest vector in χ_6 has a length ω, one can directly see that $\chi_6 \geq \omega[-N\cos(\pi/N)]-(1-\omega)4$. This proves Proposition 12. □

A5.2: More general POVMs

Now we consider a general dichotomic positive operator valued measure (POVM) on a qubit system. This is characterized by two effects E^+ and E^-, where $E^+ + E^- = \mathbb{1}$ and the probabilities of the measurement results are $p^+ = \mathrm{tr}(\varrho E^+)$ and $p^- = \mathrm{tr}(\varrho E^-)$.

These effects have to commute and one can write $E^+ = \alpha|0\rangle\langle 0| + \beta|1\rangle\langle 1|$ and $E^- = \gamma|0\rangle\langle 0| + \delta|1\rangle\langle 1|$ in an appropriate basis. We can assume that $\alpha \geq \beta$ and consequently $\delta \geq \gamma$. Furthermore, it is no restriction to choose $\beta \leq \gamma$. Then, the effects can be written as $E^+ = \beta\mathbb{1} + (\alpha-\beta)|0\rangle\langle 0|$ and $E^- = \beta\mathbb{1} + (\gamma-\beta)\mathbb{1} + (\alpha-\beta)|1\rangle\langle 1|$. This means that one can interpret the probabilities of the POVM as coming from the following procedure: With a probability of 2β one assigns a random outcome, with a probability of $\gamma-\beta$ one assigns the fixed value -1, and with a probability of $(\alpha-\beta)$ one performs the projective measurement.

This motivates the following measurement model: Instead of performing the projective measurement A, one of three possible actions are taken:

(i) with a probability p_1^A the projective measurement is performed, or

(ii) with a probability p_2^A a fixed outcome ± 1 is assigned independently of the initial state. After this announcement, the state is left in the corresponding eigenstate of A, or

(iii) with a probability p_3^A a completely random outcome ± 1 is assigned independently of the initial state.

As above, in case (iii), the physical system is left in one of two possible states ϱ^+ or ϱ^-, but we will not make any assumptions on $\varrho^{\pm}$. For this measurement model, we have:

Proposition 13. In the noise model described above, the PM operator is bounded by

$$\langle\chi_{\rm PM}\rangle \leq 1 + \sqrt{9+6\sqrt{3}} \approx 5.404. \tag{39}$$

Proof. As in the proof of Proposition 12, we only have to consider a finite set of cases. Let us first discuss the situation, where for each measurement only the possibilities (i) and (ii) are taken.

First, we have to derive some formulas for sequential measurements. The reason is that, if the option (ii) is chosen, then the original formula for sequential measurements, Eq. (15) in the main text, is not appropriate anymore and different formulas have to be used.

In the following, we write $A = (\pm)_A$ if A is a fixed assignment as described in possibility (ii) above. If not explicitly stated otherwise, the observables are measured as projective measurements. Then one can directly calculate that

$$\langle ABC\rangle = (\pm)_A\langle BC\rangle \text{ if } A = (\pm)_A, \tag{40a}$$
$$\langle ABC\rangle = \mathrm{tr}(\varrho A)\langle BC\rangle \text{ if } B = (\pm)_B, \tag{40b}$$
$$\langle ABC\rangle = (\pm)_C\langle AB\rangle \text{ if } C = (\pm)_C, \tag{40c}$$

Note that in Eq. (40b) there is no deviation from the usual formula Eq. (15) in the main text. Furthermore, we have

$$\langle ABC\rangle = (\pm)_A(\pm)_B\mathrm{tr}(C|B^{\pm}\rangle\langle B^{\pm}|) = (\pm)_A\langle BC\rangle \quad \text{if } A = (\pm)_A \text{ and } B = (\pm)_B, \tag{41a}$$
$$\langle ABC\rangle = (\pm)_A(\pm)_C\mathrm{tr}(B|A^{\pm}\rangle\langle A^{\pm}|) = (\pm)_C\langle AB\rangle \quad \text{if } A = (\pm)_A \text{ and } C = (\pm)_C, \tag{41b}$$
$$\langle ABC\rangle = (\pm)_B(\pm)_C\mathrm{tr}(\varrho A) \quad \text{if } B = (\pm)_B \text{ and } C = (\pm)_C. \tag{41c}$$

In Eqs. (41a) and (41b), $|B^{\pm}\rangle$ and $|A^{\pm}\rangle$ denote the eigenstates of B and A, which are left after the fixed assignment.

Equipped with these rules, we can discuss the different cases. First, from Eqs. (40a), (40b), and (41a) it follows that the proof of Observation 4 does not change, if fixed assignments are made only on the observables which are measured at first or second position of a sequence (i.e., the observables A, b, γ, B, c, and α).

However, the structure of the inequality changes if one of the last measurements is a fixed assignment. To give an example, consider the case that the measurement β is a fixed assignment [case (ii) above], while all other measurements are projective [case (i) above]. Using Eq. (40c) we have to estimate

$$\mathcal{X} = \langle A\rangle\langle BC\rangle + \langle A\rangle\langle\alpha a\rangle + \langle b\rangle\langle ca\rangle + \langle bB\rangle(\pm)_\beta + \langle\gamma\alpha\rangle(\pm)_\beta - \langle\gamma\rangle\langle cC\rangle. \tag{42}$$

On can directly see that it suffices to estimate

$$\mathcal{X}' = \langle B|C\rangle + \langle\alpha|a\rangle + \langle\varrho|b\rangle\langle c|a\rangle + \langle b|B\rangle + \langle\gamma|\alpha\rangle - \langle\varrho|\gamma\rangle\langle c|C\rangle, \tag{43}$$

where all expressions should be understood as scalar products of the corresponding Bloch vectors. Then, a direct optimization over the three-dimensional Bloch vectors proves that here

$$\mathcal{X}' \leq 1 + \sqrt{9+6\sqrt{3}} \approx 5.404 \tag{44}$$

holds. In general, the observables β, C, or a are the possible third measurements in a sequence. One can directly

check that, if one or several of them are fixed assignments, then an expression analogue to Eq. (42) arises and the bound of Eq. (44) holds. Finally, if some of the β, C, or a are fixed assignments and, in addition, some of the A, b, γ, B, c, and α are fixed assignments, then the comparison between Eq. (40c) and Eqs. (41b) and (41c) shows that no novel types of expressions occur.

It remains to discuss the case where not only the possibilities (i) and (ii) occur, but for one or more measurements also a random assignment [possibility (iii)] is realized. As in the proof of Proposition 12, one finds that only the cases where the second measurements (B, c, and α) are random are interesting. In addition to Eq. (38) one finds that $\langle ABC\rangle = (\pm_A)\mathrm{tr}(CX)$ if B is random and A is a fixed assignment, and $\langle ABC\rangle = 0$ if B is random and C is a fixed assignment. This shows that no new expressions occur, and proves the claim. □

Finally, we would like to add two remarks. First, it should be stressed that the presented noise model still makes assumptions about the measurement, especially about the post measurement state. Therefore, it is not the most general measurement, and we do not claim that the resulting dimension witnesses are device-independent.

Second, we would like to emphasize that the chosen order of the measurements in the definition in Eq. (9) in the main text is important for the proof of the bounds for noisy measurements: For other orders, it is not clear whether the dimension witnesses are robust against imperfections. In fact, for some choices one finds that the resulting inequalities are *not* robust against imperfections: Consider, for instance, a measurement order, where one observable (say, γ for definiteness) is the second observable in one context and the third observable in the other context. Furthermore, assume that γ is an assignment [case (iii) above], while all other measurements are projective. Then, we have to use Eq. (40b) for the first context of γ, and Eq. (40c) for the second context. In Eq. (40b) there is no difference to the usual formula, especially the formula does not depend on the value assigned to γ. Eq. (40c), however, depends on this value. This means that, for one term in the PM inequality, the sign can be changed arbitrarily and so $\langle \chi_{\mathrm{PM}}\rangle = 6$ can be reached.

[1] R. Horodecki, P. Horodecki, M. Horodecki, and K. Horodecki, Rev. Mod. Phys. **81**, 865 (2009).
[2] O. Gühne and G. Tóth, Phys. Rep. **474**, 1 (2009).
[3] G. Molina-Terriza, J.P. Torres, and L. Torner, Nature Physics **3**, 305 (2007).
[4] A.C. Dada, J. Leach, G.S. Buller, M.J. Padgett, and E. Andersson, Nature Physics **7**, 677 (2011).
[5] P. Neumann, N. Mizuochi, F. Rempp, P. Hemmer, H. Watanabe, S. Yamasaki, V. Jacques, T. Gaebel, F. Jelezko, and J. Wrachtrup, Science **320**, 1326 (2008).
[6] N. Brunner, S. Pironio, A. Acín, N. Gisin, A. Méthot, and V. Scarani, Phys. Rev. Lett. **100**, 210503 (2008).
[7] T. Vértesi and K. F. Pál, Phys. Rev. A **79**, 042106 (2009).
[8] S. Wehner, M. Christandl, and A.C. Doherty, Phys. Rev. A **78**, 062112 (2008).
[9] R. Gallego, N. Brunner, C. Hadley, and A. Acín, Phys. Rev. Lett. **105**, 230501 (2010).
[10] N. Brunner, M. Navascus, and T. Vrtesi, Phys. Rev. Lett. **110**, 150501 (2013).
[11] M. Hendrych, R. Gallego, M. Mičuda, N. Brunner, A. Acín, and J.P. Torres, Nature Physics **8**, 588 (2012).
[12] J. Ahrens, P. Badziąg, A. Cabello, and M. Bourennane, Nature Physics **8**, 592 (2012).
[13] M.M. Wolf and D. Pérez-García, Phys. Rev. Lett. **102**, 190504 (2009).
[14] E.P. Specker, Dialectica **14**, 239 (1960).
[15] A.M. Gleason, J. Math. Mech. **6**, 885 (1957).
[16] J.S. Bell, Rev. Mod. Phys. **38**, 447 (1966).
[17] S. Kochen and E.P. Specker, J. Math. Mech. **17**, 59 (1967).
[18] Y.-C. Liang, R.W. Spekkens, and H.M. Wiseman, Phys. Rep. **506**, 1 (2011).
[19] A.A. Klyachko, M.A. Can, S. Binicioğlu, and A.S. Shumovsky, Phys. Rev. Lett. **101**, 020403 (2008).
[20] A. Cabello, Phys. Rev. Lett. **101**, 210401 (2008).
[21] A. Peres, Phys. Lett. A **151**, 107 (1990).
[22] N.D. Mermin, Phys. Rev. Lett. **65**, 3373 (1990).
[23] A. Peres, *Quantum Theory: Concepts and Methods* (Kluwer, Dordrecht, 1995).
[24] M. Araújo, M. T. Quintino, C. Budroni, M. Terra Cunha, and A. Cabello, Phys. Rev. A **88**, 022118 (2013).
[25] R. Łapkiewicz, P. Li, C. Schaeff, N.K. Langford, S. Ramelow, M. Wieśniak, and A. Zeilinger, Nature (London) **474**, 490 (2011).
[26] J. Ahrens, E. Amselem, A. Cabello, and M. Bourennane, Sci. Rep. **3**, 2170 (2013).
[27] T. Fritz, New J. Phys. **12**, 083055 (2010).
[28] G. Kirchmair, F. Zähringer, R. Gerritsma, M. Kleinmann, O. Gühne, A. Cabello, R. Blatt, and C.F. Roos, Nature (London) **460**, 494 (2009).
[29] E. Amselem, M. Rådmark, M. Bourennane, and A. Cabello, Phys. Rev. Lett. **103**, 160405 (2009).
[30] O. Moussa, C.A. Ryan, D.G. Cory, and R. Laflamme, Phys. Rev. Lett. **104**, 160501 (2010).
[31] O. Gühne, M. Kleinmann, A. Cabello, J.-Å. Larsson, G. Kirchmair, F. Zähringer, R. Gerritsma, and C.F. Roos, Phys. Rev. A **81**, 022121 (2010).
[32] C. Budroni, T. Moroder, M. Kleinmann, and O. Gühne, Phys. Rev. Lett. **111**, 020403 (2013).
[33] A. Cabello, Phys. Rev. A **82**, 032110 (2010).
[34] S. Yu and C.H. Oh, Phys. Rev. Lett. **108**, 030402 (2012).
[35] M. Kleinmann, C. Budroni, J.-Å. Larsson, O. Gühne, and A. Cabello, Phys. Rev. Lett. **109**, 250402 (2012).
[36] M. Barbieri, Phys. Rev. A **80**, 034102 (2009).

Sequences of projective measurements in generalized probabilistic models

Matthias Kleinmann

Naturwissenschaftlich-Technische Fakultät, Universität Siegen, Walter-Flex-Straße 3, 57068 Siegen, Germany and

Departamento de Matemática, Universidade Federal de Minas Gerais, Caixa Postal 702, Belo Horizonte, Minas Gerais 31270-901, Brazil

We define a simple rule that allows to describe sequences of projective measurements for a broad class of generalized probabilistic models. This class embraces quantum mechanics and classical probability theory, but, for example, also the hypothetical Popescu-Rohrlich box. For quantum mechanics, the definition yields the established Lüders's rule, which is the standard rule how to update the quantum state after a measurement. In the general case it can be seen as the least disturbing or most coherent way to perform sequential measurements. As example we show that Spekkens's toy model[1] is an instance of our definition. We also demonstrate the possibility of strong post-quantum correlations as well as the existence of triple-slit correlations for certain non-quantum toy models.

I. INTRODUCTION

It is a fundamental property of quantum mechanics that any nontrivial measurement disturbs the system it acts on. This disturbance is responsible for very particular phenomena like the quantum Zeno effect[2,3], where the time-evolution of a system is frozen due to repeated measurements, or the contextual behavior of a quantum system[4], where measurement outcomes depend on the choice of previous compatible measurements. Compared to the classical world, where a measurement—at least in principle—may leave the system unchanged, this quantum property seems to be very particular and at the same time very fundamental.

The most common formulation of the this disturbance is due to Lüders[5,6] and determines how the state of a system changes after a measurement: $\rho \mapsto \Pi\rho\Pi/\operatorname{tr}(\rho\Pi)$. But this is only one out of many possible state changes that may occur in an experiment. In the most general case the post-measurement state can be seen as the result of a coherent evolution involving an auxiliary system and a destructive measurement on that auxiliary system. This fundamental result by Ozawa[7,8] does, however, not explain the special role of Lüders's rule. Conversely, Ozawa's result gives a very particular model of a measurement and one might argue that giving up Lüders's rule as a fundamental entity might actually make too strong assumptions on the peculiarities of the measurement process in quantum mechanics.

In this work we provide a very small set of assumptions that uniquely singles out Lüders's rule within quantum mechanics on the one hand, and on the other hand has many desirable properties when applied to hypothetical non-quantum models. These two aspects have been discussed for a long time[9–12], and some consensus seems to exist that the mathematical concept of a filter is an appropriate approach. We advertise that the axioms that we suggest here are significantly simpler then those that have appeared before while at the same time they imply more favorable physical properties.

We proceed as follows. The introduction is completed by a detailed reminder on how post-measurement states are treated in quantum mechanics, cf. Sec. I A, and a summary of the mathematical framework of ordered vector spaces in Sec. I B, enriched with examples in Sec. I C. In Sec. II we introduce the notion of projective, neutral, and coherent f-compatible maps, the latter of which we propose as a generalized definition of Lüders's rule. We investigate fundamental properties of this definition and give examples, in particular we study the case of quantum mechanics in Sec. III A, a large class of toy models in Sec. III B, and the n-slit experiment in Sec. III C. We conclude with a discussion of our findings in Sec. IV.

A. Quantum instruments

Before we start to formulate the behavior of measurement sequences in generalized probabilistic models, let us first recall the established formalism in quantum mechanics[8].

We consider a situation where first an observable A and then an observable B is measured. (In order to simplify the discussion, we assume that A and B have pure point spectrum.) The system subject to the measurements is initially described by a density operator ρ and the measurement of A is assumed to have yielded the result a. With the spectral decomposition as $A = \sum_a a\Pi_a$, according to Lüders[5,6], the expected value of B is given by

$$\langle B|A = a\rangle_\rho = \mathrm{tr}[\Pi_a\rho\Pi_a B]/\,\mathrm{tr}(\rho\Pi_a) = \mathrm{tr}[\rho\phi_a(B)]/\,\mathrm{tr}[\rho\phi_a(\mathbb{1})]. \tag{1}$$

For the second equality we introduced the map $\phi_a\colon X \mapsto \Pi_a X \Pi_a$, so that it becomes manifest that the conditioned expectation value on the l.h.s. arises directly from the laws of conditional probabilities and the quantum instrument $\mathcal{I}_\mathrm{L}\colon a \mapsto \phi_a$. (In literature, the notion of a Lüders instrument has been established, but it covers a broader set of instruments then those that follow Lüders's rule.)

The situation described in Eq. (1) can be further formalized. With the spectral decomposition $B = \sum b\mathrm{P}_b$, the probability to get firstly the outcome a and then the outcome b is

$$\mathbb{P}_\omega(\Pi_a \triangleright \mathrm{P}_b) = \omega[\phi_a(\mathrm{P}_b)], \tag{2}$$

where $\omega\colon X \mapsto \mathrm{tr}(\rho X)$ is a way to write the quantum state and $\Pi_a \triangleright \mathrm{P}_b$ is the event "Π_a then P_b."

Depending on the experimental implementation, the actual instrument $\mathcal{I}'$ will deviate from the instrument that has been described by Lüders. But there is confidence that $\mathcal{I}_\mathrm{L}$ can be approximated to an arbitrary precision, since on a formal level[7] one can implement $\mathcal{I}_\mathrm{L}$ by virtue of an ancilla system in a pure state, an entangling unitary between the probe and ancilla system, and a destructive measurement solely on the ancilla system. This shows that $\mathcal{I}_\mathrm{L}$ can be implemented as an immediate consequence of

(i) independent pure state preparation $\rho \mapsto \rho \otimes |\psi\rangle\langle\psi|$,

(ii) unitary evolution,

(iii) Born's rule, $\mathbb{P}_\omega(A = a) = \omega(\Pi_a)$.

However, any instrument can be implemented with the ingredients (i)–(iii). The question that drives our subsequent analysis is which of the properties of the instrument $\mathcal{I}_\mathrm{L}$ corresponding to Lüders's rule are most characteristic. Within the framework of quantum mechanics there would be a variety of possible characteristics that single out Lüders's rule

and without comparing to other possibilities, it would be difficult to argue in favor of one or another. Our approach is to broaden the mathematical concepts, so that not only quantum mechanics can be described but also a wider set of generalized probabilistic models is covered.

B. Positivity and generalized probabilistic models

Quantum events as well as classical events can be mathematical described by ordered vector spaces. This is based on the observation that the main characteristics of either theory is dominated by the notion of positivity. In particular in quantum mechanics, the (mixed) states are given by maps $\omega\colon X \mapsto \mathrm{tr}(\rho X)$ which obey $\omega(\mathbb{1}) = 1$ and $\omega(F) \geq 0$ for all positive semi-definite operators F. Conversely, a generalized measurement in quantum mechanics is a family of positive semi-definite operators (F_a) with $\sum_a F_a = \mathbb{1}$. The operators F_a are then called effects. This positivity structure is largely motivated from the probabilistic interpretation $\mathbb{P}_\omega(F_a) = \omega(F_a)$. The class of models which follows a similar interpretation is captured by the mathematical concept of an ordered vectors space. In turn, the set of models that can be fitted into this mathematical concept contains instances that are in conflict with the predictions of quantum mechanics[13,14]. For this reason, these models are called generalized probabilistic models.

We now discuss the mathematical concepts related to ordered vectors spaces while in Sec. I C we present explicit examples. For a more verbose introduction into the mathematical concepts we particularly recommend the introduction of Ref. 15 and the books by Alfsen [16] and Paulsen [17]. A real order unit vector space is a triple (V, V^+, e), such that

(i) V is a real vector space (not necessarily finite-dimensional).

(ii) $V^+ \subset V$ is a cone, i.e., $V^+ + V^+ = V^+ = \mathbb{R}^+ V^+$ and $V^+ \cap -V^+ = \{\, 0 \,\}$.

(iii) $e \in V^+$ is an order unit, i.e., for any $x \in V$ there is an $r \in \mathbb{R}^+$ such that $re + x \in V^+$.

We wrote $\mathbb{R}^+$ for the set of non-negative reals. It follows[15] that $V^+ - V^+ = V$. For two elements $x, y \in V$ the condition $x - y \in V^+$ defines a partial order and one writes $x \geq y$.

The order unit e is Archimedean provided that for any $x \in V$ the property $x + \mathbb{R}^+ e \subset V^+ \cup \{\, x \,\}$ implies $x \in V^+$. This property in some sense requires that V^+ is "closed." While we use this property merely for technical reasons, also note, that an order unit vector space can always be modified in such a way that it has an Archimedean order unit. This Archimedeanization[15] works by constructing the "closure" of the cone and identifying operationally indistinguishable elements. These operations are physically benign and hence we only consider Archimedean order unit vector (AOU) spaces.

We continue to fix notation. Within the dual space $V^* = \{\, \alpha\colon V \to \mathbb{R} \mid \alpha \text{ is linear} \,\}$ the set

$$\mathcal{S}(V, V^+, e) = \left\{\, \omega \in V^* \;\middle|\; \omega(e) = 1 \text{ and } \omega(V^+) \subset \mathbb{R}^+ \,\right\} \tag{3}$$

is the convex set of states and the definition

$$\|x\| = \inf\left\{\, r \in \mathbb{R}^+ \;\middle|\; -re \leq x \leq re \,\right\} \tag{4}$$

provides the order norm of $x \in V$. It is convenient to define the set of effects, i.e., the convex set of positive elements bounded by e,

$$V_e^+ = V^+ \cap (e - V^+), \tag{5}$$

and to write for the normalized representatives of the extremal rays of V^+ the symbol

$$\partial^+ V^+ = \{\, f \in V^+ \;|\; \|f\| = 1 \text{ and } (0 \leq g \leq f \text{ implies } g \in \mathbb{R}^+ f) \,\} \tag{6}$$

We occasionally construct V^+ from a finite set $\mathcal{A} \subset V$ of extremal rays via

$$\operatorname{cone} \mathcal{A} = \{\, x \in V \;|\; x = \textstyle\sum_{a \in \mathcal{A}} r_a\, a, \text{ where all } r_a \in \mathbb{R}^+ \,\}\,. \tag{7}$$

For two AOU spaces (V, V^+, e) and (W, W^+, e'), a linear map $\phi\colon V \to W$ is positive, provided that it maps positive elements to positive elements, $\phi(V^+) \subset W^+$. (When we let ϕ be a map, we always imply that ϕ is linear.) If $\phi(e) = e'$ then ϕ is unital. The spaces are order isomorphic, if there exists a positive unital bijection $\psi\colon V \to W$ such that its inverse is also positive.

Proposition 1. We recall three results from Ref. 15.

(i) $f \in V^+$ if and only if $\omega(f) \geq 0$ for all $\omega \in \mathcal{S}$.
(ii) If $f \in V^+$, then there exists a state $\omega \in \mathcal{S}$, such that $\omega(f) = \|f\|$.
(iii) For $x \in V$ we have $-\|x\| e \leq x \leq \|x\| e$.

In principle one is free to choose the AOU space (V, V^+, e) or the states $\mathcal{S} \subset U$ with some embedding vector space U as fundamental object. If $\mathcal{S}$ is fundamental, then[10] we can define V to be the space of affine functions on U, let $V^+ = \{\, \xi \in V \mid \xi(\mathcal{S}) \subset \mathbb{R}^+ \,\}$, and choose e with $e(\mathcal{S}) = \{\, 1 \,\}$. Since we do not want to make any particular point out of which space is fundamental, we may assume that V is reflexive, $V = V^{**}$. By virtue of Proposition 1 (i) this would imply that (V, V^+, e) and $[V^{**}, (V^{**})^+, e^{**}]$ are order isomorphic.

C. Examples of ordered vectors spaces

The reason why AOU spaces are considered to be a good framework to describe generalized probabilistic models is that classical events and quantum events can be described by means of AOU spaces[18,19]. For a recent introduction into the physical interpretation we refer to Ref. 20.

Classical events. A set of discrete classical events—e.g. the outcomes when rolling a dice—defines a so-called AOU lattice. It is the n-fold Cartesian product of $(\mathbb{R}, \mathbb{R}^+, 1)$, where n is the number of outcomes. The set of states is given by the maps $\mathbf{v} \mapsto \mathbf{p} \cdot \mathbf{v}$ with $\mathbf{p}_k \geq 0$ for all k, and $\sum_k \mathbf{p}_k = 1$. The order norm reads $\|\mathbf{v}\| = \max_k |\mathbf{v}_k|$, turning V into the Banach space ℓ_n^∞.

Quantum events. For quantum mechanics, we choose the bounded self-adjoint operators as vector space V and we identify V^+ to be the set of positive semi-definite operators. With the choice $e = \mathbb{1}$ this forms an AOU space, cf. Theorem 1.95 in Ref. 21. The set of quantum effects is V_e^+. The quantum states can be represented by the maps $X \mapsto \operatorname{tr}(\rho X)$ where ρ is positive semi-definite with $\operatorname{tr} \rho = 1$. (For infinite-dimensional Hilbert spaces, however, not all functionals in $\mathcal{S}$ can be written this way.) The order norm $\|X\|$ yields the operator norm of X and the extremal set $\partial^+ V^+$ is exactly the set of rank-one projections.

Dichotomic norm cones. A simple class of examples is constructed as $V = \mathbb{R} \times \mathbb{R}^d$, $V^+ = \{\, (t, \mathbf{x}) \mid t \geq \|\mathbf{x}\| \,\}$, and $e = (1, \mathbf{0})$, where $\|\mathbf{x}\|$ is a norm in $\mathbb{R}^d$. Such cones only allow

dichotomic observables in the sense that $e - \partial^+V^+ = \partial^+V^+$. However several interesting cases are instances of this example: the event space of tossing a coin (classical bit, $d = 1$ and $\|\mathbf{x}\| = |\mathbf{x}_1|$), the local part of a Popescu-Rohrlich box[13] (generalized bit[22], $d = 2$ and $\|\mathbf{x}\| = |\mathbf{x}_1| + |\mathbf{x}_2|$), the quantum mechanical two-level system (quantum bit, $d = 3$ and $\|\mathbf{x}\| = \sqrt{\mathbf{x} \cdot \mathbf{x}}$), and "hyperbits"[23] which generalize the quantum bit by allowing for $d > 3$ while keeping the Euclidean norm. The states for a dichotomic norm cone are the maps $(t, \mathbf{x}) \mapsto t + \mathbf{w} \cdot \mathbf{x}$ with $\|\mathbf{w}\|_* \leq 1$, where $\|\mathbf{w}\|_* \equiv \sup\{\, \mathbf{w} \cdot \mathbf{y} \mid \|\mathbf{y}\| \leq 1 \,\}$ is the dual norm. The order norm is also easy to evaluate, $\|(t, \mathbf{x})\| = |t| + \|\mathbf{x}\|$.

A pathological example. We define $V^+ = \operatorname{cone}\{\, a_1, a_2, \ldots, a_6 \,\}$ where $a_1, \ldots, a_4$ is a basis of V, $a_5 = a_1 - a_3 + a_4$, and $a_6 = a_2 + a_3 - a_4$. The order unit is chosen to be $e = a_1 + a_2 + \frac{1}{2}(a_3 + a_4)$. This case is pathological in the sense that there is no way to write $e = \sum_{v \in \mathcal{A}} v$ for any $\mathcal{A} \subset \{\, a_1, \ldots, a_6 \,\} = \partial^+V^+$.

II. SEQUENTIAL MEASUREMENTS

We now discuss sequential measurements for such generalized probabilistic models for which the measurement effects can be squeezed into an AOU space (V, V^+, e). That is, any measurement can be described by a family of effects $(f_k) \subset V_e^+$ with $\sum_k f_k = e$—this is in analogy to the generalized measurements that occur in quantum mechanics. Following the discussion in Sec. I A, we consider the situation that a sequence of two measurements has been performed and the consecutive outcomes $f, g \in V_e^+$ have occurred. What is the prediction for the probability $\mathbb{P}_\omega(f \triangleright g)$ for the event $f \triangleright g$, given that the system was in a state $\omega \in \mathcal{S}$?

This probability will clearly depend on the actual implementation of the first measurement and this implementation is readily summarized by a map $\phi\colon V \to V$, so that $\mathbb{P}_\omega(f \triangleright g) = \omega[\phi(g)]$. This implies that ϕ is positive and for consistency we assume $\phi(e) = f$, i.e., the all-embracing outcome e occurs with unit probability, given that previously the outcome f has occurred. We also assumed that ϕ is linear, so that performing with probability p a measurement with outcome g and with probability $1 - p$ a measurement with outcome h obeys $\mathbb{P}[f \triangleright pg + (1-p)h)] = p\mathbb{P}(f \triangleright g) + (1-p)\mathbb{P}(f \triangleright h)$. A positive map ϕ with $\phi(e) = f$ is called f-compatible[8].

In principle, any choice of an f-compatible map[1] may be suitable to describe $f \triangleright g$. Here we are concerned about the projective measurements which generalize Lüders's rule. The following notions capture important properties of Lüders's rule.

Definition 2. Let ϕ be an f-compatible map for $f \in V_e^+$, i.e., $\phi(e) = f$ and $\phi(V^+) \subset V^+$.

(i) ϕ is projective, if $\phi \circ \phi = \phi$.

(ii) ϕ is neutral, if $\omega \circ \phi = \omega$ for any $\omega \in \mathcal{S}$ with $\omega(f) = 1$.

(iii) ϕ is coherent, if $\phi(g) = g$ for any $g \in V^+$ with $g \leq f$.

One might be tempted to use f-compatible projections for defining a generalization of Lüders's rule. For an extremal element, $f \in \partial^+V^+$, such a map is of the form $\phi = f\omega$, where $\omega \in \mathcal{S}$ is a state with $\omega(f) = 1$ [the existence of such a state is due to Proposition 1 (ii)].

[1] In quantum mechanics we would be restricted to completely positive maps, but this subtlety can be ignored for the discussion here.

In quantum mechanics this already yields uniquely Lüders's rule for rank-one projections. Furthermore, any family $(f_k) \subset V_e^+$ with $\sum f_k \leq e$ and f_k-compatible projections ϕ_k enjoys perfect repeatability, $\phi_k \circ \phi_\ell = \delta_{k,\ell}\phi_k$, utilizing the Kronecker symbol $\delta_{k,\ell}$. This holds, since for $k \neq \ell$ and any $h \in V_e^+$ we have $0 \leq \phi_k\phi_\ell h \leq \phi_k\phi_\ell e = \phi_k f_\ell = -\phi_k(e - f_k - f_\ell) \leq 0$.

Unfortunately, projectivity does not sufficiently fix the choices for ϕ. For example, $\phi = e\omega$ is an e-compatible projection, but any subsequent measurement will solely depend on the arbitrary choice of $\omega \in \mathcal{S}$. Previously[9–12], filters have been considered as a possible extensions of Lüders's rule to generalized probabilistic models. A filter is a neutral f-compatible projection, but it is only called a filter if there also exists a neutral f-compatible projection for $e - f$. Here, we study a different extension of Lüders's rule, namely the coherent Lüders's rules.

Definition 3. A coherent Lüders's rule (CLR) for $f \in V_e^+$ is a coherent f-compatible map.

We occasionally write $f^\sharp$ for a CLR of f, although this map is not necessarily uniquely defined by the above condition.

A possible interpretation behind the definition of coherence is that the relation $g \leq f$ indicates that the outcome g provides always a finer information than f in the sense that independent of the state ω of the system, g is always less likely to be triggered than f. Thus getting firstly the course grained information f and then the fine grained information g is assumed not to influence g. Hence f preserves all the "coherences" of g. We also refer to Proposition 5, Proposition 6, the example of a triple-slit experiment in Sec. III C, and the Discussion in Sec. IV for further reasoning in favor of this definition. In Sec. II C it is also shown that neutral f-compatible projections and coherent f-compatible maps are different concepts.

A. Basic properties of coherent Lüders's rules

There are several equivalent ways of expressing Definition 3.

Lemma 4. For a positive map ϕ and an effect $f \in V_e^+$, the following statements are equivalent.

(i) $\phi(e) = f$ and $\phi(g) = g$ for all $0 \leq g \leq f$.

(ii) $\phi(e) \leq f$ and $\phi(g) \geq g$ for all $0 \leq g \leq f$.

(iii) $a \leq \phi(g) \leq f\|g\|$ for all $g \in V^+$, whenever $0 \leq a \leq f$ and $a \leq g$.

(iv) $a \leq \phi(g) \leq f$ for all $g \in V_e^+$, whenever $0 \leq a \leq f$ and $a \leq g$.

Proof. In order to see that (i) implies (iii), note that $\phi(g) = \phi(g-a) + a \geq a$. Furthermore, $f\|g\| - \phi(g) \geq 0$ follows immediately when considering $\phi(\|g\|e - g) \geq 0$ and by fact that $\|g\|e \geq g$ holds since e is Archimedean.

Obviously (iii) implies (iv), since for $g \in V_e^+$ we have $\|g\| \leq 1$.

Statement (ii) follows from (iv) by letting $g_{(\mathrm{iv})} = e$ (yielding $\phi(e) \leq f$) and by choosing $g_{(\mathrm{iv})} = g_{(\mathrm{ii})} = a$ (yielding $\phi(g_{(\mathrm{ii})}) \geq g_{(\mathrm{ii})}$).

We finally show that (i) follows from (ii). We first use that $\phi(e - f) \geq 0$ and thus $f \geq \phi(e) \geq \phi(f) \geq f$, i.e., $\phi(e) = f = \phi(f)$. Then $\phi(g) - g \leq \phi(f) - f \equiv 0$, where the inequality follows from $f - g \leq \phi(f - g)$, which is due to $0 \leq f - g \leq f$. But $\phi(g) \leq g$ can only be compatible with $\phi(g) \geq g$ when $\phi(g) = g$. □

Note, that with statement (iv) of this lemma, we have $\phi(h) = f$ for $f \leq h \leq e$, by letting $a = f$ and $g = h$.

From a physical perspective, a CLR for f describes exactly such a measurement that does not disturb any other subsequent measurement with outcome f.

Proposition 5. Let $\mathcal{C} \supset (V^+ \otimes \mathcal{S})$ be some cone of positive maps and let ϕ be an f-compatible map for $f \in V_e^+$. Then ϕ is coherent if and only if $\phi \circ \psi = \psi$ holds for all f-compatible maps $\psi \in \mathcal{C}$.

Proof. If ψ is f-compatible, then $\psi(h) \leq \psi(e) = f$ for any $h \in V_e^+$. It follows that $\phi \circ \psi = \psi$ if ϕ is a CLR. For the converse we consider $\psi = (f-g)\omega + g\sigma \in \mathcal{C}$ with $0 \leq g \leq f$ and $\omega, \sigma \in \mathcal{S}$. This map is clearly f-compatible and we define $\Delta \equiv \phi\circ\psi - \psi = [\phi(f)-f]\omega + [\phi(g)-g](\sigma-\omega)$. From $\Delta(e) = 0$ we obtain $\phi(f) = f$ and assuming $\sigma \neq \omega$, also $\phi(g) = g$ must hold. Hence ϕ is coherent. □

A CLR in particular obeys repeatability and compatibility.

Proposition 6. Let $f^\sharp$ and $g^\sharp$ be two CLRs for $f, g \in V_e^+$, respectively. We have:

(i) $f^\sharp$ is projective.

(ii) If $g \leq f$ then $f^\sharp g = g^\sharp f$.

(iii) If $g \leq f$ and $g^\sharp$ is unique for g, then $f^\sharp g^\sharp = g^\sharp f^\sharp$.

Proof. We implicitly use Lemma 4 (iv). Then $f^\sharp h \leq f$ for any $h \in V_e^+$ and hence $f^\sharp(f^\sharp h) = f^\sharp h$. If $g \leq f$ then immediately $f^\sharp g = g = g^\sharp f$ (cf. also the remark after Lemma 4). If the CLR for g is unique then $f^\sharp g^\sharp = g^\sharp f^\sharp$, since $f^\sharp g^\sharp = g^\sharp$ and on the other hand $g^\sharp f^\sharp$ is a valid CLR for g. □

We mention that the property of being neutral or coherent is robust under sections. A section[24] is a positive unital injection τ from (W, W^+, e') to (V, V^+, e), such that there exists a positive surjection $\tau' \colon V \to W$ with $\tau' \circ \tau = \mathrm{id}_W$. If ϕ is a neutral/coherent $\tau(f)$-compatible map, then $\tau' \circ \phi \circ \tau$ is a neutral/coherent f-compatible map. An important instance of this observation is the embedding of the classical events into quantum events via $\tau \colon \mathbf{v} \mapsto \mathrm{diag}(\mathbf{v})$. In contrast, general $\tau(f)$-compatible projections do not always induce f-compatible projections.

B. Conditions on elements with a coherent Lüders's rule

Not all $f \in V_e^+$ admit a CLR as we see next. But the CLR for e is the identity mapping, while for 0 it is the zero mapping. On the other hand, if f is extremal, $f \in \partial^+ V^+$, then any f-compatible projection is a CLR. For the general situation we have

Proposition 7. For $f \in V_e^+$ consider the following statements.

(i) f admits a CLR.

(ii) $g \leq f\|g\|$ for all $0 \leq g \leq f$.

(iii) $0 \leq g \leq f$ and $g \leq e - f$ only for $g = 0$.

Then (i) implies (ii) and (ii) implies (iii).

Proof. Statement (ii) is a direct consequence of Lemma 4 (iii), $g = f^\sharp g \leq f\|g\|$. For the second part we consider $0 \leq g \leq f \leq e - g$. Then $0 \leq g \leq f\|g\| \leq \|g\|(e-g)$ and therefore $e\|g\|/(\|g\|+1) \geq g$, which contradicts $\|g\| \equiv \inf\{\, r \in \mathbb{R}^+ \mid re \geq g \,\}$ unless $\|g\| = 0$. By the Archimedean property the assertion follows. □

From part (ii) of this proposition it immediately follows that if $f = \sum_k p_k f_k$ with $(f_k) \subset \partial^+ V^+$ and real numbers $p_k > 0$ then already $f_k \leq f$. But one cannot conclude that there exists a decomposition of f into extremal elements with unit weights, cf. the pathological example form Sec. I C with $f = e$. This pathological space also provides an example where (iii) does not imply (ii). The counterexample works with $f = e - a_1 - a_2 \equiv (a_3 + a_4)/2$, which obeys (iii). But $f - pa_3 \geq 0$ only for $p \leq \frac{1}{2}$ in contradiction to (ii). At the moment it remains unclear whether (ii) implies (i), even though it does not seem plausible to hold. On the other hand, for quantum mechanics, already statement (iii) can only hold if F is a projection since $0 \leq \sqrt{F}(\mathbb{1} - F)\sqrt{F} \equiv F - F^2 \leq F$ and $0 \leq (\mathbb{1} - F)^2 \equiv \mathbb{1} - 2F + F^2$, i.e., $F - F^2 \leq \mathbb{1} - F$. By assumption we then have $F - F^2 = 0$ and hence F is a projection.

C. Neutral maps

Neutral f-compatible projections have been suggested previously[9–12] as an extension of Lüders's rule to generalized probabilistic models. For the moment we call them neutral Lüders's rules (NLRs). If f and $e - f$ allow an NLR, then an NLR for f is a filter. We observe:

1. Some elements do not have an NLR, despite being extremal. Consider the dichotomic norm cone (cf. Sec. I C) with $\|\mathbf{x}\| = \sum |\mathbf{x}_i|$ and $d \geq 2$. In this case, there exists no neutral map ϕ for any of the extremal elements $f \in \partial^+ V^+$ since states with $\omega(f) = 1$ are not unique but on the other hand $\phi = f\omega$ must hold for ϕ to be an f-compatible projection.

2. Some elements with an NLR do not have a CLR. An example occurs in the pathological example from Sec. I C for the effect $f = e - a_1 - a_2$. As demonstrated at the end of Sec. II B this element does not have a CLR. But the only state with $\omega(f) = 1$ is $\omega(a_k) = (0,0,1,1,0,0)_k$ and hence $f\omega$ is an NLR for f. One can also construct an NLR for the complement $f_\neg = e - f$, showing that $f\omega$ is a filter. The NLR for $f_\neg$ is not unique, but a possible representative is given by $a_1\omega_1 + a_2\omega_2$ with $\omega_i(a_k) = \delta_{i,k} + \delta_{i+4,k}$.

III. APPLICATIONS

A. Quantum mechanics

In quantum mechanics, $F \in V_e^+$ admits a CLR if and only if it is a projection. We have shown necessity in Sec. II B and in order to show sufficiency we assume that F is a projection and that $F^\sharp(X) = FXF$. It remains to show that $G = FGF$ for any $0 \leq G \leq F$. Although this is an easy and well-known relation, we shall spend a few lines to show it: We write $F_\neg = \mathbb{1} - F$. Then $0 \leq F_\neg(F - G)F_\neg = -F_\neg G F_\neg \leq 0$ and thus $F_\neg G = F_\neg G F$. But $0 \leq (F + \lambda F_\neg)G(F + \lambda F_\neg) = FGF + \lambda(F_\neg GF + FGF_\neg)$ for all $\lambda \in \mathbb{R}$ implies $F_\neg GF = -FGF_\neg$, i.e., $G = FGF$.

The rule $F^\sharp\colon X \mapsto FXF$ is unique as we demonstrate by construction. Assume $G \in V_e^+$. Then $0 \leq F(\mathbb{1} - G)F = F - FGF$ implying $F^\sharp(FGF) = FGF$ and $0 \leq F^\sharp[F_\neg(\mathbb{1} - G)F_\neg] =$

$-F^\sharp(F_\neg G F_\neg)$ which yields $F^\sharp(F_\neg G F_\neg) = 0$. With $G'_\lambda \equiv (F + \lambda F_\neg) G (F + \lambda F_\neg) \geq 0$ we have

$$F^\sharp(G'_\lambda) = FGF + \lambda A \geq 0, \text{ where } A = F^\sharp(F_\neg G F + F G F_\neg), \tag{8}$$

for all $\lambda \in \mathbb{R}$. This implies again $A = 0$ and hence $F^\sharp(G) \equiv F^\sharp(G'_1) = FGF$.

We mention that we did not assume that $F^\sharp$ is completely positive but nevertheless obtained the intended quantum mechanical Lüders's rule.

B. Dichotomic norm cones

As a second example, we consider the dichotomic norm cones of Sec. I C. For this AOU spaces the set of effects admitting a CLR is given by $\{0, e\} \cup \partial^+ V^+$, cf. Appendix A. This shows that dichotomic norm cones form a very convenient toy model for which basically the assumption of an f-compatible projection alone leads to a reasonable Lüders's rule. Put into an explicit form, any extremal element $f \in \partial^+ V^+$ is of the form $f = (\frac{1}{2}, \mathbf{f})$ with $\|\mathbf{f}\| = \frac{1}{2}$ and any corresponding CLR reads thus

$$f^\sharp \colon (t, \mathbf{x}) \mapsto (t + \mathbf{f}' \cdot \mathbf{x}) f, \text{ with } \mathbf{f}' \cdot \mathbf{f} = \tfrac{1}{2}, \text{ and } \|\mathbf{f}'\|_* = 1. \tag{9}$$

Since the set of CLRs for a given effect f is convex, it follows that if $\|\mathbf{x}\|$ is a p-norm with $1 < p < \infty$ then the CLR is unique. This is due to the fact that then the dual norm $\|\mathbf{x}\|_*$ is the $[p/(p-1)]$-norm, the unit-sphere of which only has convex subsets with a single vector. On the other hand, for the Manhattan Norm, $p = 1$, and e.g. $\mathbf{f} = (\frac{1}{2}, 0, \ldots, 0)$ the available choices are any of $\mathbf{f}' = (1, \xi_2, \ldots, \xi_d)$ with arbitrary coefficients $-1 \leq \xi_k \leq 1$.

As an example we compute the effective "observable" for an sequential measurement of two dichotomic observables $A = a - a_\neg$ and $B = b - b_\neg$ with $a_\neg = e - a$ and $b_\neg = e - b$. That is, with the notation $A\sharp = a^\sharp - a^\sharp_\neg$, we aim at $A\sharp B$. For simplicity we assume that in $a^\sharp$ and $a^\sharp_\neg$ we have $\mathbf{a}'_\neg = -\mathbf{a}'$, which surely holds when both CLRs are unique. Writing $b = (\beta, \mathbf{b})$ yields

$$A\sharp B = (2\beta - 1)A + 2(\mathbf{a}' \cdot \mathbf{b})e. \tag{10}$$

If $\beta = \frac{1}{2}$, e.g., because b is extremal, then the expected value $\langle A\sharp B \rangle_\omega \equiv \omega(A\sharp B)$ does not depend on the prepared state ω. For the case of the Euclidean norm, $\|\mathbf{x}\| = \sqrt{\mathbf{x} \cdot \mathbf{x}}$, and $B\sharp$ defined analogously to $A\sharp$, we find in addition $A\sharp B = B\sharp A$. Both aspects have been observed already for qubits[25] which corresponds to the dichotomic norm cone with $d = 3$ and the Euclidean norm.

Dichotomic norm cones can have strong non-quantum behavior. As an example we consider the simplest correlation term $\langle \mathrm{LG}' \rangle$,

$$\langle \mathrm{LG}' \rangle_\omega = \omega(A\sharp B + B - A). \tag{11}$$

For so-called macro-realistic systems (which are in our language CLR measurements on the classical events) the constraint $\langle \mathrm{LG}' \rangle \leq 1$ is valid[26], while for quantum mechanics the bound $\langle \mathrm{LG}' \rangle \leq \frac{3}{2}$ is in order[27]. Note, that the quantum mechanical bound only holds for CLRs[28]. For dichotomic norm cones and assuming again that always $\mathbf{a}' = -\mathbf{a}'_\neg$ we obtain the sharp bound (cf. Appendix B)

$$\langle \mathrm{LG}' \rangle \leq 2\|\mathbf{b} - \mathbf{a}\| + 2\mathbf{a}' \cdot \mathbf{b}, \text{ where } \|\mathbf{b}\| = \tfrac{1}{2}. \tag{12}$$

In the case of the Manhattan norm, $\|\mathbf{x}\| = \sum |\mathbf{x}_k|$, and $d = 2$ we find that the r.h.s. of this inequality can easily reach 3 by choosing $\mathbf{a} = (\frac{1}{2}, 0)$, $\mathbf{b} = (0, \frac{1}{2})$, and $\mathbf{a}' = (1, 1)$.

We finally mention that Spekkens's toy model[1] implements a CLR. In this model, there are six extremal elements $\partial^+ V^+ = \{ a_{\pm 1}, a_{\pm 2}, a_{\pm 3} \}$ given by $a_i = (\frac{1}{2}, \mathbf{a}_{(i)})$, with

$$\mathbf{a}_{(\pm 1)} = (\pm\tfrac{1}{2}, 0, 0),\ \mathbf{a}_{(\pm 2)} = (0, \pm\tfrac{1}{2}, 0), \text{ and } \mathbf{a}_{(\pm 3)} = (0, 0, \pm\tfrac{1}{2}). \tag{13}$$

These elements form observables $A_k = a_{+k} - a_{-k}$ and hence $e = a_{+k} + a_{-k} \equiv (1, \mathbf{0})$. This way Spekkens's toy model is the dichotomic norm cone with $d = 3$ and the Manhattan norm. Spekkens also introduced a state update rule for this model, which is such that

$$\mathbb{P}(a_i \triangleright a_j) = \mathbb{P}(a_i) \begin{cases} 1 & i = j, \\ 0 & i = -j, \\ \frac{1}{2} & \text{else.} \end{cases} \tag{14}$$

This update rule corresponds to the CLR defined in Eq. (9) with the choice $\mathbf{a}'_{(i)} = 2\mathbf{a}_{(i)}$.

C. The triple-slit experiment

While the double-slit experiment is a prime example of a quantum effect, within quantum mechanics there are no higher order interference terms, as has been found by Sorkin[29]. This absence was also verified in experiments[30]. Recently, the triple-slit experiment has been investigated as instance of sequential measurements in the context of generalized probabilistic models[12] and the (im)possibility of triple-slit correlations in such models was discussed e.g. in Refs. 31 and 32.

In an n-slit experiment with slits labeled by $\mathcal{N} = \{ 1, 2, \ldots, n \}$, detecting that the particle passed through any of the slits $\alpha \subset \mathcal{N}$ plays the role of the first measurement, described by a map ϕ_α. The measurement of the interference pattern on the screen is hence the second measurement. Each possible combination of open slits α may have its particular interference pattern as long as the integrated intensity is independent of whether the slits are opened individually or jointly, so that $\phi_\alpha(e) = \sum_{k \in \alpha} \phi_{\{k\}}(e)$. Clearly, the total intensity is bounded by unity, so that $\phi_{\mathcal{N}}(e) \in V_e^+$.

We discuss now briefly the assumption that ϕ_α is coherent for the effect $\phi_\alpha(e)$ and hence is a CLR. Assume that the probability for an effect g depends only on the integrated intensity that arrives through the slits α, i.e., $\phi_\alpha(e) \equiv \sum_{k \in \alpha} \phi_{\{k\}}(e) \geq g$. In this case, the coherence assumption $\phi_\alpha(g) = g$ assures that putting the simultaneously opened slits α in front of a measurement with outcome g does not change that outcome.

We recursively define (in general non-positive) maps η_α via

$$\phi_\alpha = \sum_{\beta \subset \alpha} \eta_\beta. \tag{15}$$

Then those maps η_α are exactly the interference terms $I_{|\alpha|}(\alpha)$ as defined by Sorkin[29], adapted to the language chosen here. In Eq. (15) we try to write the map on the l.h.s. in terms of the lower order correlations. The difference between the actual map ϕ_α and this lower order sum is then defined as η_α.

In a quantum mechanical n-slit experiment the slits are described by projections Π_k obeying $\sum \Pi_k \leq \mathbb{1}$. We let $\Pi_\alpha = \sum_{k\in\alpha} \Pi_k$ and therefore

$$\phi_\alpha \colon X \mapsto \Pi_\alpha X \Pi_\alpha \equiv \sum_{\beta\subset\alpha\colon |\beta|\leq 2} \eta_\beta(X), \tag{16}$$

that is, $\eta_\beta = 0$ whenever $|\beta| > 2$. That is, in quantum mechanics all interference terms above the second order vanish. We mention that in general this absence only occurs if the quantum instrument follows Lüders's rule, as a counterexample may serve $\phi_\alpha \colon X \mapsto \sqrt{A_\alpha} X \sqrt{A_\alpha}$ with $A_\alpha = \sum_k A_k$ and $A_1 = \mathbb{1}/2$, $A_2 = |0\rangle\langle 0|/2$, $A_3 = |1\rangle\langle 1|/2$. Such measurements, however, may fail to have a proper physical interpretation as a triple-slit experiment, since the operators A_k may act non-locally.

For generalized probabilistic models, though, we can easily have higher order correlations: Consider the AOU space with $V^+ = \operatorname{cone}\{a_1, \ldots, a_5\}$, where $a_1, \ldots, a_4$ is a basis of V, $a_5 = a_1 + a_2 + a_3 - a_4$, and $e = a_1 + a_2 + a_3 \equiv a_4 + a_5$. We choose $\phi_\alpha(e) = \sum_{k\in\alpha} a_k$ for $\alpha \subset \{1, 2, 3\} \equiv \mathcal{N}$. A brief calculation yields for $\alpha \subsetneq \mathcal{N}$,

$$\phi_\alpha = \sum_{k\in\alpha} a_k \omega_k^\alpha \tag{17}$$

where ω_k^α are arbitrary choices of states with $\omega_k^\alpha(a_k) = 1$. Since those states are not unique, we can e.g. use this freedom to achieve commutativity, $\phi_\alpha \circ \phi_\beta = \phi_\beta \circ \phi_\alpha$, or to get vanishing double-slit correlations, $\eta_{\{k,\ell\}} = 0$. In contrast, the map for the triple-slit is the identity mapping, $\phi_\mathcal{N} = e^\sharp \equiv \mathrm{id}$. From Eq. (17) we see that $a_4 \notin \eta_\alpha(V)$ except for $\alpha = \mathcal{N}$, i.e., nonvanishing triple-slit correlations occur.

IV. DISCUSSION

An important property of quantum systems is that the measurement necessarily changes the state of the system—or in a Heisenberg type-of-picture that the description of a measurement depends on previous measurements that have been performed. How this change occurs in general depends on the actual implementation of the measurement. In quantum mechanics, however, the change induced by projective measurements according to Lüders is the least disturbing and least biased implementation of a projective measurement. We re-derived this rule in quantum mechanics (cf. Sec. III A) solely from the coherence assumption stated in Definition 3. This definition of coherent Lüders rules (CLRs) can be applied to a wide class of hypothetical non-quantum models, namely the generalized probabilistic models which can described by means of Archimedean ordered vector spaces.

We showed in Proposition 5 that CLRs are exactly those maps which do not disturb any subsequent and possibly more "noisy" implementation of the same measurement. We also showed that familiar results of repeatability and compatibility hold (Proposition 6, cf. also Refs. 9 and 11).

In quantum mechanics, Lüders's rule is directly linked to and singles out the projection operators, which in turn play a key role e.g. in spectral theory. (Celebrated results for a generalized spectral theory[10,33,34] are, however, linked to neutral maps.) We find that for extremal measurement effects (a generalization of rank-one projections in quantum mechanics) an CLR always exists, while necessary conditions for existence have been given in Proposition 7. Also, in certain pathological cases, the CLR is not unique. This ambiguity might be

unsatisfactory, but for quantum mechanics and classical mechanics the conditions of being a CLR are sufficient to achieve uniqueness, so that adding any further condition is of a rather speculative kind.

Finally we demonstrated in Sec. III B that CLRs occurred already earlier in Spekkens's toy model[1] and that this toy model can now be seen as an instance of a much wider class of models with a natural notion of sequential measurements. For those models it is e.g. straightforward to compute the upper limit for the Leggett-Garg inequality in Eq. (12). As a last instance we discussed in Sec III C the triple-slit experiment, finding that generalized probabilistic models with a CLR can easily have substantial triple-slit correlations, while it is an important prediction of quantum mechanics that those are absent.

ACKNOWLEDGMENTS

The proof of Lemma 4 was simplified by one of the anonymous referees. For discussions, hints, and amendments I am particularly indebted to J. Emerson, O. Gühne, R. Hübener, J.-Å. Larsson, V.B. Scholz, M. Ziman, and Z. Zimborás. I thank the Centro de Ciencias de Benasque, where part of this work has been done, for its hospitality during the workshop on quantum information 2013. I acknowledge support from the BMBF (Chist-Era Project QUASAR), the Brazilian agency CAPES, through the program Science without Borders, the DFG, the EU (Marie Curie CIG 293993/ENFOQI), and the FQXi Fund (Silicon Valley Community Foundation).

Appendix A: Elements with a coherent Lüders's rule in dichotomic norm cones

In a dichotomic norm cone (cf. Sec. I C), the set of effects admitting a CLR is given by $\{0, e\} \cup \partial^+ V^+$, as stated in Sec. III B. For $f = (t, \mathbf{f}) \in V_e^+$ we have $\|f\| = 1$ if and only if $t = 1 - \|\mathbf{f}\|$ and $\|\mathbf{f}\| \leq \frac{1}{2}$. Assume now that f admits a CLR, but $0 \neq f \neq e$. By virtue of Proposition 7 (ii) it follows that $\|f\| = 1$ and $\|\mathbf{f}\| = \frac{1}{2}$. The first statement is obtained by choosing $g = f$ and the second statement by the choice $0 \leq g = (1 - 2\|\mathbf{f}\|)e = f - (\|\mathbf{f}\|, \mathbf{f}) \leq f$. If now $a \in \partial^+ V^+$ and $p > 0$, such that $pa \leq f$, then also $a \leq f$. This reads $\frac{1}{2} - \frac{1}{2} \geq \|\mathbf{f} - \mathbf{a}\|$ and therefore $f = a$.

Appendix B: Obtaining Eq. (12)

Under the result $A \sharp B = (2\beta - 1)A + 2(\mathbf{a}' \cdot \mathbf{b})e$ [Eq. (10)] we bound the correlation term $\langle \mathrm{LG}' \rangle_\omega = \omega(A \sharp B + B - A)$ [Eq. (11)] for dichotomic norm cones, assuming $A = a - a_\neg = (0, 2\mathbf{a})$, and $B = b - b_\neg = (2\beta - 1, 2\mathbf{b})$. Writing $\omega = (1, \mathbf{w})$, this yields for $\mathbf{b} \neq \mathbf{0}$,

$$\begin{aligned} \tfrac{1}{2}\langle \mathrm{LG}' \rangle_\omega &= \mathbf{a}' \cdot \mathbf{b} + \mathbf{w} \cdot (\mathbf{b} - \mathbf{a}) + (2\beta - 1)(\mathbf{w} \cdot \mathbf{a} + \tfrac{1}{2}) \\ &\leq \|\mathbf{b}\|[\mathbf{a}' \cdot \underline{\mathbf{b}} + \|\underline{\mathbf{b}} - 2\mathbf{a}\| - 1] + \tfrac{1}{2} \end{aligned} \tag{B1}$$

with $\underline{\mathbf{b}} = \mathbf{b}/\|\mathbf{b}\|$. The inequality is due to $\beta \leq 1 - \|\mathbf{b}\|$, $\|\mathbf{w}\|_* \leq 1$, and $\mathbf{w} \cdot \mathbf{a} \geq -\frac{1}{2}$. The bound is sharp, if $\beta = 1 - \|\mathbf{b}\|$ and $\mathbf{w} \cdot (\underline{\mathbf{b}} - 2\mathbf{a}) = \|\underline{\mathbf{b}} - 2\mathbf{a}\|$. Using the conditions from Eq. (9), we have $\|\underline{\mathbf{b}} - 2\mathbf{a}\| \geq -\mathbf{a}' \cdot (\underline{\mathbf{b}} - 2\mathbf{a}) = 1 - \mathbf{a}' \cdot \underline{\mathbf{b}}$ and hence the term in square brackets is never negative. This makes the choice $\|\mathbf{b}\| = \frac{1}{2}$ optimal and we arrive at the sharp bound of Eq. (12).

[1]R. W. Spekkens, "Evidence for the epistemic view of quantum states: A toy theory," Phys. Rev. A **75**, 032110 (2007).

[2]A. Peres, *Quantum Theory: Concepts and Methods* (Kluwer, Dordrecht, 1995).

[3]W. M. Itano, D. J. Heinzen, J. J. Bollinger, and D. J. Wineland, "Quantum Zeno effect," Phys. Rev. A **41**, 2295–2300 (1990).

[4]G. Kirchmair, F. Zähringer, R. Gerritsma, M. Kleinmann, O. Gühne, A. Cabello, R. Blatt, and C. F. Roos, "State-independent experimental test of quantum contextuality," Nature (London) **460**, 494–497 (2009).

[5]G. Lüders, "Über die Zustandsänderung durch den Meßprozeß," Ann. Phys. (Leipzig) **443**, 323–328 (1951).

[6]G. Lüders, "Concerning the state-change due to the measurement process," Ann. d. Phys. **15**, 663–670 (2006).

[7]M. Ozawa, "Quantum measuring processes of continuous observables," J. Math. Phys. **25**, 79–87 (1984).

[8]T. Heinosaari and M. Ziman, *The mathematical language of quantum theory: from uncertainty to entanglement* (Cambridge University Press, Cambridge, New York, 2012).

[9]B. Mielnik, "Theory of filters," Comm. Math. Phys. **15**, 1–46 (1969).

[10]H. Araki, "On a characterization of the state space of quantum mechanics," Comm. Math. Phys. **75**, 1–24 (1980).

[11]G. Niestegge, "A representation of quantum measurement in order-unit spaces," Found. Phys. **38**, 783–795 (2008).

[12]C. Ududec, H. Barnum, and J. Emerson, "Three slit experiments and the structure of quantum theory," Found. Phys. **41**, 396–405 (2011).

[13]S. Popescu and D. Rohrlich, "Quantum nonlocality as an axiom," Found. Phys. **24**, 379–385 (1994).

[14]P. Janotta, "Generalizations of boxworld," EPTCS **95**, 183–192 (2012).

[15]V. I. Paulsen and M. Tomforde, "Vector spaces with an order unit," Indiana Univ. Math. J. **58**, 1319–1359 (2009).

[16]E. M. Alfsen, *Compact convex sets and boundary integrals*, Ergebnisse der Mathematik und ihrer Grenzgebiete No. 57 (Springer, Berlin, 1971).

[17]V. I. Paulsen, *Completely bounded maps and operator algebras*, Cambridge Studies in Advanced Mathematics No. 78 (Cambridge University Press, Cambridge, 2002).

[18]G. Ludwig, *An Axiomatic Basis for Quantum Mechanics*, Vol. I-II (Springer-Verlag, Berlin, 1987).

[19]P. Mittelstaedt, *The Interpretation of Quantum Mechanics and the Measurement Process* (Cambridge University Press, Cambridge, 1998).

[20]H. Barnum and A. Wilce, "Information processing in convex operational theories," Electron. Notes Theor. Comput. Sci. **270**, 3–15 (2011).

[21]E. M. Alfsen and F. W. Shultz, *State spaces of operator algebras: basic theory, orientations and $C*$-products* (Birkhäuser, Boston, 2001).

[22]J. Barrett, "Information processing in generalized probabilistic theories," Phys. Rev. A **75**, 032304 (2007).

[23]M. Pawłowski and A. Winter, ""Hyperbits": The information quasiparticles," Phys. Rev. A **85**, 022331 (2012).

[24]M. Kleinmann, T. J. Osborne, V. B. Scholz, and A. H. Werner, "Typical local measurements in generalized probabilistic theories: Emergence of quantum bipartite correlations," Phys. Rev. Lett. **110**, 040403 (2013).

[25]T. Fritz, "On the existence of quantum representations for two dichotomic measurements," J. Math. Phys. **51**, 052103 (2010).

[26]A. J. Leggett and A. Garg, "Quantum mechanics versus macroscopic realism: Is the flux there when nobody looks?" Phys. Rev. Lett. **54**, 857–860 (1985).

[27]C. Budroni, T. Moroder, M. Kleinmann, and O. Gühne, "Bounding temporal quantum correlations," Phys. Rev. Lett. **111**, 020403 (2013).

[28]C. Budroni and C. Emary, "Temporal quantum correlations and leggett-garg inequalities in multilevel systems," Phys. Rev. Lett. **113**, 050401 (2014).

[29]R. D. Sorkin, "Quantum mechanics as quantum measure theory," Mod. Phys. Lett. A **9**, 3119–3127 (1994).

[30]U. Sinha, C. Couteau, T. Jennewein, R. Laflamme, and G. Weihs, "Ruling out multi-order interference in quantum mechanics," Science **329**, 418–421 (2010).

[31]G. Niestegge, "Conditional probability, three-slit experiments, and the Jordan algebra structure of quantum mechanics," Adv. Math. Phys. **2012**, 156573 (2012).

[32]B. Dakić, T. Paterek, and Č. Brukner, "Density cubes and higher-order interference theories," New J. Phys. **16**, 023028 (2014).

[33]E. M. Alfsen and F. W. Shultz, "Non-commutative spectral theroy for affine function spaces on convex sets," Memoirs AMS **6**, 1–120 (1976).

[34]E. M. Alfsen and F. W. Shultz, *Geometry of state spaces of operator algebras* (Birkhäuser, Boston, 2003).

Systematic errors in current quantum state tomography tools

Christian Schwemmer,[1,2] Lukas Knips,[1,2] Daniel Richart,[1,2] and Harald Weinfurter[1,2]
[1] *Max-Planck-Institut für Quantenoptik, Hans-Kopfermann-Str. 1, D-85748 Garching, Germany and*
[2] *Department für Physik, Ludwig-Maximilians-Universität, D-80797 München, Germany*

Tobias Moroder,[3] Matthias Kleinmann,[3] and Otfried Gühne,[3]
[3] *Naturwissenschaftlich-Technische Fakultät, Universität Siegen, Walter-Flex-Str. 3, D-57068 Siegen, Germany*

Common tools for obtaining physical density matrices in experimental quantum state tomography are shown here to cause systematic errors. For example, using maximum likelihood or least squares optimization for state reconstruction, we observe a systematic underestimation of the fidelity and an overestimation of entanglement. A solution for this problem can be achieved by a linear evaluation of the data yielding reliable and computational simple bounds including error bars.

PACS numbers: 03.65.Ud, 03.65.Wj, 06.20.Dk

Introduction.—Quantum state tomography (QST) [1] enables us to fully determine the state of a quantum system and thereby to deduce all its properties. As such QST is widely used to characterize and to evaluate numerous experimentally implemented qubit states or their dynamics, e.g., in ion trap experiments [2, 3], photonic systems [4, 5], superconducting circuits [6], or nuclear magnetic resonance systems [7, 8]. The increasing complexity of todays multiqubit/qudit quantum systems brought new challenges but also progress. Now, highly efficient methods allow an even scalable analysis for important subclasses of states [9, 10]. The calculation of errors of QST was significantly improved although the errors remain numerically expensive to evaluate for larger systems [11]. Moreover QST was used to detect systematic errors in the alignment of an experiment itself [12].

A central step in QST is to establish the state from the acquired experimental data. A direct, linear evaluation of the data returns almost for sure an unphysical density matrix with negative eigenvalues [13]. Thus, several schemes have been developed to obtain a physical state which resembles the observed data as closely as possible [4, 14, 15].

In this Letter we test whether the naïve expectation is met that QST delivers proper estimates for physical quantities. We test this for the two most commonly used reconstruction schemes—maximum likelihood (ML) [15] and least squares (LS) [4]—using Monte Carlo simulations. This expectation is not fulfilled: both schemes return states which deviate systematically from the true state, e.g., underestimate the fidelity as shown in Fig. 1. For data sizes typical in multiqubit experiments the deviation from the true value is significant, in fact it is larger than commonly deduced "error bars" [16]. We show that the constraint of physicality necessarily leads to systematic errors for the reconstruction scheme. The size of these errors depends on the experimental noise and unavoidable statistical fluctuations. We find that it is advisable to evaluate linear operators directly on the raw data. We also show how physical quantities that

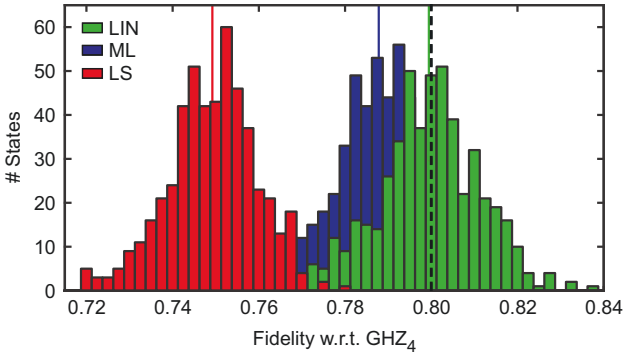

FIG. 1: (Color online) Histogram of the fidelity estimates of 500 independent simulations of QST of a noisy four-party Greenberger-Horne-Zeilinger (GHZ) state for three different reconstruction schemes. The values obtained via maximum likelihood (ML, blue) or least squares (LS, red) fluctuate around a value that is lower than the initial fidelity of 80% (dashed line). For comparison, we also show the result using linear inversion (LIN, green), which does not suffer from such a systematic error called bias.

are given by convex (concave) nonlinear functions of the density matrix like the bipartite negativity etc., can be linearized thereby providing a meaningful lower (upper) bound, namely a directly computable error bar.

Standard state tomography tools.—The aim of QST is to identify the initially unknown state ϱ_0 of a system via appropriate measurements on multiple preparations of this state. For an n-qubit system, the so-called Pauli tomography scheme consists of measuring in the eigenbases of all 3^n possible combinations of local Pauli operators, each yielding 2^n possible results [4]. In more general terms, in a tomography protocol one repeats for each measurement setting s the experiment a certain number of times N_s and obtains c_r^s times the result r. These numbers then yield the frequencies $f_r^s = c_r^s/N_s$. The probability to observe the outcome r for setting s is given by $P_{\varrho_0}^s(r) = \mathrm{tr}(\varrho_0 M_r^s)$. Here, M_r^s labels the measurement

operator corresponding to the result r when measuring setting s. The probabilities $P^s_{\varrho_0}(r)$ will uniquely identify the unknown state ϱ_0, if the set of operators M^s_r spans the space of Hermitian operators.

Provided the data f, i.e., the set of experimentally determined frequencies f^s_r one requires a method to determine the estimate $\hat{\varrho} \equiv \hat{\varrho}(f)$ of the unknown state ϱ_0. Simply inverting the relations for $P^s_{\varrho_0}(r)$ we obtain

$$\hat{\varrho}_{\mathrm{LIN}} = \sum_{r,s} A^s_r f^s_r \tag{1}$$

where A^s_r are determined from the measurement operators M^s_r [8, 17]. Note that there is a canonical construction of A^s_r even for the case of an overcomplete set of M^s_r, see SM 1. This reconstruction of $\hat{\varrho}_{\mathrm{LIN}}$ is computationally simple and has become known as linear inversion (LIN).

Yet, due to unavoidable statistical fluctuations the estimate $\hat{\varrho}_{\mathrm{LIN}}$ is not a physical density operator for typical experimental situations, i.e., generally some eigenvalues are negative. Besides the issues of a physical interpretation of such a "state" this causes further problems in evaluating interesting functions like the von Neumann entropy, the quantum Fisher information or an entanglement measure like the negativity as these functions are defined or meaningful only for valid, i.e., positive-semidefinite, quantum states.

For this reason, different methods have been introduced that mostly follow the paradigm that the reconstructed state $\hat{\varrho} = \arg\max_{\varrho \geq 0} T(\varrho|f)$ maximizes a target function $T(\varrho|f)$ *within* the set of *valid* density operators. This target function thereby measures how well a density operator ϱ agrees with the observed data f. Two common choices are maximum likelihood (ML) [15] where $T_{\mathrm{ML}} = \sum_{r,s} f^s_r \log[P^s_\varrho(r)]$, and least squares (LS) [4] where $T_{\mathrm{LS}} = -\sum_{r,s}[f^s_r - P^s_\varrho(r)]^2/P^s_\varrho(r)$. We denote the respective solutions by $\hat{\varrho}_{\mathrm{ML}}$ and $\hat{\varrho}_{\mathrm{LS}}$. From these estimates one then easily computes any physical quantity of the observed state, like e.g. the fidelities $\hat{F}_{\mathrm{ML}} = \langle\psi|\hat{\varrho}_{\mathrm{ML}}|\psi\rangle$ and $\hat{F}_{\mathrm{LS}} = \langle\psi|\hat{\varrho}_{\mathrm{LS}}|\psi\rangle$ with respect to the target state $|\psi\rangle$.

Numerical simulations.—To enable detailed analysis of the particular features of the respective state reconstruction algorithm and to exclude influence of systematic experimental errors we perform Monte Carlo simulations. For a chosen state ϱ_0 the following procedure is used: *i*) Compute the single event probabilities $P^s_{\varrho_0}(r)$, *ii*) toss a set of frequencies according to a multinomial distribution, *iii*) reconstruct the state with either reconstruction method and compute the functions of interest, *iv*) carry out steps *ii*) and *iii*) 500 times. Note that the optimality of the maximizations for ML and LS in step (ii) is certified by convex optimization [10, 18].

Exemplarily, we first consider the four-qubit Greenberger-Horne-Zeilinger (GHZ) state

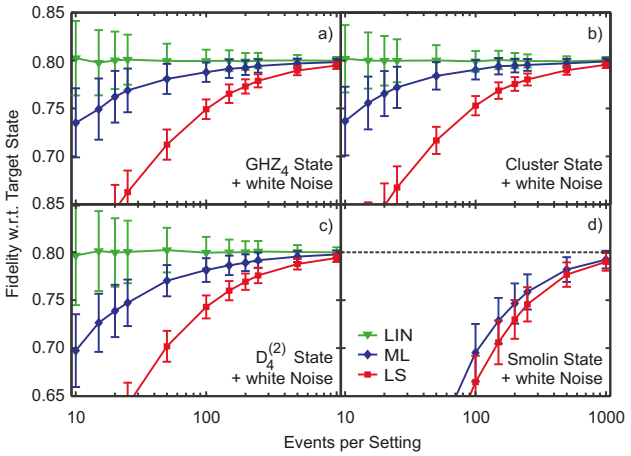

FIG. 2: (Color online) The performance of ML, LS, and LIN methods depending on the number of events N_s per setting and for four different noisy initial states ϱ_0. Note that the fidelity can only be calculated linearly if the reference state is pure which is not the case for the Smolin state [19]. Therefore only the curves for ML and LS are plotted for the Smolin state.

$|\mathrm{GHZ}_4\rangle = (|0000\rangle + |1111\rangle)/\sqrt{2}$ mixed with white noise, i.e., $\varrho_0 = p\,|\mathrm{GHZ}_4\rangle\langle\mathrm{GHZ}_4| + (1-p)\mathbb{1}/16$ where p is chosen such that the fidelity is $\langle\mathrm{GHZ}_4|\varrho_0|\mathrm{GHZ}_4\rangle = 0.8$. This state is used to simulate the Pauli tomography scheme. Fig. 1 shows an exemplary histogram of the resulting fidelities for $N_s = 100$ measurement repetitions which is a typical value used for various multiqubit experiments. The fidelities obtained via LIN reconstruction fluctuate around the initial value ($\overline{F}_{\mathrm{LIN}} = 0.799 \pm 0.012$). (The values given there are the mean and the standard deviation obtained from the 500 reconstructed states). In stark contrast, both ML ($\overline{F}_{\mathrm{ML}} = 0.788 \pm 0.010$) and even worse LS ($\overline{F}_{\mathrm{LS}} = 0.749 \pm 0.010$) systematically underestimate the fidelity, i.e., are strongly biased. Evidently, the fidelities of the reconstructed states differ by more than one standard deviation for ML and even more than five standard deviations for LS. The question arises how these systematic errors depend on the parameters of the simulation. Let us start by investigating the dependence on the number of repetitions N_s. Fig. 2a shows the mean and the standard deviations of histograms like the one shown in Fig. 1. for different N_s. As expected, the systematic errors are more profound for low number of repetitions N_s per setting s and decrease with increasing N_s. Yet, even for $N_s = 500$, a number hardly used in multiqubit experiments, $\overline{F}_{\mathrm{LS}}$ still deviates by one standard deviation from the correct value. The effect is also by no means special for the GHZ state but was equally observed for other prominent four-party states, here also chosen with a true fidelity of 80%, see Fig. 2b-2d and the Supplemental Material (SM).

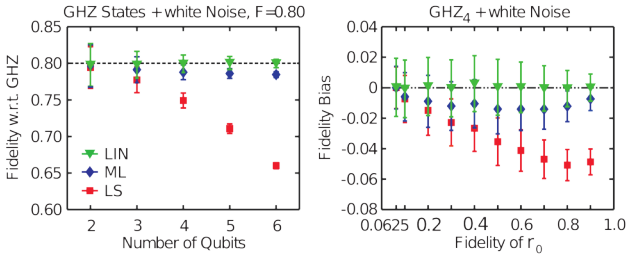

FIG. 3: (Color online) The behavior of ML, LS, and LIN depending on the number of qubits n (left) and the fidelity of ϱ_0 (right).

The systematic deviations vary also with the number of qubits or the purity of the initial state. Fig. 3a shows the respective dependencies of the fidelity for n-qubit states $\varrho_0 = p\,|\mathrm{GHZ}_n\rangle\langle\mathrm{GHZ}_n| + (1-p)\mathbb{1}/2^n$ (for $N_s = 100$). Here, a significant increase of the bias with the number of qubits is observed especially for LS. Also when varying the purity or fidelity with the GHZ state, respectively, we observe a remarkable deviation for ML and LS estimators (Fig. 3b). If the initial fidelity is very low, the effect is negligible, but large fidelity values suffer from stronger deviations, especially for LS.

The commonly specified "error bars" used in QST quantify the statistical fluctuations of the estimate $\hat{\varrho}$. Starting either from the estimate $\hat{\varrho}_{\mathrm{EST}}$ (EST $\in$ {ML, LS}) or the observed data set f this error is typically accessed by Monte Carlo sampling: One repeatedly simulates data sets $f^{(i)}$ according to the state ϱ_{EST} or f together with a representative noise model for the respective experiment and reconstructs the state $\hat{\varrho}(f^{(i)})$. From the resulting empirical distribution, one then reports the standard deviation (or a region including, say, 68% of the simulated states) for the matrix elements or for quantities of interest [16], see also SM 3. However, the problem with such error bars is that they might be too small since they reflect only statistical fluctuations of the measured frequencies, but not the systematic error which easily can be larger [20].

In summary, we observe systematic errors, which depend on the state reconstruction method and the strength of the statistical fluctuations of the count rates shown here as dependence on the number of repetitions of the experiment. Since the effect even depends on the unknown initial state any manual correction of the bias is unjustifiable. Let us emphasize that in most cases the initial value differs by more than the "error bar" determined via bootstrapping (cf. SM 3).

Biased and unbiased estimators.—The systematic offset discussed above is well-known in the theory of point estimates [20]. Expressed for QST, an estimator $\hat{\varrho}$ is called unbiased if its fluctuations are centered around the true mean, such that for its expectation value

$$\mathbb{E}_{\varrho_0}(\hat{\varrho}) \equiv \sum_f P_{\varrho_0}(f)\hat{\varrho}(f) = \varrho_0 \qquad (2)$$

holds for all possible states ϱ_0 with $P_{\varrho_0}(f)$ the probability to observe the data f. An estimator that violates Eq. (2) is called biased. Similar definitions hold for instance for fidelity estimators, $\mathbb{E}_{\varrho_0}(\hat{F}) = \langle\psi|\varrho_0|\psi\rangle \equiv F_0$. This terminology is motivated by the form of the mean squared error, which decomposes for example for the fidelity into

$$\mathbb{E}_{\varrho_0}[(\hat{F}-F_0)^2] = \mathbb{V}_{\varrho_0}(\hat{F}) + [\mathbb{E}_{\varrho_0}(\hat{F}) - F_0]^2, \qquad (3)$$

where $\mathbb{V}(\hat{F}) \equiv \mathbb{E}(\hat{F}^2) - \mathbb{E}(\hat{F})^2$ denotes the variance. Equation (3) consists of two conceptually different parts. The first being a statistical term quantifying the fluctuations of the estimator $\hat{F}$ itself. The second, purely systematic term, is called *bias* and vanishes for unbiased estimators [21]. Note that, since the expectation values of the frequencies are the probabilities, $\mathbb{E}_{\varrho_0}(f_r^s) = P_{\varrho_0}^s(r)$, and because $\hat{\varrho}_{\mathrm{LIN}}$ as given by Eq. (1) is linear in f_r^s the determination of a quantum state using LIN is unbiased. However, as shown below, for QST the bias is inherent to estimators constraint to giving only physical answers.

Proposition. *A reconstruction scheme for QST that always yields valid density operators is biased.*

Proof. For a tomography experiment on the state $|\psi_i\rangle$ with finite measurement time there is a set of possible data $\mathcal{S}_i = \{f_i | P_{|\psi_i\rangle}(f_i) > 0\}$, with $P_{|\psi_i\rangle}(f_i)$ the probability to obtain data f_i when observing state $|\psi_i\rangle$.

Consider two pure non-orthogonal states $|\psi_1\rangle$ and $|\psi_2\rangle$ ($\langle\psi_1|\psi_2\rangle \neq 0$). For these two states there exists a non-empty set of data $\mathcal{S}_{12} = \{f' | P_{|\psi_1\rangle}(f') \cdot P_{|\psi_2\rangle}(f') > 0\} = \mathcal{S}_1 \cap \mathcal{S}_2$, which can occur for both states.

Now let us assume that a reconstruction scheme $\hat{\varrho}$ provides a valid quantum state $\hat{\varrho}(f)$ for all possible outcomes f and that Eq. (2) is satisfied for $|\psi_1\rangle$, i.e., $\sum_{\mathcal{S}_1} P_{|\psi_1\rangle}(f_1)\hat{\varrho}(f_1) = |\psi_1\rangle\langle\psi_1|$. This incoherent sum over all $\hat{\varrho}(f_1)$ can be equal to the pure state $|\psi_1\rangle\langle\psi_1|$ only for the (already pathological) case that $\hat{\varrho}(f_1) = |\psi_1\rangle\langle\psi_1|$ for all $f_1 \in \mathcal{S}_1$. This means that the outcome of the reconstruction is fixed for all f_1 including all data $f' \in \mathcal{S}_{12}$. As these data also occur for state $|\psi_2\rangle$ there exist $f_2 \in \mathcal{S}_{12}$ with $\hat{\varrho}(f_2) = |\psi_1\rangle\langle\psi_1| \neq |\psi_2\rangle\langle\psi_2|$. Thus, in Eq. (2), the sum over all reconstructed states now is an incoherent mixture of at least two pure states and the condition $\sum_{\mathcal{S}_2} P_{|\psi_2\rangle}(f_2)\hat{\varrho}(f_2) = |\psi_2\rangle\langle\psi_2|$ is violated for $|\psi_2\rangle$. Hence, $\hat{\varrho}$ does not obey Eq. (2) for $|\psi_2\rangle$ and is therefore biased [22]. □

This leaves us with the trade-off: Should one necessarily use an algorithm like ML or LS to obtain a valid quantum state but suffer from a bias, or should one use LIN which is unbiased but typically delivers an unphysical result?

Parameter estimation by linear evaluation.—Here, we demonstrate that starting from $\hat{\varrho}_{\mathrm{LIN}}$ it is straightforward to provide a valid, lower/upper bound and an easily computable confidence region for many quantities of interest. For that we exploit the fact that many relevant functions are either convex, like most entanglement measures or the quantum Fisher information, or concave, like the von Neumann entropy. We linearize these operators around some properly chosen state in order to obtain a reliable lower (upper) bound. Note that typically a lower bound on an entanglement measure is often suited for evaluating experimental states whereas an upper bound does not give much additional information.

Recall that a differentiable function $g(x)$ is convex if $g(x) \geq g(x') + \nabla g(x')^T (x - x')$ holds for all x, x'. In our case we are interested in a function $g(x) = g[\varrho(x)]$ where x is a variable to parametrize a quantum state ϱ in a linear way. From convexity it follows that it is possible to find an operator L, such that

$$\mathrm{tr}(\varrho_0 L) \leq g(\varrho_0) \tag{4}$$

holds for all ϱ_0 (similarly an upper bound is obtained for concave functions). This operator can be determined from the derivatives of $g(x)$ with respect to x at a suitable point x'. For cases where the derivative is hard to compute such an operator can also be obtained from the Legendre transformation [23] or directly inferred from the definition of the function $g(x)$ [24]. A detailed discussion is given in the SM 5.

For this bound a confidence region, i.e., the error bars in the frequentistic approach, can be calculated. For example a one-sided confidence region of level γ can be described by a function $\hat{C}$ on the data f such that $\mathrm{Prob}_{\varrho_0}[\hat{C} \leq g(\varrho_0)] \geq \gamma$ holds for all ϱ_0 [20]. According to Hoeffding's tail inequality [25] and a given decomposition of $L = \sum l_r^s M_r^s$ into the measurement operators M_r^s a confidence region then is given by

$$\hat{C} = \mathrm{tr}(\hat{\varrho}_{\mathrm{LIN}} L) - \sqrt{\frac{h^2 |\log(1-\gamma)|}{2N_s}}, \tag{5}$$

where h^2 is given by $h^2 = \sum_s (l^s_{\max} - l^s_{\min})^2$, and $l^s_{\max/\min}$ denotes the respective extrema of l_r^s over r for each setting s. Although not being optimal, such error bars are easy to evaluate and valid without extra assumptions. Since we directly compute a confidence interval on $g(x)$ this is also generally a tighter error bar than those deduced from a "smallest" confidence region on density operators which tend to drastically overestimate the error (see SM 4 for an example).

In the following we show how to use a linearized operator on the example of the bipartite negativity [24]. (For the quantum Fisher information [26] and additional discussion see SM 5.) A lower bound on the negativity

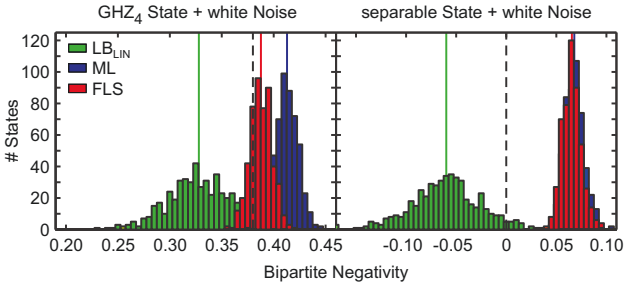

FIG. 4: (Color online) Lower bound $\mathrm{LB}_{\mathrm{LIN}}$ obtained by linearizing bipartite negativity for a four-qubit product (left) and the GHZ state (right) both mixed with white noise resulting in 80% fidelity. The ML and LS reconstruction leads to a systematic overestimation of the negativity, while the lower bound yields a valid estimate.

$N(\varrho_{AB})$ of a bipartite state ϱ_{AB} is given by

$$N(\varrho_{AB}) \geq \mathrm{tr}(\varrho_{AB} L) \tag{6}$$

for any L satisfying $\mathbb{1} \geq L^{T_A} \geq 0$, where the superscript T_A denotes partial transposition [27] with respect to party A. The inequality (6) is tight if L is the projector on the negative eigenspace of $\varrho_{AB}^{T_A}$. Using this linear expression one can directly compute the lower bound on the negativity and by using Eq. (5) the one-sided confidence region. Any choice of L is in principle valid, however for a good performance L should be chosen according to the experimental situation. We assume, however, no prior knowledge and rather estimate L by the projector on the negative eigenspace of $\hat{\varrho}_{\mathrm{ML}}^{T_A}$ deduced from an *additional* tomography again with $N_s = 100$ counts per setting. One can, of course, also start with an educated guess of L motivated by the target state one wants to prepare. In any case, in order to apply Eq. (5) and to assure a linear evaluation of the data the operator L must be chosen independently of the tomographic data [12].

Fig. 4 shows the distributions of the negativity between qubits $A = \{1, 2\}$ and $B = \{3, 4\}$ for the four-qubit GHZ state and for the separable four-qubit state $|\psi_{\mathrm{sep}}\rangle \propto (|0\rangle + |+\rangle)^{\otimes 4}$, each mixed with white noise such that the fidelity with the respective pure state is 80%. In both cases we observe that ML and LS *overestimate* the amount of entanglement. Even worse, if no entanglement is present, ML and LS clearly indicate entanglement. In contrast, the lower bound of the negativity, as given by Eq. (6), does not indicate false entanglement.

Conclusion.—Any state reconstruction algorithm enforcing physicality of the result suffers from systematic deviations. We have shown that for the commonly used methods and the typical measurement schemes this bias is significant for data sizes typical in current experiments. It leads to systematically wrong statements about derived quantities like the fidelity or the negativity which can lead to erroneous conclusions particularly for the

presence of entanglement. Equivalent statements can be inferred for process tomography.

We have demonstrated that the simple method of linear inversion can be used to overcome these problems in many cases. Expectation values being linear in ϱ do not exhibit a bias at all even if $\hat{\varrho}_{\rm LIN}$ is not physical in the overwhelming number of cases. A linearization of convex (concave) nonlinear physical quantities yields meaningful lower (upper) bounds together with easy to calculate confidence intervals restoring the trust in quantum state and process tomography.

We like to thank D. Gross, P. Drummond and M. Raymer for stimulating discussions. This work has been supported by the EU (Marie Curie CIG 293993/ENFOQI and ERC QOLAPS), the BMBF (Chist-Era project QUASAR) and QCCC of the Elite Network of Bavaria.

[1] M. G. A. Paris and J. Řeháček, eds., *Quantum state estimation* (Springer Berlin Heidelberg, 2004).

[2] H. Häffner, W. Hänsel, C. F. Roos, J. Benhelm, D. Chekal-kar, M. Chwalla, T. Körber, U. D. Rapol, M. Riebe, P. O. Schmidt et al., Nature **438**, 643 (2005).

[3] J. P. Home, D. Hanneke, J. D. Jost, J. M. Amini, D. Leibfried, and D. J. Wineland, Science **325**, 1227 (2009).

[4] D. F. V. James, P. G. Kwiat, W. J. Munro, and A. G. White, Phys. Rev. A **64**, 052312 (2001).

[5] K. J. Resch, P. Walther, and A. Zeilinger, Phys. Rev. Lett., **94**, 070402 (2005); N. Kiesel, C. Schmid, G. Tóth, E. Solano, and H. Weinfurter, Phys. Rev. Lett. **98**, 063604 (2007); M. W. Mitchell, C. W. Ellenor, S. Schneider, and A. M. Steinberg, Phys. Rev. Lett. **91**, 120402 (2003).

[6] L. DiCarlo, J. M. Chow, J. M. Gambetta, L. S. Bishop, B. R. Johnson, D. I. Schuster, A. Majer, J. Blais, L. Frunzio, S. M. Girvin, and R. J. Schoelkopf, Nature **460**, 240 (2009); M. Neeley, R. C. Bialczak, M. Lenander, E. Lucero, M. Mariantoni, A. D. O'Connell, D. Sank, H. Wang, M. Weides, J. Wenner et al., Nature **467**, 570 (2010); A. Fedorov, L. Steffen, M. Baur, M. da Silva, and A. Wallraff, Nature **481**, 170 (2012).

[7] O. Mangold, A. Heidebrecht, and M. Mehring, Phys. Rev. A **70**, 042307 (2004); M. A. Nielsen, E. Knill, and R. Laflamme, Nature **396**, 52 (1998).

[8] I. L. Chuang and M. A. Nielsen, J. Mod. Opt. **44**, 2455 (1997).

[9] D. Gross, Y.-K. Liu, S. T. Flammia, S. Becker, and J. Eisert, Phys. Rev. Lett. **105**, 150401 (2010); G. Tóth, W. Wieczorek, D. Gross, R. Krischek, C. Schwemmer, and H. Weinfurter, Phys. Rev. Lett. **105**, 250403 (2010); M. Cramer, M. B. Plenio, S. T. Flammia, D. Gross, S. D. Bartlett, R. Somma, O. Landon-Cardinal, Y.-K. Liu, and D. Poulin, Nat. Commun. **1**, 9 (2010); O. Landon-Cardinal and D. Poulin, New J. Phys. **14**, 085004 (2012).

[10] T. Moroder, P. Hyllus, G. Tóth, C. Schwemmer, A. Niggebaum, S. Gaile, O. Gühne, and H. Weinfurter, New J. Phys. **14**, 105001 (2012).

[11] M. Christandl and R. Renner, Phys. Rev. Lett. **109**, 120403 (2012); T. Sugiyama, P. S. Turner, and M. Murao, Phys. Rev. Lett. **111**, 160406 (2013); R. Blume-Kohout, arXiv:1202.5270; J. Shang, H. K. Ng, A. Sehrawat, X. Li, and B.-G. Englert, New J. Phys. **15**, 123026 (2013).

[12] T. Moroder, M. Kleinmann, P. Schindler, T. Monz, O. Gühne, and R. Blatt, Phys. Rev. Lett. **110**, 180401 (2013); D. Rosset, R. Ferretti-Schöbitz, J.-D. Bancal, N. Gisin, and Y.-C. Liang, Phys. Rev. A **86**, 062325 (2012); C. Stark, arXiv:1209.5737; N. K. Langford, New J. Phys. **15**, 035003 (2013); S. J. van Enk and R. Blume-Kohout, New J. Phys. **15**, 025024 (2013).

[13] D. Smithey, M. Beck, and M. G. Raymer, Phys. Rev. Lett. **70**, 1244 (1993); G. M. D'Ariano, C. Macchiavello, and N. Sterpi, Quantum Semiclass. Opt. **9**, 929 (1997); U. Leonhardt, M. Munroe, T. Kiss, T. Richter, and M. Raymer, Opt. Comm. **127**, 144 (1996).

[14] R. Blume-Kohout, New J. Phys. **12**, 043034 (2010); R. Blume-Kohout, Phys. Rev. Lett. **105**, 200504 (2010).

[15] Z. Hradil, Phys. Rev. A **55**, R1561 (1997).

[16] B. Efron and R. J. Tibshirani, *An introduction to the bootstrap* (Chapman & Hall, 1994).

[17] J. F. Poyatos and J. I. Cirac, Phys. Rev. Lett. **78(2)**, 390 (1997); N. Kiesel, Ph.D. thesis, Ludwig-Maximilians-Universität München (2007); T. Kiesel, Phys. Rev. A **85**, 052114 (2012).

[18] S. Boyd and S. Vandenberghe, *Convex optimization* (Cambridge University Press, 2004).

[19] J. A. Smolin, Phys. Rev. A **63**, 032306 (2001).

[20] A. F. Mood, *Introduction to the theory of statistics* (McGraw-Hill Inc., 1974).

[21] It is well-known that estimators can be biased for a finite number of samples or for particular additional conditions and constraints. An example is the estimate of the variance σ^2 of a Gaussian distribution with known mean μ. The ML estimate from N samples x_i gives $\hat{\sigma}^2_{\rm ML}(x_i) = \frac{1}{N}\sum_i (x_i-\mu)^2$, while an unbiased estimator is $\hat{\sigma}^2(x_i) = \frac{1}{N-1}\sum_i (x_i-\mu)^2$.

[22] This proof, given here for pure states, can be generalized for mixed states ϱ_1 and ϱ_2 with the ranges of the two states not sharing any vector.

[23] O. Gühne, M. Reimpell, and R. F. Werner, Phys. Rev. Lett. **98**, 110502 (2007); J. Eisert, F. G. S. L. Brandao, and K. M. R. Audenaert, New J. Phys. **9**, 46 (2007).

[24] G. Vidal and R. F. Werner, Phys. Rev. A **65**, 032314 (2002).

[25] M. Tomamichel, C. C. W. Lim, N. Gisin, and R. Renner, Nat. Commun. **3**, 634 (2012); S. T. Flammia and Y.-K. Liu, Phys. Rev. Lett. **106**, 230501 (2011); M. P. da Silva, O. Landon-Cardinal, and D. Poulin, Phys. Rev. Lett. **107**, 210404 (2011).

[26] D. Petz and C. Ghinea, QP–PQ: Quantum Probab. White Noise Anal. **27**, 261 (2011).

[27] A. Peres, Phys. Rev. Lett. **77**, 1413 (1996).

[28] R. A. Horn and C. R. Johnson, *Topics in matrix analysis* (Cambridge University Press, 1991).

Supplemental Material

SM 1: Quantum state reconstruction using linear inversion

In [4] it is explained how to obtain the estimate $\hat{\varrho}_{\mathrm{LIN}}$ for an n-qubit state from the observed frequencies of a complete set of projection measurements, i.e. 4^n results. Yet, the scheme described there is more general and can be used for any (over)complete set of projection measurements.

In the standard Pauli basis $\{\sigma_0, \sigma_x, \sigma_y\sigma_z\}$ the density matrix of the state ϱ is given by

$$\varrho = \frac{1}{2^n}\sum_{\mu} T_\mu \Gamma_\mu \tag{7}$$

where $\mu = 1...4^n$ enumerates all possible n-fold tensor products of Pauli matrices $\Gamma_1 = \sigma_0 \otimes \sigma_0 \otimes ... \otimes \sigma_0$, $\Gamma_2 = \sigma_0 \otimes \sigma_0 \otimes ... \otimes \sigma_x$, etc. and with correlations $T_\mu = \mathrm{tr}(\varrho\Gamma_\mu)$. To simplify our notation we will use the following mapping for a setting s with a respective outcome r: $(r,s) \longrightarrow \nu = 2^{n(s-1)} + r - 1$, hence for the projectors, $M_r^s \longrightarrow M_\nu$, and for the $A_r^s \longrightarrow A_\nu$, etc. Then the probabilities to observe a result r for setting s, or ν respectively, are given by

$$P_\nu = \mathrm{tr}(\varrho M_\nu) = \frac{1}{2^n}\sum_{\mu} \mathrm{tr}(M_\nu\Gamma_\mu)T_\mu. \tag{8}$$

Introducing the matrix $\hat{B}$ with elements

$$B_{\nu,\mu} = \frac{1}{2^n}\mathrm{tr}(M_\nu\Gamma_\mu) \tag{9}$$

Eq. (8) simplifies to

$$\vec{P} = \hat{B}\vec{T}. \tag{10}$$

Inverting Eq. (10), the correlations can be obtained from the probabilities P_ν, i.e., $T_\mu = \sum_\nu (\hat{B}^{-1})_{\mu,\nu}P_\nu$. Note that this is possible for any set of measurement operators. In case of a tomographically overcomplete set, i.e. $\nu > \mu$ the inverse $\hat{B}^{-1}$ has to be replaced by the pseudo inverse $\hat{B}^{-1} \longrightarrow B^+ = (B^\dagger B)^{-1}B^\dagger$. Reinserting T_μ one obtains

$$\varrho = \frac{1}{2^n}\sum_{\nu,\mu} (\hat{B}^{-1})_{\mu,\nu}\Gamma_\mu P_\nu. \tag{11}$$

For finite data sets, the P_ν are replaced by the frequencies f_ν and with

$$A_\nu = \frac{1}{2^n}\sum_{\mu} (\hat{B}^{-1})_{\mu,\nu}\Gamma_\mu \tag{12}$$

Eq. (1) is obtained.

SM 2: Bias for other prominent states

The occurrence of a bias for fidelity estimation based on ML and LS state reconstruction is by no means a special feature of the GHZ state. In Fig. 5 we show some further examples of the corresponding dependencies of the bias on the number of measurements per setting N_s for the W and the fully separable state $|\psi\rangle \propto (|0\rangle + |+\rangle)^{\otimes 4}$. For all these pure states we assume that they are mixed with white noise for an overall initial fidelity of 80%, so that the states are not at the border of the state space.

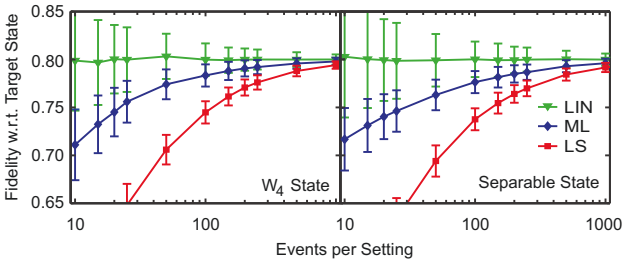

FIG. 5: The behavior of ML, LS and LIN depending on the number of events N_s per setting for different noisy initial states ϱ_0.

Furthermore we observed that the fidelity values as inferred via LS are systematically lower than those obtained using ML, see Fig. 6.

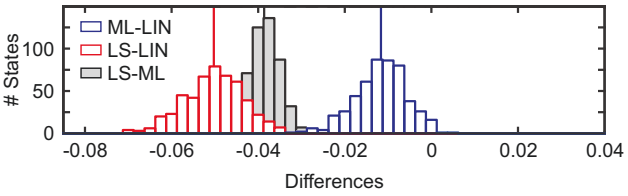

FIG. 6: Here we show the differences of the respective fidelity estimates evaluated for each single simulated tomography experiment as shown in Fig. 1 of the main text. It shows that the respective ML or LS estimate, with one rare exception, is always lower than the LIN estimate. Comparing ML and LS (gray) shows that not only on average but also for every single data set LS delivers a smaller fidelity value than ML.

SM 3: Bootstrapping

As already mentioned in the main text, in many publications where QST is performed the standard error bar is calculated by bootstrapping based on Monte Carlo methods. One can here distinguish between parametric bootstrapping, where $f^{(i)}$ are sampled according to $\hat{P}^s(r) = \mathrm{tr}(\hat{\varrho}(f_{\mathrm{obs}})M_r^s)$, and non-parametric bootstrapping, where $\hat{P}^s(r) = f_{\mathrm{obs}}$ is used instead.

We consider again the four-qubit GHZ state of 80% fidelity and $N_s = 100$. Interpreting the simulations of Fig. 1 as Monte-Carlo simulations from the parametric bootstrap with $\hat{P}^s(r) = \mathrm{tr}(\varrho_0 M_r^s)$ we have already seen that ML and LS yield fidelity estimates below the actual value. If one uses now one of these data sets f_{obs} as a seed to generate new samples $f^{(i)}$ the fidelity decreases further. As shown in Fig. 7 this happens in particular for parametric bootstrapping (0.777 ± 0.011 for ML and 0.700 ± 0.012 for LS) while non-parametric bootstrapping (0.780 ± 0.011 for ML and 0.714 ± 0.012 for LS) weakens this effect. However, in this context, one is interested in fact in the standard deviation of the simulated distribution. In our simulations it is somewhat smaller than the distribution of linearly evaluated fidelities. This means, the biasedness of ML and LS methods leads to a false estimate of the error, too.

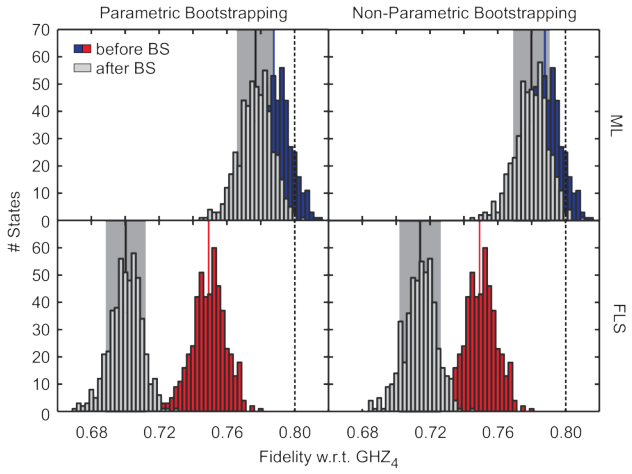

FIG. 7: Error bar computation for the fidelity of the four-qubit GHZ state via Monte-Carlo simulation using either parametric or non-parametric bootstrapping with the data from Fig. 1. For each of these 500 observations f_{obs}, 100 new data sets $f^{(i)}$ were generated and reconstructed in order to deduce the mean and standard deviation as an error bar for the fidelity. The histograms denoted by "after BS" show the distributions of these means together with an averaged error bar given by the gray shaded areas. The initial values for the fidelities are described by the dashed lines.

SM 4: Confidence regions for states vs. scalar quantities

Let us now comment on confidence regions (CR) for density operators and CR on parameter functions Q. Having a (tractable) method to compute CR for states $\hat{C}_\varrho(f)$ [11], one could think that this region of states also provides good CR for the parameter functions Q, if one manages to evaluate the minimal and maximal values of $Q(\varrho)$ for all $\varrho \in \hat{C}_\varrho(f)$. However, such CR are typically much worse than CR evaluated for Q directly, the reason being the large freedom in how to build up a CR. Let us give the following illustrative example, see also Fig. 8:

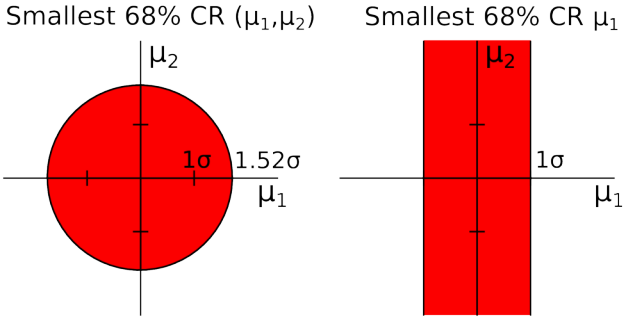

FIG. 8: Which confidence region is the smallest? If one is interested in both mean values $\vec{\mu} = (\mu_1, \mu_2)$ then clearly the left one represents the smallest one, but if $Q(\vec{\mu}) = \mu_1$ is chosen, then the right one is much better than the projected left one.

Let us consider the task to obtain a CR for the two mean values $\vec{\mu} = (\mu_1, \mu_2)$ of two independent Gaussian experiments, where the first N samples x_i are drawn from $\mathcal{N}(\mu_1, \sigma^2)$ while the remaining N instances y_i originate from $\mathcal{N}(\mu_2, \sigma^2)$, both with the same known variances. If one is interested in an 68% CR for both mean values $\vec{\mu}$ then both possible recipes

$$\hat{C}^{(1)} = \{\vec{\mu} \,:\, \|\vec{\mu} - (\bar{x}, \bar{y})\| \leq 1.52\sigma/\sqrt{N}\}, \tag{13}$$

$$\hat{C}^{(2)} = [\bar{x} - \sigma/\sqrt{N}, \bar{x} + \sigma/\sqrt{N}] \times (-\infty, \infty) \tag{14}$$

with $\bar{x} = \frac{1}{N}\sum_i x_i$ and similar for $\bar{y}$ are valid 68% CR. However, while $\hat{C}^{(1)}$ yields the smallest area for the CR, it gives a much larger confidence region for $Q(\vec{\mu}) = \mu_1$ than if we would directly use $\hat{C}^{(2)}$, which in fact is the smallest one for μ_1. Note that this effect increases roughly with $\sqrt{\dim}$ if one adds further parameters in the considered Gaussian example. Therefore we see that "error bars" associated with CR on the density operator are not the best choice if one is interested only on a few key properties of the state.

SM 5: Bounds on convex/concave functions

As mentioned in the main text, one can directly bound convex (or concave) functions $g(x)$ by linear ones using an operator L

$$\mathrm{tr}(\varrho_0 L) \leq g(\varrho_0). \tag{15}$$

Here, we want to explain in detail how the operator L can be determined from the derivatives of $g[\varrho(x)]$. Therefore, we parametrize the density operator $\varrho(x) = \mathbb{1}/\dim + \sum_i x_i S_i$ via an orthonormal basis S_i of Hermitian traceless operators. A possible choice for the

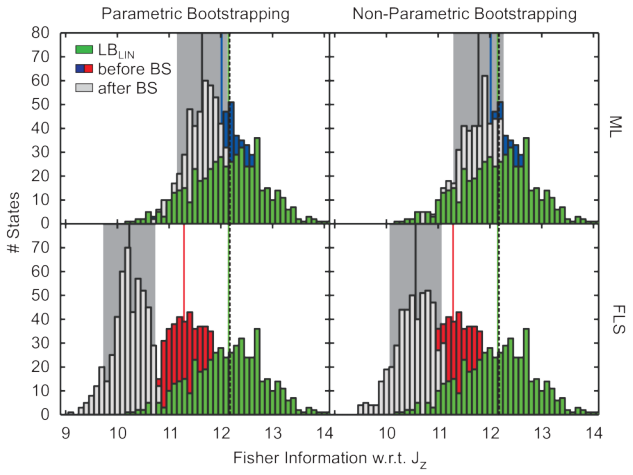

FIG. 9: Full analysis of a Pauli QST scheme with $N_s = 100$ on four qubits in order to deduce the quantum Fisher information with respect to $H = J_z$. As the true underlying state we assume again a noisy four-party GHZ state. We observe that the quantum Fisher information is underestimated from both ML and LS, while the lower bound deduced from LIN is fine.

S_i are all normalized traceless tensor products of the Pauli matrices and the identity. Since we employ an affine parametrization, the function $g(x) = g[\varrho(x)]$ is convex. Direct calculation shows that choosing the operator $L[\varrho(x')] = l_0 \mathbb{1} + \sum_i l_i S_i$ as

$$l_0 = g[\varrho_{\text{guess}}(x')] - \sum_i x'_i \frac{\partial}{\partial x_i} g[\varrho_{\text{guess}}(x')] \quad (16)$$

$$l_i = \frac{\partial}{\partial x_i} g[\varrho_{\text{guess}}(x')] \quad (17)$$

gives due to the convexity condition $g(x) \geq g(x') + \nabla g(x')^T (x - x')$ a lower bound as in Eq. (15). Here, $L[\varrho(x')]$ is computed on a "guess" x', i.e., $\varrho_{\text{guess}}(x')$ of the true state ϱ_0. Recall that while the guess ϱ_{guess} must be a valid state the lower bound $\text{tr}(\varrho_0 L)$ is well-defined also for nonphysical density operators.

As an example how to apply this linearization, let us consider the quantum Fisher information $f(x) = F(\varrho, H)$, which measures the suitability of a state ϱ to determine the parameter θ in an evolution $U(\theta, H) = e^{-i\theta H}$. More explicitly the formulae are given by

$$f(x) = 2 \sum_{jk} \frac{(\lambda_j - \lambda_k)^2}{\lambda_j + \lambda_k} H_{jk} H_{kj}, \quad (18)$$

$$\frac{\partial}{\partial x_i} f(x) = 4 \sum_{jkl} \frac{\lambda_j \lambda_k + \lambda_j \lambda_l + \lambda_k \lambda_l - 3\lambda_j^2}{(\lambda_j + \lambda_k)(\lambda_j + \lambda_l)} H_{jk} S_{i,kl} H_{lj} \quad (19)$$

where $\{\lambda_i, |\psi_i\rangle\}$ denotes the eigenspectrum of $\varrho(x)$, $H_{jk} = \langle \psi_j | H | \psi_k \rangle$ and $S_{i,kl} = \langle \psi_k | S_i | \psi_l \rangle$. In order to compute the derivative of the Fisher information one can employ the alternative form, as given for instance in Ref. [26],

$$F(\varrho, H) = \text{tr}[(H\varrho^2 + \varrho^2 H - 2\varrho H \varrho) J_\varrho^{-1}(H)], \quad (20)$$

$$J_\varrho^{-1}(H) = \int_0^\infty dt \; e^{-t/2\varrho} H e^{-t/2\varrho}. \quad (21)$$

such that the derivative can be computed via the help of matrix derivatives [28].

Now let us imagine that we want to determine the quantum Fisher information of a four-qubit state with respect to $H = J_z$, while our true underlying state ϱ_0 is once more the noisy GHZ state of 80% fidelity. Figure 9 shows the full simulation of a Pauli tomography experiment with $N_s = 100$ together with the standard error analysis using parametric or non-parametric bootstrapping. As with the other examples, we observe a systematic discrepancy between the results of standard QST tools and the true value. In this case, though the quantum Fisher information is typically larger for stronger entangled states, ML or LS underestimate the true capabilities of the state. However, if we use the described method for LIN (with an in this case optimized operator L) the lower bound via LIN is fine.

For completeness, we also give the respective derivatives for further convex functions of interest like the purity $g(x) = \text{tr}(\varrho^2)$

$$\frac{\partial}{\partial x_i} g(x) = 2 \, \text{tr}[S_i \varrho(x)] \quad (22)$$

and correspondingly for the von Neumann entropy $g(x) = -\text{tr}(\varrho \log \varrho)$

$$\frac{\partial}{\partial x_i} g(x) = -\text{tr}[S_i (\log \varrho(x) - \mathbb{1})]. \quad (23)$$

Necessary and sufficient condition for quantum state-independent contextuality

Adán Cabello,[1,*] Matthias Kleinmann,[2,†] and Costantino Budroni[3,‡]

[1]*Departamento de Física Aplicada II, Universidad de Sevilla, E-41012 Sevilla, Spain*
[2]*Department of Theoretical Physics, University of the Basque Country UPV/EHU, P.O. Box 644, E-48080 Bilbao, Spain*
[3]*Naturwissenschaftlich-Technische Fakultät, Universität Siegen, Walter-Flex-Str. 3, D-57068 Siegen, Germany*

(Dated: June 30, 2015)

We solve the problem of whether a set of quantum tests reveals state-independent contextuality and use this result to identify the simplest set of the minimal dimension. We also show that identifying state-independent contextuality graphs [R. Ramanathan and P. Horodecki, Phys. Rev. Lett. **112**, 040404 (2014)] is not sufficient for revealing state-independent contextuality.

PACS numbers: 03.65.Ud, 03.65.Ta

Introduction.—Contextuality, i.e., that the result of a measurement does not reveal a preexisting value that is independent of the set of comeasurable measurements jointly realized (i.e., the context of the measurement), is one of the most striking features of quantum theory and has been recently identified as a critical resource for quantum computing [1–3]. The earliest manifestation of contextuality in quantum theory is the Kochen-Specker theorem [4, 5], which states that, if the dimension d of the quantum system is greater than 2, there exists a finite set of elementary tests (represented by rank-one projectors in quantum theory) such that a value 1 or 0 (representing true or false, respectively) cannot be assigned to each of them respecting that: (i) result 1 cannot be assigned to two mutually exclusive tests (represented in quantum theory by mutually orthogonal projectors), and (ii) result 1 must be assigned to exactly one of d mutually exclusive tests. Sets of elementary tests in which this assignment is impossible are called *Kochen-Specker sets* [6].

Assumptions (i) and (ii) are not needed for detecting contextuality. It can be revealed by the violation of correlation inequalities satisfied by any model with noncontextual results. These inequalities are called *noncontextuality (NC) inequalities* [7]. Bell inequalities [8] are a special case of them.

Remarkably, there are NC inequalities which are violated by any quantum state for a *fixed* set of measurements [9]. A NC inequality with this property is called a *state-independent NC (SI-NC) inequality*, whereas a set of elementary tests which can be used for such a state-independent violation is called a *state-independent contextuality (SIC) set*.

Every Kochen-Specker set is a SIC set [10, 11], but there are SIC sets that are not Kochen-Specker sets [12, 13]. This observation, together with the experimental implementation of SIC sets for testing SI-NC inequalities [14–19] and the emergence of applications of SIC sets (e.g., device-independent secure communication [20], local contextuality-based nonlocality [21], Bell inequalities revealing full nonlocality [22], state-independent quantum dimension witnessing [23], and state-independent hardware certification [24]) stimulated the interest in the problem of identifying SIC sets.

In some cases, one can guess that a given set of elementary quantum tests is a SIC set. Then, to prove it, it is sufficient to construct a SI-NC inequality violated by these tests. For example, the set of elementary quantum tests associated with the Peres-Mermin square [25, 26] violates a SI-NC inequality [9]; therefore, it is a SIC set. However, in general, one cannot follow this strategy and it is convenient to adopt a more general point of view and consider not a specific set of elementary quantum tests, but all sets of elementary quantum tests with a given exclusivity graph. In this graph, vertices correspond to tests and edges occur when two tests are mutually exclusive. Since elementary tests are represented by rank-one projectors and two of them are mutually exclusive if and only if the corresponding projectors are orthogonal, the exclusivity graph is equivalent to the orthogonality graph of the corresponding projectors. This approach using graphs has been very successful in investigating the general properties of quantum contextuality [27, 28] and the separation between quantum theory and other hypothetical theories [29–33]. An open question is when, for a given orthogonality graph, there exists a realization of the graph which is a SIC set. Unfortunately, it has been notoriously difficult to answer this question [34]. The aim of this Letter is to provide a versatile tool that allows one to approach this problem.

Recently, Ramanathan and Horodecki (RH) [35] have presented a solution to a relaxation of the problem of identifying SIC sets, namely of identifying "SIC graphs." That is, whether a given graph admits, for any given state, a realization as a set of projectors (with orthogonality relations corresponding to edges in the graph) such that the correlations of such projectors on that state violate some NC inequality. This definition fits neither with the definition of a SIC set above nor with most of the previous literature (cf. Refs. [9, 10, 12, 13, 21–24, 34]). As far as we know, the only work where a similar definition has been used is Ref. [36]. Moreover, the definition of a SIC set in Ref. [35] is not state independent on an operational level. The issue is that, according to this definition, the realization of a SIC graph may depend

on the state; the set of measurements that violate the NC inequality may be different for different initial states. Therefore, the definition is not state independent on an operational level. To make an analogy, adopting a similar definition one will reach the conclusion that a pentagon is a "SIC graph for pure states" since any pure state will violate the Klyachko-Can-Binicioğlu-Shumovsky NC inequality [37] for some five rank-one projectors whose orthogonality graph is a pentagon. In contrast, the problem of identifying SIC sets not only has a long tradition (cf. Refs. [6, 12, 13]), but also an immediate experimental translation (cf. Refs. [17–19, 24]).

To prove that the result in Ref. [35] does not solve the problem of identifying SIC sets, we begin by showing that there exists a SIC graph for which no realization violates a NC inequality for every quantum state (Theorem 1). After that, we present a solution to the problem of identifying SIC sets (Theorem 3). Finally, we use it to prove a conjecture formulated by Yu and Oh in Ref. [12] on the simplest SIC set in $d = 3$ (Theorem 5).

From graph theory we will use the notions of the chromatic number and the fractional chromatic number of a graph (cf. Ref. [38]). Given a graph G, i.e., a set of vertices and the edges connecting them, a coloring of the graph is an assignment of colors to vertices such that vertices connected by an edge are associated with different colors. The chromatic number $\chi(G)$ is the minimum number of colors needed. Similarly, the fractional chromatic number $\chi_f(G)$ is the minimum of $\frac{a}{b}$ such that vertices have b associated colors, out of a colors, where vertices connected by an edge have associated disjoint sets of colors. $\chi_f(G)$ can be computed as a linear program.

Results.—The operational state *dependence* of a SIC graph as defined in Ref. [35] is apparent in the following theorem.

Theorem 1. There exists a SIC graph for which no realization is a SIC set.

Proof.—In Ref. [35] it is proven that a necessary and sufficient condition for a graph G with a $[d, r]$-realization (i.e., a realization in dimension d by means of rank-r projectors) to be a SIC graph is that the fractional chromatic number $\chi_f(G)$ is strictly larger than d/r.

However, consider the 13-vertex graph of Yu and Oh [12], $G_{\rm YO}$. This graph has a $[3, 1]$-realization and its fractional chromatic number is $\chi_f(G_{\rm YO}) = \frac{35}{11}$. Now consider the 14-vertex graph $G_{\rm YO+1}$ constructed by adding one vertex to $G_{\rm YO}$ and linking this new vertex with the 13 vertices of $G_{\rm YO}$. Clearly, this graph has a $[4, 1]$-realization and $\chi_f(G_{\rm YO+1}) = \frac{35}{11} + 1 > 4$. It is true that, for any state in $d = 4$, there is a realization which violates a NC inequality. However, whatever the realization, when the system is in the eigenstate corresponding to the new vertex, there is an obvious noncontextual assignment of results, namely, one to the 14th projector and zero to all others. ■

Now we will address the problem of identifying SIC sets. We first recall a result from Ref. [39] that helps us to identify sets of (not necessarily rank-one) projectors for which there is a SI-NC inequality.

Theorem 2. A set of observables $\{ A_1, \ldots, A_n \}$ with spectra $\{\sigma(A_1), \ldots, \sigma(A_n)\}$, and contexts C (i.e., the set of sets of comeasurable observables) violates the SI-NC inequality

$$\sum_{c \in C} \lambda_c \langle \prod_{k \in c} A_k \rangle \leq \eta \tag{1}$$

with $0 \leq \eta < 1$ and real coefficients λ_c, if and only if

$$\sum_{c \in C} \lambda_c \prod_{k \in c} a_k \leq \eta \text{ for all } a \text{ and } \sum_{c \in C} \lambda_c \prod_{k \in c} A_k \geq \mathbb{1}, \tag{2}$$

where the entries a_k in $a = (a_1, \ldots, a_n)$ assume any value from $\sigma(A_k)$.

Then, the necessary and sufficient condition for a set of rank-one projectors to constitute a SIC set is given by the following.

Theorem 3. A set of rank-one projectors $S = \{ \Pi_1, \ldots, \Pi_n \}$ is a SIC set if and only if there are nonnegative numbers $w = (w_1, w_2, \ldots)$ and a number $0 \leq y < 1$ such that

$$\sum_{j \in \mathcal{I}} w_j \leq y \text{ for all } \mathcal{I} \text{ and } \sum_i w_i \Pi_i \geq \mathbb{1}, \tag{3}$$

where $\mathcal{I}$ is any set such that $i, j \in \mathcal{I}$ implies $\Pi_i \Pi_j \neq 0$ (i.e., $\mathcal{I}$ is any independent set of the orthogonality graph of S).

In particular, w gives rise to the SI-NC inequality

$$\sum_i w_i \langle \Pi_i \rangle - \sum_i w_i \sum_{j \in \mathcal{N}(i)} \langle \Pi_i \Pi_j \rangle \leq y, \tag{4}$$

where $\mathcal{N}(i) = \{ j \mid \Pi_i \Pi_j = 0 \}$ is the orthogonality neighborhood of i.

Proof.—For proving sufficiency, we will prove that, for a given (y, w) satisfying conditions (3), with $0 \leq y < 1$, inequality (4) is a valid NC inequality and it is violated for every state. For that, it is enough to realize that among the noncontextual assignments maximizing the left-hand side of inequality (4) are those that respect the orthogonality conditions; i.e., two orthogonal projectors could not both have been assigned the value 1. Respecting the orthogonality conditions precisely amounts to assign 1 to the elements of a set $\mathcal{I}$ appearing in conditions (3) and, hence, the bound y holds for inequality (4). The proof goes as follows. Let us consider orthogonal projectors Π_i and Π_j and any noncontextual assignment $p \in \{0, 1\}^n$ such that $p_i = 1$ but $p_j = 0$. By changing the value of p_j, i.e., violating the orthogonality

condition, we get an extra contribution w_j from the first term and $-\sum_{k\in\mathcal{N}(j)}(w_j+w_k)p_k \leq -w_j$ from the second term, decreasing the total value of the left-hand side of inequality (4). This proves that inequality (4) is a valid NC inequality. By condition (3), it is violated by any quantum state.

For proving necessity, we show that if $\{\Pi_i\}$ give rise to a violation of a linear NC inequality for every state, then conditions (3) are satisfied. Let us assume, for some (λ,η), that the following inequality is violated by any state

$$\sum_{\mathcal{C}} \lambda_{\mathcal{C}} \langle \prod_{k\in\mathcal{C}} \Pi_k \rangle \leq \eta, \tag{5}$$

where the sum is over all cliques $\mathcal{C}$ different from the empty set in the orthogonality graph of S, corresponding to all possible contexts, and $\lambda_{\mathcal{C}}$ are real numbers. Notice that the use of a linear expression in inequality (5) is not a restriction as it follows from the Hahn-Banach theorem (cf., e.g., Ref. [40]). In fact, the set of quantum correlations for all states and the set of noncontextual correlations are (compact) convex sets, and hence the sets either intersect or they can be separated by a hyperplane, i.e., distinguished via a linear inequality. Notice also that inequality (5) contains all of the possible correlations that are jointly measurable; i.e., it includes all contexts $\mathcal{C}$, with a generic coefficient λ.

Since inequality (5) holds, in particular, for all assignments respecting orthogonality, we have $\sum_{k\in\mathcal{I}} \lambda_{\{k\}} \leq \eta$ for any independent set $\mathcal{I}$. At the same time, we assume a state-independent violation and hence, without loss of generality, $\sum_k \lambda_{\{k\}}\Pi_k \geq \mathbb{1}$ and $\eta < 1$. [In general we have $\sum_k \lambda_{\{k\}}\Pi_k \geq \xi\mathbb{1}$ and $\eta < \xi$. But the assignment $p \equiv (0,0,\dots)$ yields $0 \leq \eta < \xi$, which allows us to rescale $\lambda_{\mathcal{C}} \to \lambda_{\mathcal{C}}/\xi$ and $\eta \to \eta/\xi$.] Eventually, we identify $w_i = \max\{0, \lambda_{\{i\}}\}$ and $y = \eta$. Indeed, inequality (5) has to hold for any assignment $p = (p_1,\dots,p_n)$ respecting orthogonality and having $p_k = 0$ for all $\lambda_{\{k\}} < 0$. This way, the condition in Eq. (3) is obeyed by that identification. ∎

We mention that the condition in Theorem 2 as well as that in Theorem 3 can be verified by means of a semidefinite program. Semidefinite programs are a class of optimization problems that can be solved numerically with a certificate of optimality [41].

At this point, it is interesting to point out the relation between Theorem 3 and the results in Ref. [35]. According to Ref. [35], to conclude that a graph of orthogonality is a SIC graph, it is sufficient to check the expectation value of $\sum_j w_i\Pi_i$ on the maximally mixed state $\rho = \mathbb{1}/d$. Assuming rank-one projectors, we can substitute the condition $\sum_i w_i\Pi_i \geq \mathbb{1}$ with $\frac{1}{d}\sum_i w_i \geq 1$, yielding RH's result. In fact, the condition in Eq. (3) can be formulated in terms of the existence of a solution greater than d for the linear program

$$\begin{aligned} \text{maximize:} \quad & \sum_i w_i \\ \text{subject to:} \quad & \sum_{j\in\mathcal{I}} w_j \leq 1 \text{ for all } \mathcal{I}, \\ & w_i \geq 0 \text{ for all } i. \end{aligned} \tag{6}$$

Every (w,y) obeying Eq. (3) with $y < 1$ can be used to achieve $\sum_i w_i > d$ by rescaling all the weights by $1/y$. The linear program in Eq. (6) is the dual problem of the fractional chromatic number $\chi_f(G)$ of the orthogonality graph G (also known as the fractional clique number, cf. Ref. [38]); hence, both yield the same optimal value.

Together with the fact that the chromatic number $\chi(G)$ is lower bounded by the fractional chromatic number $\chi_f(G)$ [38], we have the following.

Theorem 4. Necessary conditions for a set of rank-one projectors in dimension d to be a SIC set are that for the orthogonality graph G, (i) $\chi_f(G) > d$ and (ii) $\chi(G) > d$.

Condition (i) is also a direct consequence of the results in Ref. [35], where it was demonstrated in addition that, in general, condition (ii) is strictly weaker than condition (i). However, condition (ii) has the advantage of being solvable exactly by simple integer arithmetic, while condition (i) is the solution to a linear program.

The minimal dimension in which SIC sets exist is $d = 3$ [5]. Therefore, identifying the smallest SIC set in $d = 3$ is a problem of fundamental importance. Using the previous results we can prove a conjecture from Ref. [12].

Theorem 5. In dimension $d = 3$, there exists no SIC set with less than 13 projectors. The set provided by Yu and Oh in Ref. [12] is therefore the simplest for $d = 3$.

Proof.—The orthogonality graph of a SIC set has to obey at least the following necessary conditions: (a) that the graph has a $[3,1]$-representation, and (b) that the graph has a fractional chromatic number greater than 3.

From condition (a) it follows that the graph must be square free, because for a projector represented by a vertex of the square, the other two connected to it must be in the orthogonal plane, and the fourth is orthogonal to both, so it must be the same as the first.

The first step is to generate all nonisomorphic, i.e., not obtained via a relabeling, square-free connected graphs with 12 or fewer vertices and then calculate their chromatic number. It is sufficient to consider connected graphs since for a disconnected graph the chromatic number is the largest chromatic number of its connected components.

For this, we use the utility `geng` from the software package `nauty` v2.5r9 [42], and we find 143 129 graphs with such properties. Among them, there is only one graph G with $\chi(G) > 3$, which is depicted in Fig. 1(c).

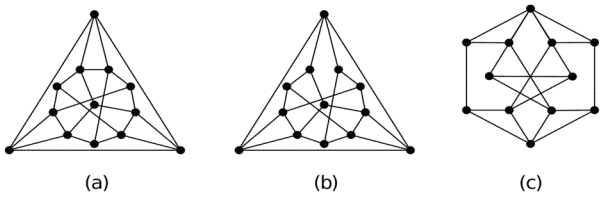

FIG. 1: (a) Yu-Oh graph $G_{\rm YO}$, (b) $G_{\rm YO}$ minus one edge. (c) The only square-free connected 12-vertex graph with chromatic number $\chi(G) > 3$.

By solving the linear program in Eq. (6) with exact arithmetic [43], one finds that its fractional chromatic number is $\chi_f(G) = 3$. ■

One can go further and ask whether there are other SIC graphs with 13 vertices aside from the Yu-Oh graph $G_{\rm YO}$, depicted in Fig. 1(a). There are in total eight square-free graphs with 13 vertices and $\chi(G) > 3$ [44], and out of these eight graphs, only three have $\chi_f(G) > 3$ [45]. Two of them are depicted in Fig. 1, (a) $G_{\rm YO}$ and (b) $G_{\rm YO}$ minus one edge, together with the 12-vertex graph (c), which is a common induced subgraph of all remaining 13-vertex graphs with $\chi(G) > 3$.

The existence of a representation in dimension $d = 3$ for a given orthogonality graph can be written as a minimization of a polynomial function. In fact, the scalar product of two complex vectors can be written as a polynomial with vector entries as variables; hence, orthogonality conditions correspond to its zeros. A numerical search was not able to find a solution for such graphs in $d = 3$.

Conclusion.—We have started arguing that the definition of "state-independent contextuality scenario" used in Ref. [35] is inconsistent with almost all of the previous literature on the topic and is not state independent on an operational level because the realization of the scenario depends on the state. Then we have shown that the criterion proposed in Ref. [35] does not solve the problem of whether or not a set of quantum tests reveals state-independent contextuality in the sense defined in most of the literature, including all experimental implementations and applications. Then we have presented a solution to this problem and explained the connection between this solution and the results in Ref. [35]. Finally, we have used our result to prove that the Yu-Oh set is the simplest set of elementary quantum tests revealing state-independent contextuality in dimension three. Our results clarify the structure of state-independent contextuality and—as we demonstrated on an example—enable the systematic investigation of state-independent contextuality sets.

The authors thank P. Horodecki, J. R. Portillo, R. Ramanathan, and S. Severini for the useful conversations. This work was supported by Project No. FIS2011-29400 (MINECO, Spain) with FEDER funds, the FQXi large grant project "The Nature of Information in Sequential Quantum Measurements," and by the European Union (ERC Starting Grant No. GEDENTQOPT). Theorems 4 and 5 incorporate results that appeared in an unpublished article [34].

* Electronic address: adan@us.es
† Electronic address: matthias.kleinmann@uni-siegen.de
‡ Electronic address: costantino.budroni@uni-siegen.de

[1] M. Howard, J. J. Wallman, V. Veitch, and J. Emerson, Contextuality supplies the "magic" for quantum computation, Nature (London) **510**, 351 (2014).
[2] R. Raussendorf, Contextuality in measurement-based quantum computation, Phys. Rev. A **88**, 022322 (2013).
[3] N. Delfosse, P. A. Guerin, J. Bian, and R. Raussendorf, Wigner function negativity and contextuality in quantum computation on rebits, Phys. Rev. X **5**, 021003 (2015).
[4] E. P. Specker, Die Logik nicht gleichzeitig entscheidbarer Aussagen, Dialectica **14**, 239 (1960) [The logic of nonsimultaneously decidable propositions, arXiv:1103.4537].
[5] S. Kochen and E. P. Specker, The problem of hidden variables in quantum mechanics, J. Math. Mech. **17**, 59 (1967).
[6] M. Pavičić, J.-P. Merlet, B. D. McKay, and N. D. Megill, Kochen-Specker vectors, J. Phys. A: Math. Gen. **38**, 1577 (2005); **38**, 3709 (2005).
[7] R. W. Spekkens, D. H. Buzacott, A. J. Keehn, Ben Toner, and G. J. Pryde, Preparation contextuality powers parity-oblivious multiplexing, Phys. Rev. Lett. **102**, 010401 (2009).
[8] J. S. Bell, On the Einstein Podolsky Rosen Paradox, Physics (Long Island City, N.Y.) **1**, 195 (1964).
[9] A. Cabello, Experimentally testable state-independent quantum contextuality, Phys. Rev. Lett. **101**, 210401 (2008).
[10] P. Badziąg, I. Bengtsson, A. Cabello, and I. Pitowsky, Universality of state-independent violation of correlation inequalities for noncontextual theories, Phys. Rev. Lett. **103**, 050401 (2009).
[11] X.-D. Yu and D. M. Tong, Coexistence of Kochen-Specker inequalities and noncontextuality inequalities, Phys. Rev. A **89**, 010101(R) (2014).
[12] S. Yu and C. H. Oh, State-independent proof of Kochen-Specker theorem with 13 rays, Phys. Rev. Lett. **108**, 030402 (2012).
[13] I. Bengtsson, K. Blanchfield, and A. Cabello, A Kochen-Specker inequality from a SIC, Phys. Lett. A **376**, 374 (2012).
[14] G. Kirchmair, F. Zähringer, R. Gerritsma, M. Kleinmann, O. Gühne, A. Cabello, R. Blatt, and C. F. Roos, State-independent experimental test of quantum contextuality, Nature (London) **460**, 494 (2009).
[15] E. Amselem, M. Rådmark, M. Bourennane, and A. Cabello, State-independent quantum contextuality with single photons, Phys. Rev. Lett. **103**, 160405 (2009).
[16] O. Moussa, C. A. Ryan, D. G. Cory, and R. Laflamme, Testing contextuality on quantum ensembles with one clean qubit, Phys. Rev. Lett. **104**, 160501 (2010).
[17] C. Zu, Y.-X. Wang, D.-L. Deng, X.-Y. Chang, K. Liu, P.-Y. Hou, H.-X. Yang, and L.-M. Duan, State-independent

experimental test of quantum contextuality in an indivisible system, Phys. Rev. Lett. **109**, 150401 (2012).

[18] V. D'Ambrosio, I. Herbauts, E. Amselem, E. Nagali, M. Bourennane, F. Sciarrino, and A. Cabello, Experimental implementation of Kochen-Specker set of quantum tests, Phys. Rev. X **3**, 011012 (2013).

[19] G. Cañas, S. Etcheverry, E. S. Gómez, C. Saavedra, G. B. Xavier, G. Lima, and A. Cabello, Experimental implementation of an eight-dimensional Kochen-Specker set and observation of its connection with the Greenberger-Horne-Zeilinger theorem, Phys. Rev. A **90**, 012119 (2014).

[20] K. Horodecki, M. Horodecki, P. Horodecki, R. Horodecki, M. Pawłowski, and M. Bourennane, Contextuality offers device-independent security, arXiv:1006.0468.

[21] A. Cabello, Proposal for revealing quantum nonlocality via local contextuality, Phys. Rev. Lett. **104**, 220401 (2010).

[22] L. Aolita, R. Gallego, A. Acín, A. Chiuri, G. Vallone, P. Mataloni, and A. Cabello, Fully nonlocal quantum correlations, Phys. Rev. A **85**, 032107 (2012).

[23] O. Gühne, C. Budroni, A. Cabello, M. Kleinmann, and J.-Å. Larsson, Bounding the quantum dimension with contextuality, Phys. Rev. A **89**, 062107 (2014).

[24] G. Cañas, M. Arias, S. Etcheverry, E. S. Gómez, A. Cabello, G. B. Xavier, and G. Lima, Applying the simplest Kochen-Specker set for quantum information processing, Phys. Rev. Lett. **113**, 090404 (2014).

[25] A. Peres, Incompatible results of quantum measurements, Phys. Lett. A **151**, 107 (1990).

[26] N. D. Mermin, Simple unified form for the major no-hidden-variables theorems, Phys. Rev. Lett. **65**, 3373 (1990).

[27] A. Cabello, S. Severini, and A. Winter, Graph-theoretic approach to quantum correlations, Phys. Rev. Lett. **112**, 040401 (2014).

[28] A. Acín, T. Fritz, A. Leverrier, and A. B. Sainz, A combinatorial approach to nonlocality and contextuality, Commun. Math. Phys. **334**, 533 (2015).

[29] A. Cabello, Simple explanation of the quantum violation of a fundamental inequality, Phys. Rev. Lett. **110**, 060402 (2013).

[30] T. Fritz, A. B. Sainz, R. Augusiak, J. Bohr Brask, R. Chaves, A. Leverrier, and A. Acín, Local orthogonality: A multipartite principle for correlations, Nat. Commun. **4**, 2263 (2013).

[31] B. Yan, Quantum correlations are tightly bound by the exclusivity principle, Phys. Rev. Lett. **110**, 260406 (2013).

[32] A. B. Sainz, T. Fritz, R. Augusiak, J. Bohr Brask, R. Chaves, A. Leverrier, and A. Acín, Exploring the local orthogonality principle, Phys. Rev. A **89**, 032117 (2014).

[33] A. Cabello, Exclusivity principle and the quantum bound of the Bell inequality, Phys. Rev. A **90**, 062125 (2014).

[34] A. Cabello, State-independent quantum contextuality and maximum nonlocality, arXiv:1112.5149v1.

[35] R. Ramanathan and P. Horodecki, Necessary and sufficient condition for state-independent contextual measurement scenarios, Phys. Rev. Lett. **112**, 040404 (2014).

[36] P. Kurzyński and D. Kaszlikowski, Contextuality of almost all qutrit states can be revealed with nine observables, Phys. Rev. A **86**, 042125 (2012).

[37] A. A. Klyachko, M. A. Can, S. Binicioğlu, and A. S. Shumovsky, Simple test for hidden variables in spin-1 systems, Phys. Rev. Lett. **101**, 020403 (2008).

[38] E. R. Scheinerman and D. H. Ullman, *Fractional Graph Theory: A Rational Approach to the Theory of Graphs* (Dover, New York, 2011).

[39] M. Kleinmann, C. Budroni, J.-Å. Larsson, O. Gühne, and A. Cabello, Optimal inequalities for state-independent contextuality, Phys. Rev. Lett. **109**, 250402 (2012).

[40] R. A. Horn and C. R. Johnson, *Matrix Analysis* (Cambridge University Press, New York, 1985).

[41] L. Vandenberghe and S. Boyd, Semidefinite programming, SIAM Rev. **38**, 49 (1996).

[42] B. D. McKay and A. Piperno, Practical graph isomorphism, II, J. Symb. Comput. **60**, 94 (2014).

[43] K. Fukuda, software library `cddlib` v094g, `http://www.ifor.math.ethz.ch/~fukuda/cdd_home/`

[44] In the `graph6` encoding (`http://cs.anu.edu.au/~ebdm/data/formats.html`), they are: "`L?AEB?oDDIQSUS`", "`L?AEB?oFDHISPS`", "`L?ABA_oo_iREJa`", "`L?ABAagF@bWgHc`", "`L?ABEagE‘gH‘‘c`" (which is G_{YO} minus one edge), "`L?AB?vOLDPHa‘o`" (which is G_{YO}), "`L?BDA_gEREHcac`, and "`L?‘D@bCUCbDgWc`".

[45] In the `graph6` encoding, "`L?ABEagE‘gH‘‘c`", having $\chi_f = 19/6$, "`L?AB?vOLDPHa‘o`", having $\chi_f = 35/11$, and "`L?‘D@bCUCbDgWc`", having $\chi_f = 13/4$.

Quantum state-independent contextuality requires 13 rays

Adán Cabello,[1, a)] Matthias Kleinmann,[2, b)] and José R. Portillo[3, c)]

[1)] *Departamento de Física Aplicada II, Universidad de Sevilla, E-41012 Sevilla, Spain*

[2)] *Department of Theoretical Physics, University of the Basque Country UPV/EHU, P.O. Box 644, E-48080 Bilbao, Spain*

[3)] *Departamento de Matemática Aplicada I, Universidad de Sevilla, E-41012 Sevilla, Spain*

We show that, regardless of the dimension of the Hilbert space, there exists no set of rays revealing state-independent contextuality with less than 13 rays. This implies that the set proposed by Yu and Oh in dimension three [Phys. Rev. Lett. **108**, 030402 (2012)] is actually the minimal set in quantum theory. This contrasts with the case of Kochen–Specker sets, where the smallest set occurs in dimension four.

I. INTRODUCTION

Fifty years ago, Kochen and Specker[1] answered the following question: Is it possible that, independently of which is the quantum state, the quantum observables each possess a definite single value, regardless of whether they are measured or not? The Kochen–Specker (KS) theorem states that this is impossible if the dimension of the underlying Hilbert space is larger than two. One consequence of this theorem is the impossibility of reproducing quantum theory in terms of noncontextual hidden variable theories, defined as those in which the outcomes are independent of the context. A context is a set of mutually compatible quantum observables. In this sense, quantum theory is said to exhibit contextuality.

The original proof of the KS theorem had two other distinctive traits: (i) It only used a finite set of observables with two outcomes, where one outcome is represented by a rank-one projection onto a ray of the Hilbert space. Hereafter, as it is common in the literature, we will use ray as synonym of self-adjoint rank-one projection. (ii) The set is KS-uncolorable, i.e., it is impossible to assign values 1 or 0 to each ray while respecting that two orthogonal rays cannot both have assigned 1, and 1 must be assigned to exactly one of d mutually orthogonal rays. These restrictions are motivated by the observation that orthogonal rays correspond to mutually exclusive outcomes of a sharp observable and d mutually orthogonal rays correspond to an exhaustive set of mutually exclusive outcomes for a Hilbert space of dimension d. KS-uncolorable sets of rays are called KS sets.[2]

The original KS set had 117 rays in $d = 3$, which can be grouped in 132 contexts. There have been many efforts for finding simpler sets exhibiting state-independent contextuality (SIC). For instance, Peres and Mermin realized that, by considering observables not represented by rank-one projections and replacing KS uncolorability by a similar condition, one can find very compact sets of observables in $d = 4$ and $d = 8$.[3,4] Still, these sets can be rewritten in terms of KS sets.[5,6] So far, it has been shown[2] that the KS set of minimum

[a)] Electronic mail: adan@us.es

[b)] Electronic mail: matthias_kleinmann001@ehu.eus

[c)] Electronic mail: josera@us.es

cardinality occurs in $d = 4$ and has 18 rays.[7] It also has been proved[2] that, in $d = 3$, the KS set with minimum cardinality has more than 22 and less than 32 rays.[8] On the other hand, the KS set with minimum number of contexts known occurs in $d = 6$ and has seven contexts (and 21 rays).[9]

A big step was the observation that SIC based on rays does not need to rely on KS-uncolorable sets. It is enough that they lead to a state-independent violation of a noncontextuality inequality. This substantially simplifies the methods for revealing SIC in $d = 3$. Specifically, Yu and Oh singled out one set with 13 rays in $d = 3$.[10] The optimal state-independent noncontextuality inequalities for this set were identified in Ref. 11. Sets of rays having a state-independent violation of a non-contextuality inequality are called SIC sets.

Recent experiments testing SIC[12–20] and an increasing number of applications, such as device-independent secure communication,[21] local contextuality,[22,23] Bell inequalities revealing full nonlocality,[24] state-independent quantum dimension witnessing,[25] and state-independent hardware certification,[19] have stimulated the interest in the following question: Which is the minimal set of rays needed for SIC? It is known that, for $d = 3$, the answer is 13,[26] but it would be well possible that the minimal set occurs in some higher dimension, as it happens for KS sets. Here we prove that this is not the case.

II. MAIN RESULT

The basis of our proof is a condition identified by Ramanathan and Horodecki[26,27] to be necessary for any SIC set in dimension d, namely that the orthogonality graph G of the set of rays has fractional chromatic number $\chi_f(G) > d$. The orthogonality graph of a SIC set is the graph in which orthogonal rays are represented by adjacent vertices. A coloring of G is an assignment of colors to the vertices such that adjacent vertices are associated with different colors. $\chi_f(G)$ is the infimum of $\frac{a}{b}$ such that vertices have a set of b associated colors, out of a colors, where adjacent vertices have associated disjoint sets of colors.

Instead of considering all possible SIC sets of size n, we rather investigate all graphs with n vertices. Then, we consider the nondegenerate orthogonal representations (ORs) of any graph G. An OR is an injection ϕ, mapping the vertices of G to rays, such that adjacent vertices in G are mapped to orthogonal rays. The OR is faithful (FOR) if, conversely, any two orthogonal rays correspond to an edge of G. We denote by $\Xi(G)$ the smallest dimension of the Hilbert space which still admits a FORs of G. It then follows from the Ramanathan–Horodecki condition that G is the orthogonality graph of a SIC set only if $\chi_f(G) > \Xi(G)$. Our main results is then as follows.

Theorem 1. *Any graph G with 12 or less vertices has $\chi_f(G) \leq \Xi(G)$.*

Hence, according to quantum theory, no SIC set with less than 13 rays exists.

III. PROOF OF THEOREM 1

We proceed by an exhaustive search for a counterexample, examining all 166 122 463 890 nonisomorphic graphs with up to 12 vertices. Applying a cascade of filters we eventually discard all graphs and prove this way Theorem 1. We start by introducing the criteria for defining these filters and then explain our procedure providing intermediate results for each of the filters.

We denote by $V(G)$ and $E(G)$ the sets of vertices and edges of G, respectively. The complement $\overline{G}$ of G is a graph that has the same vertices while the edges are the complemented set, i.e., $e \in E(\overline{G})$ if and only if $e \notin E(G)$. A subgraph S of G is any graph with $V(S) \subset V(G)$ and $E(S) \subset E(G)$. A subgraph is induced if $\overline{S}$ is also a subgraph of $\overline{G}$. It is a simple observation that any (F)OR is also a (F)OR of any (induced) subgraph. Defining ξ analogously to Ξ, but for ORs,[1] this proves the following.

Lemma 2. *By definition, $\xi(G) \leq \Xi(G)$. If S is a subgraph of G, then $\xi(S) \leq \xi(G)$. Similarly, if S is an induced subgraph of G, then $\Xi(S) \leq \Xi(G)$.*

The union of two graphs $G_1 \cup G_2$ consists of the disjoint union of the respective vertex sets and edge sets. The join $G_1 + G_2$ of two graphs is the union of both graphs adding one edge between any pair $(v_1, v_2) \in V(G_1) \times V(G_2)$. The graph K_1 with one vertex and no edge takes a special role in the following simple relations.

Lemma 3. *For two graphs G_1 and G_2 and $f \in \{ \chi_f, \Xi, \xi \}$, we have $f(G_1 \cup G_2) = \max[f(G_1), f(G_2)]$ and $f(G_1 + G_2) = f(G_1) + f(G_2)$, with the exceptions $\Xi(K_1 \cup K_1) = 2$ and $\xi(K_1 \cup K_1) = 2$.*

Proof. For χ_f the relations are well-known, cf., e.g., Ref. 29, Sec. 3.10. For Ξ and ξ and the first relation, the maximum is at least a lower bound, since any (F)OR of $G_1 \cup G_2$ must also be a (F)OR of G_1 and of G_2. Conversely, if at least one of the graphs has more than one vertex then also its (F)OR has at least dimension two. This (F)OR can then be transformed by a unitary rotation, such that the image of the (F)ORs of G_1 and G_2 are disjoint and also no rays are orthogonal. Hence one can combine any two (F)ORs of G_1 and G_2 to a (F)OR in the larger of the dimensions of both (F)ORs. The second relation follows at once, noting that $\{ v_1, v_2 \} \in E(G_1 + G_2)$ if and only if either $v_1 \in V(G_1)$ and $v_2 \in V(G_2)$, or vice versa, or $\{ v_1, v_2 \} \in E(G_1)$, or $\{ v_1, v_2 \} \in E(G_2)$. Hence ϕ is a (F)OR for $G_1 + G_2$ if and only if it is a (F)OR for G_1 and G_2, and the spans of $\phi[V(G_1)]$ and $\phi[V(G_2)]$ are mutually orthogonal. □

These relations are useful for our purposes since they imply that, if a graph or its complement is not connected and $\chi_f(G) > \Xi(G)$, then this must already be true for a subgraph of G. Hence in our search we only need to consider connected graphs the complement of whose are also connected. Another important consequence of Lemma 3 is that $\xi(n\overline{K_2} + mK_1) = 2n + m$, where K_ℓ is the completely connected graph with ℓ vertices.[30,31] This implies $\Xi(G) \geq 2n + m$ as soon as $n\overline{K_2} + mK_1$ is a subgraph of G. A weaker form of this condition is that if K_ℓ is a subgraph of G, then $\Xi(G) \geq \ell$.

As a final ingredient to our proof, we use the seven graphs listed in Table I. If any of those graphs is an induced subgraph S of G, then $\Xi(G) \geq \Xi(S)$ applies. The values of $\Xi(S)$ are obtained by construction, and due to Lemma 3 it is sufficient to study the five graphs in Fig. 1. The construction is similar for all five graphs and we demonstrate the method only for the most complicated case $\mathrm{Ci}_{11}(1, 2, 3) \setminus \{ v \}$, cf. Fig. 1 (e). The vertices $\{ 4, 5, 6, 7 \}$ form the induced subgraph K_4 and, without loss of generality, we can choose $\phi(4) = (1, 0, 0, 0, 0)$, $\phi(5) = (0, 1, 0, 0, 0)$, $\phi(6) = (0, 0, 1, 0, 0)$, and $\phi(7) = (0, 0, 0, 1, 0)$. Since vertex 3 is adjacent to the vertices $\{ 4, 5, 6 \}$ and not adjacent to vertex 7 or 8, and vertex 7 is adjacent to 8, we have $\phi(3) = (0, 0, 0, a, 1)$ with some $a \neq 0$. By similar arguments,

[1] The orthogonal rank of a graph is also sometimes denoted by ξ,[28] but there the minimum is taken without the restriction that the OR is an injection. This yields slightly different properties.

Graph name	In Fig. 1	*graph6*	Ξ	Filter	Remaining
$\overline{H}$	(a)	`Ebtw`	5	(3.1)	124 220
$\mathrm{Ci}_8(1,2)$	(b)	`Gbijmo`	5	(3.2)	124 216
$\overline{H} + K_1$	—	`Fbvzw`	6	(3.3)	4 722
$\overline{\mathrm{Caterpillar}_2^{3,2}}$	(c)	`Fbtzw`	6	(3.4)	569
$\overline{\mathrm{Caterpillar}_3^{2,1,1}}$	(d)	`Fbuzw`	6	(3.5)	400
$\mathrm{Ci}_{11}(1,2,3) \setminus \{ v \}$	(e)	`Ibgzmngjg`	6	(3.6)	366
$\overline{H} + K_2$	—	`Gzznnk`	7	(3.7)	0

TABLE I. List of graphs used for filtering via Lemma 2. The graphs $\mathrm{Caterpillar}_k^{n_1,\ldots,n_k}$ are linear graphs of length k, where n_v leafs are added to vertex v. $H = \mathrm{Caterpillar}_2^{2,2}$, $\mathrm{Ci}_n(e_1,\ldots,e_m)$ is the circulant graph, where each vertex is connected to its e_1th-, …, e_mth-next neighbor. $G \setminus \{ v \}$ is the graph G with one vertex removed. Selected graphs are displayed in Fig. 1. *graph6* is a standard graph data format widely used in computer software.[37] The number Ξ is the smallest dimension of any faithful nondegenerate orthogonal representation. The last column shows the number of graphs remaining after filtering for the induced subgraph, cf. main text.

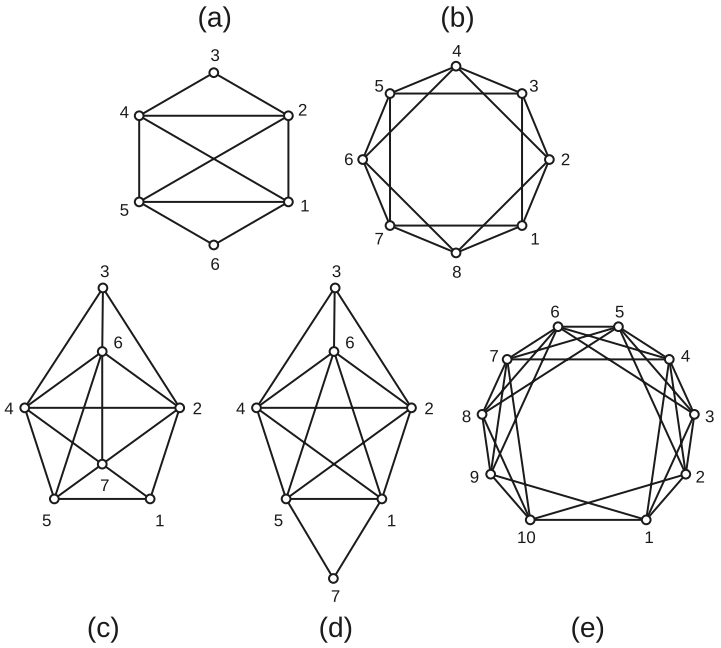

FIG. 1. Graphs from Table I. Graphs (a) and (b) have $\Xi = 5$ and graphs (c)–(e) have $\Xi = 6$. The other two graphs from Table I are obtained by adding one or two vertices to graph (a) each being connected to all other vertices.

$\phi(2) = (0, 0, b, -1/a^*, 1)$ with $b \neq 0$, and, by symmetry, $\phi(8) = (c, 0, 0, 0, 1)$ and $\phi(9) = (-1/c^*, d, 0, 0, 1)$, with $c, d \neq 0$. Using, that vertex 1 is adjacent to the vertices $\{ 4, 9, 3, 2 \}$, we have $\phi(1) = (0, -1/d^*, -x/b^*, -1/a^*, 1)$ with $x = 1 + 1/|a|^2$, and, by symmetry, $\phi(10) = (-1/c^*, -y/d^*, -1/b^*, 0, 1)$ with $y = 1 + 1/|c|^2$. Eventually, vertex 1 and 10 are adjacent, implying $y/|d|^2 + x/|b|^2 + 1 = 0$, which is a contradiction. However, it is straightforward to find a FOR in dimension 6, proving $\Xi[\mathrm{Ci}_{11}(1,2,3) \setminus \{ v \}] = 6$.

order	graphs	(1)	(2.1)	(2.2)
1	1	1	0	0
2	2	0	0	0
3	4	0	0	0
4	11	1	0	0
5	34	8	1	0
6	156	68	2	0
7	1 044	662	28	0
8	12 346	9 888	456	0
9	274 668	247 492	15 954	3
10	12 005 168	11 427 974	957 882	98
11	1 018 997 864	994 403 266	99 869 691	5 765
12	165 091 172 592	163 028 488 360	19 715 979 447	560 500

TABLE II. Number of nonisomorphic graphs with 1–12 vertices. (1)–(2.2) after filtering, cf. main text.

For all graphs with less than 13 vertices, we discard those graphs which satisfy at least one of the following filter criteria:

(1) G or $\overline{G}$ is not connected.

(2.1) G has subgraph K_ℓ, where $\chi_f(G) \leq \ell$.

(2.2) G has subgraph $n\overline{K_2}+mK_1$, where $\chi_f(G) \leq 2n+m < \chi_f(G)+1$ and $m \in \{0, 1\}$.

(3.1)–(3.7) G has an induced subgraph S from Table I with $\chi_f(G) \leq \Xi(S)$.

For obvious reasons, we fall back to a computer-based proof. We use *geng* from the software package *nauty*[32,33] to generate all nonisomorphic graphs. The fractional chromatic number can be obtained by solving the linear program,[29,34]

$$\begin{aligned} \text{maximize: } & \sum_{v \in V(G)} x_v \\ \text{subject to: } & \sum_{v \in \mathcal{I}} x_v \leq 1, \text{ for all } \mathcal{I} \text{ of } G \\ & x_v \geq 0 \text{ for all } v \in V(G), \end{aligned} \tag{1}$$

where $\mathcal{I}$ are independent sets of G, i.e., sets of vertices where all vertices are mutually nonadjacent. We find optimal solutions to this program using the software package *GLPK*[35] and verify the correctness of the solution by applying the strong duality of linear programs, using an accuracy threshold of $\epsilon = 10^{-12}$. We approximate the floating-point value obtained for χ_f by a rational number with less than ϵ deviation, while constraining the denominator to be not larger than nm, where n is the number vertices of G and m is the number of maximal independent sets. This procedure always succeeds and ensures that the calculation of χ_f is exact, despite floating-point arithmetic being used in intermediate steps.

We apply all filters (1)–(3.7) consecutively so that each filter reduces the number of candidate graphs. The numbers of graphs remaining after each step are shown in Table II, for filters (1), (2.1), and (2.2), and as a function of the number of vertices of the graph. The list of 566 366 graphs remaining after filter (2.2) is available in *graph6*-format.[36] For the filters (3.1)–(3.7), we show in Table I the total number of remaining graphs after each filter. No graph remains after applying all filters, which proves Theorem 1.

IV. CONCLUSIONS

Contextuality is a fundamental feature of quantum observables and can be completely detached from any features of the quantum state of the system. This state-independent contextuality already occurs for the most elementary case of observables being sharp and having only two outcomes, one of which is nondegenerate; such observables can be represented by rays in a Hilbert space. Here we have shown that state-independent contextuality with elementary observables requires at least 13 different observables by performing an exhaustive search over all cases with less observables. The Yu–Oh set is an example of such 13 observables and is already realizable on a three-level quantum system, which is the smallest quantum system allowing for contextuality. This is in contrast to the first instances of state-independent contextuality, the Kochen–Specker sets, where the smallest set cannot be realized on a three-level system. Therefore, fifty years after the discovery of state-independent contextuality in quantum theory, we finally have the answer to the question of which is the simplest way to reveal it, i.e., which is the smallest set of elementary observables exhibiting state-independent contextuality.

ACKNOWLEDGMENTS

We thank the team of the Scientific Computing Center of Andalusia (CICA) for their help with the distributed computing. This work was supported by Project No. FIS2014-60843-P, "Advanced Quantum Information" (MINECO, Spain), with FEDER funds, the project "Photonic Quantum Information" (Knut and Alice Wallenberg Foundation, Sweden), the EU (ERC Starting Grant GEDENTQOPT), and by the DFG (Forschungsstipendium KL 2726/2–1).

[1] S. Kochen and E. P. Specker, The problem of hidden variables in quantum mechanics, J. Math. Mech. **17**, 59 (1967).

[2] M. Pavičić, J.-P. Merlet, B. D. McKay, and N. D. Megill, Kochen–Specker vectors, J. Phys. A: Math. Gen. **38**, 1577 (2005).

[3] A. Peres, Incompatible results of quantum measurements, Phys. Lett. A **151**, 107 (1990).

[4] N. D. Mermin, Simple unified form for the major no-hidden-variables theorems, Phys. Rev. Lett. **65**, 3373 (1990).

[5] A. Peres, Two simple proofs of the Kochen–Specker theorem, J. Phys. A: Math. Gen. **24**, L175 (1991).

[6] M. Kernaghan and A. Peres, Kochen–Specker theorem for eight-dimensional space. Phys. Lett. A **198**, 1 (1995).

[7] A. Cabello, J. M. Estebaranz, and G. García-Alcaine, Bell–Kochen–Specker theorem: A proof with 18 vectors, Phys. Lett. A **212**, 183 (1996).

[8] J. H. Conway and S. Kochen, reported in A. Peres, *Quantum Theory: Concepts and Methods* (Kluwer, Dordrecht, 1995), p. 114.

[9] P. Lisoněk, P. Badziąg, J. R. Portillo, and A. Cabello, Kochen–Specker set with seven contexts, Phys. Rev. A **89**, 042101 (2014).

[10] S. Yu and C. H. Oh, State-independent proof of Kochen–Specker theorem with 13 rays, Phys. Rev. Lett. **108**, 030402 (2012).

[11] M. Kleinmann, C. Budroni, J.-Å. Larsson, O. Gühne, and A. Cabello, Optimal inequalities for state-independent contextuality, Phys. Rev. Lett. **109**, 250402 (2012).

[12]G. Kirchmair, F. Zähringer, R. Gerritsma, M. Kleinmann, O. Gühne, A. Cabello, R. Blatt, and C. F. Roos, State-independent experimental test of quantum contextuality, Nature (London) **460**, 494 (2009).

[13]E. Amselem, M. Rådmark, M. Bourennane, and A. Cabello, State-independent quantum contextuality with single photons, Phys. Rev. Lett. **103**, 160405 (2009).

[14]O. Moussa, C. A. Ryan, D. G. Cory, and R. Laflamme, Testing contextuality on quantum ensembles with one clean qubit, Phys. Rev. Lett. **104**, 160501 (2010).

[15]C. Zu, Y.-X. Wang, D.-L. Deng, X.-Y. Chang, K. Liu, P.-Y. Hou, H.-X. Yang, and L.-M. Duan, State-independent experimental test of quantum contextuality in an indivisible system, Phys. Rev. Lett. **109**, 150401 (2012).

[16]X. Zhang, M. Um, J. Zhang, S. An, Y. Wang, D.-L. Deng, C. Shen, L.-M. Duan, and K. Kim, State-independent experimental test of quantum contextuality with a single trapped ion, Phys. Rev. Lett. **110**, 070401 (2013).

[17]V. D'Ambrosio, I. Herbauts, E. Amselem, E. Nagali, M. Bourennane, F. Sciarrino, and A. Cabello, Experimental implementation of a Kochen–Specker set of quantum tests, Phys. Rev. X **3**, 011012 (2013).

[18]G. Cañas, S. Etcheverry, E. S. Gómez, C. Saavedra, G. B. Xavier, G. Lima, and A. Cabello, Experimental implementation of an eight-dimensional Kochen–Specker set and observation of its connection with the Greenberger–Horne–Zeilinger theorem, Phys. Rev. A **90**, 012119 (2014).

[19]G. Cañas, M. Arias, S. Etcheverry, E. S. Gómez, A. Cabello, G. B. Xavier, and G. Lima, Applying the simplest Kochen–Specker set for quantum information processing, Phys. Rev. Lett. **113**, 090404 (2014).

[20]M. Jerger, Y. Reshitnyk, M. Oppliger, A. Potočnik, M. Mondal, A. Wallraff, K. Goodenough, S. Wehner, K. Juliusson, N. K. Langford, and A. Fedorov, Contextuality without nonlocality in a superconducting quantum system, arXiv:1602.00440.

[21]K. Horodecki, M. Horodecki, P. Horodecki, R. Horodecki, M. Pawłowski, and M. Bourennane, Contextuality offers device-independent security, arXiv:1006.0468.

[22]A. Cabello, Proposal for revealing quantum nonlocality via local contextuality, Phys. Rev. Lett. **104**, 220401 (2010).

[23]B.-H. Liu, X.-M. Hu, J.-S. Chen, Y.-F. Huang, Y.-J. Han, C.-F. Li, G.-C. Guo, and A. Cabello, Experimental test of the free will theorem, arXiv:1603.08254.

[24]L. Aolita, R. Gallego, A. Acín, A. Chiuri, G. Vallone, P. Mataloni, and A. Cabello, Fully nonlocal quantum correlations, Phys. Rev. A **85**, 032107 (2012).

[25]O. Gühne, C. Budroni, A. Cabello, M. Kleinmann, and J.-Å. Larsson, Bounding the quantum dimension with contextuality, Phys. Rev. A **89**, 062107 (2014).

[26]A. Cabello, M. Kleinmann, and C. Budroni, Necessary and sufficient condition for quantum state-independent contextuality, Phys. Rev. Lett. **114**, 250402 (2015).

[27]R. Ramanathan and P. Horodecki, Necessary and sufficient condition for state-independent contextual measurement scenarios, Phys. Rev. Lett. **112**, 040404 (2014).

[28]P. J. Cameron, A. Montanaro, M. W. Newman, S. Severini, and A. Winter, On the quantum chromatic number of a graph, Electr. J. Comb. **14**, #R81 (2007).

[29]E. R. Scheinerman and D. H. Ullman, *Fractional Graph Theory. A Rational Approach to the Theory of Graphs* (John Wiley & Sons, New York, 1997).

[30]A. Solís, *Algoritmos para la Resolución del Problema de Representación Ortogonal* (Master Thesis, Universidad de Sevilla, 2012)

[31]A. Solís and J. R. Portillo, Orthogonal representation of graphs, arXiv:1504.03662.

[32]B. D. McKay and A. Piperno, Practical graph isomorphism, II, J. Symb. Comput. **60**, 94 (2014).

[33]nauty and Traces, `http://pallini.di.uniroma1.it/`.

[34]D. Bertsimas and J. N. Tsitsiklis, *Introduction to Linear Optimization* (Athena Scientific, Belmont, Massachusetts, 1997).

[35]GNU Linear Programming Kit, `http://www.gnu.org/software/glpk/`.

[36]`http://personal.us.es/josera/minSIC/`, *sha256*-digest `a23b d030 d126 a3e5 44c0 f820 afcf aa9a ac31 a991 4ae1 416a 6a1a 682f 9bbe 2535`.

[37]B. D. McKay, Description of graph6 and sparse6 encodings, `http://cs.anu.edu.au/~bdm/data/formats.txt`.

Quantum correlations are stronger than all nonsignaling correlations produced by n-outcome measurements

Matthias Kleinmann*
Department of Theoretical Physics, University of the Basque Country UPV/EHU, P.O. Box 644, E-48080 Bilbao, Spain

Adán Cabello†
Departamento de Física Aplicada II, Universidad de Sevilla, E-41012 Sevilla, Spain

We show that, for any n, there are m-outcome quantum correlations, with $m > n$, which are stronger than any nonsignaling correlation produced from selecting among n-outcome measurements. As a consequence, for any n, there are m-outcome quantum measurements that cannot be constructed by selecting locally from the set of n-outcome measurements. This is a property of the set of measurements in quantum theory that is not mandatory for general probabilistic theories. We also show that this prediction can be tested through high-precision Bell-type experiments and identify past experiments providing evidence that some of these strong correlations exist in nature. Finally, we provide a modified version of quantum theory restricted to having at most n-outcome quantum measurements.

Introduction.—The violation of Bell inequalities [1–6] does not only show the impossibility of local realism [7], but also demonstrates (i) the existence of entangled states, i.e., states which cannot be produced by choosing among states produced locally, and (ii) the existence of incompatible measurements, i.e., measurements whose outcomes cannot be obtained from a single joint measurement. Remarkably, this holds not only assuming quantum theory (QT) but also holds for the much broader set of general probabilistic theories (GPTs) [8–11]. GPTs include classical probability theory and QT, and also theories admitting supraquantum nonsignaling correlations, such as, e.g., Popescu-Rohrlich boxes [12].

Svetlichny pointed out that (i) can be refined and that for any number of parties n, there are correlations predicted by QT that cannot be explained by any GPT in which all states are produced by choosing among $(n-1)$-partite entangled states [13–15]. Hence, the violation of n-partite Svetlichny inequalities [16–19] demonstrates the existence of genuinely n-partite entangled states, and therefore puts strong constraints on which GPTs are suitable to describe nature.

Here we address the problem of whether there is a sensible way to go beyond (ii) and, assuming that QT is correct, constrain more rigidly the structure of the set of measurements in any GPT describing nature. Our main result is the proof that, according to QT, nature does produce correlations which cannot be generated by shared randomness (e.g., by means of local hidden variables) and nonsignaling correlations for which the number of outcomes is limited to n. In this sense, we show that quantum correlations are not n-chotomic, for any $n = 2, 3, \ldots$. This implies that, the same way Bell inequality experiments exclude all local realistic theories, QT predicts that certain experiments can exclude all GPTs in which

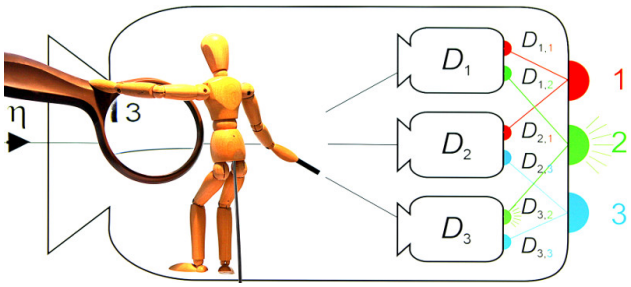

FIG. 1. Illustration of a three-outcome measurement which can be explained as selecting one from three two-outcome measurements. From the outside, the measurement apparatus (represented by the outer box) has three outcomes (represented by three lights of different colors). The state of a physical system tested by the apparatus is described by η_α, where $\alpha = 1, 2, 3$ is a variable that is hidden to the experimenter but can be read off by the measurement apparatus (illustrated by a robot inside the box using a magnifying glass), without disturbing the state of the system. From the inside, the measurement apparatus works as follows: based on the value of α (here: $\alpha = 3$) a corresponding two-outcome measurement D_α is selected (as the robot does by operating the switch selecting the measurement D_3).

measurements are locally selected from n-outcome measurements. A possible selection mechanism, in which all measurements are produced from two-outcome measurements with the help of hidden variables, is illustrated in Fig. 1.

However, according to our analysis, such experiments require visibilities beyond what is currently feasible. This motivates us to consider a particular subclass of GPTs: those in which measurements are locally selected from n-outcome *quantum* measurements. We identify past experiments which, for $n = 2$ and $n = 3$ and under some assumptions, may be taken as experimental falsifications of this subclass of GPTs. Finally, we take the possibility seriously that QT does not account for correlations in na-

* matthias_kleinmann001@ehu.eus
† adan@us.es

ture and provide a modified version of QT restricted to having at most n-outcome quantum measurements. This theory shows that nonsignaling correlations for which the number of outcomes is limited to n constitute an alternative that should be experimentally tested.

Quantum correlations are not n-chotomic.—For $m > n$, the set of m-outcome measurements in QT is strictly larger than the convex hull of the n-outcome measurements [20]. Hence, there are, e.g., three-outcome quantum measurements which cannot be implemented by choosing one from a set of two-outcome quantum measurements. Here we present a result which goes beyond this observation. We demonstrate that if QT is correct, then any GPT describing nature needs to share this property. For this, we prove the yet more general result that any GPT not having this property cannot reproduce the correlations predicted by QT. This result only depends on properties of correlations and does not rely on how the preparation and measurement devices work. Therefore, it enables us to exclude all those GPTs in a device-independent way.

Suppose that two parties can perform several measurements on a bipartite system and that each party can independently choose among the measurement settings. For a fixed measurement setting μ on the first party and ν on the second party, we write $P_{\mu,\nu}(k,\ell)$ for the probability to obtain the corresponding outcomes k and ℓ. A set of such correlations is nonsignaling, if $\sum_\ell P_{\mu,\nu}(k,\ell) \equiv P_{\mu,\_}(k)$ is independent of ν and $\sum_k P_{\mu,\nu}(k,\ell) \equiv P_{\_,\nu}(\ell)$ is independent of μ. We are now interested in the case where the number of measurement outcomes is limited to n, i.e., the measurements are n-chotomic. An n-chotomic local measurement obeys $P_{\mu,\_}(k) = 0$ for all k, except for a subset of size n, or, similarly, $P_{\_,\nu}(\ell) = 0$ for all ℓ, except for a subset of size n. The set of nonsignaling n-chotomic correlations $\mathcal{P}_n$ is then the convex hull of the set of nonsignaling correlations where all measurements are, at most, n-chotomic.

We address the question of whether the set of quantum correlations contains correlations that are not in $\mathcal{P}_n$ by considering the combinations of correlations in the Collins–Gisin–Linden–Massar–Popescu inequalities [21] in the formulation of Zohren and Gill [22], namely,

$$I'(\boldsymbol{P}) = P_{2,2}(k<\ell) + P_{1,2}(k>\ell) + P_{1,1}(k<\ell) + P_{2,1}(k\geq\ell), \quad (1)$$

where $P_{2,2}(k<\ell) = \sum_{k<\ell} P_{2,2}(k,\ell)$, and similarly for the other terms. I' can be evaluated for any set of bipartite correlations $\boldsymbol{P}$ which features at least two measurement settings per party. We can now state our main result.

Theorem 1. For any n, there is an $m > n$ and quantum correlations $\boldsymbol{Q} \in \mathcal{P}_m$, such that $I'(\boldsymbol{Q}) < \inf[I'(\mathcal{P}_n)]$.

Proof. It has been shown [23] that for any $\varepsilon > 0$, there exists an m and some quantum correlations $\boldsymbol{Q} \in \mathcal{P}_m$ such that $I'(\boldsymbol{Q}) < \varepsilon$. In Appendix A we prove that $q_n \equiv \inf[I'(\mathcal{P}_n)] > 0$ for any n. Therefore, by choosing $\varepsilon = q_n/2$, the assertion follows. □

This proves that, for any n, there are quantum correlations which are not nonsignaling n-chotomic. For example, the hypothetical Popescu–Rohrlich box [12] is a GPT predicting correlations that are impossible according to QT. However, this GPT only contains dichotomic measurements. Hence, Theorem 1 reveals that QT contains correlations that are impossible to achieve for a Popescu–Rohrlich box.

Consequence 2. QT contains correlations that cannot be explained by dichotomic GPTs, even if we admit supraquantum correlations, such as Popescu–Rohrlich boxes.

Experiments.—Theorem 1 gives rise to the question: Is it feasible to experimentally demonstrate the existence of correlations which cannot be explained by n-chotomic GPTs with current quantum technology? As shown in Theorem 1, in principle, we could use experiments aiming to violate I' for this purpose. However, in practice, this approach is rather unfeasible since, even for excluding dichotomic GPTs, we would need to observe a value of I' below $\frac{1}{2}$, something that requires quantum measurements with at least ten outcomes [22]. Further investigation is therefore needed in order to identify inequalities with more modest experimental demands.

As a first step in this direction, we explore whether it is possible to experimentally exclude GPTs in which measurements are produced by selecting from, at most, n-outcome *quantum* measurements. These GPTs constitute interesting variants of QT in which the sets of measurements are arguably simpler than the one of QT, as we discuss below. In addition, unlike most alternatives to QT investigated in the past (e.g., local realistic theories), they share most of the predictions of QT, including the violation of Bell inequalities.

For this purpose, we compute the upper bounds on $1 - I'$ for GPTs for dichotomic and trichotomic quantum measurements when the outcomes k, l take values $1, 2, 3$ (I_3) or values $1, 2, 3, 4$ (I_4). We observe that although violating the resulting inequalities is experimentally demanding, there is already experimental evidence [27, 28, 30] supporting that there are measurements which cannot be explained choosing from quantum dichotomic or quantum trichotomic measurements. Interestingly, when we compute the upper bounds for the bipartite all-versus-nothing Bell inequality with three four-outcome measurements [26], we observe that the results of a previous experiment, show a clear violation of the quantum trichotomic bound [29]. This suggests that this inequality can be a powerful tool to provide conclusive evidence of the existence of genuinely nontrichotomic quantum measurements. We also compute the upper bounds of an inequality due to Vértesi and Bene [24] which, so far, has not been tested experimentally. However, it is *a priori* interesting for our considerations,

	VB [24]	I_3 [21, 25]	I_4 [21]	AN [26]
2-outcome	21.068*	0.20711	0.20711	8.1962
3-outcome	—	—	0.30495	8.1962
Quantum	21.090*	0.30495*	0.36476*	9.0000*
2-visibility	99.97%	90%	86%	92%
3-visibility	—	—	95%	92%
Experiment	none	Ref. [27]	Ref. [28]	Ref. [29]
2-violation		5.5σ	16σ	70σ
3-violation	—	—	4.3σ	70σ

TABLE I. Upper bounds on correlations, required visibility, and experimental results. Values with an asterisk* have been established in prior work. VB stands for the combination of correlations in the Vértesi–Bene inequality [24], I_n for $1 - I'$ with possible outcomes $k, \ell = 1, 2, \ldots, n$, and AN for the correlations in an all-versus-nothing inequality [26]. The rows "2-outcome," "3-outcome," and "Quantum" list upper bounds when quantum measurements have only two, only three or an unrestricted number of outcomes, respectively. In the rows "2-visibility" and "3-visibility" the required visibility (absence of white noise, i.e., minimal p if the prepared state is a mixture of the target state and a completely depolarized state, $\varrho_{\text{prepared}} = p\varrho_{\text{target}} + (1-p)\varrho_{\text{depolarized}}$) is shown, where the former is for violating the two-outcome bound and the latter for violating the three-outcome bound. In the last rows, observed experimental violations of the two-outcome and three-outcome bounds are shown, in terms of multiples of statistical standard deviations.

since it can be violated by a two-qubit system. Unfortunately, we find that the visibility required to falsify dichotomic quantum measurements using the Vértesi–Bene inequality is too high for current experiments.

We have summarized all our calculations and the significant experimental results in Table I. The methods that we have used for calculating the upper bounds are described in Appendix B. It is important to remark that all mentioned experiments fail to satisfy several of the conditions needed to extract loophole-free conclusions. For example, all of them require the fair sampling assumption due to the low detection efficiency. Furthermore, in all of these experiments, locality is assumed rather than enforced by spacelike separation. Most critically, in all studied cases, the n-outcome measurements are actually implemented using dichotomic measurements due to a limited number of detectors. But the existing experiments suggest that a loophole-free version of these experiments is within current experimental reach and can demonstrate the existence of genuinely nondichotomic and nontrichotomic quantum measurements.

At this point, the conclusion is that there is already evidence that there are correlations in nature which cannot be explained by GPTs with dichotomic and trichotomic quantum measurements. However, more experimental effort is needed for a loophole-free confirmation of this result, and even more theoretical and experimental effort is needed for demonstrating correlations which cannot be explained by more general GPTs with dichotomic measurements.

Probabilistic theories with n-chotomic measurements.—Our main result, Theorem 1, establishes that nonsignaling n-chotomic correlations $\boldsymbol{P} \in \mathcal{P}_n$ cannot explain all quantum correlations. In this section, we take the possibility seriously that QT does *not* account for correlations in nature and we argue how n-chotomic measurements with fixed n may constitute a plausible alternative to the construction used in QT.

The first argument is the observation that, even in the everyday use of QT, we find situations in which the set of actual measurements is only a subset of the set of measurements possible *a priori*. One example is the superselection rules arising from the nonexistence of certain ways of manipulating a system and the constraints on its time evolution [31]. Another example arises when quantum systems can only be manipulated locally. There, the standard paradigm is the paradigm of local operations and classical communication in which several separated parties have access to a shared composite quantum system but there is no quantum interaction between the parts. Consequently, there are outcomes of two-outcome measurements that cannot participate in certain measurements with more than two outcomes [32, 33].

The second argument why n-chotomic measurements may be a plausible alternative to QT is its simplicity. From the perspective of GPTs, the fact that a theory includes measurements which cannot be created by choosing from two-outcome measurements is surprising: Any measurement with more than two outcomes can be coarse-grained to a two-outcome measurement (k, not k), simply by only distinguishing between the outcome labeled k and any other outcome. Now, consider the converse problem. Suppose that we have the set of all two-outcome measurements of a GPT and we want to construct the set of all measurements with any number of outcomes. Then, the arguably simplest way to do it is as it is illustrated in Fig. 1, i.e., by selecting from two-outcome measurements. The fact that this is not the case in QT tells us that QT is, in this sense, very special. Fortunately, Theorem 1 shows that we can test whether nature is special in this sense.

The third argument is that there is nothing *a priori* problematic in a dichotomic theory. To illustrate this point, we develop a dichotomic theory based on QT. For this purpose, it is enough to consider experiments consisting of two stages, the preparation stage and the measurement stage. In standard QT, a preparation is described by a density operator ϱ and a measurement by a family of positive semidefinite operators $(E_1, E_2, \ldots)$ summing to $\mathbb{1}$, so that the probability to obtain outcome k is given by $\operatorname{tr}(E_k\varrho)$.

A straightforward example where two-outcome measurements are insufficient is a measurement which can perfectly distinguish between more than two states so that $\operatorname{tr}(\varrho_\ell E_k) = \delta_{\ell,k}$, where $\delta_{\ell,k}$ denotes the Kronecker delta. However, there is nothing particularly characteristic of QT in this example as already in our everyday

classical experience we can easily distinguish different preparations—for example, the six distinct outcomes of a die. In order to be able to separate this trivial example from the case we are interested in, we consider a modification of QT. Imagine that the state preparation does not only prepare the quantum state but, in addition, transmits some information, e.g., an integer value α. In turn, the measurement apparatus is sensitive to α and can exhibit different behavior depending on α. This means that α carries some classical information, e.g., which state ϱ_k was prepared or which side of the die is up, covering the aforementioned situation, cf. also Fig. 1. In fact, this scenario is more realistic than it may seem. For example, in a photon experiment, the halfwave plate used to prepare different polarization states may introduce a slight shift in momentum, and it may happen that the analyzing setup is sensible to this shift and gives a different response depending on the momentum.

A general formalism to capture this situation is to modify the standard formulation of QT by replacing the density operator ϱ by positive semidefinite operators $(\eta_1, \eta_2, \dots) \equiv \boldsymbol{\eta}$ obeying $\sum_\alpha \mathrm{tr}(\eta_\alpha) = 1$ and to substitute each operator E_k by positive semidefinite operators $(D_{1,k}, D_{2,k}, \dots) \equiv \boldsymbol{D}$ such that $\sum_k D_{\alpha,k} = \mathbb{1}$ for each α. If there is no other sensitivity to α, then outcome k will have probability $P(k) = \sum_\alpha \mathrm{tr}(\eta_\alpha D_{\alpha,k})$. If we restrict the quantum part of the measurements to be trivial, i.e., all $D_{\alpha,k}$ are either $\mathbb{1}$ or 0, then, effectively, we would have a hidden variable model. If, for each α, at most two operators $D_{\alpha,k}$ are nonzero, then, on a fundamental level, all measurements are dichotomic, and similarly for the n-chotomic case.

Let us now use the above example to illustrate why at least bipartite correlations are required to falsify these GPTs. For a single party, we can always explain *a posteriori* any experiment in which the correlations of certain states $\boldsymbol{\eta}^{(\mu)}$ and measurements $\boldsymbol{D}^{(\nu)}$ are considered. Indeed, we may let $D^{(\nu)}_{\alpha,k} = p_k^{(\alpha,\nu)}$ and $\eta^{(\mu)}_\alpha = \delta_{\alpha,\mu}$, where $p_k^{(\mu,\nu)}$ are probability distributions that do not contradict the observations. A way to inhibit such constructions is to move into a setup in which a system is distributed between two parties and each of them performs local measurements. Then, instead of preparing states $\boldsymbol{\eta}^{(\mu)}$ and performing measurements $\boldsymbol{D}^{(\nu)}$, both parties perform independent local measurements $\boldsymbol{D}'^{(\mu)}$ and $\boldsymbol{D}^{(\nu)}$, respectively, on a fixed bipartite state $\boldsymbol{\eta}$. The resulting observations are then distributed according to the correlations

$$P_{\mu,\nu}(k,\ell) = \sum_{\alpha',\alpha} \mathrm{tr}(\eta_{\alpha',\alpha}\, D'^{(\mu)}_{\alpha',k} \otimes D^{(\nu)}_{\alpha,\ell}). \qquad (2)$$

When all local measurements are at most n-chotomic, then, by construction, these correlations are nonsignaling n-chotomic and are therefore subject to Theorem 1.

Conclusions.—Quantum theory (QT) is in agreement with all existing experimental evidence. Therefore, when exploring alternative theories to QT, it is sensible to focus on those giving similar predictions. In this Letter we have studied a large class of such alternative theories. We have considered a class of general probabilistic theories in which the set of measurements is constructed by selecting from measurements with n outcomes. For any n, these theories satisfy Bell-type inequalities which are violated by QT. Testing this prediction is a fundamental challenge for the future, as it would demonstrate that correlations in nature are stronger than those allowed by theories which, in other experiments, produce correlations exceeding those of QT, e.g., as it is the case for Popescu–Rohrlich boxes. However, this challenge is difficult and will require further efforts both in theory and experiments.

Meanwhile, as an example of the kind of tools that will be needed, we have considered theories with the same set of n-outcome measurements than QT for a fixed n, but such that any measurement with more outcomes is constructed by selecting measurements with only n outcomes. These theories share meany features with QT and can, e.g., explain the violation of Bell inequalities. However, we have shown that these alternative theories satisfy certain Bell-type inequalities which are violated by QT. The violations predicted by QT are very small and testing them requires high-precision experiments. We have identified previous experiments which, up to some assumptions, seem to rule out these theories for $n = 2$ and $n = 3$.

ACKNOWLEDGMENTS

We thank Géza Giedke, Gustavo Lima, Géza Tóth, and Tamás Vértesi for discussions. This work was supported by the FQXi large grant project "The Nature of Information in Sequential Quantum Measurements", project No. FIS2014-60843-P "Advanced Quantum Information" (MINECO, Spain) with FEDER funds, the Project "Photonic Quantum Information" (Knut and Alice Wallenberg Foundation, Sweden), the EU (ERC Starting Grant GEDENTQOPT), and the DFG (Forschungsstipendium KL 2726/2–1).

Appendix A: Proof of Theorem 1.

For the remaining step in the proof of Theorem 1 we assume without loss of generality that all measurement outcomes are labeled $k, \ell = 1, 2, \dots$, and we define $\mathcal{P}_{n,r}$ as the subset of $\mathcal{P}_n$ for which the maximal index k or ℓ is at most r. We show that (a) $\inf[I'(\mathcal{P}_{n,r})] \geq 2^{1-r}$ for any r and (b) $I'(\mathcal{P}_{n,r'}) = I'(\mathcal{P}_n)$ for some r'. It follows that $\inf[I'(\mathcal{P}_n)] = \inf[I'(\mathcal{P}_{n,r'})] \geq 2^{1-r'} > 0$ holds, which is the statement needed in order to complete the proof in the main text.

(a) For arbitrary correlations $\boldsymbol{P} \in \mathcal{P}_{n,r}$ we denote by $\boldsymbol{P}' \in \mathcal{P}_{n,r-1}$ the correlations where in $\boldsymbol{P}$ the rth outcomes are merged with the first outcomes. This

implies $P'_{\mu,\nu}(k \geq \ell) = P_{\mu,\nu}(k \geq \ell) + P_{-,\nu}(r) - P_{\mu,-}(r) + P_{\mu,\nu}(r,1)$, and therefore, $I'(\boldsymbol{P'}) = I'(\boldsymbol{P}) - [P_{2,2}(r,1) + P_{1,2}(1,r) + P_{1,1}(r,1) - P_{2,1}(r,1)] \leq I'(\boldsymbol{P}) + P_{2,1}(r,1) \leq 2I'(\boldsymbol{P})$. By induction and due to $I'(\mathcal{P}_{n,1}) = \{1\}$, we have $2^{1-r} \leq I'(\boldsymbol{P})$.

(b) We consider the set $\tilde{\mathcal{P}}_n$ of those correlations which can be created from the correlations in $\mathcal{P}_{n,n}$ by applying all changes of the labels of the outcomes $\lambda'_\mu \colon \{1,\ldots,n\} \to \mathbb{N}$, and similarly λ_ν, via $P_{\mu,\nu}(k,\ell) \mapsto P_{\mu,\nu}(\lambda'_\mu(k), \lambda_\nu(\ell))$, while all other correlation terms are zero. This does not yield more than $4n^2$ logical relations like $\lambda_\mu(k) < \lambda_\nu(l)$ in I' and hence, at most 2^{4n^2} different labelings are needed to reach all logical relations. Since this is a finite set, there is an integer r' denoting the maximal resulting index in the labelings, and therefore $I'(\mathcal{P}_{n,r'}) \supseteq I'(\tilde{\mathcal{P}}_n)$. By definition, $\mathcal{P}_n$ is the convex hull of $\tilde{\mathcal{P}}_n$, so that $I'(\tilde{\mathcal{P}}_n) = I'(\mathcal{P}_n)$ follows from the fact that I' is affine. Therefore, $I'(\mathcal{P}_{n,r'}) = I'(\mathcal{P}_n)$ holds due to $\mathcal{P}_{n,r'} \subseteq \mathcal{P}_n$.

Appendix B: Quantum n-chotomic bounds in Table I.

The maximal quantum value is known for some inequalities or it can be numerically approximated by a hierarchy of semidefinite programs suggested by Navascués, Pironio, and Acín [34]. For n-chotomic quantum measurements, one can proceed similarly, since it is enough to maximize the value of the inequality, but with the additional assumption that at most n measurement outcomes are nontrivial. By exploring all possible combinations with n nontrivial outcomes and calculating the maximal bound for each of these cases, we obtain the n-chotomic bounds provided in Table I.

We used the third level of the hierarchy for the values in the rows "2-outcome" and "3-outcome." Since this is an upper approximation on the true value, these values are at most too pessimistic. For the values in the row "Quantum," the given values are for certain quantum states and measurements. This value is optimal for AN, and the value coincides with the bound from the second level of the hierarchy for I_3 and I_4. Only for VB, the third level of the hierarchy gives a slightly larger value, $21.092 > 21.090$.

[1] S. J. Freedman and J. F. Clauser, "Experimental test of local hidden-variable theories," Phys. Rev. Lett. **28**, 938–941 (1972).

[2] A. Aspect, J. Dalibard, and G. Roger, "Experimental test of Bell's inequalities using time-varying analyzers," Phys. Rev. Lett. **49**, 1804–1807 (1982).

[3] G. Weihs, T. Jennewein, C. Simon, H. Weinfurter, and A. Zeilinger, "Violation of Bell's inequality under strict Einstein locality conditions," Phys. Rev. Lett. **81**, 5039–5043 (1998).

[4] B. Hensen, H. Bernien, A. E. Dréau, A. Reiserer, N. Kalb, M. S. Blok, J. Ruitenberg, R. F. L. Vermeulen, R. N. Schouten, C. Abellán, W. Amaya, V. Pruneri, M. W. Mitchell, M. Markham, D. J. Twitchen, D. Elkouss, S. Wehner, T. H. Taminiau, and R. Hanson, "Loophole-free Bell inequality violation using electron spins separated by 1.3 kilometres," Nature (London) **526**, 682–686 (2015).

[5] M. Giustina, M. A. M. Versteegh, S. Wengerowsky, J. Handsteiner, A. Hochrainer, K. Phelan, F. Steinlechner, J. Kofler, J.-Å. Larsson, C. Abellán, W. Amaya, V. Pruneri, M. W. Mitchell, J. Beyer, T. Gerrits, A. E. Lita, L. K. Shalm, S. W. Nam, T. Scheidl, R. Ursin, B. Wittmann, and A. Zeilinger, "Significant-loophole-free test of Bell's theorem with entangled photons," Phys. Rev. Lett. **115**, 250401 (2015).

[6] L. K. Shalm, E. Meyer-Scott, B. G. Christensen, P. Bierhorst, M. A. Wayne, M. J. Stevens, T. Gerrits, S. Glancy, D. R. Hamel, M. S. Allman, K. J. Coakley, S. D. Dyer, C. Hodge, A. E. Lita, V. B. Verma, C. Lambrocco, E. Tortorici, A. L. Migdall, Y. Zhang, D. R. Kumor, W. H. Farr, F. Marsili, M. D. Shaw, J. A. Stern, C. Abellán, W. Amaya, V. Pruneri, T. Jennewein, M. W. Mitchell, P. G. Kwiat, J. C. Bienfang, R. P. Mirin, E. Knill, and S. W. Nam, "Strong loophole-free test of local realism," Phys. Rev. Lett. **115**, 250402 (2015).

[7] J. S. Bell, "On the Einstein Podolsky Rosen paradox," Physics **1**, 195–200 (1964).

[8] G. Ludwig, *An Axiomatic Basis for Quantum Mechanics*, Vol. I (Springer-Verlag, Berlin, 1985).

[9] P. Mittelstaedt, *The Interpretation of Quantum Mechanics and the Measurement Process* (Cambridge University Press, Cambridge, England, 1998).

[10] G. Chiribella, G. M. D'Ariano, and P. Perinotti, "Probabilistic theories with purification," Phys. Rev. A **81**, 062348 (2010).

[11] A. Acín, R. Augusiak, D. Cavalcanti, C. Hadley, J. K. Korbicz, M. Lewenstein, Ll. Masanes, and M. Piani, "Unified framework for correlations in terms of local quantum observables," Phys. Rev. Lett. **104**, 140404 (2010).

[12] S. Popescu and D. Rohrlich, "Quantum nonlocality as an axiom," Found. Phys. **24**, 379–385 (1994).

[13] G. Svetlichny, "Distinguishing three-body from two-body nonseparability by a Bell-type inequality," Phys. Rev. D **35**, 3066–3069 (1987).

[14] D. Collins, N. Gisin, S. Popescu, D. Roberts, and V. Scarani, "Bell-type inequalities to detect true n-body nonseparability," Phys. Rev. Lett. **88**, 170405 (2002).

[15] M. Seevinck and G. Svetlichny, "Bell-type inequalities for partial separability in N-particle systems and quantum mechanical violations," Phys. Rev. Lett. **89**, 060401 (2002).

[16] J. Lavoie, R. Kaltenbaek, and K. J. Resch, "Experimental violation of Svetlichny's inequality," New J. Phys. **11**, 073051 (2009).

[17] C. Erven, E. Meyer-Scott, K. Fisher, J. Lavoie, B. L. Hig-

gins, Z. Yan, C. J. Pugh, J.-P. Bourgoin, R. Prevedel, L. K. Shalm, L. Richards, N. Gigov, R. Laflamme, G. Weihs, T. Jennewein, and K. J. Resch, "Experimental three-photon quantum nonlocality under strict locality conditions," Nat. Photonics **8**, 292–296 (2014).

[18] D. R. Hamel, L. K. Shalm, H. Hübel, A. J. Miller, F. Marsili, V. B. Verma, R. P. Mirin, S. W. Nam, K. J. Resch, and T. Jennewein, "Direct generation of three-photon polarization entanglement," Nat. Photonics **8**, 801–807 (2014).

[19] J. T. Barreiro, J.-D. Bancal, P. Schindler, D. Nigg, M. Hennrich, T. Monz, N. Gisin, and R. Blatt, "Demonstration of genuine multipartite entanglement with device-independent witnesses," Nat. Phys. **9**, 559–562 (2013).

[20] P. Busch, M. Grabowski, and P. J. Lahti, *Operational Quantum Physics* (Springer, Berlin, 1995).

[21] D. Collins, N. Gisin, N. Linden, S. Massar, and S. Popescu, "Bell inequalities for arbitrarily high-dimensional systems," Phys. Rev. Lett. **88**, 040404 (2002).

[22] S. Zohren and R. D. Gill, "Maximal violation of the Collins-Gisin-Linden-Massar-Popescu inequality for infinite dimensional states," Phys. Rev. Lett. **100**, 120406 (2008).

[23] S. Zohren, P. Reska, R. D. Gill, and W. Westra, "A tight Tsirelson inequality for infinitely many outcomes," Europhys. Lett. **90**, 10002 (2010).

[24] T. Vértesi and E. Bene, "Two-qubit Bell inequality for which positive operator-valued measurements are relevant," Phys. Rev. A **82**, 062115 (2010).

[25] A. Acín, T. Durt, N. Gisin, and J. I. Latorre, "Quantum nonlocality in two three-level systems," Phys. Rev. A **65**, 052325 (2002).

[26] A. Cabello, ""All versus nothing" inseparability for two observers," Phys. Rev. Lett. **87**, 010403 (2001).

[27] A. Vaziri, G. Weihs, and A. Zeilinger, "Experimental two-photon, three-dimensional entanglement for quantum communication," Phys. Rev. Lett. **89**, 240401 (2002).

[28] T. Ikuta and H. Takesue, "Enhanced violation of the Collins-Gisin-Linden-Massar-Popescu inequality with optimized time-bin-entangled ququarts," Phys. Rev. A **93**, 022307 (2016).

[29] T. Yang, Q. Zhang, J. Zhang, J. Yin, Z. Zhao, M. Żukowski, Z.-B. Chen, and J.-W. Pan, "All-versus-nothing violation of local realism by two-photon, four-dimensional entanglement," Phys. Rev. Lett. **95**, 240406 (2005).

[30] A. C. Dada, J. Leach, G. S. Buller, M. J. Padgett, and E. Andersson, "Experimental high-dimensional two-photon entanglement and violations of generalized Bell inequalities," Nat. Phys. **7**, 677–680 (2011).

[31] G. C. Wick, A. S. Wightman, and E. P. Wigner, "The intrinsic parity of elementary particles," Phys. Rev. **88**, 101–105 (1952).

[32] C. H. Bennett, D. P. DiVincenzo, C. A. Fuchs, T. Mor, E. Rains, P. W. Shor, J. A. Smolin, and W. K. Wootters, "Quantum nonlocality without entanglement," Phys. Rev. A **59**, 1070–1091 (1999).

[33] M. Kleinmann, H. Kampermann, and D. Bruß, "Asymptotically perfect discrimination in the local-operation-and-classical-communication paradigm," Phys. Rev. A **84**, 042326 (2011).

[34] M. Navascués, S. Pironio, and A. Acín, "Bounding the set of quantum correlations," Phys. Rev. Lett. **98**, 010401 (2007).

Analysing multiparticle quantum states

Otfried Gühne[1], Matthias Kleinmann[2], and Tobias Moroder[1]

[1]Naturwissenschaftlich-Technische Fakultät, Universität Siegen,
Walter-Flex-Straße 3, 57068 Siegen, Germany

[2] Department of Theoretical Physics, University of the Basque Country UPV/EHU,
P.O. Box 644, E-48080 Bilbao, Spain

Abstract. The analysis of multiparticle quantum states is a central problem in quantum information processing. This task poses several challenges for experimenters and theoreticians. We give an overview over current problems and possible solutions concerning systematic errors of quantum devices, the reconstruction of quantum states, and the analysis of correlations and complexity in multiparticle density matrices.

1. Introduction

The analysis of quantum states is important for the advances in quantum optics and quantum information processing. Many experiments nowadays aim at the generation and observation of certain quantum states and quantum effects. For instance, in quantum simulation experiments thermal or ground states of certain spin models should be observed. Another typical problem is the demonstration of advanced quantum control by preparing certain highly entangled states using systems such as trapped ions, superconducting qubits, nitrogen-vacancy centers in diamond, or polarized photons.

All these experiments require a careful analysis in order to verify that the desired quantum phenomenon has indeed been observed. This analysis does not only concern the final data reported in the experiment but in fact, many more questions have to be considered in parallel. Did the experimenter align the measurement devices correctly? Have the count rates been evaluated properly in order to obtain the mean values of the measured observables? Such questions are relevant and, as we demonstrate below, ideas from theoretical physics can help the experimenters answer them.

Many experiments in quantum optics can be divided in several steps (see also Fig. 1). In the beginning, some experimental procedures are carried out and measurements are taken. The results of the measurements are collected as data. These data are then processed to obtain a quantum state or density matrix ϱ, which is often viewed as the best description of the "actual state" generated in the experiment. This quantum state can then be further analysed, for instance, its entanglement properties may be determined.

In this article, we show how ideas from statistics and entanglement theory can be used for analysing the transitions between the four building blocks in Fig. 1. First, we

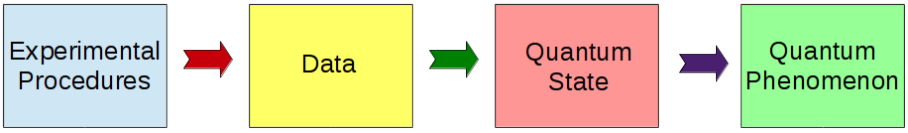

Figure 1. The analysis of many experiments in quantum physics can be divided into several steps, from the experimental procedures to the verification of quantum mechanical properties of the generated states.

consider the transition from the experimental procedures to the data. We show that applying statistical tests to the data can be used to recognize systematic errors in the experimental procedures, such as a misalignment of the measurement devices. Then, we consider the reconstruction of a quantum state from the experimental data. We explain why many frequently used state reconstruction schemes, such as the maximum-likelihood reconstruction, lead to a bias in the resulting state. This can, for instance, result in a fake detection of entanglement, meaning that the reconstructed state is entangled, while the original state, on which the measurements were carried out, was not entangled. We also show how such a bias can be avoided. Finally, we discuss the characterization of quantum states on a purely theoretical level. Assuming a multiparticle density matrix ϱ we show how its entanglement can be characterized and how the complexity of the state can be quantified using tools from information geometry and exponential families.

2. Systematic errors in quantum experiments

In this first part of the article, we discuss what assumptions are typically used in quantum experiments. The violation of these assumptions leads to systematic errors and we show how these systematic errors can be identified using statistical methods and hypothesis tests.

2.1. Assumptions underlying quantum experiments

Before explaining the assumptions, it is useful to discuss a simple example. Consider a two-photon experiment, where a quantum state should be analysed by performing state tomography. For that, Alice and Bob have to measure all the nine possible combinations of the Pauli matrices $\sigma_i \otimes \sigma_j$ for $i, j \in \{x, y, z\}$. In practice, this can be done as follows: Alice and Bob measure the three Pauli matrices $\sigma_x, \sigma_y, \sigma_z$ by measuring the polarization in different directions, getting the possible results $+$ and $-$. These results correspond to the projectors on the eigenvectors of the observable. By combining the results, they obtain one of four possible outcomes from the set $\{++, +-, -+, --\}$. The measurement is repeated N times on copies of the state, where the outcome $++$ occurs $N_{++|ij}$ times etc. From that, one can obtain the relative frequencies $F_{++|ij} = N_{++|ij}/N$ and estimate the expectation values as $\langle \sigma_i \otimes \sigma_j \rangle_{\text{exp}} = (N_{++|ij} - N_{+-|ij} - N_{-+|ij} + N_{--|ij})/N$. In addition, the expectation values of the marginals

$\sigma_i \otimes \sigma_0$ (here and in the following, we set $\sigma_0 = \mathbb{1}$) can be determined from the same data. Given all the experimental results, Alice and Bob may then reconstruct the quantum state via the formula

$$\hat{\varrho} = \frac{1}{4} \sum_{i,j \in \{0,x,y,z\}} \lambda_{ij} \sigma_i \otimes \sigma_j, \text{ where } \lambda_{ij} = \langle \sigma_i \otimes \sigma_j \rangle_{\text{exp}}. \tag{1}$$

This simple quantum state reconstruction scheme is often called linear inversion. It assumes that the observed frequencies equal the probabilities, we will discuss its advantages and disadvantages below. For the moment, we just use it as an example to illustrate the definitions and discussion concerning systematic errors in experiments.

Now we can formulate the assumptions that lead to the statistical model typically used in quantum experiments. We consider a scenario where one actively chooses between different measurements (e.g., the $\sigma_i \otimes \sigma_j$), each having a finite number of results. We use the label s to denote the measurement setting and r to denote the result. It is important to note that, if in an experiment using the setting s one registers the result r, then this outcome $r|s$ is not just treated as a classical result. In addition, each outcome is tied to an operator $M_{r|s}$ (e.g., the projectors onto the eigenstates corresponding to the results $\{++, +-, -+, --\}$ of $\sigma_i \otimes \sigma_j$) that serves as the object to compute probabilities within quantum mechanics: If the underlying quantum state is characterized by the density operator ϱ, then the probability to observe $r|s$ is given by $P(r|s;\varrho) = \text{tr}(\varrho M_{r|s})$. Therefore, this quantum mechanical description is one of the essential ingredients to connect the observed samples with the parameters of the system that one likes to infer. Knowledge about this description can come from previous calibration measurements or from other expertise that one has acquired with the equipment. But one thing should be obvious: If one assumes a description $M_{r|s}$, which deviates from the true description in the experiment $\tilde{M}_{r|s}$, then things can go terribly wrong and these type of errors are the ones that we like to address in the following.

Clearly, such deviations are presumably present in any model, but they are usually assumed to be small. However, considering the increased complexity of present experiments, one can ask the question, whether or not these deviations show up significantly in the data. Well known examples, like different detection efficiencies or dark-count rates in photo-detectors or non-perfect gate fidelities for single-qubit rotations preceding the readout of a trapped ion, could support this scepticism. However, these effects are hardly ever considered in the description of $M_{r|s}$.

Let us complete the list of assumptions. Most often each experiment of setting s is repeated N times, which are assumed to be independent and identically distributed trials. So one further assumes that one always prepares the same quantum state ϱ, measures the same observables $M_{r|s}$, and that both are completely independent ‡.

‡ This means that both, measurements and states are described by the corresponding N-fold tensor products. While such a property can be inferred for the states with the help of the de Finetti theorem [1], one should be aware that its exchangeability requirements do not apply to experiments where one actively measures first all the $s = 1$ measurements, followed by all $s = 2$ measurements and so on.

Clearly, also in all these steps there can be errors, for instance, due to drifts in the measuring devices or dead-times in detectors coming from previous triggering events. However, if everything works as planned, then it is not necessary anymore to keep track of the individual measurement results, since every information that can be inferred about the state parameters is already included in the count rates $N_{r|s}$ of the individual measurement results $r|s$. Their probability is then given by a multinomial distribution $\mathrm{Mult}[N, P(r|s;\varrho)]$ for each setting, which is the distribution characterizing N repetitions of independent trials. Here, the single event probabilities $P(r|s;\varrho) = \mathrm{tr}(\varrho M_{r|s})$ are calculated according to quantum mechanics and these are the only parameters that depend on the quantum state.

Finally, the whole collection of distributions for all measurement settings is the exact parametric model used for most quantum experiments. These distributions are given by the set

$$\mathcal{P}_{\mathrm{QM}} = \Big\{ P(\{N_{r|s}\}_{r,s};\varrho) = \prod_s \mathrm{Mult}\left[N, \mathrm{tr}(\varrho M_{r|s})\right] \text{, for all } \varrho \text{ with } \varrho \geq 0, \mathrm{tr}(\varrho) = 1 \Big\}, \tag{2}$$

and the observed probabilities are assumed to be an element of this set. In the following, we discuss how the validity of this model can be tested.

2.2. Testing the assumptions

How can one test in this framework whether the assumed measurement description is correct for the experiment? As a first try, we could intersperse the experiment with test measurements, in which one prepares previously characterized states. But such an option seems very cumbersome, independent of problems like how to characterize the test states in the first place and to ensure that they are well prepared in between the true experiment. In contrast, we want to do it more directly and this becomes possible, at least partially, by exploiting that quantum states only allow a restricted set of event probabilities.

Let us first discuss the idea for the case where one has access to the true event probabilities $P_0(r|s)$ which can be attained from the relative frequencies $F_{r|s} = N_{r|s}/N \to P_0(r|s)$ in the limit $N \to \infty$. We want to know whether these observed probabilities are at all compatible with the assumed measurement description. This boils down to the question whether there exists a quantum state ϱ_0 with $P_0(r|s) = \mathrm{tr}(\varrho_0 M_{r|s})$ for all r, s. Since quantum states must respect the positivity constraint $\varrho \geq 0$, not all possible probabilities are accessible: For instance, if one measures a qubit along the x, y, z directions, its corresponding probabilities will be constrained by the requirement that the Bloch vector must lie within the Bloch ball. To make this more general, assume that we have a certain set of numbers $w_{r|s}$ such that the observable $\sum_{r|s} w_{r|s} M_{r|s} \geq 0$ has no negative eigenvalues and is, therefore, positive semidefinite. If the probabilities

$P_0(r|s)$ can indeed by realized by a quantum state, one has

$$w \cdot P_0 \equiv \sum_{r,s} w_{r|s} P_0(r|s) = \sum_{r,s} w_{r|s} \operatorname{tr}(\varrho_0 M_{r|s}) = \operatorname{tr}[\varrho_0 \big(\sum_{r,s} w_{r|s} M_{r|s} \big)] \geq 0, \tag{3}$$

where the inequality holds because both operators are positive semidefinite. Thus, if everything is correct one must get a non-negative value for $w \cdot P_0 \geq 0$. Consequently, whenever one observes $w \cdot P_0 < 0$, one knows that something must be wrong and that the description of the measurements $M_{r|s}$ has some flaws. This type of inequalities is similar in spirit to Bell inequalities for local hidden variable models or entanglement witnesses for separable states [2, 3]. Let us point out that the above inequalities are necessary and sufficient. So, indeed any $P_0(r|s)$ which cannot originate from a quantum state, can be detected by appropriately chosen coefficients $w_{r|s}$ by $w \cdot P_0 < 0$ [4]. Finally, we add that besides the positivity, some other constraints for the measurement description are conceivable. For instance, in the example of state tomography from above, the marginal $\langle \sigma_x \otimes \sigma_0 \rangle$ should not depend on whether it has been derived from the measurement $\sigma_x \otimes \sigma_x$ or $\sigma_x \otimes \sigma_y$. This can be formulated as a linear dependency of the form $\sum_{r,s} w_{r|s} M_{r|s} = 0$ and the corresponding constraint even becomes an equality $w \cdot P_0 = 0$.

Note that, with this test we ask the question whether the data $P_0(r|s)$ *fit at all* to the assumed measurement model $M_{r|s}$. But it should be clear that this approach can never serve as a proof that everything is correct in the experiment. For example, one can consider again the Bloch ball, where the measurement model assumes perfectly aligned measurements in the x, y, z directions, but in the true experiment one measures in slightly tilted directions which distorts the resulting Bloch ball. All states from this tilted Bloch ball, which lie outside the standard sphere, will be detected by the above method as being incompatible with the assumed model. For all other states, however, we do not see the difference because they are still consistent with the model.

Finally, let us address the point that we only collect count rates in the experiment. Since the relative frequencies $F_{r|s}$ are only approximations to the true probabilities $P(r|s)$, it is clear that a similar inequality as Eq. (3) does not need to hold anymore for $w \cdot F$, even if everything is correct. One would expect, however, that larger negative values are much less likely. This is indeed the case and is made more quantitative via Hoeffding's inequality [5].

This inequality states the following: Consider N independent, not necessarily identically distributed, bounded random variables $X_i \in [a_i, b_i]$. Then the sample mean $\bar{X} = \sum_i X_i / N$ satisfies

$$\operatorname{Prob}[\bar{X} - \mathbb{E}(\bar{X}) \leq -t] \leq \exp\Big(\frac{-2t^2 N^2}{\sum_i (b_i - a_i)^2} \Big) \tag{4}$$

for all $t > 0$, where $\mathbb{E}(\bar{X})$ denotes the expectation value of $\bar{X}$. In practice, the main statement of this inequality is that for N independent repetitions of an experiment, the probability of deviations from the mean value by a difference t scales like $\exp(-t^2 N)$.

It is important to stress that this result uses no extra assumptions, like N being large, at all.

For our case, we can use Hoeffding's inequality to bound the probability of observing data that violate positivity constraints as in Eq. (3). More precisely, we can derive the following statement [6]: For all distributions compatible with quantum mechanics, the probability to observe frequencies $\{F_{r|s}\}_{r,s}$ such that $w \cdot F < -\varepsilon$ is bounded by

$$\mathrm{Prob}_P\big[w \cdot F < -\varepsilon\big] \equiv \sum_{\substack{\{n_{r|s}\}_{r,s}:\\ w\cdot F<-\varepsilon}} P(\{n_{r|s}\}_{r,s}) \leq \exp\Big(-\frac{2\varepsilon^2 N}{C_w^2}\Big), \text{ for all } P \in \mathcal{P}_{QM} \qquad (5)$$

with $C_w^2 = \sum_s (w_{\max|s} - w_{\min|s})^2$ and $w_{\max|s}$, $w_{\min|s}$ being the extreme values of $\{w_{r|s}\}_r$. Again, this can be interpreted as showing that if everything is correct, then the probability of finding a violation of the positivity constraint is exponentially suppressed.

We can use this statement as follows: Suppose that we should reach a conclusion whether the observed data are "compatible" or "incompatible" with our assumed model. Of course, if we say "incompatible", we do not want to reach this conclusion too often, if indeed everything is perfect. For definiteness, we may assume that the probability of claiming incompatibility if everything is correct should be at maximum $\alpha = 1\%$. We then use Eq. (5) to deduce the threshold value that we need to beat, $\varepsilon_\alpha = \sqrt{C_w^2 |\log(\alpha)|/2N}$. If we now carry out the experiment and register click rates with $w \cdot F < -\varepsilon_\alpha$, we know that there was at most a $\alpha = 1\%$ chance that we would have registered such badly looking data, if everything is correct. Since this would be really bad luck we would rather say "incompatible", and assume that some systematic error was present §.

In practice, this test can be used to detect systematic errors in various scenarios: In ion trap experiments, a typical systematic error comes from the cross talk between the ions, i.e. the fact that a laser focused on one ion also influences the neighbouring ions. This phenomenon can be detected with the presented method [6]. The second application are Bell experiments: In these experiments, the choice of the measurements on one party should ideally not influence the results of the other party and a violation of this condition completely invalidates the result of a Bell test. Again, this non-signalling condition can be formulated as linear constraints on the probabilities and this can be tested with the presented method. In all these applications, the determination of the vector w characterizing the positivity constraint or the linear constraint can be done as follows: One splits the observed data into two parts. From the first part one determines the w leading to the maximal violation of the respective constraint for the first half. Then, one applies this w as a test to the second part of the data. If the violations of the constraint are only due to statistical fluctuations, the respective w for the two parts of the data are uncorrelated and the test will not find a significant violation of the constraint.

§ Since one typically likes to leave the choice of appropriate levels of α to the reader one can also report the p-value [7] of the observed data: It is the smallest α with which we would have still said "incompatible" with the test.

Let us point out that the mathematical framework just described is called a hypothesis test [7], in which one tests the null-hypothesis N_0: "compatible", against the alternative A: "incompatible". The special property of such a test is that there is an asymmetry about the two types of errors that can occur. As already explained, our concern is that, when saying "incompatible", then this statement is more or less correct. The other error can occur when we respond "compatible" to incompatible data. Naturally, this error characterizing the detection strength of our test, ideally, should also be made small. However, it is not possible to reduce both errors equally simultaneously. Nevertheless, since we cannot detect all possible systematic deviations from the assumed model, anyway, one should not be too euphoric about the statement "compatible" in this sense.

Note that, while the presented test has been build up by first deriving specific inequalities for event probabilities and then equipping it with the necessary statistical rigour to arrive at an hypothesis test, one can also take the other direction, by using techniques which are known to be good for hypothesis tests and apply them to the special statistical model of the quantum experiments. We have done this for the so-called generalized likelihood-ratio test [7] and details can be found in Ref. [6]. Finally, other tests for systematic errors can be found in Refs. [8–10].

3. Performing state tomography

In the previous section, we have seen that care has to be taken when making the measurements on the quantum system. In this section, we show that the interpretation of tomographic data, such as the reconstruction of the quantum state, has to be done with care, too. Otherwise, one introduces yet another class of systematic errors.

3.1. Problems with state estimates

We are used to summarize experimental data by an estimate together with an error margin. In quantum state tomography this corresponds to an estimate for the density matrix together with an error region. So, the first question is how one can obtain an estimate $\hat{\varrho}$ for the experimentally prepared density matrix ϱ_{exp} from the observed frequencies $F_{r|s}$. The simplest approach is to use linear inversion, that is, the method given in Eq. (1). This has, however, at first sight some disadvantages: Due to statistical fluctuations the observed frequencies are not equal to the true probabilities and this leads to the consequence that the reconstructed "density matrix" will typically have some negative eigenvalues. This makes the further analysis of the experiment, e.g. the evaluation of entanglement measures, not straightforward. In order to circumvent this, one often makes a density matrix reconstruction by setting

$$\hat{\varrho} = \arg\max_{\sigma \geq 0} \mathcal{F}(F_{r|s}, \sigma). \tag{6}$$

Here, one optimizes a target function $\mathcal{F}$ over all density matrices σ and the optimal σ will obviously be a valid density matrix. Examples for this type of state reconstruction

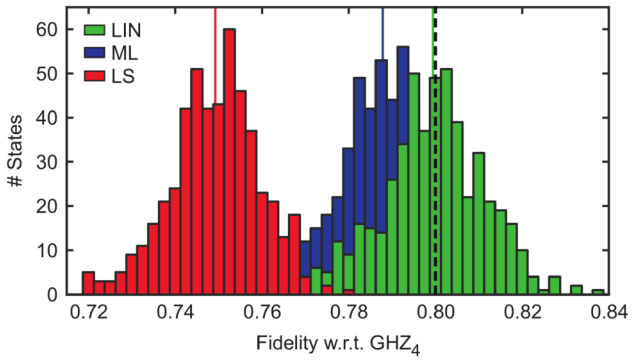

Figure 2. Demonstration of the bias for different state estimators. A given state ϱ_{exp} having 80% fidelity with the GHZ state was used to sample the distribution of the estimator $\hat{\varrho}$ in state space, and from these samples the fidelities with the GHZ state were computed. The maximum-likelihood (ML) and least-square (LS) estimators clearly underestimate the fidelity, while the linear inversion (LIN) is unbiased. The figure is taken from Ref. [11].

are the maximum-likelihood reconstruction or the least-squares reconstruction, both are frequently used for experiments in quantum optics.

An important property of such an estimator is the question whether it is biased or unbiased. This means the following: The underlying state ϱ_{exp} leads via the multinomial distribution to a probability distribution over the frequencies $F_{r|s}$. The estimator $\hat{\varrho}$ is a function from the observed data (the frequencies $F_{r|s}$) to the state space. In this way, the original state ϱ_{exp} induces a probability distribution over the estimators $\hat{\varrho}$, and one can ask whether the expectation value of this equals the original state, $\mathbb{E}[\hat{\varrho}] \stackrel{?}{=} \varrho_{\text{exp}}$. If this is the case, the estimator is unbiased, otherwise it is biased. It must be stressed, however, that biased estimators are not necessarily useless or bad, as it all depends on the purpose the estimator is used for.

For quantum state reconstruction one can prove the following: Any state reconstruction scheme that yields a density matrix from experimental data will be biased, i.e., on average, the reconstructed state $\hat{\varrho}$ will not be the state used in the experiment, $\mathbb{E}[\hat{\varrho}] \neq \varrho_{\text{exp}}$. A proof of this statement was given in Ref. [11], but the following example demonstrates that the problem in finding an unbiased estimator comes from the fact that the quantum mechanical state space is bounded by the positivity constraint. Consider a coin toss where we are interested in the modulus of the difference between the probability of obtaining heads or tails, $\Delta = |p_h - p_t| = 1 - 2\min\{p_h, 1-p_h\}$. This quantity cannot be negative, so also an estimator should not be negative. Let us assume that an estimator $\hat{\Delta}$ is unbiased, $\mathbb{E}[\hat{\Delta}] = \Delta_{\text{exp}}$. Then, for any experimental data that could come from a fair coin ($\Delta_{\text{exp}} = 0$) we cannot have $\hat{\Delta} > 0$ since this would imply $\mathbb{E}[\hat{\Delta}] = \sum_k (1/2)^n \binom{n}{k} \hat{\Delta}(k) > 0$, where k denotes the number of occurrences of heads. On the other hand, any possible number of heads and tails is compatible with

a fair coin. So, the estimate $\hat{\Delta}$ for *any* data must be 0. Then in particular $\mathbb{E}[\hat{\Delta}] = 0$, which means that $\hat{\Delta}$ is a biased estimator whenever the coin is *not* fair.

Apart from this theoretical argument, the question arises whether this effect plays a significant role in practical quantum state reconstruction. Unfortunately, this is the case and this effect can causes substantial fidelity underestimation or spurious entanglement detection in realistic scenarios [11]. This problem applies to the established schemes for reconstructing a density matrix, in particular to the maximum-likelihood method [12] and the constrained least-squares method [13]. So, how large is the bias? For example, in a tomography of a four-qubit GHZ state with fidelity 0.8, when reconstructing from a total number of 8100 samples, the state from a maximum-likelihood estimate has a fidelity of 0.788 ± 0.010 [11], i.e., the fidelity is systematically underestimated (see also also Fig. 2). Such an underestimation may be considered to be unfortunate, but acceptable. However, it was also demonstrated that maximum-likelihood and least-square methods tend to *overestimate* the entanglement. In fact, for a clearly separable state the reconstructed states can be always entangled, thus leading to spurious entanglement detection [11]. This is not acceptable for many experiments.

A way to avoid the bias is to accept that the reconstructed density matrix is not always a valid quantum state and can have negative eigenvalues. The simplest unbiased method is linear inversion explained above. More generally, if $M_{r|s}$ are the operators corresponding to the measurement outcomes in a complete tomographic measurement scheme, then one can find operators $X_{r|s}$ such that for all states $\varrho = \sum_{r|s} X_{r|s} P(r|s;\varrho)$ holds, generalizing Eq. (1) ‖. The estimate given by linear reconstruction is then $\hat{\varrho} = \sum_{r|s} X_{r|s} F_{r|s}$, where $F_{r|s}$ are the relative frequencies of the result r for setting s. This estimate is unbiased but it comes with the price that in all realistic scenarios $\hat{\varrho}$ has some negative eigenvalues and hence it is not a valid density matrix. Depending on the intended use of the reconstructed density matrix this may be problematic, but it was shown in Ref. [11] that entanglement measures or the Fisher information can still be estimated. In addition, we stress that the eigenvectors corresponding to these negative eigenvalues are randomly distributed in the following sense: If we choose a rank one projection $|\alpha\rangle\langle\alpha|$ independently of the data, then the probability that $\mathrm{tr}(\hat{\varrho}|\alpha\rangle\langle\alpha|) < -\epsilon$ is exponentially suppressed, as can be seen from the inequality in (3).

3.2. Problems with error regions

Any report of an experiment has to equip the reported results with error bars. In the case of a density matrix, this will be a high-dimensional error region. When specifying an error region, one first has to decide between the Bayesian framework and the frequentistic framework. A Bayesian analysis gives a credible region, which has the property that with high probability the actual state is in this region. A frequentist's analysis gives a confidence region, which is a map from the data to a region in state space such that with high probability the region contains the actual state. There is a long debate

‖ The new operators $X_{r|s}$ may be necessary, since the $M_{r|s}$ can be overcomplete or not orthogonal.

in mathematical statistics which method is appropriate, but most of the subsequent discussion is independent of this dispute.

Before discussing the advantages and disadvantages of an error region, it is important to remember, that the variance does in general not give an appropriate error region. This occurs in particular if the underlying distributions are far from being Gaussian. But for state tomography, the data is sampled from a multinomial distribution, typically with a very low number of events. Indeed, in many experiments the number of clicks per measurement outcome is about ten, but sometimes even below one. Also the method of bootstrapping may yield an inappropriate error region. In bootstrapping, one uses an estimate $\hat{\varrho}$ for the state (parametric bootstrapping) or the empirical distributions of the outcomes of the measurements $F_{r|s}$ (non-parametric bootstrapping) in order to estimate the variance of the estimate. This estimate is usually obtained by Monte Carlo sampling from the corresponding distributions. There is no particular reason that this should be a good error region, and it was also demonstrated that the most commonly used schemes yield invalid error regions.

Methods to obtain valid error regions both in the Bayesian [14] and in the frequentistic framework [15] have been suggested, however, they turn out to be notoriously difficult to compute. But even when it is possible to achieve a proper error region, one has to keep in mind that the size of the error region scales with the dimension of the underlying Hilbert space, i.e., exponentially with the number of qubits. This makes it very difficult to perform state tomography of a large system with a reasonable sized error region. Fortunately, in many situations the error region for the state is not of uttermost importance. Often one is only interested in certain scalar quantities like a measure of entanglement or the fidelity with the (pure) target state. In this cases it is possible to infer an appropriate confidence region directly from the data, without taking the detour over an error region for the density operator. This is particularly simple, if the quantity of interest is linear in the density matrix, e.g., the fidelity with a pure state $F = \langle\psi|\varrho|\psi\rangle$. One can again use Hoeffding's tail inequality in order to obtain a lower bound $\hat{F}_l$ on the fidelity. The promise is then that $P(\hat{F}_l > \langle\psi|\varrho_{\text{exp}}|\psi\rangle) < 1\%$ for any state ϱ_{exp}. A general method to provide such confidence regions for convex functions, like the bipartite negativity or the quantum Fisher information, has been introduced in Ref. [11].

4. Analysing density matrices

In the last section of this article, we assume that a valid multiparticle density matrix ϱ is given and the task is to analyse its properties. Naturally, many questions can be asked about a density matrix, but we concentrate on two of them. First, we consider the question whether the state is genuinely multiparticle entangled or not. We explain a powerful approach for characterizing multiparticle entanglement with the help of so-called PPT mixtures and semidefinite programming. Second, we consider the problem of characterizing the complexity of a given quantum state and explain an approach using

exponential families. For example, in this approach a state that is a thermal state of a Hamiltonian with two-body interactions only, is considered to be of low complexity and the distance to these thermal states can be considered as a measure of complexity. The underlying techniques also allow to characterize pure states which are not ground states of a two-body Hamiltonian.

4.1. Characterizing entanglement with PPT mixtures

4.1.1. Notions of entanglement — Before explaining the characterization of multiparticle entanglement, we have to explain some basic facts about entanglement on a two-particle system. The definition of entanglement is based on the notion of local operations and classical communication (LOCC). If a quantum state can be prepared by LOCC, it is called separable, otherwise it is entangled. For pure states, this just means that product states of the form $|\phi\rangle = |\alpha\rangle \otimes |\beta\rangle$ are separable and all other states (e.g. the singlet state $|\psi^-\rangle = (|01\rangle - |10\rangle)/\sqrt{2}$) are entangled. If mixed states are considered, a density matrix ϱ is separable, if it can be written as a convex combination of product states,

$$\varrho = \sum_k p_k \varrho_A^k \otimes \varrho_B^k, \tag{7}$$

where the p_k form a probability distribution, so they are non-negative and sum up to one. Physically, the convex combination means that Alice and Bob can prepare the global state by fixing the joint probabilities with classical communication and then preparing the states ϱ_k^A and ϱ_k^B separately. The question whether or not a given quantum state is entangled is, however, in general difficult to answer. This is the so-called separability problem [2, 3].

Many separability criteria have been proposed, but none of them delivers a complete solution of the problem. The most famous separability test is the criterion of the positivity of the partial transpose (PPT criterion) [16]. For that, one considers the partial transposition of a density matrix $\varrho = \sum_{ij,kl} \varrho_{ij,kl} |i\rangle\langle j| \otimes |k\rangle\langle l|$, given by

$$\varrho^{T_A} = \sum_{ij,kl} \varrho_{ij,kl} |j\rangle\langle i| \otimes |k\rangle\langle l|. \tag{8}$$

In an analogous manner, one can also define the partial transposition ϱ^{T_B} with respect to the second system. The PPT criterion states that for any separable state ϱ the partial transpose ϱ^{T_A}, (and consequently also $\varrho^{T_B} = (\varrho^{T_A})^T$) has no negative eigenvalues and is therefore positive semidefinite. So, if one finds a negative eigenvalue of ϱ^{T_A}, then the state ϱ must necessarily be entangled. The PPT criterion solves the separability problem for low dimensional systems (that is, two qubits or one qubit and one qutrit) [2], but in all other cases the set of separable states is a strict subset of the PPT states. The entangled states which are PPT are of great theoretical interest: It has been shown that their entanglement can never be distilled to pure state entanglement, even if many copies of the state are available. This weak form of entanglement is then also called *bound*

entanglement and bound entangled states are central for many challenging questions in quantum information theory.

The characterization of entanglement becomes significantly more complicated, if more than two particles are involved. Let us consider three particles (A, B, C). First, a state can be fully separable, meaning that it does not contain any entanglement and is of the form $|\phi^{\text{fs}}\rangle = |\alpha\rangle \otimes |\beta\rangle \otimes |\gamma\rangle$. If a state is entangled, one can further ask whether only two parties are entangled or all three parties. For instance, in the state $|\phi^{\text{bs}}\rangle = |\psi^-\rangle_{AB} \otimes |\gamma\rangle_C$ the parties A and B are entangled, but C is not entangled with A or B, therefore the state is called biseparable. Alternatively, if all parties are entangled with each other, the state is called genuine multipartite entangled [3]. For the simplest case of three two-level systems (qubits) it has been shown that even the genuine multipartite entangled states can be divided into two subclasses, represented by the GHZ state $|GHZ\rangle = (|000\rangle + |111\rangle)/\sqrt{2}$ and the W state $|W\rangle = (|001\rangle + |010\rangle + |100\rangle)/\sqrt{3}$. These subclasses are distinguished by the fact that a single copy of a state in one class cannot be converted via LOCC into a state in the other class, even if this transformation is not required to be performed with probability one [3].

The classification of entanglement for pure states can be extended to mixed states by considering convex combinations as in Eq. (7). First, a mixed state is fully separable, if it can be written as a convex combination of fully separable states

$$\varrho^{\text{fs}} = \sum_k p_k \varrho_A^k \otimes \varrho_B^k \otimes \varrho_C^k, \tag{9}$$

and a state is biseparable, if it can be written as a mixture of biseparable states, which might be separable with respect to different partitions,

$$\varrho^{\text{bisep}} = p_1 \varrho_{A|BC}^{\text{sep}} + p_2 \varrho_{B|AC}^{\text{sep}} + p_3 \varrho_{C|AB}^{\text{sep}}. \tag{10}$$

The different notions of entanglement in the multipartite case and the different bipartitions that have to be taken into account imply that the question whether a given mixed multipartite state is entangled or not is extraordinarily complicated.

4.1.2. The approach of PPT mixtures — A systematic approach for characterizing genuine multiparticle entanglement makes use of so-called PPT mixtures [17]. Instead of asking whether a state is a mixture of separable states with respect to different partitions as in Eq. (10), one asks whether it is a mixture of states which are PPT for the bipartitions

$$\varrho^{\text{pptmix}} = p_1 \varrho_{A|BC}^{\text{ppt}} + p_2 \varrho_{B|AC}^{\text{ppt}} + p_3 \varrho_{C|AB}^{\text{ppt}}. \tag{11}$$

Since the separable states are a subset of the PPT states, any biseparable state is also a PPT mixture. This means that if a state is no PPT mixture, then it must be genuine multipartite entangled (see also Fig. 3).

At first, it is not clear what can be gained by this redefinition of the problem. First, the condition for PPT mixtures is a relaxation of the definition of biseparability and it

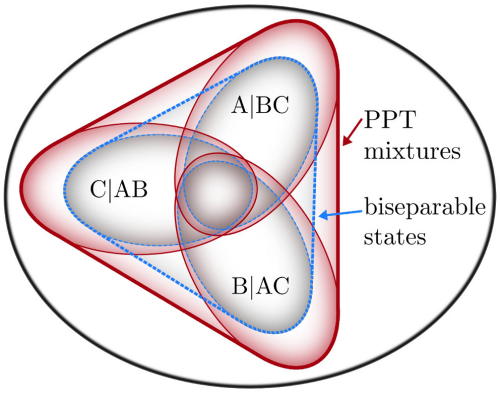

Figure 3. Schematic view of the states which are PPT mixtures and the biseparable states for three particles. There are three possible bipartitions, and the corresponding sets of states which are separable or PPT for the bipartition. The figure is taken from Ref. [17].

might be that the conditions are relaxed too much, implying that not many states can be detected by this method. Second, it is not clear how the criterion for PPT mixtures can be evaluated in practice and whether this is easier than evaluating the conditions for separability directly. In the following, however, we will see that the question whether a state is a PPT mixture or not can directly be checked with a technique called semidefinite programming. Furthermore, the approximation to the biseparable states is rather tight, and for many families of states the property of being a PPT mixture coincides with the property of being biseparable.

4.1.3. Evaluation of the criterion — Let us discuss the evaluation of the condition for PPT mixtures. For that, we need to introduce the notion of entanglement witnesses. In the two-particle case, an entanglement witness $\mathcal{W}$ is an observable with the property that the expectation value is positive for all separable states, $\mathrm{tr}(\varrho^{\mathrm{sep}}\mathcal{W}) \geq 0$. This implies that a measured negative expectation value signals the presence of entanglement. In this way, the concept of an entanglement witness bears some similarity to a Bell inequality, where correlations are bounded for classical states admitting a local hidden variable model, while entangled states may violate the bound.

How can entanglement witnesses be constructed? For the two-particle case a simple method goes as follows: Consider an observable of the form

$$\mathcal{W} = P + Q^{T_A}, \tag{12}$$

where $P \geq 0$ and $Q \geq 0$ are positive semidefinite operators. Using the fact that $Tr(XY^{T_A}) = Tr(X^{T_A}Y)$ for arbitrary operators X, Y, we find that for a separable state $Tr(\mathcal{W}\varrho^{\mathrm{sep}}) = Tr(P\varrho^{\mathrm{sep}}) + Tr(Q(\varrho^{\mathrm{sep}})^{T_A}) \geq 0$, since ϱ^{sep} has to be PPT. Therefore, the observable $\mathcal{W}$ is an entanglement witness, which may be used to detect the entanglement in states that violate the PPT criterion.

This construction can be used to decide whether a given three-particle state is a PPT mixture or not. For that, consider the optimization problem

$$\begin{aligned} \underset{\mathcal{W},P_i,Q_i}{\text{minimize}} \quad & Tr(\varrho\mathcal{W}) \\ \text{subject to:} \quad & \mathcal{W} = P_1 + Q_1^{T_A} = P_2 + Q_2^{T_B} = P_3 + Q_3^{T_C} \text{ and} \\ & P_i \geq 0 \text{ for } i = 1,2,3 \text{ and} \\ & \mathbb{1} \geq Q_i \geq 0 \text{ for } i = 1,2,3. \end{aligned} \tag{13}$$

The constraints guarantee that the observable $\mathcal{W}$ is of the form as in Eq. (12) for any of the three bipartitions. This means, that if a state is a PPT mixture as in Eq. (11), the expectation value $Tr(\varrho\mathcal{W})$ has to be non-negative. On the other hand, one can show that if a state is not a PPT mixture, then the minimization problem will always result in a strictly negative value [17]. In this way, the question whether a state is a PPT mixture or not, can be transformed into a optimization problem under certain constraints.

The point is that the optimization problem belongs to the class of semidefinite programs (SDP). An SDP is an optimization problem of the type

$$\begin{aligned} \underset{x_i}{\text{minimize}} \quad & \sum_i c_i x_i \\ \text{subject to:} \quad & F_0 + \sum_i x_i F_i \geq 0, \end{aligned} \tag{14}$$

where the c_i are real coefficients defining the target function, the F_i are hermitean matrices defining the constraints and the x_i are real coefficients which are varied. This type of optimization problem has two important features [18]. First, using the so-called dual problem one can derive a lower bound on the solution of the minimization, which equals the exact value under weak conditions. This means that the optimality of a solution found numerically can be demonstrated. In this way, one can prove rigorously by computer whether a given state is a PPT mixture or not. Second, for implementing an SDP in practice there are ready-to-use computer algebra packages available and therefore the practical solution of the SDP is straightforward.

4.1.4. Results — Concerning the characterization of PPT mixtures, the following results have been obtained:

- First, the practical evaluation of the SDP in Eq. (13) can be carried out easily with standard numerical routines. A free ready-to-use package called `PPTMixer` is available online [19], and it solves the problem for up to six qubits on standard computers. For a larger number of particles, the numerical evaluation becomes difficult, but analytical approaches are also feasible [17, 22].
- For many families of states, the approach of the PPT mixtures delivers the strongest criterion of entanglement known so far. For many cases it even solves the problem of characterizing multiparticle entanglement. For instance, three-qubit permutation-invariant states are biseparable, if and only if they are PPT mixtures [20]. The

same holds for states with certain symmetries, like GHZ diagonal states or four-qubit states diagonal in the graph-state basis [21, 22].

- Nevertheless, the approach of PPT mixtures can not detect all multiparticle entangled states. There are examples of genuinely entangled three-qubit and three-qutrit states, which are PPT mixtures [23, 24]. For an increasing dimension and number of particles one can even show that the probability that a given multiparticle entangled state can be detected by the PPT mixture approach decreases [25]. This finding, however, is in line with the observation that also in bipartite high-dimensional systems no single entanglement criterion detects a large fraction of states [26].
- The value $\mathcal{N}(\varrho) = -Tr(\varrho\mathcal{W})$, that is, the amount of violation of the witness condition is a computable entanglement monotone for genuine multiparticle entanglement [22]. It can be called the genuine multiparticle negativity, as it generalizes the entanglement measure of bipartite negativity.
- An interesting feature of the PPT mixer approach is that it can also be evaluated, if only partial information on the state ϱ is available. Namely, if only the expectation values $\langle A_i\rangle$ of some observables A_i are known, one can add in the SDP in Eq. (13) that the witness $\mathcal{W}$ should be a linear combination of the measured observables $\mathcal{W} = \sum_i \lambda_i A_i$. It can be shown that this is then still a complete solution of the problem, meaning that the SDP returns a negative value, if and only if all states that are compatible with the data $\langle A_i\rangle$ are not PPT mixtures.

4.2. Characterizing the complexity of quantum states

Besides the question whether a given multiparticle quantum state is entangled or not, one may also be interested in other questions about a reconstructed quantum state ϱ. For instance, one may ask: Is the given state is a ground state or thermal state of a simple Hamiltonian? In the following, we will explain how this question can be used to characterize the complexity of a many-body quantum state.

4.2.1. Exponential families — First, one can consider the set of all possible two-body Hamiltonians. For multi-qubit systems they are of the form

$$H_2 = \sum_{i,\alpha} \lambda_\alpha^{(i)} \sigma_\alpha^{(i)} + \sum_{i,j,\alpha,\beta} \mu_{\alpha\beta}^{(ij)} \sigma_\alpha^{(i)} \sigma_\beta^{(j)} + \nu\mathbb{1}, \tag{15}$$

where $\sigma_\alpha^{(i)}$ is the Pauli matrix σ_α acting on the i-th qubit. This Hamiltonian H_2 contains, apart from the identity, single-particle terms and two-particle interactions. However, no geometrical arrangement of the particles is assumed and the two-particle interactions are between arbitrary particles and not restricted to nearest-neighbour interactions. We also denote the set of all two-particle Hamiltonians by $\mathcal{H}_2$, and in a similar manner one can define the sets of k-particle Hamiltonians $\mathcal{H}_k$.

Given the set of k-particle Hamiltonians, we can define the so-called exponential family of all thermal states

$$\mathcal{Q}_k = \{\exp\{H_k\} \text{ with } H_k \in \mathcal{H}_k\}, \tag{16}$$

where the normalization of the state has been included into the Hamiltonian via the term $\nu\mathbb{1}$.

If a given quantum state is in the family $\mathcal{Q}_k$ for small k, then one can consider it to be less complex, since only a simple Hamiltonian with few parameters are required to describe the interaction structure. One the other hand, if a state is not in the exponential family, one can consider the distance

$$D_k(\varrho||\mathcal{Q}_k) := \inf_{\eta\in\mathcal{Q}_k} D(\varrho||\eta) \tag{17}$$

with $D(\varrho||\eta) = \mathrm{tr}[\varrho\log(\varrho)] - \mathrm{tr}[\varrho\log(\eta)]$ being the relative entropy, as a measure of the complexity of the quantum state. The optimal η is also called the information projection $\tilde{\varrho}_k$ and one can show that this $\tilde{\varrho}_k$ is the maximum likelihood approximation of ϱ within the family $\mathcal{Q}_k$ [27]. Below, we will explain several further equivalent characterizations which can help to solve the underlying minimization problem.

This type of complexity measure has been first discussed for the case of classical probability distributions in the context of information geometry [28]. The measure D_1 is also known as the multi-information in complexity theory [29]. For classical complex systems, these quantities have been used to study the onset of synchronization and chaos in coupled maps or cellular automata [27]. For the quantum case, this measure and its properties have been discussed in several recent works [30–33].

At this point, it is important to note that in the quantum case as well as in the classical case the quantity D_k does not necessarily decrease under local operations [31, 32]. Simple examples for this fact follow from observation that taking a thermal state of a two-body Hamiltonian and tracing out one particle typically leads to a state that is not a thermal state of a two-body Hamiltonian anymore. Therefore, the quantity D_k should not be considered as a measure of correlations in the quantum state, it is more appropriate to consider it as a measure of the complexity of the state.

4.2.2. Characterizing the approximation — For the characterization of the information projection $\tilde{\varrho}_k$, the following result is quite helpful [31]. First, let ϱ be an arbitrary quantum state, and $\tilde{\varrho}_k$ be the information projection onto the exponential family $\mathcal{Q}_k$. Furthermore, let M_k be the set of all quantum states that have the same k-body marginals as ϱ. M_k is, contrary to $\mathcal{Q}_k$, a linear subspace of the space of all density matrices (see Fig. 4). Then, the following statements are equivalent:

(a) The state $\tilde{\varrho}_k$ is the closest state to ϱ in $\mathcal{Q}_k$ with respect to the relative entropy.

(b) The state $\tilde{\varrho}_k$ has the maximal entropy among all states in M_k.

(c) The state $\tilde{\varrho}_k$ is the intersection $\mathcal{Q}_k \cap M_k$.

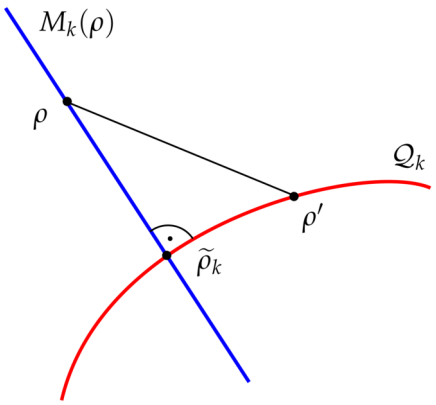

Figure 4. The information projection $\tilde{\varrho}_k$ of the state ϱ is the closest state to ϱ within the exponential family $\mathcal{Q}_k$. M_k denotes the set of all quantum states that have the same k-body marginals as ϱ, and can also be used to characterize $\tilde{\varrho}_k$. For arbitrary states ϱ' within $\mathcal{Q}_k$ the relation $D(\varrho||\varrho') = D(\varrho||\tilde{\varrho}_k) + D(\tilde{\varrho}_k||\varrho')$ holds, which resembles the Pythagorean Theorem. The figure is taken from Ref. [33]

This equivalence can be used for many purposes. For example, it is useful for developing an algorithm for computing the information projection [33, 34]. Instead of minimizing the relative entropy as a highly nonlinear function over $\mathcal{Q}_k$, one can do the following: One optimizes over all states in $\mathcal{Q}_k$ with the aim to make the k-body marginals the same as for the state ϱ. The resulting algorithm converges well and allows the computation of the complexity measure D_k for up to six qubits [33].

Second, from the equivalences it follows that the multi-information D_1 can directly be calculated, since the closest state to ϱ in the family $\mathcal{Q}_1$ is the product state $\tilde{\varrho}_1 = \varrho_1 \otimes \varrho_2 \otimes ... \otimes \varrho_N$ built out of the reduced single-particle density matrices of ϱ. Clearly, $\tilde{\varrho}_1$ has the same marginals as ϱ and maximizes the entropy.

4.2.3. A five-qubit example — As a final example, let us discuss how the notion of exponential families can help to characterize ground states of two-body Hamiltonians. For that, consider the five-qubit ring-cluster state $|R_5\rangle$. This state is defined to be the unique eigenstate fulfilling

$$|R_5\rangle = g_i|R_5\rangle, \tag{18}$$

where $g_1 = \sigma_x\sigma_z\mathbb{1}\mathbb{1}\sigma_z, g_2 = \sigma_z\sigma_x\sigma_z\mathbb{1}\mathbb{1}, g_3 = \mathbb{1}\sigma_z\sigma_x\sigma_z\mathbb{1}, g_4 = \mathbb{1}\mathbb{1}\sigma_z\sigma_x\sigma_z$, and $g_5 = \sigma_z\mathbb{1}\mathbb{1}\sigma_z\sigma_x$. Here, the tensor product symbols have been omitted. After appropriate local transformations, the ring-cluster state can also be written as

$$|R_5\rangle = \frac{1}{\sqrt{8}}\big[|00000\rangle + |00110\rangle - |01011\rangle + |01101\rangle + |10001\rangle - |10111\rangle + |11010\rangle + |11100\rangle\big]. \tag{19}$$

The ring-cluster state is an example of a so-called graph state, and plays an important role in quantum error correction as a codeword of the five-qubit Shor code. It was known

before that the state $|R_5\rangle$ cannot be the unique ground state of a two-body Hamiltonian [35]. This, however, leaves the question open whether it can be approximated by ground states of two-body Hamiltonians. For instance, for three qubits it was shown that not all pure states are ground states of two-body Hamiltonians, but all pure states can be approximated arbitrarily well by such ground states [36].

The characterization of the exponential families from the previous section can indeed help to prove that the state has $|R_5\rangle$ has finite distance to all thermal states of two-body Hamiltonians. For that, first note that the two-body marginals of the state $|R_5\rangle\langle R_5|$ are all maximally mixed two-qubit states. Then, one can directly find states which have the same two-body marginals, but their entropy is larger than the entropy the state $|R_5\rangle\langle R_5|$. This last property is, of course, not surprising, since $|R_5\rangle\langle R_5|$ has as a pure state the minimal possible entropy. According to the previous section, this already implies that $|R_5\rangle\langle R_5|$ cannot be the thermal or ground state of any two-body Hamiltonian.

Furthermore, if an arbitrary state ϱ has a high fidelity with $|R_5\rangle$ then the two-body marginals will be close to the maximally mixed states, and in addition the entropy of ϱ will be small. This implies that one can find again states with the same marginals and higher entropy. Using these ideas and some detailed calculations one can prove that if a state fulfils

$$F = \langle R_5|\varrho|R_5\rangle \geq \frac{31}{32} \approx 0.96875. \tag{20}$$

then it cannot be a thermal state of a two-body Hamiltonian [37]. This shows that the state $|R_5\rangle$ cannot be approximated by thermal states of two-body Hamiltonians. In principle, this bound can also be used to prove experimentally that a given state is not a thermal state of a two-body Hamiltonian.

5. Conclusion

In conclusion we have explained several problems occurring in the analysis of multiparticle quantum states, ranging from systematic errors of the measurement devices to the characterization of ground states of two-body Hamiltonians. We believe that several of the explained topics are important to be addressed in the future. First, since the current experiments in quantum optics are getting more and more complex, advanced statistical methods need to be applied in order to reach solid conclusions. Second, the analysis of ground states and thermal states of simple Hamiltonians is relevant for quantum simulation and quantum control, so direct characterizations would be very helpful.

6. Acknowledgements

We thank Rainer Blatt, Tobias Galla, Bastian Jungnitsch, Martin Hofmann, Lukas Knips, Thomas Monz, Sönke Niekamp, Daniel Richart, Philipp Schindler, Christian Schwemmer, and Harald Weinfurter for discussions and collaborations on the presented

topics. Furthermore, we thank Mariami Gachechiladze, Felix Huber, and Nikolai Miklin for comments on the manuscript. This work has been supported by the EU (Marie Curie CIG 293993/ENFOQI, ERC Starting Grant GEDENTQOPT, ERC Consolidator Grant 683107/TempoQ), the FQXi Fund (Silicon Valley Community Foundation), and the DFG (Forschungsstipendium KL 2726/2-1).

References

[1] R. Renner, Nature Physics **3**, 645 (2007).
[2] R. Horodecki, P. Horodecki, M. Horodecki, and K. Horodecki, Rev. Mod. Phys. **81**, 865 (2009).
[3] O. Gühne and G. Tóth, Phys. Rep. **474**, 1 (2009).
[4] T. Moroder, M. Keyl, and N. Lütkenhaus, J. Phys. A: Math. Theor. **41**, 275302 (2008).
[5] W. Hoeffding, J. Am. Stat. Assoc. **58**, 301 (1963).
[6] T. Moroder, M. Kleinmann, P. Schindler, T. Monz, O. Gühne, and R. Blatt, Phys. Rev. Lett. **110**, 180401 (2013).
[7] A. F. Mood, *Introduction to the theory of statistics*, McGraw-Hill Inc., 1974.
[8] L. Schwarz and S. J. van Enk, Phys. Rev. Lett. **106**, 180501 (2011).
[9] N. K. Langford, New J. Phys. **15**, 035003 (2013).
[10] S. J. van Enk and R. Blume-Kohout, New J. Phys. **15**, 025024 (2013).
[11] C. Schwemmer, L. Knips, D. Richart, H. Weinfurter, T. Moroder, M. Kleinmann, and O. Gühne, Phys. Rev. Lett. **114**, 080403 (2015).
[12] Z. Hradil, Phys. Rev. A **55**, 1561(R) (1997).
[13] D. F. V. James, P. G. Kwiat, W. J. Munro, and A. G. White, Phys. Rev. A **64**, 052312 (2001).
[14] J. Shang, H. K. Ng, A. Sehrawat, X. Li, and B.-G. Englert, New J. Phys. **15**, 123026 (2013).
[15] M. Christandl and R. Renner, Phys. Rev. Lett. **109**, 120403 (2012).
[16] A. Peres, Phys. Rev. Lett. **77**, 1413 (1996).
[17] B. Jungnitsch, T. Moroder and O. Gühne, Phys. Rev. Lett. **106**, 190502 (2011).
[18] L. Vandenberghe and S. Boyd, SIAM Review **38**, 49 (1996).
[19] See the program `PPTmixer`, available at `mathworks.com/matlabcentral/fileexchange/30968`.
[20] L. Novo, T. Moroder, and O. Gühne, Phys. Rev. A **88**, 012305 (2013).
[21] X. Chen, P. Yu, L. Jiang, and M. Tian, Phys. Rev. A **87**, 012322 (2013).
[22] M. Hofmann, T. Moroder, and O. Gühne. J. Phys. A: Math. Theor. **47**, 155301 (2014).
[23] G. Tóth, T. Moroder, and O. Gühne. Phys. Rev. Lett. **114**, 160501 (2015).
[24] M. Huber and R. Sengupta, Phys. Rev. Lett. **113**, 100501 (2014).
[25] C. Lancien, O. Gühne, R. Sengupta, and M. Huber, J. Phys. A: Math. Theor. **48** 505302 (2015).
[26] S. Beigi and P. W. Shor, J. Math. Phys. **51**, 042202 (2010).
[27] T. Kahle, E. Olbrich, J. Jost and N. Ay, Phys. Rev. E **79**, 026201 (2009).
[28] S. Amari, IEEE Trans. Inf. Theory **47**, 1701 (2001).
[29] N. Ay and A. Knauf, Kybernetika **42**, 517 (2007).
[30] D. L. Zhou, Phys. Rev. Lett. **101**, 180505 (2008).
[31] D. L. Zhou, Phys. Rev. A **80**, 022113 (2009).
[32] T. Galla and O. Gühne, Phys. Rev. E **85**, 046209 (2012).

[33] S. Niekamp, T. Galla, M. Kleinmann, and O. Gühne, J. Phys. A: Math. Theor. **46**, 125301 (2013).
[34] D. L. Zhou, Commun. Theor. Phys. **61**, 187 (2014).
[35] M. Van den Nest, K. Luttmer, W. Dür, and H. J. Briegel, Phys. Rev. A **77**, 012301 (2008).
[36] N. Linden, S. Popescu, and W. K. Wootters, Phys. Rev. Lett. **89**, 207901 (2002).
[37] F. Huber and O. Gühne, Phys. Rev. Lett. **117**, 010403 (2016).

Device-independent certification of a nonprojective qubit measurement

Esteban S. Gómez,[1,2,3] Santiago Gómez,[1,2,3] Pablo González,[1,2,3] Gustavo Cañas,[1,2,3]
Johanna F. Barra,[1,2,3] Aldo Delgado,[1,2,3] Guilherme B. Xavier,[2,3,4]
Adán Cabello,[5] Matthias Kleinmann,[6] Tamás Vértesi,[7] and Gustavo Lima[1,2,3,*]

[1]*Departamento de Física, Universidad de Concepción, 160-C Concepción, Chile*
[2]*Center for Optics and Photonics, Universidad de Concepción, 160-C Concepción, Chile*
[3]*MSI-Nucleus for Advanced Optics, Universidad de Concepción, 160-C Concepción, Chile*
[4]*Departamento de Ingeniería Eléctrica, Universidad de Concepción, 160-C Concepción, Chile*
[5]*Departamento de Física Aplicada II, Universidad de Sevilla, E-41012 Sevilla, Spain*
[6]*Department of Theoretical Physics, University of the Basque Country UPV/EHU, P.O. Box 644, E-48080 Bilbao, Spain*
[7]*Institute for Nuclear Research, Hungarian Academy of Sciences, H-4001 Debrecen, P.O. Box 51, Hungary*

Quantum measurements on a two-level system can have more than two independent outcomes, and in this case, the measurement cannot be projective. Measurements of this general type are essential to an operational approach to quantum theory, but so far, the nonprojective character of a measurement could only be verified experimentally by already assuming a specific quantum model of parts of the experimental setup. Here, we overcome this restriction by using a device-independent approach. In an experiment on pairs of polarization-entangled photonic qubits we violate by more than 8 standard deviations a Bell-like correlation inequality which is valid for all sets of two-outcome measurements in any dimension. We combine this with a device-independent verification that the system is best described by two qubits, which therefore constitutes the first device-independent certification of a nonprojective quantum measurement.

The qubit is the abstract notion for any system which can be modeled in quantum theory by a two-level system. In such a system, any observable has at most two eigenvalues and hence any projective measurement can have at most two outcomes. Still, a qubit allows for an infinite number of different two-outcome measurements, the value of which, in general, cannot be known to the observer beforehand, but rather follows a binomial distribution. In quantum information theory, additional properties reflecting this binary structure have been revealed, e.g., the information capacity of a qubit is one classical bit, even when using entangled qubits [1]. Nonetheless, the properties of a qubit sometimes break with the binary structure, e.g., transferring the quantum state of a qubit is only possible with the communication of two classical bits and the help of entanglement [2]. Moreover, it is well-known that general quantum measurements can be nonprojective and have more than two irreducible outcomes [3]. The most general quantum measurement with n outcomes is described by positive semidefinite, possibly nonprojective, operators $E_1, E_2, \ldots, E_n$ with $\sum E_k = \mathbb{1}$. The number of outcomes is reducible, if it is possible to write $E_k = \sum_\lambda p_\lambda E_k^{(\lambda)}$ so that $E_1^{(\lambda)}, \ldots, E_n^{(\lambda)}$ are measurements for each λ, p_λ is a probability distribution over λ, and for each λ there is at least one k_λ with $E_{k_\lambda}^{(\lambda)} = 0$. Nonprojective measurements found first applications in quantum information processing in the context of the discrimination of nonorthogonal quantum states. Ivanovic [4] found that it is possible to discriminate two pure qubit states without error even if the two states are nonorthogonal, but at the cost of allowing a third measurement outcome that indicates a failure of the discrimination procedure. The strategy with the lowest failure probability can be shown to be an irreducible three-outcome measurement [5]. Also recently, nonprojective measurements proved to be essential in purely information theoretical tasks like improving randomness certification [6].

A peculiarity of nonprojective qubit measurements with more than two irreducible outcomes is that there is no known way to implement them within a qubit system. Rather, the measurement apparatus needs to manifestly work outside of what would be modeled by a qubit alone. To some extent it is therefore a matter of perspective whether, at all, one is willing to admit such nonprojective measurements on a qubit system. However, device-independent self-testing [7] allows us to demonstrate that a qubit description is appropriate for the tested system, by showing that, with high precision, any measurement on the system can be modeled as a qubit measurement.

A key observation is that it is not possible to show that a measurement is irreducibly nonbinary insofar we consider a single quantum system, as the outcomes of measurements on a single system can always be explained in terms of a hidden variable model where all $E_k^{(\lambda)}$ are either $\mathbb{1}$ or 0 and p_λ depends on the preparation of the system. The situation changes when considering the correlations between independent measurements on an entangled system [8], but still, a violation of a conventional Bell inequality on qubits—however high—can always be explained by locally selecting from binary quantum measurements [9]. Yet, there are specialized Bell-like inequalities, where qubit measurements with more than three outcomes outperform the maximal violation attainable when only binary measurements are considered [10]. An analysis of this advantage reveals that this effect is very small and would require an overall visibility of more than

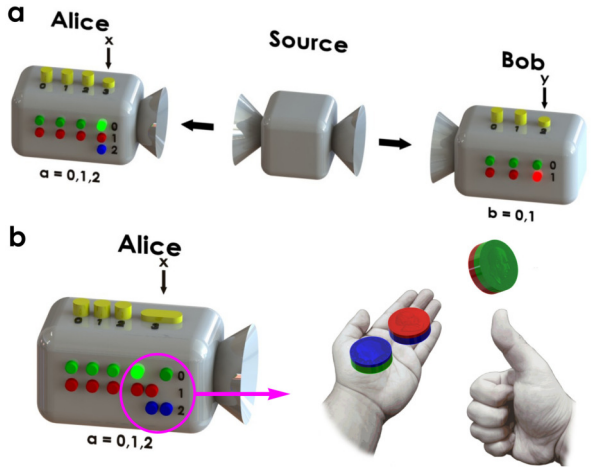

FIG. 1. Testing correlations that cannot be explained in terms of binary measurements. (a) Scheme of the test performed. Pairs of entangled systems are sent to Alice's and Bob's laboratories (represented by boxes with yellow buttons at the top and lights of different color in the side). In each laboratory one system is submitted to a measurement (represented by the yellow button pressed) and produces an outcome (represented by a light flashing). All possible measurements have two outcomes, except for Alice's measurement $x = 3$ which has three outcomes (represented by lights of different color, green for 0, red for 1, and blue for 2). (b) Discarded scenario. Our experiment excludes that the outcomes of Alice's measurement $x = 3$ are produced by a measurement apparatus that selects one out of three binary quantum measurements with outcomes 0/1, 1/2, or 2/0 (represented by three coins with green/red, red/blue, and blue/green sides, respectively).

0.992 [9–11].

Here we introduce an inequality where this threshold is lowered to 0.9845, enabling the device-independent certification of a nonbinary measurement on a qubit. We consider a bipartite scenario, cf. Fig. 1(a), where one party, Alice, chooses one among four measurements $x = 0, 1, 2, 3$ while the other party, Bob, chooses one among three measurements $y = 0, 1, 2$. All measurements have two outcomes, $a = 0, 1$ and $b = 0, 1$, except Alice's measurement $x = 3$, which has three outcomes, $a = 0, 1, 2$. We denote by $P(ab|xy)$ the probability for outcome a and b when the setting x and y were chosen and consider the expression

$$\begin{aligned} I = {} & P(00|00) + P(00|11) + P(00|22) \\ & - P(00|01) - P(00|12) - P(00|20) \\ & - P(00|30) - P(10|31) - P(20|32). \end{aligned} \quad (1)$$

When restricted to binary quantum measurements, not necessarily on a qubit, then the value of I is upper bounded by 1.2711. Without this restriction, the maximal quantum value of I is $3\sqrt{3}/4 \approx 1.2990$ and can be achieved for two qubits using a maximally entangled state. Thus, an experiment violating the inequality $I < 1.2711$ proves that Alice's measurement $x = 3$ cannot have been a measurement composed of binary quantum measurements on whatever quantum system and selected by the measurement apparatus, as shown in Fig. 1(b).

Since projective measurements on a qubit necessarily are binary or trivial, a violation of $I < 1.2711$ certifies the implementation of a nonprojective measurement. This requires, however, that the system at Alice's laboratory is actually a qubit, which is manifestly the case in our experimental set-up, as we explain below. In addition, this assertion of Alice's system being a qubit, can also be verified in a device-independent way by measuring the violation of the Clauser–Horne–Shimony–Holt (CHSH) Bell inequality [12]. If this violation is maximal, the joint state has to be a maximally entangled qubit-qubit state [13–15], independently of what measurement apparatuses are used. If the observed value for the CHSH violation deviates by ϵ from the maximum $2\sqrt{2}-2$, the state must still have a fidelity of at least $1 - 2.2\epsilon$ with a maximally entangled qubit-qubit state [16]. A description of the system in the corresponding qubit-qubit-space is hence accurate up to 2.2ϵ.

The set-up of our experiment is shown in Fig. 2. Degenerate 810 nm photon pairs, with orthogonal polarisations, are produced from spontaneous parametric down-conversion (SPDC) in a bulk type-II nonlinear periodically poled potassium titanyl phosphate (PPKTP) 20 mm long crystal. The crystal is pumped by a single-longitudinal mode continuous wave 405 nm laser with 1 mW of optical power. We resort to an ultra-bright source architecture, where the type-II nonlinear crystal is placed inside an intrinsically phase-stable Sagnac interferometer [17–19]. This interferometer is composed of two laser mirrors, a half-wave plate (HWP_2) and a polarizing beamsplitter cube (PBS_1). HWP_2 and PBS_1 are both dual-wavelength with anti-reflection coatings at 405 nm and 810 nm. The fast axis of the HWP_2 is set at 45 degree with respect to the horizontal, such that down-converted photons are generated in the clockwise and counter-clockwise directions. The clockwise and counter-clockwise propagating modes overlap inside the polarizing beamsplitter and, by properly adjusting the pump beam polarization mode, the two-photon state emerging at the output ports is $|\psi^+\rangle = (|HV\rangle + |VH\rangle)/\sqrt{2}$, where $|H\rangle$ ($|V\rangle$) denotes the horizontal (vertical) polarization of a down-converted photon. Due to the phase-matching conditions, there may be entanglement between other degrees of freedom of the generated photons, or coupling between the polarization and the momentum of these photons that would compromise the quality of the polarization entanglement. To avoid this we add extra spectral and spatial filtering. To remove the remaining laser light we adopt a series of dichroic mirrors followed by a long-pass color glass filter. Then, Semrock high-quality (peak transmission greater than 90%) narrow bandpass (full-width-half-maximum of 0.5 nm) interference filters centered at 810 nm are used to ensure that phase-matching

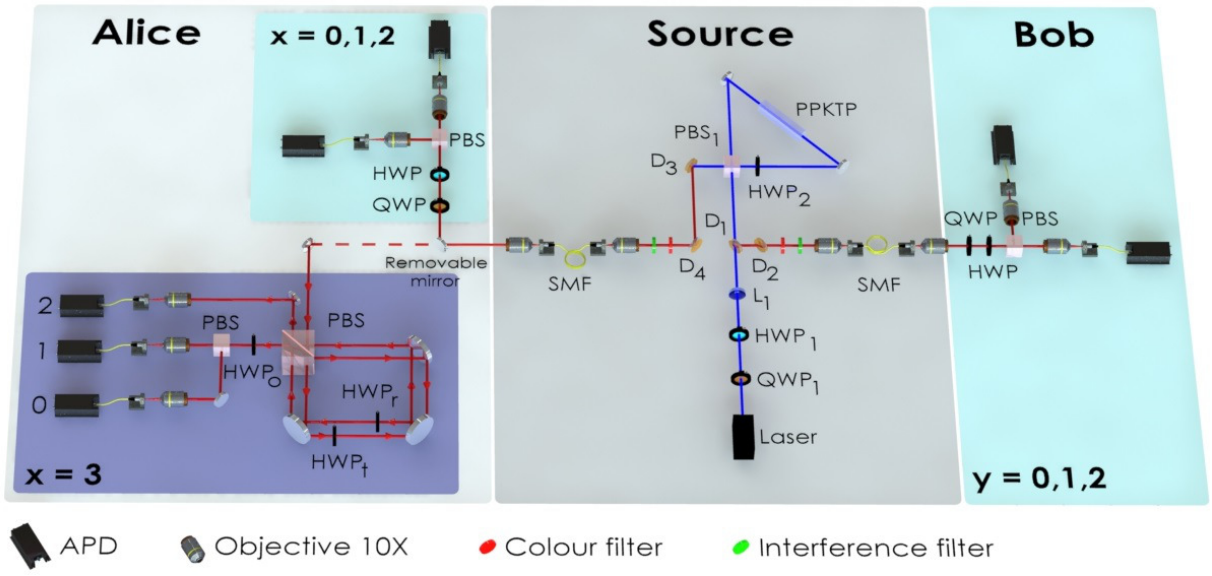

FIG. 2. Experimental set-up. A PPKTP nonlinear crystal placed into a phase-stable Sagnac interferometer is pumped by a single mode laser operating at 405 nm to produce pairs of polarization-entangled photons at 810 nm. The quarter-wave plate QWP_1 and the half-wave plate HWP_1 are used to control the polarization mode of the pump beam. Dichroic mirrors (D) and longpass color filters are used to remove the pump beam light. The generated photons are then sent to Alice and Bob through single-mode fibers (SMF). Alice (Bob) can choose among three different binary measurements (depicted in blue boxes) labeled by $x = 0, 1, 2$ ($y = 0, 1, 2$). These measurements are performed using a set of a QWP, a HWP, and a PBS. Besides, Alice also performs a three-outcome measurement $x = 3$ using a polarization based two-path Sagnac interferometer (depicted in the Alice's violet box). The elements of the three-outcome qubit measurement are defined by HWP_r, HWP_t, and HWP_o. The coincidence counts between Alice's and Bob's detectors are recorded using a coincidence electronics unit based on a field programmable gate array device.

conditions are achieved with the horizontal and vertical polarization modes at degenerated frequencies.

The indistinguishability of the photon pair modes ("HV" and "VH") is guaranteed by coupling the generated down-converted photons into single mode fibers. These fibers implement a spatial mode filtering of the down-converted light, destroying any residual spatial entanglement or polarization-momentum coupling. To maximize the source's spectral brightness, we resort to a numerical model [20]. In our case, the beam waist w_p of the pump beam, and w_{SPDC} of the selected down-converted modes, at the center of the PPKTP crystal, are adjusted by using a 20 cm focal length lens (L_1) and $10X$ objective lenses. The optimal condition for maximal photon-par yield is obtained when $w_{\mathrm{SPDC}} = \sqrt{2}w_p$, with $w_p = 40\,\mu$m. The observed source spectral brightness was 410000 photon pairs (s mW nm)$^{-1}$. The quality of the polarization entanglement generated at the source site was measured by observing a mean two-photon visibility of 0.987 ± 0.002 while measuring over the logical and diagonal polarization bases.

Due to the demand of a high overall visibility we built a coincidence electronics based on a field programmable gate array platform and capable of implementing up to 1 ns coincidence windows, thus reducing the probability for an accidental coincidence count to less than 0.00025. Therefore, the evaluation of the data does not require a separate treatment for accidental coincidence counts. The down-converted photons are registered using PerkinElmer single-photon avalanche detectors with an overall detection efficiency of 15%. We account for this by including the assumption into our analysis that the detected coincides are a fair sample from the set of all photon pairs.

Alice's and Bob's binary measurements are implemented using a set composed of a quarter wave plate (QWP), a HWP, and a PBS for each party, cf. Fig. 2. A high-quality film polarizer is also used in front of the detectors (not shown for sake of clarity) to obtain a total extinction ratio of the polarizers equal to 10^7:1. Therefore, in our experiment the two-photon visibility is not upper limited by the polarization contrast of our measurement apparatuses. Alice's three-outcome measurement $x = 3$ is implemented using the propagation modes of Alice's down-converted photon. With this purpose, Alice's photons are sent, after displacing a removable mirror, through a polarization based two-path Sagnac interferometer. The propagation modes of a photon within this interferometer are not co-propagating and depend on its polarization state. This allows for conditional polar-

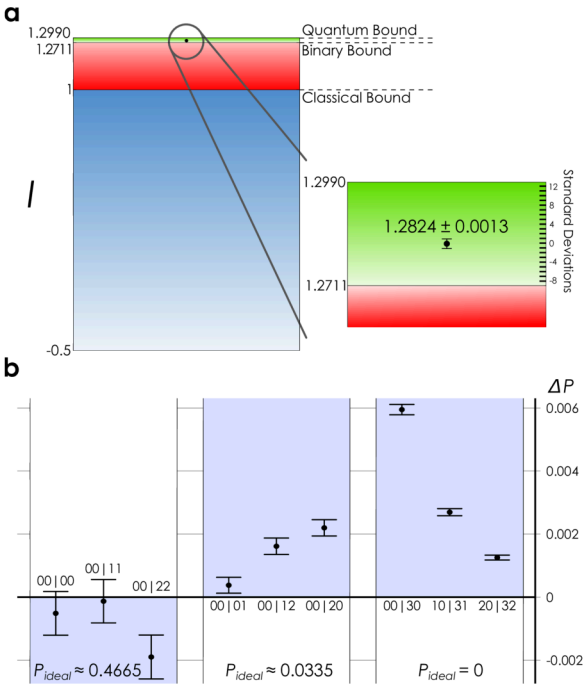

FIG. 3. Experimental results. (a) Critical values and experimental value of I, cf. Eq. (1). Uncorrelated, uniformly random events yield $-1/2$, general local hidden variable models cannot exceed 1, binary quantum measurements do not reach 1.2711, and $3\sqrt{3}/4 \approx 1.2990$ is the universal bound according to quantum theory. The experimental value obtained is $I = 1.2824 \pm 0.0013$, violating the bound for binary quantum measurements by more than 8 standard deviations. (b) Correlation measurements. For each correlation $P(ab|xy)$ in I, the deviation of the measured value from the ideal value is shown, $\Delta P = P_{\text{exp}} - P_{\text{ideal}}$. Deviations in the blue shaded areas decrease the experimental value of I. Error bars correspond to 1 standard deviation and are calculated assuming fair samples from Poissonian distributions.

ization transformations implemented with HWPs placed inside the interferometer, as shown in Fig. 2. The plate located at the clockwise reflected mode is denoted by HWP_r and the plate at the counter-clockwise transmitted mode by HWP_t. The fast axis of HWP_r is oriented in the direction of the horizontal axis, while HWP_t is oriented at an angle of 117.37°. The two propagation modes are then superposed again at the PBS, and at one of the output ports of the interferometer an extra HWP_o, oriented at 112.5°, and a PBS is used to conclude the three-outcome measurement. Further details on the implementation of the Alice's three-outcome measurement $x = 3$ are given in the appendix.

In the experiment, the correlations $P(ab|xy)$ in I were measured by integrating coincidences over a time of 240 s for each outcome and normalizing over the total number of coincidences per setting. The results are shown in Fig. 3 and yield a measured value of $I = 1.2824 \pm 0.0013$. The measurement settings were implemented independently for Alice and Bob, justifying the assumption that Alice's measurements also act independently of Bob's measurement setting y and vice versa. Hence, any explanation in terms of binary measurements on an arbitrary quantum system is excluded by 8.7 standard deviations, which corresponds to a p-value of 1.6×10^{-18}.

In order to prove that Alice's measurement $x = 3$ is a nonprojective quantum measurement, we need also to verify that Alice's system can be properly described as a qubit. We rely here on two complementary arguments. First, one can resort to the design of the experiment where the source is designed to produce entanglement in polarization, i.e., qubit-qubit entanglement. Second, we measured the CHSH correlations with our set-up and observed a violation of $2\sqrt{2} - 2 - \epsilon$ with $\epsilon = 0.0253 \pm 0.0014$ and hence the fidelity with a maximally entangled qubit-qubit state is guaranteed in a device-independent way to be at least 0.9351 within 3 standard deviations [16]. Note, that we measured the CHSH correlations using the same source and the same measurement set-up as we used for the measurement of I—except that different angles at the HWPs are adopted. Except for some ubiquitous adversary ad-hoc models we can hence conclude that also in the measurement of I, the fidelity of the state with a maximally entangled qubit-qubit state is at least 0.9351. Notice that the estimate for the fidelity is pessimistic since imperfections in the measurement apparatuses reduce the CHSH violation and therefore lower the bound on the fidelity. Still, in an alternative explanation where 93.51% of the times binary measurement was used, a bound of $I < 0.9351 \times 1.2711 + 0.0649 \times 3\sqrt{3}/4 < 1.2730$ would have to be obeyed, which is clearly violated in the experiment.

Our result shows that three-outcome nonprojective measurements can produce strictly stronger correlations between two qubits than projective two-outcome measurements on any quantum system and, therefore, that nature cannot be described in terms of binary quantum tests, not even when these tests are performed on two-level quantum systems. Quantum theory predicts also qubit-qubit correlations that cannot be explained as produced by three-outcome measurements. Observing them requires an overall visibility above 0.9927, which is beyond what is currently feasible in our set-up. Further theoretical and experimental efforts will be needed to identify and produce qubit correlations which can only be explained by four-outcome nonprojective measurements. This will be the farthest we can go, as qubit correlations can always be accounted that way [21].

We thank Antonio Acín, Marcelo Terra-Cunha, Paolo Mataloni, Valerio Scarani, Jaime Cariñe, Miguel Solís-Prosser and Omar Jiménez for conversations and assistance. This work was supported by FONDECYT grants 1160400, 11150325, 11150324, 1140635, 1150101, Milenio grant RC130001, PIA-CONICYT grant PFB0824, OTKA grant K111734, the FQXi large grant project

"The Nature of Information in Sequential Quantum Measurements", the project FIS2014-60843-P, "Advanced Quantum Information" (MINECO, Spain), with FEDER funds, the Knut and Alice Wallenberg Foundation, Sweden (Project "Photonic Quantum Information"), the EU (ERC Starting Grant GEDENTQOPT), and the DFG (Forschungsstipendium KL 2726/2-1). P.G. and J.F.B. acknowledge the financial support of CONICYT.

Maximal value of I for binary quantum measurements.

To obtain the bound for I while considering only binary quantum measurements, we note that I contains the chained Bell inequality [22, 23] $I_{\text{chain}} \leq 1$ with three settings, where

$$I_{\text{chain}} = P(00|00) + P(00|11) + P(00|22) - P(00|01) - P(00|12) - P(00|20). \quad (2)$$

The remainder, $I - I_{\text{chain}} = -P(00|30) - P(10|31) - P(20|32)$ only involves correlations of Alice's three-outcome measurement $x = 3$. There are three possibilities for replacing Alice's measurement $x = 3$ by a binary measurement, by omitting $a = 0$, $a = 1$, or $a = 2$. Taking into account the permutation symmetry of I, all of them are equivalent to $I' = I_{\text{chain}} - P(00|30) - P(10|31)$. We used the Navascués–Pironio–Acín (NPA) hierarchy [24] to obtain an upper bound on the maximal value I'. Running level 2 of the hierarchy, we obtain 1.271045 for this bound. Within the numerical precision, this value can be attained with a partially entangled qubit-qubit state showing that 1.2711 also corresponds to the maximal value of I with binary qubit measurements.

Maximal value of I for arbitrary quantum measurements.

An upper bound on the maximal value of I attainable in quantum theory can be obtained by upper bounding I_{chain} and the remainder $I - I_{\text{chain}}$ separately. The maximal value of I_{chain} is $3\sqrt{3}/4$ and can be attained with a qubit-qubit maximally entangled state [25]. On the other hand, by construction, $I - I_{\text{chain}}$ cannot be greater than zero since it only contains nonpositive terms. Put together, the maximal value of I is upper bounded by $3\sqrt{3}/4$.

This value is tight and can be attained by preparing the qubit-qubit state $|\psi^+\rangle = (|01\rangle + |10\rangle)/\sqrt{2}$ and choosing the following measurements: Alice's binary measurements $x = 0, 1, 2$ are defined by $M_{0|x} = P(\alpha_x)$ and $M_{1|x} = \mathbb{1} - P(\alpha_x)$, with $P(\theta) = (\mathbb{1} + \sigma_z \cos\theta + \sigma_x \sin\theta)/2$, where σ_z and σ_x are Pauli matrices, and the angles are given by $\alpha_0 = 3\pi/2$, $\alpha_1 = \pi/6$, and $\alpha_2 = 5\pi/6$. Alice's three-outcome measurement $x = 3$ is defined by $M_{a|3} = 2P(\gamma_a)/3$ for $a = 0, 1, 2$, with angles $\gamma_0 = 2\pi/3$, $\gamma_1 = 4\pi/3$, and $\gamma_2 = 0$. Bob's measurements are defined by $M_{0|y} = P(-\gamma_y)$ and $M_{1|y} = \mathbb{1} - P(-\gamma_y)$ for $y = 0, 1, 2$.

Implementation of Alice's three-outcome measurement.

The three-outcome measurement is implemented by sending Alice's down-converted photon through a polarization based two-path Sagnac interferometer, cf. Fig. 2. We write $|H\rangle$ ($|V\rangle$) for the horizontal (vertical) polarization. The mode entering the interferometer, rotating counter-clockwise and leaving for outcomes 0 and 1 is denoted by $|a\rangle$. $|b\rangle$ denotes the clockwise rotating mode leaving for outcome 3. In this way, the action of the PBS within the interferometer is given by

$$U_{\text{PBS}} = |H\rangle\langle H|(|a\rangle\langle a| + |b\rangle\langle b|) + i|V\rangle\langle V|(|a\rangle\langle b| + |b\rangle\langle a|). \quad (3)$$

The actions of the HWP_t and HWP_r of the interferometer in the transmitted and reflected mode, respectively, combine to $U_{t,r} = U_{\text{HWP}}(\gamma_t')|a\rangle\langle a| + U_{\text{HWP}}(\gamma_r')|b\rangle\langle b|$, where $U_{\text{HWP}}(\gamma')$ is the Jones matrix of a HWP whose fast axis is oriented at an angle γ' with respect to the horizontal axis

$$U_{\text{HWP}}(\gamma') = \cos(2\gamma')(|H\rangle\langle H| - |V\rangle\langle V|) + \sin(2\gamma')(|V\rangle\langle H| + |H\rangle\langle V|). \quad (4)$$

Therefore, the Sagnac interferometer is described by $U_{\text{S}} = U_{\text{PBS}} U_{t,r} U_{\text{PBS}}$.

After the interferometer, the photon in mode $|a\rangle$ is transmitted through HWP_o and an additional PBS. On the polarization degree of freedom, the three outcome modes 0, 1, and 2 are hence mediated by $|\psi\rangle \to A_k|\psi\rangle$ with the Kraus operators

$$\begin{aligned} A_0 &= \langle b|U_{\text{PBS}} U_{\text{HWP}}(\gamma_o')|a\rangle\langle a|U_{\text{S}}|a\rangle\,, \\ A_1 &= \langle a|U_{\text{PBS}} U_{\text{HWP}}(\gamma_o')|a\rangle\langle a|U_{\text{S}}|a\rangle\,, \text{ and} \\ A_2 &= \langle b|U_{\text{S}}|a\rangle\,, \end{aligned} \quad (5)$$

so that the implemented three-outcome measurement is given by $M_{k|3} = A_k^\dagger A_k$. The measurement required for a maximal violation of I is achieved with $\gamma_r' = 0$, $\gamma_t' \approx 117.37°$, and $\gamma_o' = 112.5°$.

Qubit-qubit correlation inexplicable by three-outcome nonprojective measurements.

We consider a scenario where Alice chooses among the binary measurements $x = 0, 1, 2$ and the four-outcome measurement $x = 3$ and Bob chooses among the binary

measurement $y = 0, 1, 2, 3$. The expression

$$L = \beta_{\rm el} - 8\sum_{i=0}^{3} P(i, 0|3, i), \tag{6}$$

has been used in Ref. [6] in the context of randomness extraction. The term $\beta_{\rm el}$ was introduced by Bechmann-Pasquinucci and Gisin [26] in the Bell inequality $\beta_{\rm el} \leq 6$, where

$$\begin{aligned}\beta_{\rm el} = &+P(10|02) + P(10|03) + P(10|11) + P(10|13)\\ &+ P(10|21) + P(10|22) + 2P(00|00)\\ &+ 2P(00|10) + 2P(00|20) + 4P(00|01)\\ &+ 4P(00|12) + 4P(00|23) - 2P(10|00)\\ &- 2P(10|10) - 2P(10|20) - 3P(00|02)\\ &- 3P(00|03) - 3P(00|11) - 3P(00|13)\\ &- 3P(00|21) - 3P(00|22). \end{aligned}\tag{7}$$

Applying the methods developed in Section and Section , one finds, using the third level of the NPA-hierarchy, that the value of L is upper bounded by 6.6876 for binary measurement and by 6.8489 for three-outcome measurements. Using four-outcome qubit measurements, L can reach a value of $4\sqrt{3} > 6.9282$. Therefore, a verification of an irreducible four-outcome qubit measurements requires a visibility of 0.9928.

* glima@udec.cl

[1] A. S. Holevo, "Bounds for the quantity of information transmitted by a quantum communication channel," Probl. Inf. Transm. **9**, 177–183 (1973).

[2] Charles H. Bennett, Gilles Brassard, Claude Crépeau, Richard Jozsa, Asher Peres, and William K. Wootters, "Teleporting an unknown quantum state via dual classical and Einstein-Podolsky-Rosen channels," Phys. Rev. Lett. **70**, 1895–1899 (1993).

[3] Paul Busch, Marian Grabowski, and Pekka J. Lahti, *Operational Quantum Physics* (Springer, Berlin, 1995).

[4] I. D. Ivanovic, "How to differentiate between non-orthogonal states," Phys. Lett. A **123**, 257–259 (1987).

[5] Asher Peres, "How to differentiate between non-orthogonal states," Phys. Lett. A **128**, 19 (1988).

[6] Antonio Acín, Stefano Pironio, Tamás Vértesi, and Peter Wittek, "Optimal randomness certification from one entangled bit," Phys. Rev. A **93**, 040102 (2016).

[7] C.-E. Bardyn, T. C. H. Liew, S. Massar, M. McKague, and V. Scarani, "Device-independent state estimation based on Bell's inequalities," Phys. Rev. A **80**, 062327 (2009).

[8] John S. Bell, "On the Einstein Podolsky Rosen paradox," Physics **1**, 195–200 (1964).

[9] Matthias Kleinmann and Adán Cabello, "Quantum correlations are stronger than all nonsignaling correlations produced by n-outcome measurements," Phys. Rev. Lett. **117**, 150401 (2016).

[10] T. Vértesi and E. Bene, "Two-qubit Bell inequality for which positive operator-valued measurements are relevant," Phys. Rev. A **82**, 062115 (2010).

[11] J. F. Barra, E. S. Gómez, G. Cañas, W. A. T. Nogueira, L. Neves, and G. Lima, "Higher quantum bound for the Vértesi-Bene-Bell inequality and the role of positive operator-valued measures regarding its threshold detection efficiency," Phys. Rev. A **86**, 042114 (2012).

[12] John F. Clauser, Michael A. Horne, Abner Shimony, and Richard A. Holt, "Proposed experiment to test local hidden-variable theories," Phys. Rev. Lett. **23**, 880–884 (1969).

[13] Stephen J. Summers and Reinhard Werner, "Maximal violation of Bell's inequalities is generic in quantum field theory," Comm. Math. Phys. **110**, 247–259 (1987).

[14] Sandu Popescu and Daniel Rohrlich, "Which states violate Bell's inequality maximally?" Phys. Lett. A **169**, 411–414 (1992).

[15] B. S. Tsirelson, "Some results and problems on quantum Bell-type inequalities," Hadronic J. Suppl. **8**, 329–345 (1993).

[16] Jean-Daniel Bancal, Miguel Navascués, Valerio Scarani, Tamás Vértesi, and Tzyh Haur Yang, "Physical characterization of quantum devices from nonlocal correlations," Phys. Rev. A **91**, 022115 (2015).

[17] Taehyun Kim, Marco Fiorentino, and Franco N. C. Wong, "Phase-stable source of polarization-entangled photons using a polarization Sagnac interferometer," Phys. Rev. A **73**, 012316 (2006).

[18] F. N. C. Wong, J. H. Shapiro, and T. Kim, "Efficient generation of polarization-entangled photons in a nonlinear crystal," Laser Physics **16**, 1517–1524 (2006).

[19] Alessandro Fedrizzi, Thomas Herbst, Andreas Poppe, Thomas Jennewein, and Anton Zeilinger, "A wavelength-tunable fiber-coupled source of narrowband entangled photons," Opt. Express **15**, 15377–15386 (2007).

[20] Daniel Ljunggren and Maria Tengner, "Optimal focusing for maximal collection of entangled narrow-band photon pairs into single-mode fibers," Phys. Rev. A **72**, 062301 (2005).

[21] Giulio Chiribella, Giacomo Mauro D'Ariano, and Dirk Schlingemann, "How continuous quantum measurements in finite dimensions are actually discrete," Phys. Rev. Lett. **98**, 190403 (2007).

[22] Philip M. Pearle, "Hidden-variable example based upon data rejection," Phys. Rev. D **2**, 1418–1425 (1970).

[23] Samuel L. Braunstein and Carlton M. Caves, "Wringing out better Bell inequalities," Ann. Phys. **202**, 22–56 (1990).

[24] Miguel Navascués, Stefano Pironio, and Antonio Acín, "Bounding the set of quantum correlations," Phys. Rev. Lett. **98**, 010401 (2007).

[25] Stephanie Wehner, "Tsirelson bounds for generalized Clauser-Horne-Shimony-Holt inequalities," Phys. Rev. A **73**, 022110 (2006).

[26] H. Bechmann-Pasquinucci and N. Gisin, "Intermediate states in quantum cryptography and Bell inequalities," Phys. Rev. A **67**, 062310 (2003).

1. Introduction

With an interest towards fundamental questions in quantum physics, as well as applications, larger and larger entangled quantum systems have been realized with photons, trapped ions, and cold atoms [1–11]. Entanglement is needed for certain quantum information processing tasks [12, 13], and it is also necessary to reach the maximum sensitivity in a wide range of interferometric schemes in quantum metrology [14]. Hence, the verification of the presence of entanglement is a crucial but exceedingly challenging task, especially in an ensemble of many, say 10^3 or 10^{12} particles [5–11]. Moreover, in such experiments it is not sufficient to claim that "the state is entangled", we need also to know how entangled the system is. Hence, quantifying entanglement in large ensembles has recently been at the center of attention. In several experiments the *entanglement depth* (i.e., the minimal number of mutually entangled particles consistent with the measurement data) was determined, reaching to the thousands [7–11].

In the many-particle case, especially in large ensembles of cold atoms, it is typically very difficult or even impossible to address the particles individually, while measuring collective quantities is still feasible. In this context, one of the most successful approaches to detect entanglement is based on the criterion [15]

$$\xi_{\rm s}^2 := N\frac{(\Delta J_x)^2}{\langle J_y\rangle^2+\langle J_z\rangle^2} \geq 1, \tag{1}$$

where N is the number of the spin-1/2 particles, $J_l = \sum_{n=1}^{N} j_l^{(n)}$ for $l = x, y, z$ are the collective spin components, and $j_l^{(n)}$ are single particle spin components acting on the nth particle. Every multiqubit state that violates (1) must be entangled [15]. The criterion (1) is best suited for states with a large collective spin in the $(\hat{y}, \hat{z})$-plane and a small variance $(\Delta J_x)^2$ in the orthogonal direction. For such states the variance of a spin component is reduced below what can be achieved with fully polarized spin-coherent states, hence they have been called *spin squeezed* in the context of metrology [16, 17].

As a generalization of (1), a criterion has also been derived by Sørensen and Mølmer [18] to detect the depth of entanglement of spin-squeezed states in an ensemble of particles with a spin j. For the criterion, we have to consider a subgroup of $k \leq N$ particles and define its total spin as

$$J = kj. \tag{2}$$

We also need to define a function F_J via a minimization over quantum states of such a group as

$$F_J(X) := \frac{1}{J}\min_{\varrho:\frac{1}{J}\langle L_z\rangle_\varrho = X}(\Delta L_x)_\varrho^2, \tag{3}$$

where L_l are the spin components of the group. In practice, the minimum will be the same if we carry out the minimization over states of a single particle with a spin J [19]. Then, for all pure states with an entanglement depth of at most k

$$(\Delta J_x)^2 \geq NjF_J\left(\frac{\langle J_z\rangle}{Nj}\right) \tag{4}$$

holds. It is easy to see that (4) is valid even for mixed states with an entanglement depth of at most k since the variance is concave in the state and $F_J(X)$ is convex ‡. Thus, every state that violates (4) must have a depth of entanglement of $(k+1)$ or larger. It is important to stress that the criterion (4) provides a tight lower bound on $(\Delta J_x)^2$ based on $\langle J_z \rangle$. Spin squeezing has been demonstrated in many experiments, from cold atoms [7, 20–26] to trapped ions [27], magnetic systems [28] and photons [29], and in many of these experiments even multipartite entanglement has been detected using the condition (4) [7, 23–26, 29].

Recently, the concept of spin squeezing has been extended to unpolarized states [30–34]. In particular, Dicke states are attracting increasing attention, since their multipartite entanglement is robust against particle loss, and they can be used for high precision quantum metrology [8]. Dicke states are produced in experiments with photons [35, 36] and Bose-Einstein condensates [8, 37, 38]. Suitable criteria to detect the depth of entanglement of Dicke states have also been derived. However, either they are limited to spin-1/2 particles [8, 39] or they do not give a tight lower bound on $(\Delta J_x)^2$ based on the expectation value measured for the criterion, concretely, $\langle J_y^2 + J_z^2 \rangle$ [40].

In this paper, we present a general condition that: (i) provides a lower bound on the entanglement depth, (ii) is applicable to spin-j systems, for any j, (iii) works both for spin-squeezed states and Dicke states, and, (iv) is close to provide a tight bound in the sense mentioned above in the large particle number limit. Such a criterion can be applied immediately, for instance, in experiments producing Dicke states in spinor condensates [41].

We now summarize the main results of our paper. With a method similar to the one used for obtaining Eq. (4), we show that the condition

$$(\Delta J_x)^2 \geq Nj G_J \left(\frac{\langle J_y^2 + J_z^2 \rangle - Nj(kj+1)}{N(N-k)j^2} \right) \tag{5}$$

holds for states with an entanglement depth of at most k of an ensemble of N spin-j particles, where we introduced the notation

$$G_J : X \mapsto F_J(\sqrt{X}), \tag{6}$$

with $F_J(X)$ defined as in Eq. (3) and $J = kj$ as in (2). Our approach is motivated by the fact that Eq. (4) fails to be a good criterion for mixed states with a low polarization $\langle J_y \rangle^2 + \langle J_z \rangle^2 \ll N^2 j^2$. Thus, we consider the second moments $\langle J_y^2 + J_z^2 \rangle$ instead, which are still large for many useful unpolarized quantum states, such as Dicke states. Using the second moments is advantageous even for states with a large spin polarization since criteria with second moments are more robust to noise, which will be demonstrated later on concrete examples. We also analyze the performance of our condition compared to other criteria in the literature.

‡ The convexity of $F_J(X)$ is observed numerically [18]. In case the right-hand side of (3) results in a non-convex function in X, then the convex hull of the right-hand side of (3) must be used in the place of $F_J(X)$.

In general, the function $G_J(X)$ appearing on the right-hand side of (5) has to be evaluated numerically. However, due to its convexity properties we can bound it from below with the two lowest nontrivial orders of its Taylor expansion around $X = 0$, yielding a spin-squeezing parameter similar to the one defined in (1). While states saturating (5) determine a curve in the $(\langle J_y^2 + J_z^2\rangle, (\Delta J_x)^2)$-plane, such an analytic condition corresponds to tangents to this curve. Hence, we will refer to it as a linear criterion. Such a criterion for states with an entanglement depth k or smaller is given by the inequality

$$\xi^2 := (kj+1)\frac{2(N-k)j(\Delta J_x)^2}{\langle J_y^2 + J_z^2\rangle - Nj(kj+1)} \geq 1, \tag{7}$$

where we require that kj is an integer. A similar condition can be obtained from the Sørensen–Mølmer criterion (4) as

$$\xi^2_{\mathrm{SM}} := (kj+1)\frac{2Nj(\Delta J_x)^2}{\langle J_y\rangle^2 + \langle J_z\rangle^2} \geq 1, \tag{8}$$

again requiring that kj is integer. A direct comparison between ξ^2 and ξ^2_{SM} shows that the former is more suitable for detecting the depth of entanglement of unpolarized states, such as Dicke states. Note also the similarity between (8) and the original criterion for spin-1/2 particles (1). All these criteria are also generalized to the case when the particle number is not fixed, following [19].

Our paper is organized as follows. In section 2, we discuss how to evaluate our criteria numerically, while we also discuss cases where analytical formulas can be used instead of numerics. In section 3, we derive our nonlinear entanglement criterion. In section 4, we present linear criteria leading to new spin-squeezing parameters. In section 5, we compare our entanglement conditions to other conditions existing in the literature. Finally, in section 6, we discuss how to generalize our methods to the case of a fluctuating number of particles.

2. Numerical computation of $G_J(X)$

Before describing how to obtain $F_J(X)$ and $G_J(X)$ numerically, we define some notions necessary for our discussion. We distinguish various levels of multipartite entanglement based on the following definitions. A pure quantum state is k-producible if it can be written as

$$|\psi^{(1)}\rangle \otimes |\psi^{(2)}\rangle \otimes \cdots \otimes |\psi^{(M)}\rangle, \tag{9}$$

where $|\psi^{(l)}\rangle$ are states of $k_l \leq k$ particles, and M stands for the number of particle groups. A mixed quantum state is k-producible, if it can be written as a mixture of pure k-producible states. Clearly, 1-producible states are separable states. A state that is not k-producible is called $(k+1)$-entangled. The entanglement depth is $k+1$ whenever the state is $(k+1)$-producible but not k-producible [18, 42].

Next, we will show a simple method to calculate $F_J(X)$ and $G_J(X)$. We will discuss both numerical and analytical approaches. Knowing the properties of these functions is

necessary to prove later the relation (5). For an integer J, the function $F_J(X)$ given in (3) can be efficiently computed for some interval of X as follows [18]. We just need to calculate the ground states $|\phi_\lambda\rangle$ of the Hamiltonian

$$H_\lambda = L_x^2 - \lambda L_z \tag{10}$$

for a sufficiently wide interval of λ. Note that the ground states of (10) are the extreme spin-squeezed states studied in [18]. Then, the points of the curve $F_J(X)$ are obtained as $X = \frac{1}{J}\langle L_z\rangle_{\phi_\lambda}$ and $F_J(X) = \frac{1}{J}\langle L_x^2\rangle_{\phi_\lambda}$. Note that the method takes into account that the state minimizing $(\Delta J_x)^2$ for a given $\langle L_z\rangle$ has $\langle L_x\rangle = 0$, which is a property numerically observed to be true for integer J [18]. The algorithm can be extended to half-integer J's by adding a Lagrange multiplier term $\lambda_2 L_x$ that constraints $\langle L_x\rangle$ to some value, the details can be found in Appendix A. In practice, $F_J(X)$ is computed typically for an integer J only, which makes it possible to detect $(k+1)$-particle entanglement for any k for an integer j and for an even k for a half-integer j. In the latter case, it is not a large restriction to consider only even k, since the entanglement depth in cold atom experiments can be quite large [7–9].

In a similar fashion, we can also obtain the curve for $G_J(X)$ defined in (6). The points of the curve are given as $X = \frac{1}{J^2}\langle L_z\rangle_{\phi_\lambda}^2$ and $G_J(X) = \frac{1}{J}\langle L_x^2\rangle_{\phi_\lambda}$. In figure 1, we drew $G_J(X)$ for various values of J. Based on these, the boundary for k-producible states in the $(\langle J_y^2 + J_z^2\rangle, (\Delta J_x)^2)$-plane is given by

$$\begin{aligned}\langle J_y^2 + J_z^2\rangle_\lambda &= \frac{N(N-k)j^2}{k^2 j^2}\langle L_z\rangle_{\phi_\lambda}^2 + Nj(kj+1),\\ (\Delta J_x)_\lambda^2 \quad &= \frac{N}{k}(\Delta L_x)_{\phi_\lambda}^2.\end{aligned} \tag{11}$$

In the numerical calculations, L_l are Hermitian matrices of size $(2kj+1)\times(2kj+1)$. Hence, it is possible to draw the boundaries for various levels of multipartite entanglement for kj reaching up to the thousands, and for an arbitrarily large N.

We mention that for $J = 1$ we have $G_1(X) = \frac{1}{2}(1-\sqrt{1-X})$, i.e., the function on the right-hand side of the criteria can be obtained analytically. Substituting $F_1(X) = G_1(X^2)$ into (5), we can obtain an analytic 2-producibility condition for qubits and an analytic separability condition for qutrits. In figure 2, we plotted the curves for k-producible states for some examples with spin-$\frac{1}{2}$ and spin-1 particles. For higher J, the function $G_J(X)$ is not known analytically. Based on uncertainty relations of angular momentum operators, a lower bound on $G_J(X)$ for any J can be obtained as

$$\tilde{G}_J(X) = \frac{1}{2}\left[(J+1) - JX - \sqrt{(J+1-JX)^2 - X}\right], \tag{12}$$

which is not tight for small J and small X, but becomes tight for large J and X close to 1 [18].

3. Nonlinear criterion

In this section, we present our first main result.

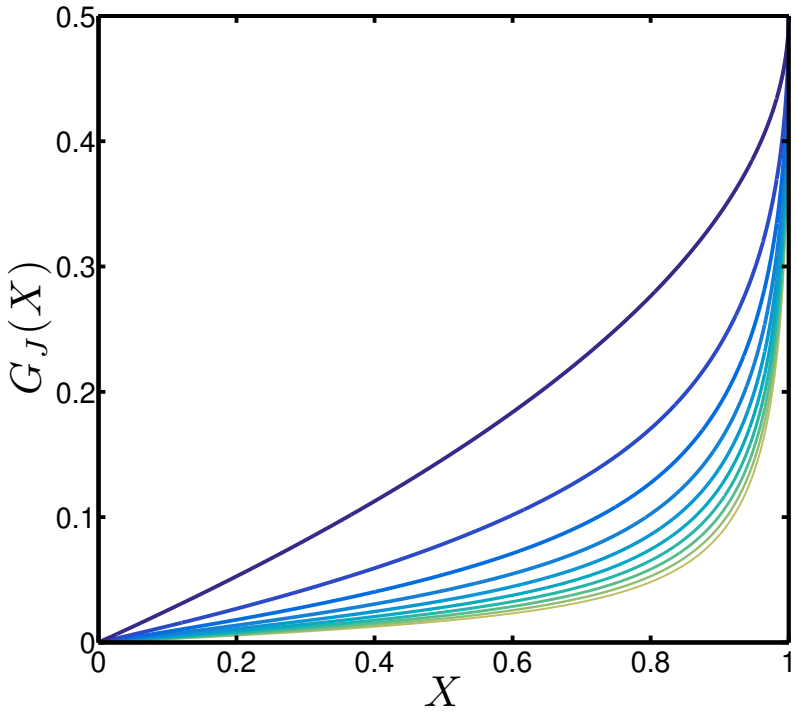

Figure 1. The function $G_J(X)$ defined in (6) for (left to right) $J = 1, 3, 5, \ldots, 19$.

Observation 1. The inequality in (5) holds for all k-producible states of N spin-j particles. Thus, every state of N spin-j particles that violates (5) must be $(k+1)$-entangled. The condition (5) can be used if $\langle J_y^2 + J_z^2 \rangle \geq Nj(kj+1)$, while otherwise there is a k-producible quantum state for which $(\Delta J_x)^2 = 0$.

Proof. The key argument of the proof is that for pure k-producible states of N spin-j particles

$$\frac{\sqrt{\langle J_y \rangle^2 + \langle J_z \rangle^2}}{Nj} \geq \sqrt{\frac{\langle J_y^2 + J_z^2 \rangle - Nj\,(kj+1)}{N(N-k)j^2}} \tag{13}$$

holds, which is proven in Appendix B.1. Then, based on (13) and on the monotonicity of $F_J(X)$ in X, we have for pure k-producible states

$$F_J(\text{LHS}) \geq F_J(\text{RHS}). \tag{14}$$

Here, we used the notation LHS and RHS for the left-hand side and right-hand side of the relation (13), respectively. On the other hand, the Sørensen–Mølmer criterion (4) can be rewritten as

$$(\Delta J_x)^2 \geq Nj F_J(\text{LHS}). \tag{15}$$

From (14) and (15) follows that (5) holds for pure k-producible states.

Next, we will consider mixed states. In the formula (5) the argument of G is linear in the state. Then, our criterion (5) can be extended to mixed k-producible states via

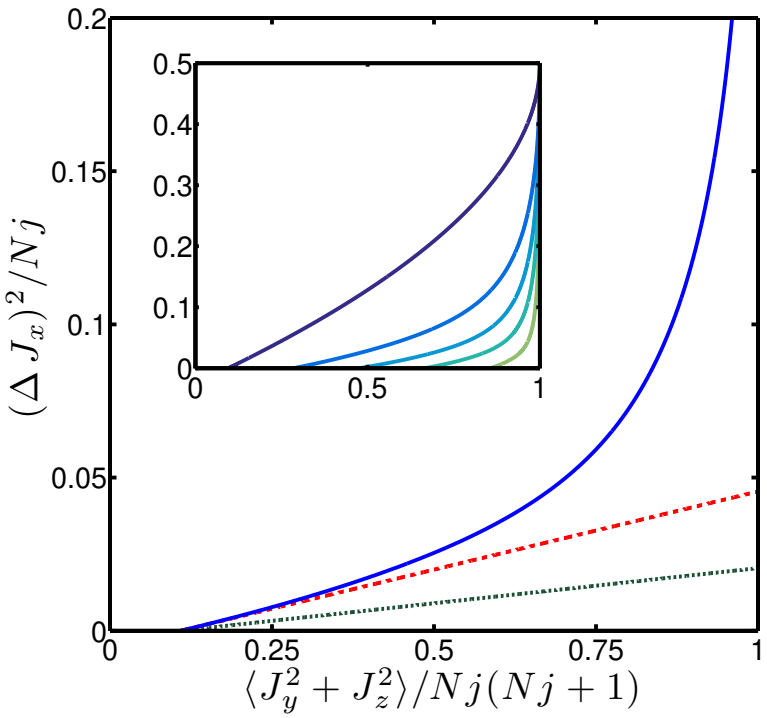

Figure 2. 20-producibility criteria for $N = 200$ qubits. (solid) The boundary given by (5). (dashed) Criterion (7), i.e., the tangent to the curve given by (5). (dotted) Criterion (22) given in [39]. (inset) Curves for k-producibility for $N = 20$ spin-1 particles, for (left to right) $k = 1, 5, 9, 13, 17$.

a convex hull of $G_J(X)$. However we can observe numerically that $G_J(X)$ is convex already by itself. The tightness of (5) is discussed in Appendix B.2, while the convexity of $G_J(X)$ is considered in detail in Appendix B.3. □

The criterion (5) is especially suited to detect states for which $\langle J_y^2 + J_z^2\rangle$ is large and $(\Delta J_x)^2$ is small. A paradigmatic example for such a state is the unpolarized Dicke state in the x-basis

$$\rho_{\text{Dicke}} = |J = Nj, m_x = 0\rangle\langle J = Nj, m_x = 0|, \tag{16}$$

that satisfies $(\Delta J_x)^2 = 0$ and $\langle J_y^2 + J_z^2\rangle = Nj(Nj+1)$ and is detected as N-entangled. In fact, substituting these quantities in the criterion (5) the left-hand side is zero, while the right-hand side is positive for $k = N - 1$. Note also that the Dicke states violate maximally even the relation (13) for pure k-producible states §.

4. Linear analytic criteria

In this section, we will derive the spin-squeezing parameters (7) and (8). Complementary to the approximation (12), our approach is based on a lower bound on $G_J(X)$ that is

§ We stress that (13) is not an entanglement criterion, since it does not hold for mixed states.

tighy for $X \approx 0$ and improves $\tilde{G}_J$ at small X by a factor of 2. For our derivation, we will compute the first terms of the Taylor expansion of $G_J(X)$ around $X = 0$. Using the convexity of $G_J(X)$, we will obtain the bound $G_J(X) \geq (G_J(0) + XG'_J(0))$, with $G_J(0) = 0$. In other words, we will compute the tangent to the k-producibility boundaries, near their intersection point with the horizontal axis.

In what follows, we present the details of the derivation. The expansion of $G_J(X)$ can be obtained by employing the perturbation series for H_λ in powers of the parameter $\lambda \ll 1$, taking advantage of the fact that $X = 0$ corresponds to $\lambda = 0$. The ground state of H_λ is then given by $|\phi_\lambda\rangle = |\phi^{(0)}\rangle + \lambda|\phi^{(1)}\rangle + O(\lambda^2)$ ‖, where $|\phi^{(0)}\rangle$ is the ground state of the unperturbed Hamiltonian $H^{(0)} = L_x^2$, i.e., the eigenstate of L_x with eigenvalue zero. As in usual perturbation theory, the first order term is obtained by imposing $\langle\phi^{(0)}|\phi^{(1)}\rangle = 0$ and results in $|\phi^{(1)}\rangle = \sum_{m\neq 0} c_m|E_m^{(0)}\rangle$, where $c_m = -\langle E_m^{(0)}|H^{(1)}|E_0^{(0)}\rangle/(E_m^{(0)} - E_0^{(0)})$ and $E_m^{(0)}$ are the energy levels of the unperturbed Hamiltonian. In our case, we obtain $|\phi^{(1)}\rangle = \sum_{m\neq 0} c_m|m\rangle_x$ with $c_m = -\langle m|_x L_z|0\rangle_x/m^2$, where $|m\rangle_x$ are the eigenstates of L_x with eigenvalue m. The expansion of the ground state explicitly is as follows

$$|\phi_\lambda\rangle = |0\rangle_x - i\lambda\frac{\sqrt{J(J+1)}}{2}\left(|1\rangle_x - |-1\rangle_x\right) + O(\lambda^2). \tag{17}$$

Based on (17), we obtain for the dependence of X and $G_J(X)$ on λ, respectively, $X(\lambda) = \frac{1}{J^2}\langle L_z\rangle^2_{\phi_\lambda} \approx \lambda^2(J+1)^2$ and $G_J(X(\lambda)) = \frac{1}{J}\langle L_x^2\rangle_{\phi_\lambda} \approx \frac{1}{2}\lambda^2(J+1)$. Hence, we arrive at

$$G_J(X) \geq \frac{X}{2(J+1)}, \tag{18}$$

by employing the chain rule for $\frac{\mathrm{d}G_J(X(\lambda))}{\mathrm{d}X}$ near $X = \lambda = 0$. Based on this, we can derive an analytic criterion that becomes tight close to the point $(\Delta J_x)^2 = 0$. Note that we could also use $\tilde{G}_J(X)$ defined in (12) instead of $G_J(X)$ for constructing our linear entanglement condition. However, taking the derivative of $\tilde{G}_J(X)$ one obtains $G_J(X) \geq \tilde{G}_J(X) \geq X\tilde{G}'_J(0) = \frac{X}{4(J+1)}$, which underestimates (18) by a factor of 2. Note that we computed the leading terms for the Taylor expansion of $G_J(X)$ analytically, while the function itself is known only numerically.

Observation 2. The criteria in (7) and (8) hold for all k-producible states of N spin-j particles such that J given in (2) is an integer number. Every state of N spin-j particles that violates one of the criteria must be $(k+1)$-entangled, i.e., has an entanglement depth at least $k+1$.

Proof. From (18) we can bound the criterion (5) from below with (7) by substituting $X = \left[\langle J_y^2 + J_z^2\rangle - Nj(kj+1)\right]/[N(N-k)j^2]$. Analogously, by rewriting (4) in terms of G_J and using the bound (18) with $X = \langle J_z\rangle^2/N^2j^2$ we obtain (8). □

‖ $O(x)$ is the usual Landau symbol used to describe the asymptotic behavior of a quantity for small x

In figure 2, we plot the criterion (7) as the tangent to the boundary of 20-producibility for $N = 200$ particles with spin $j = \frac{1}{2}$ in the $(\langle J_y^2 + J_z^2\rangle, (\Delta J_x)^2)$-plane.

5. Comparison with similar criteria

Next, we compare our criteria with other similar entanglement conditions. First let us consider the Sørensen-Mølmer criterion (4).

Observation 3. Whenever the condition

$$\frac{(\Delta J_y)^2 + (\Delta J_z)^2}{Nj} > kj\left(1 - \frac{\langle J_y\rangle^2 + \langle J_z\rangle^2}{N^2 j^2}\right) + 1 \tag{19}$$

holds then our criterion (5) is strictly stronger than the Sørensen–Mølmer criterion (4).

Proof. (a) Since $F_J(X)$ is a monotonously increasing function of X, the inequality $F_J(X) \geq F_J(Y)$ holds if and only if $X \geq Y$. Hence, for comparing (4) and (5) it suffices to compare the arguments of the function F in the two conditions. It is then straightforward to prove that (5) implies (4) whenever (19) holds. Then, let us now present a family of states that are detected by (5), but not detected by (4). We consider states of the form

$$\rho_{\text{Dicke},p} \;=\; (1-p)\rho_{\text{Dicke}} + p\frac{\mathbb{1}}{(2j+1)^N}, \tag{20}$$

where the unpolarized Dicke state is given in (16). From the linear criterion (7) we obtain that if $p < \frac{3(N-k)j}{2j(j+1)(kj+1)(N-k)-2(j+1)+3(Nj+1)}$ then the state $\rho_{\text{Dicke},p}$ is detected by (5). On the other hand, $\rho_{\text{Dicke},p}$ is not detected by the Sørensen–Mølmer criterion (4), since $\langle J_l\rangle = 0$ for $l = x, y, z$ for this state for all p. □

From Observation 3, we can immediately see that our criterion (5) is much stronger than the original spin-squeezing criterion (4) for states close to Dicke states (16) since for such states $(\Delta J_y)^2 + (\Delta J_z)^2 \gg Nkj^2$. Here, we assumed that k is much smaller than N, which is consistent with experiments, where criterion (4) always detects an entanglement depth much smaller than N due to noise [7, 9].

Let us now study numerically how our criterion works for a relevant class of states. We consider spin-squeezed states of spin-$\frac{1}{2}$ particles obtained from ground states of the Hamiltonian

$$H_\mu = J_x^2 - \mu J_z, \tag{21}$$

for simplicity assuming an even particle number. The Dicke state (16) corresponds to $\mu = 0$, while the usual spin-squeezed states with a large spin polarization correspond to a large μ. For such states without noise, our criterion (5) is not stronger than (4).

Simple calculations show that if some small noise is present in the system then (5) detect an entanglement depth higher than the original criterion (4). First we consider spin-squeezed states for $N = 1000$ spin-$\frac{1}{2}$ particles, such that 10 particles are decohered into the fully mixed state. Such a noise is typical in cold atom experiments

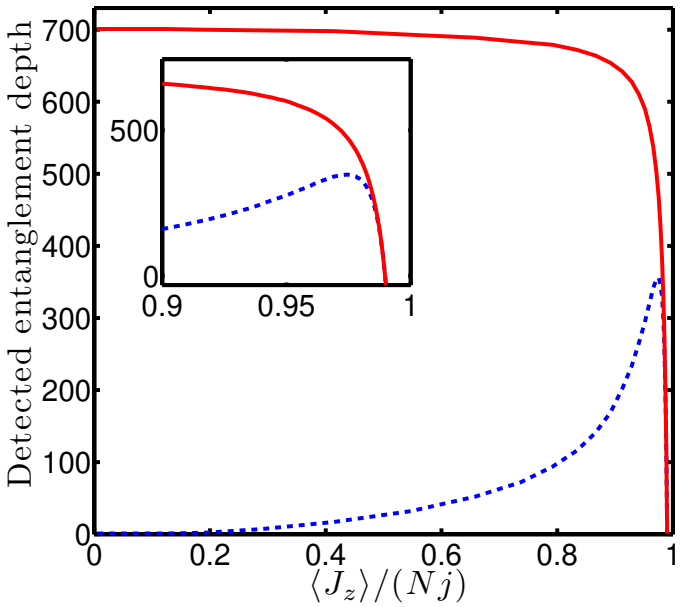

Figure 3. Multiparticle entanglement for spin-squeezed states of $N = 1000$ spin-$\frac{1}{2}$ particles, after 10 particles decohered into the completely mixed state. (solid) Entanglement depth detected by our criterion (5) and (dashed) the Sørensen-Mølmer criterion (4).

[43]. The results can be seen in figure 3. Our criterion (5) and the Sørensen-Mølmer criterion (4) detect the same entanglement depth for almost completely polarized spin-squeezed states. On the other hand, as the squeezing increases, our criterion detects a monotonically increasing entanglement depth, while the other criterion detects smaller and smaller multipartite entanglement. While we considered a noise affecting a few particles, still the detected entanglement depth is much smaller than N. Other types of noise, such as particle loss, small added white noise, or noise effects modelled considering the thermal states of (21) lead to a similar situation.

Next, we compare our criteria with another important condition that is designed to detect the depth of entanglement near unpolarized Dicke states (16). It is a linear criterion derived by Duan in [39], stating that

$$N(k+2)(\Delta J_x)^2 \geq \langle J_y^2 + J_z^2\rangle - \frac{N}{4}(k+2) \tag{22}$$

holds for all k-producible states of N spin-$\frac{1}{2}$ particles. Any state that violates (22) is detected as $(k+1)$-entangled. In this case, we can compare it with the linear criterion (7), specialized to qubit-systems, i.e., for $j = \frac{1}{2}$

$$\frac{(N-k)}{2}(k+2)\,(\Delta J_x)^2 \geq \langle J_y^2 + J_z^2\rangle - \frac{N}{4}(k+2)\,. \tag{23}$$

It is easy to see that a violation of (22) implies a violation of (23). Thus, our condition detects more states, which can be seen in figure 2.

Finally, we note that (5) with $j = 1/2$ is similar to the criterion for spin-1/2 particles used in the experiment described in [8]. A key difference is that in (5), in the denominator of the fraction, the term $N(N-k)j^2 = N(N-k)/4$ appears, while in the formula of [8] there is the term $N^2/4$. The difference between the two criteria is the largest when we examine highly entangled Dicke states or spin-squeezed states, and in the argument of $F_J(X)$ we have a value close to $X = 1$. In the vicinity of this point, the derivative of $F_J(X)$ is very large, hence some improvement in the argument of $F_J(X)$ makes the bound on the right-hand side of (5) significantly higher. As a consequence, the criterion (5) can be used to detect the noisy Dicke states of many particles even in $k \sim N$ case, while the criterion of [8] can be used only when $k \ll N$, and it does not detect the Dicke state as N-entangled.

6. Extension to fluctuating number of particles

For macroscopic ensembles of particles, e.g., for $N \sim 10^6$, the total particle number is not under perfect control. In this section, we will generalize our entanglement criteria to such a situation. The quantum state of a large particle ensemble with a fluctuating particle number is given as

$$\rho = \sum_N Q_N \rho_N, \tag{24}$$

where ρ_N are the density matrices corresponding to a subspace with a particle number N and Q_N are probabilities. We also have to consider collective spin operators defined as $J_l = \sum_N J_{l,N}$ for $l = x, y, z$, where $J_{l,N}$, act on the subspace with N particles. In principle, one could evaluate an entanglement condition, e.g., (4) for one of the fixed-N subspaces. If ρ_N has an entanglement depth k for some N, then the state ρ has also at least an entanglement depth k. However, in practice, we would not have sufficient statistics to evaluate our entanglement criteria for some fixed N. This issue has been studied by Hyllus *et al.* [19], who generalized the definition of entanglement depth to the case of a fluctuating number of particles. They also showed how spin-squeezing criteria can be used in this case such that all the collected statistics is used, not only data for a given particle number N. For instance, (4) can be transformed to [19]

$$(\Delta J_x)^2 \geq \langle N \rangle j F_J \left(\frac{\langle J_z \rangle}{\langle N \rangle j} \right). \tag{25}$$

Here, (25) could be obtained from (4) simply with the substitution $N \to \langle N \rangle$.

Using methods similar to the ones in [19], we will now obtain the criterion (4) for fluctuating particle numbers.

Observation 4. All k-producible states with a fluctuating particle number must satisfy the following inequality

$$(\Delta J_x)^2 \geq \langle N \rangle j G_J \left(\frac{\langle W \rangle}{\langle N \rangle j} \right), \tag{26}$$

where we define the operator

$$W = \sum_N (Nj - kj)^{-1} \left[J_{y,N}^2 + J_{z,N}^2 - Nj(kj+1)\mathbb{1}_N \right], \tag{27}$$

$\langle W \rangle \geq 0$ is required, and J is the total spin of a k-particle group given in (2).

Proof. We have to start from a state of the form (24). Due to the concavity of the variance, the variance of the mixed state can be bounded from below with the variances of ϱ_N as $(\Delta J_k)^2 \geq \sum_N Q_N (\Delta J_{k,N})^2$. Moreover, since $G_J(X)$ is convex in X, it has to satisfy Jensen's inequality. Thus,

$$\frac{1}{\sum_N Q_N N} \sum_N Q_N N G_J\left(X_N\right) \geq G_J\left(\frac{\sum_N Q_N N X_N}{\sum_N Q_N N} \right) \tag{28}$$

with $X_N = \frac{\langle W \rangle_{\varrho_N}}{N}$ and $\langle N \rangle = \sum_N Q_N N$ must hold. Based on these, the statement of the Observation follows. □

Note that the operator W defined in (27) is simply a sum of $J_{y,N}^2 + J_{z,N}^2$ over all fixed-N subspaces, normalized with $(Nj - kj)$. Thus, to apply our condition in experiments with fluctuating number of particles, one needs to measure the spin operators and the particle number jointly at each shot, and then average over an ensemble.

Finally, let us consider how to apply the ideas above for the spin-squeezing parameters defined in this paper. The parameter (8) can be extended to fluctuating particle numbers simply by replacing N with $\langle N \rangle$. Similarly, for the parameter (7), we have to replace $\frac{\langle J_y^2 + J_z^2 \rangle - Nj(kj+1)}{(N-k)j}$ by $\langle W \rangle$.

7. Conclusions

We derived a set of criteria to determine the depth of entanglement of spin-squeezed states and unpolarized Dicke states, extending and completing the results of Refs. [8, 18]. These generalized spin-squeezing conditions are valid even for an ensemble of spin-j particles with $j > \frac{1}{2}$, which is very useful, since most experiments are carried out with particles with a higher spin, e.g., with spin-1 ^{87}Rb atoms. Since theory is mostly available for the spin-$\frac{1}{2}$ case, pseudo spin-$\frac{1}{2}$ particles are created artificially such that only two of the levels are populated. While the spin-squeezing approach to entanglement detection is already widely used in such systems [7, 8, 20–26, 33, 38], our criteria make it possible to study spin-squeezing in fundamentally new experiments. A clear advantage of using the physical spin is that it is typically much easier to manipulate than the pseudo spin-$\frac{1}{2}$ particles [33]. In future, it would be interesting to clarify the relation between generalized spin squeezing and metrological usefulness [44–49], and also compare our results with the complete set of spin-squeezing criteria of [50], which contain one additional collective observable, related to single-spin average squeezing.

Acknowledgments

We thank G. Colangelo, L. M. Duan, O. Gühne, P. Hyllus, M. W. Mitchell, and J. Peise for discussions. This work was supported by the EU (ERC Starting Grant 258647/GEDENTQOPT, CHIST-ERA QUASAR, COST Action CA15220) the Spanish MINECO (Project No. FIS2012-36673-C03-03 and No. FIS2015-67161-P), the Basque Government (Project No. IT4720-10), the National Research Fund of Hungary OTKA (Contract No. K83858), the DFG (Forschungsstipendium KL 2726/2-1), and the FQXi (Grant No. FQXi-RFP-1608). We also acknowledge support from the Centre QUEST, the DFG through RTG 1729 and CRC 1227 (DQ-mat), project A02, and the EMRP.

Appendix A. Computing $F_J(X)$ and $G_J(X)$ for half-integer spin

For half-integer spins, we have to calculate $F_J(X)$ numerically as follows. We consider the Hamiltonian [18]

$$H_{\lambda,\lambda_2} = L_x^2 - \lambda L_z - \lambda_2 L_x, \tag{A.1}$$

and denote its ground state by ϕ_{λ,λ_2}. Then, $F_J(X)$ can be obtained as

$$F_J(X) = \min_{\lambda,\lambda_2:\frac{1}{J}\langle L_z\rangle = X} (\Delta J_x)^2_{\psi_{\lambda,\lambda_2}}, \tag{A.2}$$

which is a two-parameter optimization with the constraint $\frac{1}{J}\langle L_z\rangle = X$.

Appendix B. Details of the proof of Observation 1

Appendix B.1. Proof. of (13)

To prove (13), let us consider the expression $(\Delta J_y)^2+(\Delta J_z)^2$ on pure k-producible states (9). Due to the additivity of the variance for tensor products

$$\begin{aligned}(\Delta J_y)^2 + (\Delta J_z)^2 &= \sum_l \left[(\Delta j_y^{(l)})^2 + (\Delta j_z^{(l)})^2\right] \\ &\leq \sum_l \left[k_l j\,(k_l j+1) - \langle (j_x^{(l)})^2\rangle - \langle j_y^{(l)}\rangle^2 - \langle j_z^{(l)}\rangle^2\right]\end{aligned} \tag{B.1}$$

holds, where the superscript (l) indicates the lth group, that is composed of k_l particles. The inequality (B.1) is saturated by all quantum states for which $\langle (j_x^{(l)})^2+(j_y^{(l)})^2+(j_z^{(l)})^2\rangle$ is maximal, i.e., equal to $k_l j\,(k_l j+1)$, for all l.

For simplifying our expression, we neglect the non-negative quantity

$$\mathcal{X} := \sum_l \langle (j_x^{(l)})^2\rangle, \tag{B.2}$$

and after some rearrangement of the terms in (B.1) we arrive at

$$\begin{aligned}\langle J_y^2 + J_z^2\rangle \leq\ & \langle J_y\rangle^2 + \langle J_z\rangle^2 \\ &+ \sum_l k_l j \left[(k_l j+1) - k_l j \frac{\left(\langle j_y^{(l)}\rangle^2 + \langle j_z^{(l)}\rangle^2\right)}{k_l^2 j^2}\right].\end{aligned} \tag{B.3}$$

From (B.3), we can obtain a simpler bound as

$$\langle J_y^2 + J_z^2\rangle \leq \langle J_y\rangle^2 + \langle J_z\rangle^2 + Nj + \sum_l k_l j \left[kj\left(1 - \frac{\langle j_y^{(l)}\rangle^2 + \langle j_z^{(l)}\rangle^2}{k_l^2 j^2}\right)\right], \tag{B.4}$$

due to the fact that $k_l \leq k, \sum_l k_l = N$, and that the expression inside the round brackets in (B.4) is positive. Furthermore, using Jensen's inequality in the form

$$-\sum_l k_l f_l^2 \leq -\frac{1}{N}\left(\sum_l k_l f_l\right)^2, \ \sum_l k_l = N, \tag{B.5}$$

with $f_l = \frac{\langle j_m^{(l)}\rangle}{k_l}$ for $m = x, y, z$ we obtain

$$\langle J_y^2 + J_z^2\rangle - Nj(kj+1) \leq \left(1 - \frac{k}{N}\right)(\langle J_y\rangle^2 + \langle J_z\rangle^2). \tag{B.6}$$

Hence, we proved (13).

Appendix B.2. Tightness of (13) and (5)

We will now examine, how the relation (13) would look for pure k-producible states (9) without neglecting $\mathcal{X}$ defined in (B.2). Simply, $\langle J_y^2 + J_z^2\rangle$ would be substituted by $\langle J_y^2 + J_z^2\rangle + \mathcal{X}$. With a derivation similar to the one in Appendix B.1, it can be shown that such a condition would be saturated by all quantum states of the form $|\psi\rangle\otimes|\psi\rangle\otimes...\otimes|\psi\rangle$, if $|\psi\rangle$ are k-qubit states and $\langle j_x^2 + j_y^2 + j_z^2\rangle_\psi$ is maximal, i.e., it is $kj\,(kj+1)$. (Here we assumed that $\mathcal{X}$ is defined such that all particle groups contain k particles, i.e, $k_l = k$ for all l.)

Let us now see how large $\mathcal{X}$ is for relevant states. For the state fully polarized in the z-direction, we have

$$\mathcal{X} = \sum_l (\Delta j_x^{(l)})^2 = Nj^2/2, \tag{B.7}$$

where we used the fact that $\langle j^{(l)}\rangle = 0$ for such a state. Let us consider now the ground states of the Hamiltonian (21) for a given parameter μ. Such states include usual spin-squeezed states, as well as Dicke states (16). For any μ,

$$\mathcal{X} < Nj^2/2 \tag{B.8}$$

holds, since for such states the variance of the x-components of the collective angular momentum is squeezed below that of the completely polarized state for any particle group. Note that the upper bound in (B.8) does not grow with k.

Let us now consider the other relevant quantity, $\langle J_y^2 + J_z^2\rangle$. For the state fully polarized in the x-direction, we have $\langle J_y^2 + J_z^2\rangle = Nj(Nj + 1/2)$. For the Dicke state (16), $\langle J_y^2 + J_z^2\rangle = Nj(Nj+1)$. For ground states of (21) for $\mu > 0$, $\langle J_y^2 + J_z^2\rangle$ is in between these two values. This can be seen noticing that $\langle J_x^2 + J_y^2 + J_z^2\rangle = Nj(Nj+1)$ for these states.

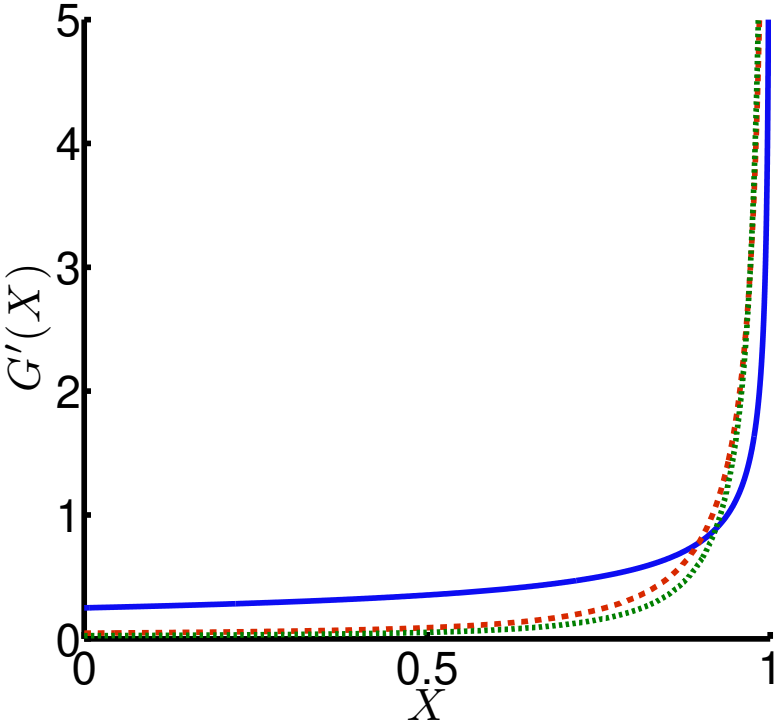

Figure B1. The derivative $G'(X) = \frac{J}{2\langle L_z\rangle_{\phi_\lambda}}\lambda$ as a function of $X = \frac{1}{J^2}\langle L_z\rangle^2_{\phi_\lambda}$ for (solid) $J = 1$, (dashed) $J = 10$, and (dotted) $J = 19$.

Based on the previous discusion, it is clear that $\mathcal{X} \ll \langle J_y^2 + J_z^2\rangle$ holds for large N. Hence, in practical cases the relation (5) provides a tight bound on $(\Delta J_x)^2$ based on $\langle J_y^2 + J_z^2\rangle$ in the large N limit.

Appendix B.3. Properties of F_J and G_J

The functions $F_J(X)$ can be obtained from the optimal states ρ for the problem defined in (3), i.e., the states that minimize $(\Delta L_x)^2$ for a given $\langle L_z\rangle$. As discussed in section 2, for an integer spin J, such states are the ground states of (10), where λ is a parameter. They have $\langle L_x\rangle = 0$ [18]. Thus, $F_J(X)$ yields the minimal $\langle J_x^2\rangle$ for a given value of $\langle J_z\rangle$. Since the set of physical states is convex, the set of points in the $(\langle J_z\rangle, \langle J_x^2\rangle)-$space corresponding to physical states is also convex. Hence, $F_J(X)$ is also a convex function and in particular its derivative $\lambda(X)$ is monotonously increasing with X. Note that in [18] a different proof was presented for this fact. In principle, the derivative $F'_J(X)$ can be computed by numerical derivation of $F_J(X)$. However, it is much simpler to obtain $F'_J(X)$ for some range of X by plotting $(\frac{1}{J}\langle L_z\rangle_{\phi_\lambda}, \lambda)$ for some range of λ [18]. In other words, for $X = \frac{1}{J}\langle L_z\rangle_{\phi_\lambda}$ the derivative is $F'_J(X) = \lambda$.

To show that also $G_J(X)$ is convex we observe that $G'_J(X) = \frac{1}{2\sqrt{X}}F'_J(\sqrt{X})$ is a monotonously increasing function of X. We evaluate numerically the derivative $G'_J(X)$ by plotting $(\frac{1}{J^2}\langle L_z\rangle^2_{\phi_\lambda}, \frac{J}{2\langle L_z\rangle_{\phi_\lambda}}\lambda)$ for a wide range of λ, cf. figure B1, and see explicitly

its monotonicity. More generally, one can check whether or not $F_J(X^{\frac{1}{\alpha}})$ is convex for any exponent α. It can then be observed numerically (not shown) that $F_J(X^{\frac{1}{\alpha}})$ is not convex for any $\alpha > 2$.

So far we discussed the case of integer spin. For half-integer spin, the ideas mentioned before cannot be used. Then, the derivative of G_J can be obtained via the numerical derivation of $F_J(X)$. Based on numerics, we can make the same statements about the convexity of $G_J(X)$ and $F_J(X^{\frac{1}{\alpha}})$ as for the case of an integer spin.

References

[1] Schwemmer C, Tóth G, Niggebaum A, Moroder T, Gross D, Gühne O and Weinfurter H 2014 *Phys. Rev. Lett.* **113** 040503

[2] Gao W B, Lu C Y, Yao X C, Xu P, Gühne O, Goebel A, Chen Y A, Peng C Z, Chen Z B and Pan J W 2010 *Nat. Phys.* **6** 331–335

[3] Leibfried D, Barrett M, Schaetz T, Britton J, Chiaverini J, Itano W, Jost J, Langer C and Wineland D 2004 *Science* **304** 1476–1478

[4] Huang Y F, Liu B H, Peng L, Li Y H, Li L, Li C F and Guo G C 2011 *Nat. Commun.* **2** 546

[5] Appel J, Windpassinger P J, Oblak D, Hoff U B, Kjærgaard N and Polzik E S 2009 *PNAS* **106** 10960–10965

[6] Sewell R J, Koschorreck M, Napolitano M, Dubost B, Behbood N and Mitchell M W 2012 *Phys. Rev. Lett.* **109** 253605

[7] Gross C, Zibold T, Nicklas E, Esteve J and Oberthaler M K 2010 *Nature* **464** 1165–1169

[8] Lücke B, Peise J, Vitagliano G, Arlt J, Santos L, Tóth G and Klempt C 2014 *Phys. Rev. Lett.* **112** 155304

[9] Hosten O, Engelsen N J, Krishnakumar R and Kasevich M A 2016 *Nature* **529** 505–508

[10] McConnell R, Zhang H, Hu J, Ćuk S and Vuletić V 2015 *Nature* **519** 439–442

[11] Haas F, Volz J, Gehr R, Reichel J and Esteve J 2014 *Science* **344** 180–183

[12] Horodecki R, Horodecki P, Horodecki M and Horodecki K 2009 *Rev. Mod. Phys.* **81** 865–942

[13] Gühne O and Tóth G 2009 *Phys. Rep.* **474** 1–75

[14] Pezzé L and Smerzi A 2009 *Phys. Rev. Lett.* **102** 100401

[15] Sørensen A, Duan L M, Cirac J and Zoller P 2001 *Nature* **409** 63–66

[16] Kitagawa M and Ueda M 1993 *Phys. Rev. A* **47** 5138–5143

[17] Wineland D J, Bollinger J J, Itano W M and Heinzen D J 1994 *Phys. Rev. A* **50** 67–88

[18] Sørensen A S and Mølmer K 2001 *Phys. Rev. Lett.* **86** 4431–4434

[19] Hyllus P, Pezzé L, Smerzi A and Tóth G 2012 *Phys. Rev. A* **86** 012337

[20] Hald J, Sørensen J L, Schori C and Polzik E S 1999 *Phys. Rev. Lett.* **83** 1319–1322

[21] Fernholz T, Krauter H, Jensen K, Sherson J F, Sørensen A S and Polzik E S 2008 *Phys. Rev. Lett.* **101** 073601

[22] Orzel C, Tuchman A K, Fenselau M L, Yasuda M and Kasevich M A 2001 *Science* **291** 2386–2389

[23] Riedel M F, Böhi P, Li Y, Hänsch T W, Sinatra A and Treutlein P 2010 *Nature* **464** 1170–1173

[24] Esteve J, Gross C, Weller A, Giovanazzi S and Oberthaler M 2008 *Nature* **455** 1216–1219

[25] Bohnet J G, Cox K C, Norcia M A, Weiner J M, Chen Z and Thompson J K 2014 *Nat. Photon* **8** 731–736

[26] Cox K C, Greve G P, Weiner J M and Thompson J K 2016 *Phys. Rev. Lett.* **116** 093602

[27] Meyer V, Rowe M A, Kielpinski D, Sackett C A, Itano W M, Monroe C and Wineland D J 2001 *Phys. Rev. Lett.* **86** 5870–5873

[28] Auccaise R, Araujo-Ferreira A G, Sarthour R S, Oliveira I S, Bonagamba T J and Roditi I 2015 *Phys. Rev. Lett.* **114** 043604

[29] Mitchell M W and Beduini F A 2014 *New J. Phys.* **16** 073027

[30] Tóth G, Knapp C, Gühne O and Briegel H J 2007 *Phys. Rev. Lett.* **99** 250405

[31] He Q Y, Peng S G, Drummond P D and Reid M D 2011 *Phys. Rev. A* **84** 022107

[32] Reis M S, Soriano S, dos Santos A M, Sales B C, Soares-Pinto D O and Brandão P 2012 *Europhys. Lett.* **100** 50001

[33] Behbood N, Ciurana F M, Colangelo G, Napolitano M, Tóth G, Sewell R J and Mitchell M W 2014 *Phys. Rev. Lett.* **113** 093601

[34] Vitagliano G, Apellaniz I, Egusquiza I L and Tóth G 2014 *Phys. Rev. A* **89** 032307

[35] Wieczorek W, Krischek R, Kiesel N, Michelberger P, Tóth G and Weinfurter H 2009 *Phys. Rev. Lett.* **103** 020504

[36] Prevedel R, Cronenberg G, Tame M S, Paternostro M, Walther P, Kim M S and Zeilinger A 2009 *Phys. Rev. Lett.* **103** 020503

[37] Lücke B, Scherer M, Kruse J, Pezzé L, Deuretzbacher F, Hyllus P, Peise J, Ertmer W, Arlt J, Santos L, Smerzi A and Klempt C 2011 *Science* **334** 773–776

[38] Hamley C, Gerving C, Hoang T, Bookjans E and Chapman M 2012 *Nat. Phys.* **8** 305–308

[39] Duan L M 2011 *Phys. Rev. Lett.* **107** 180502

[40] Zhang Z and Duan L M 2013 *Phys. Rev. Lett.* **111** 180401

[41] Hoang T M, Anquez M, Boguslawski M J, Bharath H M, Robbins B A and Chapman M S 2016 *Proc. Natl. Acad. Sci.* **113** 9465

[42] Gühne O, Tóth G and Briegel H J 2005 *New J. Phys.* **7** 229

[43] de Echaniz S R, Mitchell M W, Kubasik M, Koschorreck M, Crepaz H, Eschner J and Polzik E S 2005 *J. Opt. B: Quantum and Semiclassical Opt.* **7** S548

[44] Hyllus P, Laskowski W, Krischek R, Schwemmer C, Wieczorek W, Weinfurter H, Pezzé L and Smerzi A 2012 *Phys. Rev. A* **85** 022321

[45] Tóth G 2012 *Phys. Rev. A* **85** 022322

[46] Zhang Z and Duan L M 2014 *New J. Phys.* **16** 103037

[47] Tóth G and Apellaniz I 2014 *J. Phys. A: Math. Theor.* **47** 424006

[48] Apellaniz I, Lücke B, Peise J, Klempt C and Tóth G 2015 *New J. Phys.* **17** 083027

[49] Apellaniz I, Kleinmann M, Gühne O and Tóth G (*Preprint* `1511.05203`)

[50] Vitagliano G, Hyllus P, Egusquiza I L and Tóth G 2011 *Phys. Rev. Lett.* **107** 240502

Optimal witnessing of the quantum Fisher information with few measurements

Iagoba Apellaniz,[1] Matthias Kleinmann,[1] Otfried Gühne,[2] and Géza Tóth[1,3,4,*]

[1]*Department of Theoretical Physics, University of the Basque Country UPV/EHU, E-48080 Bilbao, Spain*
[2]*Naturwissenschaftlich-Technische Fakultät, Universität Siegen, Walter-Flex-Str. 3, 57068 Siegen, Germany*
[3]*IKERBASQUE, Basque Foundation for Science, E-48013 Bilbao, Spain*
[4]*Wigner Research Centre for Physics, Hungarian Academy of Sciences, H-1525 Budapest, Hungary*

(Published: 28 March 2017)

We show how to verify the metrological usefulness of quantum states based on the expectation values of an arbitrarily chosen set of observables. In particular, we estimate the quantum Fisher information as a figure of merit of metrological usefulness. Our approach gives a tight lower bound on the quantum Fisher information for the given incomplete information. We apply our method to the results of various multiparticle quantum states prepared in experiments with photons and trapped ions, as well as to spin-squeezed states and Dicke states realized in cold gases. Our approach can be used for detecting and quantifying metrologically useful entanglement in very large systems, based on a few operator expectation values. We also gain new insights into the difference between metrological useful multipartite entanglement and entanglement in general.

DOI: 10.1103/PhysRevA.95.032330

I. INTRODUCTION

Entanglement lies at the heart of many problems in quantum mechanics and has attracted increasing attention in recent years. There are now efficient methods to detect it with a moderate experimental effort [1,2]. However, in spite of intensive research, many of the intriguing properties of entanglement are not fully understood. One such puzzling fact is that, while entanglement is a sought after resource, not all entangled states are useful for some particular quantum information processing task. For instance, it has been realized recently that entanglement is needed in very general metrological tasks to achieve a high precision [3]. Remarkably, this is true even in the case of millions of particles, which is especially important for characterizing the entanglement properties of cold atomic ensembles [4–9]. However, there are highly entangled pure states that are useless for metrology [10].

In the light of the these results, besides verifying that a quantum state is entangled, we should also show that it is useful for metrology. This is possible if we know the quantum Fisher information $\mathcal{F}_{\mathrm{Q}}[\varrho, J_l]$ for the state. Here ϱ is a density matrix of an ensemble of N two-level systems (i.e., qubits), $J_l = \frac{1}{2}\sum_n \sigma_l^{(n)}$ for $l = x, y, z$ are the angular momentum components and $\sigma_l^{(n)}$ are the Pauli spin matrices acting on qubit n.

The quantum Fisher information is a central quantity of quantum metrology. It is connected to the task of estimating the phase θ for the unitary dynamics of a linear interferometer $U = \exp(-iJ_l\theta)$, assuming that we start from ϱ as the initial state. It provides a tight bound for the precision of phase estimation as [11,12]

$$(\Delta\theta)^2 \geqslant 1/\mathcal{F}_{\mathrm{Q}}[\varrho, J_l]. \tag{1}$$

It has been shown that if $\mathcal{F}_{\mathrm{Q}}[\varrho, J_l]$ is larger than the value achieved by product states [3], then the state ϱ is entangled. Higher values of the quantum Fisher information indicate even multipartite entanglement [13]; this fact has been used to analyze the results of several experiments [8,9,14].

In this paper, we suggest estimating the quantum Fisher information based on a few measurements [15]. Our method can be called "witnessing the quantum Fisher information" since our estimation scheme is based on measuring operator expectation values similarly to how entanglement witnesses work [1, 2]. Our findings are expected to simplify the experimental determination of metrological sensitivity since the proposed set of a few measurements is much easier to carry out than the direct determination of the metrological sensitivity, which has been applied in several experiments [8, 9, 16, 17]. The archetypical criterion in this regard is [3]

$$\mathcal{F}_{\mathrm{Q}}[\varrho, J_y] \geqslant \frac{\langle J_z\rangle^2}{(\Delta J_x)^2}, \tag{2}$$

which is expected to work best for states that are almost completely polarized in the z direction and spin-squeezed in the x direction. Apart from spin-squeezed states, there are conditions similar to Eq. (2) for symmetric states close to Dicke states [18–21] and for two-mode squeezed states [22].

After finding criteria for various systems, it is crucial to develop a general method that provides an *optimal* lower bound on the quantum Fisher information in a wide class of cases, especially for the states most relevant for experiments such as spin-squeezed states [23], Greenberger-Horne-Zeilinger (GHZ) states [24], and symmetric Dicke states [18]. It seems that such a method would involve a numerical minimization over all density matrix elements constrained for some operator expectation values, which would be impossible except in very small systems.

In this paper, we demonstrate that tight lower bounds on the quantum Fisher information can still be computed efficiently. Remarkably, our method works for thousands of particles. We show how to obtain a bound on the quantum Fisher information from fidelity measurements for GHZ states [25–32] and for symmetric Dicke states [14,33–37]. We also discuss how to obtain such bounds based on collective measurements for spin-squeezed states of thousands of atoms [6,7,38] and for sym-

* toth@alumni.nd.edu; http://www.gtoth.eu

metric Dicke states prepared recently in cold gases [8,39–41]. We stress that the method is very general, and needs only the expectation values of a set of operators chosen by the experimenter. Then it provides a tight lower bound on the quantum Fisher information.

Due to the relation between the quantum Fisher information and entanglement mentioned above, our method can also be used for entanglement detection and quantification based on an arbitrary set of operator expectation values in very large systems. So far, methods that can be used for large systems, such as spin-squeezing inequalities [42–44], work only for a specific set of observables. In addition, methods that can quantify entanglement based on the expectation values of an arbitrary set of observables, such as semidefinite programming [45–47], work only for small systems.

The paper is organized as follows. In Sec. II, we show how to bound the quantum Fisher information based on the knowledge of some operator expectation values. In Sec. III, we test our method on theoretical examples in small systems. In Sec. IV, we present calculations for experimental data. Finally, in Sec. V, we discuss how the quantum Fisher information is expected to scale with the particle number in the limit of large particle numbers.

II. ESTIMATION OF THE QUANTUM FISHER INFORMATION

In this section, first we review some important properties of the quantum Fisher information. Then we present our method for estimating it based on a few measurements.

A. Entanglement quantification with the quantum Fisher information

In Sec. I, we mentioned briefly, how quantum Fisher information connects quantum metrology and entanglement theory. In more detail, the bounds on the quantum Fisher information make it possible to detect metrologically useful entanglement. It has been shown that if

$$\mathcal{F}_{\mathrm{Q}}[\varrho, J_l] > (k-1)N, \tag{3}$$

where k is an integer, then the state has a better metrological performance than any state with at most $(k-1)$–particle entanglement, hence it possesses at least k-particle metrologically useful entanglement [3,13]. We can immediately see that a perfect N-particle GHZ state possesses metrologically useful N-particle entanglement. Based on the ideas above, it is possible to use the quantum Fisher information for entanglement detection [8,9,14].

Let us analyze the condition, Eq. (3), further. A simple calculation shows that for a tensor product of $(k-1)$–particle GHZ states the two sides of Eq. (3) are equal. Hence, a state is detected by Eq. (3) if it performs better than a state in which all particles are in GHZ states of $(k-1)$ particles. For instance, if in an experiment with 10 000 particles we detect five-particle metrologically useful entanglement, then the state is better metrologically than a tensor product of 2500 four-particle GHZ states. Based on this example, it is easy to see that the requirements for metrologically useful k-particle entanglement are much stricter than for general k-particle entanglement.

B. Estimation of a general function of ϱ

First, we review a method that can be used to find a lower bound on a convex function $g(\varrho)$ based on only a single operator expectation value $w = \langle W\rangle_\varrho = \mathrm{Tr}(W\varrho)$. Theory tells us that a tight lower bound can be obtained as [48–50]

$$g(\varrho) \geqslant \mathcal{B}(w) := \sup_r \left[rw - \hat{g}\,(rW)\right], \tag{4}$$

where $\hat{g}$ is the Legendre transform, in this context defined as

$$\hat{g}(W) = \sup_\varrho [\langle W\rangle_\varrho - g(\varrho)]. \tag{5}$$

Equation (4) has been applied to entanglement measures [49, 50]. Since those are defined as convex roofs over all possible decompositions of the density matrix, it is sufficient to carry out the optimization in Eq. (4) for pure states only. However, still an optimization over a general pure state, i.e., over many variables, has to be carried out, which is practical only for small systems.

Based on this method, we would like to estimate the quantum Fisher information, which is strongly connected to entanglement, while it also has a clear physical meaning in metrological applications. As the first step, we note that $\mathcal{F}_{\mathrm{Q}}[\varrho, J_l]$ can be obtained as a closed formula with ϱ and J_l [12], however, this is a highly nonlinear expression which would make the computation of the Legendre transform very demanding. A key point in our approach is using a very recent finding showing that $\mathcal{F}_{\mathrm{Q}}[\varrho, J_l]$ is the convex roof of $4(\Delta J_y)^2$ [51], and hence the optimization may be carried out only for pure states. With this, however, we are still facing an optimization problem that cannot be solved numerically for system sizes relevant for quantum metrology.

We now arrive at our first main result. We show that, for the quantum Fisher information, Eq. (5) can be rewritten as an optimization over a *single* real parameter.

Observation 1. The quantum Fisher information can be estimated using the Legendre transform

$$\hat{\mathcal{F}}_{\mathrm{Q}}(W) = \sup_\mu \left\{\lambda_{\max}\left[W - 4(J_l-\mu)^2\right]\right\}, \tag{6}$$

where $\lambda_{\max}(A)$ denotes the maximal eigenvalue of A.

Proof. Based on the previous discussion, we can rewrite the right-hand side of Eq. (5) for our case as

$$\hat{\mathcal{F}}_{\mathrm{Q}}(W) = \sup_\Psi [\langle W - 4J_l^2\rangle_\Psi + 4\,\langle J_l\rangle_\Psi^2]. \tag{7}$$

Equation (7) is quadratic in operator expectation values. It can be rewritten as an optimization linear in operator expectation values as

$$\hat{\mathcal{F}}_{\mathrm{Q}}(W) = \sup_{\Psi,\mu} [\langle W - 4J_l^2\rangle_\Psi + 8\mu\,\langle J_l\rangle_\Psi - 4\mu^2], \tag{8}$$

which can be reformulated as Eq. (6). At the extremum, the derivative with respect to μ must be 0, hence at the optimum $\mu = \langle J_l \rangle_\Psi$. This also means that we have to test μ values in the interval $-N/2 \leqslant \mu \leqslant N/2$ only. ■

In this paper, we use Eq. (6) to calculate the Legendre transform [52]. The full optimization problem to be solved consists of Eq. (6) and Eq. (4) with the substitutions $g(\varrho) = \mathcal{F}_\mathrm{Q}[\varrho, J_l]$ and $\hat{g}(W) = \hat{\mathcal{F}}_\mathrm{Q}(W)$.

We want to stress the generality of our findings beyond the linear interferometers covered in this article. For nonlinear interferometers [53–58], the phase θ must be estimated in a unitary dynamics $U = \exp(-iA\theta)$, where A is not a sum of single spin operators and, hence, is different from the angular momentum components. Using Observation 1, we can obtain lower bounds for the corresponding quantum Fisher information $\mathcal{F}_\mathrm{Q}[\varrho, A]$ if we replace J_l with A in Eq. (6).

C. Measuring several observables

We now consider the estimation of the quantum Fisher information based on several expectation values. We can generalize the method described by Eqs. (4) and (5) for measuring several observables W_k as [49]

$$\mathcal{F}_\mathrm{Q}[\varrho, J_y] \geqslant \sup_{r_1, r_2, \ldots, r_K} \left[\sum_{k=1}^{K} r_k w_k - \hat{\mathcal{F}}_\mathrm{Q} \left(\sum_{k=1}^{K} r_k W_k \right) \right], \qquad (9)$$

where $w_k = \langle W_k \rangle_\varrho$. As we can see, we now have several parameters r_k. Combining Eq. (9) with the Legendre transform (6), we arrive at the formula

$$\mathcal{F}_\mathrm{Q}[\varrho, J_l] \geqslant \sup_{\{r_k\}} \left[\sum_k r_k w_k - \sup_\mu \lambda_\mathrm{max}\,(M) \right], \qquad (10)$$

where

$$M = \sum_k r_k W_k - 4(J_l - \mu)^2. \qquad (11)$$

Since $\hat{\mathcal{F}}_\mathrm{Q}(\sum r_k W_k)$ is a convex function in r_k, in Eq. (10) the quantity to be maximized in r_k is concave [48]. Thus, we can easily find the maximum with the gradient method. If we do not find the optimal r_k, then we underestimate the real bound. Hence, we will still have a valid lower bound. This does not hold for the optimization over μ. The function to be optimized is not a convex function of μ, and not finding the optimal μ leads to overestimating the bound. Thus, great care must be taken when optimizing over μ.

III. EXAMPLES

In this section, we show how to use our method to estimate the quantum Fisher information based on fidelity measurements, as well as collective measurements.

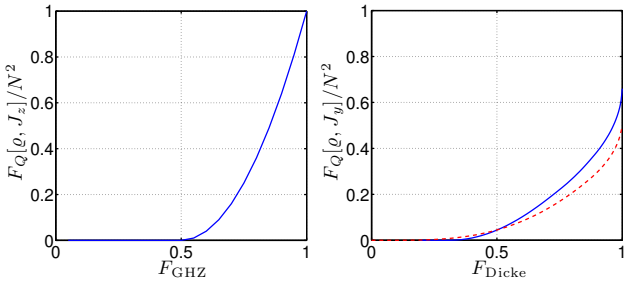

FIG. 1. (a) Fidelity vs. lower bound on the quantum Fisher information for GHZ states of N qubits. The quantum Fisher information is 0 if the fidelity is less than 0.5. (b) The same, but for Dicke states for with $N = 6$ (solid line) and $N = 40$ (dashed line).

A. Exploiting symmetries

When making calculations for quantum systems with an increasing number of qubits, we soon run into difficulties when computing the largest eigenvalue of Eq. (6). The reason is that for N qubits, we need to handle $2^N \times 2^N$ matrices, hence we are limited to systems of 10–15 qubits.

We can obtain bounds for much larger particle numbers, if we restrict ourselves to the symmetric subspace [59]. This approach can give optimal bounds for many systems, such as Bose-Einstein condensates of two-state atoms, which are in a symmetric multiparticle state. The bound computed for the symmetric subspace might not be correct for general states.

Finally, it is important to note that if the operator W is permutationally invariant and the eigenstate with the maximal eigenvalue of the matrix in Eq. (6) is nondegenerate, then the two bounds coincide, as shown in Appendix B.

B. Fidelity measurements

Let us examine the case where W is a projector onto a pure quantum state. First, we consider GHZ states [24]. We choose $W = |\mathrm{GHZ}\rangle\langle\mathrm{GHZ}|$, hence $\langle W \rangle$ is equal to F_GHZ, the fidelity with respect to the GHZ state. Based on knowing F_GHZ, we would like to estimate $\mathcal{F}_\mathrm{Q}[\varrho, J_z]$.

Observation 2. A sharp lower bound on the quantum Fisher information with the fidelity F_GHZ is given by

$$\frac{\mathcal{F}_\mathrm{Q}[\varrho, J_z]}{N^2} \geqslant \begin{cases} (1 - 2F_\mathrm{GHZ})^2 & \text{if } F_\mathrm{GHZ} > 1/2, \\ 0 & \text{if } F_\mathrm{GHZ} \leqslant 1/2. \end{cases} \qquad (12)$$

The proof is based on carrying out the optimization described above analytically and can be found in Appendix A [60]. Equation (12) is plotted in Fig. 1(a). Note that the bound on the quantum Fisher information normalized by N^2 in Eq. (12) is independent of the number of particles. Moreover, the bound is 0 for $F_\mathrm{GHZ} \leqslant 0.5$. This is consistent with the fact that for the product state $|111\ldots11\rangle$ we have $F_\mathrm{GHZ} = 1/2$, while $\mathcal{F}_\mathrm{Q}[\varrho, J_z] = 0$.

Next, let us consider symmetric Dicke states. An N-qubit

symmetric Dicke state is given as

$$|\mathrm{D}_N^{(m)}\rangle = \binom{N}{m}^{-\frac{1}{2}} \sum_k \mathcal{P}_k(|1\rangle^{\otimes m} \otimes |0\rangle^{\otimes(N-m)}), \qquad (13)$$

where the summation is over all the different permutations of the product state having m particles in the $|1\rangle$ state and $(N-m)$ particles in the $|0\rangle$ state.

From the point of view of metrology, we are interested mostly in the symmetric Dicke state for even N and $m = \frac{N}{2}$. This state is known to be highly entangled [61,62] and allows for Heisenberg limited interferometry [63]. In the following, we omit the superscript giving the number of $|1\rangle$'s and use the notation

$$|\mathrm{D}_N\rangle \equiv |\mathrm{D}_N^{(\frac{N}{2})}\rangle. \qquad (14)$$

The witness operator that can be used for noisy Dicke states is $W = |\mathrm{D}_N\rangle\langle\mathrm{D}_N|$, hence for the expectation value of the witness it is just the fidelity with respect to Dicke states, i.e., $\langle W\rangle = F_{\mathrm{Dicke}}$. In Fig. 1(b), we plot the results for Dicke states of various numbers of qubits. Now the normalized curve is not the same for all particle numbers. $F_{\mathrm{Dicke}} = 1$ corresponds to $\mathcal{F}_{\mathrm{Q}}[\varrho, J_y] = N(N+2)/2$. At this point note that for the examples presented above, the quantum Fisher information scales as $O(N^2)$ if the quantum state has been prepared perfectly, where $O(x)$ is the usual Landau notation used to describe the asymptotic behavior of a quantity for large x [13].

Note that estimating $\mathcal{F}_{\mathrm{Q}}[\varrho, J_y]$ based on F_{Dicke} was possible for 40 qubits in Fig. 1(b), since we carried out the calculations for the symmetric subspace. For our case, the witness operator W is permutationally invariant and it has a nondegenerate eigenstate corresponding to the maximal eigenvalue. Hence, based on the arguments in Sec. III A the bound is valid even for general, i.e., nonsymmetric states. Further calculations for the large-N limit are given in Appendix C.

C. Spin-squeezed states

In the case of spin-squeezing, the quantum state has a large spin in the z direction, but a decreased variance in the x direction. By measuring $\langle J_z\rangle$ and $(\Delta J_x)^2$ we can estimate the quantum Fisher information by Eq. (2). However, this formula does not necessarily give the best lower bound for all values of the collective observables. With our approach we can find the best bound.

To give a concrete example, we choose $W_1 = J_z$, $W_2 = J_x^2$, and $W_3 = J_x$ for the operators to be measured. We change w_1 and w_2 in some interval. We also require that $w_3 = 0$, since we assume that the mean spin points in the z direction [64]. This is reasonable since in most spin-squeezing experiments we know the direction of the mean spin.

Our results are shown in Fig. 2(a). We chose $N = 4$ particles since for small N the main features of the plot are clearly visible. The white areas correspond to nonphysical combinations of expectation values. States at the boundary can be obtained as ground states of $H_{\mathrm{bnd}}^{(\pm)}(\mu) = \pm J_x^2 - \mu J_z$ (Appendix D). In

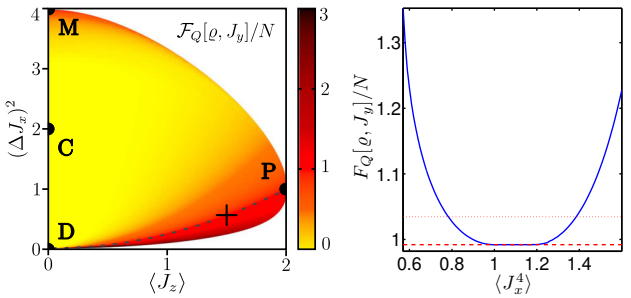

FIG. 2. (a) Optimal lower bound on the quantum Fisher information $\mathcal{F}_{\mathrm{Q}}[\varrho, J_y]$ based on collective measurements for spin-squeezing with $N = 4$. The mean spin points in the z direction. Below the dashed line we have $\mathcal{F}_{\mathrm{Q}}[\varrho, J_y]/N > 1$. For the description of points P, D, M, and C, see the text. (b) Lower bound on $\mathcal{F}_{\mathrm{Q}}[\varrho, J_y]$ for $\langle J_z\rangle = 1.5$ and $(\Delta J_x)^2 = 0.567$, as a function of $\langle J_x^4\rangle$. The corresponding point in (a) is denoted by a cross. Dashed horizontal line: Lower bound without constraining $\langle J_x^4\rangle$. Dotted horizontal line: Lower bound for states in the symmetric subspace. As shown, an additional constraint or assuming symmetry improves the bound.

Fig. 2(a), the state fully polarized in the z direction, an initial state for spin-squeezing experiments, corresponds to point P. The Dicke state, (14), corresponds to point D [65]. Spin-squeezing makes $(\Delta J_x)^2$ decrease, while $\langle J_z\rangle$ also decreases somewhat. Hence, at least for small squeezing, it corresponds to moving down from point P towards point D on the boundary of the plot, while the metrological usefulness is increasing. Below the dashed line $\mathcal{F}_{\mathrm{Q}}[\varrho, J_y]/N > 1$, hence the state possesses metrologically useful entanglement [3]. The equal mixture of $|000..00\rangle_x$ and $|111..11\rangle_x$ corresponds to point M, with $\mathcal{F}_{\mathrm{Q}}[\varrho_M, J_y] = N$. Finally, the completely mixed state corresponds to point C. It cannot be used for metrology, hence $\mathcal{F}_{\mathrm{Q}}[\varrho_C, J_y] = 0$.

We now compare the difference between our bound and Eq. (2). First, we consider the experimentally relevant region for which $(\Delta J_x)^2 < 1$. We find that for points that are away from the boundary at least by 0.01 on the vertical axis, the difference between the two bounds for $\mathcal{F}_{\mathrm{Q}}[\varrho, J_y]$ is smaller than 2×10^{-6}. For points at the boundary the difference is somewhat larger but still small; the relative difference is less than 2% (see Appendix E). Hence, Eq. (2) practically coincides with the optimal bound for $(\Delta J_x)^2 < 1$. We now consider the region in Fig. 2(a) for which $(\Delta J_x)^2 > 1$. The difference between the two bounds is now larger. It is largest at point M, for which the bound, (2), is 0. Hence, for measurement values corresponding to points close to M, our method could improve formula (2). It is important from the point of view of applying our method to spin-squeezing experiments that the bound, (2), can be substantially improved even for $(\Delta J_x)^2 < 1$, if we assume a bosonic symmetry or we measure an additional quantity, such as $\langle J_x^4\rangle$ as shown in Fig. 2(b).

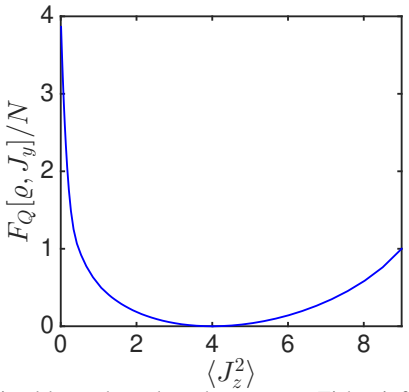

FIG. 3. Optimal lower bound on the quantum Fisher information for symmetric states close to Dicke states for $N = 6$.

D. Dicke states

In this section, we use our method to find lower bounds on the quantum Fisher information for states close to the Dicke states, (14), based on collective measurements. We discuss what operators have to be measured to estimate the metrological usefulness of the state. In Sec. IV B 2, we test our approach for a realistic system with very many particles.

In order to estimate the metrological usefulness of states created in such experiments, we choose to measure $W_1 = J_x^2$, $W_2 = J_y^2$, and $W_3 = J_z^2$ since the expectation values of these operators uniquely define the ideal Dicke state, and they have already been used for entanglement detection [39]. In cold gas experiments it is common that the state created is invariant under transformations of the type $U_z(\phi) = \exp(-iJ_z\phi)$ [21]. For such states $\langle J_x^2 \rangle = \langle J_y^2 \rangle$, which we also use as a constraint in our optimization.

Let us demonstrate how our method works in an example for small systems. Figure 3 shows the results for $N = 6$ particles for symmetric states for which

$$\langle J_x^2 + J_y^2 + J_z^2 \rangle = \tfrac{N}{2}\left(\tfrac{N}{2} + 1\right) =: \mathcal{J}_N. \qquad (15)$$

It can be seen that the lower bound on the quantum Fisher information is the largest for $\langle J_z^2 \rangle = 0$. It reaches the value corresponding to the ideal Dicke state, $N(N + 2)/2 = 24$. It is remarkable that the state is also useful for metrology if $\langle J_z^2 \rangle$ is very large. In this case $\langle J_x^2 \rangle$ and $\langle J_y^2 \rangle$ are smaller than $\langle J_z^2 \rangle$, and this cigar-shaped uncertainty ellipse can be used for metrology.

IV. CALCULATIONS FOR EXPERIMENTAL DATA

In this section, we use our method to find tight lower bounds on the quantum Fisher information based on experimental data. First, we determine the quantum Fisher information for several experiments in photons and trapped ions creating GHZ states and Dicke states, in which the fidelity has been measured [14,27,29–36,66–68]. Our method is much simpler than obtaining the quantum Fisher information from the density matrix [14] or estimating it from a metrological procedure [8]. Second, we obtain a bound on the quantum Fisher information for a spin-squeezing experiment with thousands of particles [7]. Based on numerical examples, we see that the bound, (2), is close to optimal even if the state is not completely polarized. Assuming symmetry or knowing additional expectation values can improve the bound (2). Finally, we also obtain the bound for the quantum Fisher information for a recent experiment with Dicke states [39]. The estimate of the precision based on considering the particular case where $\langle J_z^2 \rangle$ is measured for parameter estimation [21] is close to the optimal bound computed by our method.

A. Few-particle experiments

We now estimate the quantum Fisher information based on the fidelity with respect to Dicke states and GHZ states for several experiments with photons and trapped cold ions, following the ideas in Sec. III B.

Our results are summarized in Table I. For the experiments aiming to create Dicke states, the lower bound on $\mathcal{F}_Q[\varrho, J_y]/N^2$ is shown, while for the experiments with GHZ states we estimate $\mathcal{F}_Q[\varrho, J_z]/N^2$. In [29,36] several logical qubits are stored in a particle, but in the rest of the experiments only a single qubit. Reference [32] describes experiments with 2–14 ions, of which we analyze the 8-qubit and 10-qubit GHZ sates. Finally, for the experiment in Ref. [66] we used the fidelity estimated using reasonable assumptions discussed in that paper, while the worst-case fidelity is lower.

We can compare our estimate to the quantum Fisher information of the state for the experiment in Ref. [14], where the quantum Fisher information for the density matrix was obtained as $\mathcal{F}_Q[\varrho, J_y]/N^2 = (10.326 \pm 0.093)/N^2 = (0.6454 \pm 0.0058)$. As reported in Table I, this value is larger than the one we obtained, however, it was calculated by knowing the entire density matrix, while our bound is obtained from the fidelity alone.

B. Many-particle experiments

So far, we have studied the quantum state of few particles. Next we turn to experiments with very many particles, in which a fidelity measurement is not practical. In such systems, the quantum Fisher information must be estimated based on collective measurements.

By far the most relevant quantum states in many-particle experiments are spin-squeezed states, which can be used to increase the precision in magnetometry and in atomic clocks [42]. We also discuss Dicke states, since they have been realized in several experiments [8,39–41]. Dicke states realized in cold gases are the focus of our attention, since they can be used for high-precision interferometry [63].

1. *Spin-squeezing experiment*

We now use our method to find lower bounds on the quantum Fisher information for a recent spin-squeezing experiment in cold gases, following the ideas in Sec. III C. With it

Physical system	Targeted quantum state	Fidelity	$\frac{\mathcal{F}_Q}{N^2} \geqslant$	Ref. No.
Photons	$\|D_4\rangle$	0.844 ± 0.008	0.358 ± 0.011	[33]
		0.78 ± 0.005	0.281 ± 0.059	[36]
		0.8872 ± 0.0055	0.420 ± 0.009	[14]
		0.873 ± 0.005	0.351 ± 0.006	[69]
	$\|D_6\rangle$	0.654 ± 0.024	0.141 ± 0.019	[34]
		0.56 ± 0.02	0.0761 ± 0.012	[35]
Photons	$\|GHZ_4\rangle$	0.840 ± 0.007	0.462 ± 0.019	[27]
	$\|GHZ_5\rangle$	0.68	0.130	[66]
	$\|GHZ_8\rangle$	0.59 ± 0.02	0.032 ± 0.016	[67]
	$\|GHZ_8\rangle$	0.776 ± 0.006	0.305 ± 0.013	[29]
	$\|GHZ_{10}\rangle$	0.561 ± 0.019	0.015 ± 0.011	[29]
Trapped ions	$\|GHZ_3\rangle$	0.89 ± 0.03	0.608 ± 0.097	[30]
	$\|GHZ_4\rangle$	0.57 ± 0.02	0.020 ± 0.013	[31]
	$\|GHZ_6\rangle$	$\geqslant 0.509 \pm 0.004$	0.0003 ± 0.0003	[68]
	$\|GHZ_8\rangle$	0.817 ± 0.004	0.402 ± 0.010	[32]
	$\|GHZ_{10}\rangle$	0.626 ± 0.006	0.064 ± 0.006	[32]

TABLE I. Fidelity values and the corresponding bounds on the quantum Fisher information for several experiments with Dicke states and GHZ states. For experiments targeting Dicke states, bounds on $\mathcal{F}_Q[\varrho, J_y]/N^2$ are listed. The maximal value of this quantity is 0.75 and 0.67 for $N = 4$ and $N = 6$, respectively. For experiments with GHZ states, bounds on $\mathcal{F}_Q[\varrho, J_z]/N^2$ are shown, and, in this case, the maximal value is 1.

we show that the lower bound given in Eq. (2) is close to optimal in this case. We also demonstrate that we can carry out calculations for real systems.

In particular, for our calculations we use the data from the spin-squeezing experiment in Ref. [7]. The particle number is $N = 2300$, and the spin-squeezing parameter, defined as

$$\xi_s^2 = N\frac{(\Delta J_x)^2}{\langle J_z\rangle^2}, \tag{16}$$

has the value $\xi_s^2 = -8.2\text{dB} = 10^{-8.2/10} = 0.1514$. The spin length $\langle J_z\rangle$ has been close to maximal. In our calculations, we choose

$$\langle J_z\rangle = \alpha\tfrac{N}{2}, \tag{17}$$

where we test our method with various values for α. For each α, we use a value for $(\Delta J_x)^2$ such that we get the experimentally obtained spin-squeezing parameter, (16). Moreover, we assume that $\langle J_x\rangle = 0$, as the $z$direction was the direction of the mean spin in the experiment. Based on Eq. (2), the bound for the quantum Fisher information is obtained as

$$\frac{\mathcal{F}_Q[\varrho_N, J_y]}{N} \geqslant \frac{1}{\xi_s^2} = 6.605. \tag{18}$$

where ϱ_N is the state of the system in the sxperiment satisfying Eqs. (16) and (17).

We carry out the calculations for symmetric states. This way we obtain a lower bound on the quantum Fisher information, which we denote $\mathcal{B}_{\text{sym}}(\langle J_z\rangle_{\varrho_N}, \langle J_x^2\rangle_{\varrho_N})$. As mentioned in Sec. III B, we could obtain a bound for the quantum Fisher information that is valid even for general, not necessarily symmetric states if the matrix in Eq. (6) had nondegenerate eigenvalues. This is not the case for the spin-squeezing problem. However, we still know that the bound obtained with our calculations restricted to the symmetric subspace cannot be smaller than the optimal bound for general states, $\mathcal{B}(\langle J_z\rangle_{\varrho_N}, \langle J_x^2\rangle_{\varrho_N})$. On the other hand, we know that bound (2) cannot be larger than the optimal bound for general states. These relations can be summarized as

$$\begin{aligned}\mathcal{B}_{\text{sym}}(\langle J_z\rangle_{\varrho_{N'}}, \langle J_x^2\rangle_{\varrho_N}) &\geq \mathcal{B}(\langle J_z\rangle_{\varrho_N}, \langle J_x^2\rangle_{\varrho_N}) \\ &\geq \frac{\langle J_z\rangle_{\varrho_N}^2}{(\Delta J_x)_{\varrho_N}^2},\end{aligned} \tag{19}$$

where on the right-hand side of Eq. (19) there is just the bound in Eq. (2).

Our calculations lead to

$$\mathcal{B}_{\text{sym}}(\langle J_z\rangle_{\varrho_N}, \langle J_x^2\rangle_{\varrho_N}) = 6.605 \tag{20}$$

for almost completely polarized spin-squeezed states with $\alpha = 0.85$, as well as for not fully polarized ones with $\alpha = 0.5$. That is, based on numerics, the left-hand side and the right-hand side of Eq. (19) seem to be equal. This implies that the lower bound, (2), for the quantum Fisher information is optimal for the system. In Appendix G 1, the details of the calculations are given, and we also show examples where we can improve the bound, (2), with our approach, if symmetry is assumed.

2. *Experiment creating Dicke states*

We now present our calculations for an experiment aimed at creating Dicke states in cold gases [39]. The basic ideas are similar to the ones explained in Sec. III D for small systems. The experimental data are $N = 7900, \langle J_z^2\rangle_N = 112 \pm 31, \langle J_x^2\rangle_N = \langle J_y^2\rangle_N = 6 \times 10^6 \pm 0.6 \times 10^6$ [21]. Applying some simple transformations, we can obtain a lower bound on $\mathcal{F}_Q[\varrho_n, J_y]$ for this very large number of particles, even for general, nonsymmetric systems.

For many particles we can make calculations directly only in the symmetric subspace. Thus, we transform the collective quantities such that they are compatible with symmetric states, i.e., they have to fulfill

$$\langle J_x^2\rangle_{\text{sym},N} + \langle J_y^2\rangle_{\text{sym},N} + \langle J_z^2\rangle_{\text{sym},N} = \mathcal{J}_N, \tag{21}$$

where $\mathcal{J}_N$ is given in Eq. (15). This can be done by multiplying all the second moments by the same number as

$$\langle J_l^2\rangle_{\text{sym},N} = \gamma\langle J_l^2\rangle_N, \tag{22}$$

where $l = x, y, z$, and we defined the coefficient

$$\gamma = \frac{\mathcal{J}_N}{\langle J_x^2 + J_y^2 + J_z^2\rangle_N}. \tag{23}$$

For a symmetric state, $\gamma = 1$. In practice, $\gamma \leq 1$, but close to 1. From this we can see that there are no symmetric states that are compatible with the experimentally observed expectation values. This is the reason why we needed to apply the transformation (22).

Based on the ideas of Sec. III D, we calculate the lower bound on the quantum Fisher information for symmetric systems, which we denote $\mathcal{B}_{\mathrm{sym},N}(\langle J_x^2\rangle_{\mathrm{sym},N}, \langle J_y^2\rangle_{\mathrm{sym},N}, \langle J_z^2\rangle_{\mathrm{sym},N})$.

Finally, to obtain the results for the original, non-symmetric case, we need the following observation.

Observation 3. For the bounds for original system and symmetric system, respectively, the inequality

$$\mathcal{B}_N \leqslant \tfrac{1}{\gamma}\mathcal{B}_{\mathrm{sym},N} \tag{24}$$

holds, where γ is given in Eq. (23). Here, for brevity we have omitted the arguments of $\mathcal{B}_N$ and $\mathcal{B}_{\mathrm{sym},N}$.

Proof. For our proof we need to know that for an N-qubit singlet state $\varrho_{\mathrm{singlet},N}$ the relations $\langle J_l^2\rangle_{\varrho_{\mathrm{singlet},N}} = 0$ hold for $l = x, z, y$. Due to the well-known inequality for the quantum Fisher information $\mathcal{F}_{\mathrm{Q}}[\varrho_{\mathrm{singlet},N}, J_l] \leqslant 4(\Delta J_l)^2$, we have $\mathcal{F}_{\mathrm{Q}}[\varrho_{\mathrm{singlet},N}, J_y] = 0$. In other words, the singlet is not useful for metrology with linear interferometers. Let us now consider the mixture

$$\tilde{\varrho}_N = \left(1 - \tfrac{1}{\gamma}\right)\varrho_{\mathrm{singlet},N} + \tfrac{1}{\gamma}\varrho_{\mathrm{sym},N}, \tag{25}$$

where $\varrho_{\mathrm{sym},N}$ is a symmetric state having the second moments $\langle J_l^2\rangle_{\mathrm{sym},N}$. We can easily see from Eq. (22) that for the state $\tilde{\varrho}_N$, we have $\langle J_l^2\rangle_{\tilde{\varrho}_N} = \langle J_l^2\rangle_N$. In other words, $\tilde{\varrho}_N$ has the same values for the second moments that have been measured experimentally.

We can relate the bound for general systems to the quantum Fisher information for symmetric systems as

$$\mathcal{B}_N \leqslant \mathcal{F}_{\mathrm{Q}}[\tilde{\varrho}_N, J_y] = \tfrac{1}{\gamma}\mathcal{F}_{\mathrm{Q}}[\varrho_{\mathrm{sym},N}, J_y]. \tag{26}$$

The inequality in Eq. (26) holds because our bound cannot be larger than the quantum Fisher information of state $\tilde{\varrho}_N$ having the expectation values $\langle J_l^2\rangle_N$. The equality in Eq. (26) is due to the fact that both $\tilde{\varrho}_N$ and J_y can be written as a block-diagonal matrix of blocks corresponding to different eigenvalues of $J_x^2 + J_y^2 + J_z^2$. Moreover, $\varrho_{\mathrm{singlet},N}$ and $\varrho_{\mathrm{sym},N}$ have nonzero elements in different blocks. Then we can use the general formula [70]

$$\mathcal{F}_{\mathrm{Q}}[\bigoplus_k p_k\varrho_k, \bigoplus_k A_k] = \sum_k p_k \mathcal{F}_{\mathrm{Q}}[\varrho_k, A_k], \tag{27}$$

where ϱ_k are density matrices with a unit trace and $\sum_k p_k = 1$. ■

Extensive numerics for small systems show Eq. (24) is very close to an equality, hence it can be used as a basis for making calculations for nonsymmetric states. In this way, we arrive at the bound for the experimental system,

$$\frac{\mathcal{B}_N}{N} \approx 2.94. \tag{28}$$

The "≈" sign is used referring to the fact that we assume that the inequality in Eq. (26) is close to being saturated. The details of the calculations are given in Appendix G 2.

It is instructive to compare the value, (28), to the one obtained in Ref. [21], where the metrological usefulness has been estimated based on the second and fourth moments of the collective angular momentum components, and assuming that $\langle J_z^2\rangle$ is used for parameter estimation. The result implies that $\mathcal{F}_{\mathrm{Q}}[\varrho_N, J_y]/N \geqslant 3.3$. Our result in Eq. (28) is somewhat smaller, as we did not use the knowledge of the fourth moment, only the second moments. The closeness of the two results is a strong argument for the correctness of our calculations.

V. SCALING OF $\mathcal{F}_{\mathrm{Q}}[\varrho, J_l]$ WITH N.

Recent important works examine the scaling of the quantum Fisher information with the particle number for metrology under the presence of decoherence [71]. They consider the quantum Fisher information defined for nonunitary, noisy evolution. They find that for small N it is close to the value obtained considering coherent dynamics. Hence, even the Heisenberg scaling, $O(N^2)$, can be reached. However, if N is sufficiently large, then, due to the decoherence during the parameter estimation, the quantum Fisher information scales as $O(N)$.

In contrast, we do not consider the usefulness of a quantum state in some noisy metrological process, but we estimate the quantum Fisher information assuming a perfect unitary dynamics. Hence, the quantum Fisher information can be smaller than what we expect ideally only due to imperfect state preparation [72]. We can even find simple conditions for the state preparation that lead to a Heisenberg scaling. Based on Eq. (12), if one could realize quantum states ϱ_N such that $F_{\mathrm{GHZ}}(\varrho_N) \geqslant 0.5 + \epsilon$ for $N \to \infty$ for some $\epsilon > 0$, then we would reach $\mathcal{F}_{\mathrm{Q}}[\varrho_N, J_z] = O(N^2)$. Strong numerical evidence suggests that a similar relation holds for the fidelity F_{Dicke} and $\mathcal{F}_{\mathrm{Q}}[\varrho_N, J_y]$, but with a smaller threshold value for F_{Dicke} (see Appendix C). From another point of view, our method can estimate $\mathcal{F}_{\mathrm{Q}}[\varrho, J_z]$ for large particle numbers, while a direct measurement of the metrological sensitivity considerably underestimates it.

VI. CONCLUSIONS

We have reported a general method to estimate the metrological usefulness of quantum states based on a few measurements, such as measurements of the fidelity or some collective observables. We tested our approach on extensive experimental data from photonic and cold-gas experiments and demonstrated that it works even for the case of thousands particles [73]. In the future, it would be interesting to use our method to test the optimality of various recent formulas giving a lower bound on the quantum Fisher information [19,22]. Another important question is how to improve the lower bounds on the quantum Fisher information in various experiments by using the knowledge of further operator expectation values.

ACKNOWLEDGMENTS

We thank S. Altenburg, F. Fröwis, R. Demkowicz-Dobrzański, P. Hyllus, J. Kołodińsky, O. Marty, M.W. Mitchell, M. Modugno, L. Pezze, L. Santos, A. Smerzi, I. Urizar-Lanz, and G. Vitagliano for stimulating discussions. We thank the organizers, M. Oberthaler and P. Treutlein, and the participants of the 589. Heraeus-Seminar on "Continuous Variable Entanglement in Atomic Systems" for scientific exchange. We acknowledge the support of the EU (ERC Starting Grant 258647/GEDENTQOPT, ERC Consolidator Grant 683107/TempoQ, CHIST-ERA QUASAR, Marie Curie CIG 293993/ENFOQI, COST Action CA15220), the Spanish Ministry of Economy, Industry and Competitiveness and the European Regional Development Fund FEDER through Grant No. FIS2015-67161-P (MINECO/FEDER), the Basque Government (Project No. IT986-16), the OTKA (Contract No. K83858), the UPV/EHU program UFI 11/55, the FQXi Fund (Grant No. FQXi-RFP-1608), and the DFG (Forschungsstipendium KL 2726/2-1, Project "Precise and efficient characterization of multi-qubit quantum states and gates with trapped ions").

Appendix A: Proof of Observation 2

In this section, using Eqs. (4) and (6), we obtain analytically a tight lower bound on the quantum Fisher information based on the fidelity with respect to the GHZ state, F_{GHZ}.

The calculation that we have to carry out is computing the bound,

$$\mathcal{B}(F_{\mathrm{GHZ}}) = \sup_r \{ r F_{\mathrm{GHZ}} - \sup_\mu [\lambda_{\max}(M_{\mathrm{GHZ}})] \}, \tag{A1}$$

where

$$M_{\mathrm{GHZ}} = r|\mathrm{GHZ}\rangle\langle\mathrm{GHZ}| - 4(J_z - \mu)^2 \mathbb{1}. \tag{A2}$$

We make our calculations in the J_z basis, which is defined with the 2^N basis vectors $b_0 = |00\ldots000\rangle$, $b_1 = |00\ldots001\rangle$, $b_2 = |00\ldots010\rangle$, ..., $b_{(2^N-2)} = |11\ldots110\rangle$, and $b_{(2^N-1)} = |11\ldots111\rangle$. It is easy to see that the matrix, (A2), is almost diagonal in the J_z basis. To be more specific, it can then be written as

$$M_{\mathrm{GHZ}} = M_{2\times 2} \oplus D, \tag{A3}$$

where $\oplus$ denotes the direct sum and

$$M_{2\times 2} = \begin{pmatrix} \frac{r}{2} - 4(\frac{N}{2} - \mu)^2 & \frac{r}{2} \\ \frac{r}{2} & \frac{r}{2} - 4(\frac{N}{2} + \mu)^2 \end{pmatrix} \tag{A4}$$

is given in the $\{b_0, b_{(2^N-1)}\}$ basis, while D is a diagonal matrix given in the basis of the rest of the b_k vectors as

$$D_k = -4(\langle b_k|J_z|b_k\rangle - \mu)^2 \tag{A5}$$

for $k = 1, 2, \ldots, (2^N - 2)$. This means that M_{GHZ} can be diagonalized as

$$\mathrm{diag}[\lambda_+, \lambda_-, D_1, D_2, ..., D_{(2^N-2)}], \tag{A6}$$

where the two eigenvalues of $M_{2\times 2}$ are

$$\lambda_\pm = \frac{r}{2} - N^2 - 4\mu^2 \pm \sqrt{16\mu^2 N^2 + \frac{r^2}{4}}. \tag{A7}$$

Next, we show a way that can simplify our calculations considerably. As indicated in Eq. (A1), we have to look for the maximal eigenvalue of M_{GHZ} and then optimize it over μ. We exchange the order of the two steps, that is, we look for the maximum of each eigenvalue over μ and then find the maximal one. Clearly, based on Eq. (A5) we obtain

$$\sup_\mu D_k = 0, \tag{A8}$$

since we can always choose a value for μ that makes D_k 0, while it is clear that it cannot be positive. Thus, the maximal eigenvalue, maximized also over μ, can be obtained as

$$\begin{aligned} \sup_\mu [\lambda_{\max}(M_{\mathrm{GHZ}})] &:= \max[0, \sup_\mu(\lambda_+)] \\ &= \begin{cases} 0, & \text{if } r < 0, \\ \frac{r}{2} + \frac{r^2}{16N^2}, & \text{if } 0 \leqslant r \leqslant 4N^2, \\ -N^2 + r, & \text{if } r > 4N^2, \end{cases} \end{aligned} \tag{A9}$$

where we did not have to look for the maximum of λ_- over μ since clearly $\lambda_+ \geq \lambda_-$. Finally, we have to substitute Eq. (A9) into Eq. (A1), and carry out the optimization over r, considering $F_{\mathrm{GHZ}} \in [0, 1]$. This way we arrive at Eq. (12). ■

Appendix B: Calculations in the symmetric subspace

In this section, we prove an important fact, which can be used to simplify our calculations.

Observation 4. If a permutationally invariant N-qubit Hamiltonian H has a nondegenerate ground state, then the ground state is in the symmetric subspace if $N > 2$. An analogous statement holds for the maximal eigenvalue.

Proof. This is a well-known fact; we give a proof only for completeness. Let $|\Psi\rangle$ denote the nondegenerate ground state. This is at the same time the $T = 0$ thermal ground state, hence it must be a permutationally invariant pure state. For such states $S_{kl}|\Psi\rangle\langle\Psi|S_{kl} = |\Psi\rangle\langle\Psi|$, where S_{kl} is the swap operator exchanging qubits k and l. Based on this, it follows that $S_{kl}|\Psi\rangle = c_{kl}|\Psi\rangle$, and $c_{kl} \in \{-1, +1\}$. There are three possible cases to consider.

(i) All $c_{kl} = +1$. In this case, for all permutation operators Π_j we have

$$\Pi_j|\Psi\rangle = |\Psi\rangle, \tag{B1}$$

since any permutation operator Π_j can be constructed as $\Pi_j = S_{k_1 l_1} S_{k_2 l_2} S_{k_3 l_3} \ldots S_{k_m l_m}$, where $m \geqslant 1$. Equation (B1) means that the state $|\Psi\rangle$ is symmetric.

(ii) All $c_{kl} = -1$. This means that the state is antisymmetric, however, such a state exists only for $N = 2$ qubits.

(iii) Not all c_{kl} are identical to each other. In this case, there must be k_+, l_+, k_-, l_- such that

$$S_{k_+l_+}|\Psi\rangle = +|\Psi\rangle,$$
$$S_{k_-l_-}|\Psi\rangle = -|\Psi\rangle. \tag{B2}$$

Let us assume that k_+, l_+, k_- and l_- are indices different from each other. In this case, $|\Psi'\rangle = S_{k_+k_-}S_{l_+l_-}|\Psi\rangle$ is another ground state of Hamiltonian H such that

$$S_{k_+l_+}|\Psi'\rangle = -|\Psi'\rangle,$$
$$S_{k_-l_-}|\Psi'\rangle = +|\Psi'\rangle. \tag{B3}$$

Comparing Eq. (B2) and Eq. (B3) we can conclude that $|\Psi'\rangle \neq |\Psi\rangle$, while due to the permutational invariance of H we must have $\langle\Psi|H|\Psi\rangle = \langle\Psi'|H|\Psi'\rangle$. Thus, $|\Psi\rangle$ is not a nongenerate ground state. Let us now see what happens if k_+, l_+, k_-, and l_- are not all different from each other. The proof works in an analogous way for the only nontrivial case, $k_+ = k_-$, when $S_{k_+k_-} = \mathbb{1}$.

Hence, if $N > 2$, then only (i) is possible and $|\Psi\rangle$ must be symmetric. ∎

Appendix C: Estimating the quantum Fisher information based on the fidelity with respect to Dicke states

In this section, we show that if the fidelity with respect to the Dicke state, (C3), is larger than a bound, then $\mathcal{F}_Q[\varrho, J_y] > 0$. Moreover, Fig. 1(b) shows that the lower bound on $\mathcal{F}_Q[\varrho, J_y]$ as a function of the fidelity F_{Dicke} normalized by N^2 is not the same curve for all N. In this section, we demonstrate with numerical evidence that the lower bound normalized by N^2 collapses to a nontrivial curve for large N.

As the first step, let us consider the state completely polarized in the y direction,

$$|\Psi_y\rangle = |1\rangle_y^{\otimes N}. \tag{C1}$$

State (C1) does not change under a rotation around the y axis, hence $\mathcal{F}_Q[\varrho, J_y] = 0$. Its fidelity with respect to the Dicke state, (14), is

$$F_{\text{Dicke}}(|\Psi_y\rangle) = \frac{1}{2^N}\binom{N}{N/2} \approx \sqrt{\frac{2}{\pi N}}. \tag{C2}$$

From the convexity of the bound on the quantum Fisher information in F_{Dicke}, it immediately follows that for F_{Dicke} smaller than Eq. (C2) the optimal lower bound on $\mathcal{F}_Q[\varrho, J_y]$ will give 0. For the examples shown in Fig. 1(b), this fidelity limit is 0.3125 and 0.1254 for $N = 6$ and $N = 40$, respectively.

Next, we examine what happens if the fidelity is larger than Eq. (C2).

Observation 5. If for some state ϱ we have

$$F_{\text{Dicke}}(\varrho) \equiv \text{Tr}(|D_N\rangle\langle D_N|\varrho) > F_{\text{Dicke}}(|\Psi_y\rangle), \tag{C3}$$

then $\mathcal{F}_Q[\varrho, J_y] > 0$. [The state $|D_N\rangle$ is given in Eq. (14), and $F_{\text{Dicke}}(|\Psi_y\rangle)$ is given in Eq. (C2).]

Proof. We have to determine the maximum for $F_{\text{Dicke}}(\varrho)$ for states that are not useful for metrology, i.e., $\mathcal{F}_Q[\varrho, J_y] = 0$. We know that $\mathcal{F}_Q[\varrho, J_y]$ is the convex roof of $4(\Delta J_y)^2$ [51]. Hence, if we have a mixed state for which $\mathcal{F}_Q[\varrho, J_y] = 0$, then it can always be decomposed into the mixture of pure states $|\Psi_k\rangle$ for which $\mathcal{F}_Q[\Psi_k, J_y] = 0$. As a consequence, the extremal states of the set of states for which $\mathcal{F}_Q[\varrho, J_y] = 0$ are pure states, and we can restrict our search for pure states. The optimization problem we have to solve can be given as

$$\max_{|\Psi\rangle:\mathcal{F}_Q[|\Psi\rangle,J_y]=0} |\langle\Psi|D_N\rangle|^2. \tag{C4}$$

Pure states $|\Psi\rangle$ for which $\mathcal{F}_Q[|\Psi\rangle, J_y] = 0$ must be invariant under $U_\phi = \exp(-iJ_y\phi)$ for any ϕ. Such states are the eigenstates of J_y. In order to maximize the overlap with the symmetric Dicke state $|D_N\rangle$ in Eq. (C4), we have to look for symmetric eigenstates of J_y. These are the symmetric Dicke states in the y basis $|\text{D}_N^{(m)}\rangle_y$. [See Eq. (13).] In order to proceed, we have to write down $|\text{D}_N^{(m)}\rangle_y$ in the z basis. Then, using the formula

$$\sum_k \binom{n}{k}\binom{n}{q-k}(-1)^k = \begin{cases}\binom{n}{q/2}(-1)^{q/2} & \text{for even } N,\\ 0 & \text{for odd } N,\end{cases} \tag{C5}$$

one finds that the squared overlap is given by

$$|\langle \text{D}_N^{(N/2)}|\text{D}_N^{(m)}\rangle_y|^2 = \begin{cases}\frac{\binom{N/2}{m/2}^2\binom{N}{N/2}}{2^N\binom{N}{m}} & \text{for even } N,\\ 0 & \text{for odd } N,\end{cases} \tag{C6}$$

which is maximal for $m = 0$. ∎

Next, we examine the behavior of our lower bound on $\mathcal{F}_Q[\varrho, J_y]$ based on F_{Dicke} for large N. In Fig. 4, the calculations up to $N = 500$ present strong evidence that for the fidelity values $F_{\text{Dicke}} = 0.2$, 0.5, and 0.8 the lower bound on the quantum Fisher information $\mathcal{F}_Q[\varrho, J_y]$ has an $O(N^2)$ scaling. If this is correct, then reaching a fidelity larger than a certain bound for large N would imply Heisenberg scaling for the bound on the quantum Fisher information. Note that it is difficult to present similar numerical evidence for small values of F_{Dicke}, since in that case the bound for the quantum Fisher information is nonzero only for large N due to Observation 5.

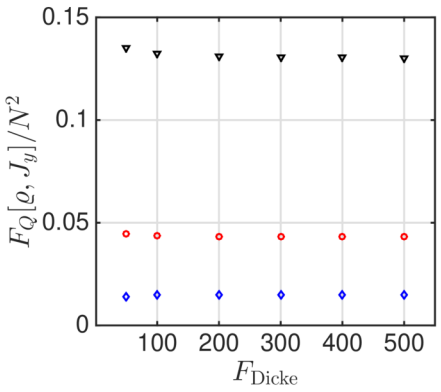

FIG. 4. (Color online) The lower bound on $\mathcal{F}_Q[\varrho, J_y]$, denoted $\mathcal{B}(F_{\text{Dicke}})$, for various particle numbers, for $F_{\text{Dicke}} = 0.2$ (diamonds), 0.5 (circles), and 0.7 (triangles). For $F_{\text{Dicke}} = 0.2$, 10 the calculated values times 10are shown, for better visibility.

Appendix D: Boundary of physical states in the $(\langle J_z\rangle, \langle J_x^2\rangle)$-plane.

In this section, we discuss how to find the physical region in the $(\langle J_z\rangle, \langle J_x^2\rangle)$ plane, which was used to prepare Fig. 2(a).

The physical region must be a convex one, since the set of quantum states is convex and the coordinates depend linearly on the density matrix. Hence, we look for the minimal or maximal $\langle J_x^2\rangle$ for a given $\langle J_z\rangle$ by looking for the ground states of the Hamiltonians [59],

$$H_{\rm bnd}^{(\pm)}(\mu) = \pm J_x^2 - \mu J_z. \tag{D1}$$

The points of the boundary can be obtained by evaluating $\langle J_x^2\rangle$ and $\langle J_z\rangle$ for the ground states of Eq. (D1). In particular, the ground states of $H_{\rm bnd}^{(+)}$ correspond to boundary points below point P corresponding to the fully polarized state in Fig. 2(a). The ground states of $H_{\rm bnd}^{(-)}$ correspond to boundary points above point P.

For $0 < \mu < \infty$, the Hamiltonian $H_{\rm bnd}^{(+)}$ has nondegenerate ground states with $\langle J_x\rangle = 0$. For even N, the ground state of $H_{\rm bnd}^{(+)}$ minimizes both $\langle J_x^2\rangle$ and $(\Delta J_x)^2$ for a given $\langle J_z\rangle$. For odd N, this is not the case for small μ [59].

On the other hand, $H_{\rm bnd}^{(-)}(\mu)$ has doubly degenerate ground states. For the ground-state subspace, we have $\langle J_x\rangle = 0$. Hence, for both even N and odd N, the ground state of $H_{\rm bnd}^{(-)}$ maximizes both $\langle J_x^2\rangle$ and $(\Delta J_x)^2$ for a given $\langle J_z\rangle$.

Appendix E: Quantum Fisher information for states at the boundary of the physical region in the $(\langle J_z\rangle, \langle J_x^2\rangle)$-plane

We show that, for even N, the ground states of $H_{\rm bnd}^{(+)}(\mu)$ defined in Eq. (D1) are close to saturating Eq. (2). As a consequence, for the boundary of the physical region in the $(\langle J_z\rangle, \langle J_x^2\rangle)$ plane below point P in Fig. 2, bound (2) is close to the optimal lower bound.

We carry out numerical calculations. Let us denote by $|\Psi_\mu\rangle$ the ground state of $H_{\rm bnd}^{(+)}(\mu)$. Moreover, let us denote the relevant expectation values for this state $\langle J_x^2\rangle_\mu$ and $\langle J_z\rangle_\mu$. We know that under the constraint $\langle J_z\rangle = \langle J_z\rangle_\mu$, the state $|\Psi_\mu\rangle$ minimizes $\langle J_x^2\rangle$. For $H_{\rm bnd}^{(+)}(\mu)$, the ground state is unique for $0 < \mu < \infty$. Thus, there is no other quantum state with the same value for $\langle J_z\rangle$ and $\langle J_x^2\rangle$.

There is a very important consequence of the uniqueness of the ground state of $H_{\rm bnd}^{(+)}(\mu)$ for the lower bound on the quantum Fisher information. We have discussed that our method based on the Legendre transform gives the optimal lower bound for the quantum Fisher information

$$\mathcal{F}_{\rm Q}[\varrho, J_y] \geq \mathcal{B}(\langle J_z\rangle_\varrho, \langle J_x^2\rangle_\varrho), \tag{E1}$$

where $\mathcal{B}$ denotes the optimal bound. Since there is a unique state corresponding to the boundary points, we must have for the states at the boundary

$$\mathcal{B}(\langle J_z\rangle_\mu, \langle J_x^2\rangle_\mu) = \mathcal{F}_{\rm Q}[\Psi_\mu, J_y]. \tag{E2}$$

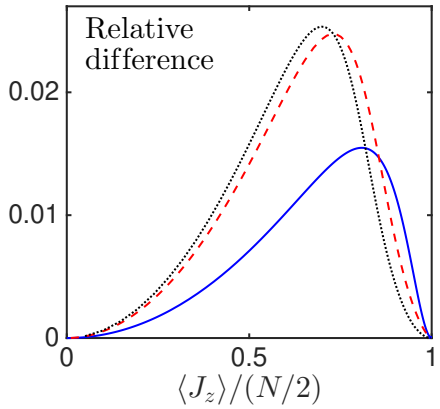

FIG. 5. Behavior of the bound in Eq. (2) for points at the boundary of physical states. The relative difference with respect to the optimal lower bound is plotted for $N = 4$ (solid line), $N = 20$ (dashed line), and $N = 1000$ (dotted line).

Thus, for the boundary points we do not have to compute the lower bound with the method based on the Legendre transform. We can just calculate the right-hand side of Eq. (E2) instead. Since we have a pure state, the quantum Fisher information is proportional to the variance $\mathcal{F}_{\rm Q}[\varrho, J_y] = 4(\Delta J_y)^2$ [11].

We add that, for even N, state $|\Psi_\mu\rangle$ not only minimizes $\langle J_x^2\rangle$ for a given value of $\langle J_z\rangle$, but also minimizes $(\Delta J_x)^2$, and this state is unique [59]. Hence, for the points on the boundary of physical states in the $(\langle J_z\rangle, (\Delta J_x)^2)$-space we have

$$\mathcal{B}(\langle J_z\rangle_\mu, (\Delta J_x)^2_\mu) = \mathcal{F}_{\rm Q}[\Psi_\mu, J_y], \tag{E3}$$

where $\mathcal{B}$ denotes the optimal bound if the expectation value $\langle J_z\rangle$ and the variance $(\Delta J_x)^2$ are constrained. Note that bound (E3) is monotonous in $(\Delta J_x)^2_\mu$ [59].

In Fig. 5, we plot the relative difference between the quantum Fisher information of $|\Psi_\mu\rangle$ and the lower bound (2) given as

$$\frac{\mathcal{F}_{\rm Q}[\Psi_\mu, J_y] - \frac{\langle J_z\rangle_\mu^2}{(\Delta J_x)^2_\mu}}{\mathcal{F}_{\rm Q}[\Psi_\mu, J_y]} \tag{E4}$$

for various particle numbers. It can be seen that for an almost fully polarized state the difference is small, but even for a state that is not fully polarized the relative difference is smaller than 3% for the particle numbers considered.

Appendix F: Why we can assume $\langle J_x\rangle = 0$ for the discussion of spin-squeezed states

We show that for the state minimizing $\mathcal{F}_{\rm Q}[\varrho, J_y]$ for given $\langle J_z\rangle$ and $\langle J_x^2\rangle$ we have $\langle J_x\rangle = 0$. Hence, if we constrain only $\langle J_z\rangle$ and $\langle J_x^2\rangle$, then we get the same bound as if we constrained $\langle J_z\rangle$ and $\langle J_x^2\rangle$, and we used an additional constraint $\langle J_x\rangle = 0$.

For spin-squeezed states, we have to solve the following optimization task. We have to find a tight lower bound on the quantum Fisher information

$$\mathcal{F}_{\rm Q}[\varrho, J_y] \geqslant \mathcal{B}(\vec{w}_\varrho) \tag{F1}$$

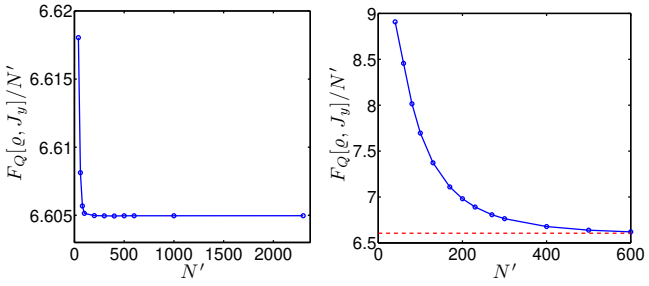

FIG. 6. (Color online) Lower bound on the quantum Fisher information based on $\langle J_z\rangle$ and $(\Delta J_x)^2$ obtained for different particle numbers making calculations in the symmetric subspace. $N = 2300$ corresponds to the spin-squeezing experiment in Ref. [7]. (a) Almost fully polarized spin-squeezed state. Even for a moderate N', the bound is practically identical to the right-hand side of Eq. (18). (b) Spin-squeezed state that is not fully polarized. For large N', the bound converges to the right-hand side of Eq. (18), represented by the dashed line. In both panels, circles correspond to the results of our calculations, which are connected by straight lines to guide the eye.

where $\vec{w}_\varrho = (\langle J_z\rangle_\varrho, \langle J_x^2\rangle_\varrho, \langle J_x\rangle_\varrho)$. For any ϱ, we can define a state $\varrho_- = \sigma_z^{\otimes N}\varrho\sigma_z^{\otimes N}$, for which $\vec{w}_{\varrho_-} = (\langle J_z\rangle_\varrho, \langle J_x^2\rangle_\varrho, -\langle J_x\rangle_\varrho)$. The metrological usefulness of ϱ and ϱ_- are the same, i.e., $\mathcal{F}_Q[\varrho, J_y] = \mathcal{F}_Q[\varrho_-, J_y]$. Then, for any ϱ, we can define a state $\varrho_0 = \frac{1}{2}(\varrho + \varrho_-)$, for which we have $\vec{w}_{\varrho_0} = (\langle J_z\rangle_\varrho, \langle J_x^2\rangle_\varrho, 0)$. Due to the convexity of the quantum Fisher information, ϱ_0 cannot be better metrologically than ϱ or ϱ_-, that is, $\mathcal{F}_Q[\varrho, J_y] = \mathcal{F}_Q[\varrho_-, J_y] \geqslant \mathcal{F}_Q[\varrho_0, J_y]$.

Since for any ϱ there is a corresponding ϱ_0 with the above properties, it follows that $\mathcal{B}(\vec{v}_\varrho) = \mathcal{B}(\vec{v}_{\varrho_-}) \geqslant \mathcal{B}(\vec{w}_{\varrho_0}) = \mathcal{B}(\langle J_z\rangle_\varrho, \langle J_x^2\rangle_\varrho, 0)$. Thus, the worst-case bound for given $\langle J_z\rangle$ and $\langle J_x^2\rangle$ is $\mathcal{B}(\langle J_z\rangle, \langle J_x^2\rangle, 0)$. Hence,

$$\mathcal{B}(\langle J_z\rangle, \langle J_x^2\rangle) = \mathcal{B}(\langle J_z\rangle, \langle J_x^2\rangle, \langle J_x\rangle = 0), \tag{F2}$$

and our claim is proved.

Appendix G: Many-particle experiments

In this section, we consider cold-gas experiments creating spin-squeezed states and Dicke states.

1. Spin-squeezing experiment

We now give the details of the calculations described in Sec. IV B 1. We present a simple scheme that we need to handle large systems. We do not make calculations directly for $N = 2300$, but we start with smaller systems and make calculations for larger and larger system sizes. This is motivated as follows. First, we can use the output of an optimization for a smaller particle number as an initial guess for a larger particle number. Thus, we need fewer steps for the numerical optimization for large system sizes, which makes our computations faster. Second, while we are able to carry out the calculation for the particle number of the experiment, we also see that we could even extrapolate the results from the results obtained for lower particle numbers. This is useful for future application of our method to very large systems.

The basic idea is that we transform the collective quantities from N to a smaller particle number N' using the scaling relation

$$\langle J_z\rangle = \frac{N'}{2}\alpha,$$
$$(\Delta J_x)^2 = \xi_s^2\frac{N'}{4}\alpha^2. \tag{G1}$$

We see that for the scaling we consider, for all N' the bound in Eq. (2) is obtained as

$$\frac{\mathcal{F}_Q[\varrho_{N'}, J_y]}{N'} \geqslant \frac{1}{\xi_s^2} = 6.605. \tag{G2}$$

where $\varrho_{N'}$ is a state satisfying Eq. (G1). Let us first take $\alpha = 0.85$, which is somewhat lower than the experimental value, however, it helps us to see various characteristics of the method. At the end of the section we also discuss the results for other values of α. Based on these ideas, we compute the bound $\mathcal{B}_{\rm sym}(\langle J_z\rangle_{\varrho_{N'}}, \langle J_x^2\rangle_{\varrho_{N'}})$, described in Sec. IV B 1, for the quantum Fisher information for an increasing system size N'.

The results are shown in Fig. 6(a). The bound obtained in this way is close to the bound in Eq. (18) even for small N'. For a larger particle number, i.e., $N' > 200$, it is constant and coincides with the bound in Eq. (18). This also strongly supports the idea that we could have used the results from small particle numbers to extrapolate the bound for N. Since for the experimental particle numbers we obtain that $\mathcal{B}_{\rm sym}(\langle J_z\rangle_{\varrho_N}, \langle J_x^2\rangle_{\varrho_N})$ equals the bound in (2), we find that for $N' = N$ all three lower bounds in Eq. (19) must be equal. Hence, Eq. (2) is optimal for the experimental system considered in this section. Besides, these results also present a strong argument for the correctness of our approach.

We now give more details of the calculation. We were able to carry out the optimization up to $N' = 2300$ with a usual laptop computer using the MATLAB programming language [74]. We started the calculation for each given particle number with the r_k parameters obtained for the previous simulation with a smaller particle number.

Let us consider a spin-squeezed state that is not fully polarized and $\alpha = 0.5$. In Fig. 6(b), we can see that for small particle numbers we have a bound on $\mathcal{F}_Q[\varrho, J_y]$ larger than the one obtained from Eq. (2). Thus for this case we could improve bound (2) by assuming symmetry. On the other hand, for large particle numbers we approach Eq. (2).

After seeing the results of the calculations for $\alpha = 0.85$ and $\alpha = 0.5$, the question arises, what would the result be for larger α, that is, for even more polarized states? It turns out that if we choose α larger than 0.85, then the convergence of $\mathcal{F}_Q[\varrho_{N'}, J_y]/N'$ will be even faster than in Fig. 6(a), and for the particle number of the experiment we obtain again that Eq. (2) is saturated.

Finally, we add a note on a technical detail. We carried out our calculations with the constraints on $(\Delta J_x)^2$, and $\langle J_z\rangle$, with the additional constraint $\langle J_x\rangle = 0$. For the experimental particle numbers, one can show that our results are valid even if we

constrain only $(\Delta J_x)^2$ and $\langle J_z\rangle$, and do not use the $\langle J_x\rangle = 0$ constraint. This way, in principle, we can only get a bound that is equal to or lower than one we obtained before. However, we previously obtained a value identical to the analytical bound, (2). The optimal bound cannot be below the analytic bound, since then the analytic bound would overestimate the quantum Fisher information, and it would not be a valid bound. Hence, even an optimization without the $\langle J_x\rangle = 0$ constraint could not obtain a smaller value than our results.

2. Experiment creating Dicke states

We now give the details for the calculations described in Sec. IV B 2. As in Appendix G 1, we compute the bound for quantum Fisher information for an increasing system size N'. However, now we are not able to do the calculation for the experimental particle number, and we use extrapolation from the results obtained for smaller particle numbers.

First, we transform the measured second moments to values corresponding to a symmetric system using Eq. (22) and Eq. (23). For our case, $\gamma = 1.301$. In this way, we obtain

$$\begin{aligned}\langle J_z^2\rangle_{\mathrm{sym},N} &= 145.69,\\ \langle J_x^2\rangle_{\mathrm{sym},N} &= \langle J_y^2\rangle_{\mathrm{sym},N} = 7.8\times 10^6.\end{aligned} \tag{G3}$$

Next, we carry out calculations for symmetric systems. We consider a scaling that keeps expectation values such that the corresponding quantum state must be symmetric. Hence, we use the relations

$$\begin{aligned}\langle J_z^2\rangle_{\mathrm{sym},N'} &= \langle J_z^2\rangle_{\mathrm{sym},N},\\ \langle J_x^2\rangle_{\mathrm{sym},N'} &= \langle J_y^2\rangle_{\mathrm{sym},N'} = \tfrac{1}{2}(\mathcal{J}_{N'} - \langle J_z^2\rangle_{\mathrm{sym},N'}),\end{aligned} \tag{G4}$$

where $\mathcal{J}_{N'}$ is defined in Eq. (15). Note that with Eq. (G4), $\langle J_x^2 + J_y^2 + J_z^2\rangle_{\mathrm{sym},N'} = \mathcal{J}_{N'}$ holds for all N', hence the state must be symmetric. The main characteristics of the scaling relation, Eq. (G4), can be summarized as follows. $\langle J_z^2\rangle_{\mathrm{sym},N'}$ remains equal to $\langle J_z^2\rangle_{\mathrm{sym},N}$, while $\langle J_x^2\rangle_{\mathrm{sym},N'}$ and $\langle J_y^2\rangle_{\mathrm{sym},N'}$ are chosen such that they are equal to each other and the state is symmetric. For large N, Eq. (G4) implies a scaling of $\langle J_z^2\rangle \sim$ const. and $\langle J_x^2\rangle = \langle J_z^2\rangle \sim N(N+2)/8$.

Let us now turn to the central quantities of our paper, the lower bounds on the quantum Fisher information. The quantum Fisher information for the experimentally obtained state ϱ_N is bounded from below as

$$\mathcal{F}_{\mathrm{Q}}[\varrho_N, J_y] \geqslant \mathcal{B}_N, \tag{G5}$$

where $\mathcal{B}_N$ denotes a bound based on $\langle J_l^2\rangle_N$ for $l = x, y, z$. An analogous relation for the symmetric state $\varrho_{\mathrm{sym},N'}$ is

$$\mathcal{F}_{\mathrm{Q}}[\varrho_{\mathrm{sym},N'}, J_y] \geqslant \mathcal{B}_{\mathrm{sym},N'}, \tag{G6}$$

where $\mathcal{B}_{\mathrm{sym},N'}$ denotes a bound based on $\langle J_l^2\rangle_{\mathrm{sym},N'}$ for $l = x, y, z$.

A central point in our scheme is that due to the scaling properties of the system we can obtain the value for the particle

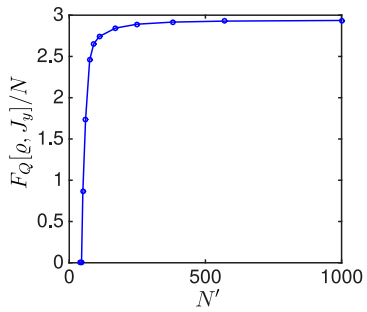

FIG. 7. (Color online) Quantum Fisher information extrapolated to $N = 7900$ from calculations with different particle numbers N' in an experiment creating Dicke states. Circles correspond to the results of our calculations, which are connected by straight lines to guide the eye.

number N from the value for a smaller particle number N' as [19]

$$\mathcal{B}_{\mathrm{sym},N} \approx \frac{\mathcal{J}_N}{\mathcal{J}_{N'}}\mathcal{B}_{\mathrm{sym},N'}, \tag{G7}$$

which we verify numerically. Note that for large N, we have $\mathcal{J}_N/\mathcal{J}_{N'} \sim N^2/(N')^2$.

As the last step, we have to return from the symmetric system to our real, not fully symmetric one. Based on Eq. (G7), and assuming that Eq. (24) is close to being saturated, a relation for the lower bound for the original problem can be obtained from the bound on the symmetric problem with N' particles as

$$\mathcal{B}_N \approx \frac{1}{\gamma}\frac{\mathcal{J}_N}{\mathcal{J}_{N'}}\mathcal{B}_{\mathrm{sym},N'}. \tag{G8}$$

In Fig. 7, we plot the right-hand side of Eq. (G8) as a function of N'. We can see that $\mathcal{B}_{N'}$ is constant or slightly increasing for $N' > 400$. This is strong evidence that Eq. (G7) is valid for large particle numbers. With this, we arrive at Eq. (28).

[1] R. Horodecki, P. Horodecki, M. Horodecki, and K. Horodecki, Rev. Mod. Phys. **81**, 865 (2009).
[2] O. Gühne and G. Tóth, Phys. Rep. **474**, 1 (2009).
[3] L. Pezzé and A. Smerzi, Phys. Rev. Lett. **102**, 100401 (2009).
[4] A. Louchet-Chauvet, J. Appel, J. J. Renema, D. Oblak, N. Kjaergaard, and E. S. Polzik, New J. Phys. **12**, 065032 (2010).

[5] J. Appel, P. J. Windpassinger, D. Oblak, U. B. Hoff, N. Kjærgaard, and E. S. Polzik, PNAS **106**, 10960 (2009).

[6] M. F. Riedel, P. Böhi, Y. Li, T. W. Hänsch, A. Sinatra, and P. Treutlein, Nature **464**, 1170 (2010).

[7] C. Gross, T. Zibold, E. Nicklas, J. Esteve, and M. K. Oberthaler, Nature **464**, 1165 (2010).

[8] B. Lücke, M. Scherer, J. Kruse, L. Pezzé, F. Deuretzbacher, P. Hyllus, J. Peise, W. Ertmer, J. Arlt, L. Santos, A. Smerzi, and C. Klempt, Science **334**, 773 (2011).

[9] H. Strobel, W. Muessel, D. Linnemann, T. Zibold, D. B. Hume, L. Pezzé, A. Smerzi, and M. K. Oberthaler, Science **345**, 424 (2014).

[10] P. Hyllus, O. Gühne, and A. Smerzi, Phys. Rev. A **82**, 012337 (2010).

[11] V. Giovannetti, S. Lloyd, and L. Maccone, Science **306**, 1330 (2004); M. G. A. Paris, Int. J. Quant. Inf. **07**, 125 (2009); R. Demkowicz-Dobrzanski, M. Jarzyna, and J. Kolodynski, Prog. Optics **60**, 345 (2015), arXiv:1405.7703; L. Pezze and A. Smerzi, in *Atom Interferometry (Proc. Int. School of Physics 'Enrico Fermi', Course 188, Varenna)*, edited by G. Tino and M. Kasevich (IOS Press, Amsterdam, 2014) pp. 691–741, arXiv:1411.5164.

[12] C. Helstrom, *Quantum Detection and Estimation Theory* (Academic Press, New York, 1976); A. Holevo, *Probabilistic and Statistical Aspects of Quantum Theory* (North-Holland, Amsterdam, 1982); S. L. Braunstein and C. M. Caves, Phys. Rev. Lett. **72**, 3439 (1994); D. Petz, *Quantum information theory and quantum statistics* (Springer, Berlin, Heilderberg, 2008); S. L. Braunstein, C. M. Caves, and G. J. Milburn, Ann. Phys. **247**, 135 (1996).

[13] P. Hyllus, W. Laskowski, R. Krischek, C. Schwemmer, W. Wieczorek, H. Weinfurter, L. Pezzé, and A. Smerzi, Phys. Rev. A **85**, 022321 (2012); G. Tóth, Phys. Rev. A **85**, 022322 (2012).

[14] R. Krischek, C. Schwemmer, W. Wieczorek, H. Weinfurter, P. Hyllus, L. Pezzé, and A. Smerzi, Phys. Rev. Lett. **107**, 080504 (2011).

[15] In another context, the measurement of the quantum Fisher information has recently been considered in systems in thermal equilibrium. P. Hauke, M. Heyl, L. Tagliacozzo, and P. Zoller, Nat. Phys. **12**, 778 (2016);T. Shitara and M. Ueda, Phys. Rev. A **94**, 062316 (2016).

[16] L. Pezze, Y. Li, W. Li, and A. Smerzi, PNAS **113**, 11459 (2016).

[17] F. Fröwis, P. Sekatski, and W. Dür, Phys. Rev. Lett. **116**, 090801 (2016).

[18] R. H. Dicke, Phys. Rev. **93**, 99 (1954).

[19] Z. Zhang and L. M. Duan, New J. Phys. **16**, 103037 (2014).

[20] F. Fröwis, R. Schmied, and N. Gisin, Phys. Rev. A **92**, 012102 (2015).

[21] I. Apellaniz, B. Lücke, J. Peise, C. Klempt, and G. Tóth, New J. Phys. **17**, 083027 (2015).

[22] E. Oudot, P. Sekatski, F. Fröwis, N. Gisin, and N. Sangouard, J. Opt. Soc. Am. B **32**, 2190 (2015).

[23] M. Kitagawa and M. Ueda, Phys. Rev. A **47**, 5138 (1993); D. J. Wineland, J. J. Bollinger, W. M. Itano, and D. J. Heinzen, Phys. Rev. A **50**, 67 (1994).

[24] D. M. Greenberger, M. A. Horne, A. Shimony, and A. Zeilinger, Am. J. Phys. **58**, 1131 (1990).

[25] D. Bouwmeester, J.-W. Pan, M. Daniell, H. Weinfurter, and A. Zeilinger, Phys. Rev. Lett. **82**, 1345 (1999).

[26] J.-W. Pan, D. Bouwmeester, M. Daniell, H. Weinfurter, and A. Zeilinger, Nature **403**, 515 (2000).

[27] Z. Zhao, T. Yang, Y.-A. Chen, A.-N. Zhang, M. Żukowski, and J.-W. Pan, Phys. Rev. Lett. **91**, 180401 (2003).

[28] C.-Y. Lu, X.-Q. Zhou, O. Gühne, W.-B. Gao, J. Zhang, Z.-S. Yuan, A. Goebel, T. Yang, and J.-W. Pan, Nat. Phys. **3**, 91 (2007).

[29] W.-B. Gao, C.-Y. Lu, X.-C. Yao, P. Xu, O. Gühne, A. Goebel, Y.-A. Chen, C.-Z. Peng, Z.-B. Chen, and J.-W. Pan, Nat. Phys. **6**, 331 (2010).

[30] D. Leibfried, M. Barrett, T. Schaetz, J. Britton, J. Chiaverini, W. Itano, J. Jost, C. Langer, and D. Wineland, Science **304**, 1476 (2004).

[31] C. Sackett, D. Kielpinski, B. King, C. Langer, V. Meyer, C. Myatt, M. Rowe, Q. Turchette, W. Itano, D. Wineland, and C. Monroe, Nature **404**, 256 (2000).

[32] T. Monz, P. Schindler, J. T. Barreiro, M. Chwalla, D. Nigg, W. A. Coish, M. Harlander, W. Hänsel, M. Hennrich, and R. Blatt, Phys. Rev. Lett. **106**, 130506 (2011).

[33] N. Kiesel, C. Schmid, G. Tóth, E. Solano, and H. Weinfurter, Phys. Rev. Lett. **98**, 063604 (2007).

[34] W. Wieczorek, R. Krischek, N. Kiesel, P. Michelberger, G. Tóth, and H. Weinfurter, Phys. Rev. Lett. **103**, 020504 (2009).

[35] R. Prevedel, G. Cronenberg, M. S. Tame, M. Paternostro, P. Walther, M. S. Kim, and A. Zeilinger, Phys. Rev. Lett. **103**, 020503 (2009).

[36] A. Chiuri, C. Greganti, M. Paternostro, G. Vallone, and P. Mataloni, Phys. Rev. Lett. **109**, 173604 (2012).

[37] P. Schindler, M. Müller, D. Nigg, J. T. Barreiro, E. Martinez, M. Hennrich, T. Monz, S. Diehl, P. Zoller, and R. Blatt, Nat. Phys. **9**, 361 (2013).

[38] C. Gross, J. Phys. B: At. Mol. Opt. Phys. **45**, 103001 (2012); J. Ma, X. Wang, C. P. Sun, and F. Nori, Phys. Rep. **509**, 89 (2011); J. Hald, J. L. Sørensen, C. Schori, and E. S. Polzik, Phys. Rev. Lett. **83**, 1319 (1999); S. R. de Echaniz, M. W. Mitchell, M. Kubasik, M. Koschorreck, H. Crepaz, J. Eschner, and E. S. Polzik, J. Opt. B: Quantum and Semiclassical Opt. **7**, S548 (2005); R. J. Sewell, M. Koschorreck, M. Napolitano, B. Dubost, N. Behbood, and M. W. Mitchell, Phys. Rev. Lett. **109**, 253605 (2012).

[39] B. Lücke, J. Peise, G. Vitagliano, J. Arlt, L. Santos, G. Tóth, and C. Klempt, Phys. Rev. Lett. **112**, 155304 (2014).

[40] C. Hamley, C. Gerving, T. Hoang, E. Bookjans, and M. Chapman, Nat. Phys. **8**, 305 (2012).

[41] X.-Y. Luo, Y.-Q. Zou, L.-N. Wu, Q. Liu, M.-F. Han, M. K. Tey, and L. You, Science **355**, 620 (2017).

[42] A. Sørensen, L.-M. Duan, J. Cirac, and P. Zoller, Nature **409**, 63 (2001).

[43] J. K. Korbicz, J. I. Cirac, and M. Lewenstein, Phys. Rev. Lett. **95**, 120502 (2005).

[44] G. Tóth, C. Knapp, O. Gühne, and H. J. Briegel, Phys. Rev. Lett. **99**, 250405 (2007).

[45] A. C. Doherty, P. A. Parrilo, and F. M. Spedalieri, Phys. Rev. Lett. **88**, 187904 (2002).

[46] H. Wunderlich and M. B. Plenio, J. Mod. Opt. **56**, 2100 (2009).

[47] G. Tóth, T. Moroder, and O. Gühne, Phys. Rev. Lett. **114**, 160501 (2015).

[48] R. T. Rockafellar, *Convex analysis* (Princeton University Press, Princeton, 1997).

[49] O. Gühne, M. Reimpell, and R. F. Werner, Phys. Rev. Lett. **98**, 110502 (2007).

[50] J. Eisert, F. G. S. L. Brandao, and K. M. R. Audenaert, New J. Phys. **9**, 46 (2007).

[51] G. Tóth and D. Petz, Phys. Rev. A **87**, 032324 (2013); S. Yu, arXiv:1302.5311 .

[52] An alternative definition is $\mathcal{F}_{\mathrm{Q}}(W) = \sup_{\nu} \langle W \rangle_{\psi_\nu} - 4(\Delta J_l)^2_{\psi_\nu}$, where $|\psi_\nu\rangle$ is the eigenstate with the maximal eigenvalue of the

operator $W - 4J_l^2 - \nu J_l$. In certain cases, this form can be calculated numerically more easily than Eq. (6).
[53] A. Luis, Physics Letters A **329**, 8 (2004).
[54] S. Boixo, S. T. Flammia, C. M. Caves, and J. Geremia, Phys. Rev. Lett. **98**, 090401 (2007).
[55] S. Choi and B. Sundaram, Phys. Rev. A **77**, 053613 (2008).
[56] S. M. Roy and S. L. Braunstein, Phys. Rev. Lett. **100**, 220501 (2008).
[57] M. Napolitano, M. Koschorreck, B. Dubost, N. Behbood, R. Sewell, and M. W. Mitchell, Nature **471**, 486 (2011).
[58] M. J. W. Hall and H. M. Wiseman, Phys. Rev. X **2**, 041006 (2012).
[59] A. S. Sørensen and K. Mølmer, Phys. Rev. Lett. **86**, 4431 (2001).
[60] A not tight lower bounds on the quantum Fisher based on the fidelity has been presented in R. Augusiak, J. Kołodyński, A. Streltsov, M. N. Bera, A. Acín, and M. Lewenstein, Phys. Rev. A **94**, 012339 (2016).
[61] G. Tóth, J. Opt. Soc. Am. B **24**, 275 (2007).
[62] G. Tóth, W. Wieczorek, R. Krischek, N. Kiesel, P. Michelberger, and H. Weinfurter, New J. Phys. **11**, 083002 (2009).
[63] M. J. Holland and K. Burnett, Phys. Rev. Lett. **71**, 1355 (1993).
[64] Due to symmetries of the problem, when minimizing $\mathcal{F}_{\mathrm{Q}}[\varrho, J_y]$ with the constrains on $\langle J_z\rangle$ and $\langle J_x^2\rangle$, we do not have to add explicitly the constraint $\langle J_x\rangle = 0$. Optimization with only the first two constraints will give the same bound (see Appendix F).
[65] Outside the symmetric subspace, there are other states with $\langle J_z\rangle = \langle J_x^2\rangle = 0$, which also correspond to point D. For example, such a state is the multiparticle singlet. However, usual spin-squeezing procedures remain in the symmetric subspace, thus we discuss only the Dicke state.
[66] Z. Zhao, Y.-A. Chen, A.-N. Zhang, T. Yang, H. J. Briegel, and J.-W. Pan, Nature **430**, 54 (2004).
[67] Y.-F. Huang, B.-H. Liu, L. Peng, Y.-H. Li, L. Li, C.-F. Li, and G.-C. Guo, Nat. Commun. **2**, 546 (2011).
[68] D. Leibfried, E. Knill, S. Seidelin, J. Britton, R. B. Blakestad, J. Chiaverini, D. B. Hume, W. M. Itano, J. D. Jost, C. Langer, R. Ozeri, R. Reichle, and D. J. Wineland, Nature **438**, 639 (2005).
[69] G. Tóth, W. Wieczorek, D. Gross, R. Krischek, C. Schwemmer, and H. Weinfurter, Phys. Rev. Lett. **105**, 250403 (2010).
[70] G. Tóth and I. Apellaniz, J. Phys. A: Math. Theor. **47**, 424006 (2014).
[71] B. Escher, R. de Matos Filho, and L. Davidovich, Nat. Phys. **7**, 406 (2011); R. Demkowicz-Dobrzański, J. Kołodyński, and M. Guţă, Nat. Commun. **3**, 1063 (2012).
[72] This is also relevant for Ref. [60], where $\mathcal{F}_{\mathrm{Q}} = O(N^2)$ is reached with weakly entangled states.
[73] For some of the programs used for this article, see the actual version of the QUBIT4MATLAB package at `http://www.mathworks.com/matlabcentral/`. The 3.0 version of the package is described in G. Tóth, Comput. Phys. Commun. **179**, 430 (2008) .
[74] For MATLAB R2015a, see `http://www.mathworks.com`.

Memory cost for simulating all quantum correlations from the Peres–Mermin scenario

Gabriel Fagundes[1, 2, *] and Matthias Kleinmann[2]

[1] *Departamento de Física, Universidade Federal de Minas Gerais UFMG, P.O. Box 702, 30123–970, Belo Horizonte, MG, Brazil*

[2] *Department of Theoretical Physics, University of the Basque Country UPV/EHU, P.O. Box 644, 48080 Bilbao, Spain*

Sequences of compatible quantum measurements can be contextual and any simulation with a classical model conforming with the quantum predictions needs to use internal memory. Kleinmann *et al.* [New J. Phys. **13**, 113011 (2011)] showed that simulating the sequences from the Peres–Mermin scenario requires at least three different internal states in order to be not in contradiction with the deterministic predictions of quantum theory. We extend this analysis to the probabilistic quantum predictions and ask how much memory is required to simulate the correlations generated for sequences of compatible observables by any quantum state. We find that even in this comprehensive approach only three internal states are required for a perfect simulation of the quantum correlations in the Peres–Mermin scenario.

I. INTRODUCTION

In the standard formulation of quantum theory (QT) the individual outcomes of measurements are, in general, not predetermined by the state of the system. Consequently, QT allows us to asses only the probability distribution over the measurement outcomes. Specker [1] noted that this is a fundamental property of QT and if quantum measurements had predetermined outcomes it would imply that these values depend on the measurement context. In this sense, QT is contextual and the mathematical formulation of this observation is the Kochen–Specker theorem [2].

Significant effort has been undertaken to understand the connection between quantum contextuality and quantum information theory, for example, with respect to the advantage of quantum computing over classical computing [3, 4]. Similarly, a quantum system distributed over several parties can be used to reduce the communication complexity over what is possible with classical systems alone [5, 6] and the communication advantage has been identified as a resource [7–9]. A related concept is the memory cost in sequential measurements [10, 11], i.e., the memory needed to simulate the correlations occurring in sequences of quantum measurements by means of a classical automaton with memory. It has been found that the memory cost can exceed the amount of information that can be stored in the quantum system yielding a quantum memory advantage [10–12]. We are here interested in the analysis of the memory cost with respect to quantum contextuality, i.e., to determine the memory cost when the measurements in a sequence only embraces mutually compatible measurements [10]. In this strict form the question of whether there exists a quantum memory advantage due to contextuality is still open.

In this paper we investigate the situation for one of the most natural candidates for a quantum memory advantage, the Peres–Mermin square. We ask, what is the smallest memory for a classical model to reproduce all contextuality predictions from the Peres–Mermin scenario, for any quantum state. Our focus here is to stay strictly in the regime of quantum contextuality, i.e., sequences of compatible measurements, and to take into account also the probabilistic predictions of quantum theory, while at the same time to admit the most versatile classical automaton models.

II. THE PERES–MERMIN SQUARE

A simple proof of the Kochen–Specker theorem was found by Peres [13] and Mermin [14] and uses 9 quantum observables arranged in the Peres–Mermin square,

$$\begin{bmatrix} A & B & C \\ a & b & c \\ \alpha & \beta & \gamma \end{bmatrix} = \begin{bmatrix} \sigma_z \otimes \mathbb{1} & \mathbb{1} \otimes \sigma_z & \sigma_z \otimes \sigma_z \\ \mathbb{1} \otimes \sigma_x & \sigma_x \otimes \mathbb{1} & \sigma_x \otimes \sigma_x \\ \sigma_z \otimes \sigma_x & \sigma_x \otimes \sigma_z & \sigma_y \otimes \sigma_y \end{bmatrix}, \quad (1)$$

where σ_x, σ_y, and σ_z are the Pauli operators. The proof of the theorem consists of the observations (i) that the operators within each row and each column form a context, i.e., they are mutually compatible, and (ii) that the condition

$$ABC = abc = \alpha\beta\gamma = Aa\alpha = Bb\beta = -Cc\gamma = \mathbb{1} \quad (2)$$

holds. Therefore, according to QT, the expected value of the product of the outcomes of observables in one context is always $+1$, with the exception $\langle Cc\gamma\rangle = -1$. In order to obtain this behavior if the values of the observables are predetermined, at least one observable needs to have a context-dependent value, so that, for example, γ has value $+1$ in the context $\alpha\beta\gamma$ but value -1 in the context $Cc\gamma$.

In QT, the outcomes of all observables within a context can be obtained in a joint measurement. For the three dichotomic observables in each context of the Peres–Mermin square, the joint measurement on two qubits has four distinct outcomes, taken from the set of the 8 possible combinations of outcomes

* gabrielf@fisica.ufmg.br

$\{(+1,+1,+1),(+1,+1,-1),\ldots,(-1,-1,-1)\}$. Alternatively, the outcomes can be obtained by measuring the observables in a context sequentially. This approach has been preferred in recent experiments on quantum contextuality [15–20]. When an observable X from the Peres–Mermin square is measured, then the quantum state ρ changes according to

$$\rho \mapsto \frac{\Pi_{x|X}\rho\Pi_{x|X}}{\mathrm{tr}(\rho\Pi_{x|X})}, \tag{3}$$

with $\Pi_{x|X} = \frac{1}{2}(\mathbb{1} + xX)$ depending on the measurement outcome $x = \pm 1$ of X. In a sense, sequential measurements with this Lüders transformation [21] are a special way to implement a joint measurement. Since the quantum state changes according to the choice of the observable and the measurement outcome, one can argue that the quantum state serves as a memory and the contextual behavior is achieved due to the very presence of this memory.

However, in an extended variant of the Peres–Mermin square, it has been shown [10] that even if one takes this perspective, a classical model mimicking the quantum behavior would need more than four internal states. This extended scenario uses quantum predictions for all combinations of Pauli matrices on two qubits, resulting in 15 dichotomic observables. The classical model must then reproduce the predictions from any sequence of compatible observables as well as respect conditions of compatibility and repeatability. The latter include conditions on sequences of incompatible measurements, and thus are outside the contextuality paradigm. Since the extended variant also operates on a quantum four-level system and such systems can carry at most two bits of classical information [22], this has been identified as an instance of memory advantage [10–12].

The analysis in Ref. [10] concerns classical models which reproduce the deterministic predictions of QT within a sequence. Such predictions are, for example, that the product of outcomes in the sequence A, B, C is always $+1$ or that the value of A is repeated in the sequence A, B, A. For the case of the Peres–Mermin square and when any sequence of measurements consists of observables from one context, there is a classical model consistent with QT in this sense and which only uses three internal states. This analysis does not cover the probabilistic predictions of QT, for example, that $\langle A\rangle = 0$ for certain quantum states and it is not known how much memory is needed to reproduce also the probabilistic predictions of QT in the Peres–Mermin square. Since the Peres–Mermin scenario is tightly linked to contextuality, we only consider sequences of observables taken from one context. This includes predictions like $\langle BBA\rangle = \langle A\rangle$, but excludes predictions involving incompatible observables as in $\langle ABc\gamma\rangle = -1$. In this paper our aim is hence to determine the smallest memory for a classical model to reproduce the nondeterministic contextual quantum predictions from the Peres–Mermin scenario, for any quantum state.

III. SEQUENTIAL CORRELATIONS AND STOCHASTIC AUTOMATA

The outcomes of a sequence of quantum measurements may be viewed as an input–output process operating on a quantum system. The input is the choice of the observable X and the output is the outcome x of the measurement of the observable. The overall probability for an output sequence $x_1, x_2, \ldots$ for a given input sequence $X_1, X_2, \ldots$ is $P(x_1, x_2, \ldots|X_1, X_2, \ldots)$ and within standard QT only such correlations can be predicted.

The classical counterpart is modeled by an automaton which operates on classical memory. This memory is represented by a set M of internal memory states. In addition, the automaton has access to an external source of randomness, modeled by an external parameter λ which is fixed throughout a measurement sequence but randomly distributed among different sequences according to a distribution function $p(\lambda)$. We use the model of a stochastic sequential automaton [23] where the output x and the state $s' \in M$ after the output only depend on the input X, the value of λ, and the internal state $s \in M$ before the output, cf. Fig 1. The behavior of the automaton is hence summarized by the probability distribution $p(x, s'|X, s, \lambda)$. It represents the probability of the output x and subsequent transition to the internal state s', given the input X, the current internal state s and the value of the parameter λ. Similarly, the initial state of the automaton has a distribution depending on λ, which we write as $p(s_0|\lambda)$. With this model, the correlations achieved by the automaton are

$$\begin{aligned} P(x_1, x_2, \ldots|X_1, X_2, \ldots) = \\ \sum_{\lambda, s_0, s_1, s_2, \ldots} p(\lambda)p(s_0|\lambda)p(x_1, s_1|X_1, s_0, \lambda) \\ \times\, p(x_2, s_2|X_2, s_1, \lambda)\cdots . \end{aligned} \tag{4}$$

For a given automaton, i.e., $p(x, s'|X, s, \lambda)$ and $p(s_0|\lambda)$, the choice of $p(\lambda)$ yields different correlations, so that the correlations predicted by different quantum states can be reproduced using different choices of the probability distribution $p(\lambda)$.

Clearly, it is possible to reproduce all noncontextual correlations with only one internal state, $|M| = 1$, since in this case the right hand side of Eq. (4) reduces to a hidden variable model [24], $\sum_\lambda p(\lambda)p(x_1|X_1, \lambda)p(x_2|X_2, \lambda)\cdots$. The external parameter λ is not always included in such an analysis, see, for example, the ϵ-transducers studied in Ref. [25]. However, then even noncontextual scenarios could require memory, since, for example, measuring the sequence σ_x, σ_x on an eigenstate of σ_z gives a random outcome for the first measurement, but the second measurement has to repeat the value of the first measurement. Consequently, if λ does not occur, the simulation requires two internal states, while when λ can take two values, no memory is required. The automaton is allowed to be intrinsically random, i.e., the distributions $p(x, s'|X, s, \lambda)$ and

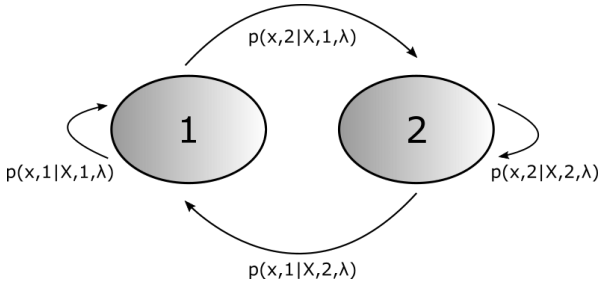

FIG. 1. Stochastic sequential machine with two internal states, $M = \{1, 2\}$. The transitions between the states s and s' are represented by arrows. The probability $p(x, s'|X, s, \lambda)$ for the output x and the transition from state s to state s' can depend on the input X and the external parameter λ.

$p(s_0|\lambda)$ may be nondeterministic. As it is evident from our analysis below, this intrinsic randomness is not required for simulating the quantum correlations from the Peres–Mermin scenario.

IV. A MEMORY-OPTIMAL AUTOMATON FOR THE PERES–MERMIN SCENARIO

As explained above, quantum contextuality is a feature of sets of compatible observables and we therefore only consider sequences of measurements where all observables are taken from one context. That is, the observables are either taken from one row or one column of the Peres–Mermin square. Our first concern is the simulation of quantum measurements of a single sequence of compatible observables. According to QT, certain events can never occur, examples are the output $+1, -1$ in the sequence A, A or the output $+1, +1, -1$ in the sequence A, B, C. In Ref. [10], it has been shown that any automaton which obeys all such quantum predictions must have memory with at least three internal states. An explicit example of such an automaton is given by [10]

$$
\begin{aligned}
o_1 &= \begin{bmatrix} +1 & +1 & +1 \\ +1 & +1 & +1 \\ +1 & +1 & +1 \end{bmatrix}, \quad t_1 = \begin{bmatrix} 1 & 1 & 2 \\ 1 & 1 & 3 \\ 1 & 1 & 1 \end{bmatrix}, \\
o_2 &= \begin{bmatrix} +1 & +1 & +1 \\ -1 & +1 & -1 \\ -1 & -1 & +1 \end{bmatrix}, \quad t_2 = \begin{bmatrix} 2 & 1 & 2 \\ 2 & 2 & 2 \\ 2 & 3 & 2 \end{bmatrix}, \\
o_3 &= \begin{bmatrix} +1 & -1 & -1 \\ +1 & +1 & +1 \\ -1 & -1 & +1 \end{bmatrix}, \quad t_3 = \begin{bmatrix} 3 & 3 & 3 \\ 1 & 3 & 3 \\ 2 & 3 & 3 \end{bmatrix}.
\end{aligned} \tag{5}
$$

This notation is supposed to be read as follows. Each matrix o_i, $i \in M$, represents the deterministic output for each of the three internal states $M = \{1, 2, 3\}$. Similarly, the transition matrices t_i represent the internal state after the output. In terms of Eq. (4), the distribution $p(x, s'|X, s)$ is 1 if the entry in the output matrix o_s at the position of the observable X is x and the entry in the transition matrix t_s in the same position is s'; the distribution is 0 otherwise. Here, $x \in \{+1, -1\}$, $s, s' \in M = \{1, 2, 3\}$, and $X \in \{A, B, C, a, b, c, \alpha, \beta, \gamma\}$. For example, if the automaton is in state $s = 1$ and we provide the observable C as input, then the measurement outcome is $x = +1$ and the automaton changes to the state $s' = 2$. It is straightforward to verify that this automaton obeys all deterministic predictions of QT for any sequence of compatible observables [10] and for any initial state s_0.

However, no quantum state gives deterministic predictions for all 9 observables in the Peres–Mermin square, because these observables are not all mutually compatible and no common eigenstate can exist. In the following we extend the automaton from Eq. (5) to use the external parameter λ, so that a statistical mixture $p(\lambda)$ can reproduce the quantum predictions.

A. Other valid automata

Starting from the automaton in Eq. (5), there are several transformations which lead to other automata with the same properties. First, it is possible to flip the signs for the output under the constraint that for each row and each column there is either no flip of signs or there are exactly two flips of signs. This generates 15 additional automata. Second, it is possible to make any permutation of the rows or a permutation of the first and second column. We restrict ourselves to the three permutations of rows which leave one row unchanged and to the permutation of the first and second column. This yields 4 additional automata and combined with the first set of transformations we get in total $16 \times 5 = 80$ automata. In addition, we are free to choose the initial state s_0 and get this way 240 different behaviors. We combine all these behaviors into a single automaton by allowing 240 different values for λ, i.e., the value of λ determines the behavior of the automaton.

B. Example: Singlet state

As an example, we reproduce all quantum correlations for the singlet state (the quantum state yielding $\langle C\rangle = \langle c\rangle = \langle\gamma\rangle = -1$) by choosing a distribution $p(\lambda)$ for $\lambda = 1, 2, \ldots, 240$. We choose $p(\lambda) = \frac{1}{4}$ if $\lambda \in \{\lambda_1, \lambda_2, \lambda_3, \lambda_4\}$ and $p(\lambda) = 0$ else. For λ_k, $k = 1, 2, 3$, the transition matrices $t_1^{(k)}$, $t_2^{(k)}$, $t_3^{(k)}$ are as in Eq. (5) and the outcome matrices $o_s^{(k)}$ are given by

$$
\begin{aligned}
o_1^{(1)} &= \begin{bmatrix} -1 & +1 & -1 \\ -1 & -1 & +1 \\ +1 & -1 & -1 \end{bmatrix}, \; o_2^{(1)} = \begin{bmatrix} -1 & +1 & -1 \\ +1 & -1 & -1 \\ -1 & +1 & -1 \end{bmatrix}, \\
& \qquad\qquad o_3^{(1)} = \begin{bmatrix} -1 & -1 & +1 \\ -1 & -1 & +1 \\ -1 & +1 & -1 \end{bmatrix},
\end{aligned} \tag{6a}
$$

$$o_1^{(2)} = \begin{bmatrix} -1 & +1 & -1 \\ +1 & +1 & +1 \\ -1 & +1 & -1 \end{bmatrix}, \; o_2^{(2)} = \begin{bmatrix} -1 & +1 & -1 \\ -1 & +1 & -1 \\ +1 & -1 & -1 \end{bmatrix}, \; o_3^{(2)} = \begin{bmatrix} -1 & -1 & +1 \\ +1 & +1 & +1 \\ +1 & -1 & -1 \end{bmatrix}, \tag{6b}$$

$$o_1^{(3)} = \begin{bmatrix} +1 & -1 & -1 \\ -1 & -1 & +1 \\ -1 & +1 & -1 \end{bmatrix}, \; o_2^{(3)} = \begin{bmatrix} +1 & -1 & -1 \\ +1 & -1 & -1 \\ +1 & -1 & -1 \end{bmatrix}, \; o_3^{(3)} = \begin{bmatrix} +1 & +1 & +1 \\ -1 & -1 & +1 \\ +1 & -1 & -1 \end{bmatrix}, \tag{6c}$$

$$o_1^{(4)} = \begin{bmatrix} +1 & -1 & -1 \\ +1 & +1 & +1 \\ +1 & -1 & -1 \end{bmatrix}, \; o_2^{(4)} = \begin{bmatrix} +1 & -1 & -1 \\ -1 & +1 & -1 \\ -1 & +1 & -1 \end{bmatrix}, \; o_3^{(4)} = \begin{bmatrix} +1 & +1 & +1 \\ +1 & +1 & +1 \\ -1 & +1 & -1 \end{bmatrix}. \tag{6d}$$

The initial state for all four cases is $s_0 = 2$, i.e., we have $p(s_0|\lambda) = 1$ if $s_0 = 2$ and zero else. In principle one can now verify that for sequences of compatible observables, all quantum correlations from the singlet state are indeed reproduced. However, there is an infinite number of input sequences which needs to be considered and it is our next step to reduce the number of sequences to a finite set.

C. A finite set of sufficient input sequences

We show in this section that a finite number of input sequences suffices to determine all correlations for all sequences. Since we only consider sequences of observables from one context, as soon as two different observables occur in a sequence, it is already possible to predict the reminder of the sequence from the outcome of these two observables. This is because the product of outcomes of the three observables of each context is always $+1$ or -1, depending on the context, and due to the requirement that repeated occurrences of an observable in a sequence produce repeated values.

Hence, it remains to consider sequences where initially one observable is measured repeatedly, for example, X, X, Y. In quantum mechanics we have

$$P(x, x, \ldots, x, y|X, X, \ldots, X, Y) = \operatorname{tr}(\Pi_{y|Y}\Pi_{x|X}\rho\Pi_{x|X}\Pi_{y|Y}) = P(x, y|X, Y), \tag{7}$$

for any number of repetitions of the input X and output x. However, for the automaton model we could have different values for outcome y in the sequences $X, X, \ldots, X, Y$, depending on the number of repetitions of x, since the value of Y does not need to be fixed until Y is actually measured. Thus, we have to consider how our specific model behaves in this situation. For any value of λ, the behavior of our automaton is analogous to the automaton in Eq. (5) and for this automaton one observes that the internal state s' after an ℓ-fold measurement of X does not depend on ℓ, if $\ell \geq 1$. Hence, the outcome of $X, X, \ldots, X, Y$ is $x, x, \ldots, x, y$ if and only if X, Y has outcome x, y.

In summary, our automaton with any choice of $p(\lambda)$ reproduces the quantum correlations for a state ρ for all sequences of compatible observables, if and only if it does so for all sequences of length two. For practical reasons, instead of dealing with the correlations $P(x, y|X, Y)$ we use the equivalent set of expectation values

$$\langle X \rangle = \sum_{x,y} x P(x, y|X, Y), \tag{8a}$$

$$\langle XYX \rangle = \sum_{x,y} y P(x, y|X, Y), \text{ and} \tag{8b}$$

$$\langle XY \rangle = \sum_{x,y} xy P(x, y|X, Y), \tag{8c}$$

where in the second equation we used that the value of X in the first and in the last position are the same. Note, that while in QT, we always have $\langle XYX \rangle = \langle Y \rangle$, this does not hold for all ensembles $p(\lambda)$ in our automaton, as, for example, in Eq. (5) with initial internal state $s = 1$, we have $\langle c \rangle = 1$, but $\langle CcC \rangle = -1$. However, we observe that $\langle XY \rangle = \langle XY \rangle$ for all $p(\lambda)$ and all compatible X and Y, a relation that also holds in QT for any state.

Therefore, we have to take into account 9 values $\langle X \rangle$, 18 values $\langle XY \rangle$, and 36 values $\langle XYX \rangle$. We enumerate these values by $j = 1, \ldots, 63$ and collect for each j the values for all 240 values of λ in a vector $\vec{v}_j$. Then the expectation values $\vec{q} = (q_1, \ldots, q_{63})$ can be achieved if and only if $q_j = \vec{v}_j \cdot \vec{p}$ for some probabilities $\vec{p}$ with $p_\lambda \equiv p(\lambda)$. The set of achievable expectation values $\vec{q}$ is hence given by the polytope

$$P = \{ \vec{q} \mid q_j = \vec{v}_j \cdot \vec{p} \text{ for all } j \text{ and some } \vec{p} \}. \tag{9}$$

Similarly, for the quantum correlations we have 63 hermitian operators Z_j, such that the expectation values $\vec{q}$ can be attained according to QT if and only if $q_j = \operatorname{tr}(\rho Z_j)$ for all j and some quantum state ρ. The set of achievable expectation values $\vec{q}$ according to QT is consequently the convex set

$$Q = \{ \vec{q} \mid q_j = \operatorname{tr}(\rho Z_j) \text{ for all } j \text{ and some } \rho \}. \tag{10}$$

This allows us to easily verify the correctness of the example in Sec. IV B, by comparing $\vec{v}_j \cdot \vec{p}$ with $\operatorname{tr}(\rho Z_j)$ for all j and for any quantum state ρ, finding a corresponding distribution $p(\lambda)$ reduces to find probabilities $\vec{p}$ with $\vec{v}_j \cdot \vec{p} = \operatorname{tr}(\rho Z_j)$ for all j. This can be solved by means of linear programming and was in fact our method to find $p(\lambda)$ for the singlet state in Sec. IV B.

D. Simulation of the correlations of any quantum state

We are now equipped with the necessary tools to prove that the correlations of any quantum state can be simulated with a construction analogous to the one in Sec. IV B. According to our previous analysis, the question whether the quantum predictions can be simulated by an appropriate distribution $p(\lambda)$ reduces to the question whether the convex set Q is contained in the polytope P. In order to make this question tractable, we use an equivalent representation of the polytope, where it is written as a finite intersection of half-spaces [26] parametrized by vectors $\vec{h}_\ell$ and numbers α_ℓ, so that

$$P = \{\, \vec{q} \mid \vec{h}_\ell \cdot \vec{q} \leq \alpha_\ell \text{ for all } \ell \,\}. \tag{11}$$

Using this half-space representation, P contains Q if and only if $\vec{h}_\ell \cdot \mathrm{tr}(\rho \vec{Z}) \leq \alpha_\ell$ for all ℓ and all ρ. By writing

$$W_\ell = \alpha_\ell \mathbb{1} - \vec{h}_\ell \cdot \vec{Z}, \tag{12}$$

this further simplifies to $\mathrm{tr}(\rho W_\ell) \geq 0$ for all ℓ and all ρ. That is, $Q \subset P$ holds if and only if all W_ℓ are positive semidefinite. Conversely, if we find a state with $\mathrm{tr}(\rho W_\ell) < 0$ for some ℓ, and hence W_ℓ is not positive semidefinite, then our automaton cannot simulate all quantum predictions for this state.

In principle, this can be tested directly. However, since the polytope P is given in the form of Eq. (9), we need to compute the half-space representation in Eq. (11). This can be achieved by using the Fourier–Motzkin elimination, but is known to be a computationally hard task and for our problem we were not able to find a direct solution. The central observation to solve the problem nonetheless is that Q spans a rather low-dimensional affine space. In particular, Q is contained in the affine space $\vec{a} + U \equiv \{\, \vec{a} + \vec{u} \mid \vec{u} \in U \,\}$, where $a_j = \mathrm{tr}(\rho Z_j)$ for some fixed ρ_0 (for example, $\rho_0 = \frac{1}{4}\mathbb{1}$) and U is the linear space $U = \{\, \vec{u} \mid u_j = \mathrm{tr}(G Z_j) \text{ for some } G \,\}$ with G any hermitian operator obeying $\mathrm{tr}(\rho_0 G) = 0$. This holds true since we can always write $\rho = \rho_0 + G$ for some G. The dimension of the linear space U is only $\dim U = 9$, as can be found by using the linear independence relations of the operators Z_j. Therefore, $Q \subset P$ is equivalent to $Q \subset P \cap (\vec{a} + U)$ and our problem reduces to calculate a half-space representation for the polytope $P \cap (\vec{a} + U)$. This problem is easily tractable, as we discuss in Appendix A. We obtain 24 nonzero operators W_ℓ, each of which is positive semidefinite. This proves $Q \subset P$ and thus our automaton can simulate the quantum correlations for any quantum state. We mention that the nonzero operators W_ℓ are, up to an arbitrary positive factor, exactly those 24 projectors of unit rank which commute with all observables from one out of the six contexts in the Peres–Mermin square.

V. CONCLUSIONS

Quantum contextuality is considered as one of the key differences between the microscopic world and the world governed by classical mechanics. Recent experimental demonstrations of this phenomenon proceed by measuring sequences of observables and yield a contradiction to the assumption of noncontextuality, i.e., the assumption that the value of an observable does not depend of which other compatible observables are measured alongside. We revisited this conclusion for the case of the Peres–Mermin scenario in the light of classical models which utilize internal memory in order to reproduce the quantum behavior. We showed that for this scenario an automaton using only three internal states can reproduce the quantum correlations from any quantum state for any sequence of compatible observables. This model is also optimal, since a lower bound of three internal states was already established [10]. The memory cost of the Peres–Mermin scenario is therefore actually lower than the canonical quantum implementation, which requires two qubits. Since for quantum correlations involving sequences of incompatible observables, the memory cost can also be larger than the memory of the quantum system, this leaves open the question, whether there can be a quantum memory advantage when restricted to sequences of compatible observables and if so, for which contextuality scenario this occurs.

ACKNOWLEDGMENTS

We thank Costantino Budroni, Adán Cabello, Marcelo Terra Cunha, Jan-Åke Larsson, Marco Túlio Quintino, and Géza Tóth, for discussions. This work was supported by CNPq, Conselho Nacional de Desenvolvimento Científico e Tecnológico, Brazil, the FQXi Large Grant "The Observer Observed: A Bayesian Route to the Reconstruction of Quantum Theory", the EU (ERC Starting Grant GEDENTQOPT), and by the DFG (Forschungsstipendium KL 2726/2–1).

Appendix A: Low-dimensional section of a polyhedral cone

A central step in Sec. IV D is to compute the half-space representation of the polytope $P \cap (\vec{a} + U)$, where P is a polytope, $\vec{a} \in P$ is a vector and U is a linear subspace of low dimension.

We first consider the equivalent problem for a polyhedral cone $\mathcal{P} = \{\, A\vec{r} \mid \vec{r} \succeq 0 \,\}$, where $\vec{r} \succeq 0$ abbreviates $r_k \geq 0$ for all k and A is some matrix with real entries. For a matrix K, let F be a matrix the range of which is

the kernel of KA. We have

$$\begin{aligned}\mathcal{P}\cap\ker(K) &= \{\, A\vec{r} \mid \vec{r}\succeq 0,\, K(A\vec{r})=0\,\}\\ &= \{\, A\vec{r} \mid \vec{r}\succeq 0,\, \vec{r}=F\vec{s} \text{ for some } \vec{s}\,\}\\ &= \{\, AF\vec{s} \mid F\vec{s}\succeq 0\,\}\\ &= AF\,\{\, \vec{s} \mid F\vec{s}\succeq 0\,\},\end{aligned} \tag{A1}$$

where we used that $KA\vec{r}=0$ implies $\vec{r}=F\vec{s}$ for some $\vec{s}$ and, conversely, $(KA)F\vec{s}=0$ for any $\vec{s}$. It follows that if we can obtain a matrix F', such that $\{\,\vec{s}\mid F\vec{s}\succeq 0\,\} = \{\,F'\vec{s}\mid \vec{s}\succeq 0\,\}$, then $\mathcal{P}\cap\ker(K) = \{\,AFF'\vec{s}\mid\vec{s}\succeq 0\,\}$.

For our case, we extend the polytope P from Eq. (9) to a polyhedral cone $\mathcal{P}$ by adding $\vec{e}=(1,1,\ldots,1)$ to the vectors $\vec{v}_j$ and by dropping the constraint $\sum_i p_i = 1$, i.e., $\mathcal{P} = \{\,A\vec{r}\mid\vec{r}\succeq 0\,\}$ and A is the matrix with rows $[e, v_1, \ldots, v_{63}]$. Then $(1,\vec{q})\in\mathcal{P}$ if and only if $\vec{q}\in P$. Similarly, we define the linear subspace $\mathcal{U} = \{\,(\lambda,\lambda\vec{a}+\vec{u}) \mid \lambda\in\mathbb{R} \text{ and } \vec{u}\in U\,\}$, so that $(1,\vec{x})\in\mathcal{U}$ is equivalent to $\vec{x}\in\vec{a}+U$.

In order to apply Eq. (A1), we choose some matrix K such that $\ker(K)=\mathcal{U}$ and some matrix F with range $\ker(KA)$. Despite F^T being a larger matrix than A, we find that F' is rather easy to compute. The matrix $B=AFF'$ is then only of rank $\dim(\mathcal{U})=10$ and a matrix B' with $\{\,B\vec{s}\mid\vec{s}\succeq 0\,\} = \{\,\vec{y}\mid B'\vec{y}\succeq 0\,\}$ can be computed at an instance. We use the software `cddlib` [27] to generate the matrices F' and B' and `iml` [28] to compute K and F. Both packages work with unlimited exact integer arithmetic and hence our computation of B' is exact. We verify independently our results by using `porta` [29] to compute K, F, F' and B'.

Finally, we have that $\vec{q}\in P$ and $\vec{q}\in\vec{a}+U$ if and only if $(1,\vec{q})\in\mathcal{P}\cap\mathcal{U}$, i.e., if and only if $B'_{\ell,1}+\sum_j B'_{\ell,j+1}q_j\geq 0$ for all ℓ. Therefore, the operators W_ℓ defined in Eq. (12) are given by

$$W_\ell = B'_{\ell,1}\mathbb{1} - \sum_j B'_{\ell,j+1}Z_j. \tag{A2}$$

As we showed in the main text, $Q\subset P\cap(\vec{a}+U)$ is equivalent to all W_ℓ being positive semidefinite. In our analysis, all operators W_ℓ satisfy this condition.

[1] Ernst Specker, "Die Logik nicht gleichzeitig entscheidbarer Aussagen," Dialectica **14**, 239–246 (1960).

[2] Simon Kochen and Ernst P. Specker, "The problem of hidden variables in quantum mechanics," J. Math. Mech. **17**, 59–87 (1967).

[3] Robert Raussendorf, "Contextuality in measurement-based quantum computation," Phys. Rev. A **88**, 022322 (2013).

[4] Mark Howard, Joel Wallman, Victor Veitch, and Joseph Emerson, "Contextuality supplies the 'magic' for quantum computation," Nature (London) **510**, 351–355 (2014).

[5] B. F. Toner and D. Bacon, "Communication cost of simulating Bell correlations," Phys. Rev. Lett. **91**, 187904 (2003).

[6] Harry Buhrman, Richard Cleve, Serge Massar, and Ronald de Wolf, "Nonlocality and communication complexity," Rev. Mod. Phys. **82**, 665–698 (2010).

[7] Rodrigo Gallego, Lars Erik Würflinger, Antonio Acín, and Miguel Navascués, "Operational framework for nonlocality," Phys. Rev. Lett. **109**, 070401 (2012).

[8] Julio I de Vicente, "On nonlocality as a resource theory and nonlocality measures," J. Phys. A: Math. Theo. **47**, 424017 (2014).

[9] Jonathan Barrett, Noah Linden, Serge Massar, Stefano Pironio, Sandu Popescu, and David Roberts, "Nonlocal correlations as an information-theoretic resource," Phys. Rev. A **71**, 022101 (2005).

[10] Matthias Kleinmann, Otfried Gühne, José R. Portillo, Jan-Åke Larsson, and Adán Cabello, "Memory cost of quantum contextuality," New J. Phys. **13**, 113011 (2011).

[11] Stephen Brierley, Adrian Kosowski, Marcin Markiewicz, Tomasz Paterek, and Anna Przysiężna, "Nonclassicality of temporal correlations," Phys. Rev. Lett. **115**, 120404 (2015).

[12] Ernesto F. Galvão and Lucien Hardy, "Substituting a qubit for an arbitrarily large number of classical bits," Phys. Rev. Lett. **90**, 087902 (2003).

[13] Asher Peres, "Incompatible results of quantum measurements," Phys. Lett. A **151**, 107–108 (1990).

[14] N. David Mermin, "Simple unified form for the major no-hidden-variables theorems," Phys. Rev. Lett. **65**, 3373–3376 (1990).

[15] G. Kirchmair, F. Zähringer, R. Gerritsma, M. Kleinmann, O. Gühne, A. Cabello, R. Blatt, and C. F. Roos, "State-independent experimental test of quantum contextuality," Nature (London) **460**, 494–497 (2009).

[16] Elias Amselem, Magnus Rådmark, Mohamed Bourennane, and Adán Cabello, "State-independent quantum contextuality with single photons," Phys. Rev. Lett. **103**, 160405 (2009).

[17] Radek Łapkiewicz, Peizhe Li, Christoph Schaeff, Nathan K. Langford, Sven Ramelow, Marcin Wieśniak, and Anton Zeilinger, "Experimental non-classicality of an indivisible quantum system," Nature (London) **474**, 490–493 (2011).

[18] Xiang Zhang, Mark Um, Junhua Zhang, Shuoming An, Ye Wang, Dong-ling Deng, Chao Shen, Lu-Ming Duan, and Kihwan Kim, "State-independent experimental test of quantum contextuality with a single trapped ion," Phys. Rev. Lett. **110**, 070401 (2013).

[19] Vincenzo D'Ambrosio, Isabelle Herbauts, Elias Amselem, Eleonora Nagali, Mohamed Bourennane, Fabio Sciarrino, and Adán Cabello, "Experimental implementation of a Kochen-Specker set of quantum tests," Phys. Rev. X **3**, 011012 (2013).

[20] Markus Jerger, Yarema Reshitnyk, Markus Oppliger, Anton Potočnik, Mintu Mondal, Andreas Wallraff, Kenneth Goodenough, Stephanie Wehner, Kristinn Juliusson, Nathan K. Langford, and Arkady Fedorov, "Contextuality without nonlocality in a superconducting quantum system," Nat. Commun. **7**, 12930 (2016).

[21] Gerhart Lüders, "Über die Zustandsänderung durch den Meßprozeß," Ann. Phys. (Leipzig) **443**, 322–328 (1951).
[22] A. S. Holevo, "Bounds for the quantity of information transmitted by a quantum communication channel," Probl. Inf. Transm. **9**, 177–183 (1973).
[23] Azaria Paz, *Introduction to Probabilistic Automata* (Academic Press, New York, London, 1971).
[24] J. S. Bell, "On the Einstein Podolsky Rosen paradox," Physics **1**, 195–200 (1964).
[25] Nix Barnett and James P. Crutchfield, "Computational mechanics of input–output processes: Structured transformations and the ϵ-transducer," J. Stat. Phys. **161**, 404–451 (2015).
[26] Branko Grünbaum, *Convex polytopes*, 2nd ed. (Springer, New York, 2003).
[27] K. Fukuda, "cddlib v094h," `https://www.inf.ethz.ch/personal/fukudak/cdd_home/`.
[28] Z. Chen, A. Storjohann, and C. Fletcher, "Integer Matrix Library v1.0.5," `https://cs.uwaterloo.ca/~astorjoh/iml.html`.
[29] T. Christof and A. Löbel, "POlyhedron Representation Transformation Algorithm v1.4.1," `http://porta.zib.de/`.

Proposed experiment to test fundamentally binary theories

Matthias Kleinmann,[1,*] Tamás Vértesi,[2,†] and Adán Cabello[3,‡]

[1] *Department of Theoretical Physics, University of the Basque Country UPV/EHU, P.O. Box 644, E-48080 Bilbao, Spain*
[2] *Institute for Nuclear Research, Hungarian Academy of Sciences, H-4001 Debrecen, P.O. Box 51, Hungary*
[3] *Departamento de Física Aplicada II, Universidad de Sevilla, E-41012 Sevilla, Spain*

Fundamentally binary theories are nonsignaling theories in which measurements of many outcomes are constructed by selecting from binary measurements. They constitute a sensible alternative to quantum theory and have never been directly falsified by any experiment. Here we show that fundamentally binary theories are experimentally testable with current technology. For that, we identify a feasible Bell-type experiment on pairs of entangled qutrits. In addition, we prove that, for any n, quantum n-ary correlations are not fundamentally $(n-1)$-ary. For that, we introduce a family of inequalities that hold for fundamentally $(n-1)$-ary theories but are violated by quantum n-ary correlations.

I. INTRODUCTION

Quantum theory (QT) is the most successful theory physicists have ever devised. Still, there is no agreement on which physical reasons force its formalism [1]. It is therefore important to test "close-to-quantum" alternatives, defined as those which are similar to QT in the sense that they have entangled states, incompatible measurements, violation of Bell inequalities, and no experiment has falsified them, and sensible in the sense that they are in some aspects simpler than QT. Examples of these alternatives are theories allowing for almost quantum correlations [2], theories in which measurements are fundamentally binary [3], and theories allowing for a higher degree of incompatibility between binary measurements [4].

Each of these alternatives identifies a particular feature of QT that we do not fully understand and, as a matter of fact, may or may not be satisfied by nature. For example, we still do not know which principle singles out the set of correlations in QT [5]. In contrast, the set of almost quantum correlations satisfies a list of reasonable principles and is simple to characterize [2]. Similarly, we do not know why in QT there are measurements that cannot be constructed by selecting from binary measurements [3]. However, constructing the set of measurements of the theory would be simpler if this would not be the case. Finally, we do not know why the degree of incompatibility of binary measurements in QT is bounded as it is, while there are theories that are not submitted to such a limitation [4].

Unfortunately, we do not yet have satisfactory answers to these questions. Therefore, it is important to test whether nature behaves as predicted by QT also in these particular aspects. However, this is not an easy task. Testing almost quantum theories is difficult because we still do not have a well-defined theory; thus, there is not a clear indication on how we should aim our experiments. Another reason, shared by theories with larger binary incompatibility, is that the only way to test them is by proving that QT is wrong, which is, arguably, very unlikely. The case of fundamentally binary theories is different. We have explicit theories [3] and we know that fundamentally binary theories predict supraquantum correlations for some experiments but subquantum correlations for others. That is, if QT is correct, there are experiments that can falsify fundamentally binary theories [3]. The problem is that all known cases of subquantum correlations require visibilities that escape the scope of current experiments.

This is particularly unfortunate now that, after years of efforts, we have loophole-free Bell inequality tests [6–10], tests touching the limits of QT [11, 12], and increasingly sophisticated experiments using high-dimensional two-photon entanglement [13–15]. Therefore, a fundamental challenge is to identify a feasible experiment questioning QT beyond the local realistic theories [16].

The main aim of this work is to present a feasible experiment capable of excluding fundamentally binary theories. In addition, the techniques employed to identify that singular experiment will allow us to answer a question raised in Ref. [3], namely, whether or not, for some n, quantum n-ary correlations are fundamentally $(n-1)$-ary.

A. Device-independent scenario

Consider a bipartite scenario where two observers, Alice and Bob, perform independent measurements on a joint physical system. For a fixed choice of measurements x for Alice and y for Bob, $P(a,b|x,y)$ denotes the joint probability of Alice obtaining outcome a and Bob obtaining outcome b. We assume that both parties act independently in the sense that the marginal probability for Alice to obtain outcome a does not depend on the choice of Bob's measurement y, i.e., $\sum_b P(a,b|x,y) \equiv P(a,\_|x,\_)$, and analogously $\sum_a P(a,b|x,y) \equiv P(\_,b|\_,y)$. These are the nonsignaling conditions, which are obeyed by QT

* matthias_kleinmann001@ehu.eus
† tvertesi@atomki.mta.hu
‡ adan@us.es

whenever both observers act independently, in particular, if the operations of the observers are spacelike separated. However, QT does not exhaust all possible correlations subject to these constraints [17].

The strength of this scenario lies in the fact that the correlations can be obtained without taking into account the details of the experimental implementation and hence it is possible to make statements that are independent of the devices used. This device-independence allows us to test nature without assuming a particular theory—such as QT—for describing any of the properties of the measurement setup. This way, it is also possible to make theory-independent statements and, in particular, to analyze the structure of any probabilistic theory that obeys the nonsignaling conditions.

B. Fundamentally binary theories

One key element of the structure of any probabilistic theory was identified in Ref. [3] and concerns how the set of measurements is constructed, depending on the number of outcomes. According to Ref. [3], it is plausible to assume that a theory describing nature has, on a fundamental level, only measurements with two outcomes while situations where a measurement has more outcomes are achieved by classical postprocessing of one or several two-outcome measurements. To make this a consistent construction, it is also admissible that the classical postprocessing depends on additional classical information and, in the bipartite scenario, this classical information might be correlated between both parties. The total correlation attainable in such a scenario are the binary nonsignaling correlations, which are characterized by the convex hull of all nonsignaling correlations obeying $P(a,\_|x,\_) = 0$ for all measurements x and all but two outcomes a, and $P(\_,b|\_,y) = 0$ for all measurements y and all but two outcomes b. The generalization to n-ary nonsignaling correlations is straightforward.

In Ref. [3], it was shown that for no n the set of n-ary nonlocal correlations covers all the set of quantum correlations. Albeit this being a general result, the proof in Ref. [3] has two drawbacks: (i) It does not provide a test which is experimentally feasible. (ii) It does not allow us to answer whether or not quantum n-ary correlations are still fundamentally $(n-1)$-ary. For example, the proof in Ref. [3] requires 10-outcome quantum measurements for excluding the binary case. In this work, we address both problems and provide (i') an inequality that holds for all binary nonsignaling correlations, but can be violated using three-level quantum systems (qutrits) with current technology, and (ii') a family of inequalities obeyed by $(n-1)$-ary nonsignaling correlations but violated by quantum measurements with n outcomes.

II. RESULTS

A. Feasible experiment to test fundamentally binary theories

We first consider the case where Alice and Bob both can choose between two measurements, $x = 0, 1$ and $y = 0, 1$, and each measurement has three outcomes $a, b = 0, 1, 2$. For a set of correlations $P(a, b|x, y)$, we define

$$I_a = \sum_{k,x,y=0,1} (-1)^{k+x+y} P(k, k|x, y), \tag{1}$$

where the outcomes with $k = 2$ do not explicitly appear. With the methods explained in Sec. III A, we find that, up to relabeling of the outcomes,

$$I_a \leq 1 \tag{2}$$

holds for nonsignaling correlations if and only if the correlations are fundamentally binary. However, according to QT, the inequality in Eq. (2) is violated, and a value of

$$I_a = 2(2/3)^{3/2} \approx 1.0887 \tag{3}$$

can be achieved by preparing a two-qutrit system in the pure state

$$|\psi\rangle = \frac{1}{2}(\sqrt{2}\,|00\rangle + |11\rangle - |22\rangle) \tag{4}$$

and choosing the measurements $x, y = 0$ as $M_{k|0} = V|k\rangle\langle k|V^\dagger$, and the measurements $x, y = 1$ as $M_{k|1} = U|k\rangle\langle k|U^\dagger$, where, in canonical matrix representation,

$$V = \frac{1}{\sqrt{12}} \begin{pmatrix} 2 & 2 & 2 \\ -\sqrt{3}-1 & \sqrt{3}-1 & 2 \\ \sqrt{3}-1 & -\sqrt{3}-1 & 2 \end{pmatrix}, \tag{5}$$

and $U = \mathrm{diag}(-1, 1, 1)V$.

Using the second level of the Navascués–Pironio–Acín (NPA) hierarchy [18], we verify that the value in Eq. (3) is optimal within our numerical precision of 10^{-6}. The visibility required to observe a violation of the inequality in Eq. (2) is 91.7%, since the value for the maximally mixed state is $I_a = 0$. The visibility is defined as the minimal p required to obtain a violation assuming that the prepared state is a mixture of the target state and a completely mixed state, $\rho_{\mathrm{prepared}} = p|\psi\rangle\langle\psi| + (1-p)\rho_{\mathrm{mixed}}$.

We show in Sec. III A that the inequality in Eq. (2) holds already if only one of the measurements of either Alice or Bob is fundamentally binary. Therefore, the violation of the inequality in Eq. (2) allows us to make an even stronger statement, namely, that none of the measurements used is fundamentally binary, thus providing a device-independent certificate of the genuinely ternary character of all measurements in the experimental setup.

The conclusion at this point is that the violation of the inequality in Eq. (2) predicted by QT could be experimentally observable even achieving visibilities that have

been already attained in previous Bell-inequality experiments on qutrit–qutrit systems [13–15]. It is important to point out that, in addition, a compelling experiment requires that the local measurements are implemented as measurements with three outcomes rather than measurements that are effectively two-outcome measurements. That is, there should be a detector in each of the three possible outcomes of each party. The beauty of the inequality in Eq. (2) and the simplicity of the required state and measurements suggest that this experiment could be carried out in the near future.

B. Quantum n-ary correlations are not fundamentally $(n-1)$-ary

If our purpose is to test whether or not one particular measurement is fundamentally binary (rather than all of them), then it is enough to consider a simpler scenario where Alice has a two-outcome measurement $x = 0$ and a three-outcome measurement $x = 1$, while Bob has three two-outcome measurements $y = 0, 1, 2$. We show in Sec. III A that for the combination of correlations

$$I_b = -P(0,\_|0,\_) + \sum_{k=0,1,2} [P(0,0|0,k) - P(k,0|1,k)], \quad (6)$$

up to relabeling of the outcomes and Bob's measurement settings,

$$I_b \leq 1 \quad (7)$$

holds for nonsignaling correlations if and only if the correlations are fundamentally binary. According to QT, this bound can be violated with a value of

$$I_b = \sqrt{16/15} \approx 1.0328, \quad (8)$$

by preparing the state

$$|\psi\rangle = \frac{1}{\sqrt{(3\zeta+1)^2+2}}(|00\rangle + |11\rangle + |22\rangle + \zeta\,|\phi\rangle|\phi\rangle), \quad (9)$$

where $\zeta = -\frac{1}{3} + \frac{1}{6}\sqrt{10\sqrt{15} - 38} \approx -0.19095$, $|\phi\rangle = |0\rangle + |1\rangle + |2\rangle$, and choosing Alice's measurement $x = 0$ as $A_{0|0} = \mathbb{1} - A_{1|0}$, $A_{1|0} = |\phi\rangle\langle\phi|/3$, and measurement $x = 1$ as $A_{k|1} = |k\rangle\langle k|$, for $k = 0, 1, 2$, and Bob's measurements $y = 0, 1, 2$ as $B_{0|y} = \mathbb{1} - B_{1|y}$ and $B_{1|k} = |\eta_k\rangle\langle\eta_k|/\langle\eta_k|\eta_k\rangle$, where $|\eta_k\rangle = |k\rangle + \xi\,|\phi\rangle$, for $k = 0, 1, 2$, and $\xi = -\frac{1}{3} + \frac{1}{6}\sqrt{6\sqrt{15} + 22} \approx 0.78765$. [Another optimal solution is obtained by flipping the sign before the $(\frac{1}{6}\sqrt{})$-terms in ξ and ζ, yielding $\xi \approx -1.4543$ and $\zeta \approx -0.47572$.]

We use the third level of the NPA hierarchy to confirm that, within our numerical precision of 10^{-6}, the value in Eq. (8) is optimal. Notice, however, that the visibility required to observe a violation of the inequality in Eq. (7) is 96.9%. This contrasts with the 91.7% required for the inequality in Eq. (2) and shows how a larger number of outcomes allows us to certify more properties with a smaller visibility.

Nevertheless, what is interesting about the inequality in Eq. (7) is that it is a member of a family of inequalities and this family allows us to prove that, for any n, quantum n-ary correlations are not fundamentally $(n-1)$-ary, a problem left open in Ref. [3]. For that, we modify the scenario used for the inequality in Eq. (7), so that now Alice's measurement $x = 1$ has n outcomes, while Bob has n measurements with two outcomes. We let $I_b^{(n)}$ be as I_b defined in Eq. (6), with the only modification that in the sum, k takes values from 0 to $n-1$. Then,

$$I_b^{(n)} \leq n - 2 \quad (10)$$

is satisfied for all fundamentally $(n-1)$-ary correlations. The proof is given in Sec. III B. Clearly, the value $I_b^{(n)} = n - 2$ can already be reached by choosing the fixed local assignments where all measurements of Alice and Bob always have outcome $a, b = 0$. According to QT, it is possible to reach values of $I_b^{(n)} > (n-2) + 1/(4n^3)$, as can be found by generalizing the quantum construction from above to n-dimensional quantum systems with $\xi = \sqrt{2}$ and $\zeta = -1/n + 1/(\sqrt{2}n^2)$. Thus, the $(n-1)$-ary bound is violated already by n-ary quantum correlations. Note, that the maximal quantum violation is already very small for $n = 4$ as the bound from the third level of the NPA hierarchy is $I_b^{(4)} < 2.00959$.

III. METHODS

A. Restricted nonsignaling polytopes

We now detail the systematic method that allows us to obtain the inequalities in Eqs. (2), (7), and (10). We write $S = [a_1, a_2, \ldots, a_n : b_1, b_2, \ldots, b_m]$ for the case where Alice has n measurements and the first measurement has a_1 outcomes, the second a_2 outcomes, etc., and similarly for Bob and his m measurements with b_1, b_2,..., outcomes. The nonsignaling correlations for such a scenario form a polytope $C(S)$. For another bipartite scenario S' we consider all correlations $P' \in C(S')$ that can be obtained by local classical postprocessing from any $P \in C(S)$. The convex hull of these correlations is again a polytope and is denoted by $C(S \to S')$.

The simplest nontrivial polytope of fundamentally binary correlations is then $C([2, 2 : 2, 2] \to [3, 3 : 3, 3])$. We construct the vertices of this polytope and compute the 468 facet inequalities (i.e., tight inequalities for fundamentally binary correlations) with the help of the Fourier-Motzkin elimination implemented in the software `porta` [19]. We confirm the results by using the independent software `ppl` [20]. Up to relabeling of the outcomes, only the facet $I_a \leq 1$ is not a face of the set the nonsignaling correlations $C([3, 3 : 3, 3])$, which concludes our construction of I_a. In addition, we find that

$$C([2, 3 : 3, 3]) = C([2, 2 : 2, 2] \to [2, 3 : 3, 3]), \quad (11)$$

and therefore the inequality in Eq. (2) holds for all nonsignaling correlations where at least one of the measurements is fundamentally binary.

As a complementary question we consider the case where only a single measurement has three outcomes. According to Eq. (11), the smallest scenarios where such a verification is possible are $[2,3:2,2,2]$ and $[2,2:2,2,3]$. We first find that $C([2,2:3,3,3]) = C([2,2:2,2,2] \to [2,2:3,3,3])$, i.e., even if all of Bob's measurements would be fundamentally ternary, the correlations are always within the set of fundamentally binary correlations. Hence, we investigate the polytope $C([2,2:2,2,2] \to [2,3:2,2,2])$ and its 126 facets. Up to symmetries, only the facet $I_b \leq 1$ is not a face of $C([2,3:2,2,2])$.

Our method also covers other scenarios. As an example we study the polytope $C([2,4:2,4] \to [2,2,2:2,2,2])$ with its 14052 facets. In this case, the four-outcome measurements have to be distributed to two-outcome measurements (or the two-outcome measurement is used twice). Hence, this scenario is equivalent to the requirement that for each party at least two of the three measurements are compatible. The polytope has, up to relabeling, 10 facets that are not a face of $C([2,2,2:2,2,2])$. According to the fourth level of the NPA hierarchy, two of the facets may intersect with the quantum correlations. While for one of them the required visibility (with respect to correlations where all outcomes are equally probable) is at least 99.94%, the other requires a visibility of at least 97.88%. This latter facet is $I_c \leq 0$, where

$$\begin{aligned} I_c = &-P(10|00) - P(00|01) - P(00|10) - P(00|11) \\ &- P(10|12) - P(01|20) - P(01|21) + P(00|22). \end{aligned} \quad (12)$$

For arbitrary nonsignaling correlations, $I_c \leq 1/2$ is tight, while within QT, $I_c < 0.0324$ must hold. We can construct a numeric solution for two qutrits which matches the bound from the third level of the NPA hierarchy up to our numerical precision of 10^{-6}. The required quantum visibility then computes to 97.2%. The quantum optimum is reached for measurements $A_{0|k} = |\alpha_k\rangle\langle\alpha_k|$, $A_{1|k} = \mathbb{1} - A_{0|k}$, and $B_{0|k} = |\beta_k\rangle\langle\beta_k|$, $B_{1|k} = \mathbb{1} - B_{0|k}$, where all $|\alpha_k\rangle$ and $|\beta_k\rangle$ are normalized and $\langle\alpha_0|\alpha_1\rangle \approx 0.098$, $\langle\alpha_0|\alpha_2\rangle \approx 0.630$, $\langle\alpha_1|\alpha_2\rangle \approx 0.572$, and $\langle\beta_k|\beta_\ell\rangle \approx 0.771$ for $k \neq \ell$. A state achieving the maximal quantum value is $|\psi\rangle \approx 0.67931\,|00\rangle + 0.67605\,|11\rangle + 0.28548\,|22\rangle$. Note, that $I_c \approx 0.0318$ can still be reached according to QT, when Alice has only two incompatible measurements by choosing $\langle\alpha_0|\alpha_1\rangle = 0$. Curiously, the facet $I_c \leq 0$ is equal to the inequality M_{3322} in Ref. [21] and a violation of it has been observed recently by using photonic qubits [12]. However, while M_{3322} is the only nontrivial facet of the polytope investigated in Ref. [21], it is just one of several nontrivial facets in our case.

B. Proof of the inequality in Eq. (10)

Here, we show that for $(n-1)$-ary nonsignaling correlations, the inequality in Eq. (10) holds. We start by letting for some fixed index $0 \leq \ell < n$,

$$F = -\sum_b R_{0,b|0,\ell} + \sum_k [R_{0,0|0,k} - R_{k,0|1,k}], \quad (13a)$$

$$X_{1;a|x,y} = \sum_b (R_{a,b|x,y} - R_{a,b|x,\ell}), \quad (13b)$$

$$X_{2;b|x,y} = \sum_a (R_{a,b|x,y} - R_{a,b|0,y}), \quad (13c)$$

where all $R_{a,b|x,y}$ are linearly independent vectors from a real vector space V. Clearly, for any set of correlations, we can find a linear function $\phi\colon V \to \mathbb{R}$ with $\phi(R_{a,b|x,y}) = P(a,b|x,y)$. For such a function, $I_b^{(n)} = \phi(F)$ holds and $\phi(X_\tau) = 0$ are all the nonsignaling conditions. The maximal value of $I_b^{(n)}$ for $(n-1)$-ary nonsignaling correlations is therefore given by

$$\begin{aligned} \max_{\ell'} \max\{\phi(F) \mid\ & \phi\colon V \to \mathbb{R}, \text{ linear}, \\ & \phi(X_\tau) = 0, \text{ for all } \tau, \\ & \phi(R_{\ell',b|1,y}) = 0, \text{ for all } b, y, \\ & \textstyle\sum_\upsilon \phi(R_\upsilon) = 2n, \text{ and} \\ & \phi(R_\upsilon) \geq 0, \text{ for all } \upsilon\}. \end{aligned} \quad (14)$$

Since the value of the inner maximization does not depend on the choice of ℓ, we can choose $\ell = \ell'$. Equation (14) is a linear program, and the equivalent dual to this program can be written as

$$\max_\ell \min_{t,\boldsymbol{\xi},\boldsymbol{\eta}} \{\, t \mid t \geq \zeta_\upsilon \text{ for all } \upsilon \,\}, \quad (15)$$

where $\boldsymbol{\zeta}$ is the solution of

$$2nF - \sum_\tau \xi_\tau X_\tau - \sum_{b,y} \eta_{b,y} R_{\ell,b|1,y} = \sum_\upsilon \zeta_\upsilon R_\upsilon. \quad (16)$$

To obtain an upper bound in Eq. (15), we choose $\boldsymbol{\eta} \equiv 2n$ and all $\xi_\tau = 0$, but $\xi_{1;a|0,k} = 4$, $\xi_{1;k|1,k} = -2n$, $\xi_{2;b|1,\ell} = -3n+2$, and $\xi_{2;b|1,k} = -(-1)^b n + 2$, for $k \neq \ell$. This yields $\max_\upsilon \zeta_\upsilon = n-2$ for all ℓ and hence the $(n-1)$-ary nonsignaling correlations obey $I_b^{(n)} \leq n-2$.

IV. CONCLUSIONS

There was little chance to learn new physics from the recent loophole-free experiments of the Bell inequality [6–10]. Years of convincing experiments [22–24] allowed us to anticipate the conclusions: nature cannot be explained by local realistic theories [16], there are measurements for which there is not a joint probability distribution [25], and there are states that are not a convex combination of local states [26].

Here we have shown how to use Bell-type experiments to gain insights into QT. In Ref. [3], it was shown that QT predicts correlations that cannot be explained by nonsignaling correlations produced by fundamentally binary measurements (including Popescu–Rohrlich boxes

[17]). We proposed a feasible experiment which will allow us to either exclude all fundamentally binary probabilistic theories or to falsify QT. If the results of the experiment violate the inequality in Eq. (2), as predicted by QT, then we would learn that no fundamentally binary theory can possibly describe nature. In addition, it would prove that all involved measurements are genuine three-outcome measurements. If the inequality in Eq. (2) is not violated despite visibilities would *a priori* lead to such a violation, then we would have evidence that QT is wrong at a fundamental level (although being subtle to detect in experiments). We have also gone beyond Ref. [3] by showing that, for any n, already n-ary quantum correlations are not fundamentally $(n-1)$-ary.

ACKNOWLEDGMENTS

This work is supported by Project No. FIS2014-60843-P, "Advanced Quantum Information" (MINECO, Spain), with FEDER funds, the FQXi Large Grant "The Observer Observed: A Bayesian Route to the Reconstruction of Quantum Theory", the project "Photonic Quantum Information" (Knut and Alice Wallenberg Foundation, Sweden), the Hungarian National Research Fund OTKA (Grants No. K111734 and No. KH125096), the EU (ERC Starting Grant GEDENTQOPT), and the DFG (Forschungsstipendium KL 2726/2-1).

[1] G. Chiribella and R. W. Spekkens (eds.), *Quantum Theory: Informational Foundations and Foils*, Fundamental Theories of Physics, Vol. 181 (Springer, Dordrecht, Holland, 2016).

[2] M. Navascués, Y. Guryanova, M. J. Hoban, and A. Acín, Almost quantum correlations, Nat. Comm. **6**, 6288 (2015).

[3] M. Kleinmann and A. Cabello, Quantum Correlations Are Stronger Than All Nonsignaling Correlations Produced by n-Outcome Measurements, Phys. Rev. Lett. **117**, 150401 (2016).

[4] P. Busch, T. Heinosaari, J. Schultz, and N. Stevens, Comparing the degrees of incompatibility inherent in probabilistic physical theories, EPL **103**, 10002 (2013).

[5] A. Cabello, Simple Explanation of the Quantum Limits of Genuine n-Body Nonlocality, Phys. Rev. Lett. **114**, 220402 (2015).

[6] B. Hensen, H. Bernien, A. E. Dréau, A. Reiserer, N. Kalb, M. S. Blok, J. Ruitenberg, R. F. L. Vermeulen, R. N. Schouten, C. Abellán, W. Amaya, V. Pruneri, M. W. Mitchell, M. Markham, D. J. Twitchen, D. Elkouss, S. Wehner, T. H. Taminiau, and R. Hanson, Loophole-free Bell inequality violation using electron spins separated by 1.3 kilometres, Nature (London) **526**, 682 (2015).

[7] M. Giustina, M. A. M. Versteegh, S. Wengerowsky, J. Handsteiner, A. Hochrainer, K. Phelan, F. Steinlechner, J. Kofler, J.-Å. Larsson, C. Abellán, W. Amaya, V. Pruneri, M. W. Mitchell, J. Beyer, T. Gerrits, A. E. Lita, L. K. Shalm, S. W. Nam, T. Scheidl, R. Ursin, B. Wittmann, and A. Zeilinger, Significant-Loophole-Free Test of Bell's Theorem with Entangled Photons, Phys. Rev. Lett. **115**, 250401 (2015).

[8] L. K. Shalm, E. Meyer-Scott, B. G. Christensen, P. Bierhorst, M. A. Wayne, M. J. Stevens, T. Gerrits, S. Glancy, D. R. Hamel, M. S. Allman, K. J. Coakley, S. D. Dyer, C. Hodge, A. E. Lita, V. B. Verma, C. Lambrocco, E. Tortorici, A. L. Migdall, Y. Zhang, D. R. Kumor, W. H. Farr, F. Marsili, M. D. Shaw, J. A. Stern, C. Abellán, W. Amaya, V. Pruneri, T. Jennewein, M. W. Mitchell, P. G. Kwiat, J. C. Bienfang, R. P. Mirin, E. Knill, and S. W. Nam, Strong Loophole-Free Test of Local Realism, Phys. Rev. Lett. **115**, 250402 (2015).

[9] B. Hensen, N. Kalb, M. S. Blok, A. E. Dréau, A. Reiserer, R. F. L. Vermeulen, R. N. Schouten, M. Markham, D. J. Twitchen, K. Goodenough, D. Elkouss, S. Wehner, T. H. Taminiau, and R. Hanson, Loophole-free Bell test using electron spins in diamond: Second experiment and additional analysis Sci. Rep. **6**, 30289 (2016).

[10] W. Rosenfeld, D. Burchardt, R. Garthoff, K. Redeker, N. Ortegel, M. Rau, and H. Weinfurter, Event-Ready Bell Test Using Entangled Atoms Simultaneously Closing Detection and Locality Loopholes Phys. Rev. Lett. 119, 010402 (2017).

[11] H. S. Poh, S. K. Joshi, A. Cerè, A. Cabello, and C. Kurtsiefer, Approaching Tsirelson's Bound in a Photon Pair Experiment, Phys. Rev. Lett. **115**, 180408 (2015).

[12] B. G. Christensen, Y.-C. Liang, N. Brunner, N. Gisin, and P .G. Kwiat, Exploring the Limits of Quantum Nonlocality with Entangled Photons, Phys. Rev. X **5**, 041052 (2015).

[13] A. Vaziri, G. Weihs, and A. Zeilinger, Experimental Two-Photon, Three-Dimensional Entanglement for Quantum Communication, Phys. Rev. Lett. **89**, 240401 (2002).

[14] S. Gröblacher, T. Jennewein, A. Vaziri, G. Weihs, and A. Zeilinger, Experimental quantum cryptography with qutrits, New. J. Phys. **8**, 75 (2006).

[15] A. C. Dada, J. Leach, G. S. Buller, M. J. Padgett, and E. Andersson, Experimental high-dimensional two-photon entanglement and violations of generalized Bell inequalities, Nat. Phys. **7**, 677 (2011).

[16] J. S. Bell, On the Einstein Podolsky Rosen paradox, Physics (Long Island City, NY) **1**, 195 (1964).

[17] S. Popescu and D. Rohrlich, Quantum nonlocality as an axiom, Found. Phys. **24**, 379 (1994).

[18] M. Navascués, S. Pironio, and A. Acín, Bounding the Set of Quantum Correlations, Phys. Rev. Lett. **98**, 010401 (2007).

[19] POlyhedron Representation Transformation Algorithm, retrieved from `http://porta.zib.de/`.

[20] Parma Polyhedra Library, retrieved from `http://bugseng.com/products/ppl/`.

[21] N. Brunner, N. Gisin, and V. Scarani, Entanglement and non-locality are different resources, New. J. Phys. **7**, 88 (2005).

[22] S. J. Freedman and J. F. Clauser, Experimental Test of Local Hidden-Variable Theories,

Phys. Rev. Lett. **28**, 938 (1972).

[23] A. Aspect, J. Dalibard, and G. Roger, Experimental Test of Bell's Inequalities Using Time-Varying Analyzers, Phys. Rev. Lett. **49**, 1804 (1982).

[24] G. Weihs, T. Jennewein, C. Simon, H. Weinfurter, and A. Zeilinger, Violation of Bell's Inequality under Strict Einstein Locality Conditions, Phys. Rev. Lett. **81**, 5039 (1998).

[25] A. Fine, Hidden Variables, Joint Probability, and the Bell Inequalities, Phys. Rev. Lett. **48**, 291 (1982).

[26] R. F. Werner, Quantum states with Einstein-Podolsky-Rosen correlations admitting a hidden-variable model, Phys. Rev. A **40**, 4277 (1989).

Observation of Stronger-than-Binary Correlations with Entangled Photonic Qutrits

Xiao-Min Hu,[1,2] Bi-Heng Liu,[1,2,*] Yu Guo,[1,2] Guo-Yong Xiang,[1,2] Yun-Feng Huang,[1,2]
Chuan-Feng Li,[1,2,†] Guang-Can Guo,[1,2] Matthias Kleinmann,[3,4,‡] Tamás Vértesi,[5,§] and Adán Cabello[6,¶]

[1]*CAS Key Laboratory of Quantum Information, University of Science and Technology of China, Hefei, 230026, People's Republic of China*
[2]*Synergetic Innovation Center of Quantum Information and Quantum Physics, University of Science and Technology of China, Hefei, 230026, People's Republic of China*
[3]*Naturwissenschaftlich-Technische Fakultät, Universität Siegen, Walter-Flex-Straße 3, D-57068 Siegen, Germany*
[4]*Department of Theoretical Physics, University of the Basque Country UPV/EHU, P.O. Box 644, E-48080 Bilbao, Spain*
[5]*Institute for Nuclear Research, Hungarian Academy of Sciences, H-4001 Debrecen, P.O. Box 51, Hungary*
[6]*Departamento de Física Aplicada II, Universidad de Sevilla, E-41012 Sevilla, Spain*

(Dated: May 8, 2018)

We present the first experimental confirmation of the quantum-mechanical prediction of stronger-than-binary correlations. These are correlations that cannot be explained under the assumption that the occurrence of a particular outcome of an $n \geq 3$-outcome measurement is due to a two-step process in which, in the first step, some classical mechanism precludes $n-2$ of the outcomes and, in the second step, a binary measurement generates the outcome. Our experiment uses pairs of photonic qutrits distributed between two laboratories, where randomly chosen three-outcome measurements are performed. We report a violation by 9.3 standard deviations of the optimal inequality for nonsignaling binary correlations.

Introduction.—Quantum mechanics is so successful that it is difficult to imagine how to go beyond the present theory without contradicting existing experiments. However, going beyond our present understanding of quantum mechanics can enable us to solve long-standing problems like the formulation of quantum gravity. Some of the most puzzling questions in quantum theory are connected to the measurement process [1]. To go beyond our present understanding of measurements we use recent axiomatizations of quantum theory [2–6] that identify quantum theory as a special case within the general probabilistic theories. We identify an axiom related to the structure of measurements that can be modified in a way not contradicting existing experimental evidence, but making different predictions.

In quantum theory, two-outcome measurements are described by pairs of operators, $(E, \mathbb{1}-E)$. A quantum measurement is feasible whenever both operators are positive semidefinite. Conversely, in any general probabilistic theory, if $(\mathcal{E}_1, \mathcal{E}_2, \ldots, \mathcal{E}_n)$ represents a feasible n-outcome measurement, then any postprocessing to a two-outcome measurement $(\mathcal{E}'_1, \mathcal{E}'_2)$ is also a feasible measurement. However, according to quantum theory, $(E_1, E_2, \ldots, E_n)$ is already a feasible n-outcome measurement whenever all postprocessings to a two-outcome measurement $(E', \mathbb{1}-E')$ are feasible. This suggests a natural alternative, namely, that feasible n-outcome measurements are only those that can be implemented by selecting from two-outcome measurements. Such measurements are hence *binary* [7] and can be implemented as a two-step process in which, in the first step, some classical mechanism excludes all but two of the outcomes and, in a second step, the final output is produced by a genuine two-outcome measurement. The concept is illustrated in Fig. 1.

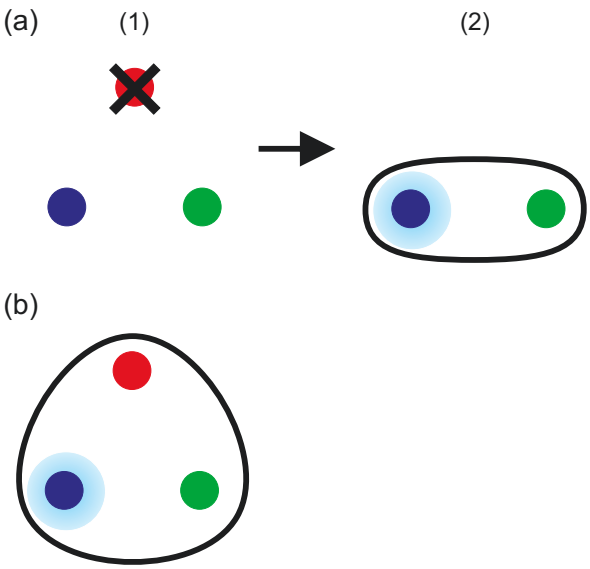

FIG. 1. Two possible explanations for the measurement process. Suppose a measurement with three possible outcomes represented by red, green, and blue lights. The process that generates the final outcome (represented by the blue light flashing) can be either (a) a sequence of two steps: (1) The red outcome is precluded by a classical mechanism (e.g., the initial position of the measured system). (2) A general two-outcome measurement selects between the two remaining outcomes. Or (b), the measurement is genuinely ternary in the sense that it cannot be explained as in (a).

Correlations between the outcomes of measurements performed by two parties, called Alice and Bob, are described by joint probabilities $P(a,b|x,y)$, where x and y are Alice's and Bob's measurement settings, respectively, and a and b are Alice's and Bob's measurement outcomes, respectively. *Binary nonsignaling correlations* are those which are both nonsignaling, i.e., $\sum_b P(a,b|x,y) \equiv P_A(a|x)$ and $\sum_a P(a,b|x,y) \equiv P_B(b|y)$, and have only two nontrivial outcomes, i.e., $P_A(a|x) = 0$ except for two outcomes a and $P_B(b|y) = 0$ except for two outcomes b, and the convex hull

thereof [7]. Such correlations also include cases that are forbidden in quantum theory as, for example, Popescu-Rohrlich boxes [8] maximally violating the Clauser-Horne-Shimony-Holt inequality [9]. Interestingly, according to quantum theory, there exist stronger-than-binary nonsignaling correlations [7]. A major problem, however, has been to identify how they can be actually observed.

The experiment presented here aims at the maximum violation predicted by quantum theory of the optimal and unique inequality [10] satisfied by binary nonsignaling correlations. The experiment is a bipartite Bell-type experiment in which Alice randomly chooses between two different measurements, $x = 0, 1$, each of them with three possible outcomes, $a = 0, 1, 2$, and Bob randomly chooses between two different measurements, $y = 0, 1$, each of them with three possible outcomes, $b = 0, 1, 2$. Binary nonsignaling correlations satisfy the inequality

$$I_a \leq 1, \tag{1}$$

where

$$I_a = \sum_{k,x,y=0,1} (-1)^{k+x+y} P(k, k|x, y), \tag{2}$$

and the outcomes $a = 2$ and $b = 2$ do not occur explicitly (see below). In contrast, according to quantum theory, the maximal value for I_a is

$$I_a = 2(2/3)^{3/2} \approx 1.089. \tag{3}$$

This maximum quantum value can be achieved by preparing two qutrits in a particular state and making some particular three-outcome local measurements (see below).

In the experiment we have obtained

$$I_a = 1.066 \pm 0.007 \tag{4}$$

which implies a violation of the inequality in Eq. (1) with a statistical significance corresponding to 9.4 standard deviations. A further analysis of the data (see below) shows that residual systematic errors do not explain this violation.

Consequently, general probabilistic theories in which n-outcome measurements are only binary are falsified by showing that there are correlations that are not binary nonsignaling. This also shows that, in nature, there are genuinely ternary measurements, thus demonstrating that the measurement process in quantum theory cannot be explained as a two-step process as in Fig. 1(a). In fact, the result of the experiment demonstrates that none of the four measurements (Alice's or Bob's) can be binary.

Bound on binary nonsignaling correlations.—The bound $I_a \leq 1$ in Eq. (1) has been proved in Ref. [10] by computer-based methods. Here we prove explicitly that the bound $I_a \leq 1$ in Eq. (1) is valid for binary nonsignaling correlations. We proceed by defining the auxiliary quantities

$$X_A = \sum_{a,b,x,y:\ a\neq 2} (-1)^{a+x+y} P(a, b|x, y) \text{ and} \tag{5a}$$

$$X_B = \sum_{a,b,x,y:\ b\neq 2} (-1)^{b+x+y} P(a, b|x, y). \tag{5b}$$

These clearly obey $X_A = 0$ and $X_B = 0$ for all nonsignaling correlations. We then have the inequality

$$3I_a - X_A - X_B \leq \sum_{a,b,x,y} P(a, b|x, y) \equiv 4, \tag{6}$$

which holds because the left-hand side of Eq. (6) has only coefficients ± 1. Consequently, $I_a \leq \frac{4}{3}$ holds for all nonsignaling correlations.

For the bound on binary nonsignaling correlations, it is enough to consider the extremal correlations. By definition, for those there exist certain indices $a_x \in \{0, 1, 2\}$ for $x = 0, 1$ and $b_y \in \{0, 1, 2\}$ for $y = 0, 1$ such that $P(a, b|x, y) = 0$ holds whenever $a = a_x$ or $b = b_y$. The reminder of the entries are then extremal two-outcome correlations and hence are either deterministic, $P(a, b|x, y) \in \{0, 1\}$, or they form a Popescu-Rohrlich box [8], implying $P(a, b|x, y) \in \{0, \frac{1}{2}\}$. As a consequence, the bound on I_a must be a multiple of $\frac{1}{2}$ and must not exceed $\frac{4}{3}$. This proves $I_a \leq 1$ for binary nonsignaling correlations. This bound is also tight as can be seen by considering the outcome assignment $a = x$ and $b = 2y$.

Experimental test.—Our experimental setup is described in Fig. 2 and further develops techniques from Refs. [11–13] optimized for testing the prediction in Eq. (3). The source generates the two-photon state

$$|\psi\rangle = (\sqrt{2}\,|H_u H_u\rangle + |V_u V_u\rangle - |H_l H_l\rangle)/2, \tag{7}$$

where H_u (V_u) denotes horizontal (vertical) polarization in the upper path and H_l denotes horizontal polarization in the lower path. Consequently, $|H_u\rangle$, $|V_u\rangle$, and $|H_l\rangle$ define a qutrit for Alice and for Bob. The visibility of the entangled state is 0.98 ± 0.01. Each photon of the pair is distributed to a different laboratory and measured there locally.

In each laboratory, the settings 0 and 1 are chosen randomly by means of a random number generator. The measurement outcomes for setting 0 are projectors onto the one-dimensional spaces spanned by

$$\begin{aligned}
|\eta_{0|0}\rangle &= (2\,|H_u\rangle - (1+\sqrt{3})\,|V_u\rangle - (1-\sqrt{3})\,|H_l\rangle)/\sqrt{12},\\
|\eta_{1|0}\rangle &= (2\,|H_u\rangle - (1-\sqrt{3})\,|V_u\rangle - (1+\sqrt{3})\,|H_l\rangle)/\sqrt{12},\\
|\eta_{2|0}\rangle &= (|H_u\rangle + |V_u\rangle + |H_l\rangle)/\sqrt{3},
\end{aligned} \tag{8}$$

where the projector onto $|\eta_{k|0}\rangle$ corresponds to outcome k. Similarly, for setting 1,

$$\begin{aligned}
|\eta_{0|1}\rangle &= (2\,|H_u\rangle + (1+\sqrt{3})\,|V_u\rangle + (1-\sqrt{3})\,|H_l\rangle)/\sqrt{12},\\
|\eta_{1|1}\rangle &= (2\,|H_u\rangle + (1-\sqrt{3})\,|V_u\rangle + (1+\sqrt{3})\,|H_l\rangle)/\sqrt{12},\\
|\eta_{2|1}\rangle &= (|H_u\rangle - |V_u\rangle - |H_l\rangle)/\sqrt{3}.
\end{aligned} \tag{9}$$

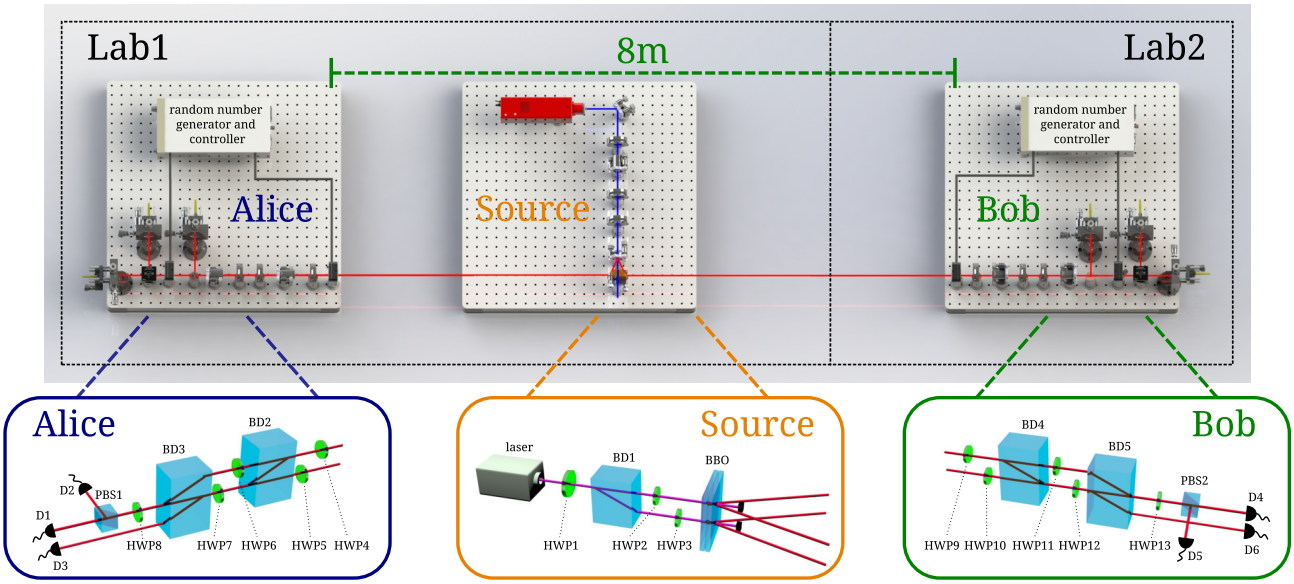

FIG. 2. **Experimental setup.** The source of pairs of photons and the first measurement party, Alice, are in laboratory Lab1, while the second measurement party, Bob, is in laboratory Lab2. The distance between Alice's and Bob's measurement setups is approximately 8 m. The pump laser is a continuous wave laser of 404 nm wavelength and 100 mW power. Subsequently, beam displacers are used to construct phase-stable interferometers. The beam displacers introduce a 4.21 mm displacement of the vertically polarized component; beam displacer BD1 operates at 404 nm and is approximately 36.41 mm long, beam displacers BD2–BD5 operate at 404 nm and are approximately 39.70 mm long. The pump beam is separated into two paths by means of the half wave plates HWP1–HWP3 and BD1, where the fast axis of HWP1 is oriented at 15° with respect to the horizontal axis, HWP2 is oriented at 27.37°, and HWP3 at 0°. After BD1 and HWP1–HWP3, the pump state is $(\sqrt{2}\,|V_u\rangle + |H_u\rangle - |V_l\rangle)/2$, where H (V) stands for horizontal (vertical) polarization and u (l) denotes the upper (lower) path. The two paths of the pump beam are then focused on two spots of two 0.5 mm thick type-I cut β-borate crystals (BBO) to generate the spatial mode and polarization mode hybrid entangled two-photon state $|\psi\rangle$; see Eq. (7). The local measurement setting 0, see Eq. (8), and 1, see Eq. (9), for Alice and Bob are constructed using the polarizing beam splitters PBS1 and PBS2, the half wave plates HWP4–HWP13, and BD2–BD4. The orientations of HWP4–HWP13 depend on the measurement setting and are chosen according to Table I. HWP4, HWP8, HWP9, and HWP13 are mounted in electric rotators to switch the measurement settings automatically and the random number generators Quantis-USB-4M (ID Quantique) are used to locally select the measurement basis. Six fiber coupled single photon detectors D1–D6 are used to detect the photons. Interference filters with a bandwidth of 3 nm are used before each detector to remove background photon noise (not shown). Coincidences between D1–D3 and D4–D6 are detected with the coincidence logic ID800 (ID Quantique, not shown), using a coincidence window of 3.2 ns.

These settings together with the state $|\psi\rangle$ yield the maximal quantum value of I_a; see Eq. (3). In our setup, the detectors D1–D3 correspond to outcomes 0–2 for Alice and the detectors D4–D6 correspond to outcomes 0–2 for Bob. The measurements are complete with respect to the qutrit space spanned by $|H_u\rangle$, $|V_u\rangle$, and $|H_l\rangle$, while any component of the incoming photon that is outside of the qutrit space remains undetected. In addition, the imperfect efficiency of the detectors, together with the coincidence logic, yield an overall detection efficiency of 0.087 ± 0.001. We account for both effects by implementing the fair sampling assumption, that the coincidences recorded are a representative subsample of what would have been recorded, if all photons were detected.

Data are collected in 4500 runs, with a collection time of 0.5 s for each run. Within each run, the measurement settings of Alice and Bob remain fixed. In total, 75 544 coincidences have been recorded.

Evaluation of the data.—The 4500 runs with random measurement settings for Alice and Bob, combine to 1060 complete data sets with all four combinations of settings and an average of 67.1 coincidences and for each complete set. We evaluate three conditions on the data: (i) normalization, i.e., whether $\sum_{a,b} N_r(a,b|x,y)$ is independent of x and y; (ii) nonsignaling, i.e., whether $\sum_a N_r(a,b|x,y)$ is independent of x and $\sum_b N_r(a,b|x,y)$ is independent of y; and (iii) binary correlations, tested by means of the inequality

$$\sum_{k,x,y=0,1} (-1)^{k+x+y} N_r(k,k|x,y) - \frac{1}{4} \sum_{a,b,x,y} N_r(a,b|x,y) \leq 0. \tag{10}$$

Hereby $N_r(a,b|x,y)$ denotes the number of coincidences for each of the complete data sets $r = 1, \ldots, 1060$ when the outcome of Alice (Bob) is a (b) and the setting is x (y). We compute the mean m and the variance v over the 1060 runs for each condition, so that $t = m\sqrt{1060/v}$ is distributed according to the Student-t distribution with $g = 1059$ degrees of

TABLE I. Angles of the fast axis of the half wave plates (HWPs) with respect to the horizontal axis as used in the measurement setups of Alice and Bob; see Fig. 2.

Measurement	HWP4 HWP9	HWP5 HWP10	HWP6 HWP11	HWP7 HWP12	HWP8 HWP13
Setting 0 (deg)	-22.5	0	45	17.63	37.5
Setting 1 (deg)	22.5	0	45	17.63	-37.5

TABLE II. p-values for (i) joint normalization conditions, (ii) joint nonsignaling conditions, and (iii) the inequality in Eq. (10). "Coin tosses" is q if the condition to hold is as plausible as obtaining q times heads in a row when tossing a fair coin. "Standard deviations" is s if the condition to hold is as plausible as obtaining a modulus greater than s from a normal distributed random variable.

Condition	p-value	Coin tosses	Standard deviations
Full data set using al 1060 repetitions: $I_a = 1.066 \pm 0.007$			
(i)	0.213	2.23	1.25
(ii)	3.66×10^{-4}	11.4	3.56
(iii)	5.95×10^{-21}	67.2	9.39
Reduced data set using every fifth data set: $I_a = 1.08 \pm 0.02$			
(i)	0.340	1.56	0.954
(ii)[a]	0.0592	4.08	1.89
(iii)	4.72×10^{-6}	17.7	4.58

[a] The χ^2 value is unexpectedly below the median of the χ^2 distribution and the p-value has been multiplied with a conservative factor of 2.

freedom. In this regime, after rescaling by $\sqrt{(g-2)/g}$, the Student-t distribution is very close to a normal distribution. We therefore obtain the p-value of the joint conditions (i) or (ii) using the χ^2 distribution, where there are three independent conditions in (i) and 11 independent conditions in (ii). The obtained values are given in Table II as "Full data set."

The full data set shows a violation of the inequality in Eq. (10) with a significance corresponding to 9.4 standard deviations. However, also the nonsignaling conditions (ii) are violated by 3.6 standard deviations. The origin of this apparent signaling is the unavoidable fluctuations in the pumping laser. This leads to statistically significant (apparent) signaling since the statistical error is smaller than the error due to the imperfections. A maximum-likelihood fit imposing the nonsignaling constraints increases the value of I_a, so that we conclude that the significance of the violation of I_a is nonetheless genuine. To further support this assertion, we reduce the set of samples so that the statistical error is again dominant and consider a reduced data set with only one-fifth of the complete data sets; see Table II, "Reduced data set." There, although the shot noise is increased by a factor of $\sqrt{5} \approx 2.2$, a violation of the inequality in Eq. (10) by 4.6 standard deviations remains, while the violation of the nonsignaling conditions becomes negligible.

Finally, we compute the empirical frequencies

$$P_r(a,b|x,y) = \frac{N_r(a,b|x,y)}{\sum_{a',b'} N_r(a',b'|x,y)} \tag{11}$$

for each r. This allows us to compute for each repetition the value of I_a. In Eq. (4) and Table II, we report the resulting mean value and standard error.

Conclusion.—We have presented an experimental violation with pairs of entangled qutrits of the optimal inequality for nonsignaling binary correlations. Our result (i) provides compelling evidence against two-step explanations of the measurement process, (ii) falsifies nonsignaling binary theories as possible descriptions of nature, apart from the detection and locality loopholes, and (iii) shows, apart from these loopholes, that in nature there exist stronger-than-binary nonsignaling correlations, i.e., correlations that, in particular, cannot be reproduced using Popescu-Rohrlich boxes. The experiment also illustrates how the maturity and refinement achieved by the experimental techniques developed for quantum communication and quantum information processing can be used to test subtle predictions of quantum theory and obtain detailed insights about how nature works.

Data repository.—The complete data set is publicly available by following the link in Ref. [14]. We encourage readers who want to expand our work with further data analysis to do so.

This work was supported by the National Key Research and Development Program of China (No. 2017YFA0304100), the National Natural Science Foundation of China (No. 11374288, No. 11274289, No. 61327901, No. 11474268, No. 11325419), the Key Research Program of Frontier Sciences, CAS (No. QYZDY-SSW-SLH003), the Fundamental Research Funds for the Central Universities, Projects No. FIS2014-60843-P, "Advanced Quantum Information," and No. FIS2015-67161-P, "Quantum Matter: From Principles to Applications" (MINECO, Spain), with FEDER funds, the FQXi Large Grant "The Observer Observed: A Bayesian Route to the Reconstruction of Quantum Theory," the DFG (Forschungsstipendium No. KL 2726/2-1), the Basque Government (Project No. IT986-16), the ERC (Starting Grant No. 258647/GEDENTQOPT and Consolidator Grant No. 683107/TempoQ), the National Research, Development and Innovation Office NKFIH (Hungary) (No. K111734 and No. KH125096), and by the Project "Photonic Quantum Information" (Knut and Alice Wallenberg Foundation, Sweden).

* bhliu@ustc.edu.cn
† cfli@ustc.edu.cn
‡ matthias.kleinmann@uni-siegen.de

§ tvertesi@atomki.mta.hu
¶ adan@us.es

[1] *Quantum Theory and Measurement*, edited by J. A. Wheeler and W. H. Zurek (Princeton University Press, Princeton, New Jersey, 1983).

[2] L. Hardy, Quantum theory from five reasonable axioms, quant-ph/0101012.

[3] B. Dakić and Č. Brukner, Quantum theory and beyond: Is entanglement special?, in *Deep Beauty. Understanding the Quantum World through Mathematical Innovation*, edited by H. Halvorson (Cambridge University Press, New York, 2011), p. 365.

[4] L. Masanes and M. P. Müller, A derivation of quantum theory from physical requirements, New J. Phys. **13**, 063001 (2011).

[5] G. Chiribella, G. M. D'Ariano, and P. Perinotti, Informational derivation of quantum theory, Phys. Rev. A **84**, 012311 (2011).

[6] L. Hardy, Reformulating and reconstructing quantum theory, arXiv:1104.2066.

[7] M. Kleinmann and A. Cabello, Quantum Correlations are Stronger than All Nonsignaling Correlations Produced by n-Outcome Measurements, Phys. Rev. Lett. **117**, 150401 (2016).

[8] S. Popescu and D. Rohrlich, Quantum nonlocality as an axiom, Found. Phys. **24**, 379 (1994).

[9] J. F. Clauser, M. A. Horne, A. Shimony, and R. A. Holt, Proposed Experiment to Test Local Hidden-Variable Theories, Phys. Rev. Lett. **23**, 880 (1969).

[10] M. Kleinmann, T. Vértesi, and A. Cabello, Proposed experiment to test fundamentally binary theories, Phys. Rev. A **96**, 032104 (2017).

[11] P. G. Kwiat, K. Mattle, H. Weinfurter, A. Zeilinger, A. V. Sergienko, and Y. Shih, New High-Intensity Source of Polarization-Entangled Photon Pairs, Phys. Rev. Lett. **75**, 4337 (1995).

[12] Y.-F. Huang, M. Li, D.-Y. Cao, C. Zhang, Y.-S. Zhang, B.-H. Liu, C.-F. Li, and G.-C. Guo, Experimental test of state-independent quantum contextuality of an indivisible quantum system, Phys. Rev. A **87**, 052133 (2013).

[13] X. M. Hu, J. S. Chen, B. H. Liu, Y. Guo, Y. F. Huang, Z. Q. Zhou, Y. J. Han, C. F. Li, and G. C. Guo, Experimental Test of Compatibility-Loophole-Free Contextuality with Spatially Separated Entangled Qutrits, Phys. Rev. Lett. **117**, 170403 (2016).

[14] See `http://personal.us.es/adan/binary.htm`.

Entanglement between two spatially separated atomic modes

Karsten Lange,[1] Jan Peise,[1] Bernd Lücke,[1] Ilka Kruse,[1] Giuseppe Vitagliano,[2,3]
Iagoba Apellaniz,[3] Matthias Kleinmann,[3] Géza Tóth,[3,4,5] Carsten Klempt[1*]
[1] *Institut für Quantenoptik, Leibniz Universität Hannover, Welfengarten 1, D-30167 Hannover, Germany*
[2] *Institute for Quantum Optics and Quantum Information (IQOQI), Austrian Academy of Sciences, Boltzmanngasse 3, A-1090 Vienna, Austria*
[3] *Department of Theoretical Physics, University of the Basque Country UPV/EHU, P.O. Box 644, E-48080 Bilbao, Spain*
[4] *IKERBASQUE, Basque Foundation for Science, E-48013 Bilbao, Spain*
[5] *Wigner Research Centre for Physics, Hungarian Academy of Sciences, P.O. Box 49, H-1525 Budapest, Hungary*
[*] *E-mail: klempt@iqo.uni-hannover.de*

Modern quantum technologies in the fields of quantum computing, quantum simulation and quantum metrology require the creation and control of large ensembles of entangled particles. In ultracold ensembles of neutral atoms, highly entangled states containing thousands of particles have been generated, outnumbering any other physical system by orders of magnitude. The entanglement generation relies on the fundamental particle-exchange symmetry in ensembles of identical particles, which lacks the standard notion of entanglement between clearly definable subsystems. Here we present the generation of entanglement between two spatially separated clouds by splitting an ensemble of ultracold identical particles. Since the clouds can be addressed individually, our experiments open a path to exploit the available entangled states of indistinguishable particles for quantum information applications.

The progress towards large ensembles of entangled particles is pursued along two different paths. In a bottom-up approach, the precise control and characterization of small systems of ions and photons is pushed towards increasingly large system sizes, reaching entangled states of 14 ions [1] or 10 photons [2]. Complementary, large numbers of up to 3,000 entangled ultracold atoms [3–5] can be generated, where the state characterization is advanced top-down towards resolving correlations on the single-particle level. Because the atoms cannot be addressed individually, ultracold atomic ensembles are controlled by global ensemble parameters, such as the total spin. Ideally, the atoms are indistinguishable, either with respect to the observable, such as the spin in hot vapor cells [6], or in all quantum numbers in Bose-Einstein condensates (BECs) [7–12]. Is it possible to make these particles distinguishable — and addressable — again, while keeping the high level of entanglement?

The generation of entanglement in these systems is deeply connected with the fundamental indistinguishability of the particles [13]. As an example, two indistinguishable bosons 1 and 2, that are prepared in two independent modes a and b, are described by an entangled triplet state $\frac{1}{\sqrt{2}}(|\mathrm{a}\rangle_1 |\mathrm{b}\rangle_2 + |\mathrm{b}\rangle_1 |\mathrm{a}\rangle_2)$ due to bosonic symmetrization. Although this type of entanglement seems to be artificial, the state presents a resource for a Bell measurement [14]. Equivalently, an ensemble containing the same number of distinguishable spin-up and spin-down atoms is not necessarily entangled, while a twin-Fock state, the corresponding ensemble with indistinguishable bosons, exhibits full

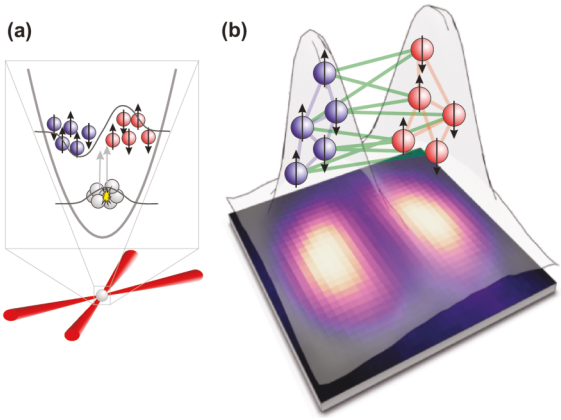

FIG. 1. **Generation of entanglement between two spatially separated atomic clouds. (a)** A Bose-Einstein condensate of atoms in the Zeeman level $m_F = 0$ is prepared in a crossed-beam optical trap. Collisions generate entangled pairs of atoms in the levels $m_F = \pm 1$ (spin up/down), in the first spatially excited mode. The created multi-particle entangled ensemble is naturally divided into two clouds (red and blue). **(b)** The atomic density profile obtained from an average over 3,329 measurements is shown in the background. The entanglement between the two clouds (indicated by green lines) in the system can be detected by analyzing spin correlations.

many-particle entanglement [15, 16]. This form of entanglement is directly applicable for atom interferometry beyond the Standard Quantum Limit [10]. However, most quantum information tasks require an individual addressing of sub-systems. Despite the experimental progress in entanglement creation in BECs, including the demonstration of Einstein-Podolsky-Rosen correlations [17] and Bell correlations [18–20], as well as the demonstration of strongly correlated momentum states [21–23], a proof of entanglement between spatially separated and individually addressable subsystems has not been realized so far. The possible applications of such a resource reach far beyond quantum information, ranging from spatially resolved quantum metrology to tests for fundamental sources of decoherence or Bell tests of quantum nonlocality.

In this Letter, we report the creation of particle entanglement in an ensemble of up to 5,000 indistinguishable atoms and prove entanglement between two spatially separated clouds. We utilize spin dynamics in a spinor BEC to create highly entangled twin-Fock states in a single spatial mode, which naturally splits into two independent parts. We record strong spin correlations between the resulting two atomic clouds, and derive a criterion to prove their entanglement. Our results thus demonstrate that the created entanglement of indistinguishable particles can be converted into entanglement of spatially separated clouds, which can be addressed individually. The concept can be extended to larger numbers of subsystems, down to single particles in an optical lattice, and opens a path to create highly entangled states for numerous applications in quantum information. For example, it presents a resource to synthesize any pure symmetric state with only single-particle projective measurements [24, 25].

Our experiments start with the preparation of a ^{87}Rb Bose-Einstein condensate in a crossed-beam optical dipole trap. The ensemble of 20,000 particles is transferred to the hyperfine level $F = 1, m_F = 0$. Spin-changing collisions create entangled atom pairs in the Zeeman levels $m_F = \pm 1$, where both atoms reside in a spatially excited mode of the dipole trap [26, 27] (see Fig. 1). The output state consists of a superposition of twin-Fock states with an equal number of atoms $N_{\pm 1}$ in the two Zeeman levels $m_F = \pm 1$ [10]. Since the total number of particles is measured during detection, the system is well described by single twin-Fock states with one defined particle number. Self-similar expansion [27] allows for an imaging of the undistorted but magnified density profiles. An inhomogeneous magnetic field separates the atoms to record the atomic densities for each Zeeman level.

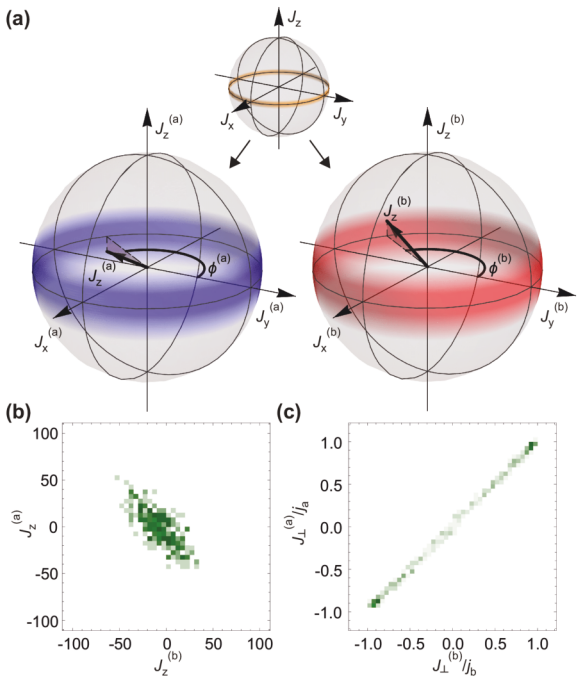

FIG. 2. **Spin correlations between the clouds a and b.** **(a)** A twin-Fock state is represented by a narrow ring on the equator of the multi-particle Bloch sphere (orange). When the system is split into two parts a (blue) and b (red), the states in the single subsystems seem to gain uncertainty. However, a measurement of $J_z^{(b)}$ or $\phi^{(b)}$ on cloud b allows for a prediction of the measurement outcome of cloud a, such that $J_z^{(a)} = -J_z^{(b)}$ or $\phi^{(a)} \approx \phi^{(b)}$. **(b)** Histogram of 506 measurements of $J_z^{(a)}$ and $J_z^{(b)}$ for a mean total number of 3,460 atoms. The data show the anticipated anti-correlation between $J_z^{(a)}$ and $J_z^{(b)}$. **(c)** The strong correlations between the angles $\phi^{(a)}$ and $\phi^{(b)}$ are recorded by a measurement of their projection on an arbitrary axis $J_\perp$ in the $x-y$ plane. The histogram of $J_\perp^{(a)}/j_a$ and $J_\perp^{(b)}/j_b$ (487 measurements) also reflects the projection of a ring onto its diameter.

The spatially excited mode of the ensembles in $m_F = \pm 1$ provides a natural splitting into a left and right cloud along a line of zero density. Hence, we divide the initial twin-Fock state into two spatially separated parts $|a\rangle$ (left side) and $|b\rangle$ (right side). This process can be described as a beam splitter of the initially populated antisymmetric input mode $\frac{1}{\sqrt{2}}(|a\rangle - |b\rangle)$.

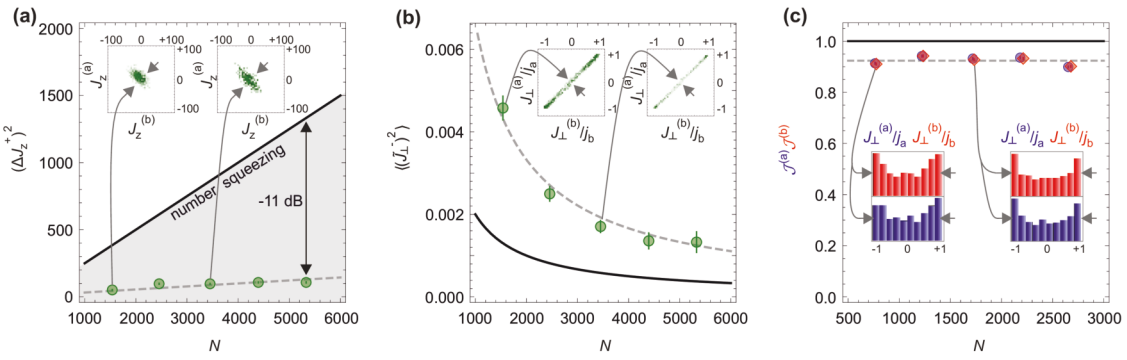

FIG. 3. **Spin correlations as a function of the total number of atoms N. (a)** The prediction variance $(\Delta J_z^+)^2$ (green circles) surpasses the shot-noise limit (black solid line), indicating number squeezing of up to $-11.0(5)$ dB. The number-dependent detection noise is modeled by a linear fit (gray dashed line). **(b)** The fluctuations $\langle(\tilde{J}_\perp^-)^2\rangle = \langle(\tilde{J}_x^-)^2\rangle = \langle(\tilde{J}_y^-)^2\rangle$ (green circles), corresponding to the phase prediction variance in the experiment, show excess noise, which increases the standard deviation by a factor of 1.8 (gray dashed line) above the shot-noise limited case (black solid line). **(c)** $\mathcal{J}^{(a)}$ and $\mathcal{J}^{(b)}$ quantify the symmetry of the states. The value 1 for purely symmetric states is indicated in black, the mean experimental value in gray. In all panels, the total number of atoms N equals the mean of all experimental realizations within an interval of 1,000. The error bars represent one standard deviation of the statistical fluctuations and are obtained via a bootstrapping method (see Supplemental Material).

The splitting introduces additional quantum noise due to a coupling with the (empty) symmetric input mode $\frac{1}{\sqrt{2}}(|\mathrm{a}\rangle + |\mathrm{b}\rangle)$. In principle, an ideal twin-Fock state shows a maximal entanglement depth [15], i.e. all atoms that make up a twin-Fock state are entangled with each other. Therefore, any splitting results in the appearance of quantum correlations between the clouds.

The resulting quantum correlations can be visualized on the multi-particle Bloch sphere (see Fig. 2(a)). Here, the atoms in the levels $m_F = \pm 1$ are represented by spin-$\frac{1}{2}$ particles, whose spins $\mathbf{j}^{(k)}$ sum up to a total spin $\mathbf{J}$. On the Bloch sphere, the lines of latitude represent the number imbalance between the two levels and the lines of longitude represent the phase difference. An ensemble in a twin-Fock state can be depicted as a ring on the Bloch sphere, characterized by a vanishing imbalance, $J_\mathrm{z} = (N_{+1} - N_{-1})/2 = 0$, and an undetermined phase difference.

If we divide the cloud, the collective spins $\mathbf{J}^{(\mathrm{a})}, \mathbf{J}^{(\mathrm{b})}$ of the two parts have to sum up to the original collective spin of the full ensemble $\mathbf{J} = \mathbf{J}^{(\mathrm{a})} + \mathbf{J}^{(\mathrm{b})}$. Therefore, the z components of the collective spins are perfectly anti-correlated $J_\mathrm{z}^{(\mathrm{a})} + J_\mathrm{z}^{(\mathrm{b})} = 0$. Furthermore, since the spin length $|\mathbf{J}|$ is maximal, the collective spins of the two parts have to point in a similar direction in the $\mathrm{x}-\mathrm{y}$ plane and thus have similar azimuthal angles $\phi^{(\mathrm{a})} \approx \phi^{(\mathrm{b})}$.

Hence, if the particle number difference of cloud b is measured to yield $J_\mathrm{z}^{(\mathrm{b})}$, the conditioned state of cloud a satisfies $J_\mathrm{z}^{(\mathrm{a})} = -J_\mathrm{z}^{(\mathrm{b})}$. If the value $J_\mathrm{x}^{(\mathrm{b})}$ ($J_\mathrm{y}^{(\mathrm{b})}$) is measured on cloud b, the state of cloud a has to fulfill $J_\mathrm{x}^{(\mathrm{a})} \approx J_\mathrm{x}^{(\mathrm{b})}$ ($J_\mathrm{y}^{(\mathrm{a})} \approx J_\mathrm{y}^{(\mathrm{b})}$). In summary, the different possible measurements on cloud b yield precise predictions for the measurement results of cloud a, which cannot be explained by a single quantum state that is independent of the chosen type of measurement. In this sense, the described system is analogous to the thought experiment by Einstein, Podolsky and Rosen [28], where entanglement is witnessed by the variances of the predictions [29, 30]. Is it thus possible to detect entanglement between the spatially separated parts of a twin-Fock state?

To this end, we derive an entanglement criterion, which optimally exploits the described spin correlations (see Supplemental Material). The spin correlations are represented by prediction operators $J_\mathrm{z}^+ = J_\mathrm{z}^{(\mathrm{a})} + J_\mathrm{z}^{(\mathrm{b})}$, and $\tilde{J}_m^- = \tilde{J}_m^{(\mathrm{a})} - \tilde{J}_m^{(\mathrm{b})}$ for $m = \mathrm{x}, \mathrm{y}$. Here, the x and y components are normalized, such that the optimal value is 1, according to $\tilde{J}_m^{(n)} = \frac{J_m^{(n)}/j_n}{\mathcal{J}^{(n)}}$

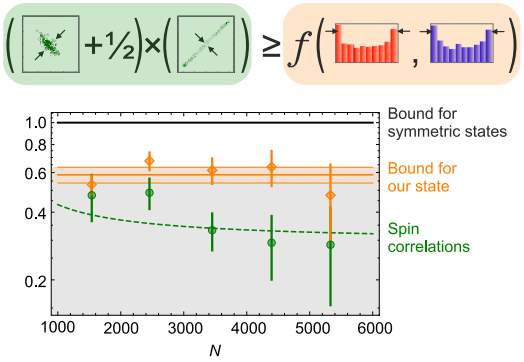

FIG. 4. **Violation of the separability criterion as a function of the total number of atoms N.** The black line represents the right-hand side (RHS) of equation (1) for the ideal case. The orange line represents the mean of the experimental results (orange diamonds) of the RHS of equation (1), where the spin length is reduced. The green circles show the experimental results for the left-hand side (LHS) of equation (1). The dashed green line indicates the prediction of the LHS corresponding to the gray lines in Fig. 3. The spin correlations clearly violate the criterion by 2.8 standard deviations at a mean total number of 3,460 atoms. The error bars and shaded orange area indicate one standard deviation and are obtained via a bootstrapping method (see Supplemental Material).

with $\mathcal{J}^{(n)} = \left\langle \frac{(J_{\mathrm{x}}^{(n)})^2+(J_{\mathrm{y}}^{(n)})^2}{j_n^2} \right\rangle^{\frac{1}{2}}$ and the spin length $j_n = N_n/2$ for $n = \mathrm{a}, \mathrm{b}$. We arrive at a simple separability criterion

$$\left[(\Delta J_{\mathrm{z}}^{+})^2 + \tfrac{1}{2}\right]\left[\langle(\tilde{J}_{\mathrm{x}}^{-})^2 + (\tilde{J}_{\mathrm{y}}^{-})^2\rangle\right] \geq f\left(\mathcal{J}^{(\mathrm{a})}, \mathcal{J}^{(\mathrm{b})}\right), \tag{1}$$

where $f(x,y) = \frac{(x^2+y^2-1)^2}{xy}$. Any separable state, including mixtures of product states of the form $\sum_k p_k |\Psi_k^{(\mathrm{a})}\rangle\langle\Psi_k^{(\mathrm{a})}| \otimes |\Psi_k^{(\mathrm{b})}\rangle\langle\Psi_k^{(\mathrm{b})}|$ with a fluctuating number of particles, fulfills this inequality. A violation of this criterion indicates that the state is inseparable and therefore entangled. For perfectly symmetric states, as we would expect in the ideal case, the right-hand side (RHS) of the equation is equal to 1. Any deterioration from perfect symmetry is quantified by $\mathcal{J}^{(\mathrm{a})}$ and $\mathcal{J}^{(\mathrm{b})}$. The inequality has similarities to the famous EPR criterion [31] due to the characteristic product of the uncertainties. It presents a general entanglement criterion, which is particularly sensitive for a spatially separated twin-Fock state.

An application of criterion (1) requires an evaluation of the spin correlations between the two clouds a and b. The measurement results for $J_{\mathrm{z}}^{(\mathrm{a})}$ and $J_{\mathrm{z}}^{(\mathrm{b})}$ are readily obtained from the absorption images. The measurement of the orthogonal direction is performed by a sequence of resonant microwave pulses prior to the particle number detection (see Supplemental Material). The pulses lead to an effective rotation of the spins by $\pi/2$. Because the microwave phase is independent of the atomic phases, the rotation yields a measurement of the spin component $J_\perp$ along an arbitrary angle in the $\mathrm{x}-\mathrm{y}$ plane. Since our quantum state is symmetric under rotations around the z axis, both due to the initial symmetry and the influence of magnetic field noise, the measured distributions of $J_\perp$ can be identified with both J_{x} and J_{y}. Interestingly, the performed measurement of $J_\perp$ is the realization of a measurement scheme to demonstrate the violation of a Bell inequality [32], if local addressing and a single-particle-resolving atom counting is added.

Figure 2 shows the histograms of J_{z} and $J_\perp/j$ for a mean total number of 3,460 particles in both clouds. The J_{z} data show the expected anti-correlation, while the $J_\perp$ measurements are strongly correlated. The $J_\perp$ histogram also shows pronounced peaks at the edges, reflecting the projection of a ring onto its diameter. The strength of these correlations can be quantified by evaluating the prediction uncertainties — the width of the distributions in the diagonal directions in the histograms, i.e. $(\Delta J_{\mathrm{z}}^{+})^2$ and $\langle(\tilde{J}_\perp^{-})^2\rangle$.

Figure 3(a) presents the prediction variance $(\Delta J_{\mathrm{z}}^{+})^2$ as a function of the total number of atoms. The shown fluctuations, obtained by subtracting independent detection noise, remain well below the shot-noise limit, and are equivalent to a number squeezing of $-11.0(5)$ dB. The orthogonal quantities (Fig. 3(b)) are slightly influenced by technical noise due to small position fluctuations of the clouds, increasing the standard deviation by a factor of 1.8 above shot noise. Figure 3(c) shows the quantities $\mathcal{J}^{(\mathrm{a})}$, $\mathcal{J}^{(\mathrm{b})}$. We obtain a value of up to 0.94, close to the ideal value of 1, indicating a sufficiently clean preparation of an almost symmetric state.

From these results, we can test a violation of the separability criterion. In Fig. 4, the orange diamonds correspond to an evaluation of the RHS of the criterion, which would ideally be 1 (black line). The left-hand side (LHS), represented by the green circles, is well below the RHS, signaling entanglement in the system. At the best value at a total number of 3,460

atoms, the experimental data violates the separability criterion by 2.8 standard deviations. Therefore, our measurements cannot result from classical correlations and prove the generation of entanglement between spatially separated clouds from particle-entangled, indistinguishable atoms.

Complementary to our work, the group of M. Oberthaler has observed spatially distributed multipartite entanglement and the group of P. Treutlein has observed spatial entanglement patterns.

ACKNOWLEDGMENTS

C.K. thanks M. Cramer for the discussion at the 589. Heraeus seminar that led to the initial idea for the experiments, and A. Smerzi for regular discussions and a review of the manuscript. This work was supported by the EU (ERC Starting Grant 258647/GEDENTQOPT, CHIST-ERA QUASAR, COST Action CA15220), the Spanish Ministry of Economy, Industry and Competitiveness and the European Regional Development Fund FEDER through Grant No. FIS2015-67161-P (MINECO/FEDER), the Basque Government (Project No. IT986-16), the National Research Fund of Hungary OTKA (Contract No. K83858), the DFG (Forschungsstipendium KL 2726/2-1), the FQXi (Grant No. FQXi-RFP-1608), and the Austrian Science Fund (FWF) through the START project Y879-N27. We also acknowledge support from the Deutsche Forschungsgemeinschaft (DFG) through RTG 1729 and CRC 1227 (DQ-mat), project A02.

SUPPLEMENTAL MATERIAL

Experimental sequence and analysis. The experimental procedure and evaluation, as well as a discussion of the number-dependent detection noise can be found in detail in the Supplemental Material of Ref. [15].

We alternate between the experiments for the two measurement directions J_z and $J_\perp$ to minimize the influence of changing ambiance conditions. Both measurements start with the same experimental sequence. A BEC is prepared in a crossed-beam optical dipole trap in the state $F = 1, m_F = 0$.

A red-detuned microwave dressing field with a detuning of 206 kHz couples the levels $F = 1, m_F = -1$ and $F = 2, m_F = -2$. This induces an energy shift of the levels such that a resonance condition for spin-changing collisions from $F = 1, m_F = 0$ to $F = 1, m_F = \pm 1$ is reached [15]. At the resonance, the energy of two atoms in the $m_F = 0$ state is equal to the energy of two atoms in $m_F = \pm 1$ plus the energy of the excitation to the first spatially excited mode. This pair creation process, producing a pair of entangled atoms in $m_F = \pm 1$, is subject to bosonic enhancement, creating further pairs in the same mode during an interaction time of $t = 180\,\mathrm{ms}$. Due to the nature of the spin-changing collisions, the $F = 1, m_F = \pm 1$ levels are populated with a two-mode squeezed state. The two-mode squeezed state consists of a superposition of twin-Fock states $\sum_n c_n \left|n\right\rangle_{+1} \left|n\right\rangle_{-1}$ with an equal number of atoms $N_{\pm 1}$ in the two Zeeman levels $m_F = \pm 1$. The weight $c_n = \frac{(-i \tanh \xi)^n}{\cosh \xi}$ corresponds to a squeezing strength $\xi = \Omega t$ and a spin dynamics rate $\Omega = 2\pi \times 6.6\,\mathrm{Hz}$. The final measurement of the total number of atoms collapses the state onto a twin-Fock state. The measurement of J_z is now a measurement of the atom numbers in the two levels $m_F = \pm 1$ of the $F = 1$ manifold. However, to keep the two experimental procedures as similar as possible, the ensembles are transferred to the $F = 2$ manifold before detection. To this end, the pulse sequence of the transfer pulses (II-IV) is reversed for the J_z measurements with respect to the $J_\perp$ measurement (see Fig. 5).

The measurement in the orthogonal direction requires a rotation around an axis perpendicular to J_z. This is achieved by a coupling of the ensembles in $F = 1, m_F = \pm 1$ by an effective $\pi/2$ pulse. Since the microwave phase is not synchronized to the atomic phases, the rotation leads to a measurement of $J_\perp$ along an arbitrary direction in the x − y plane. However, the state is fully characterized due to its perfect symmetry under rotations around the z axis. Firstly, an ideal twin-Fock state is symmetric itself, and secondly, the experimentally realized state is randomized over J_z rotations due to the influence of magnetic field noise. Therefore, the measurement of $J_\perp$ is sufficient. The detection is again realized in the $F = 2$ manifold with the $m_F = \pm 1$ ensembles occupying $F = 2, m_F = -2$ and $F = 2, m_F = 0$. The large condensate from $m_F = 0$ is mainly transferred to $F = 2, m_F = -1$ with a small fraction transferred to $F = 2, m_F = 1$.

The experimental sequence ends with the detection of the atomic ensembles. The dipole trap is switched off to allow for 7.5 ms of self-similar expansion. The mode profiles remain undistorted but magnified due to

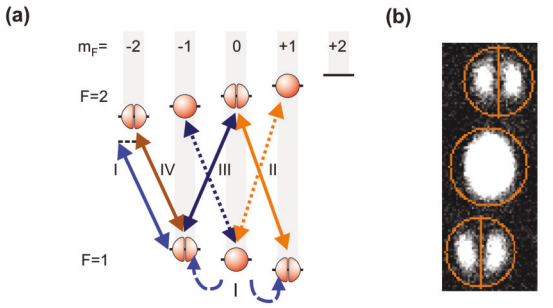

FIG. 5. **Experimental techniques. (a)** Experimental procedure for the measurement of $J_\perp$. The sequence starts with a BEC in the $|F = 1, m_F = 0\rangle$ Zeeman level .(I) A microwave dressing field (solid blue line) induces a resonance condition for spin-changing collisions, allowing for the population of the $|1, \pm 1\rangle$ levels with a twin-Fock state (dashed blue line). (II) The population in $|1, 1\rangle$ is completely transferred to $|2, 0\rangle$ via a microwave transfer (solid orange arrows). This also leads to a population of $|2, 1\rangle$ with atoms from $|1, 0\rangle$ (dotted orange line). (III) A coupling between the two levels populated by the twin-Fock state is induced by a $\pi/2$ microwave pulse (solid dark blue line). This coupling is also resonant to the transition $|1, 0\rangle \rightarrow |2, -1\rangle$, populating the $|2, -1\rangle$ level (dotted dark blue line). (IV) To avoid an overlap in the detection of the atoms in $|1, -1\rangle$ and $|2, 1\rangle$ the ensemble from $|1, -1\rangle$ is transferred to $|2, -2\rangle$ (solid dark orange line). **(b)** Single-shot absorption image with read-out masks indicated in orange. The position of the masks is determined by the center of mass of the central atomic cloud. The other two masks, as well as the cutting lines, are fixed with respect to the central cloud. The atom numbers in all four sub-masks are evaluated by summing over the column densities in the appropriate sub-masks.

the interaction of the ensembles with the large condensate remaining in the $F = 2, m_F = -1$ state [33]. After the initial mean-field dominated expansion, a strong magnetic field gradient is applied to spatially separate the atoms in the populated Zeeman levels. Finally, the number of atoms in the clouds is detected by absorption imaging on a CCD camera with a large quantum efficiency.

The absorption images are used to detect the number of atoms in the two spatially separated clouds. The center of mass of the large condensate in the $F = 2, m_F = -1$ level is used as a reference for the position of all clouds (see Fig. 5(b)). This is necessary due to slight shot-to-shot variations of the position, which result from minute position changes of the dipole trap. The position of the masks for the ensembles in $F = 2, m_F = \{-2, 0\}$ (formerly $F = 1, m_F = \pm 1$), as well as the cutting line for the parts a (left) and b (right), is fixed with respect to this reference. The number of atoms in the four resulting sub-masks is then obtained by summing over the column density of the absorption image to record the spin fluctuations and prove entanglement between the spatially separated atomic clouds.

To utilize the created state for quantum information tasks, it can be transferred into an optical lattice, where all constituent particles are individually addressable. As a concrete example, single-atom projective measurements on one half of this highly entangled ensemble allow to synthesize any pure symmetric quantum state in the second half [24, 25].

Bootstrapping. The error bars in Figs. 3 and 4 are obtained via a bootstrapping method. We created 10,000 random data sets on the basis of the distributions of the experimental data. We then calculated the standard deviations of the measured quantities from these 10,000 samples and checked that the percentage of violations of equation (1) was consistent with the reported significance.

Proof of equation (1).

We start from the sum of two Heisenberg uncertainty relations $(\Delta J_\mathrm{z})^2[(\Delta J_\mathrm{x})^2 + (\Delta J_\mathrm{y})^2] \geq \frac{1}{4}(\langle J_\mathrm{x}\rangle^2 + \langle J_\mathrm{y}\rangle^2)$. Simple algebra yields

$$\left[(\Delta J_\mathrm{z})^2 + \frac{1}{4}\right] \times \frac{(\Delta J_\mathrm{x})^2 + (\Delta J_\mathrm{y})^2}{\langle J_\mathrm{x}^2\rangle + \langle J_\mathrm{y}^2\rangle} \geq \frac{1}{4}. \qquad (2)$$

Here, the first factor represents the fluctuations in the particle number difference and the second term represents the fluctuations in the phase difference.

Product states. First, we consider product states of the form $|\Psi^{(\mathrm{a})}\rangle \otimes |\Psi^{(\mathrm{b})}\rangle$. For such states

$$\begin{aligned}\left[(\Delta J_\mathrm{z}^+)^2 + \frac{1}{2}\right] &\times \left[(\Delta \tilde{J}_\mathrm{x}^-)^2 + (\Delta \tilde{J}_\mathrm{y}^-)^2\right] \\ &= [(\mathcal{U}^{(\mathrm{a})} + \tfrac{1}{4}) + (\mathcal{U}^{(\mathrm{b})} + \tfrac{1}{4})] \cdot (\mathcal{V}^{(\mathrm{a})} + \mathcal{V}^{(\mathrm{b})}) \\ &\geq 4\sqrt{(\mathcal{U}^{(\mathrm{a})} + \tfrac{1}{4})(\mathcal{U}^{(\mathrm{b})} + \tfrac{1}{4})\mathcal{V}^{(\mathrm{a})}\mathcal{V}^{(\mathrm{b})}} \geq 1 \quad (3)\end{aligned}$$

holds, where we used the notation $\mathcal{U}^{(n)} = (\Delta J_\mathrm{z}^{(n)})^2$ and $\mathcal{V}^{(n)} = (\Delta \tilde{J}_\mathrm{x}^{(n)})^2 + (\Delta \tilde{J}_\mathrm{y}^{(n)})^2$ for $n = \mathrm{a}, \mathrm{b}$. For product states, the variance of a collective observable is the sum of the sub-system variances, i.e. $[\Delta(A^{(\mathrm{a})} + A^{(\mathrm{b})})]^2 = (\Delta A^{(\mathrm{a})})^2 + (\Delta A^{(\mathrm{b})})^2$, leading to the equality in equation (3). The first inequality is obtained from the inequality between the arithmetic and the geometric mean. Equation (2) is valid for both part a and b of the state, leading to the second inequality.

Using $\langle (\tilde{J}_\mathrm{x}^{(n)})^2\rangle + \langle (\tilde{J}_\mathrm{y}^{(n)})^2\rangle = 1$ for $n = \mathrm{a}, \mathrm{b}$, equation (3) yields

$$2\left[(\Delta J_\mathrm{z}^+)^2 + \frac{1}{2}\right](\mathcal{S} - \mathcal{C}) \geq \mathcal{S}, \qquad (4)$$

where correlations between the two subsystems are characterized by $\mathcal{C} = \left\langle \frac{J_\mathrm{x}^{(\mathrm{a})} J_\mathrm{x}^{(\mathrm{b})} + J_\mathrm{y}^{(\mathrm{a})} J_\mathrm{y}^{(\mathrm{b})}}{j_\mathrm{a} j_\mathrm{b}} \right\rangle$, and $\mathcal{S} = \mathcal{J}^{(\mathrm{a})}\mathcal{J}^{(\mathrm{b})}$. Note that $\mathcal{C}$ can be negative and $|\mathcal{C}| \leq \mathcal{S}$. The normalization with the total spin will make it easier to adapt our criterion to experiments with a varying particle number in the ensembles.

Separable states. We now consider a mixed separable state of the form $\varrho_\mathrm{sep} = \sum_k p_k |\Psi_k^{(\mathrm{a})}\rangle \otimes |\Psi_k^{(\mathrm{b})}\rangle$.

For such states, we can write the following series of inequalities

$$\begin{aligned}2\left[(\Delta J_\mathrm{z}^+)^2 + \frac{1}{2}\right]&(\mathcal{S} - \mathcal{C}) \\ &\geq 2\left[\sum_k p_k (\Delta J_\mathrm{z})_k^2 + \frac{1}{2}\right]\left[\sum_k p_k (\mathcal{S}_k - \mathcal{C}_k)\right] \\ &\geq 2\left[\sum_k p_k \sqrt{\left((\Delta J_\mathrm{z})_k^2 + \frac{1}{2}\right)(\mathcal{S}_k - \mathcal{C}_k)}\right]^2 \\ &\geq \left(\sum_k p_k \sqrt{\mathcal{S}_k}\right)^2, \qquad (5)\end{aligned}$$

where the subscript k indicates that the quantity is computed for the k^th sub-ensemble $|\Psi_k^{(\mathrm{a})}\rangle \otimes |\Psi_k^{(\mathrm{b})}\rangle$. The first inequality in equation (5) is due to $(\Delta J_\mathrm{z}^+)^2$ and

$\mathcal{S}$ being concave in the quantum state. The second inequality is based on the Cauchy-Schwarz inequality $\left(\sum_k p_k a_k\right)\left(\sum_k p_k b_k\right) \geq \left(\sum_k p_k \sqrt{a_k b_k}\right)^2$, where $a_k, b_k \geq 0$. The third inequality is the application of equation (4) for all sub-ensembles. Next, we find a lower bound on the RHS of equation (5) based on the knowledge of $\mathcal{J}^{(\mathrm{a})}$ and $\mathcal{J}^{(\mathrm{b})}$.

We find that

$$\sum_k p_k \left(\mathcal{J}_k^{(\mathrm{a})} \mathcal{J}_k^{(\mathrm{b})}\right)^{1/2} \geq (\mathcal{J}^{(\mathrm{a})})^2 + (\mathcal{J}^{(\mathrm{b})})^2 - 1, \quad (6)$$

which is based on noting $(xy)^{1/4} \geq x + y - 1$ for $0 \leq x, y \leq 1$. Using equation (6) to bound the RHS of equation (5) from below and dividing by $\mathcal{S}$ we obtain

$$\left[(\Delta J_{\mathrm{z}}^+)^2 + \frac{1}{2}\right] \times \left[2 - 2\frac{\mathcal{C}}{\mathcal{S}}\right] \geq \frac{\left[(\mathcal{J}^{(\mathrm{a})})^2 + (\mathcal{J}^{(\mathrm{b})})^2 - 1\right]^2}{\mathcal{S}}. \quad (7)$$

Non-zero particle number variance. So far, we assumed that the particle number of the two clouds a and b are known constants. In practice, the particle number is not a constant, but varies from experiment to experiment. In principle, one could postselect experiments for a given particle number, and test entanglement only in the selected experiments. However, this leads to discarding most experiments, increasing the number of repetitions needed tremendously. Hence, we modify our condition to handle non-zero particle number variances [34]. In this case, the state of the system can be written as $\varrho = \sum_{j_{\mathrm{a}}, j_{\mathrm{b}}} Q_{j_{\mathrm{a}}, j_{\mathrm{b}}} \varrho_{j_{\mathrm{a}}, j_{\mathrm{b}}}$, where $\varrho_{j_{\mathrm{a}}, j_{\mathrm{b}}}$ are states with $2j_{\mathrm{a}}$ and $2j_{\mathrm{b}}$ particles in the two clouds, $Q_{j_{\mathrm{a}}, j_{\mathrm{b}}} \geq 0$, $\sum_{j_{\mathrm{a}}, j_{\mathrm{b}}} Q_{j_{\mathrm{a}}, j_{\mathrm{b}}} = 1$. The state ϱ is separable if and only if all ϱ_N are separable. Then, expectation values for ϱ are computed as $\langle A f(\hat{j}_{\mathrm{a}}, \hat{j}_{\mathrm{b}})\rangle_\varrho = \sum_{j_{\mathrm{a}}, j_{\mathrm{b}}} Q_{j_{\mathrm{a}}, j_{\mathrm{b}}} \langle A\rangle_{\varrho_{j_{\mathrm{a}}, j_{\mathrm{b}}}} f(j_{\mathrm{a}}, j_{\mathrm{b}})$, where the operator is separated into one part that depends only on the particle number operators of the two clouds represented by $\hat{j}_{\mathrm{a}}$ and $\hat{j}_{\mathrm{b}}$, and another part that does not depend on them. $f(x)$ denotes some function. The proof from equation (3) to equation (7) can then be repeated, assuming that j_{a} and j_{b} are operators. Hence, we arrive at the criterion that can be used for the case of varying particle numbers given in equation (1).

Note that we choose the normalization of the variances such that the criterion is robust against fluctuations of the total number of particles. For a constant particle number one could simplify the fractions on the LHS of equation (1) by multiplying both the denominator and the numerator by j_{a}, and for the other fractions by j_{b}.

[1] T. Monz, P. Schindler, J. T. Barreiro, M. Chwalla, D. Nigg, W. A. Coish, M. Harlander, W. Hänsel, M. Hennrich, and R. Blatt, Phys. Rev. Lett. **106**, 130506 (2011).

[2] X.-L. Wang, L.-K. Chen, W. Li, H.-L. Huang, C. Liu, C. Chen, Y.-H. Luo, Z.-E. Su, D. Wu, Z.-D. Li, H. Lu, Y. Hu, X. Jiang, C.-Z. Peng, L. Li, N.-L. Liu, Y.-A. Chen, C.-Y. Lu, and J.-W. Pan, Phys. Rev. Lett. **117**, 210502 (2016).

[3] R. McConnell, H. Zhang, J. Hu, S. Ćuk, and V. Vuletić, Nature **519**, 439 (2015).

[4] F. Haas, J. Volz, R. Gehr, J. Reichel, and J. Estève, Science **344**, 180 (2014).

[5] O. Hosten, N. J. Engelsen, R. Krishnakumar, and M. A. Kasevich, Nature **529**, 505 (2016).

[6] B. Julsgaard, A. Kozhekin, and E. S. Polzik, Nature **413**, 400 (2001).

[7] J. Estève, C. Gross, A. Weller, S. Giovanazzi, and M. K. Oberthaler, Nature **455**, 1216 (2008).

[8] C. Gross, T. Zibold, E. Nicklas, J. Estève, and M. K. Oberthaler, Nature **464**, 1165 (2010).

[9] M. F. Riedel, P. Böhi, Y. Li, T. Hänsch, A. Sinatra, and P. Treutlein, Nature **464**, 1170 (2010).

[10] B. Lücke, M. Scherer, J. Kruse, L. Pezzé, F. Deuretzbacher, P. Hyllus, O. Topic, J. Peise, W. Ertmer, J. Arlt, L. Santos, A. Smerzi, and C. Klempt, Science **334**, 773 (2011).

[11] C. D. Hamley, C. S. Gerving, T. M. Hoang, E. M. Bookjans, and M. S. Chapman, Nature Phys. **8**, 305 (2012).

[12] T. Berrada, S. van Frank, R. Bcker, T. Schumm, J.-F. Schaff, and J. Schmiedmayer, Nat. Commun. **4**, 2077 (2013).

[13] N. Killoran, M. Cramer, and M. B. Plenio, Phys. Rev. Lett. **112**, 150501 (2014).

[14] B. Yurke and D. Stoler, Phys. Rev. A **46**, 2229 (1992).

[15] B. Lücke, J. Peise, G. Vitagliano, J. Arlt, L. Santos, G. Tóth, and C. Klempt, Phys. Rev. Lett. **112**, 155304 (2014).

[16] X.-Y. Luo, Y.-Q. Zou, L.-N. Wu, Q. Liu, M.-F. Han, M. K. Tey, and L. You, Science **355**, 620 (2017).

[17] J. Peise, I. Kruse, K. Lange, B. Lücke, L. Pezzè, J. Arlt, W. Ertmer, K. Hammerer, L. Santos, A. Smerzi, and C. Klempt, Nat. Commun. **6**, 8984 (2015).

[18] J. Tura, R. Augusiak, A. B. Sainz, T. Vértesi, M. Lewenstein, and A. Acín, Science **344**, 1256 (2014).

[19] J. Tura, R. Augusiak, A. B. Sainz, B. Lücke, C. Klempt, M. Lewenstein, and A. Acín, Ann. Phys. **362**, 370 (2015).

[20] R. Schmied, J.-D. Bancal, B. Allard, M. Fadel, V. Scarani, P. Treutlein, and N. Sangouard, Science **352**, 441 (2016).

[21] R. Bucker, J. Grond, S. Manz, T. Berrada, T. Betz, C. Koller, U. Hohenester, T. Schumm, A. Perrin, and J. Schmiedmayer, Nature Phys. **7**, 608 (2011).

[22] R. Lopes, A. Imanaliev, A. Aspect, M. Cheneau, D. Boiron, and C. I. Westbrook, Nature **520**, 66 (2015).
[23] P. Dussarrat, M. Perrier, A. Imanaliev, R. Lopes, A. Aspect, M. Cheneau, D. Boiron, and C. Westbrook, arXiv:1707.01279 (2017).
[24] W. Wieczorek, R. Krischek, N. Kiesel, P. Michelberger, G. Tóth, and H. Weinfurter, Phys. Rev. Lett. **103**, 020504 (2009).
[25] N. Kiesel, W. Wieczorek, S. Krins, T. Bastin, H. Weinfurter, and E. Solano, Phys. Rev. A **81**, 032316 (2010).
[26] C. Klempt, O. Topic, G. Gebreyesus, M. Scherer, T. Henninger, P. Hyllus, W. Ertmer, L. Santos, and J. J. Arlt, Phys. Rev. Lett. **103**, 195302 (2009).
[27] M. Scherer, B. Lücke, G. Gebreyesus, O. Topic, F. Deuretzbacher, W. Ertmer, L. Santos, J. J. Arlt, and C. Klempt, Phys. Rev. Lett. **105**, 135302 (2010).
[28] A. Einstein, B. Podolsky, and N. Rosen, Phys. Rev. **47**, 777 (1935).
[29] L.-M. Duan, G. Giedke, J. I. Cirac, and P. Zoller, Phys. Rev. Lett. **84**, 2722 (2000).
[30] R. Simon, Phys. Rev. Lett. **84**, 2726 (2000).
[31] M. D. Reid, Phys. Rev. A **40**, 913 (1989).
[32] F. Laloë and W. J. Mullin, Eur. Phys. J. B **70**, 377 (2009).
[33] Y. Castin and R. Dum, Phys. Rev. Lett. **77**, 5315 (1996).
[34] P. Hyllus, L. Pezzé, A. Smerzi, and G. Tóth, Phys. Rev. A **86**, 012337 (2012).

Bound entangled states fit for robust experimental verification

Gael Sentís[1,2], Johannes N. Greiner[3], Jiangwei Shang[4,1], Jens Siewert[5,6], and Matthias Kleinmann[1,2]

[1]Naturwissenschaftlich-Technische Fakultät, Universität Siegen, 57068 Siegen, Germany

[2]Departamento de Física Teórica e Historia de la Ciencia, Universidad del País Vasco UPV/EHU, E-48080 Bilbao, Spain

[3]3rd Institute of Physics, University of Stuttgart and Institute for Quantum Science and Technology, IQST, Pfaffenwaldring 57, D-70569 Stuttgart, Germany

[4]Beijing Key Laboratory of Nanophotonics and Ultrafine Optoelectronic Systems, School of Physics, Beijing Institute of Technology, Beijing 100081, China

[5]Departamento de Química Física, Universidad del País Vasco UPV/EHU, E-48080 Bilbao, Spain

[6]IKERBASQUE Basque Foundation for Science, E-48013 Bilbao, Spain

December 17, 2018

Preparing and certifying bound entangled states in the laboratory is an intrinsically hard task, due to both the fact that they typically form narrow regions in state space, and that a certificate requires a tomographic reconstruction of the density matrix. Indeed, the previous experiments that have reported the preparation of a bound entangled state relied on such tomographic reconstruction techniques. However, the reliability of these results crucially depends on the extra assumption of an unbiased reconstruction. We propose an alternative method for certifying the bound entangled character of a quantum state that leads to a rigorous claim within a desired statistical significance, while bypassing a full reconstruction of the state. The method is comprised by a search for bound entangled states that are robust for experimental verification, and a hypothesis test tailored for the detection of bound entanglement that is naturally equipped with a measure of statistical significance. We apply our method to families of states of 3×3 and 4×4 systems, and find that the experimental certification of bound entangled states is well within reach.

Gael Sentís: gael.sentis@uni-siegen.de
Jiangwei Shang: jiangwei.shang@bit.edu.cn
Jens Siewert: jens.siewert@ehu.eus
Matthias Kleinmann: matthias.kleinmann@uni-siegen.de

1 Introduction

To experimentally prepare, characterize and control entangled quantum states is an essential item in the development of quantum-enhanced technologies, but it also serves the indispensable purpose of testing the predictions of entanglement theory in the laboratory. Among the most intriguing features of this theory stands the existence of *bound* entanglement [1], a form of entanglement that cannot be distilled into singlet states by any protocol that uses only local operations and classical communication. Originally considered as useless for quantum information processing, bound entangled states were later established as a valid resource in the contexts of quantum key distribution [2], entanglement activation [3, 4], metrology [5, 6], steering [7], and nonlocality [8], and their nondistillability has been linked to irreversibility in thermodynamics [9, 10].

Complementing these theoretical achievements, substantial efforts have been devoted to experimentally producing and verifying bound entanglement. The first experimental report on the preparation of a bound entangled state was presented in [11], although the result was disputed [12] and subsequently amended [13]. The state prepared was the four-qubit Smolin state [14], thus it showcases a multipartite instance of bound entanglement, which is fundamentally distinct from the bipartite case: when multiple parties are present, entanglement can still potentially be distilled if two of the

parties work together. Further experimental works on multipartite bound entanglement include Refs. [15–20]. Examples of experimental bipartite setups are more scarce. In Ref. [21] bipartite bound entanglement was produced using four-mode continuous-variable Gaussian states, and Ref. [22] focuses on a family of two-qutrit states.

Since the property of nondistillability is experimentally inaccessible in a direct manner, a natural route to verify a state as bound entangled is to do a full tomographic reconstruction of the density matrix from the experimental data [23] and apply the only known computable criterion on it [1]: if an entangled state has positive partial transpose (PPT), then it is nondistillable and therefore bound entangled[1]. However, it has recently been pointed out that widely used reconstruction methods like maximum likelihood and least squares [24, 25] inevitably suffer from bias [26, 27], caused by imposing a positivity constraint over compatible density matrices. In some cases, the bias can be large enough to drastically change the entanglement properties of the estimator with respect to the true state. In addition to this state of affairs, the variance of the estimator is usually calculated by bootstrapping [28], which only accounts for statistical fluctuations, and can result in a smaller variance than the actual bias of the estimator [27]. In contrast, a direct reconstruction of the state by linear inversion produces an unbiased estimator, but at the cost of admitting unphysical density matrices. Then, the PPT criterion simply looses all meaning.

All the experimental works cited above support their claims on some combination of maximum likelihood or least squares reconstruction and bootstrapping. There exist more informative methods to derive errors from tomographic data, such as credibility [29] and confidence [30, 31] regions, and also the alternative of using linear inversion in addition to a sufficiently large number of measurements that guarantees physical estimates [32]. Should these methods be applied to the detection of a bound entangled state, more robust results may be generated, although they might come at the expense of being computationally expensive or even intractable [33]. However, regardless of the reconstruction method of choice, the problem of experimentally testing bound entanglement is intrinsically challenging. This is so because bound entangled regions of the state space are typically very small in volume [34]. Furthermore, at least for the known cases in low-dimensional systems, bound entangled states are close to both the sets of separable states and distillable entangled states. This translates into the requirement of a highly precise experimental setup, and the deepening of the potential pitfalls of biased tomographic reconstructions.

In this paper, we set ourselves to improve on the above situation by devising methods that enable robust experimental certification of bound entanglement. Instead of advocating for a particular tomographic method for detecting bound entanglement or considering the preparation of a specific state, we address the more generic question: Which are the best candidate states for an experimental verification of bound entanglement? In other words, for bipartite systems, we aim at finding states that have the largest ball of bound entangled states around them [35]. To this end, we construct simple lower bounds that the radius r of such a ball (in Hilbert–Schmidt distance) has to obey for a given state, and formulate an optimization problem that maximizes r over parametrized families of states. Having a value for the maximum radius, r^*, allows us to assert the robustness of the target state at the center of the ball, and in turn gives us an idea of the required number of preparations of the state in a potential experiment. We proceed by designing a χ^2 hypothesis test directly applicable over unprocessed tomographic data that provides a certificate for bound entanglement within some statistical significance. We show that our proposed method, combining the search of a robust candidate state with a statistical analysis through a hypothesis test, makes rigorous bound entanglement verification not only experimentally feasible with current technology, but also computationally cheap.

The paper is structured as follows. First we derive the constraints for the existence of a ball of bound entangled states of radius r around a generic bipartite state of dimension d. Then, we apply our method to two families of states of dimensions 3×3 and 4×4, known to contain bound entanglement, and find robust candidates for its

[1] It is still an open question whether the PPT criterion completely characterizes bound entanglement, namely whether all nondistillable states are PPT.

experimental verification. We proceed to devise a hypothesis test for bound entanglement, and test the robustness of the selected candidate states in terms of the necessary number of samples to achieve a statistically significant certification under realistic experimental conditions.

2 A bound entangled ball

Verifying the bound entangled character of a bipartite state ρ requires, on the one hand, showing that it is entangled, and on the other hand proving that the entanglement of ρ is nondistillable. Non-distillability is usually verified via the (sufficient) PPT condition, which we denote by $\Gamma(\rho) \geq 0$. Throughout this paper, we identify bound entangled states with PPT entangled states. As for verifying that ρ is entangled, there exist several inequivalent criteria. We choose the violation of the *computable cross norm* or *realignment* criterion (CCNR) [36], since it is simple and is generally tight enough to detect bound entanglement. The CCNR criterion dictates that, for some local orthonormal basis [with respect to the Hilbert–Schmidt inner product $(A, B) = \mathrm{tr}(A^\dagger B)$] of the Hermitian matrices $\{g_k\}$, ρ is entangled if the matrix $R(\rho)_{k,l} = \mathrm{tr}(\rho\, g_k \otimes g_l)$ obeys $\|R(\rho)\|_1 > 1$, where $\|Y\|_1 = \mathrm{tr}\sqrt{Y^\dagger Y}$ is the trace norm of Y. The points in the state space that violate CCNR, fulfill PPT, and correspond to physical states (that is, satisfy the positivity condition $\rho \geq 0$), thus define a volume of bound entangled density matrices.

Given a bound entangled state ρ that obeys these conditions, we inquire how far we can move away from it while remaining in the bound entangled region. We construct a new state $\tau = \rho + rX$, where $r \geq 0$, and X is a traceless Hermitian matrix with bounded Hilbert–Schmidt norm $\|X\|_2 = \sqrt{\mathrm{tr}\, X^\dagger X} \leq 1$. The set of all such matrices forms a Hilbert–Schmidt ball that we denote by $\mathcal{B}'$. We then define the set of all states τ as $\mathcal{B}(\rho, r) := \rho + r\mathcal{B}'$. Note that $\|\rho - \tau\|_2 \leq r$. We can bound the minimum eigenvalue of τ as

$$\begin{aligned} \lambda_{\min}(\tau) &\geq \lambda_{\min}(\rho) - r\|X\|_\infty \\ &\geq \lambda_{\min}(\rho) - r\sqrt{(d-1)/d}\,, \end{aligned} \tag{1}$$

where $\|X\|_\infty = \lambda_{\max}(X)$ is the uniform norm of X. The first inequality holds since, in the extreme case, the eigenvector associated to the minimal eigenvalue of X is aligned with the corresponding one for ρ. For the second inequality we have used that

$$\max\{\, \|X\|_\infty \mid X \in \mathcal{B}' \,\} = \sqrt{(d-1)/d} \tag{2}$$

(we provide a proof of this equation in Appendix A).

Similarly, since the partial transpose $\Gamma(\tau)$ does not change the Hilbert–Schmidt ball, $\Gamma(\mathcal{B}) = \mathcal{B}$, we have

$$\lambda_{\min}[\Gamma(\tau)] \geq \lambda_{\min}[\Gamma(\rho)] - r\sqrt{(d-1)/d}\,. \tag{3}$$

We can bound the value of the CCNR criterion over τ in a similar fashion. We have

$$\begin{aligned} \|R(\tau)\|_1 &\geq \|R(\rho)\|_1 - r\|R(X)\|_1 \\ &\geq \|R(\rho)\|_1 - r\sqrt{d}\,, \end{aligned} \tag{4}$$

where we first applied the triangle inequality, and for the last inequality we used that

$$\max\{\, \|R(X)\|_1 \mid X \in \mathcal{B}' \,\} = \sqrt{d} \tag{5}$$

(we refer to Appendix A for a proof).

Our goal is to find a state ρ such that, if we depart from it by a distance r in any direction, the resulting τ still fulfils PPT and violates CCNR, that is, $\lambda_{\min}[\Gamma(\tau)] \geq 0$ and $\|R(\tau)\|_1 > 1$. Then, using Eqs. (3) and (4), we search for a state ρ which admits the largest r under the constraints

$$\lambda_{\min}[\Gamma(\rho)] \geq r\sqrt{(d-1)/d}\,, \tag{6a}$$

$$\|R(\rho)\|_1 > 1 + r\sqrt{d}\,. \tag{6b}$$

For any admissible r, all states in $\mathcal{B}$ are bound entangled. Note that, while the optimization is naturally performed over physical target states ρ, the resulting ball $\mathcal{B}$ can well be partly outside of the state space, cf. Fig. 1, as the positivity of all states inside $\mathcal{B}$ is not imposed as a constraint.

3 Symmetric families

The method described in the previous section is completely general, but for the optimization to actually become feasible one has to restrict the free parameters in ρ. We consider two symmetric families of bipartite states which are characterized by few parameters, and nevertheless contain fairly large regions of bound entanglement.

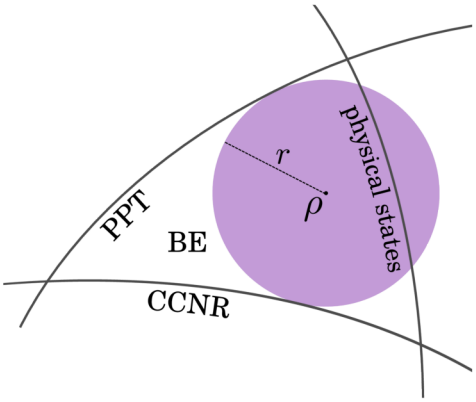

Figure 1: Schematic picture of the state space, where the boundaries of the PPT, CCNR and physical sets enclose a bound entangled region (BE). A region of points $\tau = \rho + rX$, where X is a traceless Hermitian matrix with $\|X\|_2 \leq 1$, is depicted in violet. The parameter r is the radius of a Hilbert–Schmidt ball around a target state ρ such that all physical states τ are bound entangled.

The first case that we consider is a family of two-qutrit states of the form

$$\rho = a\,|\phi_3\rangle\langle\phi_3| + b\sum_{k=0}^{2}|k, k\oplus 1\rangle\langle k, k\oplus 1| + c\sum_{k=0}^{2}|k, k\oplus 2\rangle\langle k, k\oplus 2|\,, \quad (7)$$

where $|\phi_3\rangle = \sum_{k=0}^{2}|kk\rangle/\sqrt{3}$, the symbol $\oplus$ denotes addition modulo 3, and a, b, c are real parameters. A similar three-parameter family of two qutrits, known to contain bound entanglement and arise from symmetry conditions, was analyzed in Refs. [37–42], and considered in the experiment reported in Ref. [22]. We search for the optimal values of $\{a, b, c\}$ that parametrize an optimal target state ρ^*. This state will admit any $r \leq r^*$, where r^* is the maximum radius compatible with the constraints (6a) and (6b). An exact solution for this optimization can be found (see Appendix B.1 for details). We obtain the optimal parameters

$$a \approx 0.21289\,,\ b \approx 0.04834\,,\ \text{and}\ c \approx 0.21403\,, \quad (8)$$

yielding a maximal radius $r^* \approx 0.02345$. The resulting ρ^* is a rank-7 state.

Since the ball $\mathcal{B}$ may contain unphysical states, it is in principle possible that our estimate for the maximal r^* is not tight. To explore this, we move away from ρ^* by a distance r^* in suitable directions and evaluate the position of the resulting state with respect to the boundaries of the PPT and the CCNR sets. We provide the details of this analysis in Appendix B.1. As a result, we obtain that our estimate of r^* is indeed tight with respect to the PPT boundary, but we observe that it slightly underestimates the distance with respect to the CCNR boundary.

As our second case, we consider the two-ququart states that are Bloch-diagonal, i.e., of the form

$$\rho = \sum_k x_k g_k \otimes g_k\,, \quad (9)$$

where $g_k = (\sigma_\mu \otimes \sigma_\nu)/2$, $\mu, \nu = 0, 1, 2, 3$, with $\sigma_0 = \mathbb{1}$, $\sigma_1, \sigma_2, \sigma_3$ the Pauli matrices, and the index k enumerates pairs of indices $\{\mu, \nu\}$ in lexicographic order. Bound entangled Bloch-diagonal states have already been described in Ref. [43]. The optimization over this family of states, despite having more free parameters, is much simpler than in the two-qutrit case discussed above. The reason is that the problem can be reshaped as a linear program over the coefficients x_k, and thus it can also be solved exactly (see Appendix B.2 for details). A vertex enumeration of the corresponding feasibility polytope is possible, and leads us to a set of 4224 optimal states achieving a maximal radius $r^* \approx 0.0214$. One example of such optimal state, ρ^*, is given by coefficients

$$\begin{aligned} &x_1 = \frac{1}{4}\,,\\ &x_\alpha \approx -0.0557066\,, \quad \alpha \in \{2, 3, 4, 5, 6, 9, 12, 14, 16\}\,,\\ &x_\beta \approx 0.0142664\,, \quad \beta \in \{7, 11, 13\}\,,\\ &x_\gamma \approx 0.0971467\,, \quad \gamma \in \{8, 10, 15\}\,. \end{aligned} \quad (10)$$

where x_1 is fixed by normalization. The state ρ^* has rank 10, which is the minimal rank among bound entangled states achieving r^* that are of the form (9) and are detectable by CCNR. As a byproduct of our analysis, we also obtain that the overall minimal rank for such bound entangled states is 9, albeit with a fairly smaller radius.

4 Statistical analysis

In this section we put our method for finding optimal target states to work in a practical scenario. That is, for an experiment aiming at the certification of bound entanglement, we design a statis-

tical analysis of the experimental data that crucially hinges on knowing the radius of the bound entangled ball around the target state. The idea is to judge whether the data was obtained from a bound entangled state by considering the membership of the preparation to the bound entangled ball. In order to endow the certification with a measure of statistical significance, we design a hypothesis test for this membership problem.

Our null hypothesis, H_0, is that the prepared state is outside the bound entangled ball $\mathcal{B}(\rho_0, r_0)$ of radius r_0 centered at the target state ρ_0. We make the assumption that an instance of experimental data, $\vec{x}$, is drawn from a multivariate normal distribution $N(\vec{\xi}, \Sigma)$ with offset $\vec{\xi}$ and covariance matrix Σ. This is a good approximation for realistic scenarios. Here the vector notation is used over variables that belong to the same space as the experimental data, that is, e.g., the space of frequencies of measurement outcomes. When H_0 holds true, then the offset $\vec{\xi}$ is the expected value of the data when a state ρ_{exp} is prepared such that $\|\rho_0 - \rho_{\text{exp}}\|_2 \geq r_0$. The covariance matrix Σ is determined by the particular experimental procedure used.

The goal is to design an appropriate hypothesis test for H_1 of the form $\hat{t}(\vec{x}) \leq t$, where t is a threshold parameter, and the function $\hat{t}$ is called a test statistic. If the hypothesis test is true, the data $\vec{x}$ is accepted as fulfilling the hypothesis H_1, that is, the state is bound entangled. The quantity through which we assess the significance of the hypothesis test is the worst-case probability of the test accepting H_1 while H_0 is true. This is formally written as

$$p(t, r_0) = \sup_{\rho} \left\{ \mathbb{P}[\hat{t} \leq t] \mid \|\rho_0 - \rho\|_2 \geq r_0 \right\}, \quad (11)$$

where $\mathbb{P}[\hat{t} \leq t]$ is the probability for the hypothesis test to accept data sampled from $N(\vec{\xi}, \Sigma)$, $\vec{\xi}$ depends to ρ, and $\|\rho_0 - \rho\|_2 \geq r_0$ is the assertion that H_0 holds true. For given data $\vec{x}$, the probability $p[\hat{t}(\vec{x}), r_0]$ is the p-value of this hypothesis test.

Now, let us define

$$\hat{t} \colon \vec{x} \mapsto \|\Sigma^{-1/2}[T(\rho_0) - \vec{x}]\|_2 \,, \quad (12)$$

where T is a map that takes a density matrix to the expected data (e.g., to a vector of probabilities), thus it is determined by the experimental procedure. Hence, $\hat{t}(\vec{x})$ gives some notion of distance between the standardized versions of the experimental data and the expected data of a perfect measurement performed over the target state. In Appendix C we show that, if $\hat{t}$ is of the form in Eq. (12), the probability (11) is naturally upper-bounded by

$$p(t, r_0) \leq q_m(t^2, r_1^2) \,, \quad (13)$$

where $s \mapsto q_m(s, u)$ is the cumulative distribution function of the noncentral χ^2-distribution with m degrees of freedom and noncentrality parameter u, and r_1 is the equivalent distance in the experimental data space of the Hilbert–Schmidt distance r_0, or, more precisely, $r_1 := \inf_{\Delta \notin \mathcal{B}} \hat{t}[T(\Delta)]$, where Δ is any Hermitian matrix with unit trace. Naturally, the value of r_1 scales with r_0 and strongly depends on the experimental procedure, that is, on T and Σ.

In the following, we show how to evaluate the hypothesis test for the two-qutrit state from Eq. (8) as an example of a target state ρ_0, and assess the necessary experimental requirements for a desired level of significance. For this, we need to make some assumptions about the experimental procedure. We associate the measurement outcomes in the experiment to semidefinite-positive Hermitian operators E_k. We consider a complete set of such operators, that is, the real linear span of $\{E_k\}$ is the set of all Hermitian operators. The probability of obtaining the outcome corresponding to E_k when measuring the state ρ is given by $p_k = \text{tr}(E_k \rho)$, and we assume that $T(\rho)_k \equiv p_k$. The connection between the probabilities p_k and the data gathered in the experiment crucially depends on how the experiment is performed. A straightforward theoretical association can be established if one assumes that measurement outcomes correspond to independent Poissonian trials with parameters $nT(\rho)_k$, renormalized by n, where n is the mean total number of events per measurement setting. That is, if we obtain n_k events for the outcome k, we use as data $x_k = n_k/n$. Note, however, that in a realistic experiment $T(\rho)$ and n are not known exactly. A reasonable alternative is to use the total number of observed events $\sum_k n_k$ as an estimate of n, but then the connection between p_k and x_k is more involved. For our examples below we use this latter approach (a detailed discussion is presented in Appendix C).

In order to get specific predictions, we assume that mutually unbiased bases are used as local

measurements (refer to Appendix C for an explicit construction) and that the experimental state ρ_{exp} has 5% white noise over the target, that is, $\rho_{\text{exp}} = 0.95\rho_0 + 0.05\mathbb{1}/9$. This amount of noise still results in a state within $\mathcal{B}$, since $\|\rho_0 - \rho_{\text{exp}}\|_2 \approx 0.6r_0$, where $r_0 \approx 0.02345$ is the optimal radius associated to ρ_0 (cf. Section 3). Then, one obtains $r_1^2 \approx 0.0664^2 n$ (see Appendix C for details on how to compute this value). We now set a critical t_0 below which the p-value will be larger than some acceptable threshold p_0, so that $q_m(t_0^2, r_1^2) = p_0$. To obtain t_0, one inverts the equation $q_m(t^2, r_1^2) = p$ to get $t^2(p)$, called the quantile function. Then, $t_0 := t(p_0)$. Once t_0 is fixed, we compute the probability p_{fail} that the test fails to certify bound entanglement over data obtained by measuring the prepared state ρ_{exp}, i.e., that $\hat{t}(\vec{\xi}) > t_0$ given $\vec{\xi} = T(\rho_{\text{exp}})$. We can write this probability as

$$p_{\text{fail}} = 1 - q_m\left(t_0^2, r_2^2\right) , \tag{14}$$

where $r_2^2 := \hat{t}(\vec{\xi})^2 \approx 0.0416^2 n$. Note that, while r_1 is used to determine t_0 considering a worst case scenario for a false positive, r_2 is a distance between standardized probabilities given the particular preparation ρ_{exp}. Therefore, $r_1 > r_2$ means that the test $\hat{t}$ has a chance to single out the particular experimental preparation as bound entangled from the worst-case state outside $\mathcal{B}$, and hence p_{fail} will decrease with the number of samples n, which is the case of interest. In Fig. 2 we plot p_{fail} as a function of n, for various levels of significance p_0 expressed as multiples of the standard deviation $k\sigma$, so that $p_0 = 1 - \text{erf}(k/\sqrt{2})$.

Similarly, we carry out the same analysis for the two-ququart target state specified in Eq. (10). In this case we construct our measurement settings by regarding each ququart as two qubits and performing local Pauli measurements on them. With $r_1^2 \approx 0.0856^2 n$, $r_2^2 \approx 0.0469^2 n$, and an admixture of 2.5% white noise over the target ρ_0, we obtain the results shown in Fig. 2. In both cases, for the selected target states of two qutrits and two ququarts given by Eqs. (8) and (10), our analysis shows that their experimental certification as bound entangled states under realistic assumptions is within reach, with around 70000 samples per measurement setting to reach a 3σ level of significance. Note that this number of samples justifies a posteriori our analysis assuming that experimental data $\vec{x}$ is normal-distributed.

5 Discussion

We have developed a comprehensive method for the experimental characterization of bipartite bound entanglement, from the selection of robust target states to the statistical analysis of the data. Previous experimental works were based on preparing a bound entangled state and inferring its properties from those of the reconstructed density matrix via maximum likelihood or least squares. Unfortunately, such techniques have been shown to produce unreliable results, particularly for entanglement certification [26, 27], which casts a shadow of doubt over past experimental demonstrations of bound entanglement. Instead of using a (necessarily) biased reconstruction of the density matrix and assuming that it shares the same properties that the true prepared state, we show that it is feasible to perform a hypothesis test over the unprocessed experimental tomographic data to test for membership of the preparation to a subset of the state space that is guaranteed to only contain bound entangled states. The hypothesis test is naturally equipped with a measure of statistical significance, which is easy to compute. The subset of bound entangled states is specified as a ball of radius r, and the design of the hypothesis test directly depends on this parameter. We have shown, through explicit examples of families of bipartite qutrit states and bipartite ququart states, how the certification of bound entanglement with high statistical significance is well within current experimental capabilities by using our method.

While our statistical analysis of the data in the form of a hypothesis test is a standalone technique applicable to the preparation and measurement of any state, we would like to stress that the value of the radius r has an important effect in its detection power, hence it is worth aiming at target states with maximal r. To show this, we run our analysis for the two-qutrit state prepared in Ref. [22], assuming a noiseless experimental preparation. This state has a ball of bound entangled states around it of radius $r \approx 0.01182$. This value is computed as the maximal r that satisfies Eqs. (6a) and (6b). We obtain that the required number of samples for achiev-

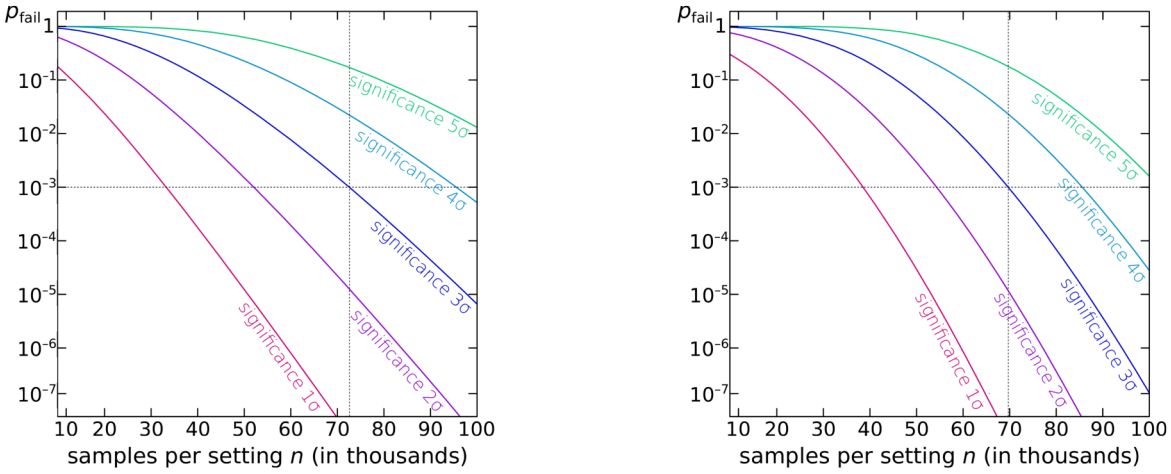

Figure 2: Probability p_{fail} to obtain data which does not confirm bound entanglement at a level of significance corresponding to at least $k\sigma$ standard deviations. The experiments consist of locally measuring (a) mutually unbiased bases over preparations of the two-qutrit state in Eq. (8) with 5% white noise, and (b) local Pauli measurements over the two-ququart state in Eq. (10) with 2.5% white noise.

ing a 3σ level of significance with a failure probability $p_{\text{fail}} \approx 10^{-3}$ is roughly twice as much as for the two-qutrit state in Eq. (8) (which admits a radius $r \approx 0.02345$) when assuming a noisy preparation. As a comparison, optimizing over the one-parameter Horodecki family [1]—which is part of the family in Eq. (7)—yields a radius $r \approx 0.01681$, for the parameters $a \approx 0.28571$, $b \approx 0.07931$, and $c \approx 0.15879$.

As a concluding remark, some comments on the generality of our result are in order. If one has prior knowledge of the expected amount and type of experimental noise, this could be incorporated into the statistical analysis by assuming the noisy state as the target. As a result, one should expect a smaller value of the test statistic $\hat{t}(\vec{x})$ for a given set of data $\vec{x}$ and hence a smaller p-value. However, our calculations for several examples indicate that this advantage does not compensate in general the drawback of having a smaller bound entangled ball. A refinement of our method could also be achieved by taking into account the form of the covariance matrix Σ into the optimization over target states, as we did incorporate it into the design of the hypothesis test. This would generally yield an ellipsoid around the target, instead of a ball, potentially capturing a larger volume of bound entangled states and thus leading to a stronger test. The possible disadvantage is that the bounds (6a) and (6b) will likely be much more complicated (if computable at all), hence the optimization step will be much harder to carry out. We leave the question open of whether such refinement provides a significant reduction in the experimental requirements.

Acknowledgments

We acknowledge Otfried Gühne, Géza Tóth, Beatrix Hiesmayr, Wolfgang Löffler, and Dagmar Bruß for useful discussions. This project was funded by the ERC Starting Grant No. 258647/GEDENTQOPT, the Basque Government grant No. IT986-16, the Spanish MINECO/FEDER/UE grant FIS2015-67161-P, the UPV/EHU program UFI 11/55, the ERC Consolidator Grant 683107/TempoQ, the DFG (No. KL 2726/2-1), and the Beijing Institute of Technology Research Fund Program for Young Scholars.

A Proofs of Eqs. (2) and (5)

Given a target state ρ, we construct the displaced state $\tau = \rho + rX$, where $r \geq 0$, and X is a bounded traceless Hermitian matrix fulfilling $\|X\|_2 \leq 1$. We claim that the minimal eigenvalue of τ can be lower bounded as [cf. Eq. (1)]

$$\lambda_{\min}(\tau) \geq \lambda_{\min}(\rho) - r\|X\|_\infty \geq \lambda_{\min}(\rho) - r\sqrt{(d-1)/d}\,, \tag{15}$$

where for the second inequality we have used that [cf. Eq. (2)]

$$\max\{\,\|X\|_\infty \mid X \in \mathcal{B}'\,\} = \sqrt{(d-1)/d}\,, \tag{16}$$

and $\mathcal{B}' = \{X | \|X\|_2 \leq 1, \operatorname{tr} X = 0, X = X^\dagger\}$. This holds from the following reasoning. Clearly, the maximum is attained for $X = \operatorname{diag}(x, y_1, \ldots, y_{d-1})$ with some vector $\vec{y}$ fulfilling $\|\vec{y}\|_\infty \leq x = -\vec{y}\cdot\vec{e}$ and $x^2 + \vec{y}^2 \leq 1$. Here, $e_k = 1$ for $k = 1, \ldots, d-1$. Note that the choice of $\vec{y}$ that allows x to be largest is the uniform vector $\vec{y} = -x\vec{e}/\vec{e}^2 \equiv \vec{z}$, since it minimizes $\vec{y}^2$. The maximization now reduces to

$$\max\{\,x \mid x^2 + x^2/\vec{e}^2 \leq 1\,\}\,,$$

which immediately yields the assertion due to $\vec{e}^2 = d-1$.

In a similar fashion, we then obtain a lower bound of the 1-norm of the realigned state τ as [cf. Eq. (4)]

$$\|R(\tau)\|_1 \geq \|R(\rho)\|_1 - r\|R(X)\|_1 \geq \|R(\rho)\|_1 - r\sqrt{d}\,, \tag{17}$$

where we use that [cf. Eq. (5)]

$$\max\{\,\|R(X)\|_1 \mid X \in \mathcal{B}'\,\} = \sqrt{d}\,. \tag{18}$$

This immediately follows from the facts that the 1-norm is bounded by the 2-norm as $\|A\|_1 \leq \sqrt{\operatorname{rank}(A)}\|A\|_2$, via e.g. Cauchy-Schwarz inequality, and that $\|R(X)\|_2 = \|X\|_2 \leq 1$. Hence $\sqrt{d}$ is an upper bound. It remains to show that this bound is attainable. For arbitrary d, we see that $\operatorname{tr} X = 0 \Leftrightarrow [R(X)]_{1,1} = 0$ (choosing the local basis such that $g_1 = \mathbb{1}$). Then, $R(X)$ is a constant anti-diagonal matrix.

B Optimally detectable bound entangled states

B.1 A state of two-qutrits

The first case that we consider is a family of two-qutrit states of the form

$$\begin{aligned}\rho = a\,|\phi_3\rangle\langle\phi_3| + b\sum_{k=0}^{2}|k, k\oplus 1\rangle\langle k, k\oplus 1| \\ + c\sum_{k=0}^{2}|k, k\oplus 2\rangle\langle k, k\oplus 2|\,,\end{aligned} \tag{19}$$

where $|\phi_3\rangle = \sum_{k=0}^{2}|kk\rangle/\sqrt{3}$, the symbol $\oplus$ denotes addition modulo 3, and a, b, c are real and non-negative. We denote the dimension of the total Hilbert space by $d = 9$. There are three distinct eigenvalues for ρ,

$$\lambda(\rho) = \{a, b, c\}\,, \tag{20}$$

which satisfy the constraint

$$a + 3(b + c) = 1\,. \tag{21}$$

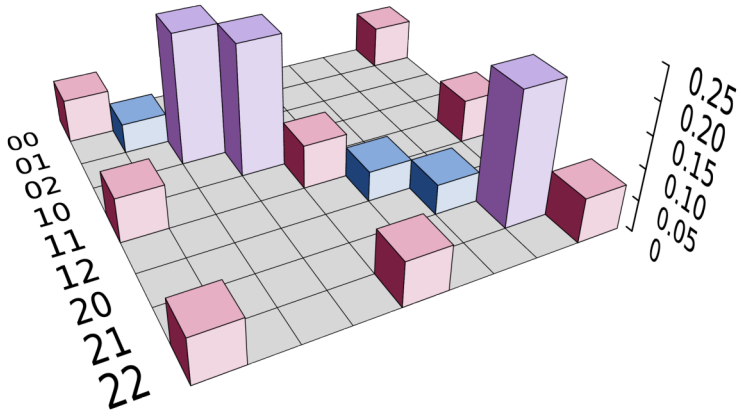

Figure 3: The density matrix of our optimal two-qutrit state ρ^* in the computational basis. The heights of the bars correspond to the entries of the density matrix. Note that all entries of ρ^* are real-valued.

Then, the three distinct eigenvalues of its partial transpose $\Gamma(\rho)$ are given by

$$\lambda(\Gamma(\rho)) = \left\{\frac{a}{3}, \frac{1}{6}\left(1 - a \pm \sqrt{4a^2 + 9(b-c)^2}\right)\right\} . \tag{22}$$

Now, the trace-norm of the realigned matrix $R(\rho)$ is given by

$$\|R(\rho)\|_1 = \frac{1}{3} + 2a + 2\sqrt{3(b^2 + c^2 + bc) - (b+c) + \frac{1}{9}} . \tag{23}$$

Plugging in Eqs. (22) and (23) in the bounds (6a) and (6b) one obtains two inequalities that, together with Eqs. (21) and $\lambda(\rho) \geq 0$, form the set of constraints that a valid target state should obey. The maximization over r such that these constraints hold can be solved exactly, although the analytical form of the optimal parameters is rather involved. Here we give the approximate values $a \approx 0.21289$, $b \approx 0.04834$, and $c \approx 0.21403$ that yield an optimal state ρ^*, which admits any $r \leq r^* \approx 0.02345$. Note that the optimization is invariant under the interchange $b \leftrightarrow c$, therefore r^* is also not affected by it. A visual representation of the density matrix of ρ^* is shown in Fig. 3.

As argued in the main text, since we do not require in our optimization that the full ball $\mathcal{B}$ is contained in the state space, an analysis of the tightness of our estimate for r^* is in order. To do so, we move away from ρ^* by a distance r^* in suitable directions and evaluate the position of the resulting state with respect to the boundaries of the PPT and the CCNR sets. We first move towards the PPT boundary. To this end, we take a normalized eigenvector $|\eta\rangle$ from the eigenspace of $\Gamma(\rho^*)$ with minimal eigenvalue and find, for the matrix after the displacement $\tilde{\rho} = \rho^* - r^*\Pi[\Gamma^{-1}(|\eta\rangle\langle\eta|)]$, the values

$$\lambda_{\min}[\Gamma(\tilde{\rho})] \approx 0\,, \quad \|R(\tilde{\rho})\|_1 \approx 1.094\,, \quad \text{and} \quad \lambda_{\min}(\tilde{\rho}) \approx -0.005\,, \tag{24}$$

where we wrote $\Pi[X]$ for $[X - \mathrm{tr}(X)\mathbb{1}/9]/\xi$ for some appropriate ξ, so that $\|\Pi[X]\|_2 = 1$. Hence, $\tilde{\rho}$ is effectively sitting on the PPT boundary, it is still detected as bound entangled by the CCNR criterion, and it is slightly outside the space of physical states. This shows that our estimate for r^* is tight with respect to PPT.

Similarly, we now consider a displacement towards the CCNR boundary. With a singular value decomposition $UDV^\dagger = R(\rho^*)$, we let $\bar{\rho} = \rho^* - r^*\Pi[R^{-1}(UV^\dagger)]$ and find the values

$$\lambda_{\min}[\Gamma(\bar{\rho})] \approx 0.03\,, \quad \|R(\bar{\rho})\|_1 \approx 1.004\,, \quad \text{and} \quad \lambda_{\min}(\bar{\rho}) \approx 0.01\,. \tag{25}$$

Therefore, it is possible that our state ρ^* is not yet optimal for obtaining the largest value r^*, since we are still not touching the CCNR boundary.

B.2 States of two-ququarts

We consider two-ququart states that are Bloch-diagonal, i.e., of the form

$$\rho = \sum_k x_k g_k \otimes g_k \,, \tag{26}$$

where $g_k = (\sigma_\mu \otimes \sigma_\nu)/2$, $\mu, \nu = 0, 1, 2, 3$, with $\sigma_0 = \mathbb{1}$, $\sigma_1, \sigma_2, \sigma_3$ the Pauli matrices, and the index k enumerates pairs of indices $\{\mu, \nu\}$ in lexicographic order. Since $\mathrm{tr}(\rho) = 1$, we get $x_1 = 1/4$.

By making the assumption that $|x_k| = s$ for $k = 2, \ldots, 16$, the optimization can be easily carried out analytically. We will see later that the maximum radius r^* for the general states (26) is indeed achieved under this assumption. The trace norm of the realignment is

$$\|R(\rho)\|_1 = \sum_k |x_k| = \frac{1}{4} + 15s \,. \tag{27}$$

Computing the minimal eigenvalue of $\Gamma(\rho)$ is not so straightforward, as the signs of the coefficients in Eq. (26) ought to be taken into account. We consider all possible sign combinations, and we see that the minimal eigenvalue of $\Gamma(\rho)$ is always of the form $\lambda_{\min}[\Gamma(\rho)] = \frac{1}{16}[1 - 4(2k-1)s]$, where $k = 1, 2, \ldots, 8$. Further, we check that $k = 2$ is the only combination with which the constraints $\rho \geq 0$, $\Gamma(\rho) \geq 0$, and $\|R(\rho)\|_1 > 1$ are satisfied, so we have

$$\lambda_{\min}[\Gamma(\rho)] = \frac{1}{16} - \frac{3}{4}s \,. \tag{28}$$

Let us denote

$$\begin{aligned} r_a &:= \sqrt{d/(d-1)}\, \lambda_{\min}[\Gamma(\rho)] = \frac{4}{\sqrt{15}} \left(\frac{1}{16} - \frac{3}{4}s \right) , \\ r_b &:= (\|R(\rho)\|_1 - 1)/\sqrt{d} = \frac{1}{4} \left(15s - \frac{3}{4} \right) . \end{aligned}$$

Since r_a and r_b are affine functions of the parameter s, the solution to the equation $r_a = r_b$ will single out a unique s^*, and the radius r^* associated to it will be maximal. These are

$$\begin{aligned} s^* &= \frac{1}{12} \frac{4 + 3\sqrt{15}}{4 + 5\sqrt{15}} \approx 0.05571 \,, \\ r^* &= \frac{1}{4} \left(15 s^* - \frac{3}{4} \right) \approx 0.0214 \,. \end{aligned} \tag{30}$$

As argued before, the parameter s^* is not enough to characterize a state of the form (26), as sign combinations of the coefficients x_k matter. An example of a state that achieves r^* is given by the parameters $x_1 = 1/4$, $x_k = s^*$ for $k \in S = \{2, 3, 4, 5, 6, 7, 9, 10, 12, 14\}$, and $x_k = -s^*$ for $k \in S^c \setminus \{1\}$.

Let us now tackle the optimization over the family of states in Eq. (26) without any extra assumption, for which we will resort to an exact but computer-aided method. First, note that the search for the optimal state can be concisely expressed as

$$\begin{aligned} \text{maximize} \quad & r \\ \text{subject to} \quad & Mx + \frac{1}{4} \geq 0 \\ & MDx + \frac{1}{4} \geq \sqrt{15} r \\ & \sum_k |x_k| - \frac{3}{4} \geq 4r \end{aligned} \tag{31}$$

where $x = \{x_k\}_{k=2}^{16}$ is a 15-dimensional real vector, r is a real nonnegative number, D is a diagonal matrix of signs such that the map $x \mapsto Dx$ effectively induces the map $\rho \mapsto \Gamma(\rho)$, M is a 16×15

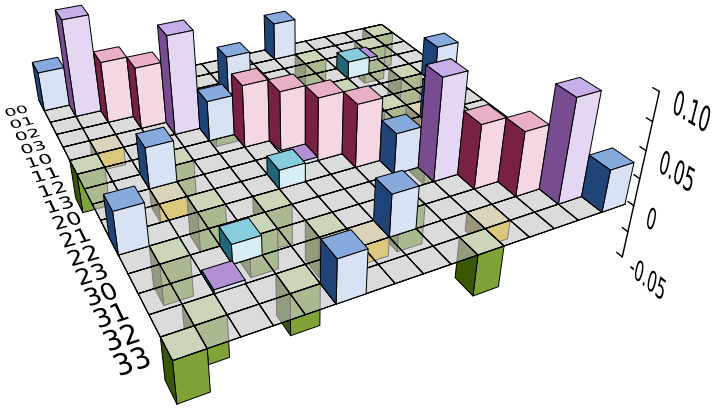

Figure 4: The density matrix of the optimal two-ququart state with parameters given in Eq. (32) in the computational basis. The heights of the bars correspond to the entries of the density matrix. Note that these are all real-valued.

matrix of signs such that $\frac{1}{4}Mx + \frac{1}{16}$ is a vector of eigenvalues of ρ, and recall that $x_1 = 1/4$ is fixed by normalization. Under these considerations it becomes apparent that the constraints in Eq. (31) correspond to semidefinite-positiveness, PPT, and CCNR, respectively.

In order to solve Eq. (31), we linearize the CCNR constraint by removing the absolute values and considering all the 2^{15} possible sign combinations in the sum. Moreover, we incorporate the constraint $r \geq 0$ and regard r as an extra free parameter, instead of as an objective function. Then, each sign combination chosen in the CCNR constraint results in a linear constraint that, along with positivity, PPT, and $r \geq 0$, will define a polytope of feasible parameters and, since all constraints are linear in r, its maximal value will occur for one of the vertices. Of course, each single linear program of this kind is in principle more restrictive than Eq. (31), but it is granted that the solution we are looking for will correspond to a vertex of the feasibility polytope of one of them. We enumerate the vertices of all the 2^{15} polytopes using the polyhedral computation library `cddlib`[2]. We then take the union of all vertices, eliminate redundant and nonextremal ones, and end up with a set of 4224 vertices with a maximal radius $r^* \approx 0.0214$, which coincides with the value analytically obtained above. The advantage of this method is that we obtain a much larger set of optimal states with varying rank. Having optimal states with smaller rank can significantly simplify their experimental preparation. In contrast, note that any state for which the assumption made in the analytical calculation above, $|x_k| = s$ for all $k = 2, \ldots, 16$, holds, is full-rank. The minimal rank for states of the form (26) achieving a maximal radius r^* is 10. An example of such a rank-10 optimal state is given by parameters

$$\begin{aligned} x_1 &= \frac{1}{4}\,, \\ x_\alpha &\approx -0.0557066\,, \quad \alpha \in \{2,3,4,5,6,9,12,14,16\}\,, \\ x_\beta &\approx 0.0142664\,, \quad \beta \in \{7,11,13\}\,, \\ x_\gamma &\approx 0.0971467\,, \quad \gamma \in \{8,10,15\}\,. \end{aligned} \tag{32}$$

In Fig. 4 we depict the resulting density matrix as a bar plot.

The vertex enumeration of all feasibility polytopes contained in Eq. (31) allows us to go beyond the set of optimal states and characterize states with even smaller ranks, naturally at the expense of sacrificing some volume of bound entangled states around them. With this in mind, we see that the absolute minimal rank for a Bloch-diagonal two-ququart bound entangled state is 9, with associated

[2] `cddlib` version 0.94h, https://www.inf.ethz.ch/personal/fukudak/cdd_home/

radius $r_9 \approx 0.0128$. An example of such state is given by parameters

$$\begin{aligned} x_1 &= \frac{1}{4}\,, \\ x_\alpha &\approx 0.0999184\,, \quad \alpha \in \{2,5\}\,, \\ x_\beta &\approx 0.0750408\,, \quad \beta \in \{3,4,6,10,14\}\,, \\ x_\gamma &\approx 0.0501632\,, \quad \gamma \in \{7,9\}\,, \\ x_\delta &\approx -0.0252856\,, \quad \delta \in \{8,13\}\,, \\ x_\epsilon &= -x_\gamma\,, \quad \epsilon \in \{11,15,16\}\,, \\ x_{12} &= -x_\delta\,. \end{aligned} \tag{33}$$

C A hypothesis test for bound entanglement

In this appendix we give a proof of Eq. (13) and show how to compute the parameters r_1, r_2, and m, needed to reproduce Fig. 2. Let us start with the proof.

The χ^2-distribution arises naturally in a hypothesis test where the hypotheses are defined in terms of bounds on Euclidean distances in a vector space of normal-distributed random variables. To see this, we consider a generic situation where we draw a sample $\vec{x}$ from an m-variate normal distribution $N(\vec{\xi}, \Sigma)$ with offset $\vec{\xi}$ and covariance matrix Σ. The offset shall be of the form $\vec{\xi} = S\lambda + \vec{\eta}$ with a matrix S and a constant vector $\vec{\eta}$. We denote by $p(t, r)$ the maximal probability that the hypothesis test $\hat{t}(\vec{x}) \leq t$ holds true under the hypothesis $\|\mu - \lambda\|_2 \geq r$ for some fixed μ, where $\vec{x}$ is sampled from $N(\vec{\xi}, \Sigma)$, and $\hat{t}$ is a test statistic. Then, for a given sample $\vec{x}$, the probability $p[\hat{t}(\vec{x}), r]$ is a p-value for the hypothesis test $\hat{t}(\vec{x}) \leq t$. By choosing

$$\hat{t}\colon \vec{x} \mapsto \|\Sigma^{-1/2}(S\mu + \vec{\eta} - \vec{x})\|_2\,, \tag{34}$$

the following lemma holds:

Lemma 1. *We have*

$$p(t, r) = q_m[t^2, r^2\, \lambda_{\min}(S^T \Sigma^{-1} S)]\,, \tag{35}$$

where $s \mapsto q_m(s, u)$ is the cumulative distribution function of the noncentral χ^2-distribution with m degrees of freedom and noncentrality parameter u. Here, $\lambda_{\min}(X)$ denotes the smallest eigenvalue of the symmetric matrix X.

Proof. By our assumptions, we have

$$p(t, r) = \sup_\lambda \{\, \mathbb{P}[\hat{t} \leq t] \mid \|\mu - \lambda\|_2 \geq r \,\}\,, \tag{36}$$

where $\hat{t}$ takes $\vec{x}$ distributed according to the normal distribution $N(\vec{\xi}, \Sigma)$. Then, $\vec{y} = \Sigma^{-1/2}(\vec{x} - \vec{\xi})$ is normal-distributed with offset $\vec{0}$ and covariance matrix $\mathbb{1}$, and we find

$$\begin{aligned} p(t, r) &= \sup_v \{\, \mathbb{P}[\|\vec{y} - \Sigma^{-1/2} S v\|_2 \leq t : \vec{y} \sim N(\vec{0}, \mathbb{1})] \mid \|v\|_2 \geq r \,\} \\ &\equiv \sup_v \{\, q_m(t^2, \|\Sigma^{-1/2} S v\|_2^2) \mid \|v\|_2 \geq r \,\}\,, \end{aligned} \tag{37}$$

where we used the definition of $q_m(s, u)$ in the second step. In order to see that this yields Eq. (35), it is enough to note that $q_m(s, u)$ is a monotonously decreasing function in u [44]. □

The cumulative distribution function of the noncentral χ^2- distribution is given in terms of Marcum's Q-function as $q_m(s, u) = 1 - Q_{m/2}(\sqrt{u}, \sqrt{s})$. In particular,

$$q_m(s, u) = \mathrm{e}^{-u/2} \sum_{l=0}^{\infty} \frac{(u/2)^l}{l!} \tilde{\gamma}(l + \tfrac{m}{2}, \tfrac{s}{2})\,, \tag{38}$$

where $\tilde{\gamma}$ is the regularized lower incomplete gamma function, so that $s \mapsto q_m(s,0)$ is the cumulative distribution function of the central χ^2-distribution[3].

Lemma 1 is presented in a generic form. At variance with the p-value defined in the main text [cf. Eq. (11)], note that the supremum in Eq. (36) is taken over a larger space, as λ is not affected by any positivity constraint. Hence, Eq. (35) is an upper bound of Eq. (11). In the context of the quantum experiment at hand, μ and λ are Hermitian operators, and we make the identifications $T(\rho_0) \equiv S(\mu) + \vec{\eta}$ and $T(\rho_{\text{exp}}) \equiv S(\lambda) + \vec{\eta}$, where ρ_0 is the target state with associated radius r_0, and ρ_{exp} is the actual state prepared in the experiment. Then, we find that $r_0^2\, \lambda_{\min}(S^T \Sigma^{-1} S) \equiv r_1^2$ [cf. Eq. (13)].

We now assume that the data is of the form $x_k^\ell = n_k^\ell / \sum_j n_j^\ell$, where n_k^ℓ is the number of events for outcome k and measurement setting ℓ. Then, the elements of the vector $T(X)$ are $\text{tr}(E_k^\ell X)$, given the effects $\{E_k^\ell\}$ with $\sum_k E_k^\ell = \mathbb{1}$, i.e., T takes quantum states to probabilities, and S is the restriction of T to the traceless operators. This determines $\vec{\eta} = T[\mathbb{1}/\,\text{tr}(\mathbb{1})]$. Note that one effect per measurement setting shall not be included in S, since its associated outcome will not be independent and this will lead to $r_1 = 0$. Note also that introducing the restricted map S is necessary in order to have a nonsingular covariance matrix Σ with a well defined inverse. With this in mind, one can determine the number of degrees of freedom m for the examples of qutrits and ququarts described in the main text. In the case of qutrits, measuring locally a complete set of mutually unbiased bases[4] (MUBs) in principle produces data of dimension 144 (we have 4 settings per party with 3 outcomes per setting), but eliminating dependent outcomes reduces this dimension to $m = 128$. For the sake of completeness, we give an explicit construction of the MUBs $\{M_\ell\}_{\ell=0}^3$, where each row in M_ℓ corresponds to a basis vector. Then, M_0 is the identity matrix,

$$M_1 = \frac{1}{\sqrt{3}} \begin{pmatrix} 1 & 1 & 1 \\ 1 & \omega^2 & \omega \\ 1 & \omega & \omega^2 \end{pmatrix}, \quad M_2 = \frac{1}{\sqrt{3}} \begin{pmatrix} 1 & 1 & \omega \\ 1 & \omega^2 & \omega^2 \\ 1 & \omega & 1 \end{pmatrix}, \quad M_3 = \frac{1}{\sqrt{3}} \begin{pmatrix} 1 & 1 & \omega^2 \\ 1 & \omega^2 & 1 \\ 1 & \omega & \omega \end{pmatrix}, \tag{39}$$

and $\omega = \exp(2\pi i/3)$. Likewise, for the ququart case we assume that the measurement settings for each party are built as pairs of local Pauli measurements $\{\sigma_\mu, \sigma_\nu\}$, with $\mu, \nu = 1, 2, 3$, hence we have 9 settings per party with 4 outcomes per setting, which leads to a reduced dimension of $m = 1215$.

For the moment, let us assume that the measurement outcomes k for each setting ℓ follow a Poisson distribution with parameters $N^\ell T(\rho)_k^\ell$, so that data is now of the form $x_k^\ell = n_k^\ell / N^\ell$, where N^ℓ is the mean total value of events for measurement setting ℓ. Then, the covariance matrix is a simple diagonal matrix with entries $T(\rho)_k^\ell / N^\ell$. In this situation, also the elimination of dependent outcomes is not necessary since Σ is invertible. This procedure is not optimal. If N^ℓ is large enough, we can well approximate N^ℓ by $\sum_k n_k^\ell$, at the cost of Σ becoming singular. However, after the dimensional reduction introduced above, the reduced covariance matrix is again invertible. The advantage of this approach is that we reduced the dimension m without discarding data, and hence the overall statistical performance is increased. This is due to the fact that r_1 and r_2 in this approach are the same as in the previous one. Note that an analysis using multinomial statistics yields the same reduced covariance matrix and hence the same parameters m, r_1, and r_2. For our examples in the main text we use the latter approach and assume $N^\ell \equiv n$ for all settings ℓ. The parameters used for computing p_{fail} in Fig. 2 are computed to be $r_1^2 \approx 0.0664^2 n$ and $r_2^2 \approx 0.0416^2 n$ for the qutrit example, and $r_1^2 \approx 0.0856^2 n$ and $r_2^2 \approx 0.0469^2 n$ in the ququart case.

[3] From Eq. (38) it is also easy to see that $f_k \colon u \mapsto q_{2k}(s, 2u)$ is a decreasing function in u, since $\partial_u f_k(u) = f_{k+1}(u) - f_k(u)$ and $\tilde{\gamma}(a,z) - \tilde{\gamma}(a+1,z) = \partial_z \tilde{\gamma}(a+1,z) = \mathrm{e}^{-z} z^a / \Gamma(a+1) \geq 0$.

[4] Two orthonormal bases $\{|e_i\rangle\}_{i=1}^d$ and $\{|f_i\rangle\}_{i=1}^d$ are called *mutually unbiased* if it holds that $|\langle e_j | f_k \rangle|^2 = 1/d \;\forall j, k = 1, \ldots, d$.

References

[1] M. Horodecki, P. Horodecki, and R. Horodecki, *Mixed-State Entanglement and Distillation: Is there a "Bound" Entanglement in Nature?*, Physical Review Letters **80**, 5239 (1998), DOI: 10.1103/PhysRevLett.80.5239.

[2] K. Horodecki, M. Horodecki, P. Horodecki, and J. Oppenheim, *Secure Key from Bound Entanglement*, Physical Review Letters **94**, 160502 (2005), DOI: 10.1103/PhysRevLett.94.160502.

[3] P. Horodecki, M. Horodecki, and R. Horodecki, *Bound Entanglement Can Be Activated*, Physical Review Letters **82**, 1056 (1999), DOI: 10.1103/PhysRevLett.82.1056.

[4] L. Masanes, *All Bipartite Entangled States Are Useful for Information Processing*, Physical Review Letters **96**, 150501 (2006), DOI: 10.1103/PhysRevLett.96.150501.

[5] Ł. Czekaj, A. Przysiężna, M. Horodecki, and P. Horodecki, *Quantum metrology: Heisenberg limit with bound entanglement*, Physical Review A **92**, 062303 (2015), DOI: 10.1103/PhysRevA.92.062303.

[6] G. Tóth and T. Vértesi, *Quantum States with a Positive Partial Transpose are Useful for Metrology*, Physical Review Letters **120**, 020506 (2018), DOI: 10.1103/PhysRevLett.120.020506.

[7] T. Moroder, O. Gittsovich, M. Huber, and O. Gühne, *Steering Bound Entangled States: A Counterexample to the Stronger Peres Conjecture*, Physical Review Letters **113**, 050404 (2014), DOI: 10.1103/PhysRevLett.113.050404.

[8] T. Vértesi and N. Brunner, *Disproving the Peres conjecture by showing Bell nonlocality from bound entanglement*, Nature Communications **5**, 5297 (2014), DOI: 10.1038/ncomms6297.

[9] M. Horodecki, J. Oppenheim, and R. Horodecki, *Are the Laws of Entanglement Theory Thermodynamical?*, Physical Review Letters **89**, 240403 (2002), DOI: 10.1103/PhysRevLett.89.240403.

[10] F. G. S. L. Brandao and M. B. Plenio, *Entanglement theory and the second law of thermodynamics*, Nature Physics **4**, 873 (2008), DOI: 10.1038/nphys1100.

[11] E. Amselem and M. Bourennane, *Experimental four-qubit bound entanglement*, Nature Physics **5**, 748 (2009), DOI: 10.1038/nphys1372.

[12] J. Lavoie, R. Kaltenbaek, M. Piani, and K. J. Resch, *Experimental bound entanglement?*, Nature Physics **6**, 827 (2010), DOI: 10.1038/nphys1832.

[13] J. Lavoie, R. Kaltenbaek, M. Piani, and K. J. Resch, *Experimental Bound Entanglement in a Four-Photon State*, Physical Review Letters **105**, 130501 (2010), DOI: 10.1103/PhysRevLett.105.130501.

[14] J. A. Smolin, *Four-party unlockable bound entangled state*, Physical Review A **63**, 032306 (2001), DOI: 10.1103/PhysRevA.63.032306.

[15] J. T. Barreiro, P. Schindler, O. Gühne, T. Monz, M. Chwalla, C. F. Roos, M. Hennrich, and R. Blatt, *Experimental multiparticle entanglement dynamics induced by decoherence*, Nature Physics **6**, 943 (2010), DOI: 10.1038/nphys1781.

[16] H. Kampermann, D. Bruß, X. Peng, and D. Suter, *Experimental generation of pseudo-bound-entanglement*, Physical Review A **81**, 040304 (2010), DOI: 10.1103/PhysRevA.81.040304.

[17] K. Dobek, M. Karpiński, R. Demkowicz-Dobrzański, K. Banaszek, and P. Horodecki, *Experimental Extraction of Secure Correlations from a Noisy Private State*, Physical Review Letters **106**, 030501 (2011), DOI: 10.1103/PhysRevLett.106.030501.

[18] F. Kaneda, R. Shimizu, S. Ishizaka, Y. Mitsumori, H. Kosaka, and K. Edamatsu, *Experimental Activation of Bound Entanglement*, Physical Review Letters **109**, 040501 (2012), DOI: 10.1103/PhysRevLett.109.040501.

[19] E. Amselem, M. Sadiq, and M. Bourennane, *Experimental bound entanglement through a Pauli channel*, Scientific Reports **3**, 1966 (2013), DOI: 10.1038/srep01966.

[20] K. Dobek, M. Karpiński, R. Demkowicz-Dobrzański, K. Banaszek, and P. Horodecki, *Experimental generation of complex noisy photonic entanglement*, Laser Physics **23**, 025204 (2013), DOI: 10.1088/1054-660X/23/2/025204.

[21] J. DiGuglielmo, A. Samblowski, B. Hage, C. Pineda, J. Eisert, and R. Schnabel, *Experimental Unconditional Preparation and Detection of a Continuous Bound Entangled State of Light*, Physical Review Letters **107**, 240503 (2011), DOI: 10.1103/PhysRevLett.107.240503.

[22] B. C. Hiesmayr and W. Löffler, *Complementarity reveals bound entanglement of two twisted photons*, New Journal of Physics **15**, 083036 (2013), DOI: 10.1088/1367-2630/15/8/083036.

[23] M. Paris and J. Řeháček (eds.), *Quantum State Estimation*, vol. 649 of *Lecture Notes in Physics* (Springer Berlin Heidelberg, Berlin, Heidelberg) (2004), ISBN 978-3-540-22329-0, DOI: 10.1007/b98673.

[24] Z. Hradil, *Quantum-state estimation*, Physical Review A **55**, R1561 (1997), DOI: 10.1103/PhysRevA.55.R1561.

[25] D. F. V. James, P. G. Kwiat, W. J. Munro, and A. G. White, *Measurement of qubits*, Physical Review A **64**, 052312 (2001), DOI: 10.1103/PhysRevA.64.052312.

[26] T. Sugiyama, P. S. Turner, and M. Murao, *Effect of non-negativity on estimation errors in one-qubit state tomography with finite data*, New Journal of Physics **14**, 085005 (2012), DOI: 10.1088/1367-2630/14/8/085005.

[27] C. Schwemmer, L. Knips, D. Richart, H. Weinfurter, T. Moroder, M. Kleinmann, and O. Gühne, *Systematic Errors in Current Quantum State Tomography Tools*, Physical Review Letters **114**, 080403 (2015), DOI: 10.1103/PhysRevLett.114.080403.

[28] B. Efron and R. J. Tibshirani, *An introduction to the bootstrap* (Chapman & Hall/CRC) (1994), ISBN 0-412-04231-2.

[29] J. Shang, H. K. Ng, A. Sehrawat, X. Li, and B.-G. Englert, *Optimal error regions for quantum state estimation*, New Journal of Physics **15**, 123026 (2013), DOI: 10.1088/1367-2630/15/12/123026.

[30] M. Christandl and R. Renner, *Reliable Quantum State Tomography*, Physical Review Letters **109**, 120403 (2012), DOI: 10.1103/PhysRevLett.109.120403.

[31] R. Blume-Kohout, *Robust error bars for quantum tomography*, arXiv:1202.5270 [quant-ph] (2012).

[32] L. Knips, C. Schwemmer, N. Klein, J. Reuter, G. Tóth, and H. Weinfurter, *How long does it take to obtain a physical density matrix?*, arXiv:1512.06866 [quant-ph] (2015).

[33] D. Suess, Ł. Rudnicki, T. O. Maciel, and D. Gross, *Error regions in quantum state tomography: computational complexity caused by geometry of quantum states*, New Journal of Physics **19**, 093013 (2017), DOI: 10.1088/1367-2630/aa7ce9.

[34] K. Życzkowski, *Volume of the set of separable states. II*, Physical Review A **60**, 3496 (1999), DOI: 10.1103/PhysRevA.60.3496.

[35] S. Bandyopadhyay, S. Ghosh, and V. Roychowdhury, *Robustness of entangled states that are positive under partial transposition*, Physical Review A **77**, 032318 (2008), DOI: 10.1103/PhysRevA.77.032318.

[36] O. Gühne and G. Tóth, *Entanglement detection*, Physics Reports **474**, 1 (2009), DOI: 10.1016/j.physrep.2009.02.004.

[37] B. Baumgartner, B. C. Hiesmayr, and H. Narnhofer, *State space for two qutrits has a phase space structure in its core*, Physical Review A **74**, 032327 (2006), DOI: 10.1103/PhysRevA.74.032327.

[38] R. A. Bertlmann and P. Krammer, *Bloch vectors for qudits*, Journal of Physics A: Mathematical and Theoretical **41**, 235303 (2008), DOI: 10.1088/1751-8113/41/23/235303.

[39] R. A. Bertlmann and P. Krammer, *Bound entanglement in the set of Bell-state mixtures of two-qutrits*, Physical Review A **78**, 014303 (2008), DOI: 10.1103/PhysRevA.78.014303.

[40] R. A. Bertlmann and P. Krammer, *Geometric entanglement witnesses and bound entanglement*, Physical Review A **77**, 024303 (2008), DOI: 10.1103/PhysRevA.77.024303.

[41] R. A. Bertlmann and P. Krammer, *Entanglement witnesses and geometry of entanglement of two-qutrit states*, Annals of Physics **324**, 1388 (2009), DOI: 10.1016/j.aop.2009.01.008.

[42] G. Sentís, C. Eltschka, and J. Siewert, *Quantitative bound entanglement in two-qutrit states*, Physical Review A **94**, 020302(R) (2016), DOI: 10.1103/PhysRevA.94.020302.

[43] T. Moroder and O. Gittsovich, *Calibration-robust entanglement detection beyond Bell inequalities*, Physical Review A **85**, 032301 (2012), DOI: 10.1103/PhysRevA.85.032301.
[44] N. L. Johnson, S. Kotz, and N. Balakrishnan, *Continuous Univariate Distributions*, 2nd ed. (John Wiley & Sons, New York) (1994), ISBN 978-0-471-58495-7.